GEMS & GEMOLOGY

WINTER 2019
VOLUME LV

THE QUARTERLY JOURNAL OF THE GEMOLOGICAL INSTITUTE OF AMERICA

Geographic Origin Special Issue

GIA®

Gems & Gemology Journals, Charts and More Available Through the GIA Store

GEMS & GEMOLOGY®

Visit our website to order. It's quick, easy and secure.

store.GIA.edu

store.gia.edu

GEMS & GEMOLOGY®
Winter 2019
VOLUME 55, No. 4


p. 569


p. 581


p. 637


p. 655


p. 663


p. 492

GEMS & GEMOLOGY®

gia.edu/gems-gemology

Subscriptions
Copies of the current issue may be purchased for $29.95 plus shipping. Subscriptions are $79.99 for one year (4 issues) in the U.S. and $99.99 elsewhere. Canadian subscribers should add GST. Discounts are available for renewals, group subscriptions, GIA alumni, and current GIA students. To purchase print subscriptions, visit store.gia.edu or contact Customer Service. For institutional rates, contact Customer Service.

Database Coverage
Gems & Gemology's impact factor is 1.844, according to the 2017 Thomson Reuters Journal Citation Reports (issued July 2018). *G&G* is abstracted in Thomson Reuters products (Current Contents: Physical, Chemical & Earth Sciences and Science Citation Index—Expanded, including the Web of Knowledge) and other databases. For a complete list of sources abstracting *G&G*, go to gia.edu/gems-gemology, and click on "Publication Information."

Manuscript Submissions
Gems & Gemology, a peer-reviewed journal, welcomes the submission of articles on all aspects of the field. Please see the Author Guidelines at gia.edu/gems-gemology or contact the Managing Editor. Letters on articles published in *G&G* are also welcome. Please note that Field Reports, Lab Notes, Gem News International, Micro-World, and Charts are not peer-reviewed sections but do undergo technical and editorial review.

Gems & Gemology is published quarterly by the Gemological Institute of America, a nonprofit educational organization for the gem and jewelry industry.

Postmaster: Return undeliverable copies of *Gems & Gemology* to GIA, The Robert Mouawad Campus, 5345 Armada Drive, Carlsbad, CA 92008.

Our Canadian goods and service registration number is 126142892RT.

About the Cover

This special issue is devoted to the geographic origin of specific colored stones. On the front cover, clockwise from left: a 64.45 mm Sri Lankan sapphire crystal, a 24.34 ct Sri Lankan blue sapphire, two cuprian tourmalines from Mozambique (55.52 and 45.74 ct), a 16.65 mm pink-purple Sri Lankan sapphire crystal, a 10.90 ct Burmese ruby, and an 11.11 ct Sri Lankan alexandrite. Courtesy of B&B Fine Gems and Evan Caplan. The back cover shows emeralds from the Chivor mine in Colombia (3.90 ct faceted stone and 2.35 cm crystal), courtesy of William Larson, Pala International. Photos by Robert Weldon/GIA.

Printing is by L+L Printers, Carlsbad, CA.
GIA World Headquarters The Robert Mouawad Campus 5345 Armada Drive Carlsbad, CA 92008 USA

ISSN 0016-626X

The Geographic Origin Dilemma

Shane F. McClure, Thomas M. Moses, and James E. Shigley

Welcome to the Winter 2019 edition of *Gems & Gemology*. This issue is special in that it is devoted exclusively to one timely subject: the determination of geographic origin for specific colored stones.

Geographic origin determination is one of the most pressing issues facing the industry—a subject with many facets and complexities that should be addressed if the discussion is to be thorough.

As part of GIA's consumer protection mission of ensuring the public trust in gems and jewelry, our purpose with this issue is to lay out what we know about determining geographic origin and how we arrive at those opinions. These articles will present every aspect of geographic origin as these authors understand it—including full transparency on the approaches and testing methods typically applied in GIA's gemological laboratories.

We intend for this issue to promote healthy and useful discussion and debate—fueled by our collective interest in bringing more understanding and consistency to the reporting of the geographic origin of colored stones.

THE CHALLENGES THAT FACE US

Geographic origin is, today, one of the least understood subjects the industry has ever experienced. Most people, other than the experts in the gemological laboratories who perform this service, do not understand the complexities accompanying the determination process. Many, including consumers, tend to misunderstand what geographic origin reports represent. Some in the industry use this lack of understanding to market stones carrying these reports in unethical ways.

The colored stone trade wants the laboratories to be able to tell them with 100% accuracy where their colored gemstones come from, and for these determinations to be consistent between all the major laboratories. Unfortunately, science cannot provide this capability. In fact, science by itself cannot even come close to this for certain gemstones—most notably blue sapphires.

Thus, laboratories must rely on the experience of their most senior gemologists, and their familiarity with gem material from the many different deposits around the world, to arrive at these determinations. This skill takes decades to develop, and even then only the most dedicated gemologists will become experts at it. This is the reason all gem labs emphasize that geographic origin determinations on reports are *opinions*—they are not indisputable facts. Because they are opinions, there will sometimes be differences in reports from different organizations.

These articles will present and discuss every part of this subject as these authors understand it. This will include exactly how the GIA laboratory approaches the issue and what testing methods are typically applied. We have chosen to use this platform to present what we know and do from our perspective. As one can see, this still results in a very large edition of *G&G*.

WHAT DETERMINES THE VALUE OF A COLORED GEMSTONE?

The main factors that determine the value of a gemstone are usually recognized as rarity, size, and durability. Also important to this equation are other factors such as beauty and mystique or lore. A stone may be large and rare and durable but unattractive for multiple reasons—poor clarity, color, or cut, for example. This clearly will affect its value. Gemstones often come from exotic places that are very remote and inaccessible. Some of these mines have a long history and may no longer exist. Historical occurrences may also have legends or interesting tales associated with them. All of these things add to the interest and therefore the desirability of a particular gem, which will add to its value.

Geographic origin may also be an indicator of the rarity and beauty of a gemstone. Some deposits only lasted for a short term, so the supply is limited. The most notable example is blue sapphire from Kashmir. Some deposits are historically perceived as producing

This Cartier bracelet from 1927 features a 47.07 ct cabochon sapphire between two pear-shaped diamonds weighing 8.60 and 9.27 ct. The sapphire is accompanied by two identification reports stating a Burmese origin, with no indications of heating. In November 2019, the bracelet sold at Sotheby's in Geneva for nearly $6.3 million. Courtesy of Sotheby's.

the finest quality of a specific gemstone (e.g., ruby from Myanmar). This may or may not still hold true, but as with many things, perception is everything, so a Burmese origin becomes more desirable and therefore more valuable.

REQUIREMENTS FOR GEOGRAPHIC ORIGIN DETERMINATION

The first prerequisite for a laboratory to issue geographic origin reports is access to adequate scientific instrumentation. With very few exceptions, this equipment is essential to the process. There is no question that this equipment is costly, which makes it out of reach for many smaller labs, but that does not change the fact that a lab must have it to competently offer this service.

The second requirement is experienced gemologists. Extensive familiarity with the material from mines around the world is absolutely required. This is the most difficult part of the equation. Equipment can be purchased—all it takes is money. Laboratory gemologists with enough experience to competently make geographic origin determinations are much rarer and are almost always unavailable. The only real way to get them is to recruit the people with the right background, determination, and desire to learn and to train them. However, this takes many years and the examination of thousands of samples.

Third is a comprehensive collection of samples that are known to originate from specific mines. The only way to obtain this is to go to those mines and collect samples as close to the source as possible. This process is the topic of the field gemology article in this issue. From these samples the data are collected and a database is formed, which becomes the underlying basis for geographic origin determinations.

THE HISTORY OF GEOGRAPHIC ORIGIN

The first to offer this service was the Gübelin laboratory in Switzerland in the 1950s. They based their determinations on Dr. Edward Gübelin's studies on how inclusions can help identify gems and their sources. Most analytical equipment was not available at that time, so gemological properties were all they had to go on.

At that time there were still relatively few deposits, so separation was not as complicated as it is today. Back then rubies came from Mogok, Burma (now Myanmar), and Thailand, two deposits completely unlike one another, so they were easy to separate. There were also some rubies found in Ceylon (now Sri Lanka), which had more in common with Burmese rubies but were still different enough to allow separation. Emeralds were mostly from Colombia and Russia, with other world sources insignificant in comparison. Sapphires had more sources even then. Kashmir and Burma were the most important, followed by Ceylon. Darker basaltic sapphires came mostly from Thailand and Australia.

Geographic origin gradually became more important in the trade over time—in some instances more important than quality. Even now, a lower-quality sapphire from Kashmir might be more expensive than a much finer sapphire from Sri Lanka simply based on the provenance.

Of course, over time, more gemstone deposits were found, some with similar geologic formation conditions as older deposits. This made separation more complicated. Even so, for a long time origin determination was not requested on reports for locations with less prestige. Today this has changed in many cases.

As demand for independent reports on gemstones increased, more laboratories came into existence, to the point where there are literally hundreds of them around the world today. Most of these are small, with few staff and even fewer resources to invest in analytical equipment.

Nevertheless, most of these laboratories try to issue geographic origin reports, regardless of their level of instrumentation and experience. There is not even much information available for them to work from. Most laboratories that have independently developed criteria for geographic origin determination through their own research consider this information proprietary and do not publish it, at least not in any detail. There is a significant investment of time and money involved that they feel must be protected. It is also the reason why there is so much inconsistency in origin determination among labs.

The question of whether or not geographic origin reports should be issued has become irrelevant. For many years there were industry leaders who actively opposed the growing trend toward country of origin reporting. In his editorial for the Winter 1990 *G&G*, GIA chairman Richard T. Liddicoat wrote:

> It would appear that if a ruby originated in Burma, it has a mystical property that makes it worth appreciably more than an identical ruby from another source. The same situation applies to sapphires from Kashmir. Yet, if two stones are identical in appearance, with no hidden faults, it is difficult to understand why one should have greater value than the other.

Indeed, these authors have privately had conversations with many dealers in the industry, who almost unanimously agree that gemstones should be valued based on their beauty, not the location of the hole in the ground they came from. However, we are all forced to acknowledge that the "ship has sailed" in this regard. There are far too many stones that have been sold for a price based on their origin for the industry to go back. The industry has fully embraced this pricing system, so much so that fairness or lack of logic no longer matters.

The industry had the opportunity to not go down this road with a more recent find of a new and valuable gemstone. When copper-bearing tourmaline was discovered in the Brazilian state of Paraíba in the late 1980s, it was the only location known for this material. When similar material was described in Nigeria in 2001 and Mozambique in 2004, the trade could have priced the material on its own merit, but that did not happen. It was somehow decided that the material from Brazil was worth substantially more, even for extremely similar stones from the other sources.

THE PROBLEM WITH GEOGRAPHIC ORIGIN REPORTS

Gem deposits are about geology, not geography. Where lines have been placed on a map to mark country boundaries is completely irrelevant to where gems form. The geologic conditions needed to form gemstones can occur in many countries and often do not respect geographic boundaries. Sometimes deposits have unique characteristics that make separation from other deposits possible. Other times they do not. Regardless, laboratories are tasked with separating them. Geographic origin determination is based on the idea that gemstones from different deposits will have different properties, which is not always true. Deposits in different countries may produce gems with similar properties (some blue sapphires from Myanmar are virtually identical to some blue sapphires from Sri Lanka). Conversely, deposits within the same country may differ in their geology and so their gems will be different. For instance, most blue sapphires from

Madagascar are from metamorphic deposits, but the deposits in Ambondromifehy are formed in alkali basalts—two very different deposits, yet both from Madagascar.

As stated earlier, when geographic origin determination began there were relatively few deposits, and those could usually be separated without much difficulty. Since that time, many more deposits have been found. As each of these deposits started to produce marketable gemstones, the issue of geographic origin became more complicated. In addition, as historical deposits have aged or become deeper or wider, their properties may vary. What used to be achievable with standard gemological tests and a microscope is no longer possible. The collection of additional analytical data such as chemistry and spectroscopy has become essential. Today these kinds of tests are routine and the search continues for other, more advanced techniques that might help.

As instruments become more complex, more knowledge is needed to operate them and interpret the data that comes from them. Instruments have become much more expensive to acquire and maintain. Often this requires people with advanced degrees in subjects such as chemistry, solid-state physics, geology, and mineralogy. This is particularly true with some techniques used for chemical analysis such as laser ablation–inductively coupled plasma–mass spectrometry (LA-ICP-MS), where continual calibration with well-known standards is essential to accurately analyze trace elements at increasingly lower concentrations (now down to parts per billion in some cases).

For years, orange fluorescence in blue sapphire was thought to exclusively indicate a Sri Lankan origin. Photo by Tino Hammid.

Another significant issue is acquiring reliable samples to test in constructing a database. Even with the best intentions, it is possible for stones from a dealer to get mixed up. Samples acquired in this way might not be accurate. The only sure way to get reliable samples is to visit the mines and collect them yourself. Even then it is difficult to be certain the stones came from the mine where they were collected. Careful documentation of how, when, where, and from whom the samples were acquired is essential to building a reliable database. GIA has a permanent field gemology department whose job it is to collect these samples as close to the mines as possible and process them. Everything about how they were collected, along with all the spectra, chemistry, and gemological data, is added to the origin database.

Of course, building such a database and gathering terabytes of information on the samples sometimes forces us to change commonly held ideas about criteria for geographic origin. A simple example would be orange fluorescence in blue sapphire. It was long thought that this property pointed to a Sri Lankan origin. However, as more deposits were found and more research was done, it became clear that orange fluorescence can occur in blue sapphire from several marble-type, relatively low-iron metamorphic deposits. So this property is now known to be mostly unhelpful in separating origin.

No matter how hard we try, sometimes we simply cannot tell where a stone came from. This could happen because of an extreme overlap of properties or because the properties do not match anything in our database. In such cases, we will say the origin is "inconclusive," which is never a popular conclusion. Regardless, in such situations it is the truth.

EXPERT OPINIONS

For all the reasons already mentioned and more, geographic origin reports are an opinion, not fact. Granted, some localities are easier to separate, but still the determination is an opinion. The quality of this opinion is based on the rigor of all of the points noted above. Every major laboratory has a comment stating this on their reports. This being an opinion, there are bound to be differences between laboratories, particularly with the more difficult determinations such as blue sapphire. Despite this fact, many in the industry treat these reports as fact and are surprised and frustrated that they sometimes get differ-

Rough and cut ruby: The crystal measures 23.4 mm in length, and the faceted stone weighs 5.22 ct. The cut stone carries four different identification reports, with the country of origin listed as either Afghanistan or Vietnam. Rubies from these two sources have similar characteristic properties. Photo by Robert Weldon/GIA; courtesy of Edward Boehm/RareSource.

ent results from different laboratories on the same stone. They should not be, but they often are.

Auction houses have begun to understand this. When selling a stone that has conflicting reports, they will often list all the reports in their catalog. In this way they let the buyer decide how much importance to give each report.

ETHICAL ISSUES

It should not be surprising that this situation allows openings for people whose ethics are less than honorable. Make no mistake: It is our opinion that the vast majority of people in the jewelry trade are honest and do their best to uphold a high ethical standard. As with any business, however, there will be some who do not let ethics get in the way of profit. The fact that certain origins can add value creates a situation where some dealers will sell a stone with a laboratory report that they know is incorrect. A dealer once told one of these authors, "It does not matter where a stone actually come from. It only matters where the labs say it comes from."

We know that some blue sapphires from Sri Lanka are almost identical to Burmese sapphires, and because of this they are often called Burmese. Some who trade in these stones call them "lucky Burma"

Gemstone classics from sources old and new: A 2.50 ct Colombian emerald ring, courtesy of Ronald Ringsrud; a 7.04 ct Madagascar sapphire, courtesy of Mayer & Watt; and an exceptional 4.10 ct concave-facet ruby from Winza, Tanzania, courtesy of Mark Gronlund. Photo by Robert Weldon/GIA.

and will sell them as Burmese even though they know it is not true.

We feel compelled to mention that some in the industry will do just the opposite. These people, if faced with a "lucky Burma" situation or something comparable, would come back to the lab and disclose the true origin, even though it might affect the value of the stone. Such honesty is uncommon in any trade.

These last paragraphs may seem overly critical of some in the industry, but that is not our intent. However, it is necessary to point out all the various pieces of this issue, as they all have a part in understanding the numerous complexities that affect this subject.

In everything we do, we are driven to bring awareness, education, and trust in gems and jewelry. In doing so, we work to support the producers, dealers, manufacturers, and retailers that make up this great industry.

In the coming pages, we lay out a thorough examination of our perspective on this complex subject—striving to be transparent about how GIA approaches geographic origin determination.

We hope this issue will spark a constructive discussion between laboratories, gemologists, experts, and members of the colored stone trade who may see things differently or have different ideas on this subject, resulting in a betterment of the industry and protection of the public—GIA's ultimate mission.

Mr. McClure is global director of colored stone services, Mr. Moses is chief laboratory and research officer, and Dr. Shigley is a distinguished research fellow, at the Gemological Institute of America.

JOIN US FOR

GIA Science Talks

A New Quarterly Series on
Gem Research Discoveries

UPCOMING SESSIONS

February 19, 2020

Natural Diamonds and Continent Formation

With Dr. Karen Smit

May 2020 (exact dates to come)

Oxygen Isotopes in Pearls and Paleoclimate

With Dr. Chunhui Zhou

August 2020 (exact dates to come)

Transition Metals Causing Gemstone and Diamond Color

With Dr. Chloe Peaker

The hour-long sessions begin at 5:00 p.m. at GIA's New York education campus and are free and open to the public. Registration in advance is required to attend.

Learn more at GIA.edu/science-talks

GIA®

The World's Foremost Authority in Gemology™

Geology of Corundum and Emerald Gem Deposits: A Review

Gaston Giuliani and Lee A. Groat

The great challenge of geographic origin determination is to connect the properties and features of individual gems to the geology of their deposits. Similar geologic environments can produce gems with similar gemological properties, making it difficult to find unique identifiers. Over the last two decades, our knowledge of corundum and emerald deposit formation has improved significantly.

The mineral deposits are classically separated into primary and secondary deposits. Primary corundum deposits are subdivided into two types based on their geological environment of formation: (1) magmatic and (2) metamorphic. Magmatic deposits include gem corundum in alkali basalts as in eastern Australia, and sapphire in lamprophyre and syenite as in Montana (United States) and Garba Tula (Kenya), respectively. Metamorphic deposits are divided into two subtypes (1) *metamorphic deposits sensu stricto* (in marble; mafic and ultramafic rocks, or M-UMR), and (2) *metamorphic-metasomatic deposits* characterized by high fluid-rock interaction and metasomatism (i.e., plumasite or desilicated pegmatites in M-UMR and marble, skarn deposits, and shear zone–related deposits in different substrata, mainly corundum-bearing Mg-Cr-biotite schist). Examples of the first subtype include the ruby deposits in marble from the Mogok Stone Tract or those in M-UMR from Montepuez (Mozambique) and Aappaluttoq (Greenland). The second subtype concerns the sapphire from Kashmir hosted by plumasites in M-UMR.

Secondary corundum deposits (i.e., present-day placers) result from the erosion of primary corundum deposits. Here, corundum is found in the following types of deposits: eluvial (derived by in situ weathering or weathering plus gravitational movement), diluvial (scree or talus), colluvial (deposited at the base of slopes by rainwash, sheetwash, slow continuous downslope creep, or a combination of these processes), and alluvial (deposited by rivers). Today, most sapphires are produced from gem placers related to alkali basalts, as in eastern Australia or southern Vietnam, while placers in metamorphic environments, such as in Sri Lanka (Ratnapura, Elahera) and Madagascar (Ilakaka), produce the highest-quality sapphires. The colluvial Montepuez deposit in Mozambique provides a huge and stable supply of clean and very high-quality rubies.

Primary emerald deposits are subdivided into two types based on their geological environment of formation: (1) tectonic-magmatic-related (Type I) and (2) tectonic-metamorphic-related (Type II). Several subtypes are defined and especially Type IA, hosted in M-UMR, which accounts for about 70% of worldwide production (Brazil, Zambia, Russia, and others). It is characterized by the intrusion of pegmatites or quartz veins in M-UMR accompanied by huge hydrothermal fluid circulation and metasomatism with the formation of emerald-bearing desilicated pegmatite (plumasite) and biotite schist. Type IB in sedimentary rocks (China, Canada, Norway, Kazakhstan, and Australia) and Type IC in granitic rocks (Nigeria) are of minor importance.

The subtype Type IIA of metamorphic deposits is related to hydrothermal fluid circulation at high temperature, in thrust fault and/or shear zones within M-UMR of volcano-sedimentary series, such as at the Santa Terezinha de Goiás deposit in Brazil. The subtype Type IIB is showcased by the Colombian emerald deposits located in the Lower Cretaceous black shales of the Eastern Cordillera Basin. These are related to the circulation of hydrothermal basinal fluids in black shales, at 300–330°C, that dissolved evaporites in (1) thrust and tear faults for the deposits of the western emerald zone (Yacopi, Coscuez, Muzo, Peñas Blancas, Cunas, and La Pita mines) and (2) a regional evaporite level intercalated in the black shales or the deposits of the eastern emerald zone (Gachalá, Chivor, and Macanal mining districts).

Secondary emerald deposits are unknown because emerald is too fragile to survive erosion and transport in rivers.

See end of article for About the Authors and Acknowledgments.

Gems & Gemology, Vol. 55, No. 4, pp. 464–489,
http://dx.doi.org/10.5741/GEMS.55.4.464

PART I: RUBY AND SAPPHIRE

Ruby and sapphire are gem varieties of the mineral corundum. The chromophores are chromium (Cr^{3+}) in ruby, and iron and titanium (Fe^{2+} and Ti^{4+}) in blue sapphire. All other colors are termed *fancy sapphires* and are named on the basis of color (e.g., yellow sapphire). Another valuable colored sapphire is the orange-pink or pinkish orange variety called *padparadscha*, derived from names for the lotus blossom. In this paper, the pink corundum associated with ruby worldwide (such as in the marble-type deposits) and called "pink sapphire" in the literature is considered to be genetically associated with ruby and not sapphire of other colors.

In Brief

- The classification systems of corundum and emerald deposits are based on different mineralogical and geological features.
- Corundum deposits are subdivided into primary (magmatic and metamorphic) and secondary (i.e., present-day placer) deposits.
- Emerald deposits are only primary and are subdivided into two types: (1) tectonic-magmatic-related and (2) tectonic-metamorphic-related.
- Today most gem sapphires are produced by placers in metamorphic and alkali basalt environments. Most rubies are produced by placers in metamorphic environments (marble and amphibolite rocks).

Geographic Distribution and Economic Significance. Corundum is found on all five continents. The highest-quality ruby crystals come from Central and Southeast Asia and Mozambique (SRK Consulting, 2015). Myanmar, with the Mogok Stone Tract, has produced "pigeon's blood" rubies since 600 CE (Hughes, 1997). The world's finest blue sapphire comes from Kashmir (Sumjam), Myanmar, Sri Lanka (figure 1), and Madagascar. Sri Lanka is so far the most important producer of excellent padparadscha sapphire (Hughes, 1997).

The value of natural ruby and sapphire is based on the classic Four C's (color, clarity, cut, and carat weight) but also on the geographic origin. Enhancements and treatments are also of importance in the final evaluation, and it is very rare to find gem corundum that has not been heat-treated (Themelis, 1992).

Ruby and sapphire are the most important colored gemstones in the gem trade, and together they account for more than 50% of global colored gem production (Hughes, 1997). Top-quality ruby is perhaps the world's most expensive gemstone, and the finest Mogok rubies are more highly valued than equivalent-sized flawless colorless diamonds. The world record price for a single ruby sold at auction belongs to the Sunrise Ruby, sold by Sotheby's in 2015 for $32.42 million ($1.27 million per carat at 25.59 ct).

Figure 1. A 245.12 ct sapphire crystal from Kataragama, Sri Lanka, measuring 5.70 × 2.15 × 1.85 cm. Photo by Robert Weldon/GIA; courtesy of Brent Lockhart.

In December 2015, the 15.04 ct Crimson Flame ruby sold for $18.3 million ($1.21 million per carat). Another notable ruby is the 10.05 ct Ratnaraj, which sold for $10.2 million (just over $1 million per carat) in November 2017 ("Ratnaraj ruby ring highlight…," 2017). The world record price paid for a single blue sapphire is $17.30 million for the 392.52 ct Blue Bell of Asia ($44,063 per carat) at a 2014 Christie's auction. However, the world record price per carat belongs to an unnamed 27.68 ct Kashmir blue sapphire that sold at a 2015 Christie's auction for $6.75 million, or $243,703 per carat. Unheated ruby from the Didy mine in Madagascar also commands high prices (Pardieu and Rakotosaona, 2012). Peretti and Hahn (2013) reported that a set of eight faceted rubies, ranging from 7 to more than 14 ct apiece, had an estimated market value of $10 million.

The discovery of the Montepuez ruby deposits in Mozambique in May 2009 (Pardieu et al., 2009), and their extraction by various companies, including Gemfields (Pardieu, 2018; Simonet, 2018), changed the international ruby market. SRK Consulting (2015) forecasted production of 432 million carats over 21 years. The resource at Montepuez is divided into primary reserves of 253 million carats (a projection of 115 carats per ton) and secondary (mainly colluvial) reserves of 179 million carats (a projection of 7.07 carats per ton). Nine Montepuez auctions held since June 2014 have generated $335 million in aggregate revenue (Pardieu, 2018).

Age of the Deposits. The global distribution of corundum deposits is closely linked to plate tectonics—collision, rift, and subduction geodynamics (Giuliani et al., 2007a). Direct dating of corundum is impossible due to the absence of a suitable geochronometer. Ages are defined by indirect dating of a series of minerals (zircon, monazite, rutile, and micas), either in the host rocks or as **syngenetic** inclusions in the corundum (please refer to the Glossary for boldfaced terms). These minerals have different blocking temperatures closed to isotopic migration that make it possible to establish a cooling history for corundum.

Four main periods of corundum formation are recognized worldwide (Giuliani et al., 2007a; Graham et al., 2008). The oldest deposit is located in the Archean **metamorphic** series (2.97–2.6 billion years ago, or Ga) of southwest Greenland. The Aappaluttoq ruby deposit in the 2.97 Ga Fiskenæsset anorthosite complex contains a sequence of thick olivine-ultramafic rocks intruded by leucogabbros that underwent a high degree of metamorphism at 2.82 Ma (U-Pb dating of monazite; Fagan, 2018). The contact between the ultramafic rock and the leucogabbro was the focus of intense fluid-rock interaction at 2.66 Ga (U-Pb dating of monazite) with ruby formation in **phlogopite** rocks (Krebs et al., 2019).

The second period of corundum formation was the Pan-African **orogeny** (750–450 Ma). This includes primary ruby and sapphire deposits in the gemstone belt of East Africa, Madagascar, India, and Sri Lanka that are linked to collisional processes between eastern and western Gondwana (figure 2) during Pan-African tectonic-metamorphic events (Kröner, 1984). The metamorphic corundum deposits in southern Madagascar have numerous geological similarities with those in East Africa, Sri Lanka, and southern India (see Giuliani et al., 2014). U-Pb dating of zircon in host rocks of ruby from the John Saul mine in the Mangare area of Kenya (612 ± 6 Ma; Simonet, 2000), Longido in Tanzania (610 ± 6 Ma; Le Goff et al., 2010), and the Vohibory deposits in Madagascar (612 ± 5 Ma; Jöns and Schenk, 2008) revealed similar periods of formation related to the East African orogeny. U-Pb dating of rutile inclusions in ruby from the different ruby mines at Mangare has indicated cooling ages between 533 ± 11 and 526 ± 13 Ma (Sorokina et al., 2017a). Moreover, the U-Pb ages of zircon coeval with blue sapphire in the Andranondambo skarn deposit in southern Madagascar range from 523 to 510 Ma (Paquette et al., 1994). These different ages confirm the existence of a metamorphic corundum episode, between 600 and 500 Ma, during the late Pan-African orogenic cycle (**Cambrian** period), and corresponding to the Kuunga orogeny.

The third period corresponds to the Cenozoic Himalayan orogeny (45 Ma to the Quaternary). Examples include the marble-hosted ruby deposits in Central and Southeast Asia, which occur in metamorphic blocks that were affected by major tectonic events during the collision of the Indian and Eurasian plates (Garnier et al., 2008). The ruby has been indirectly dated by $^{40}Ar/^{39}Ar$ stepwise heating experiments performed on single grains of coeval phlogopite, and by ion-probe U-Pb analyses of zircon included in the corundum (Graham et al., 2008; Giuliani et al., 2014). All of the Oligocene to Pliocene ages (40–5 Ma) are consistent with compressional tectonic events that were active in the ruby-bearing metamorphic belt from Afghanistan to Vietnam.

The fourth period of corundum formation is dominated by the extrusion of **alkali basalts** in the Ceno-

Figure 2. Juxtaposition of Antarctica, Sri Lanka, India, Madagascar, and Eastern Africa in a reconstruction of Gondwana showing the locations of the main gem corundum deposits (see Giuliani et al., 2014). Eastern Africa: Garba Tula (GT), Mangare (M), Twiga (T), Si Ndoto (SN), Longido and Lonsogonoi (LL), Mahenge and Morogoro (MM), Kalalani and Umba (K), Songea (S), Tunduru (T). Mozambique: Montepuez (Mz); Madagascar: Ilakaka (Ila), Zazafotsy and Sahambano (ZS), deposits from the Vohibory region (Vo), Ambatomena (Am), Andranondambo (An), Andilamena (And), Didy (Dy). South India: Mysore (My), Karur-Kangayam corundum belt (KK), Orissa (Or). Sri Lanka: Ratnapura and Elahera (RE), Wanni Complex (WC), Highland Complex (HC). Antarctica: Napier Complex (NC), Rayner Complex (RC), Lützow-Holm Complex (LHC), Yamoto-Belgique Complex (YBC).

zoic (65 Ma to Quaternary). Gem corundum occurs worldwide as **xenocrysts** or **megacrysts** in **xenoliths** or enclaves incorporated in **basaltic** magmas during their ascent. Such sapphire and ruby deposits occur from Tasmania through eastern Australia, Southeast Asia, and eastern China to far eastern Russia (Graham et al., 2008). They are also found in Nigeria and Cameroon in the Aïr and Hoggar regions; the French Massif Central in the Limagne Rift; in northern, central, and eastern Madagascar (Hughes, 1997; Giuliani et al., 2014); and recently at Aksum in Ethiopia (Vertriest et al., 2019).

Classification of Corundum Deposits. Classification systems have evolved over time and are based on different mineralogical and geological features:

1. the morphology of corundum (Ozerov, 1945)
2. the geological context of the deposits (Hughes, 1997)

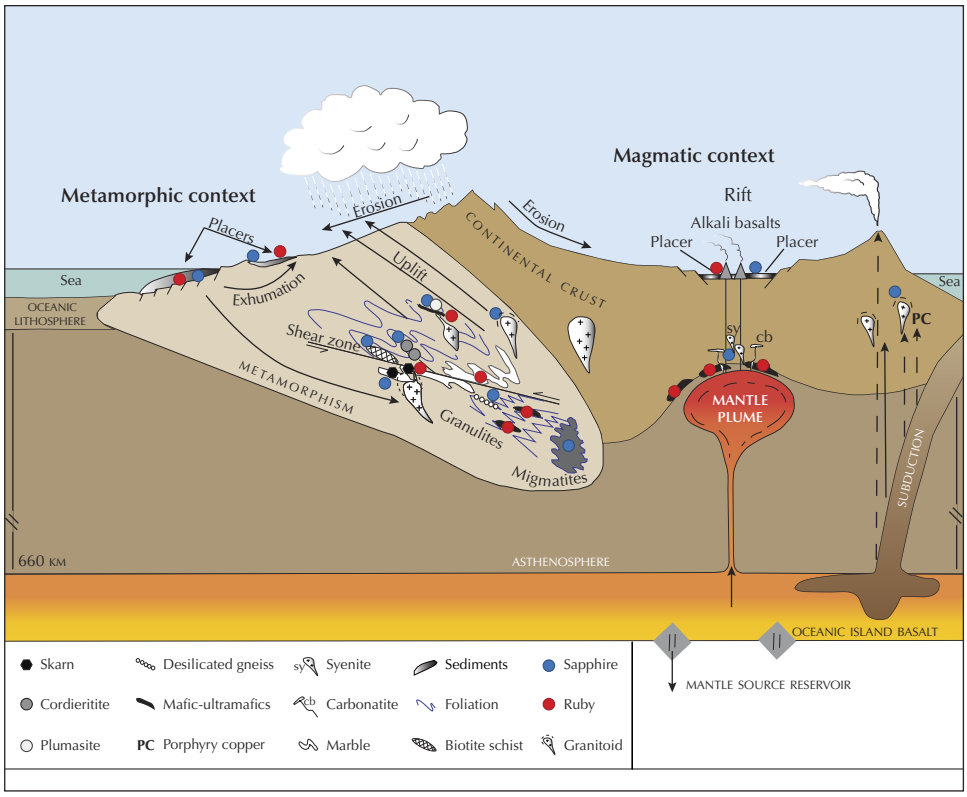

Figure 3. The different types of corundum deposits in their geological and geodynamical environments. The vertical dimension is not to scale, and the subcontinental lithosphere is not shown. Modified from Giuliani et al. (2014).

3. the lithology of the host rocks (Schwarz, 1998)
4. the genetic processes responsible for corundum formation (Simonet et al., 2008)
5. the genetic type of the deposit (Kievlenko, 2003)
6. the geological environment and nature of the corundum host rock (Garnier et al., 2004; Giuliani et al., 2007a, 2014)
7. the oxygen isotopic composition of the corundum (Giuliani et al., 2012)

Today, gem corundum deposits are classified as *primary* and *secondary* deposits. Primary deposits contain corundum either in the rock where it crystallized or as xenocrysts and in xenoliths in the rock that carried it from the zone of crystallization in the crust or mantle to the earth's surface.

Primary deposits are subdivided into two types: magmatic and metamorphic (figure 3). **Magmatic** deposits include gem corundum in alkali basalts and sapphire in **lamprophyres** and **syenites**. Metamorphic deposits are divided into *metamorphic deposits sensu stricto* (marble; M-UMR), and *metamorphic-metasomatic deposits* characterized by high fluid-rock interaction and metasomatism (i.e., **plumasite** or desilicated **pegmatites** in M-UMR and marble, skarn deposits, and **shear zone**–related deposits in different substrata, mainly corundum-bearing Mg-Cr-biotite schist).

Secondary deposits (i.e., present-day **placers**) are of two types (Dill, 2018). The first are eluvial concentrations derived by in situ weathering or weathering plus gravitational movement or accumulation. Eluvial-diluvial deposits are on slopes and in karst cavities (marble type). Colluvial deposits correspond to decomposed primary deposits that have moved vertically and laterally downslope as the hillside eroded. The second are alluvial deposits resulting from erosion of the host rock and transport of corundum by streams and rivers. Concentration occurs where water velocity drops at a slope change in the hydrographical profile of the river, such as at the base of a waterfall or in broad gullies, debris cones, meanders, and inflowing streams. Sometimes the corundum placers are marine, as at Nosy Be Island, Madagascar (Ramdhor and Milisenda, 2004).

Geology and Genesis of Primary Magmatic Corundum Deposits. Gem corundum in magmatic deposits is found in plutonic and volcanic rocks. In **plutonic** rocks, corundum is associated with rocks deficient in silica and their pegmatites, namely syen-

ite (Simonet et al., 2004) and nepheline syenite (Sorokina et al., 2017b). The corundum formed by direct crystallization from the melt as an accessory mineral phase. In volcanic rocks, sapphire and occasionally ruby are found in continental alkali basalt (Sutherland et al., 1998a). The corundum occurs as xenocrysts in lava flows and plugs of subalkaline olivine basalts, high-alumina alkali basalt, and basanite. These magmas occur in crustal extensional environments impacted by the rise of upwelling **mantle plumes**. The sapphires are either blue-green-yellow (BGY; figure 4A) or pastel-colored, and the deposits have economic importance only because advanced weathering in tropical regions concentrates the sapphires in eluvial and especially large alluvial placers. Gem sapphires also occur as xenocrysts in alkaline basic lamprophyre such as for the Yogo Gulch deposit in Montana (Brownlow and Komorowski, 1988; Renfro et al., 2018), as mafic dikes of biotite monchiquite called **ouachitite**, a lamprophyre characterized by an abundance of phlogopite and brown amphibole, olivine, clinopyroxene, and analcime. For other Montana deposits such as Missouri River, the lamprophyres have not been identified and Berg and Palke (2016) found sapphires in a basaltic trachyandesite sill. Berg (2007) postulated that the Rock Creek sapphires were transported by rhyolitic volcanism.

Research over the last decade has greatly improved our knowledge of the genesis of sapphire-bearing lamprophyres in Montana (Berg and Palke, 2016; Palke et al., 2016, 2017) and gem corundum-bearing alkali basalts (Graham et al., 2008; Sutherland et al., 2009; Uher et al., 2012; Baldwin et al., 2017; Palke et al., 2018). The sapphires and/or rubies are xenocrysts and more rarely megacrysts in xenoliths formed under metamorphic and/or magmatic conditions (figures 4B, D). Previous trace element chemistry of the alluvial sapphires from Montana suggested a metamorphic origin (Peucat et al., 2007). However, Palke et al. (2016) reported the presence of Na and Ca glassy melt inclusions in Yogo Gulch sapphires, which suggested a magmatic origin. That study related the formation of sapphire to partial lower crustal melting of plagioclase-rich magmatic rocks by the lamprophyre. In this scenario, the sapphires are not "accidental" xenocrysts originating elsewhere, but rather "in situ" xenocrysts enclaved by the lamprophyre itself before their transport to the surface (Palke et al., 2018).

Studies of the BGY sapphires and ruby in alkali basalts (figure 4) focused on solid inclusions (Sutherland et al., 2009; Baldwin et al., 2017; Palke et al., 2018), trace element geochemistry (Peucat et al., 2007), oxygen isotopes (Yui et al., 2003; Giuliani et al., 2005), and the nature of their parental xenoliths

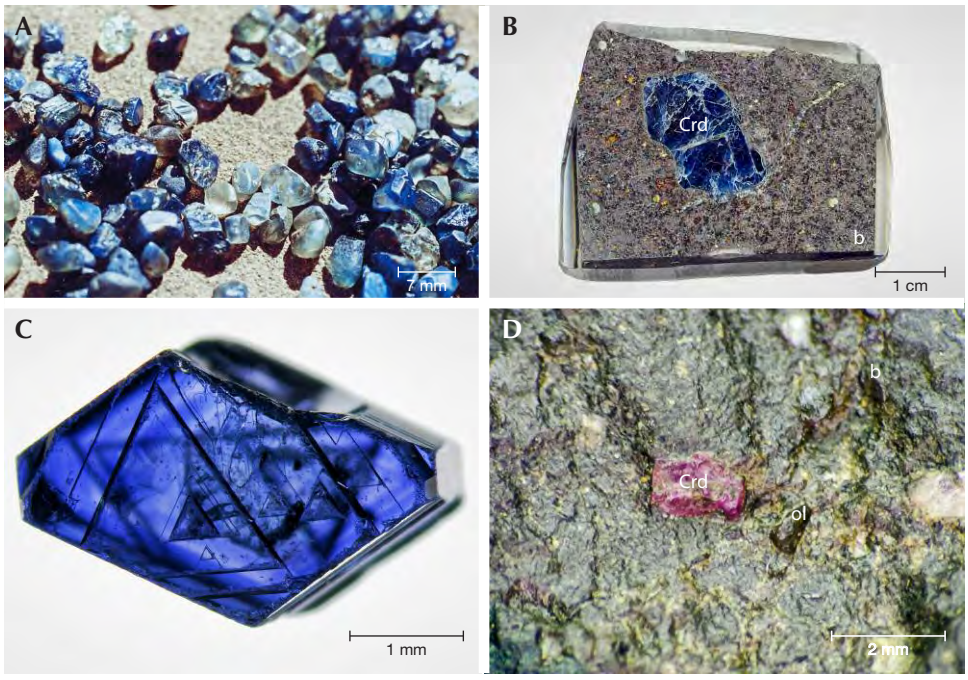

Figure 4. Gem corundum associated with alkali basalts. A: Blue-green-yellow sapphires from the Ambondromifehy placers, Antsiranana region, Madagascar; photo by G. Giuliani. B: Sapphire xenocryst (Crd) included in an alkali basalt (b) from the Changle deposit, China; photo by F. Fontan. C: Sapphire from the Souliot placer in the Massif Central, France; photo by D. Schlaefli. D: Ruby (Crd) xenocryst in an alkali basalt (b) containing a crystal of peridot (ol) from the Soamiakatra deposit in the Ankaratra Massif, central Madagascar; photo by S. Rakotosamizanany.

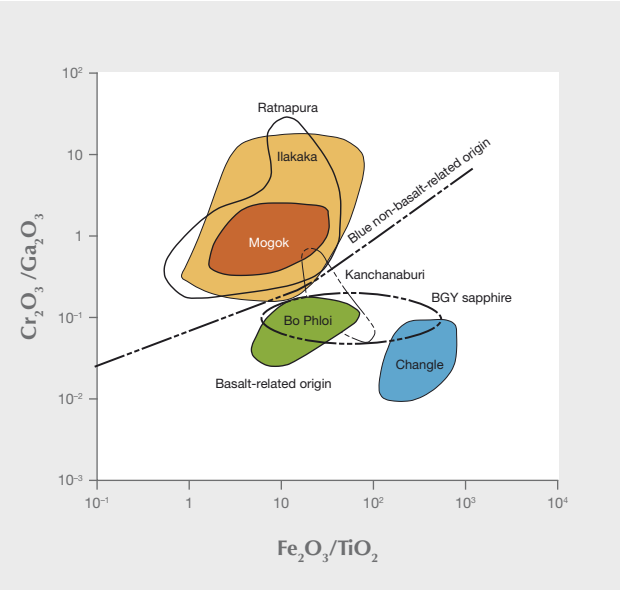

Figure 5. The Fe_2O_3/TiO_2 vs. Cr_2O_3/Ga_2O_3 diagram used for geological discrimination between blue sapphires from metamorphic and basalt-related origins. The metamorphic gem sapphires originate from the placers of Ilakaka in Madagascar, Ratnapura in Sri Lanka, and Mogok in Myanmar. The magmatic sapphires are from the placers of Bo Phloi and Kanchanaburi in Thailand, and Changle in China. The chemical field of the BGY sapphires defined by Sutherland and Schwarz (2001) is also shown.

(Rakotozamizanany et al., 2014) to show that the gem corundum may have different magmatic and metamorphic origins.

Within a single gem province in Australia, variations in color observed for corundum found ~10 km apart suggest the existence of multiple sources for the gemstones (Sutherland et al., 1998a; Sutherland and Schwarz, 2001). Studies of trace element distributions in corundum from New South Wales and Victoria found evidence for two contrasting geochemical fields, one for magmatic sapphire and one for metamorphic crystals. The same geochemical behavior was confirmed for corundum from the Kanchanaburi–Bo Rai and Nam Yuen deposits in Thailand and Pailin in Cambodia. The Fe/Ti vs. Cr/Ga chemical variation diagram proposed by Sutherland et al. (1998b) is commonly used to separate magmatic from metamorphic blue sapphires (figure 5). "Magmatic" corundum crystals have a Cr_2O_3/Ga_2O_3 ratio <1 and solid inclusions of Nb-bearing rutile, ilmenite, ferrocolumbite, ferrotantalite, pyrochlore, fersmite, samarskite, hercynite, magnetite, zircon, and iron oxides. "Metamorphic" corundum crystals have pastel (blue, pink, orange) to ruby color, are rich in chromium and poor in gallium (Cr_2O_3/Ga_2O_3 ratio >3), and have chromiferous spinel, pleonaste, Al-rich diopside, and sapphirine inclusions.

Several hypotheses have been advanced to explain the formation of magmatic sapphires: crystallization from highly evolved melts, most likely syenites (Uher et al., 2012); partial melting of amphibole-bearing lithosphere (Sutherland et al., 1998b); reaction of a fractionated silicate melt with a **carbonatitic** melt (Guo et al., 1996); partial melting of Al-rich rocks of the crust (such as anorthosites; Palke et al., 2016, 2017); and a carbonatitic melt exsolved from highly evolved **phonolites** (Baldwin et al., 2017).

The origin of ruby is always debated, and its metamorphic origin is questioned once more by recent studies showing melt inclusions in ruby from the Chanthaburi-Trat region of Thailand and Pailin in Cambodia (Palke et al., 2018). Based on the chemical composition of these melt inclusions, the protolith of ruby is suggested to be an "anorthosite" that was converted at high pressure to a garnet-**clinopyroxenite**. In this scenario, the rubies are considered to be xenocrysts of their host basalts. Xenoliths of ruby-bearing garnet-clinopyroxenite were found in alkali basalt in the primary Soamiakatra deposit in Madagascar (Rakotosamizanany et al., 2014). The associations of clinopyroxene + pyrope + scapolite + ruby and spinel + ruby + pyrope indicated formation at 1100°C and 20 kilobars, at the limit of the **eclogite** domain, corresponding to depths of approximately 60 km. The protolith of the garnet pyroxenite was proposed to be olivine-rich cumulates and/or plagioclase.

Geology and Genesis of Metamorphic Corundum Deposits. Corundum is a high-temperature mineral that forms naturally by metamorphism of alumina-rich rocks under amphibolite and **granulite** facies conditions, and at temperatures between 500° and 800°C (Simonet et al., 2008). Metamorphic gem corundum deposits are located in metamorphosed M-UMR, marble, quartzite, **gneiss**, and **metapelite** complexes that were heated either regionally or by thermal anomalies generated by local plutonic intrusions (figure 3). The various formation mechanisms depend on either isochemical metamorphism (i.e., regional metamorphism) or **metasomatic** metamorphism (i.e., contact and/or hydrothermal-infiltration processes affecting the lithology).

There are two main subtypes of metamorphic corundum deposits: (a) *metamorphic deposits sensu*

stricto, such as corundum in marbles and M-UMR; and (b) *metamorphic-metasomatic deposits* related to fluid circulation in M-UMR and Ca-rich host rocks such as limestones, marbles, and gneiss.

Metamorphic Deposits Sensu Stricto. The first metamorphic deposit sensu stricto is defined by ruby in marble from Central and Southeast Asia. This is one of the main worldwide sources for high-quality ruby with intense "pigeon's blood" color and high transparency. These deposits occur in metamorphosed platform carbonates that are generally associated with marbles intercalated with gneisses that are sometimes intruded by **granitoids** (see Giuliani et al., 2014). The ruby mineralization is restricted to peculiar impure marble horizons. The protolith of the ruby-bearing metamorphic rocks is carbonates rich in detrital clays and organic matter and intercalated evaporitic layers. Ruby crystals occur:

1. Disseminated within marble and associated with phlogopite, muscovite, scapolite, margarite, spinel, titanite, pyrite, and graphite, as in Afghanistan (Jegdalek), Nepal (Chumar and Ruyil), Pakistan (Hunza Valley and Nangimali), Myanmar (Mogok and Mong Hsu), and Vietnam (Luc Yen, Quy Chau)
2. In veinlets or gash veins, as in some occurrences in northern Vietnam, associated with phlogopite, margarite, titanite, graphite, and pyrite, and sometimes related to micro-shear zones, as at Nangimali in Pakistan
3. In pockets associated with orthoclase, phlogopite, margarite, graphite, and pyrite in some occurrences in northern Vietnam.

The ruby formed during retrograde metamorphism at T ~ 620–670°C and P ~ 2.6–3.3 kilobars (Garnier et al., 2008). The aluminum and the chromophore elements in the ruby originated from marbles (e.g., Al up to 1000 ppmw, V and Cr between 5 and 30 ppmw in the marble of the Nangimali deposit). The nature and chemical compositions of the solid (anhydrite, Na-scapolite, F-paragonite, F-Na-phlogopite, F-pargasite) and fluid inclusions highlight the major contribution of evaporites during metamorphism of the initial protolith (Giuliani et al., 2015, 2018). Fluorine probably played an important role in the extraction of the aluminum present in the impurities (clays) in the **limestone** during metamorphism.

The second metamorphic deposit sensu stricto is related to ruby in metamorphosed M-UMR (gabbroic and dunitic rocks), which is also called amphibolite-type. The majority of rubies are produced in Africa, from deposits located in the **Neoproterozoic**-age metamorphic Mozambique Belt (750–540 Ma) that extends from Somalia through Kenya, Tanzania, Malawi, Mozambique, and Madagascar. This type of deposit is found worldwide, and new deposits have been discovered in Greenland at Aappaluttoq (Fagan, 2015, 2018) and Mozambique at Montepuez, Ruambeze, and M'sawize (Pardieu et al., 2009; Pardieu and Chauviré, 2013; Simonet, 2018). The most common assemblage of these deposits is corundum, anorthite, amphibole (gedrite, pargasite), and margarite. Other index minerals are sapphirine, garnet, spinel, kornerupine, phlogopite, and zoisite. The assemblage formed under amphibolite and granulite facies conditions at P = 9–11.5 kilobars and T = 750–800°C for the ruby-bearing amphibolite in the Vohibory area of Madagascar (Nicollet, 1986), and P = 7 to 10 kilobars and T = 800–850°C for those located at Buck Creek in North Carolina (Tenthorey et al., 1996).

At the Winza deposit in central Tanzania (Peretti et al., 2008; Schwarz et al., 2008), gem corundum crystals are embedded in dark amphibolite. The corundum is locally associated with areas of brown to orangy garnet ± feldspar, with accessory Cr-spinel, mica, kyanite, and allanite. The ruby and sapphire crystals are closely associated with dikes of a garnet- and pargasite-bearing rock cross-cutting amphibolite (figure 6A). The central part of the dike is composed of garnet (pyrope-almandine) + pargasite ± plagioclase ± corundum ± spinel ± apatite. Metamorphic conditions estimated from the garnet-amphibole-corundum equilibrium assemblage show that the metamorphic overprint occurred at T ~ 800 ± 50°C and P ~ 8–10 kbar (Schwarz et al., 2008). The chemical composition of Winza ruby and sapphires (figure 6B) includes moderate contents of Cr (0.1–0.8 wt.% Cr_2O_3) and Fe (0.2–0.8 wt.% Fe_2O_3), very low to low amounts of Ti (55–192 ppmw TiO_2) and V (up to 164 ppmw V_2O_3), and low to moderate Ga (64–146 ppmw Ga_2O_3).

The gem corundum deposits of southwest Greenland are another example of ruby hosted in gabbroic rocks subjected to metamorphic metasomatism (Fagan, 2018). The geology of the Aappaluttoq deposit is dominated by an intrusive gabbro to leucogabbro sequence of rocks with significant volumes of ultramafic rocks in the Fiskenæsset Complex, a layered-cumulate igneous complex. The intrusive suite comprises layers of gabbro, ultramafic rocks, leucogabbro, and calcic anorthosite. The corundum mineralization occurs in a specific stratigraphic horizon

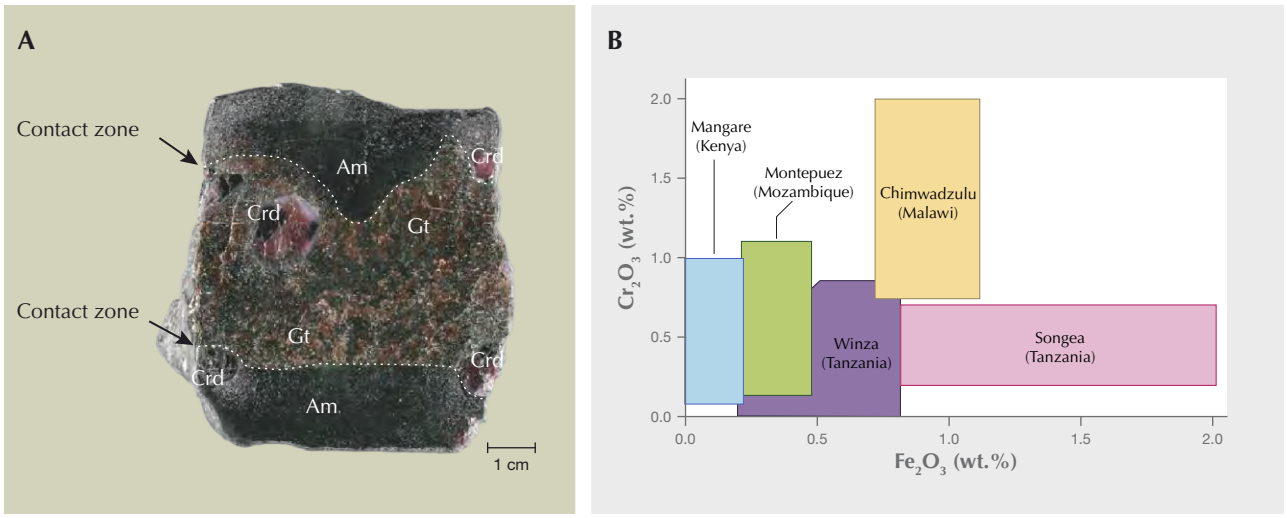

Figure 6. A: The primary ruby and sapphire mineralization at the Winza deposit in Tanzania is hosted by an orangy brown garnet-rich rock (Gt) intercalated in a fine-grained amphibolite (Am). B: Fe_2O_3 vs. Cr_2O_3 diagram showing the chemical composition of the Winza rubies compared with those from other ruby deposits hosted in mafic-ultramafic rocks, such as Chimwadzulu (Malawi), Mangare (Kenya), Montepuez (Mozambique), and the placer at Songea (Tanzania). Photo by P. Lagrange.

in the metamorphic complex; this probably represents a unit with high Al, low Si, and a high fluid flux. The ruby lies between layers of ultramafic rock and leucocratic gabbro. The main corundum-bearing ore is composed of three main rock types (figure 7): sapphirine-gedrite, leucogabbro, and a phlogopitite, which is the most important. The leucogabbro contains a large amount of pink corundum. The gabbro is rich in Al and is believed to be the unit responsible for releasing the Al to form the corundum. Its structural location, distal from the ultramafic unit, is thought to be responsible for the lack of ruby, as the Cr geochemical gradient was not sufficient to enrich the corundum within the gabbroic units enough to impart more than a pink coloration. The phlogopitite is the host for the majority of the ruby at Aappaluttoq. This is due to the proximity of this unit to the ultramafic Cr source rock, reflecting the relative mobility of Cr in a fluid-rich environment. This unit is ultimately a metasomatic product, comprising approximately 90% phlogopite, 5% biotite, and 5% corundum.

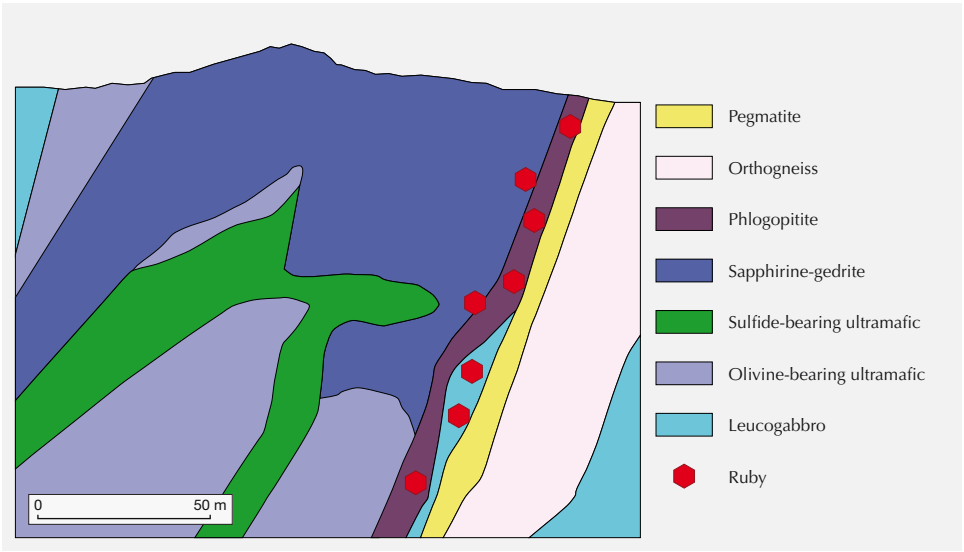

Figure 7. Schematic cross section of the ruby deposit at Aappaluttoq, in the Fiskenæsset district, Greenland. The ruby mineralization is hosted by phlogopitites, phlogopitized leucogabbro, and sapphirine-gedrite-bearing rocks. Modified from Fagan (2018).

Metamorphic-Metasomatic Deposits. Here, two main subtypes are distinguished: The first subtype corresponds to desilicated pegmatite in mafic rocks (i.e., plumasites). These deposits formed at medium to high temperatures during hydrothermal fluid circulation and metasomatism that developed at the contact of two contrasting lithologies: (1) granite or pegmatite adjoining (2) M-UMR, marble, or gneiss (figure 8A). The metasomatic reactions are related to the infiltration of post-magmatic solutions, which originated from the same granite or from other magmatic or metamorphic events. The mechanism of desilication, a loss of quartz, involves diffusion of Si from a pegmatite vein to an ultramafic rock (which plays the role of SiO_2 sink) at a rate more rapid than the diffusion of Al. The Al:Si ratio increases in the pegmatite vein, and a metasomatic plagioclase-corundum association in which the mass of alumina per unit volume is much greater than in the initial rock may develop if the volume of rock decreases at the same time and is underlain by a zone of quartz dissolution.

World-class sapphire deposits in desilicated pegmatites have been described from the Umba River (Solesbury, 1967) and Kalalani (Seifert and Hyršl, 1999) in Tanzania; the Sumjam deposit in Kashmir (Lydekker, 1883); the Mangare area in southern Kenya, including the well-known John Saul mine (Mercier et al., 1999; Simonet, 2000); and the Polar Urals in Russia (Meng et al., 2018).

The states of Jammu and Kashmir produce the blue sapphires most prized for their gorgeous blue color and velvety luster, caused by layers of microscopic liquid inclusions. The deposit is located in Cambrian metamorphic rocks showing a succession of marble, amphibolite, and gneiss that have been intruded by pegmatites (Atkinson and Kothavala, 1983). The sapphire is associated with pockets or lenses of olivine-talc-spinel-bearing metamorphic rocks. The lenses are from 1 to 100 meters in length and up to 30 meters thick and enveloped by a green aureole of tremolite, actinolite, and anthophyllite-bearing rocks. Desilicated pegmatites are located at the contact between the lenses and the amphibolite. The mineralogical association consists of plagioclase, mica, tourmaline, and sapphire. The rims of the desilicated pegmatite are composed of talc-biotite-carbonate and tourmaline-bearing rocks (Peretti et al., 1990). Study of the primary carbonic fluid inclusions in the sapphire has indicated fluctuation of the conditions of fluid trapping in the crystals: P ~ 3.7–5.6 kbar and T ~ 680–700°C at the center, and P ~ 2.9–3.1 kbar and T ~ 500°C at the periphery.

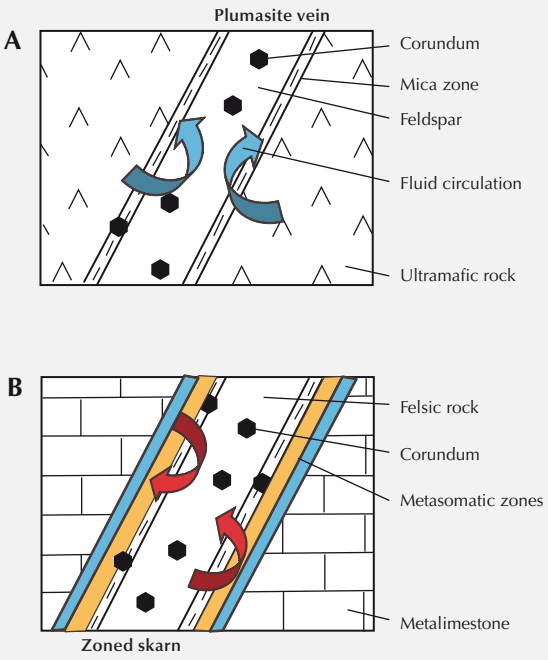

Figure 8. The formation of corundum in plumasite and skarn deposits by fluid-rock interaction. A: The metasomatic fluid circulated along the contact between two rocks of contrasting lithology, such as ultramafic or marble and pegmatite. The percolation inside the rocks induced metasomatic desilication of the silica-rich rocks and the formation of metasomatic rocks such as corundum-bearing plagioclase (plumasite), and/or phyllosilicate-rich rocks (phlogopite schist, vermiculite schist, chloritite). B: The skarn deposit is formed by a succession of different zoned rocks composed of Ca-rich silicates from the pegmatite to the Ca-rich host rock. Modified from Simonet et al. (2008).

The second metamorphic subtype deposit is formed by skarn deposits formed in marble or calc-silicate rocks. Skarns generally form when granitic intrusions (or equivalents) intrude Ca-bearing rocks such as pure or impure marbles (figure 8B). The deposits are associated with thermal metamorphism due to the temperature gradient around the intrusion. Every post-magmatic process linked to the emplacement of the pluton has a stage at which the solutions became acid, constituting a source of strong reactions with their wall rocks. As the activity of K, Na, and Al increases, these elements enter into reactions with marble or dolomitic marble, increasing the concentrations of Ca and Mg in solution.

Such reactions produce feldspar, biotite, and Ca-bearing minerals. The association of Ca-bearing, usually Fe-rich silicates (including amphibole, pyroxene, garnet, epidote, and zoisite) or Mg-rich silicates (such as phlogopite, diopside, pargasite, and forsterite) defines the so-called skarn mineralogy.

World-class sapphire-bearing skarn deposits occur at Andranondambo in the Tranomaro area of southern Madagascar (Rakotondrazafy et al., 1996, 2008); at Thammannawa, near Kataragama in southeastern Sri Lanka (Dharmaratne et al., 2012); and at Bakamuna in the Elahera area of Sri Linka (Silva and Siriwardena, 1988).

Geology and Genesis of Secondary Corundum Deposits. Climate is the major factor in the formation of secondary deposits. In tropical areas, rocks are exposed to meteoric alteration, resulting in an assemblage of clay minerals, iron and manganese oxides, and other supergene phases. Corundum and zircon are resistant minerals found in soils, **laterite**, and gravelly levels overlying bedrock.

Of particular importance are paleoplacers characterized by different mineral phases cemented in a carbonate or silica-rich matrix. Paleoplacers of corundum are known from alkali basalt deposits in Madagascar. In Antsiranana Province, the paleoplacer is composed of a carbonate-karst **breccia** in cavities in Jurassic limestone (Schwarz et al., 2000; Giuliani et al., 2007b). In the Vatomandry area, the paleoplacer is a sandstone that contains hematite, ruby, sapphire, and zircon. At Ilakaka, gem corundum is found in three gravel levels in two main alluvial terraces deposited on Isalo sandstone. The terraces are weakly consolidated, but correspond to paleoplacers (Garnier et al., 2004). The Ilakaka deposits produce very fine blue, blue-violet, violet, purple, orange, yellow, and translucent sapphire crystals along with pink and red corundum, zircon, alexandrite, topaz, garnet, spinel, andalusite, and tourmaline.

Important placers formed in marble environments are found in Myanmar, where gem-bearing levels enriched in pebbles, sand, silt, clay, and iron oxides are called "byon" (Kane and Kammerling, 1992). The gem content is closely related to the formation of karst and chemical weathering of marble and associated rocks. The corundum is trapped in eluvial, colluvial, alluvial, fracture-filling, and cave deposits.

In Australia, sapphire and ruby in alkali basalts are subjected to a tropical climate, probably more so in the past. The resulting alluvial deposits are in eastern Australia, primarily northern New South Wales and central Queensland (Sutherland and Abduriyim, 2009). The main ruby production has been from Barrington Tops, Yarrowitch, and Tumbarumba, all in New South Wales. The sapphire-bearing basaltic sediments, locally called "wash," occur in layers 1 to 3 m thick underneath dark clayey soil some 1 to 3 m below the surface (Abduriyim et al., 2012). In the Inverell district of New South Wales, at the Mary Anne Gully mine, brown basaltic sedimentary soils are extracted from an area of 10 to 40 km^2, and large-scale mining operations take place at Kings Plains.

At Montepuez in Mozambique, the main source of facet-grade material in the Gemfields properties is secondary deposits (SRK Consulting, 2015; Simonet, 2018). The secondary deposits are mainly colluvials with limited horizontal transport (more subangular fragments) and a few alluvial pebbles (smooth and round appearance). Most of the mineralized horizons are stone lines, weathering-resistant rock fragments formed by millions of years of erosion (Simonet, 2018). Composed of angular fragments of quartz and pegmatite, the stone lines are excellent traps for smaller grains of high-density minerals such as ruby. The colluvial deposits are either associated with the proximal primary deposits (as in the Maninge Nice/Glass mines) or are disconnected (as in the Mugloto mine).

PART II: EMERALD

Emerald is the green gem variety of beryl ($Be^{2+}_3Al^{3+}_2Si^{4+}_6O^{2-}_{18}$) (figure 9). The color of emerald is due to trace amounts of Cr and/or V replacing Al in the crystal structure. Beryl has a hardness of 7.5–8 on the Mohs scale.

Economic Significance. Emerald is generally the third most valuable gem after diamond and ruby. The pricing of emeralds is unique in the colored gemstone market, emphasizing color almost to the exclusion of clarity, brilliance, or other characteristics (Walton, 2004).

The highest per-carat price ever paid for an emerald was $304,878 per carat, at a total price of US$5,511,500, for the Rockefeller ring at Christie's New York in June 2017. However, Elizabeth Taylor's Bulgari emerald still holds the record for the highest total price ever paid for an emerald at $6,130,500, or $281,329 per carat at 23.46 carats. An exceptional 10.11 ct Colombian faceted stone brought US$1,149,850 in 2000 (Zachovay, 2002). In October 2017, a Gemfields auction of Zambian emeralds gen-

Figure 9. Emerald specimen from Chivor, Colombia. The carbonate matrix presents a vug with emerald, and pyrite. The top emerald measures 16.82 × 8.55 mm, the bottom emerald 11.98 × 7.96 mm. The specimen measures 76.43 × 63.44 mm. Photo by Robert Weldon/GIA; courtesy of Greg Turner, Cornerstone Minerals.

erated revenues of $21.5 million ("In the News…," 2018); the average value of the bids was $66.21 per carat (Branstrator, 2017). The auction included the 6,100 ct Insofu ("baby elephant") rough emerald from the Kagem mine. One year later Kagem produced another giant crystal, the 5,565 ct Inkalamu ("lion elephant") rough emerald (Gemfields, 2018). Giant crystals have also been discovered in Colombia, such

as El Monstro (16,020 ct) and the Emilia (7,025 ct), both from the Gachalá region. In 2017, a large piece of biotite schist with several large emerald crystals was discovered in the Carnaíba mine, Brazil. The specimen, named Bahia, weighs 341 kg, but the weight and value of the emeralds are unconfirmed (Weil, 2017).

Production. As with most gem materials, it is difficult to obtain accurate statistics for emerald production. In 2005, Colombia, Brazil, Zambia, Russia, Zimbabwe, Madagascar, Pakistan, and Afghanistan were the main producers (Yager et al., 2008). Today, the list of leading emerald producers is unchanged, with Colombia, Brazil and Zambia, at the top.

The original Colombian deposits are almost exhausted, despite Furagems' announcement of an estimated 3 million tons inferred emerald at a grade of 2 carats per ton for the Coscuez mine. Nevertheless, new finds in the Maripi area, beginning with La Pita in 1998 and then Las Cunas, should ensure that Colombia remains the most important source for years to come.

Brazil became a significant emerald producer during the 1970s, and by the end of the century it was exporting $50 million annually (Lucas, 2012) and accounting for approximately 10% of global production (Schwarz and Giuliani, 2002). Although Brazilian emeralds were not traditionally known for their quality (Lucas, 2012), stones from the Itabira/Nova Era belt (which includes the highly productive Belmont mine) reportedly sell for up to $30,000 per carat. Today, the main Brazilian production is related to emerald deposits associated with granitic intrusions in the states of Minas Gerais (74%), Bahia (22%), and Goiás (4%) (Martins, 2018).

The Kafubu mining district in Zambia accounts for most of that country's production. The mining licenses at Kafubu extend for approximately 15 km of strike length. The development of modern mining on this large scale by Gemfields, through underground and huge opencast mining, allows for large quantities of high-quality commercial-grade gems.

Other important producers are Russia, from the Izumrudnye Kopi district approximately 60 km northeast of Ekaterinburg in the Ural Mountains (Grundmann and Giuliani, 2002), and Zimbabwe, from the Sandawana (formerly Zeus) mine approximately 360 km south of Harare.

As with other colored stones, emerald deposits are often located in countries with unstable political regimes without strong mineral rights security, and smuggling tends to be rampant. Despite these problems, emerald remains one of the most sought-after colored gemstones.

The Geochemistry of Be, Cr, and V. Beryl is relatively rare because there is very little Be (2.1 ppmw) in the upper continental crust (Rudnick and Gao, 2003). Beryllium tends to be concentrated in rocks of the continental crust, such as granite, pegmatite, black shale, and their metamorphic equivalents. Chromium and V are more common (92 and 97 ppmw, respectively) in the upper continental crust (Rudnick and Gao, 2003) and are concentrated in dunite, peridotite, and basalt of the oceanic crust and upper mantle, and their metamorphic equivalents. However, high concentrations can also occur in sedimentary rocks, particularly black shale (Schwarz et al., 2002).

Unusual geologic and geochemical conditions are required for Be and Cr and/or V to meet. In the classic model, Be-bearing pegmatites interact with Cr-bearing M-UMR. However, in the Colombian deposits (see below) there is no evidence of magmatic activity, and it has been demonstrated that fluid circulation processes within the host black shale were sufficient to form emerald. In addition, researchers recognize that regional metamorphism and tectonometamorphic processes such as shear zone formation may play a significant role in certain deposits (e.g., Grundmann and Morteani, 1989, 1993; Cheilletz et al., 2001; Vapnik et al., 2005, 2006). Emeralds, though exceedingly rare, can obviously form in a wider variety of geological environments than previously thought (Walton, 2004).

Classification. Emerald deposits are found on all five continents (figure 10) and range in age from Archean (2.97 Ga for the Gravelotte deposit in South Africa) to Cenozoic (9 Ma for the Khaltaro deposit in Pakistan) (figure 11). Giuliani et al. (2019) introduced a new classification scheme in which emerald deposits are divided into two main types depending on the geological environment, and further subdivided on the basis of host rock (table 1):

Type I: Tectonic-magmatic-related, with subtypes hosted in:

- IA. **Mafic-ultramafic** rocks (Brazil, Zambia, Russia, and others)
- IB. Sedimentary rocks (China, Canada, Norway, Kazakhstan, Australia)
- IC. Granitic rocks (Nigeria)

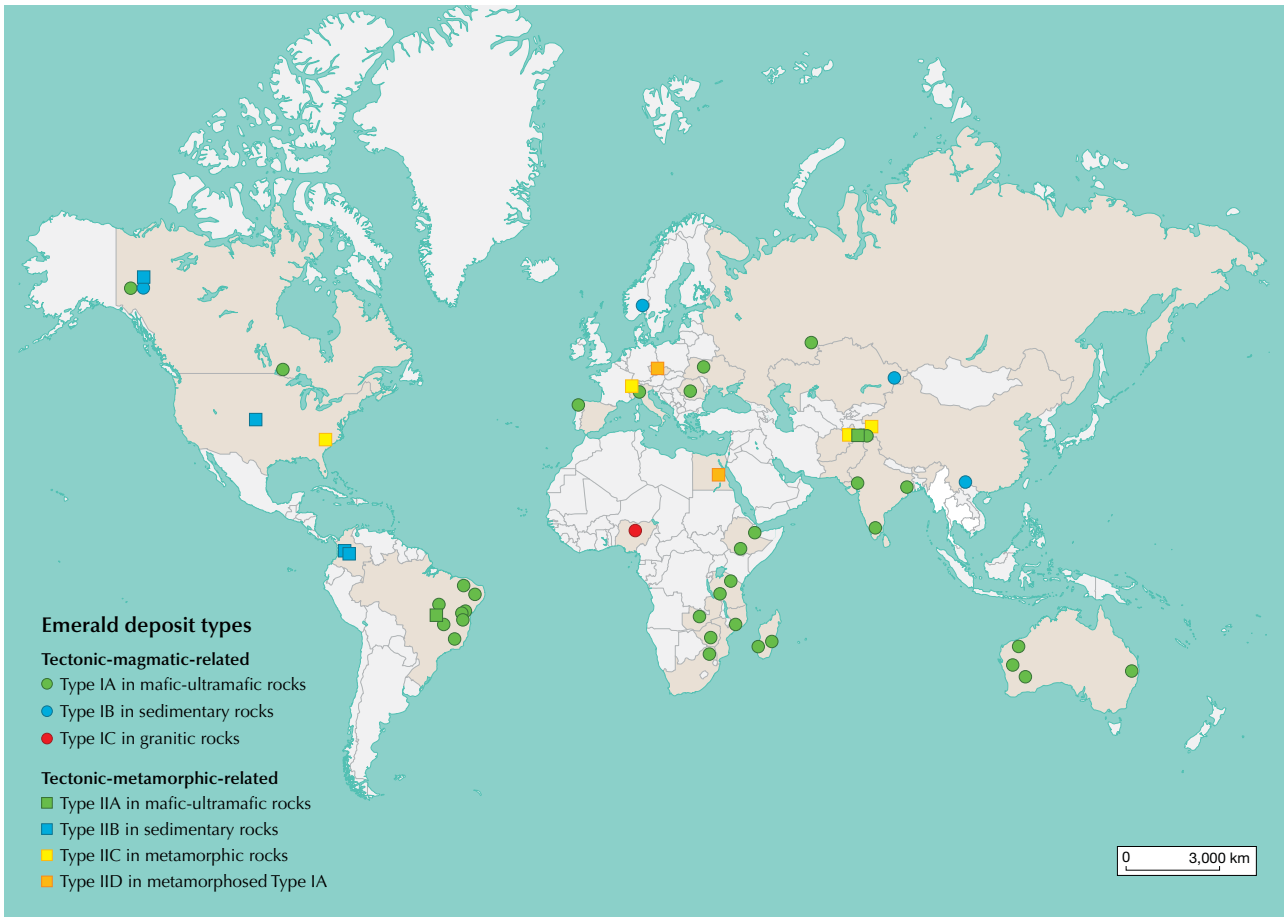

Figure 10. Map of emerald deposits and occurrences worldwide, divided into types and subtypes.

Type II: Tectonic-metamorphic-related, with subtypes hosted in:

IIA. M-UMR (Brazil, Austria)

IIB. Sedimentary rocks: black shale (Colombia, Canada)

IIC. Metamorphic rocks (China, Afghanistan, United States)

IID. Metamorphosed Type I deposits or hidden-granitic intrusion-related (Austria, Egypt, Australia, Pakistan) and some unclassified deposits

An idealized Type IA deposit is shown in figure 12. Type IA deposits are typified by the prolific emerald mines of central Zambia, of which Kagem is thought to be the world's largest open-pit mine for colored gemstones (Behling and Wilson, 2010). The emerald deposits are hosted by Cr-rich (3,000 to 4,000 ppmw) talc-chlorite ± actinolite ± magnetite metabasic rocks of the Muva Supergroup, which have been identified as metamorphosed **komatiite** (Seifert et al., 2004). The **metabasite** horizons are overlapped by a major field of Be-bearing pegmatite and hydrothermal veins ~10 km in length that was emplaced during the late stages of the Pan-African orogeny (~530 Ma; John et al., 2004). Economic emerald concentrations are almost entirely restricted to phlogopite reaction zones (typically 0.5 to 3 m wide) between quartz-tourmaline veins and metabasite (Zwaan et al., 2005). Chemical analyses (Siefert et al., 2004) indicate that the formation of phlogopite schist from metabasite involved the introduction of K_2O (8 to 10 wt.%), F (2.7 to 4.7 wt.%), Li_2O (0.1 to 0.7 wt.%), Rb (1,700 to 3,000 ppmw), Be (up to 1,600 ppmw), Nb (10 to 56 ppmw), and significant amounts of B. A fluid inclusion study suggested that the veins associated with emerald mineralization formed at 350° to 450°C and 150 to 450 kilobars (Zachariáš et al., 2005). K-Ar dating of muscovite from a pegmatite and an associated quartz-tourmaline vein gave cooling ages of 452 to 447 Ma, which is considered to approximately date the emerald mineralization (Seifert et al., 2004).

TABLE 1. Classification of emerald deposits (from Giuliani et al., 2019).

Type of deposit	Tectonic-Magmatic-Related			Tectonic-Metamorphic-Related				
Geological environment	Granitic			Sedimentary	Metamorphic			
Metamorphic conditions	Greenschist to granulite facies			Anchizone to greenschist facies	Greenschist to granulite facies			
Host rocks	Mafic-ultramafic rocks	Sedimentary rocks	Granitoids	Sedimentary rocks	Metamorphic rocks			
Type	Type IA	Type IB	Type IC	Type IIB	Type IIC		Type IIA	Type IID
	Pegmatite-aplite-quartz-greisen veins, pods, metasomatites			Carbonate platform sediments	Metamorphism of SR	Migmatites	Metamorphism of M-UMR	Metamorphosed Type IA, mixed IA and IIA in M-UMR, unknown
Mineralization style	Veins and/or metasomatites	Veins and/or metasomatites	Pods	Veins and/or metasomatites	Veins	Veins	Shear zone	Shear zone, metasomatites, veins, boudins, faults
Origin of the fluid	Metasomatic-hydrothermal	Metasomatic-hydrothermal	Metasomatic-hydrothermal	Metasomatic-hydrothermal	Metasomatic-hydrothermal	Hydrothermal	Metamorphic-metasomatic	Magmatic-metasomatic[a]
Deposits	Brazil: Carnaíba, Socotó, Itabira, Fazenda Bonfim, Pirenópolis Canada: Tsa da Gliza, Taylor 2 Bulgaria: Rila Urals (e.g., Malysheva) Pakistan: Khaltaro Afghanistan: Tawakh India: Rajasthan South Africa: Gravelotte Zambia (e.g., Kafubu) Tanzania: Manyara, Sumbawanga Mozambique (e.g., Rio Maria) Australia (e.g., Menzies, Wodgina) Ethiopia: Kenticha Madagascar: Ianapera, Mananjary Zimbabwe: Sandawana, Masvingo, Filabusi Somalia: Borama Ukraine: Wolodarsk	Norway: Eidsvoll China: Dayakou Canada: Lened Australia: Emmaville, Torrington Kazakhstan: Delgebetey	Nigeria: Kaduna	Colombia: Eastern and Western emerald zones Canada: Mountain River United States: Uinta (?)	China: Davdar Afghanistan: Panjshir	United States: Hiddenite	Austria: Habachtal Brazil: Itaberai, Santa Terezinha de Goiás Pakistan: Swat-Mingora-Gujar-Kili, Barang	Austria: Habachtal (?)[b] Brazil: Santa Terezinha de Goiás (?)[c] Pakistan: Swat-Mingora (?)[d] Australia: Poona[b] Egypt: Djebel Sikait, Zabara, Umm Kabu[b] Zambia: Musakashi[e]

[a]With a metamorphic remobilization

[b]Probably metamorphic remobilization of Type IA deposit

[c]Probably related to hidden granitic intrusive cut by thrust and emerald-bearing shear zone

[d]Probably related to undeformed hidden intrusives and accompanying hydrothermal activity.

[e]Unknown genesis: vein style, fluid inclusion indicates affinities with Types IIB and IIC

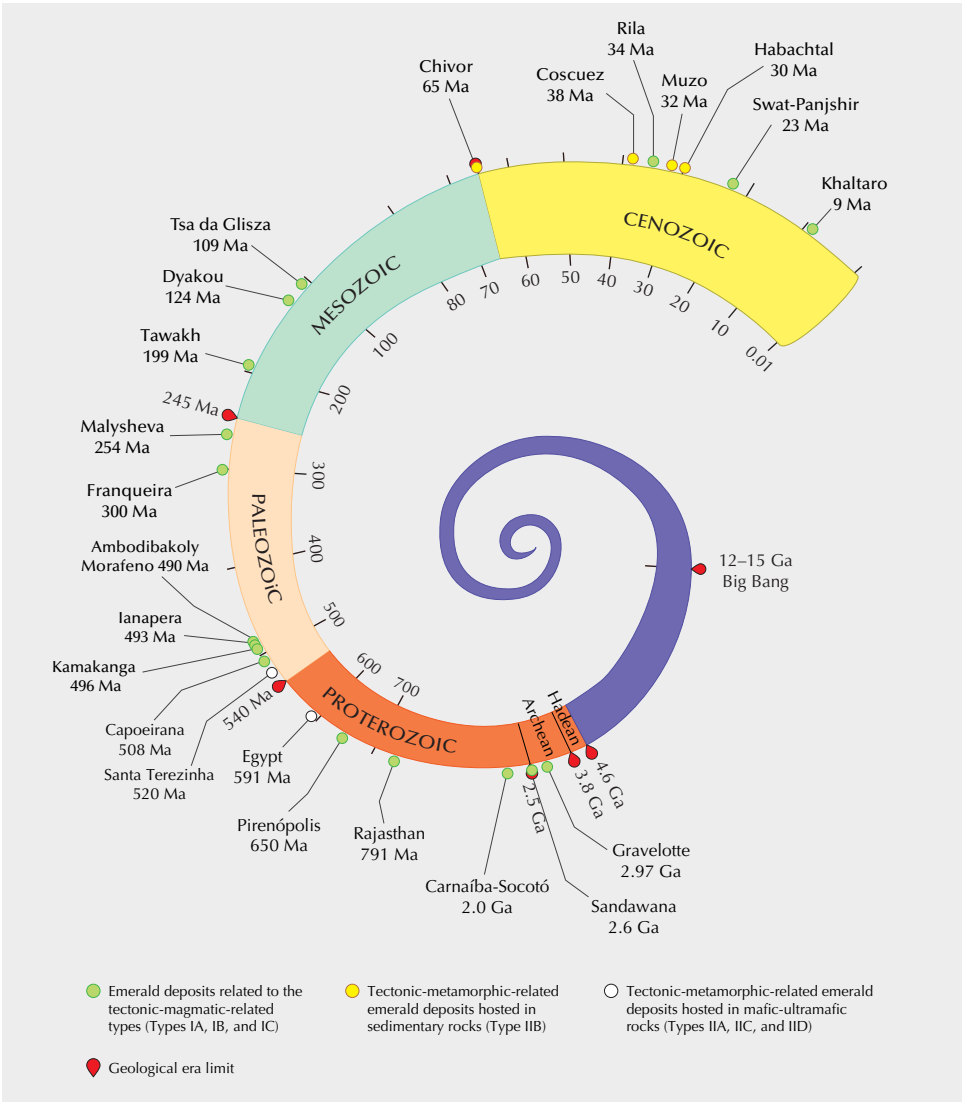

Figure 11. Spiral time diagram for emerald deposits. Modified from Giuliani (2011).

At the Lened locality in Canada's Northwest Territories, only about 5% of the beryl is transparent and bluish green (and can therefore be considered pale emerald), but it is the most recently studied Type IB occurrence. At Lened the emeralds are hosted by approximately 13 quartz veins that cut skarn in carbonate rocks and older strata. Beryllium and other incompatible elements (W, Sn, Li, B, and F) in the emerald, vein minerals, and surrounding skarn were introduced during the terminal stages of crystallization of the proximal ~100 Ma Lened pluton (Lake et al., 2017). Decarbonation during pyroxene-garnet skarn formation in the host carbonate rocks probably caused local overpressuring and fracturing that allowed ingress of magmatic-derived fluids and formation of quartz-calcite-beryl-scheelite-tourmaline-pyrite veins. The chromophoric elements (V>Cr) were mobilized by metasomatism of **metasedimentary** rocks (black shale) that underlie the emerald occurrence (Lake et al., 2017).

The only Type IC deposit identified to date is in central Nigeria, where emerald occurs as a result of early metasomatic **albitization** (see Glossary) of an alkaline granite body of the **Mesozoic** Jos Ring Complex (Vapnik and Moroz, 2000) (figure 13). The emeralds occur with quartz, feldspar, and topaz in small pegmatitic pockets up to 8 cm in size at the granite–country rock contact, and in small **miarolitic** pockets in the roof of the granite, in a zone <20 m from the contact with overlying rocks of the Nigerian Basement Complex (Schwarz et al., 1996). Chromium was likely incorporated from the basement schist or from younger volcanic rocks (Schwarz et al., 1996). Fluid inclusion data indicate emerald crystallization (of the

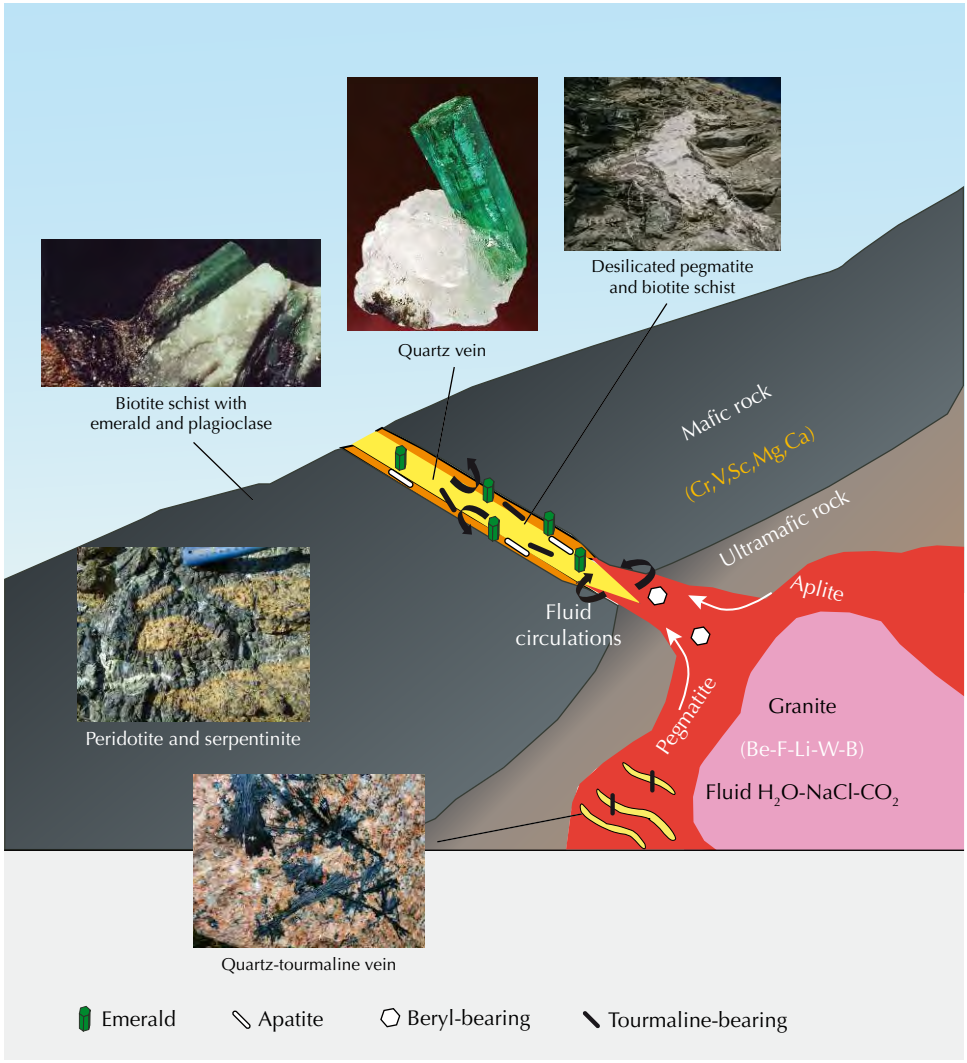

Figure 12. An idealized Type IA (tectonic-magmatic-related in mafic-ultramafic rocks) deposit, in which a granite pluton with attendant pegmatite and aplite dikes and tourmaline-bearing and/or beryl-bearing quartz veins intrude mafic (metabasalt) and/or ultramafic (metaperidotite, serpentinite) rocks. Fluid circulation (indicated by the arrows) transforms the mafic rocks into a magnesium-rich biotite schist and the pegmatite into an albite-rich plagioclasite. Emerald and apatite can precipitate in the pegmatite, aplite, plagioclasite, and quartz veins, and in their adjacent phlogopite schist zones.

early and intermediate growth phases) at 400° to 450°C and 0.2 to 0.3 kilobars (Vapnik and Moroz, 2000).

An example of a Type IIA deposit is Santa Terezinha in the Brazilian state of Goiás. This deposit, with emerald grades varying between 50 and 800 grams/ton, is associated with ductile shear zones cutting mafic and ultramafic rock formations (Giuliani et al., 1997a,b). The emeralds occur in phlogopitite and phlogopitized talc-carbonate schist (figure 14). The talc schist provided sites for thrusting that gave rise to the formation of sheath folds. Emeralds from Santa Terezinha are most commonly found in the

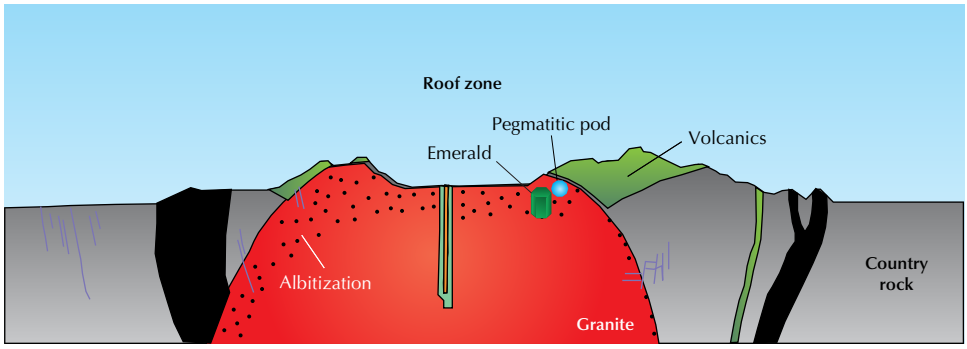

Figure 13. Geological schematic cross-section of ring complexes and their associated emerald mineralization in Nigeria. Modified from Kinnaird (1984).

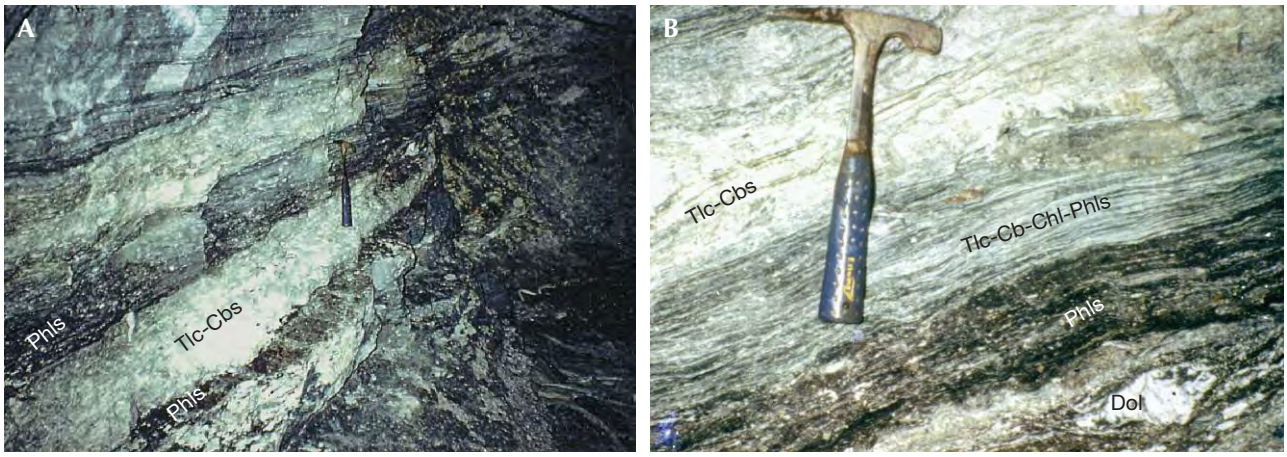

Figure 14. The Santa Terezinha de Goiás emerald deposit, Goiás State, Brazil. A: Phlogopite schist (Phls) and talc-carbonate schists (Tlc-Cbs). B: With carbonate lenses (Dol). Phlogopitization affects the Tlc-Cbs and the talc-carbonate-chlorite-phlogopite schist (Tlc-Cb-Chl-Phls). Photos by G. Giuliani.

cores of the sheath folds and along the foliations. Isotopic data ($\delta^{18}O$ and δD for emerald and coeval phlogopite) are consistent with both magmatic and metamorphic fluids. However, the absence of granite and related pegmatites, and the low Be concentration in the volcano-sedimentary sequence (<2 ppmw), exclude a magmatic origin for Be. A metamorphic origin is therefore proposed for the Santa Terezinha parental fluids (Giuliani et al., 1997a,b).

The famous Colombian deposits (figure 15) are the best examples of Type IIB deposits. In Colombia, the emeralds occur in extensional carbonate-silicate-

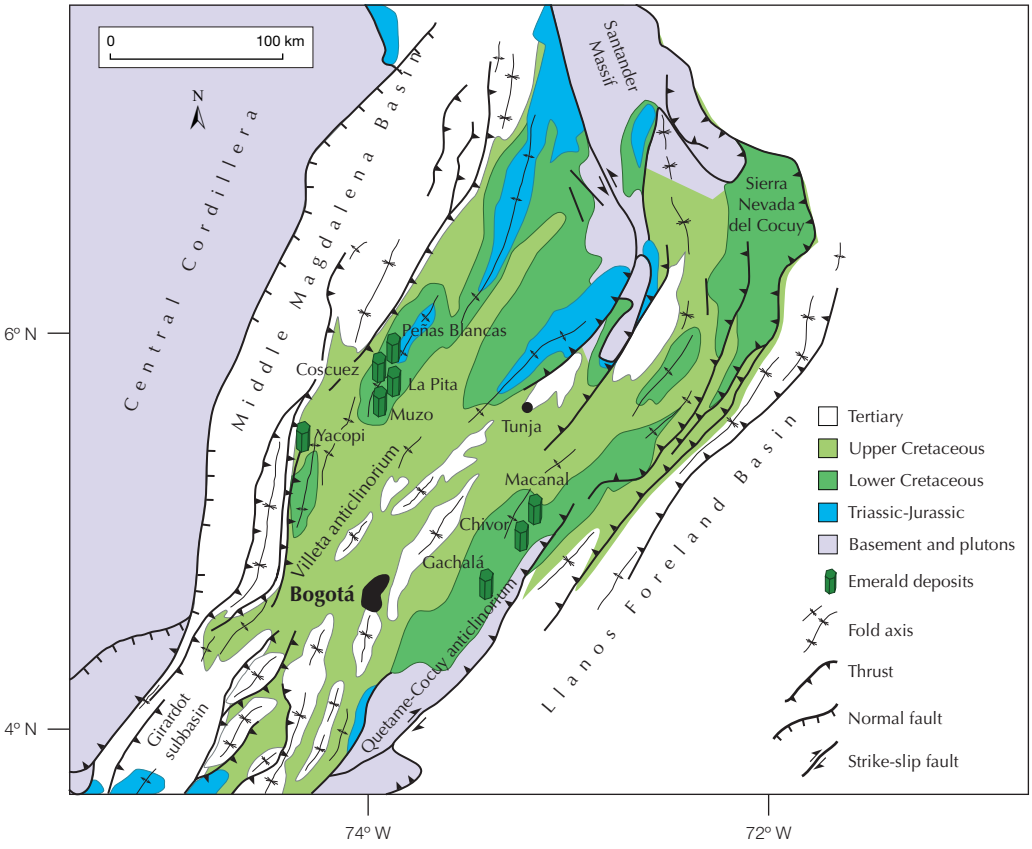

Figure 15. Generalized geological map of the Cordillera Oriental of Colombia showing the locations of the main emerald deposits.

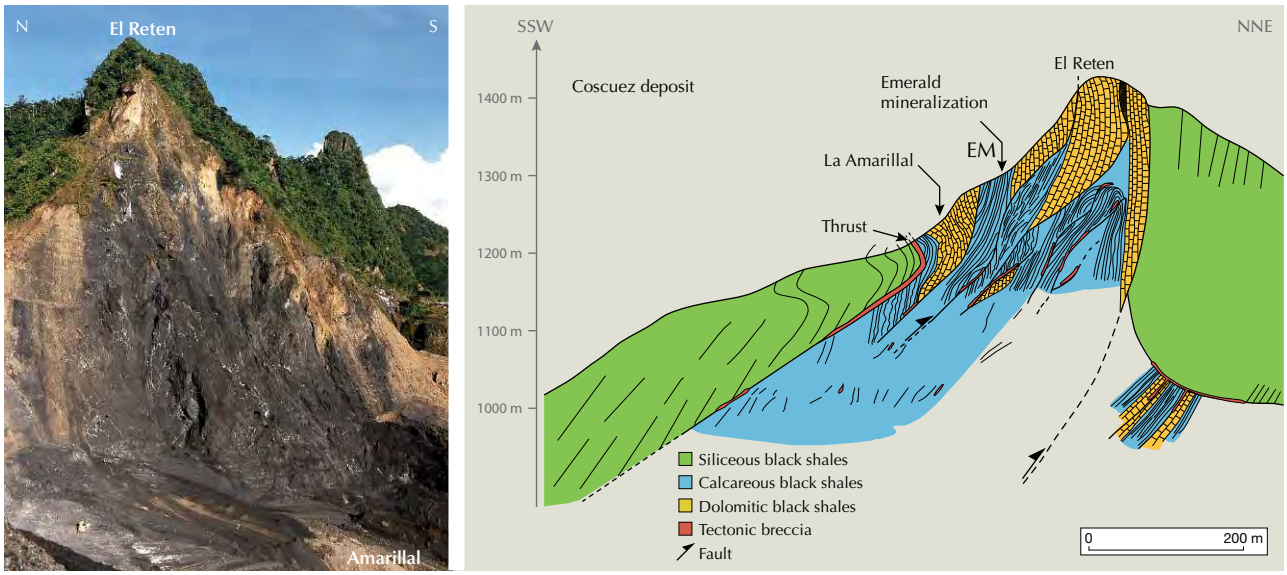

Figure 16. Left: View of the Coscuez deposit in 1996. Photo by G. Giuliani. Right: Geological cross-section of the Coscuez deposit.

pyrite veins, pockets, and breccia in an Early **Cretaceous** black shale–limestone succession (figure 16). The deposits are unusual because there is no evidence of magmatic activity. Instead, the emeralds formed as a result of hydrothermal growth associated with tectonic activity (Ottaway et al., 1994; Giuliani et al., 1995; Cheilletz and Giuliani, 1996; Branquet et al., 1999a,b). The parent fluids are thought to have formed at depth from meteoric and formational water interacting with salt beds and evaporitic sequences (Ottaway et al., 1994; Giuliani et al., 2000). These highly alkaline fluids (up to 40 wt.% equivalent NaCl) migrated upward through the sedimentary sequence along thrust planes and then interacted with the black shale. During Na and Ca metasomatism, major and trace elements (including Be, Cr, and V) were leached from the enclosing black shale; this first stage was accompanied by development of a vein system filled by fibrous calcite, bitumen, and pyrite. The second stage was characterized by extensional vein sets and hydraulic breccia development filled by muscovite, albite, calcite, dolomite, pyrite, and bitumen and by the precipitation in drusy cavities of fluorite, apatite, parisite-(Ce), dolomite, emerald, and quartz.

For many years it was assumed that Colombian deposits were unique, but in 2007 an unusual occurrence of green beryl (unfortunately not transparent enough for gem use) was discovered near Mountain River in Canada's Northwest Territories. This beryl is hosted by extensional quartz-carbonate veins cutting Neoproterozoic sandstone and siltstone. Research by Hewton et al. (2013) showed that the elements necessary to form beryl were liberated by inorganic thermochemical sulfate reduction via the circulation of warm basinal brines through siliciclastic, carbonate, and evaporitic rocks (figure 17). The Mountain River green beryl occurrence thus represents a variant of the Type IIB emerald deposit in the classification scheme of Giuliani et al. (2019) and suggests the potential for Colombian-type emerald mineralization in northwestern Canada.

Type IIC emerald deposits are further subdivided on the basis of the available examples. At the Panjshir Valley in Afghanistan (and Davdar in China) the host rock is a metamorphosed sedimentary rock and the formational fluids are metasomatic-hydrothermal in origin. At Hiddenite in northeastern North Carolina (United States), the host rock is a migmatite and the fluids are hydrothermal (Giuliani et al., 2019).

In Afghanistan the principal deposits lie within a 400 km^2 area centered on the Panjshir Valley 130 km northeast of Kabul (Bowersox et al., 1991; Fijal et al., 2004). In the Khendj and adjacent valleys on the southeast side of the Panjshir Valley, the emerald occurrences are hosted by metamorphic schist that has been subjected to intense hydrothermal alteration. The altered zones are irregularly scattered along a fracture network and characterized by the development of albite, muscovite, biotite, tourmaline, and pyrite. Fluid inclusions in the emeralds are highly saline, which suggests that the southeast Panjshir Valley occurrences, like those in Colombia, are linked to hydrothermal fluids that derived their high

salinity from leaching of evaporitic sequences (Giuliani et al., 1997a; Sabot et al., 2000; Vapnik and Moroz, 2001; Franz and Morteani, 2002; Giuliani et al., 2005). However, the metamorphic grade of the host rocks is higher than in the Colombian deposits. Sabot et al. (2000) suggested that the circulation of hydrothermal fluids resulted from tectonism that preceded uplift during the Himalayan orogeny.

At the Rist property northeast of Hiddenite, the emeralds occur in quartz veins and open cavities that occupy northeast-trending sub-vertical fractures in folded metamorphic rocks (Wise and Anderson, 2006). Emerald is associated with quartz, albite, beryl, calcite, dolomite, muscovite, rutile, spodumene, and siderite. The absence of pegmatites and the observed mineral assemblages suggest a hydrothermal origin. The source of Be and Cr, and of the Li needed to crystallize emerald and spodumene, remains unknown.

Type IID deposits are metamorphosed Type IA (Habachtal in Austria; Djebel Sikait, Zabara, and Umm Kabu in Egypt; and probably Poona in Australia), mixed Type IA and IIA deposits in mafic-ultramafic rocks, and in deposits whose origin is unknown (e.g., Musakashi in Zambia) (Giuliani et al., 2019). These deposits have no economic interest, and the origin of the Be is unknown. In the Habachtal deposit, the metamorphic Habach Formation consists of a sequence of metapelite and **metavolcanic** rocks with interlayered serpentinite. The emeralds occur within metasomatic biotite schist, called "blackwall" zones, developed between these rocks as a result of regional metamorphism involving intense deformation. Geochemical analyses show that the entire "blackwall" zone is enriched in Be, which Grundmann and Morteani (1989) suggested originated with submarine volcanic exhalations. Mass balance calculations suggested that the transformation of serpentinite and Be-rich country rocks released excess Be to form emerald in the blackwall zone (figure 18). The source of the Cr is the metasomatized ultrabasic rocks. Grundmann and Morteani (1989) argued for a regional metamorphic origin for the emeralds. Zwaan (2006) was critical of this interpretation and warned that in cases where pegmatitic sources of Be are not apparent, one must proceed with caution since fluids can travel far from pegmatites, especially along intensely sheared rocks. Zwaan (2006) also pointed out that pegmatites do occur in the Habach Formation and that the Habachtal emeralds contain up to 760 ppmw Cs (Calligaro et al., 2000), which suggests a pegmatitic source, and sulfide deposits related to submarine volcanic exhalation are not generally enriched in Be.

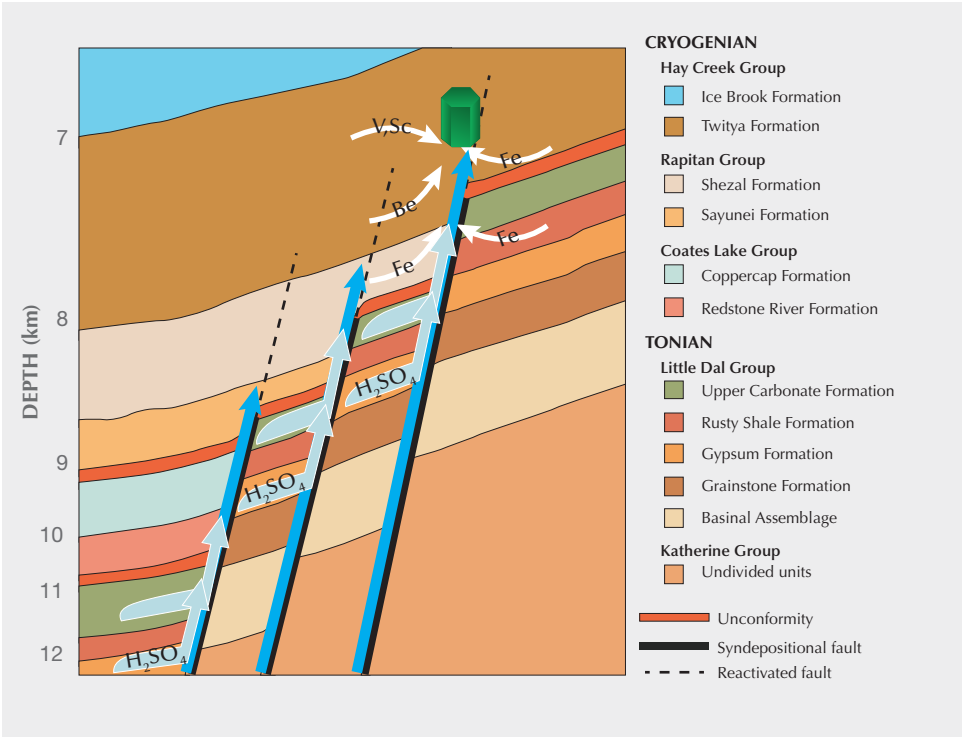

Figure 17. Genesis of the Mountain River occurrence in Canada. The blue arrows indicate fluid movement, and the light blue arrows indicate derivation of salts and sulfate. Modified from Hewton et al. (2013).

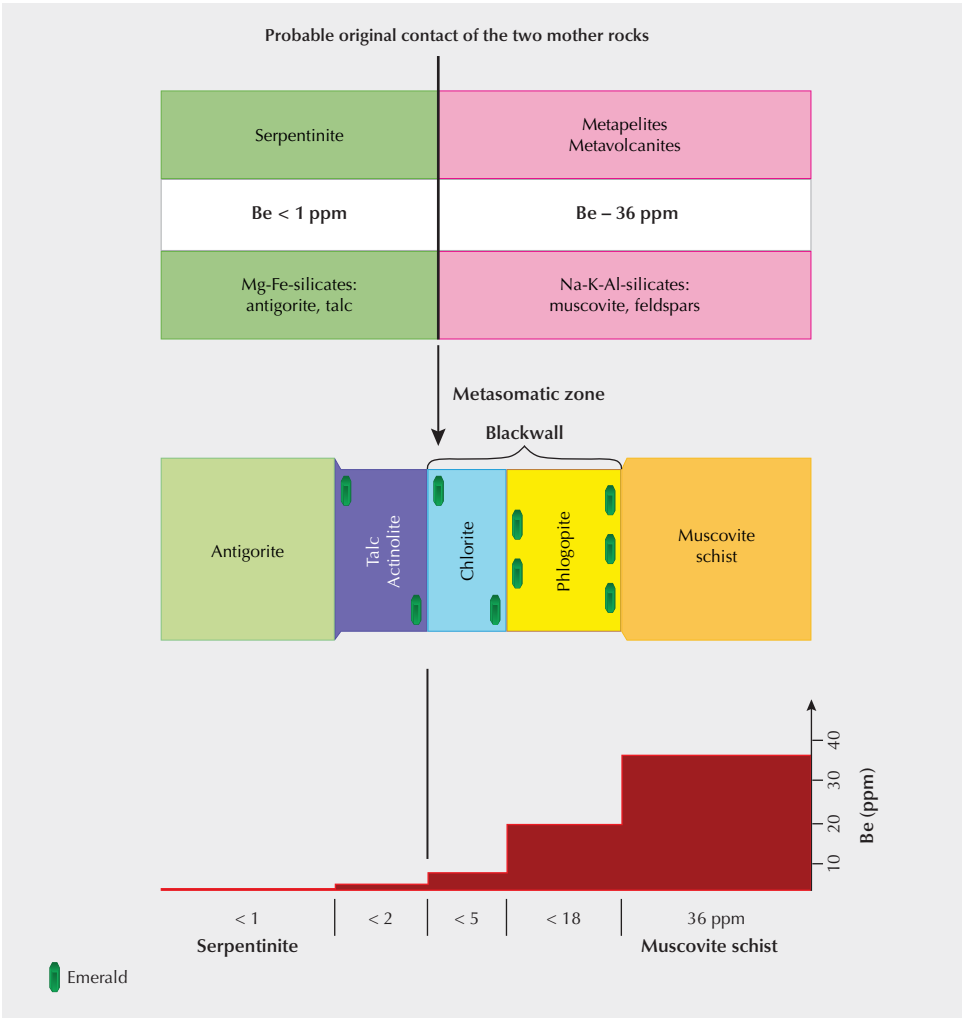

Figure 18. Model for formation of the Habachtal emerald deposit in Austria. Top: Initial stage showing the different lithologies with their respective Be contents. Middle: Final stage after regional metamorphism showing the final metasomatic rock assemblages. Bottom: Be liberated from the muscovite schists is incorporated into the emerald crystals. Modified from Grundmann and Morteani (1989).

SUMMARY

This paper is a brief review of the state of our knowledge of the geology and genesis of gem corundum and emerald deposits. The genetic models provide guidelines for prospecting and conceptual understanding, help to forecast the location of undiscovered gem deposits, and give geologic and geographic clues on the origins of ruby, sapphires, and emerald. Over the last two decades, knowledge of the formation of these deposits has improved significantly. For example, we now know that ruby in marbles in Southeast Asia and Central Asia result from the metamorphism of Al-bearing limestone and melting of evaporites. Today, most gem corundum production is from placers related to alkali basalt, plumasite, skarn, marble, and amphibolites. Sri Lanka and Madagascar remain important sources of high-quality metamorphic blue sapphire, Mozambique and northeastern Madagascar for top-quality ruby, and Southeast Asia and Australia for BGY sapphires. Most emerald production is from hard-rock mines in Colombia, Zambia, and Brazil.

ABOUT THE AUTHORS

Dr. Giuliani is a senior researcher at Université Paul Sabatier, GET/IRD and Université de Lorraine, CRPG/CNRS, Vandœuvre, France. Dr. Groat is a professor in the Department of Earth, Ocean and Atmospheric Sciences at the University of British Columbia in Vancouver.

ACKNOWLEDGMENTS

The authors would like to thank the editorial board of G&G for the invitation to contribute on the state of our knowledge on the geology and genesis of corundum and emerald deposits. We also thank two anonymous reviewers and Dr. Lin Sutherland for their constructive comments as well as the editorial support and improvement done by G&G.

GLOSSARY

Albitization: Partial or complete replacement of pre-existing plagioclase feldspar or alkali feldspar by albite in an igneous rock; commonly due to the residual water-rich vapor released during the final stages of crystallization of a granite body. The circulation of highly Na-rich saline hydrothermal fluids in fractures can also produce the albitization of rocks of different nature.

Alkali basalt: A type of basalt found in oceanic and continental areas associated with volcanic activity, such as oceanic islands, continental rifts, and volcanic fields; characterized by relatively high alkali (Na_2O and K_2O) content relative to other basalts; may originate at greater depths in the mantle (150–200 km) than most basalts (50–100 km).

Basaltic: Referring to a dark-colored, fine-grained igneous rock, composed mainly of plagioclase feldspar and pyroxene, formed by the solidification of magma near the earth's surface.

Breccia: A coarse-grained rock of sedimentary or igneous origin that is composed of angular rock fragments held together by a mineral cement or fine-grained matrix. Brecciation is the process of forming a breccia or the magma that crystallizes such a rock.

Cambrian: The first geological period of the Paleozoic Era, which spans time in the earth's history from 541 to 485.4 million years ago.

Carbonatitic: Refers to a magma composed mostly of molten carbonate minerals.

Clinopyroxenite: A rock composed dominantly of clinopyroxene. Typically refers to ultramafic igneous rocks that are often genetically related to other mafic/ultramafic rocks such as gabbros and peridotites.

Cretaceous: A geological period of the Mesozoic Era spanning in time from 145 to 66 million years ago.

Eclogite: A rock composed dominantly of pyrope-almandine garnet and Na-rich clinopyroxene. Eclogites are generally noted for their lack of plagioclase feldspar and typically form through metamorphism of mafic rocks at very high pressures, usually in the earth's mantle or in very thick sections of the crust.

Gneiss: Metamorphic rock identified by its banded appearance and texture; bands contain interlocking granular minerals or elongate minerals with evidence of preferred orientation; gneiss forms by regional metamorphism at convergent plate boundaries.

Granitoid: Coarse-grained plutonic igneous rocks composed mostly of feldspars and quartz with minor accessory minerals such as micas. *Granitoid* is a general term that includes granites and other mineralogical and compositionally similar plutonic rocks.

Granulite: Rocks that have experienced high-grade metamorphism at high temperature and medium to high pressure. Temperatures are generally high enough to initiate partial melting in granulites.

Komatiite: Ultramafic volcanic rocks with very high magnesium contents. Komatiites are very rare and generally confined to the Archean and Hadean Eons.

Lamprophyre: A group of dark-colored intrusive igneous rocks characterized by a high percentage of mafic minerals (such as biotite mica, hornblende, and pyroxene) as larger crystals, set in a fine-grained groundmass composed of the same minerals plus feldspars or feldspathoids.

Laterite: A soil rich in iron and aluminum, considered to have formed in hot and wet tropical areas.

Limestone: A sedimentary rock composed dominantly of calcium carbonate ($CaCO_3$). Limestones generally form through the gradual accumulation of the skeletal remains of marine organisms onto the seafloor over time.

Mafic: A dark-colored igneous rock chiefly composed of iron- and magnesium-rich minerals.

Mafic-ultramafic: See *mafic* and *ultramafic*.

Magmatic deposit: A deposit related to or derived from magma.

Mantle plume: An upwelling of hot rock rising up through the earth's mantle that is one of the likely mechanisms of convection and heat transfer in the earth. Mantle plumes are accompanied by extensive volcanism resulting from decompression of hot rocks originating deep within the mantle.

Megacryst: A crystal in an igneous or metamorphic rock that is significantly larger than those in the surrounding groundmass or matrix.

Mesozoic: The geological era containing the Triassic, Jurassic, and Cretaceous periods. The Mesozoic Era lasted from 252 to 66 million years ago.

Metabasite: The metamorphosed version of low-silica mafic, originally igneous rocks.

Metamorphic: Related to a process that causes mineralogical, chemical, or structural changes in solid rocks by exposing them to new pressure and temperature conditions by burial within the crust or mantle.

Metapelite: A metamorphosed fine-grained sedimentary rock (e.g., mudstone or siltstone).

Metasedimentary: A metamorphosed version of an originally sedimentary rock (e.g., marble or slate).

Metasomatic: Formed by metasomatism, a geologic process that produces new minerals in an existing rock by replacement.

Metavolcanic: A metamorphosed version of a volcanic rock.

Miarolitic: Crystal-lined irregular cavities or vugs most commonly found in granitic pegmatites, and also in a variety of other igneous rocks.

Neoproterozoic: A geological era from 1,000 to 541 million years ago belonging to the Proterozoic Eon.

Orogeny: The processes by which geologic structures in

mountainous regions are formed. These processes include thrusting, folding, faulting, and (at depth) metamorphism and igneous intrusions.

Ouachitite: Pronounced "wash-e-tite," this is a specific type of lamprophyre, predominantly composed of phenocrysts (large crystals) of mica and clinopyroxene set within a groundmass of fine-grained mica and clinopyroxene with minor analcime, calcite, corundum, and other trace accessory minerals.

Pegmatite: Intrusive igneous rock with a texture of exceptionally large mineral grains (by convention, the largest are more than about 3 cm long); most pegmatites are composed of quartz, feldspar, and mica (similar composition as granite); sometimes contain minerals that are rarely found in other types of rocks, including gems.

Phlogopite: A brown micaceous mineral that occurs chiefly in metamorphosed limestone and magnesium-rich igneous rocks. It consists of hydrous silicate of potassium and magnesium and aluminum.

Phonolite: Uncommon, fine-grained volcanic igneous rock consisting of alkaline feldspars (sanidine, anorthoclase or orthoclase) and nepheline.

Placer: A surface deposit consisting of valuable minerals that have been weathered out and then mechanically concentrated (normally by flowing water) in alluvial sediments.

Plumasite: Metasomatic rock, typically coarse-grained and found especially in dikes, consisting chiefly of corundum grains in a plagioclase feldspar matrix. It results from the circulation of hydrothermal fluids into a generally granitoid dike.

Plutonic: Igneous rock formed by slow cooling of magma that is intruded into the earth's crust.

Shear zone: The result of large-volume rock deformation due to intense regional stress, typically in continental collisional plates, as in the Himalayas today, at depths down to few kilometers; may occur at the edges of tectonic blocks, forming discontinuities that mark a distinct structure.

Skarn: Metasomatic rocks composed of calcium-magnesium-aluminum silicate minerals resulting from fluid-rock interaction of hydrothermal fluids with Ca-Mg-rich rocks. Generally, they form locally when a granitic pluton intrudes limestone or Ca-Mg-rich rocks.

Syenite: A coarse-grained intrusive igneous rock with a general composition similar to that of granite, but with a lower quartz content (typically <5%).

Syngenetic: Refers to an inclusion that formed at the same time as the host gem.

Ultramafic: An igneous rock composed mainly of mafic (iron and magnesium-rich) minerals.

Xenocryst: A large crystal in an igneous rock that is foreign to the rock in which it occurs.

Xenolith: An inclusion of a foreign rock in an igneous rock.

REFERENCES

Abduriyim A., Sutherland F.L., Coldham T. (2012) Past, present and future of Australian gem corundum. *Australian Gemmologist*, Vol. 24, No. 10, pp. 234–242.

Atkinson D., Kothavala R.Z. (1983) Kashmir sapphire. *G&G*, Vol. 19, No. 2, pp. 64–76, http://dx.doi.org/10.5741/GEMS.19.2.64

Baldwin L.C., Tomaschek F., Ballhaus C., Gerdes A., Fonseca R.O.C, Wirth R., Geisler T., Nagel T. (2017) Petrogenesis of alkaline basalt-hosted sapphire megacrysts. Petrological and geochemical investigations of in situ sapphire occurrences from the Siebengebirge Volcanic Field, Germany. *Contributions to Mineralogy and Petrology*, Vol. 172, No. 6, http://dx.doi.org/10.1007/s00410-017-1362-0

Behling S., Wilson W.E. (2010) The Kagem emerald mine: Kafubu area, Zambia. *Mineralogical Record*, Vol. 41, No. 1, pp. 59–68.

Berg R.B. (2007) Sapphires in the Butte-Deer Lodge area, Montana. *Montana Bureau of Mines and Geology Bulletin*, No. 134, 62 pp.

Berg R.B., Palke A.C. (2016) Sapphires from an eocene sill near Helena, Montana. *Geological Society of America Abstracts with Programs*, Vol. 48, No. 7, http://dx.doi.org/10.1130/abs/2016AM-278371

Bowersox G.W., Snee L.W., Foord E.F., Seal R.R. II. (1991) Emeralds of the Panjshir Valley, Afghanistan. *G&G*, Vol. 27, No. 1, pp. 26–39, http://dx.doi.org/10.5741/GEMS.27.1.26

Branquet Y., Laumonier B., Cheilletz A., Giuliani G. (1999a) Emeralds in the Eastern Cordillera of Colombia: Two tectonic settings for one mineralization. *Geology*, Vol. 27, No. 7, pp. 597–600, http://dx.doi.org/10.1130/0091-7613(1999)027%3C0597:EITECO%3E2.3.CO;2

Branquet Y., Cheilletz A., Giuliani G., Laumonier Blanco O. (1999b) Fluidized hydrothermal breccia in dilatant faults during thrusting: The Colombian emerald deposits. In K.J.W. McCaffrey, L. Lonergan, and J.J. Wilkinson, Eds., *Fractures, Fluid Flow and Mineralization*, Geological Society of London, Special Publications, Vol. 155, No. 1, pp. 183–195, http://dx.doi.org/10.1144/GSL.SP.1999.155.01.14

Branstrator B. (2017) Gemfields sells 6,100-ct rough emerald at Oct. auction. *National Jeweler*, October 11, https://www.nationaljeweler.com/diamonds-gems/supply/5911-gemfields-sells-6-100-ct-rough-emerald-at-oct-auction

Brownlow A.H., Komorowski J.-C. (1988) Geology and origin of the Yogo sapphire deposit, Montana. *Economic Geology*, Vol. 83, No. 4, pp. 875–880, http://dx.doi.org/10.2113/gsecongeo.83.4.875

Calligaro T., Dran J.-C., Poirot J.P., Querré G., Salomon J., Zwaan J.C. (2000) PIXE/PIGE characterisation of emeralds using an external micro-beam. *Nuclear Instruments and Methods in Physics Research Section B*, Vol. 161–163, pp. 769–774, http://dx.doi.org/10.1016/S0168-583X(99)00974-X

Cheilletz A., Giuliani G. (1996) The genesis of Colombian emeralds: A restatement. *Mineralium Deposita*, Vol. 31, No. 5, pp. 359–364, http://dx.doi.org/10.1007/BF00189183

Cheilletz A., Sabot B., Marchand P., De Donato P., Taylor B., Archibald D., Barres O., Andrianjaffy J. (2001) Emerald deposits in Madagascar: Two different types for one mineralising event. European Union of Geosciences Conference Abstracts, Vol. 6, p. 547.

Dharmaratne P.G.R., Premasiri H.M.R., Dillimuni D. (2012) Sapphires from Thammannawa, Kataragama area, Sri Lanka. *G&G*, Vol. 48, No. 2, pp. 98–107, http://dx.doi.org/10.5741/

GEMS.48.2.98
Dill H.G. (2018) Gems and placers–A genetic relationship par excellence. *Minerals*, Vol. 8, No. 10, pp. 470–513, http://dx.doi.org/10.3390/min8100470
Fagan A.J. (2015) True North Gems Greenland mining – The final lap. *InColor*, No. 29, pp. 36–49.
Fagan A.J. (2018) The ruby and pink sapphire deposits of SW Greenland: Geological setting, genesis, and exploration techniques. PhD Thesis, University of British Columbia, Vancouver, 747 pp.
Fijal J., Heflik W., Natkaniec-Nowak L., Szczepaniak A. (2004) Emeralds from the Panjshir Valley (Afghanistan). *Gemmologie: Zeitschrift der Deutschen Gemmologischen Gesellschaft*, Vol. 53, No. 4, pp. 127–142.
Franz G., Morteani G. (2002) Be-minerals: Synthesis, stability, and occurrence in metamorphic rocks. *Reviews in Mineralogy and Geochemistry*, Vol. 50, No. 1, pp. 551–589, http://dx.doi.org/10.2138/rmg.2002.50.13
Garnier V., Ohnenstetter D., Giuliani G., Schwarz D. (2004) Saphirs et rubis: Classification des gisements de corindon. *Le Règne Minéral*, Vol. 55, pp. 4–47.
Garnier V., Giuliani G., Ohnenstetter D., Fallick A.E., Dubessy J., Banks D., Hoàng Q.V., Lhomme T., Maluski H., Pêcher A., Bakhsh K.A., Pham V.L., Phan T.T., Schwarz D. (2008) Marble-hosted ruby deposits from central and Southeast Asia: Towards a new genetic model. *Ore Geology Reviews*, Vol. 34, No. 1-2, pp. 169–191, http://dx.doi.org/10.1016/j.oregeorev.2008.03.003
Gemfields (2018) Gemfields introduces 'Inkalamu', the 5,655 carat Lion Emerald. October 29, https://gemfields.com/gemfields-introduces-inkalamu-the-5655-carat-lion-emerald/
Giuliani G. (2011) La spirale du temps de l'émeraude. *Le Règne Minéral*, Vol. 98, pp. 31–44.
Giuliani G., Cheilletz A., Arboleda C., Carrillo V., Rueda F., Baker J.H. (1995) An evaporitic origin of the parent brines of Colombian emeralds: Fluid inclusion and sulphur isotope evidence. *European Journal of Mineralogy*, Vol. 7, No. 1, pp. 151–165, http://dx.doi.org/10.1127/ejm/7/1/0151
Giuliani G., France-Lanord C., Zimmermann J.L., Cheilletz A., Arboleda C., Charoy B., Coget P., Fontan F., Giard D. (1997a) Fluid composition, δD of channel H_2O, and $\delta^{18}O$ of lattice oxygen in beryls: Genetic implications for Brazilian, Colombian, and Afghanistani emerald deposits. *International Geology Review*, Vol. 39, No. 5, pp. 400–424, http://dx.doi.org/10.1080/00206819709465280
Giuliani G., Cheilletz A., Zimmermann J.L., Ribeiro-Althoff A.M., France-Lanord C., Féraud G. (1997b) Les gisements d'émeraude du Brésil: Genèse et typologie. *Chronique de la Recherche Minière*, Vol. 526, pp. 17–61.
Giuliani G., Christian F.L., Cheilletz A., Coget P., Branquet Y., Laumonier B. (2000) Sulfate reduction by organic matter in Colombian emerald deposits: Chemical and stable isotope (C, O, H) evidence. *Economic Geology*, Vol. 95, No. 5, pp. 1129–1153, http://dx.doi.org/10.2113/gsecongeo.95.5.1129
Giuliani G., Fallick A.E., Garnier V., France-Lanord C., Ohnenstetter D., Schwarz D. (2005) Oxygen isotope composition as a tracer for the origins of rubies and sapphires. *Geology*, Vol. 33, No. 4, pp. 249–252, http://dx.doi.org/10.1130/G21261.1
Giuliani G., Ohnenstetter D., Garnier V, Fallick A.E., Rakotondrazafy A.F.M., Schwarz D. (2007a) The geology and genesis of gem corundum deposits. In L.A. Groat, Ed., *Geology of Gem Deposits*, 1st ed., Mineralogical Association of Canada, Short Course Series 37, Yellowknife, Canada, pp. 23–78.
Giuliani G., Fallick A.E., Rakotondrazafy A.F.M., Ohnenstetter D., Andriamamonjy A., Rakotosamizanany S., Ralantoarison T., Razanatseheno M.M., Dunaigre C., Schwarz D. (2007b) Oxygen isotope systematics of gem corundum deposits in Madagascar: Relevance for their geological origin. *Mineralium Deposita*, Vol. 42, No. 3, pp. 251–270, http://dx.doi.org/10.1007/s00126-006-0105-3
Giuliani G., Ohnenstetter D., Fallick A.E., Groat L., Feneyrol J. (2012) Geographic origin of gems linked to their geological history. *InColor*, No. 19, pp. 16–27.
Giuliani G., Ohnenstetter D., Fallick A.E., Groat L.A., Fagan A.J. (2014) The geology and genesis of gem corundum deposits. In L.A. Groat, Ed., *Geology of Gem Deposits*, 2nd ed., Mineralogical Association of Canada, Short Course Series 44, pp. 29–112.
Giuliani G., Dubessy J., Banks D., Lhomme T., Ohnenstetter D. (2015) Fluid inclusions in ruby from Asian marble deposits: Genetic implications. *European Journal of Mineralogy*, Vol. 27, No. 3, pp. 393–404, http://dx.doi.org/10.1127/ejm/2015/0027-2442
Giuliani G., Dubessy J., Ohnenstetter D., Banks D., Branquet Y., Feneyrol J., Fallick A.E., Martelat J.-E. (2018) The role of evaporites in the formation of gems during metamorphism of carbonate platforms: A review. *Mineralium Deposita*, Vol. 53, No. 1, pp. 1–20, http://dx.doi.org/10.1007/s00126-017-0738-4
Giuliani G., Groat L.A., Marshall D., Fallick A.E., Branquet Y. (2019) Emerald deposits: A review and enhanced classification. *Minerals*, Vol. 9, No. 2, pp. 105–168, http://dx.doi.org/10.3390/min9020105
Graham I.T., Sutherland F.L., Webb G.B., Fanning C.M. (2004) Polygenetic corundums from New South Wales gemfields. In A.I. Khanchuk, G.A. Gonevchuk, A.N. Mitrokhin, I.F. Simanenko, N.J. Cook, R. Seltmann, Eds., *Metallogeny of the Pacific Northwest: Tectonics, Magmatism and Metallogeny of Active Continental Margins*. Dalnauka, Vladivostok, Russia, pp. 336–339.
Graham I., Sutherland L., Zaw K., Nechaev V., Khanchuk A. (2008) Advances in our understanding of the gem corundum deposits of the West Pacific continental margins intraplate basaltic fields. *Ore Geology Reviews*, Vol. 34, No 1-2, pp. 200–215, http://dx.doi.org/10.1016/j.oregeorev.2008.04.006
Grundmann G., Giuliani G. (2002) Emeralds of the world. *extraLapis English*, No. 2, pp. 24–35.
Grundmann G., Morteani G. (1989) Emerald mineralization during regional metamorphism; the Habachtal (Austria) and Leydsdorp (Transvaal, South Africa) deposits. *Economic Geology*, Vol. 84, No. 7, pp. 1835–1849, http://dx.doi.org/10.2113/gsecongeo.84.7.1835
Grundmann G., Morteani G. (1993) Emerald formation during regional metamorphism: The Zabara, Sikeit and Umm Kabo deposits (Eastern Desert, Egypt). In U. Thorweihe and H. Schandelmeir, Eds., *Geoscientific Research in Northeast Africa*, pp. 495–498, http://dx.doi.org/10.1201/9780203753392-90
Guo J., O'Reilly S.Y., Griffin W.L. (1996) Corundum from basaltic terrains: A mineral inclusion approach to the enigma. *Contributions to Mineralogy and Petrology*, Vol. 122, No. 4, pp. 368–386, http://dx.doi.org/10.1007/s004100050134
Hewton M.L., Marshall D.D., Ootes L., Loughrey L.E., Creaser R.A. (2013) Colombian-style emerald mineralization in the northern Canadian Cordillera: Integration into a regional Paleozoic fluid flow regime. *Canadian Journal of Earth Sciences*, Vol. 50, No. 8, pp. 857–871, http://dx.doi.org/10.1139/cjes-2012-0128
Hughes R.W. (1997) *Ruby & Sapphire*. RWH Publishing, Boulder, Colorado, 512 pp.
In the News: Gemfields' October emerald auction: US$21.5 million in sales (2018) *InColor*, No. 37, p. 22.
John T., Schenk V., Mezger K., Tembo F. (2004) Timing and *PT* evolution of whiteschist metamorphism in the Lufilian Arc–Zambezi Belt orogen (Zambia): Implications for the assembly of Gondwana. *Journal of Geology*, Vol. 112, No. 1, pp. 71–90, http://dx.doi.org/10.1086/379693
Jöns N., Schenk V. (2008) Relics of the Mozambique Ocean in the central East African orogen: Evidence from the Vohibory Block of southern Madagascar. *Journal of Metamorphic Geology*, Vol. 26, No. 1, pp. 17–28, http://dx.doi.org/10.1111/j.1525-1314.2007.00745.x
Kane R.E., Kammerling R.C. (1992) Status of ruby and sapphire mining in the Mogok stone tract. *G&G*, Vol. 28, No. 3, pp. 152–174, http://dx.doi.org/10.5741/GEMS.28.3.152
Kievlenko E.Y. (2003) *Geology of Gems*. Ocean Publications Ltd, Littleton, Colorado, pp. 432.

Kinnaird J.A. (1984) Contrasting styles of Sn-Nb-Ta-Zn mineralization in Nigeria. *Journal of African Earth Sciences*, Vol. 2, No. 2, pp. 81–90, http://dx.doi.org/10.1016/S0731-7247(84)80001-4

Krebs M.Y., Pearson D.G., Fagan A.J., Bussweiler Y., Sarkar C. (2019) The application of trace elements and Sr–Pb isotopes to dating and tracing ruby formation: The Aappaluttoq deposit, SW Greenland. *Chemical Geology*, Vol. 523, pp. 42–58, http://dx.doi.org/10.1016/j.chemgeo.2019.05.035

Kröner A. (1984) Late Precambrian plate tectonics and orogeny: A need to redefine the term Pan-African. In J. Klerkx and J. Michot, Eds., *African Geology*. Musée Royal de l'Afrique Centrale, Tervuren, Belgium, pp. 23–28.

Lake D.J., Groat L.A., Falck H., Cempirek J., Kontak D., Marshall D., Giuliani G., Fayek M. (2017) Genesis of emerald-bearing quartz veins associated with the Lened W-skarn mineralization, Northwest Territories, Canada. *Canadian Mineralogist*, Vol. 55, No. 4, pp. 561–593, http://dx.doi.org/10.3749/canmin.1700025

Le Goff E., Deschamps Y., Guerrot C. (2010) Tectonic implications of new single zircon Pb-Pb evaporation data in the Lossogonoi and Longido ruby-districts, Mozambican metamorphic Belt of north-eastern Tanzania. *Comptes Rendus Geoscience*, Vol. 342, No. 1, pp. 36–45, http://dx.doi.org/10.1016/j.crte.2009.10.003

Lucas A. (2012) Brazil's emerald industry. *G&G*, Vol. 48, No. 1, pp. 73–77, http://dx.doi.org/10.5741/GEMS.48.1.73

Lydekker R.L. (1883) The geology of the Kashmir and Chamba territories, and the British district of Khagan. *Memoirs of the Geological Survey of India*, Vol. 22, 344 pp.

Martins S. (2018) Brazilian emeralds. Second World Emerald Symposium, October 12–14, Bogotá.

Meng F., Shmelev V.R., Kulikova K.V., Ren Y. (2018) A red corundum-bearing vein in the Rai-Iz ultramafic rocks, Polar Urals, Russia: The product of fluid activity in a subduction zone. *Lithos*, Vol. 320-321, pp. 302–314, http://dx.doi.org/10.1016/j.lithos.2018.09.025

Mercier A., Debat P., Saul J.M. (1999) Exotic origin of the ruby deposits of the Mangari area in SE Kenya. *Ore Geology Reviews*, Vol. 14, No. 2, pp. 83–104, http://dx.doi.org/10.1016/S0169-1368(99)00002-5

Nicollet C. (1986) Saphirine et staurotide riche en magnésium et chrome dans les amphibolites et anorthosites à corindon du Vohibory Sud, Madagascar. *Bulletin de Minéralogie*, Vol. 109, No. 5, pp. 599–612, http://dx.doi.org/10.3406/bulmi.1986.7961

Ottaway T.L., Wicks F.J., Bryndzia L.T., Kyser T.K., Spooner E.T.C. (1994) Formation of the Muzo hydrothermal emerald deposit in Colombia. *Nature*, Vol. 369, No. 6481, pp. 552–554, http://dx.doi.org/10.1038/369552a0

Ozerov K. (1945) Form of corundum crystals as dependent upon chemical composition of medium. *Doklady Akademii Nauk SSSR*, Vol. 47, pp. 49–52.

Palke A.C., Renfro N.D., Berg R.B. (2016) Origin of sapphires from a lamprophyre dike at Yogo Gulch, Montana, USA: Clues from their melt inclusions. *Lithos*, Vol. 260, pp. 339–344, http://dx.doi.org/10.1016/j.lithos.2016.06.004

Palke A.C., Renfro N.D., Berg R.B. (2017) Melt inclusions in alluvial sapphires from Montana, USA: Formation of sapphires as restitic component of lower crustal melting? *Lithos*, Vol. 278-281, pp. 43–53, http://dx.doi.org/10.1016/j.lithos.2017.01.026

Palke A.C., Wong J., Verdel C., Avila J.N. (2018) A common origin for Thai/Cambodian rubies and blue and violet sapphires from Yogo Gulch, Montana, USA? *American Mineralogist*, Vol. 103, No. 3, pp. 469–479, http://dx.doi.org/10.2138/am-2018-6164

Paquette J.L., Nédelec A., Moine B., Rakotondrazafy A.F.M. (1994) U-Pb, single zircon Pb-evaporation and Sm-Nd isotopic study of a granulite domain in SE Madagascar. *Journal of Geology*, Vol. 102, No. 5, pp. 523–538, http://dx.doi.org/10.1086/629696

Pardieu V. (2018) Gemfields' November 2017 ruby auction yields record results. *InColor*, No. 37, pp. 62–63.

Pardieu V., Chauviré B. (2013) Les rubis du Mozambique. *Le Règne Minéral*, Cahier No. 2, pp. 101–108.

Pardieu V., Rakotosaona N. (2012) Ruby and sapphire rush near Didy, Madagascar (April-June 2012). *GIA Research News*, https://www.gia.edu/doc/Ruby-and-Sapphire-Rush-Near-Didy-Madagascar.pdf

Pardieu V., Jacquat S., Bryl L.P., Senoble J.B. (2009) Rubies from northern Mozambique. *InColor*, No. 12, pp. 32–36.

Peretti A., Hahn L. (2013) Record-breaking discovery of ruby and sapphire at the Didy mine in Madagascar: Investigating the source. *InColor*, No. 21, pp. 22–35.

Peretti A., Mullis J., Kündig R. (1990) Die Kaschmir-Saphire und ihr geologisches erinnerungsvermögen. *Neue Zürcher Zeitung*, Vol. 187, pp. 58–59.

Peretti A., Peretti F., Kanpraphai A., Bieri W.P., Hametner K., Günther D. (2008) Winza rubies identified. *Contributions to Gemology*, Vol. 7, pp.1–97.

Peucat J.J., Ruffault P., Fritsch E., Bouhnik-Le Coz M., Simonet C., Lasnier B. (2007) Ga/Mg ratios as a new geochemical tool to differentiate magmatic from metamorphic blue sapphires. *Lithos*, Vol. 98, No. 1-4, pp. 261–274, http://dx.doi.org/10.1016/j.lithos.2007.05.001

Rakotondrazafy A.F.M., Moine B., Cuney, M. (1996) Mode of formation of hibonite ($CaAl_{12}O_{19}$) within the U-Th skarns from the granulites of S-E Madagascar. *Contributions to Mineralogy and Petrology*, Vol. 123, pp. 190–201, http://dx.doi.org/10.1007/s004100050150

Rakotondrazafy A.F.M., Giuliani G., Ohnenstetter D., Fallick A.E., Andriamamonjy A., Rakotosamizanany S., Ralantoarison T., Razanatseheno M., Offant Y., Garnier V., Maluski H., Dunaigre C., Schwarz D., Mercier A., Ratrimo V., Ralison B. (2008) Gem corundum deposits of Madagascar: A review. *Ore Geology Reviews*, Vol. 34, No. 1-2, pp. 134–154, http://dx.doi.org/10.1016/j.oregeorev.2007.05.001

Rakotosamizanany S., Giuliani G., Ohnenstetter D., Rakotondrazafy A.F.M., Fallick A.E., Paquette J.-L., Tiepolo M. (2014) Chemical and oxygen isotopic compositions, age and origin of gem corundums in Madagascar alkali basalts. *Journal of African Earth Sciences*, Vol. 94, pp. 156–170, http://dx.doi.org/10.1016/j.jafrearsci.2013.06.003

Ramdhor R., Milisenda C.C. (2004) Neue Vorkommen von saphirseifenlager stätten auf Nosy-Bé, Madagaskar. Zeitschrift der *Deutschen Gemmologischen Gesellschaft*, Vol. 53, No. 4, pp. 143–158.

Ratnaraj ruby ring highlight of Christie's Hong Kong Magnificent Jewels sale (2017) *InColor*, No. 34, pp. 76.

Renfro N.D., Palke A.C., Berg R.B. (2018) Gemological characterization of sapphires from Yogo Gulch, Montana. *G&G*, Vol. 54, No. 2, pp. 184–201, http://dx.doi.org/10.5741/GEMS.54.2.184

Rudnick R.L., Gao S. (2003) Composition of the continental crust. In R.L. Rudnick, Ed., *The Crust*. Treatise on Geochemistry Series, Vol. 3. Elsevier Science, Amsterdam, pp. 1–64.

Sabot B., Cheilletz A., De Donato P., Banks D., Levresse G., Barrès O. (2000) Afghan emeralds face Colombian cousins. *Chronique de la Recherche Minière*, Vol. 541, pp. 111–114.

Schwarz D. (1998) Aus Basalten, Marmoren und Pegmatiten. Spezielle Ursachen formten in der Erdkruste edle Rubine und Saphire. In C. Weise, Ed., Rubin, Saphir, Korund: schön, hart, selten, kostbar. *extraLapis*, No. 15, pp. 5–9.

Schwarz D., Giuliani G. (2002) South America: Brazil. *extraLapis English*, No. 2, 46–51.

Schwarz D., Kanis J., Kinnaird J. (1996) Emerald and green beryl from central Nigeria. *Journal of Gemmology*, Vol. 25, No. 2, pp. 117–141.

Schwarz D., Kanis J., Schmetzer K. (2000) Sapphires from Antsiranana Province, Northern Madagascar. *G&G*, Vol. 36, No. 3, pp. 216–233, http://dx.doi.org/10.5741/GEMS.36.3.216

Schwarz D., Giuliani G., Grundmann G., Glas M. (2002) The origin of emerald...a controversial topic. *extraLapis English*, No. 2, 18–21.

Schwarz D., Pardieu V., Saul J.M., Schmetzer K., Laurs B.M., Giuliani G., Klemm L., Malsy A.-K., Hauzenberger C., Du Toit G., Fallick A.E., Ohnenstetter D. (2008) Ruby and sapphires from Winza, central Tanzania. *G&G*, Vol. 44, No. 4, pp. 322–347,

http://dx.doi.org/10.5741/GEMS.44.4.322
Seifert A.V., Hyršl J. (1999) Sapphire and garnet from Kalalani, Tanga Province, Tanzania. *G&G*, Vol. 35, No. 2, pp. 108–120, http://dx.doi.org/10.5741/GEMS.35.2.108
Seifert A.V., Žáček V., Vrána S., Pecina V., Zachariáš J., Zwaan J.C. (2004) Emerald Mineralization in the Kafubu area, Zambia. *Bulletin of Geosciences*, Vol. 79, No. 1, pp. 1–40.
Silva K.K.M.W., Siriwardena, C.H.E.R (1988) Geology and the origin of the corundum-bearing skarn at Bakamuna, Sri Lanka. *Mineralium Deposita*, Vol. 23, No. 3, pp. 186–190, http://dx.doi.org/10.1007/BF00204299
Simonet C. (2000) Géologie des gisements de saphir et de rubis. L'exemple de la John Saul ruby mine, Mangare, Kenya. Ph.D. thesis, Université de Nantes, 349 pp.
Simonet C. (2018) The Montepuez ruby deposits, what's next? *InColor*, No. 37, pp. 32–40.
Simonet C., Paquette J.L., Pin C., Lasnier B., Fritsch E. (2004) The Dusi (Garba Tula) sapphire deposit, Central Kenya–a unique Pan-African corundum-bearing monzonite. *Journal of African Earth Sciences*, Vol. 38, No. 4, pp. 401–410, http://dx.doi.org/10.1016/j.jafrearsci.2004.02.002
Simonet C., Fritsch E., Lasnier B. (2008) A classification of gem corundum deposits aimed towards gem exploration. *Ore Geology Reviews*, Vol. 34, No. 1-2, pp. 127–133, http://dx.doi.org/10.1016/j.oregeorev.2007.09.002
Solesbury F. (1967) Gem corundum pegmatites in NE Tanganyika. *Economic Geology*, Vol. 62, No. 7, pp. 983–991, http://dx.doi.org/10.2113/gsecongeo.62.7.983
Sorokina E.S., Rösel D., Häger T., Mertz-Kraus R., Saul J.M. (2017a) LA-ICP-MS U–Pb dating of rutile inclusions within corundum (ruby and sapphire): New constraints on the formation of corundum deposits along the Mozambique belt. *Mineralium Deposita*, Vol. 52, No. 5, pp. 641–649, http://dx.doi.org/10.1007/s00126-017-0732-x
Sorokina E.S., Karampelas S., Nishanbaev T.P., Nikandrov S.N., Semiannikov B.S. (2017b) Sapphire megacrysts in syenite pegmatites from the Ilmen Mountains, South Urals, Russia: New mineralogical data. *Canadian Mineralogist*, Vol. 55, No. 5, pp. 823–843, http://dx.doi.org/10.3749/canmin.1700016
SRK Consulting (UK) Limited (2015) A Competent Persons Report on the Montepuez Ruby Project, Mozambique. July 2015, 195 pp.
Sutherland F.L., Abduriyim A. (2009) Geographic typing of gem corundum: A test case from Australia. *Journal of Gemmology*, Vol. 31, No. 5-8, pp. 203–210.
Sutherland F.L., Schwarz D. (2001) Origin of gem corundums from basaltic fields. *Australian Gemmologist*, Vol. 21, No. 1, pp. 30–33.
Sutherland F.L., Hoskin P.W.O., Fanning C.M., Coenraads R.R. (1998a) Models of corundum origin from alkali basaltic terrains: A reappraisal. *Contributions to Mineralogy and Petrology*, Vol. 133, No. 4, pp. 356–372, http://dx.doi.org/10.1007/s004100050458
Sutherland F.L., Schwarz D., Jobbins E.A., Coenraads R.R., Webb G.B. (1998b) Distinctive gem corundum suites from discrete basalt fields: A comparative study of Barrington, Australia, and West Pailin, Cambodia, gemfields. *Journal of Gemmology*, Vol. 26, No. 2, pp. 65–85.
Sutherland F.L., Zaw K., Meffre S., Giuliani G., Fallick A.E., Graham I.T., Webb G.B. (2009) Gem-corundum megacrysts from east Australian basalt fields: Trace elements, oxygen isotopes and origins. *Australian Journal of Earth Sciences*, Vol. 56, No. 7, pp. 1003–1022, http://dx.doi.org/10.1080/08120090903112109
Tenthorey E.A., Ryan J.G., Snow E.A. (1996) Petrogenesis of sapphirine-bearing metatroctolites from the Buck Creek ultramafic body, southern Appalachians. *Journal of Metamorphic Geology*, Vol. 14, No. 2, pp. 103–114, http://dx.doi.org/10.1046/j.1525-1314.1996.05793.x
Themelis T. (1992) *The Heat Treatment of Ruby and Sapphire*. Gemlab Inc., Bangkok, 256 pp.
Uher P., Giuliani G., Szakall S., Fallick A.E., Strunga V., Vaculovic D., Ozdin D., Greganova M. (2012) Sapphires related to alkali basalts from the Cerová Highlands, Western Carpathians (southern Slovakia): Composition and origin. *Geologica Carpathica*, Vol. 63, No. 1, pp. 71–82, http://dx.doi.org/10.2478/v10096-012-0005-7
Vapnik Y., Moroz I. (2000) Fluid inclusions in emerald from the Jos Complex (central Nigeria). *Schweizerische Mineralogische und Petrographische Mitteilungen*, Vol. 80, No. 2, pp. 117–129.
Vapnik Y., Moroz I. (2001) Fluid inclusions in Panjshir emerald (Afghanistan). *Proceedings of the XVI European Current Research on Fluid Inclusions (ECROFI)*, pp. 451–454.
Vapnik Y., Sabot B., Moroz I. (2005) Fluid inclusions in Ianapera emerald, Southern Madagascar. *International Geology Review*, Vol. 47, No. 6, pp. 647–662, http://dx.doi.org/10.2747/0020-6814.47.6.647
Vapnik Y., Moroz I., Eliezri I. (2006) Formation of emeralds at pegmatite-ultramafic contacts based on fluid inclusions in Kianjavato emerald, Mananjary deposits, Madagascar. *Mineralogical Magazine*, Vol. 70, No. 2, pp. 141–158, http://dx.doi.org/10.1180/0026461067020320
Vertriest W., Girma D., Wongrawang P., Atikarnsakul U., Schumacher K. (2019) Land of origins: A gemological expedition to Ethiopia. *G&G*, Vol. 55, No. 1, pp. 72–88, http://dx.doi.org/10.5741/GEMS.55.1.72
Walton L.A. (2004) Exploration criteria for coloured gemstone deposits in the Yukon. *Yukon Geological Survey*, Open File 2004-10, 184 pp.
Weil E. (2017) The curse of the Bahia emerald, a giant green rock that ruins lives. *Wired*, March 2, www.wired.com/2017/03/curse-bahia-emerald-giant-green-rock-wreaks-havoc-ruins-lives/
Wise M.A., Anderson A.J. (2006) The emerald- and spodumene-bearing quartz veins of the Rist emerald mine, Hiddenite, North Carolina. *Canadian Mineralogist*, Vol. 44, No. 6, pp. 1529–1541, http://dx.doi.org/10.2113/gscanmin.44.6.1529
Yager T.R., Menzie W.D., Olson D.W. (2008) Weight of production of emeralds, rubies, sapphires, and tanzanite from 1995 through 2005. U.S. Geological Survey Open-File Report 2008-1013, 9 pp., https://pubs.usgs.gov/of/2008/1013/ofr2008-1013.pdf
Yui T.-F., Zaw K., Limkatrun P. (2003) Oxygen isotope composition of the Denchai sapphire, Thailand: A clue to its enigmatic origin. *Lithos*, Vol. 67, No. 1-2, pp. 153–161, http://dx.doi.org/10.1016/S0024-4937(02)00268-2
Zachariáš J., Žáček V., Pudilová M., Machovič V. (2005) Fluid inclusions and stable isotope study of quartz-tourmaline veins associated with beryl and emerald mineralization, Kafubu area, Zambia. *Chemical Geology*, Vol. 223, No. 1-3, pp. 136–152, http://dx.doi.org/10.1016/j.chemgeo.2004.12.023
Zachovay M. (2002) What is the price of an emerald? *extraLapis English*, No. 2, pp. 93–96.
Zwaan J.C. (2006) Gemmology, geology and origin of the Sandawana emerald deposits, Zimbabwe. *Scripta Geologica*, Vol. 131, pp. 1–211.
Zwaan J.C., Seifert A.V., Vrána S., Laurs B.M., Anckar B., Simmons W.B., Falster A.U., Lustenhouwer W.J., Muhlmeister S., Koivula J.I., Garcia-Guillerminet H. (2005) Emeralds from the Kafubu area, Zambia. *G&G*, Vol. 41, No. 2, pp. 116–148, http://dx.doi.org/10.5741/GEMS.41.2.116

Field Gemology: Building a Research Collection and Understanding the Development of Gem Deposits

Wim Vertriest, Aaron C. Palke, and Nathan D. Renfro

GIA's field gemology program was established in late 2008 to support research on geographic origin determination of colored gemstones. By building and maintaining an extensive collection of gem materials with known origins, GIA's research scientists have been able to study and analyze rubies, sapphires, emeralds, and other gemstones using the best available reference samples. This has led to improved origin determination services while supporting numerous research and education projects. To date the collection has accumulated during more than 95 field expeditions on six continents and currently includes more than 22,000 samples. GIA's field gemology efforts require a thorough understanding of the gem trade, including the evolution of gemstone deposits and the development of treatments. It is important to recognize potential new deposits and gemstone enhancement procedures immediately because they can change rapidly and leave a lasting impact on the trade. Field expeditions also involve documenting the mines and local conditions. These factors provide context for the gemstones and are becoming increasingly important in the eyes of the public.

Over the last decade, GIA has invested considerable resources in determining the geographic origin of certain gemstones. The field gemology program plays an essential role in these studies. Its mission is to build, maintain, and expand a reliable reference collection of scientific samples (figure 1). These stones are used for research by GIA's gemologists and research scientists.

This article explains the challenges of geographic origin research, sample collection, and the current state of GIA's colored stone reference collection. The development of gemstone deposits is also discussed, and an overview is provided of the most important localities for which GIA offers origin determination.

THE CRITICAL FACTOR IN GEOGRAPHIC ORIGIN RESEARCH

In recent years, the gem and jewelry trade has come to place a premium on the geographic origin of high-value gemstones. This has expanded the traditional role of laboratories, which is mainly gem identification and detection of treatments and synthetics, to also include geographic origin determination of certain gem species.

Geographic origin determination of colored gemstones relies heavily on advanced research. In a modern gemological lab, advanced analytical techniques and highly trained scientists are irreplaceable. But the work of a brilliant team with the most sophisticated equipment is irrelevant if the reference mate-

In Brief

- GIA's colored stone reference collection is one of the largest and best-documented collections of its kind.
- A thorough understanding of the colored stone market and available materials is required when building a reference database.
- Gem-producing areas are constantly changing: Field gemologists need to follow up on old and new sources.
- Apart from maintaining the colored stone research collection, GIA's field gemology department is responsible for documenting the mining and trading environment.

See end of article for About the Authors and Acknowledgments.
Gems & Gemology, Vol. 55, No. 4, pp. 490–511,
http://dx.doi.org/10.5741/GEMS.55.4.490

Figure 1. Aaron Palke (left) and Wim Vertriest sort through gem gravel in Mogok, Myanmar, in December 2018. Photo by Kevin Schumacher.

rial is not reliable. Dependable research samples are the critical factor to ensure solid research for geographic origin determination. The quality of the reference materials determines the quality of the data produced.

WHAT MAKES A RESEARCH COLLECTION RELIABLE?

Gemstones are small, high-value assets that are easily transportable but difficult to trace. This can lead to a lack of transparency throughout the supply chain. Procuring trustworthy samples from the trade is challenging for research institutes, especially when the trade places such high value on the results of their work. Traders might try to influence research to their own advantage by providing limited or incorrect samples.

A strong reference collection is the necessary foundation of research, but what makes a collection reliable? Naturalist and documentary filmmaker Sir David Attenborough noted that

> a research library associated with collections is almost of greater importance than the objects themselves. Unless you know where it came from *exactly*, and when it came from *exactly*, you are missing a lot of very, *very* important information. And that information can not only come from the object itself, but from the circumstances of documentation that should accompany every scientifically collected specimen.
>
> ("Sir David Attenborough…," 2017)

Building a reliable collection requires going where the stones are, as it is unsustainable to rely solely on donations from traders. GIA's field gemology department was created to establish a reliable collection to support origin determination by collecting the samples directly. Over the last decade, the department has gathered gemstones on six continents through more than 95 expeditions.

While the ultimate goal is to collect samples in the mines (figure 2), this is not always feasible: Some mines are no longer active, and others are off limits to foreigners or pose great safety risks. This means the samples in GIA's reference collection have various degrees of reliability. GIA developed the following classification scheme, which reflects the degree of confidence for origin from high to low:

- A-type samples are mined directly by the field gemologist (figure 3). This includes sampling from the host rock in the mine, washing/panning an alluvial deposit, and the like. Naturally, these have the highest degree of reliability.

Figure 2. During GIA field expedition 87 to Greenland's ruby mines, samples were collected from the host rock using a geological hammer. The samples are individually bagged and associated data, including GPS coordinates, is immediately attached on a paper label. Photo by Wim Vertriest.

- B-type samples are collected at the mine with the field gemologist witnessing the mining process but not actively removing the stones from the ground (figure 4). Miners are naturally protective of their goods—one high-value stone that goes missing could make a huge difference in a mining operation. In many places, visitors are not allowed to touch mining equipment, sorting tables, or exposed rock faces, so B-type samples are often easier to obtain than A-type. The most common scenario for this type of sample is where gravels are washed and concentrated on a large scale. In these operations, the washing plant is usually cleared at the end of the day. These stones still have a clearly established origin.
- C-type samples are collected at the mine but without witnessing the mining process for the specific stones (figure 5). Miners often possess gems that were mined in previous days. Arti-

Figure 3. A-type sampling: Author AP collects ruby and pink sapphire directly from the host rock in Aappaluttoq, Greenland. Photo by Wim Vertriest.

Figure 4. B-type sampling: Collecting samples from gravel that is being washed by a Burmese miner in the Kin area, west of Mogok. Photo by Wim Vertriest.

sanal miners also change working locations regularly. In these circumstances, the origin is already less certain since parcels might easily have been switched, added to, or mixed with production from multiple sites.

- D-type samples are collected from the miner but not at the mine (figure 6). Large-scale operations often have off-site headquarters where sorting, grading, and other steps take place. Artisanal miners often travel to central markets to sell their goods. Since these samples are collected off-site, the origin is less certain than that of stones obtained at the mines.
- E-type samples are purchased from dealers in the local market, often in close proximity to the mines (figure 7). The sellers have collected the material from the miners and often present stones from a mix of different miners and potentially sources. These are less reliable than stones obtained directly from the miners.

Figure 5. C-type sampling: Selecting rubies in the sorting house at Montepuez Ruby Mining's operation in Montepuez, Mozambique. Photo by M. Lemoux.

Figure 6. D-type sampling: The GIA team purchased samples from this artisanal miner along the road in Mogok, Myanmar. Every day he drives his motorbike into the mountains to work a small ruby deposit. Photo by Wim Vertriest.

- F-type samples are collected in international markets (figure 8). Gemstones are often traded in centers with a high volume of stones, where it is easy to obtain a variety of samples and spot goods that are new to the trade. These sites can be temporary, such as the Tucson and Hong Kong trade shows, or fixed trading hubs like Bangkok. Material from sources such as museum collections is also included in this category.

Figure 7. E-type sampling: Author WV checks blue spinel at the morning market in Luc Yen, Vietnam. Photo by Vincent Pardieu.

Figure 8. F-type sampling: Inspecting Madagascar sapphires in an office in Beruwala, Sri Lanka. Photo by Vincent Pardieu.

- Z-type samples are those that have no origin information. These can still be useful in some cases. For example, a recent study of the effect of heating on basalt-related sapphires did not require stones from specific locations. So we decided to spare the samples with known origin and use Z-type samples. Stones are also categorized as Z-type when the initial collection data are suspected to be inaccurate (everyone who buys in the field makes mistakes). On one occasion, we found a synthetic and two heat-treated stones in a C-type parcel of 90 stones. Because of this discovery, the whole parcel lost credibility and was reclassified as Z-type.

Material gathered by all of these means is valuable for research, as long as the collection circumstances are known. That is why GIA also includes other information with its samples. Every sample has GPS coordinates from the acquisition site attached to it, and the mine coordinates are added when available. Other information includes species and variety, sample price, seller identity, locality details, and the possibility of treatment (again, see figure 2). If this information is not available, valuable data are missing. Careful and precise logging of this information is critical, especially if the collection will have multiple users over time.

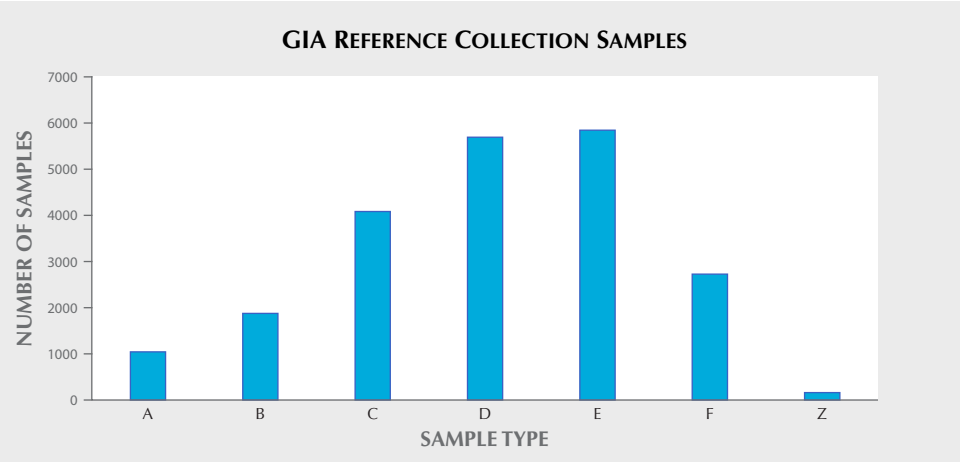

Figure 9. The number of samples of each type in GIA's reference collection.

GIA'S RESEARCH COLLECTION IN THE REAL WORLD

In an ideal world, GIA's collection would consist of only A-type stones mined by GIA field gemologists, but unfortunately gem-quality material found in these conditions is very rare. To best support origin determination services, we still collect samples in all other circumstances (figure 9). This is a common practice when new deposits are discovered. First the material becomes available in an international market, where some samples (F-type) are obtained by GIA for initial analysis. Visiting a new mining location usually involves substantial preparation and planning, so a few months could pass before sample collection at the mine (A- to C-type) occurs. In the meantime, stones from these new mines could become available in the market and be submitted to GIA's laboratories.

This is why we rely heavily on stones with different classification codes. Even if their reliability is lower than A-type, they allow us to conduct preliminary research, to later be supported with data from more reliable samples.

Field gemology supports the research on geographic origin at GIA laboratories. Traditionally, origin determination was only requested for the three most important colored stones: ruby, sapphire, and emerald. These have been the focus of the field gemology program's sampling expeditions for the first decade. Because gem corundum is also the subject of many treatment experiments, a significant part of the collection consists of ruby, sapphire, and fancy sapphire (figure 10).

With increasing demand for geographic origin determination for a wider variety of gemstones, GIA's colored stone reference collection needs to be diversified. In the last two years, significant efforts have been made to collect alexandrite, cuprian tourmaline, and other gemstones. Many of the samples used in origin determination research of cuprian tourma-

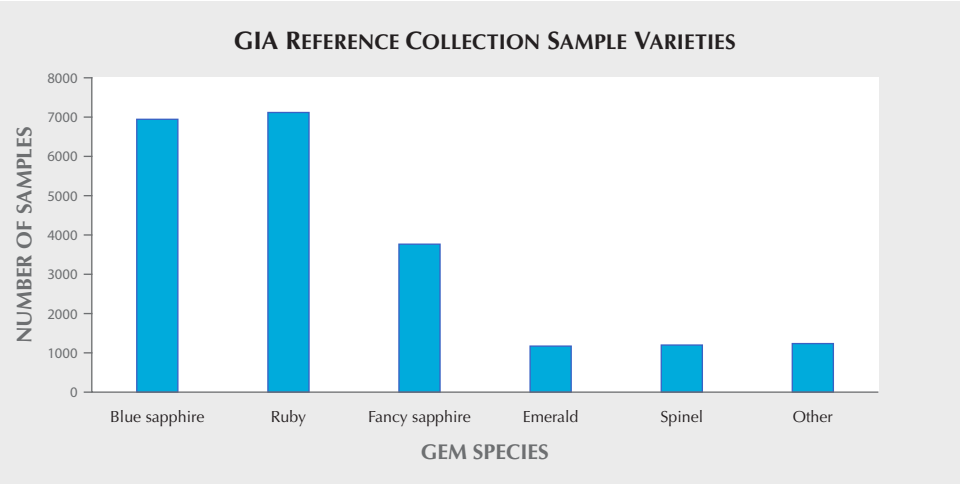

Figure 10. The number of samples of each gemstone variety in GIA's reference collection. Fancy sapphire includes yellow, green, purple, and color-change corundum as well as pink sapphires, which are used to complement ruby studies. The others are mainly rock samples but include alexandrite, tourmaline (cuprian and non-cuprian), garnet, tanzanite, and other gem minerals.

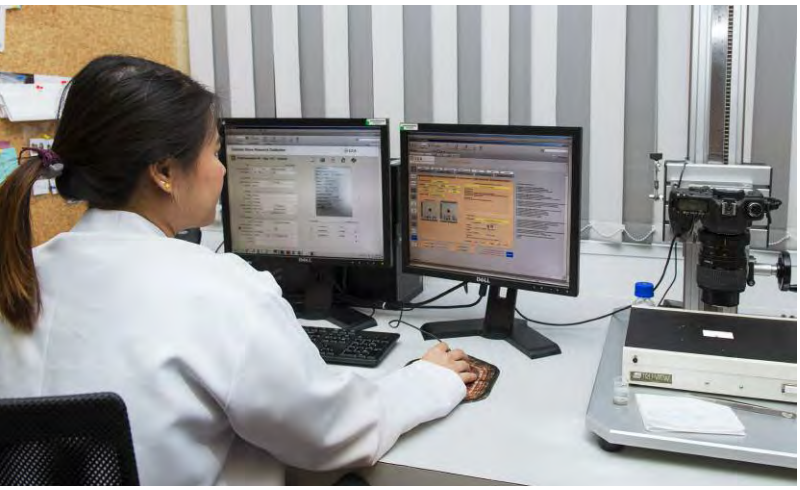

Figure 11. Stone librarians enter field data and color-calibrated photos into the digital database, which is accessible by gemologists in all GIA laboratories. Photo by Nuttapol Kitdee.

Figure 12. Before a sample can be analyzed, it must be prepared. This preparation involves polishing large, flat windows on the stone with a minimum of polish lines. This can be achieved using precision cutting machines. Photo by Nuttapol Kitdee.

line and alexandrite are still acquired in the trade (E- and F-type), but GIA is actively working on visiting the mining sites and collecting samples there.

Sample collecting is only the first step in the life of a research sample. Once the material is acquired by GIA field gemologists and shipped back to the lab, it needs to be added to a database that provides an overview for the entire collection. A GIA stone librarian enters all the available data in a digital database that is accessible to GIA colored stone identification staff around the world (figure 11). The data are accompanied by a color-calibrated photo of the rough piece. Documenting all pieces in exactly the same lighting conditions allows a preliminary color comparison of different samples based on digital images. All of the accompanying field data is printed on a labeled cassette in which the stone is stored in the physical library.

The majority of stones collected in the field are rough pebbles. This means they have some form of skin and are not fully transparent and thus need to be prepared for analytical procedures. In order to observe inclusions and obtain high-quality spectroscopic data, it is critical that windows with an excellent polish be faceted on the stones. This is done with traditional lapidary techniques using precision cutting machines to guarantee large, flat surfaces (figure 12).

However, for research samples, especially when looking at spectroscopy, orientation of the windows/facets is very important. The majority of stones in the research collection are dichroic (corundum and beryl), which means their optical properties vary depending on the direction in which they are observed. To make sure we compare every sample in the proper direction, for samples chosen for spectroscopy we align the c-axis parallel or perpendicular to the polished windows. By using a custom-made instrument that allows us to locate the c-axis position within one degree (Thomas et al., 2014), we know that all spectra collected on our stones are comparable (figure 13). For inclusion observation it is also important to have varying window orientations since some two-dimensional internal features (e.g., needles and platelets) are associated with the crystal structure and thus nearly invisible from certain angles. A variety of orientations allows more possibilities to explore the inclusion scene in a gem.

Polishing windows also removes the stone's outer layer, which might be encrusted with mud, host rock, or other material. By analyzing the trace element chemistry on a freshly polished surface, contamination by surface features such as iron staining is avoided. It also allows us to target specific zones within the crystal more precisely. This is often the case with blue sapphire, where color zoning is extremely common and the internal trace element concentration can vary considerably.

The majority of research stones go through the same analytical procedures as gems submitted by clients. Documenting inclusions with photomicrography is the first step. If the stone is extremely clean, it can be used for color analysis. In these high-quality wafers, there are no discernible internal features that can disturb light traveling through them. This allows

Figure 13. Selected samples with very high clarity are often aligned to the c-axis using this custom-built instrument. Aligning all samples allows for a precise characterization of the wavelength absorption in certain directions and guarantees that different samples can be compared. Photo by Nuttapol Kitdee.

Figure 14. GIA's colored stone reference collection is managed by the Bangkok lab, where the majority of samples are kept in the field gemology department. Photo by Nuttapol Kitdee.

for precise analysis of the absorption spectrum in the ultraviolet, visible, and near-infrared light range, which is used to identify the causes of color in the material.

FTIR spectroscopy and trace element chemistry data are also collected. All of the data associated with a research sample, ranging from refractive index to trace element concentrations, are available to GIA gemologists worldwide through the digital database.

To explore new techniques, a portion of the research samples are also used for analysis that is not routinely conducted on colored stones in gemological laboratories. In recent years, stones have been used for destructive analysis to measure rare earth element concentrations and isotope ratios as well as studies on various luminescence techniques.

Ultimately, the samples are stored in the GIA colored stone reference collection in Bangkok (figure 14). This library consists of four subsections:

- Premium gems: These stones are readily usable for routine gemological analysis. These samples are sufficiently large and free of fractures, combined with a desirable color.
- Treated gems: The GIA colored stone reference collection includes numerous stones that are known to have been subjected to treatment. Some were acquired as treated, but the majority are the result of GIA's internal treatment experiments, focused mainly on heating of rubies and blue sapphires.
- Matrix material: While visiting mines, GIA field gemologists document the host rock and collect associated minerals. This section of the collection, though currently underutilized, offers significant potential for future studies on the geology of gem deposits.
- Basic gems: Much of the material that is collected is not readily usable for routine gemological analysis due to lower quality (e.g., abundant fractures and small sizes). These samples are still valuable for studies that require destructive techniques or treatment procedures. Gem species other than the ones for which GIA offers origin determination are also included in this section.

Apart from the main library in Bangkok, there are satellite collections of most of the major gemstones in GIA's colored stone laboratories in Carlsbad, Hong Kong, New York, and Tokyo.

THE EVOLUTION OF GEMSTONE DEPOSITS

Active sources of gemstones are constantly shifting. The life of a gemstone deposit is often highly erratic and unpredictable. Some deposits, such as Ratnapura in Sri Lanka, have steadily produced high-quality material for centuries, while others have existed for only brief periods. One of the best examples is Winza, Tanzania, which produced fine rubies beginning in 2007 but was almost completely abandoned by 2010. Although deposits are routinely depleted, the material mined from them has the potential to circulate in the trade for generations.

BOX A: SURVIVAL OF THE FITTEST

Figure A-1 shows the shift of ruby mining areas on the East African mainland over the past century. The earliest ruby discovery in East Africa was near Longido, Tanzania, where ruby was found around the time of World War I. This hard-rock primary deposit is famous for specimens of ruby-in-zoisite. Mining these gemstones requires blasting and deep tunneling, making it a very expensive affair. While the material's color is good, its clarity is lacking, with most being opaque and of carving quality (Dirlam et al., 1992).

In the 1970s, ruby was discovered in the Mangare area in Kenya by John Saul. The gems are found in a primary deposit, but the ruby-hosting rock is quite weathered in the upper levels, making it fairly easy to mine. The color of this ruby was considered highly desirable, and the name "John Saul color" is sometimes used as a trade name for it. The material often lacks clarity, and the majority are cut into translucent cabochons. Most of it requires heat treatment to improve the clarity (Bridges, 1982).

In the following decades, rubies were discovered at several places in central Tanzania. However, none of those had the volume or quality to threaten Mangare's position as supreme producer on the African continent.

In 2007, fine rubies were discovered in a primary and nearby secondary deposit at Winza, Tanzania. The finest material had excellent clarity and fabulous color, but the lower-grade material could not be optimized by treatment, rendering much of the production useless as gemstones (Schwarz et al., 2008). Although there was initial optimism, the deposit was quickly abandoned. The majority of miners and buyers moved south across the border to Mozambique.

In 2009, facet-grade ruby was discovered near Montepuez, Mozambique. This material quickly became available in large volumes, various sizes, and a range of color intensities. Additionally, the material reacts well to treatments to optimize both color and clarity (Vertriest and Saeseaw, 2019). The wide availability of this material has had a dramatic impact on other ruby mining areas, which have been completely overshadowed by the giant deposit in Montepuez.

In 2017, many unlicensed buyers were expelled from Mozambique. These buyers, an important link in the supply chain, searched elsewhere in East Africa for a ruby source that met their needs. Around the same time, facet-grade rubies were discovered in Longido, the mine originally known for its carving-grade material. This new material from an old mine has highly desirable colors but is only available in smaller sizes (Pardieu, 2019). While the renewed interest has not made it a serious competitor to Montepuez in Mozambique, it has certainly revived the ruby trade in northern Tanzania and provided rough ruby buyers with an alternative source for melee and small calibrated stones.

While the deposits might have unstable histories, the gems themselves are durable and here to stay, whether a deposit produces for centuries or only a few months. A complete and reliable reference collection contains stones from all of these deposits.

Figure A-1. This map shows the locations of the mines that dominated ruby production on the East African mainland in the last century. The Longido and Mangare mines were famous for their fine-color but low-clarity stones. Several deposits produced smaller volumes of goods but were never competitors. Winza generated some excitement by producing fine faceted rubies, but its life span was rather short. The Montepuez deposit in Mozambique has overshadowed all the other deposits, but internal turmoil has forced traders to revisit old deposits such as Longido, where new types of ruby are being mined.

Understanding the evolution of a gemstone deposit is critical for a field gemologist. GIA's field gemologists aim to stay aware of new developments in sourcing and treatments because they can have a sudden impact on the global gem trade. The field gemology program allows GIA to adapt its procedures as quickly as possible to account for emerging sources and treatments.

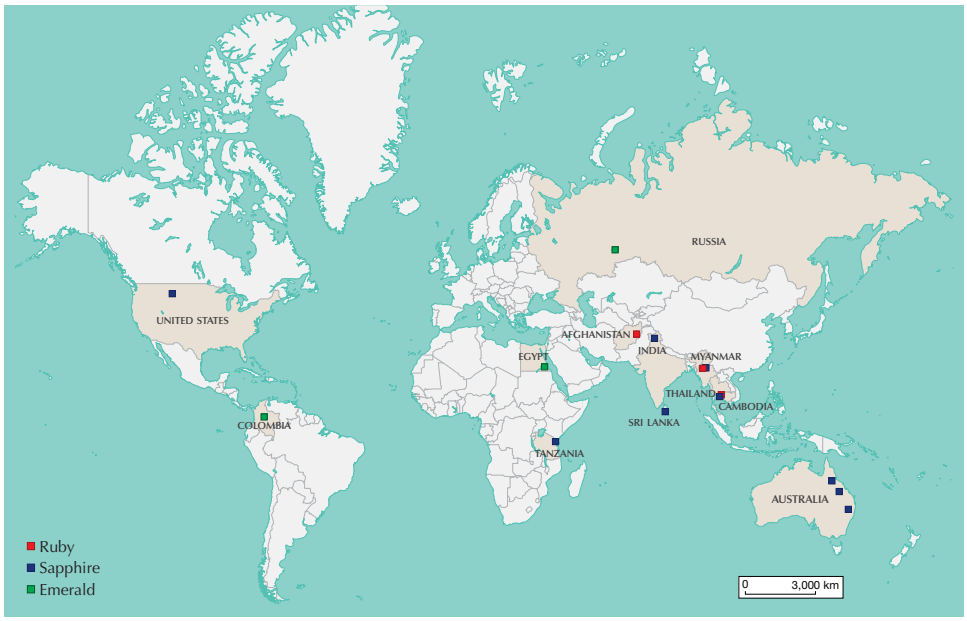

Figure 15. Map of classical ruby, sapphire, and emerald deposits that were highly influential before the rise of the modern gem trade.

The Life of a Gemstone Deposit. Many gemstone deposits have been established for several decades or even centuries, so their early histories are often unknown. In the last decades, many new sources have emerged, and GIA has been fortunate to witness their development.

Most new deposits share a similar story: It starts with an accidental discovery, usually by people who travel extensively through unexplored lands, such as gold panners, lumberjacks, or nomadic tribes. They find a beautiful rock but are unaware of its value. Eventually, someone discovers the value of these crystals. This often triggers a rush of small-scale miners, who begin a frenzied search for more of the material or anything that looks like it.

A nearby group of buyers is critical to sustain a young deposit. Production will halt quickly if no buyers are on hand to trade the stones for cash. Often these are local traders, but sometimes international buyers are also present from the start. Regardless, this all takes place close to the mines. The local buyers will provide this material to the global market, where international gem traders and wholesalers become aware of it. Sometimes this process takes a few years, but it could happen in just a few weeks. In recent years, mobile phones and social media have become popular in mining areas. This has increased the speed of information and changed the way it spreads through the trade, even though the development of a deposit is essentially still the same.

The process of gem discovery is not always constant—there are many external forces involved. A gem mining rush in a remote area is often closely related to local socioeconomic challenges, some of which can severely disrupt mining. In many cases these finds are in tropical countries with strong seasonal changes that prevent mining part of the year, which can limit the mining season to a couple of months. In some cases, mining does not resume when the weather clears. A range of situations can cause newly discovered mining areas to be abandoned.

The most serious threat to the development of gemstone deposits is probably the emergence of other deposits. Here the Darwinian principle "survival of the fittest" applies. A new deposit that is easier to work, faster to reach, delivers higher volumes, or produces more marketable stones that react better to treatments will cause others to be ruthlessly abandoned by miners and/or local buyers (see box A).

Keeping track of these developments is a critical aspect of the field gemologist's job, since deposits can show up and disappear in the most unexpected ways. This might present only a brief window to collect reliable samples, but one that is enough to produce a huge volume of gems that will influence the market and be submitted to labs for decades to come.

Overview of Important Gemstone Deposits. The use of gems in early civilizations and empires is well known: Cleopatra's emeralds, Sri Lankan sapphires in Roman signet rings, Central Asian spinels and rubies in European royal treasuries, and Colombian emeralds in Indian Mughal jewelry. Such examples show that gems traveled the planet even in times

Figure 16. Mogok, Myanmar, is the most famous of all ruby sources. Its mining history stretches over centuries, and its close connection with the red gemstone is the reason for its nickname "Ruby Land." Photo by Wim Vertriest.

when the concept of global mobility was unheard of. Back then, a single locality could have an outsized impact on the international trade.

The following is a brief overview of deposits that can be considered classical (figure 15). Gems from these areas heavily influenced the world trade before the rise of modern gemology and gem trading, roughly during the 1960s and 1970s. In the case of gem sources, *classical* does not necessarily mean exhausted. Many of these locations are still relevant gem mining regions. Most of this information is distilled from *Ruby & Sapphire: A Gemologist's Guide* (Hughes et al., 2017), supplemented with GIA's field gemology observations during expeditions in the last decade.

Ruby

- Mogok, Myanmar, is the world's most revered ruby locality. Ruby is an integral part of the local culture, and the Mogok Valley is sometimes referred to as "Ruby Land" (figure 16).
- Afghanistan's ruby mines delivered many of the rubies and pink sapphires for the treasuries of Indian rulers. For centuries, artisanal miners have extracted rubies from these hard rock mines in the marble hills just east of Kabul, although production is very limited nowadays.
- The border area between Thailand and Cambodia began supplying rubies around 200 years ago and peaked in the 1970s and '80s. By the 2000s, production had virtually halted. Rubies have been found here in alluvial deposits related to the weathering of corundum-bearing alkali basalts.

Metamorphic Sapphire

- The most famous historical sapphire source is Sri Lanka, formerly Ceylon, which still produces large volumes of high-quality

Figure 17. Sapphire mining in Sri Lanka is still dominated by artisanal, man-powered techniques to this day. They have not changed in centuries, and large-scale mining is limited. Photo by Wim Vertriest.

Figure 18. Sapphires are still being mined in the rugged mountains of Montana by the Spokane Bar Sapphire Mine. A handful of companies run mechanized and efficient mining operations to retrieve rough gems during the summer months. Photo by Nathan Renfro.

stones (figure 17). New discoveries are still being made—for example, a large rush occurred in 2012 at a new deposit near Kataragama when a large concentration of high-value sapphires was found in an area not previously known to contain such quality material (Pardieu et al., 2012; Zoysa and Rahuman, 2012).

- Along with ruby, Mogok supplies a variety of high-quality gems, including fine blue sapphires and star sapphires. Some of these rough sapphires can reach enormous sizes, although these Burmese giants usually have limited clarity and unattractive color.
- The disputed region of Kashmir produced the world's most coveted sapphires for a brief time in the late 1800s. Even today, sapphires from the original discovery are perceived as legendary. Recent output from this area is of lower quality.
- The Umba Valley in Tanzania yielded a variety of sapphires, mainly fancy-color, from World War II until the mid-1970s. A few artisanal miners are still working in the Umba River.

Igneous-Related Sapphire

- Sapphires from Pailin, Cambodia, were discovered and reached their height around the time when Kashmir sapphires were at peak production. Pailin sapphire is very limited now and consists mainly of smaller sizes.
- Australia is estimated to be one of the largest sapphire mining nations by volume. The mines have produced for over 100 years, but output peaked in the 1960s and 1970s. During this period, Australia was the main source of blue sapphire for the international trade, with large mines and many foreign buyers operating there.
- Chanthaburi, Thailand, is known as a trading and treatment center, but it was once the center of a flourishing sapphire mining community. Several hills around the city are ancient basalt volcanoes that brought dark blue and fancy sapphires to the surface. The mines near Chanthaburi are well known for their fine black star sapphires and dark yellow "Mekong whiskey" stones.
- In the United States, Montana saw millions of carats of sapphire mined from the late 1800s to early 1900s, mostly for use in the watch industry but with many entering the gem market (figure 18). The finest blue sapphires from Montana were produced in the Yogo Gulch deposit (Renfro et al., 2018). In recent years, some of the state's mining operations have been revived (Hsu et al., 2017).

Emerald

- Colombia is the world's most prized locality for emeralds because of their long history and fine quality. Pre-Columbian civilizations al-

Figure 19. The statue on Chivor's main square, in the heart of the Colombian emerald mining region, serves as a reminder of the gem's long history there. Emeralds have been important in the region for centuries and were already greatly revered by pre-Columbian civilizations. Photo by Robert Weldon/GIA.

ready held the gem in high esteem (figure 19). After their discovery by Spanish conquistadors, emeralds were brought to Europe and the rest of the world where they were highly treasured in the European royal courts as well as the Mughal palaces of India.

- Mines in southern Egypt are the presumed source of the Egyptian and Roman empires' emeralds. These mines were abandoned after their peak, and when emeralds from the New World started entering the old continent in the 1500s, the Egyptian mines were all but forgotten. In the 1800s they were rediscovered by French colonial explorers, who tried unsuccessfully to reopen them (Jennings et al., 1993; Johnson and Koivula, 1997).
- Russian emeralds have been mined near the town of Malysheva in the Ural Mountains since the 1830s (Schmetzer et al., 1991). For much of the twentieth century, the mine's emphasis was on beryllium metal for strategic and industrial applications. In 2018, the new management significantly increased production of emeralds, parallel to the mining of other minerals for beryllium extraction (Burlakov and Burlakov, 2018).

Red and Pink Spinel

- For centuries, the Central Asian region of Badakhshan, straddling the borders of Tajikistan, Afghanistan, and China, has produced magnificent spinels. They were often mistaken for rubies in medieval times and were well known by the term "Balas ruby." One of the most famous colored stones in the world, the Black Prince's "Ruby" in the United Kingdom's Imperial State Crown, is actually a Badakhshan spinel. The Kuh-i-Lal area in Tajikistan is considered the most important source of fine red spinel in the region (Pardieu and Farkhodova, 2019).
- Although Myanmar holds incredible volumes of spinel in the Mogok and Namya areas, it has always been in the shadow of the ruby and sapphire that are also found there. In the last 20 years, the mines in Man Sin (Mogok) and Namya (Hpakant) have become famous for the so-called Jedi spinel, characterized by an intense color and fluorescence (Pardieu, 2014).

Alexandrite

- Alexandrite was first documented in the Ural Mountains of Russia. The greens and reds of this newly discovered color-change chrysoberyl variety matched the Russian imperial colors, and thus the stone was named after the future Czar Alexander II. Its occurrence is closely associated with emerald. Fine Russian alexandrite is still considered the standard by which all color-change gems are measured (Schmetzer, 2010).

In recent decades, many new sources have come into the gem trade (see figure 20). There is no strict guideline for when a modern source becomes classical. As a rule of thumb, modern sources are considered to be deposits that began producing after the rise of modern gemology and whose discoveries have been well documented.

Figure 20. Map of ruby, sapphire, and emerald deposits that have emerged in recent decades.

The vast majority of modern deposits are in East Africa, a gemstone-rich area that did not historically have a strong cultural connection to gemstones, unlike the Asian countries of Sri Lanka or Myanmar. The increasing knowledge about gemstones and international travel by dealers provided an opportunity for these deposits to be discovered and establish a presence on the world market.

Ruby

- In 1973, John Saul and his team discovered ruby in the Mangare area of Kenya. This material has fine color but requires heat treatment to heal the abundant fractures. Most of the gems from this deposit were cut as cabochons. Initially production was considerable, but it has diminished greatly in the last 20 years (Bridges, 1982; Emmett, 1999).
- During the late Soviet period (1979), geologists discovered the Snezhnoe ("Snowy") ruby mine near Murghab, Tajikistan, at an altitude of 4,000 meters. Artisanal mining is restricted to the summer months, when small crews of workers break rubies out of the hard marbles. Tajik rubies are typically pinkish to purplish red but have strong fluorescence (Smith, 1998).
- In 1983, rubies were first reported near the village of An Phu in the Luc Yen District of Vietnam. In the following years, corundum was found in neighboring valleys, and in 1987 the first larger-scale operation began. These industrial operations were only profitable for a few years, and since the 1990s only artisanal miners have been able to work these deposits in the remote jungle mountains of northern Vietnam (Pardieu and Long, 2010; Trivier, 2018).
- Ruby in Mong Hsu, Myanmar, was discovered in the early 1990s. Many miners began working here and sold the material to Thai buyers across the border. Almost 100 percent of the material is heat treated to remove a dark blue core in the center of the crystals (Koivula et al., 1993; Peretti et al., 1995).
- In 2007, a Tanzanian farmer found some rubies in a river near his farm. A few months later, a massive gem rush occurred at the deposit now known as Winza. For a few short years, fabulous rubies emerged from these mines. Many have blue color zones, sometimes resulting in bicolor ruby-sapphires. They react poorly to treatment, rendering most of the low-grade material useless (Schwarz et al., 2008).
- The jungles of northeastern Madagascar have provided fine rubies for more than 20 years. However, production has not been steady, and most stones reach the market in waves due to rushes by artisanal miners. The main rushes took place at Vatomandry in the early 2000s (Schwarz and Schmetzer, 2001), Moramanga in 2004 (Hughes et al., 2006), Didy in 2012 (Pardieu and Rakotosaona, 2012), and Zahamena in 2014 (Pardieu et al., 2015).

Figure 21. Currently the majority of Mozambican ruby is mined from mechanized, large-scale mining operations. Small-scale mining plays an important role, but less so year after year. Photo by Wim Vertriest.

- The most recent ruby discovery is the most important one. Since 2009, a variety of sizes and qualities have been mined near Montepuez, Mozambique (figure 21). In less than a decade, Mozambican rubies have conquered the trade and become widely available in every price range (Pardieu et al., 2009; Vertriest and Saeseaw, 2019).
- The newest large-scale ruby source is also the world's oldest deposit. Greenland's rubies and pink sapphires formed billions of years ago but have only become available to the public in the last several years. The rubies were already described by geologists in the 1960s. However, they were probably known by the local people long before, since the area is named Aappalutoq, the Greenlandic word for "red."

Metamorphic Sapphire

- The southern Tanzanian deposits near Tunduru and Songea have produced sapphire and other gemstones such as garnets, alexandrites, and tourmalines since the early 1990s. Despite Tunduru's potential, it was never fully developed because of its remoteness and competition from other deposits. Sapphires from Songea span a full range of colors, but the majority were not seen as highly desirable due to strong modifying colors. Mining activity increased again in the early 2000s when the fancy sapphires reacted well to Be-diffusion treatment (Hughes and Pardieu, 2011).
- One of the first modern discoveries of high-quality sapphire in Madagascar was in the southeastern part of the island. Andranondambo became famous for its blue sapphires, which were initially confused with Kashmir sapphires. Some attempts to set up large-scale mining operations were quickly abandoned (Kiefert et al., 1996; Schwarz et al., 1996). In 2016, a new find near the town of Vohitany brought fresh production to the market for a few months (Pardieu et al., 2016).
- One of the most important modern colored stone discoveries took place in another part of Madagascar, near the quiet town of Ilakaka in the southwest part of the island (figure 22). In 1996, large volumes of sapphire, fancy sapphire, and other gemstones were found in extensive riverbeds and associated paleochannels. The sapphires resemble Ceylon sapphires and react similarly to treatment, and thus the area attracts many buyers from Sri Lanka.
- Along with rubies, blue sapphires are found in the hilly jungles of northeastern Madagascar. Several rushes took place, bringing large volumes of sapphire to the market in a very short time. The first deposit that produced blue sapphire was Andrebabe in 2002, but it stayed largely under the radar. It was Didy that put this area of Madagascar on the sapphire map when large, high-quality material was found alongside the rubies during a rush in 2012 (Pardieu and Rakotosaona, 2012). In 2016, the Bemainty deposits produced *padparadscha* sapphires in addition to fine blue sapphires that were initially confused with

Figure 22. The quiet town of Ilakaka was transformed in the late 1990s by the discovery of huge sapphire deposits. It has quickly become one of the world's most important gem localities. Photo by Vincent Pardieu.

Kashmir sapphires. Laboratories made concerted efforts to correctly identify the origin of these stones, but it took several months to acquire reliable samples to study and make the distinction (Pardieu et al., 2017).

Igneous-Related Sapphire

- Kanchanaburi, Thailand, produced huge volumes of blue sapphire in the 1980s and early 1990s. Production continues but at much lower levels. Most of it consists of blue sapphire, but black spinel (pleonaste) is found as a byproduct (Gunawardene and Chawla, 1984; Koivula and Kammerling, 1990).
- Sapphire can also be found in the far north of Madagascar, in the area around Ambondromifehy, also known as Diego-Suarez. Since 1995, basalt-related sapphires have been recovered by artisanal miners. The blue stones are often heat treated to optimize their colors. Fine yellow and green stones are also found (Schwarz et al., 2000).
- The West African countries of Nigeria and Cameroon hold substantial reserves of sapphires. They were largely under the radar until the discovery of fine goods on the Mambilla Plateau in 2014 (Pardieu et al., 2014). High-quality sapphires are available in

Figure 23. Ethiopian sapphire miners have been working in a remote part of the desert straddling the border with Eritrea since 2017. Photo by Wim Vertriest.

Figure 24. Zambian emeralds are mined from massive open pits that are among the largest colored stone operations in the world. Photo by Robert Weldon/GIA.

smaller volumes from other deposits in the eastern and northern parts of the country.

- The most recent discovery of good-quality basalt-related sapphire was in the northern Tigray Province of Ethiopia (2017) (figure 23). Artisanal miners work remote deposits in the desert straddling the border with Eritrea (Vertriest et al., 2017).

Emerald

- Central Asia has produced fine emeralds in the Panjshir (Afghanistan) and Swat (Pakistan) valleys since the 1970s and 1960s, respectively (Gübelin, 1982; Bowersox et al., 1991). Extraction methods are quite basic because the difficult working conditions prevent large-scale operations. Both areas produce fine quality, with the Panjshir Valley delivering well-formed crystals. The Swat Valley is mostly known for its smaller but deeply saturated clean emeralds that are in high demand in the watch industry.
- Zambian emeralds were first documented by colonial exploration geologists. It wasn't until the 1970s that gemstone mining began in the Kafubu area, which is still the world's leading emerald producer by volume. Several industrial operations are active, representing some of the largest colored stone mines in the world (figure 24) (Zwaan et al., 2005).
- Brazil has been a consistent supplier of emerald for the international market since its discovery in the 1970s. Capoeirana and Belmont in Minas Gerais State are the most important producers, with the latter being one of the world's largest and most advanced emerald mining operations. Mines in Bahia State and Santa Terezinha de Goiás are currently less important (Lucas, 2012).
- Emeralds were discovered in eastern Madagascar around the same time as in Brazil, but mining operations and production have remained limited. Nevertheless, some fine ma-

terial has been produced in the past decades (Pardieu, 2018).

- The most recent emerald source is Ethiopia, where high-quality emeralds were discovered in 2016. The mines are in the southern part of the country, 70 km from the trading town of Shakiso. In its first years, Ethiopia made a strong impression on the market, but time will tell whether it can maintain its status as an important producer (Renfro et al., 2017).

Paraíba Tourmaline

- The original discovery of Paraíba tourmaline was in Paraíba State in Brazil. The first deposit was found in 1987 at Mina da Batalha. A few years later, similar material was found in two mines in Rio Grande do Norte State (Koivula and Kammerling, 1989).
- Since 2001, copper-bearing tourmaline from western Nigeria, very similar to the Brazilian material, has been available in the market. Production is scarce, and only small volumes currently reach the market (Abduriyim et al., 2006).
- Copper-bearing tourmaline was originally discovered in Mozambique in 1991 but only became widely known in 2005. Most of the production comes from secondary deposits, resulting in tumbled rough (Laurs et al., 2008). Mining was initially limited to artisanal miners, but larger operations were set up with variable degrees of success.

Red and Pink Spinel

- Red spinel was found alongside ruby in Luc Yen, Vietnam, in the 1980s. Large crystals are found in secondary gravels mined from small streams and under rice fields, as well as in primary hard rock mines, where the crystals are mined directly from the white marbles (Pardieu and Long, 2010).
- Mahenge, Tanzania, became the first widely known spinel deposit outside Asia. In the spring of 2007, four enormous spinel crystals (ranging from 5.7 to 52 kg) were discovered in the Ipanko Valley, which produced many clean faceted stones in the double-digit range. Ever since there have been struggles over the mining licenses. Most of the production comes from small-scale operations (Hughes and Pardieu, 2011).

Alexandrite

- In the 1980s, alexandrites were found in Hematita, Minas Gerais, Brazil. This is the only modern location that has produced considerable volumes and qualities to date. After an artisanal miner rush, a larger-scale operation was developed, although this mine is small compared to some other colored stone mines (e.g., emerald mines). Other alexandrite deposits have been found in Brazil but are not as significant (Proctor, 1988).
- Indian alexandrite has been known since the 1980s (Bank, 1987; Durlabhji, 1999; Panjikar and Ramchandran, 1997). Only since 2000 has production become substantial at a few deposits. Mining is artisanal and often hindered by natural conditions, such as the intense rainy season or flooding due to the 2004 Indian Ocean tsunami.
- In recent decades, increased gemological knowledge and the discovery of large secondary deposits has led to alexandrites being recognized at several other important localities. They are occasionally found in Tunduru (Tanzania), Mogok (Myanmar), Sri Lanka, and Ilakaka (Madagascar). Anecdotal occurrences associated with emerald mineralization have been documented in Tanzania (Bank and Gübelin, 1976; Schmetzer and Malsy, 2011), Zimbabwe (Bank, 1964; Schmetzer et al., 2011), and Zambia.

FIELD GEMOLOGY CASE STUDIES

Working with Different Degrees of Reliability: Ethiopian Emeralds. In December 2016, the first high-quality Ethiopian emeralds began circulating in the Bangkok market. Some parcels were also available in California. GIA was able to analyze some of these goods (F-type samples) to obtain preliminary data such as inclusion photomicrographs and trace element chemistry. When we analyzed the research samples, we found that their characteristics were identical to two client-submitted stones that did not match our known emerald data from other locations.

In the following months, more Ethiopian samples from other independent traders were acquired, and in March 2018 GIA visited the mining area and collected emeralds under the most reliable conditions (A- to D-type). The data from these samples were

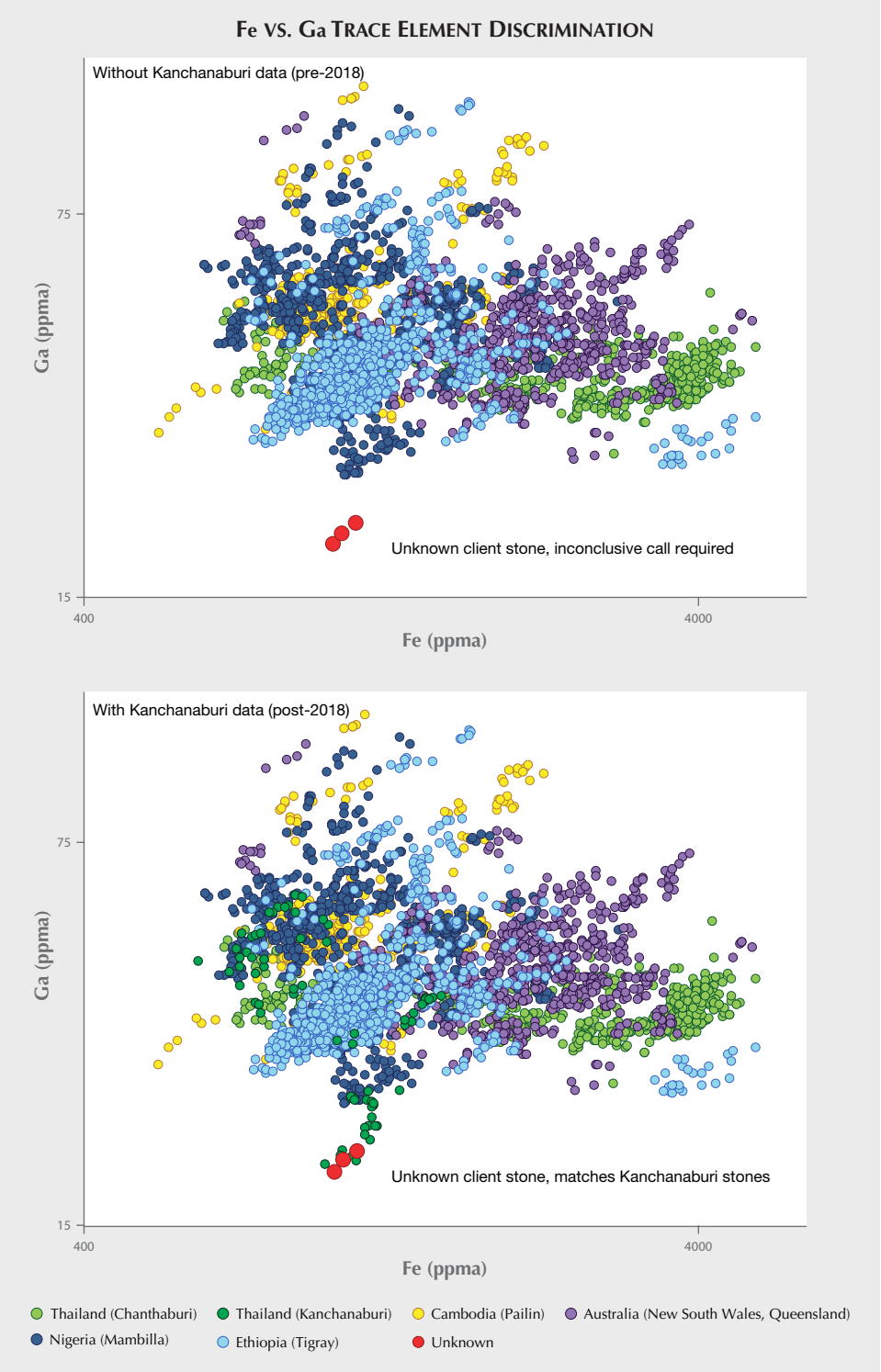

Figure 25. Trace element data of an unknown client stone compared to reference data in an Fe vs. Ga plot. Before the Kanchanaburi reference stones were analyzed, this stone did not match anything in GIA's database (top). However, a Thai origin determination was supported once the Kanchanaburi data were added (bottom).

compared with our preliminary data, and the data sets have been combined. The data collected on the new A- to D-type samples were also consistent with the first samples we studied, confirming the reliability of those F-type samples.

The Importance of Revisiting Old Sources: Kanchanaburi Sapphires. For years GIA analyzed magmatic sapphires with chemistry unlike any of the reference collection's magmatic sapphire stones. These unusual stones had much lower Ga content

Figure 26. Shane McClure (right) and miner Russ Thompson examine sapphire samples from the Eldorado Bar of the Missouri River in Helena, Montana. Photo by Nathan Renfro.

and could have been mistaken for metamorphic-type sapphires based only on chemistry. In 2017, GIA's field gemology team visited the old mines near Kanchanaburi in western Thailand. According to all published reports, they had been closed since the late 1990s, but the field visit found them still producing sapphires. The team had never visited this mine because it was considered exhausted long before GIA's field gemology department came into existence. When we eventually tested these sapphires, many of them matched the mystery stones with low Ga content that were coming through the lab (figure 25). GIA can now confidently issue origin determinations on such stones rather than an "inconclusive" origin on laboratory reports.

Future Projects: Unknown Paraíba Tourmaline. GIA's identification laboratories sometimes analyze Paraíba tourmalines with a chemical composition that does not match any of our reference data. We have not yet succeeded in matching them to any reliable reference stones. We have, however, invested significant resources in obtaining reference samples from known sources that will match these mystery stones. One of the major goals of the field gemology program is to return to the different Paraíba tourmaline mining areas in Brazil and Africa in order to identify the mine that produced these unknown stones.

VALUE OF THE COLLECTION FOR THE FUTURE

GIA's colored stone reference collection has been built with an eye on origin determination, which means that the highest priority is certainty of provenance. Knowing the stones' enhancement history (if any) also makes them valuable for treatment experiments such as spectroscopic evaluation of blue sapphire before and after heat treatment.

The focus is currently on ruby, sapphire (figure 26), and emerald, as these are the most important stones we see in the lab. But other associated minerals are also collected. Most of these other materials have not been a focus of our research until now, but they might prove valuable in the future as localities become inaccessible or exhausted. Many of the mining sites we visit for ruby, sapphire, and emerald also produce other gem species, and to not collect these materials would be a wasted opportunity. For example, the Russian demantoid deposits and emerald deposits are both located near Ekaterinburg, making it convenient to visit both sites in a single field expedition. As another example, the Longido ruby mines and the Merelani tanzanite mines are both less than half a day from Arusha, so it would be logical to visit them both during an expedition to Tanzania.

Many deposits often produce more than one variety, such as Mogok, which supplies more red spinel than blue sapphire and ruby combined. Looking ahead to the future, gemstone varieties other than the big three should be collected for future projects involving origin determination, treatments, and so on.

During our expeditions, we collect detailed information about the source. Natural conditions, cultural customs, socioeconomic situations, challenges,

mining conditions, and the like are all observed and documented with photos, videos, and interviews. This information is valuable not only for education but also to provide context about the gemstones for the trade and the public.

Other laboratories agree that a reliable origin collection is the only way to deliver high-quality research on origin determination (Gübelin Gemmological Laboratory, 2006). GIA's field gemology collection is one of the largest and most complete collections designed with origin determination in mind. Its value for gemological research and education cannot be underestimated and makes field gemology a truly remarkable part of GIA.

ABOUT THE AUTHORS

Mr. Vertriest is supervisor of GIA's field gemology department in Bangkok. Dr. Palke is senior research scientist, and Mr. Renfro is manager of identification (colored stones), at GIA in Carlsbad, California.

ACKNOWLEDGMENTS

GIA's field gemology efforts were initiated by Andy Lucas and Vincent Pardieu, who visited many gemstone mining areas on behalf of GIA's education and laboratory services, respectively. The networks, libraries, and procedures they developed formed the foundation of GIA's current field gemology department. We would like to take this opportunity to thank anyone who has helped GIA during field expeditions around the world, whether it was a simple introduction or full logistic support during a mine visit. And last, we appreciate the warm reception from gemstone miners, traders, and mining communities around the world during our expeditions.

REFERENCES

Abduriyim A., Kitawaki H., Furuya M., Schwarz D. (2006) "Paraíba"-type copper-bearing tourmaline from Brazil, Nigeria, and Mozambique: Chemical fingerprinting by LA-ICP-MS. *G&G*, Vol. 42, No. 1, pp. 4–21, http://dx.doi.org/10.5741/GEMS.42.1.4

Bank H. (1964) Alexandritvorkommen in Südrhodesien. *Zeitschrift der Deutschen Gesellschaft fur Edelsteinkunde*, Vol. 47, pp. 11–15.

—— (1987) Alexandrite from India. *Deutsche Goldschmiede Zeitung*, Vol. 3, p. 116.

Bank H., Gübelin E. (1976) Das Smaragd-Alexandritvorkommen von Lake Manyara/Tansania. *Zeitschrift der Deutschen Gemmologischen Gesellschaft*, Vol. 25, No. 3, pp. 130–147.

Bowersox G.W., Snee L.W., Foord E.E., Seal R.R. (1991) Emeralds of the Panjshir Valley, Afghanistan. *G&G*, Vol. 27, No. 1, pp. 26–39, http://dx.doi.org/10.5741/GEMS.27.1.26

Bridges C. (1982) Gems of East Africa. In D.M. Eash, Ed., *Proceedings of the First International Gemological Symposium*. Gemological Institute of America, Santa Monica, CA, pp. 266–275.

Burlakov A., Burlakov E. (2018) Emeralds of the Urals. *InColor*, No. 40, pp. 88–94.

Dirlam D.M., Misiorowski E.B., Tozer R., Stark K.B., Bassett A.M. (1992) Gem wealth of Tanzania. *G&G*, Vol. 28, No. 2, pp. 80–102, http://dx.doi.org/10.5741/GEMS.28.2.80

Durlabhji M. (1999) Indian gemstones update. *Gemworld*, Vol. 26, No. 3, pp. 18–20.

Emmett J.L. (1999) Gem News: An update on the John Saul ruby mine. *G&G*, Vol. 35, No. 4, pp. 213–215.

Gübelin E.J. (1982) Gemstones of Pakistan: Emerald, ruby and spinel. *G&G*, Vol. 18, No. 3, pp. 123–129, http://dx.doi.org/10.5741/GEMS.18.3.123

Gübelin Gemmological Laboratory (2006) A holistic method to determining gem origin. *Jewellery News Asia*, No. 264, pp. 118–126.

Gunawardene M., Chawla S.S. (1984) Sapphires from Kanchanaburi Province, Thailand. *Journal of Gemmology*, Vol. 19, No. 3, 228–239.

Hsu T., Lucas A., Kane R.E., McClure S.F., Renfro N.D. (2017) Big Sky Country sapphire: Visiting Montana's alluvial deposits. *G&G*, Vol. 53, No. 2, pp. 215–227, http://dx.doi.org/10.5741/GEMS.53.2.215

Hughes R.W., Pardieu V. (2011) Gem hunting in Tanzania. www.lotusgemology.com/index.php/library/articles/147-downtown-gem-hunting-in-tanzania

Hughes R.W., Pardieu V., Schorr D. (2006) Sorcerers & sapphires: A visit to Madagascar. https://www.ruby-sapphire.com/index.php/component/content/article/10-articles/879-madagascar-ruby-sapphire?Itemid=202

Hughes R.W., Manorotkul W., Hughes E.B. (2017) *Ruby & Sapphire: A Gemologist's Guide*. RWH Publishing, Bangkok.

Jennings R.H., Kammerling R.C., Kovaltchouk A., Calderon G.P., Baz M.K.E., Koivula J.I. (1993) Emeralds and green beryls of Upper Egypt. *G&G*, Vol. 29, No. 2, pp. 100–115, http://dx.doi.org/10.5741/GEMS.29.2.100

Johnson M.L., Koivula J.I., Eds. (1997) Gem News: Origin of ancient Roman emeralds. *G&G*, Vol. 33, No. 4, p. 303.

Kiefert L., Schmetzer K., Krzemnicki M.S., Bernhardt H.-J., Hänni H.A. (1996) Sapphires from Andranondambo area, Madagascar. *Journal of Gemmology*, Vol. 25, No. 3, pp. 185–209.

Koivula J.I., Kammerling R.C., Eds. (1989) Gem News: Paraíba tourmaline update. *G&G*, Vol. 25, No. 4, p. 248.

Koivula J.I., Kammerling R.C., Eds. (1990) Gem News: Update on sapphire mining in Kanchanaburi. *G&G*, Vol. 26, No. 4, pp. 302–303.

Koivula J.I., Kammerling R.C., Fritsch E., Eds. (1993) Gem News: Update on Monghsu ruby. *G&G*, Vol. 29, No. 4, pp. 286–287.

Laurs B.M., Zwaan J.C., Breeding C.M., Simmons W.B., Beaton D., Rijsdijk K.F., Befi R., Falster A.U. (2008) Copper-bearing (Paraíba-type) tourmaline from Mozambique. *G&G*, Vol. 44, No. 1, pp. 4–30, http://dx.doi.org/10.5741/GEMS.44.1.4

Lucas A. (2012) Brazil's emerald industry. *G&G*, Vol. 48, No. 1,

pp. 73–77, http://dx.doi.org/10.5741/GEMS.48.1.73
Panjikar J., Ramchandran K.T. (1997) New chrysoberyl deposits from India. *Indian Gemmologist*, Vol. 7, No. 1–2, pp. 3–7.
Pardieu V. (2014) Hunting for "Jedi" spinels in Mogok. *G&G*, Vol. 50, No. 1, pp. 46–57, http://dx.doi.org/10.5741/GEMS.50.1.46
Pardieu V. (2018) "Ants and kings": Emeralds from Mananjary, Madagascar. https://www.youtube.com/watch?v=qUioeFyvY_o
Pardieu V. (2019) Thailand: The undisputed ruby trading kingdom: A brief history. *InColor*, Vol. 42, pp. 14–22.
Pardieu V., Farkhodova T. (2019) Spinel from Tajikistan: The gem that made famous the word "ruby." *InColor*, No. 43, pp. 30–33.
Pardieu V., Long P.V. (2010) Gem News International: Ruby, sapphire, and spinel mining in Vietnam: An update. *G&G*, Vol. 46, No. 2, pp. 151–152.
Pardieu V., Rakotosaona N. (2012) Ruby and sapphire rush near Didy, Madagascar. *GIA Research News*, https://www.gia.edu/gia-news-research-nr101512
Pardieu V., Jacquat S., Bryl L.P., Senoble J.B. (2009) Rubies from northern Mozambique. *InColor*, No. 12, pp. 32–36.
Pardieu V., Dubinsky E.V., Sangsawong S., Chauviré B. (2012) Sapphire rush near Kataragama, Sri Lanka. *GIA Research News*, https://www.gia.edu/ongoing-research/sapphire-rush-near-kataragama-sri-lanka
Pardieu V., Sangsawong S., Muyal J., Sturman N. (2014) Blue sapphires from the Mambilla Plateau, Taraba State, Nigeria. *GIA Research News*, www.gia.edu/gia-news-research-nigerian-source-blue-sapphire
Pardieu V., Sangsawong S., Detroyat S. (2015) Gem News International: Rubies from a new deposit in Zahamena National Park, Madagascar. *G&G*, Vol. 51, No. 4, pp. 454–456.
Pardieu V., Sangsawong S., Vertriest W., Detroyat S., Raynaud V., Engniwat S. (2016) Gem News International: Blue sapphires from a new deposit near Andranondambo, Madagascar. *G&G*, Vol. 52, No. 1, pp. 96–97.
Pardieu V., Vertriest W., Weeramonkhonlert V., Raynaud V., Atikarnsakul U., Perkins R. (2017) Sapphires from the gem rush Bemainty area, Ambatondrazaka (Madagascar). *GIA Research News*, www.gia.edu/gia-news-research/sapphires-gem-rush-bemainty-ambatondrazaka-madagascar
Peretti A., Schmetzer K., Bernhardt H.-J., Mouawad F. (1995) Rubies from Mong Hsu. *G&G*, Vol. 31, No. 1, pp. 2–26, http://dx.doi.org/10.5741/GEMS.31.1.2
Proctor K. (1988) Chrysoberyl and alexandrite from the pegmatite districts of Minas Gerais, Brazil. *G&G*, Vol. 24, No. 1, pp. 16–32, http://dx.doi.org/10.5741/GEMS.24.1.16
Renfro N., Sun Z., Nemeth M., Vertriest W., Raynaud V., Weeramonkhonlert V. (2017) Gem News International: A new discovery of emeralds from Ethiopia. *G&G*, Vol. 53, No. 1, pp. 114–116.
Renfro N.D., Palke A.C., Berg R.B. (2018) Gemological characterization of sapphires from Yogo Gulch, Montana. *G&G*, Vol. 54, No. 2, pp. 184–201, http://dx.doi.org/10.5741/GEMS.54.2.184
Schmetzer K. (2010) *Russian Alexandrites*. Schweizerbart Science Publishers, Stuttgart, Germany.
Schmetzer K., Malsy A.-K. (2011) Alexandrite and colour-change chrysoberyl from the Lake Manyara alexandrite-emerald deposit in northern Tanzania. *Journal of Gemmology*, Vol. 32, No. 5–8, pp. 179–209.
Schmetzer K., Bernhardt H.J., Biehler R. (1991) Emeralds from the Ural Mountains, USSR. *G&G*, Vol. 27, No. 2, pp. 86–99, http://dx.doi.org/10.5741/GEMS.27.2.86
Schmetzer K., Malsy A.-K., Stocklmayer V., Stocklmayer S. (2011) Alexandrites from the Novello alexandrite-emerald deposit, Masvingo District, Zimbabwe. *Australian Gemmologist*, Vol. 24, No. 6, pp. 133–147.
Schwarz D., Schmetzer K. (2001) Rubies from the Vatomandry area, eastern Madagascar. *Journal of Gemmology*, Vol. 27, No. 7, pp. 409–416.
Schwarz D., Petsch E.J., Kanis J. (1996) Sapphires from the Andranondambo region, Madagascar. *G&G*, Vol. 32, No. 2, pp. 80–99, http://dx.doi.org/10.5741/GEMS.32.2.80
Schwarz D., Kanis J., Schmetzer K. (2000) Sapphires from Antsiranana Province, northern Madagascar. *G&G*, Vol. 36, No. 3, pp. 216–233, http://dx.doi.org/10.5741/GEMS.36.3.216
Schwarz D., Pardieu V., Saul J.M., Schmetzer K., Laurs B.M., Giuliani G., Klemm L., Malsy A.-K., Erel E., Hauzenberger C., Du Doit G., Fallick A.E., Ohnenstetter D. (2008) Rubies and sapphires from Winza, central Tanzania. *G&G*, Vol. 44, No. 4, pp. 322–347, http://dx.doi.org/10.5741/GEMS.44.4.322
Sir David Attenborough on Museum Collections – 360 (2017) American Museum of Natural History, August 31, https://www.amnh.org/explore/videos/at-the-museum/sir-david-attenborough-on-museum-collections-360
Smith C.P. (1998) Rubies and pink sapphires from the Pamir Mountain Range in Tajikistan, former USSR. *Journal of Gemmology*, Vol. 26, No. 2, pp. 103–109.
Thomas T., Rossman G.R., Sandstrom M. (2014) Device and method of optically orienting biaxial crystals for sample preparation. *Review of Scientific Instruments*, Vol. 85, No. 9, 093105, http://dx.doi.org/10.1063/1.4894555
Trivier A. (2018) Between rice paddies and karst pinnacles: The Luc Yen gemstone mining area. *InColor*, No. 39, pp. 16–26.
Vertriest W., Saeseaw S. (2019) A decade of ruby from Mozambique: A review. *G&G*, Vol. 55, No. 2, pp. 162–183, http://dx.doi.org/10.5741/GEMS.55.2.162
Vertriest W., Weeramonkhonlert V., Raynaud V., Bruce-Lockhart S. (2017) Gem News International: Sapphires from northern Ethiopia. *G&G*, Vol. 53, No. 2, pp. 247–248.
Zoysa E.G., Rahuman S. (2012) Sapphire rush in Kataragama. *InColor*, No. 19, pp. 56–61.
Zwaan J.C., Seifert A.V., Vrána S., Laurs B.M., Anckar B., Simmons W.B., Falster A.U., Lustenhouwer W.J., Muhlmeister S., Koivula J., Garcia-Guillerminet H. (2005) Emeralds from the Kafubu area, Zambia. *G&G*, Vol. 41, No. 2, pp. 116–148, http://dx.doi.org/10.5741/GEMS.41.2.116

A Review of Analytical Methods Used in Geographic Origin Determination of Gemstones

Lee A. Groat, Gaston Giuliani, Jennifer Stone-Sundberg, Ziyin Sun, Nathan D. Renfro, and Aaron C. Palke

Origin determination is of increasing importance in the gem trade. It is possible because there is a close relationship between the geological environment of formation and the physical and chemical properties of gemstones, such as trace element and isotopic compositions, that can be measured in the laboratory using combinations of increasingly sophisticated instrumentation. Origin conclusions for ruby, sapphire, and emerald make up the bulk of demand for these services, with growing demand for alexandrite, tourmaline, and spinel. However, establishing origin with a high degree of confidence using the capabilities available today is met with varying degrees of success. Geographic origin can be determined with a high level of confidence for materials such as emerald, Paraíba-type tourmaline, alexandrite, and many rubies. For some materials, especially blue sapphire and some rubies, the situation is more difficult. The main problem is that if the geology of two deposits is similar, then the properties of the gemstones they produce will also be similar, to the point where concluding an origin becomes seemingly impossible in some cases. Origin determination currently relies on a combination of traditional gemological observations and advanced analytical instrumentation.

In gemology, "origin" refers to the geographic locality of a gemstone deposit (Hänni, 1994). Origin determination of colored gemstones began with Gübelin and SSEF (both in Switzerland) in the 1950s and with AGL (New York) in 1977 (Schwarz, 2015). Origin determination is of increasing importance in today's market, and for many gems this information is considered either a value-adding factor or a positive for the salability of a gemstone (Hainschwang and Notari, 2015).

Origin determination is often possible because there is a close relationship between the environment of crystallization, especially the mineralogical and chemical composition of the host rock, and the properties of the gemstones that can be studied in the lab, often using sophisticated equipment (Hänni, 1994). In this paper we review the analytical techniques (figure 1) commonly used to characterize gem materials, with a specific focus on geographic origin determination. We also review the physical and chemical properties of corundum and emerald, which have the greatest demand for origin determination. Finally, we provide examples of origin determination of corundum and emerald from the literature to illustrate how these analytical methods are applied to the problem of establishing origin.

See end of article for About the Authors and Acknowledgments.
Gems & Gemology, Vol. 55, No. 4, pp. 512–535,
http://dx.doi.org/10.5741/GEMS.55.4.512

In Brief

- Origin determination is possible because there is a close relationship between the geological environment of formation and the physical and chemical properties of gemstones.
- Geographic origin can be determined with a high degree of confidence for emerald, Paraíba-type tourmaline, alexandrite, and many rubies.
- For some materials, especially blue sapphire and some rubies, the situation is more difficult.

CHARACTERISTICS OF CORUNDUM

Corundum, Al_2O_3, crystallizes in the $\bar{3}2/m$ class of the trigonal system (space group $R\bar{3}c$) with hexagonal unit cell axes of $a \approx 4.76$ Å and $c \approx 12.99$ Å (Cesbron et al., 2002). This uniaxial negative material (n_ω =

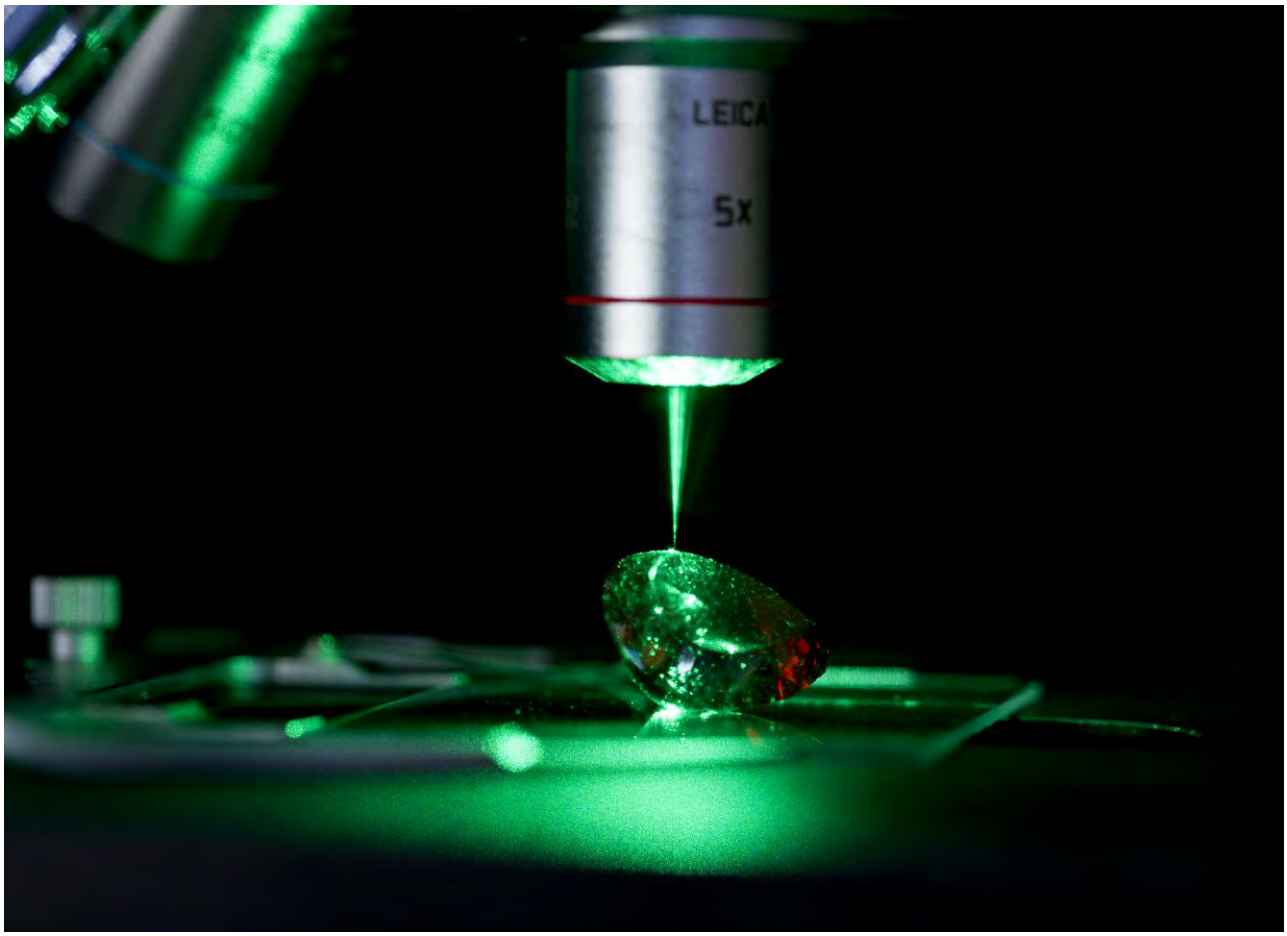

Figure 1. Confocal Raman spectroscopy, which can be used to identify mineral inclusions in gems submitted to the lab, is one of the advanced analytical methods used in geographic origin research. Photo by Kevin Schumacher.

1.767–1.772 and $n_\varepsilon \approx 1.759–1.763$) has a specific gravity of approximately 4. In corundum, the oxygen (O) anions are in a hexagonal close-packed configuration and form layers of ions arranged successively in the order ABAB...etc. (figure 2). The aluminum (Al) atoms are coordinated by six O atoms, three from layer A and three from layer B, in a slightly distorted octahedral arrangement. Because there are two Al atoms for three atoms of O, two Al sites out of every three are occupied, and one is vacant. A number of elements can substitute for Al^{3+} at the octahedral site (Mg^{2+}, Ti^{4+}, V^{3+}, Cr^{3+}, Mn^{2+}, $Fe^{2+,3+}$, Ga^{3+}).

Euhedral crystals of corundum can exhibit different faces that correspond to a number of crystalline forms (Cesbron et al., 2002) (figure 3): the rhombohedron (positive, $\{10\bar{1}1\}$, and negative, $\{01\bar{1}1\}$), the hexagonal dipyramid $\{hh\bar{2}\bar{h}l\}$, the pinacoid {0001}, first-order $\{10\bar{1}0\}$ and second-order $\{11\bar{2}0\}$ hexagonal prisms, the dihexagonal prism $\{hki0\}$, and the ditrigonal scalenohedron $\{hkil\}$.

Corundum exhibits a wide variety of colors, of which the most sought-after are red rubies, blue sapphires, and orangy pink *padparadscha* sapphires. These colors result from the substitution of chromophoric trace elements for Al in the crystal structure (Hughes et al., 2017). When chromium (Cr) replaces Al, the result, depending on the extent of the substitution, is a pink to red color. It is well known that Cr (along with vanadium, V) is the chromophore responsible for the green color in emerald (see below), but in corundum the distance between the metallic ion and O is short (1.913 Å), and as a consequence the Cr^{3+} ions show high electrostatic repulsion and absorption features are shifted to higher energies. In the optical absorption spectrum of ruby there are two large absorption bands (figure 4), with transmission windows at 480 nm (blue visible light) and 610 nm (red visible light). As the human eye is more sensitive to red than blue light above 610 nm, ruby appears red. Chromium-related red emission under ultravio-

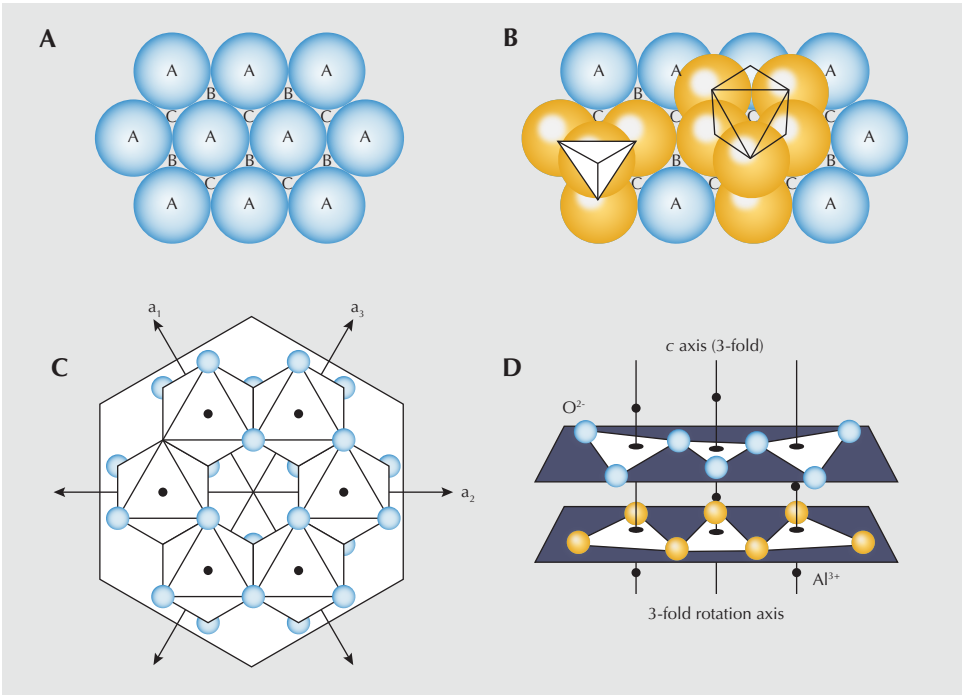

Figure 2. The crystal structure of corundum. A: A single layer of spheres representing O atoms in hexagonal close-packed coordination. In a second layer the spheres would be oriented over the B locations, and a third layer would be over the first (A locations). B: Six O atoms coordinate Al atoms at the C positions, forming an octahedron (the tetrahedrally coordinated site is vacant). Only two out of every three Al sites are occupied in the Al layers. C: The crystal structure of corundum looking down the c-axis. D: Perspective view of the crystal structure of corundum. From Giuliani et al. (2014a).

let (UV) light, and sometimes in daylight, is the cause of the fluorescence sometimes observed in (Fe-poor) rubies from certain deposits, including those from Myanmar and Vietnam.

The blue color in corundum requires the interaction of two transition metals, iron (Fe) and titanium (Ti). When Fe^{2+} and Ti^{4+} are located at neighboring Al sites, an optically induced transfer of an electron (termed "intervalence charge transfer," IVCT) creates an absorption band centered at approximately 580 nm that is responsible for the blue color (again, see figure 4) (Hughes et al., 2017). This defect assemblage is a very strong absorber and requires very few Fe-Ti pairs (on the order of 10 pairs for 1 cm of path length) to produce a reasonable saturation of blue color in corundum.

Figure 3. Crystalline forms of the $\bar{3}2/m$ class of the rhombohedral system (from Giuliani et al., 2014a; after Cesbron et al., 2002). A: Positive rhombohedron {10$\bar{1}$1}. B: Negative rhombohedron {01$\bar{1}$1}. C: Hexagonal dipyramid {hhil}. D: Pinacoid {0001}. E: First-order hexagonal prism {10$\bar{1}$0}. F: Second-order hexagonal prism {11$\bar{2}$0}. G: Dihexagonal prism {hki0}. H: Ditrigonal scalenohedron {hkil}.

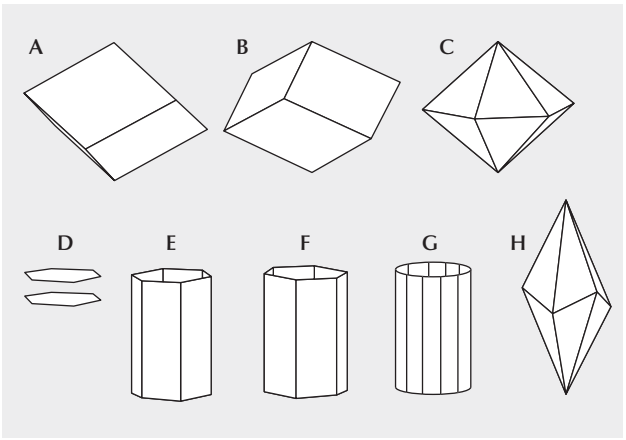

Treatment of corundum generally is focused on improving color. Patches of blue and purplish color in ruby (e.g., from Mong Hsu in Myanmar) are removed by heat treatment in order to create a "purer" red or pink color. The gems are placed in an oxidizing environment, which destroys the Fe^{2+}-Ti^{4+} IVCT that may be naturally present and leaves a more desirable pink or red color. The blue color of sapphire is often made deeper by heat treatment using a reducing atmosphere to convert Fe^{3+} to Fe^{2+} while also dissolving any Ti available in mineral inclusions (such as rutile) into the crystal lattice. Once the Ti is dissolved into the lattice, it can pair with the Fe^{2+}, producing the blue color via Fe^{2+}-Ti^{4+} IVCT. As discussed by Palke et al. (2019a), pp. 536–579 of this issue, this type of heat treatment can make origin determination more difficult as the natural inclusion scenes that might ordinarily aid in origin determination can be severely altered.

Heat treatment can also serve to improve the clarity of corundum by dissolving inclusions or fusing fractures. This often is done in the presence of a syn-

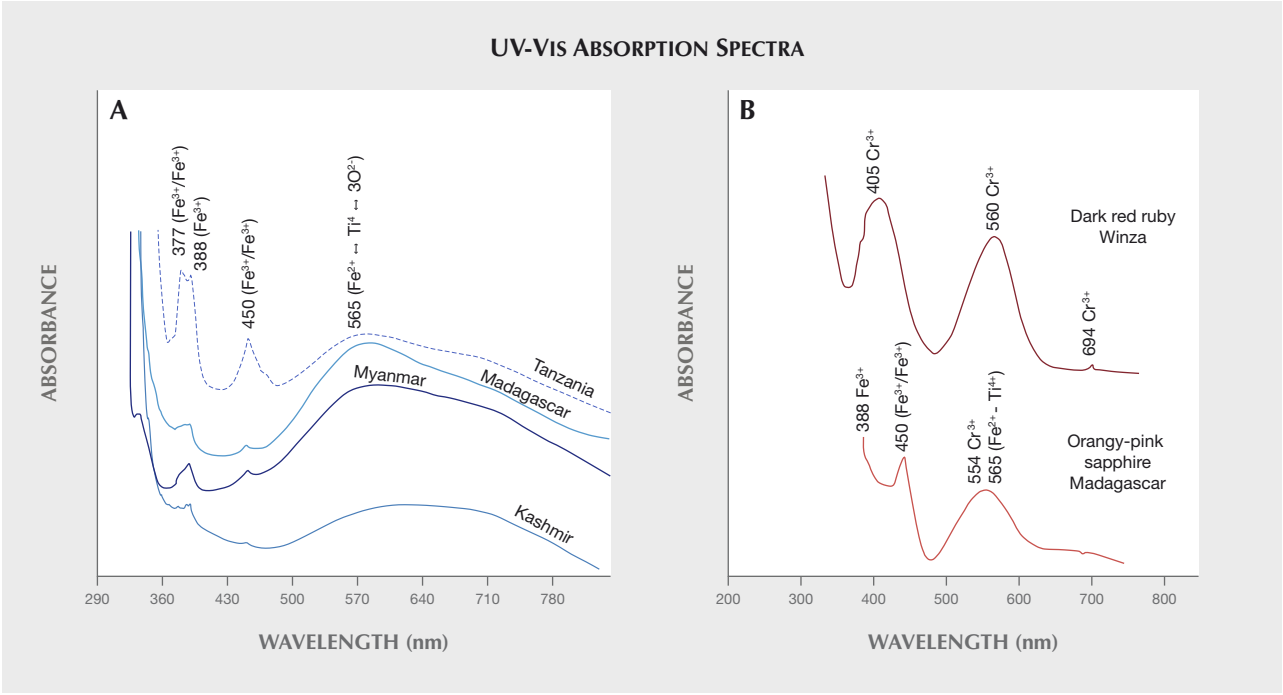

Figure 4. Typical polarized UV-Vis absorption spectra of sapphire and ruby. A: Polarized absorption spectra of four sapphires from different deposits (Notari and Grobon, 2002) showing bands corresponding to chromophores. B: Polarized absorption spectra of Winza ruby (Schwarz et al., 2008) and orangy pink sapphire from Madagascar (Peretti and Günther, 2002). The spectrum of ruby shows the well-known Cr^{3+} absorption bands at 405–410 and 560 nm, and the Cr "doublet" at 694 nm. The sapphire from Madagascar is close in color to padparadscha.

thetic flux, which facilitates this process at a temperature much lower than the melting point of corundum. Once the fractures are fused together, light can pass through the stone uninterrupted by the lower refractive index of air-filled cracks; this results in significant clarity enhancement and also serves to produce a more durable gemstone. This type of treatment is especially prevalent among rubies, and can sometimes act as a tell-tale sign of origin for certain localities such as Mong Hsu; see Palke et al. (2019b), pp. 580–612 of this issue. Diffusion treatments using Ti and beryllium (Be) are done to improve color but in the case of Ti can even be used to impart stars. Titanium diffusion into Fe-containing corundum in order to produce or enhance a blue color is a lengthy high-temperature process that produces a thin skin of color no more than 0.5 mm thick. However, Be diffuses easily into the lattice and may penetrate for several millimeters, or through the entirety of small stones. Beryllium diffusion can create many different colors in sapphire, depending upon the nature of trace elements in the gem (see Hughes, 1997; Emmett et al., 2017). GIA never provides origin reports for diffused stones, even if the original corundum was a natural stone.

CHARACTERISTICS OF EMERALD

Emerald is the green gem variety of the mineral beryl, which has the general formula $Be_3Al_2Si_6O_{18}$. This uniaxial negative material ($n_\omega \approx 1.568–1.602$, $n_\varepsilon \approx 1.564–1.595$) has a specific gravity ranging from approximately 2.6 to 2.9. Beryl is hexagonal and crystallizes in point group $6/m\ 2/m\ 2/m$ and space group $P6/m2/c2/c$. The Al or Y site is surrounded by six O atoms in octahedral coordination, and both the beryllium (Be) and silicon (Si) sites by four O atoms in tetrahedral coordination (figure 5). The SiO_4 tetrahedra share corners to form six-membered rings parallel to (001); stacking of the rings results in large channels parallel to the c crystallographic axis. The diameter of each channel varies from approximately 2.8 to approximately 5.1 Å. There are two sites in the channels; these are referred to as the 2*a* (at 0,0,0.25, in the wider part) and 2*b* (at 0,0,0, in the narrow part) positions.

Emerald crystals typically exhibit a prismatic habit characterized by six first-order $\{10\bar{1}0\}$ prismatic faces and two {0001} pinacoid faces. Small additional $\{10\bar{1}2\}$ and $\{11\bar{2}2\}$ faces can also be present.

The color of emerald is due to trace amounts of Cr and/or V replacing Al in the crystal structure. The

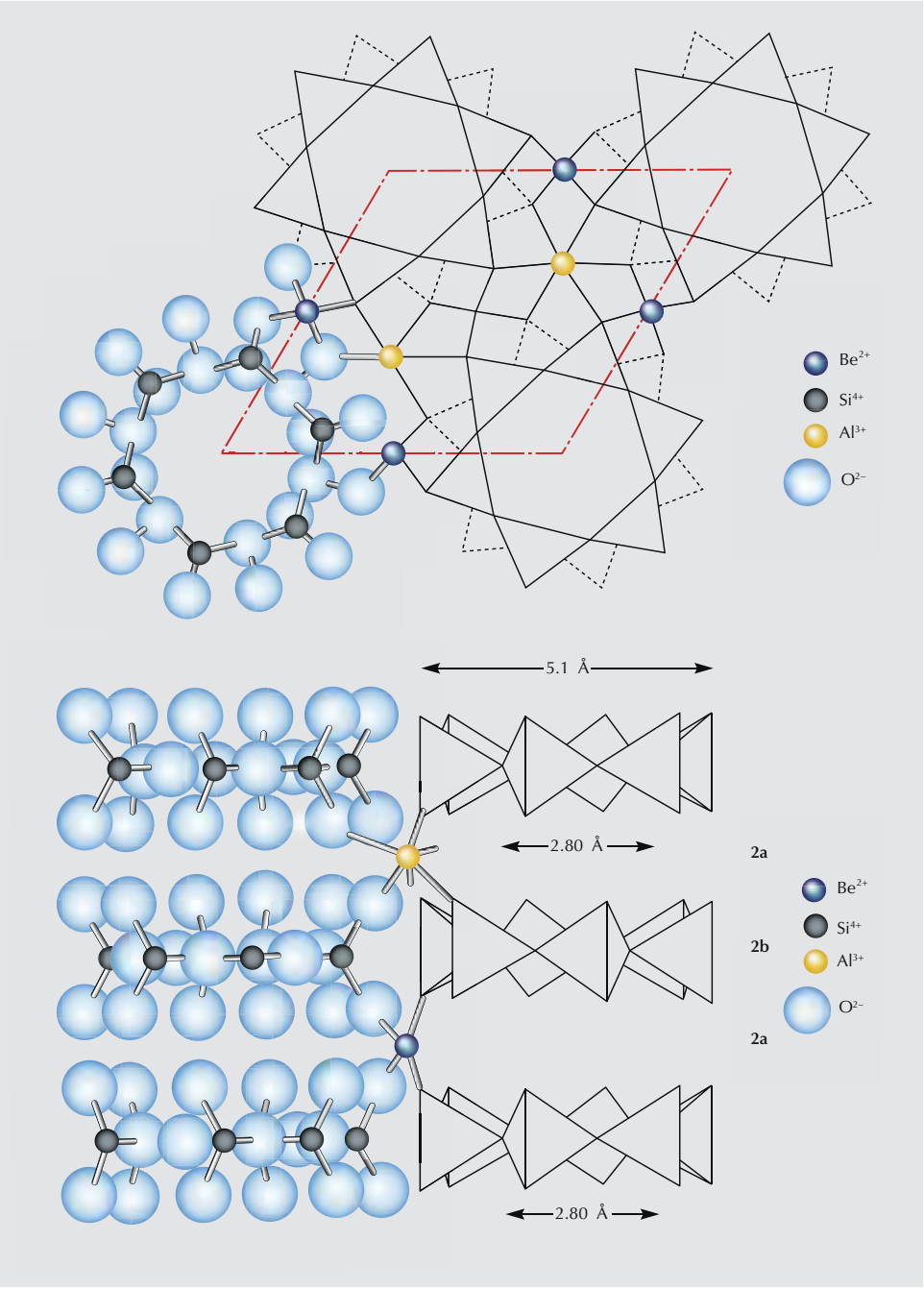

Figure 5. The crystal structure of beryl projected onto (top) (001) and (bottom) (100) showing SiO_4 tetrahedra, six-coordinated Al and four-coordinated Be atoms, and levels of the 2a and 2b sites in the channels formed by the hexagonal rings (from Giuliani et al., 2019).

presence of Cr and V in the beryl structure causes a red fluorescence that enhances the luminosity of the blue-green color, but if Fe^{3+} is present in the emerald crystal, this effect is suppressed (Nassau, 1983). There has been some debate over the difference between emerald and green beryl (see Conklin, 2002; Schwarz and Schmetzer, 2002).

In most cases the Cr_2O_3 content is much higher than that of V_2O_3; the main exceptions are for samples from the Lened deposit in Canada, the Davdar and Malipo occurrences in China, the Muzo mine in Colombia, the Mohmand district in Pakistan, and Eidsvoll in Norway.

Most elemental substitutions occur at the Al site (figure 6; see representative compositions in Groat et al., 2008). Magnesium is the main substituent in most emeralds, but other elements that can substitute for Al^{3+} include Sc^{3+}, Ti^{4+}, V^{3+}, Cr^{3+}, Mn^{2+}, $Fe^{2+,3+}$, Co^{2+}, Ni^{2+}, La^{3+}, and Ce^{3+}. Lithium (Li^{+}) can also substitute for beryllium at the Be site. To achieve charge

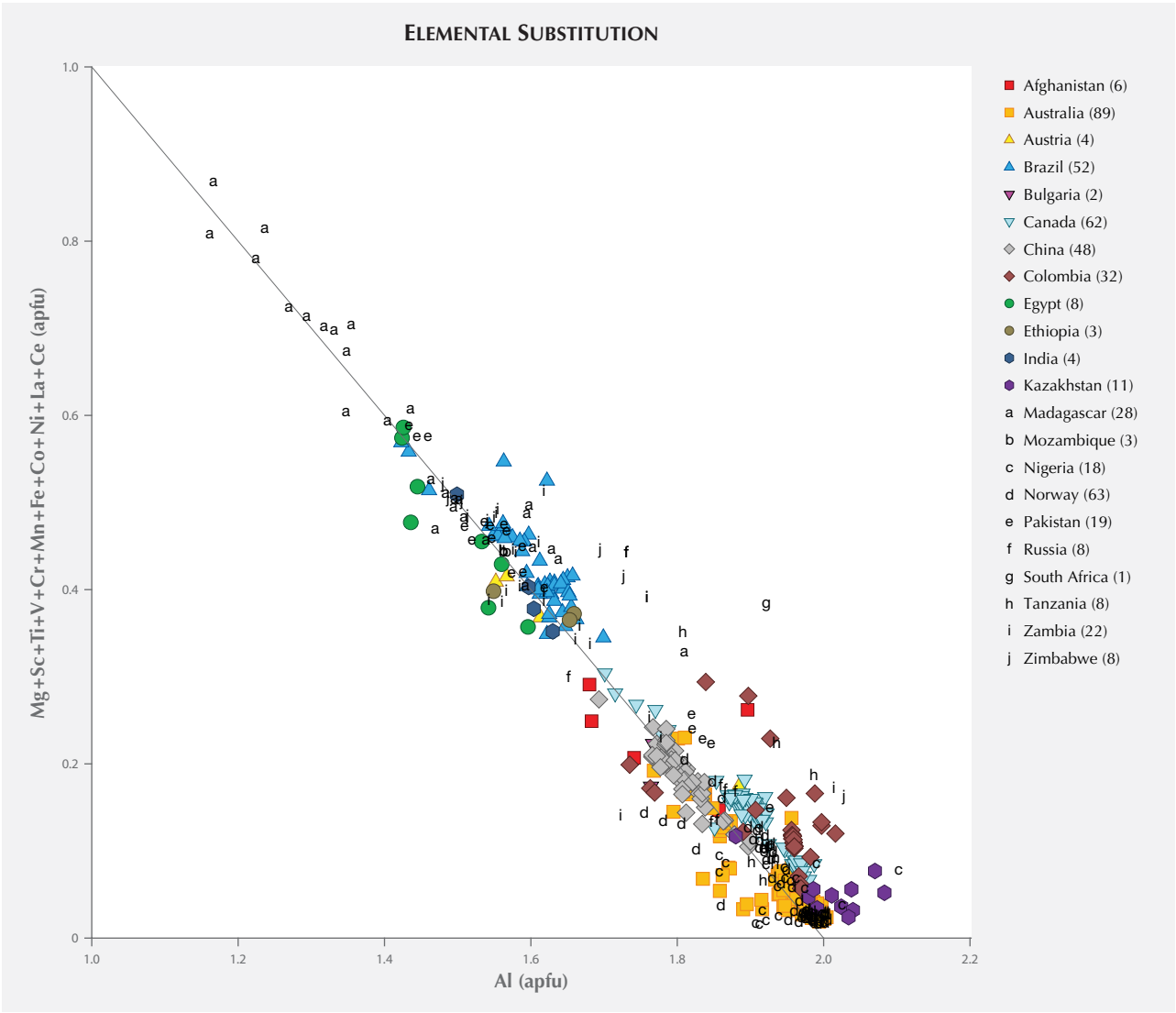

Figure 6. Al versus the sum of other Y-site cations, in atoms per formula unit, for 499 emerald analyses from the literature. The number of analyses per country is given in parentheses in the legend. Sources of data: Kovaloff (1928); Zambonini and Caglioti (1928); Leitmeier (1937); Otero Muñoz and Barriga Villalba (1948); Simpson (1948); Gübelin (1958); Vlasov and Kutakova (1960); Martin (1962); Petrusenko et al. (1966); Beus and Mineev (1972); Hickman (1972); Garstone (1981); Hänni and Klein (1982); Graziani et al. (1983); Kozlowski et al. (1988); Hammarstrom (1989); Ottaway (1991); Schwarz (1991); Artioli et al. (1993); Schwarz et al. (1996); Giuliani et al. (1997b); Abdalla and Mohamed (1999); Gavrilenko and Pérez (1999) (Kazakhstan values are averages of 11 analyses); Alexandrov et al. (2001) (average of 10 analyses), Groat et al. (2002); Marshall et al. (2004) (two averages of five analyses each), Vapnik et al. (2005, 2006); Zwaan et al. (2005); Gavrilenko et al. (2006); Zwaan et al. (2006) (average of 55 analyses); Rondeau et al. (2008); Andrianjakavah et al. (2009); Brand et al. (2009); Loughrey et al. (2012); Marshall et al. (2012); Zwaan et al. (2012); Loughrey et al. (2013); Marshall et al. (2016) (average of 37 analyses); Lake et al. (2017) (average of 88 analyses); Aurisicchio et al. (2018); Santiago et al. (2018) (average of approximately 130 analyses); Giuliani et al. (2019).

balance, the substitution of divalent cations for Al is coupled with the substitution of a monovalent cation (Na^+, Cs^+, Rb^+, and K^+) for a vacancy at a 2*a* or 2*b* site in the channel (figure 7). Artioli et al. (1993) suggested that, in alkali- and water-rich beryls, H_2O molecules and the larger alkali atoms (Cs, Rb, K) occupy the 2*a* sites and Na atoms occupy the smaller 2*b* positions, while in alkali- and water-poor beryl, both Na atoms and H_2O molecules occur at the 2*a* site and the 2*b* site is empty.

While some gems, such as aquamarine in pegmatites, crystallize in relatively stable environments that allow for continuous growth without strong perturbations, emeralds are formed in geologic environments characterized by abrupt changes and mechanical stress (Schwarz, 2015). This results in smaller crystals with considerable internal defects, such as inclusions and fractures. Therefore, the most common treatment for emeralds is clarity enhancement, which is accomplished by injecting a material (typically an oil or resin) of similar refractive index into the fractures. This is typically done under vacuum in order to completely fill the cracks with a filler of matching refractive index, lowering the relief of the once air-filled cracks. The vast majority of emeralds on the gem market are treated in this manner to varying degrees.

ANALYTICAL METHODS USED FOR ORIGIN DETERMINATION

Corundum and emerald and their inclusions are identified and characterized using a variety of methods, many of which (especially when used in combination) provide data that can also be used for origin determination. Various methods are used to identify basic physical properties, inclusions, spectroscopic characteristics, trace element chemistry, and isotopic chemistry.

Inclusion Identification. The positive identification of inclusions contained within a gemstone can hold the key to its origin. At GIA, combining this with knowledge of the trace elements present is often enough to make an origin determination. Establishing the identity of an inclusion traditionally has been done visually with reference to known inclusions. However, Raman spectroscopy is now routinely used to positively identify mineral inclusions by reference to established spectroscopic databases.

Microscopy. Optical microscopy can be used to characterize optical properties (such as refractive indices and birefringence), growth features, solid inclusions (on the basis of color and morphology), and fluid in-

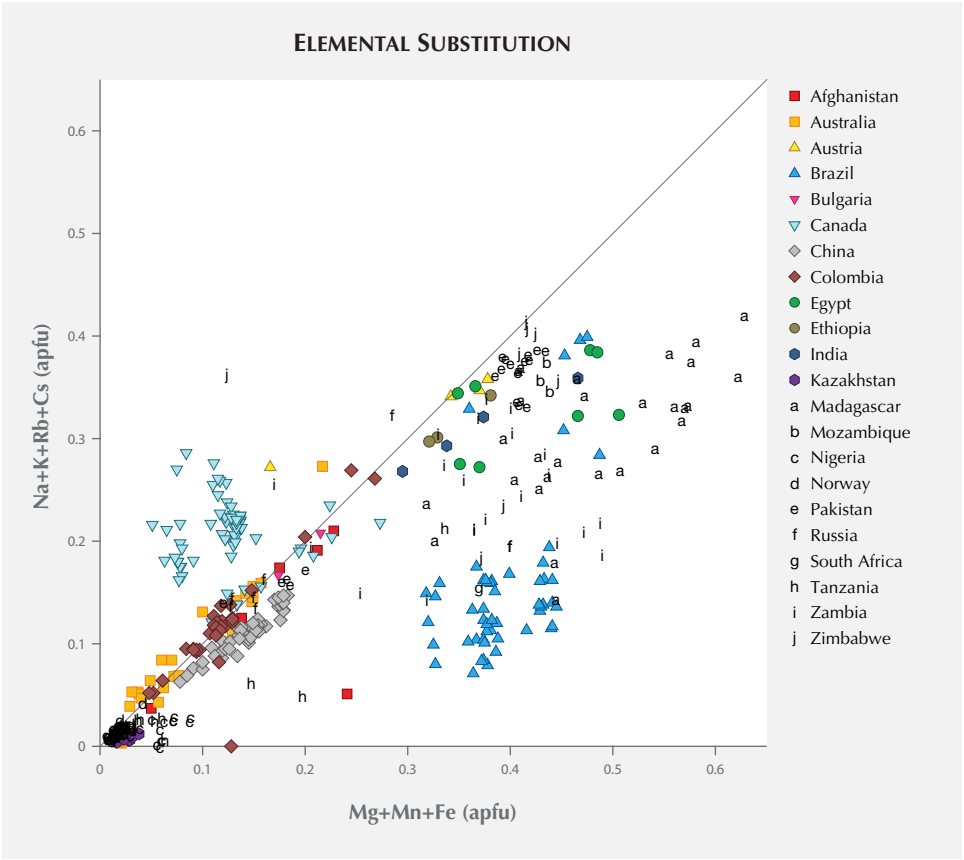

Figure 7. Mg + Mn + Fe versus monovalent channel-site cations, in atoms per formula unit, for analyses from the literature. Sources of data are the same as in figure 6. Points above the 1:1 line suggest Li substitution in the crystal structure; points below the line suggest that some of the Fe is present as Fe^{3+}.

clusions (shape and ratios of solid:liquid:vapor), if present, as the finest-quality gems will by definition exhibit few inclusions of any kind. Observation of a stone's inclusion characteristics provides some of the most important information available to the gemologist when making geographic origin calls. The most commonly used tool in the gemological lab is a binocular microscope equipped with darkfield illumination. This illumination environment provides higher contrast of a stone's inclusions by causing light to enter the stone from a wide range of angles rather than from below the stone only. This is often supplemented by the use of a strong fiber-optic light, especially when used to highlight rutile silk in sapphires and rubies. Solid and fluid inclusions in gemstones are often identified by observing their morphology, color, luster, and other properties and comparing against possible options for a given host mineral based on an understanding of their geological origins. After inclusions with a certain appearance have been confirmed with Raman spectroscopy, their identity can often be assumed when observed later by comparison.

Microscopy is also the first step in identifying heat-treated corundum and synthetics that have been erroneously submitted to the lab for origin reports. Stones that have been heated only (i.e., without Be or Ti diffusion) can be issued origin reports. However, determining origin can be more difficult for heated stones, especially metamorphic blue sapphires; see Palke et al. (2019a), pp. 536–579 of this issue.

Raman Spectroscopy. When a laser is aimed at a material, almost all of the reflected laser light undergoes Rayleigh scattering (and hence is elastically scattered light with the same wavelength as the incident laser light), but a very small percentage of the reflected laser light is at a different wavelength because of inelastic (Raman) scattering of the laser light by molecular vibrations (Zaszczak, 2013). Most materials exhibit a characteristic Raman spectrum that can be used for identification. Reliable reference spectra are available from sources such as the RRUFF database (rruff.info). Raman spectroscopy allows subsurface analyses of many types of solid inclusions and can also be used to identify solids and molecular phases in fluid inclusions.

Spectroscopy. By looking at the spectroscopic signatures of gemstones in light ranging from the ultraviolet through the visible and into the infrared, we can oftentimes determine some very basic information related to the geological formation or treatment history. These spectroscopic measurements are quick, nondestructive, and provide invaluable information to help guide our next steps in origin determination.

Ultraviolet/Visible/Near-Infrared (UV-Vis-NIR) Spectroscopy. High-quality absorption spectroscopy is a valuable tool to understand the chemical properties of a gemstone and to identify the color-causing agents in a material, which can be useful in origin determination. This technique relies on passing white light through a stone and measuring how much light gets absorbed by (or transmitted through) the stone from the ultraviolet to the near-infrared. For most colored stones, the transition metals and other defects that can cause color can also have absorption that extends into the ultraviolet and near-infrared. For origin determination, it can be important to identify certain chromophores, such as copper in tourmaline, in order to confidently apply the "Paraíba-type" tourmaline varietal name.

For other materials, the color-causing agents are not so important for origin determination, but certain absorption features can be useful to narrow down the range of possibilities; see Palke et al. (2019a,b), pp. 536–579 and pp. 580–612 of this issue; Saeseaw et al. (2019), pp. 614–646 of this issue. Specifically, emeralds can be separated into tectonic-metamorphic-related and tectonic-magmatic-related groups based on the intensity of iron-related bands, and blue sapphires can be separated into metamorphic and basalt-related groups based on the intensity and/or absence of an absorption band at 880 nm (Giuliani and Groat, 2019, pp. 464–489 of this issue).

Infrared Spectroscopy (IR). Today this almost always refers to Fourier-transform infrared spectroscopy (FTIR). This form of vibrational spectroscopy is based on the reflectance, transmittance, or absorbance of infrared light by a material. This technique relies on the fact that a sample absorbs different amounts of light at distinct frequencies that correspond to the vibrational frequencies of the bonds in the sample. However, transmission IR spectroscopy is typically used to study discrete molecules within a crystal structure, such as H_2O at the channel sites in emerald, and to observe hydroxyl bands and other features in corundum that can be useful for detection of heat treatment. Synthetic alexandrite and emerald that have been unwittingly submitted for an origin report can also often be identified by observation of specific

fingerprints in the hydroxyl-stretching region of an FTIR spectrum. Infrared spectroscopy can also be used to identify solids and molecular phases (such as H_2O, CO_2, and CH_4) in fluid inclusions. Additionally, Saeseaw et al. (2014) explored the potential of using FTIR to identify different groups of emeralds based on the structure around water molecules in the beryl channel, which might have potential in providing an additional discriminant variable for origin determination. At the moment, however, the use of this technique is still in the exploratory stage.

Trace Element Chemistry. Being able to detect the presence or absence and relative quantities of a variety of trace elements in ruby, sapphire, emerald, tourmaline, alexandrite, and spinel can sometimes quickly rule in or rule out particular origins. Determining trace element chemistry efficiently with high levels of accuracy to very low concentrations in a nondestructive manner is a considerable challenge. An overview of four different methods used by the geological and gemological communities is presented, outlining the advantages and limitations of each.

Energy-Dispersive X-Ray Fluorescence Spectroscopy (EDXRF). This technique relies on the interaction of X-rays and a sample and takes advantage of the fact that each element has a unique atomic structure, which results in a unique set of peaks on an emission spectrum. In the laboratory, this method requires no real sample preparation, and it is quick and nondestructive. The excitation source may be a beam of electrons (as in the scanning electron microscope) or an X-ray source (as in handheld X-ray fluorescence spectrometers). This technique is used to determine the elements present in a sample, and can be used to estimate their relative abundances; however, due to factors such as X-ray absorption and overlapping X-ray emission peaks, accurate estimation of the sample composition requires the application of quantitative corrections (sometimes referred to as matrix corrections). Beyond limits in accuracy, some key lighter trace elements (those lighter than sodium) cannot be detected. When applied with care, however, EDXRF can produce reliable results, although its precision and high detection limits cannot match more advanced techniques such as LA-ICP-MS (see below).

Electron Probe Micro-Analyzer (EPMA). This technique is most often used to quantify major element compositions of minerals and is accurate to the parts per million level. In the electron microprobe, the sample is attached to a stage (movable in x, y, and z axes) at one end of a column with a filament at the opposite end. Air is removed from the column until a high vacuum is achieved and then high voltage is applied to the filament, which gives off electrons. Electromagnets in the column shape the electrons into a narrow (generally 1–5 micron) beam that is directed onto the sample. The elements making up the sample emit characteristic X-rays, which are diffracted and detected by a wavelength-dispersive spectrometer. The intensity of the X-ray energy given off by an element is compared to that emitted by a standard sample of known composition (a calibration standard), and then matrix corrections are applied to this intensity ratio to yield concentrations.

Electron microprobe compositions are usually given in terms of weight percent oxides, because in most minerals O is by far the most abundant element. Although it is possible to measure oxygen, there is less error involved in measuring the cations and allocating the O for charge balance.

Much of the early research on origin determination was carried out using electron microprobe analyses (e.g., Giuliani et al. 2014b). The technique is not destructive per se, but analyzing gems requires special sample holders that generally must be custom-fabricated. As such, it is not a standard gemological laboratory instrument and is more suited for analyzing geological samples collected in the field.

Analyses of light elements are often less accurate (10–20 rel.% for Li and Be; R. Škoda, pers. comm., 2019) because of their low X-ray yield (resulting in low count rates and low peak-to-background ratios) due to X-ray absorption in the specimen, the analyzer crystal, and the detector window. This is why most published analyses of beryl are renormalized with an assumed three Be atoms per formula unit.

Electron microprobe analyses can be used to narrow down the origin of emerald—for example, to determine whether Cr or V is the principal chromophore. It is less useful for corundum, where the trace elements generally occur in much lower concentrations and interferences (peak overlap) among many of the transition elements (Ti, V, and Cr) makes them difficult to measure.

Electron microprobe instruments are very expensive to purchase, maintain, and operate, which is why they are rarely found outside the university environment. For trace element determinations, this method has largely been supplanted by the following

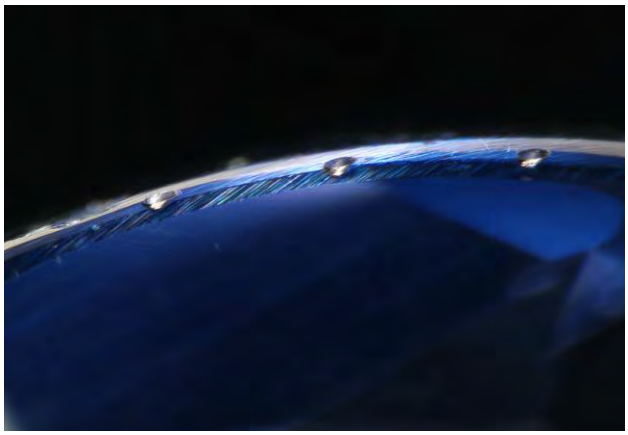

Figure 8. Typical laser ablation spots placed on the girdle of a synthetic sapphire. The field of view is 1.58 mm and the pits are 60 microns in diameter. Photo by Jonathan Muyal.

technique, which is faster and benefits from better detection limits.

Laser Ablation–Inductively Coupled Plasma–Mass Spectrometry (LA-ICP-MS). With the introduction of sapphire color enhancement via beryllium diffusion treatment around 2002 (Emmett et al., 2003), the gemological community needed an analytical method capable of detecting Be, as EDXRF and EPMA cannot. LA-ICP-MS was adopted shortly thereafter to meet this need and proved to be highly useful beyond just detecting Be diffusion treatment in sapphire. This method is fast, detects elements from Be to U at ppm to ppb levels simultaneously, and the sample chambers available allow for analyzing stones in virtually any form, including mounted in jewelry (e.g., Abduriyim and Kitawaki, 2006). In this technique, an ultraviolet laser beam (such as 213 and 193 nm) is used to generate aerosols from the sample surface. The ablated material is then transported into the plasma, where it is ionized. The ions generated in the plasma torch are then introduced to a mass analyzer for elemental and isotopic analysis. However, mass interferences must be accounted for; when the sample is ablated, species with masses similar to elements of interest can occur, generating falsely elevated levels. To have enough signal to quantify trace elements with small ablation spots, gemological labs typically employ quadrupole mass spectrometers with modest mass-resolving powers (MRP) of around 300. The MRP necessary to separate a species of interest from a close-in-mass interference is simply the ratio of the mass of the species of interest divided by the difference between that mass and the close-in-mass interference of concern.

To quantify the various trace elements in a given gem material, calibration standards must be used. There are many traditional calibration standards commercially available, such as those manufactured by the National Institutes of Standards (NIST) or the United States Geological Survey (USGS). At GIA, a desire for enhanced trace element accuracy for ruby and sapphire led to the development of its own corundum calibration standards for LA-ICP-MS (see box A).

While LA-ICP-MS is considered a semi-destructive technique in that the process leaves ablation pits, the generally small size chosen for the pits (~50 µm) means that they are impossible to see without magnification (figure 8 shows typical laser ablation spots placed on the girdle of a synthetic sapphire). As each mineral species interacts differently with the UV laser light, evaluating the ablation pits generated with different laser conditions is recommended.

Secondary Ion Mass Spectrometry (SIMS). Because LA-ICP-MS is limited by the inability to separate some close-in-mass interferences while still being able to detect to the ppm and sub-ppm levels, SIMS (figure 9) can be an attractive option. When extreme sensitivity and high mass resolution are required, SIMS is potentially the best choice. Its sensitivity for all isotopes to the ppm and ppb level is unequaled while still being able to employ MRPs of 3000 to 6000. This technique involves sputtering the surface of a sample with a primary beam of ions to generate, collect, and analyze secondary ions. As the relative signal generated varies not only by species but also by what matrix a species is in, relative sensitivity factors (RSF) need to be developed for every combination of trace element and matrix. These RSF values are derived from depth profiling primarily ion implant standards for this conversion of relative signal to concentration. The RSF values are also impacted by the choice of primary ion beam and the analytical conditions (beam polarity, current, and potential). The matrix-matched corundum standards developed by GIA (detailed in box A) were all calibrated using SIMS. In all, RSF factors were developed for 18 trace elements in corundum (Be, Mg, Si, Ca, Sc, Ti, V, Cr, Mn, Fe, Co, Ni, Cu, Zn, Ga, Ge, Zr, and Pb) to not only cover those trace elements regularly characterized for origin determination but also to further research on trace elements we expect could be present based on size and valency. However, gemological lab-

BOX A: MATRIX-MATCHED CORUNDUM STANDARDS AT GIA

The onset of beryllium diffusion treatment of sapphire signaled a need for better quantitative analysis capabilities in gemological laboratories (Emmett et al., 2003). Energy-dispersive X-ray fluorescence (EDXRF)—the traditional instrumentation used to detect trace elements in gems—was completely blind to this critical trace element being artificially introduced into natural sapphire. To address this, GIA and other gem laboratories adopted laser ablation–inductively coupled plasma–mass spectrometry (LA-ICP-MS).

At GIA, corundum (ruby and sapphire) accounts for most of the gemstones submitted for origin services. Only a small handful of trace elements are typically present (Mg, Ti, V, Cr, Fe, and Ga), and these are usually at very low concentrations (generally less than 100 ppma and often less than 10 ppma), making the chemical analyses extremely difficult. Additionally, much research at GIA involving the color origin of corundum also requires trace element quantification of chromophore chemistry with atomic-level accuracy. For this reason, the GIA laboratory has focused on producing the highest-quality and most accurate trace element analyses possible for corundum and ensuring that these results are consistent across its five global identification laboratories.

For more than a decade, GIA has invested in creating its own matrix-matched standards for ruby and sapphire. In 2006, the first set of corundum matrix-matched standards was introduced into its laboratories (Wang et al., 2006). For a decade, these standards were used to quantify Be, Mg, Ti, V, Cr, Fe, and Ga in corundum. In 2016, an updated set was developed to offer multiple and more optimal levels of some trace elements, and to reduce the number of individual standards (Stone-Sundberg et al., 2017). Additionally, a high-purity synthetic sapphire "blank" was introduced, allowing users to correct for mass interferences from the matrix itself. Currently, GIA is releasing a third set of matrix-matched corundum standards for both internal use and outside distribution (figure A-1). This third generation of corundum standards adds a calibrated value for Ni.

In comparing results from calibrating LA-ICP-MS with NIST SRM 610 and 612 against our corundum standards, we have found that using NIST SRM 610 and 612 can result in underreporting the levels of Be, Ti, V, Fe, Ni, and Ga (the levels of Mg are slightly overreported using NIST SRM 610 and 612, and Cr appears to be reasonably accurate within error). The generation of suppressed trace element concentrations with NIST standards can result from differences in the way the laser interacts with the two different matrices.

This lengthy and expensive undertaking to create single-crystal matrix-matched standards for ruby and sapphire required working with several highly specialized vendors. These included synthetic Czochralski crystal growers to produce the specifically targeted trace element contents of the crystals, secondary ion mass spectrometry (SIMS) laboratories to generate corundum-specific relative sensitivity factors for the elements of interest and calibrate the individual standards, ion implanters to create the secondary standards for SIMS, and laboratories with Rutherford backscattering spectrometry (RBS) capabilities to validate our ion implants prior to calibration efforts. This process could be replicated for other matrices if desired in the future.

Figure A-1. GIA's corundum standards set for matrix-matched LA-ICP-MS measurement of trace elements in ruby and sapphire. Each corundum standard is laser inscribed. The number 16-0524-06 corresponds to the high-purity corundum blank, 07-0687-14 and 02-1287-29 are Czochralski-grown doped synthetic corundum, and Y-1212 is a Yogo sapphire wafer used for Fe and Ni measurements.

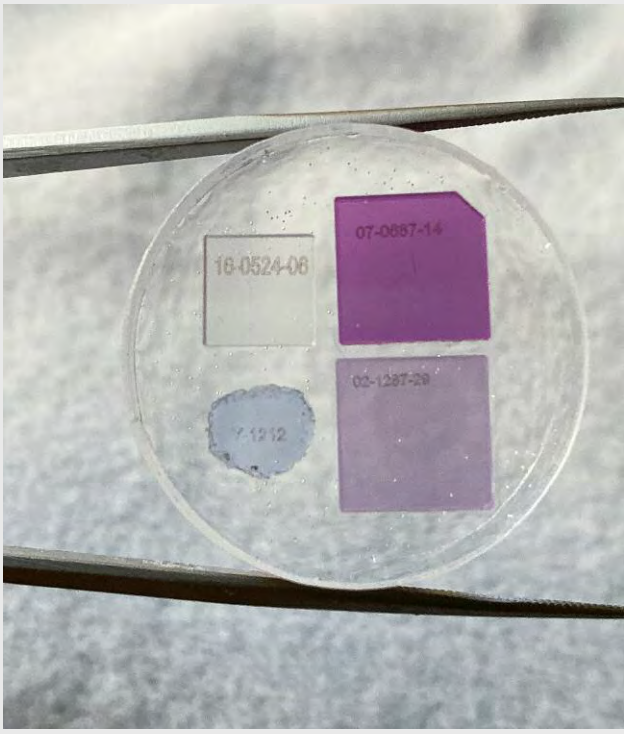

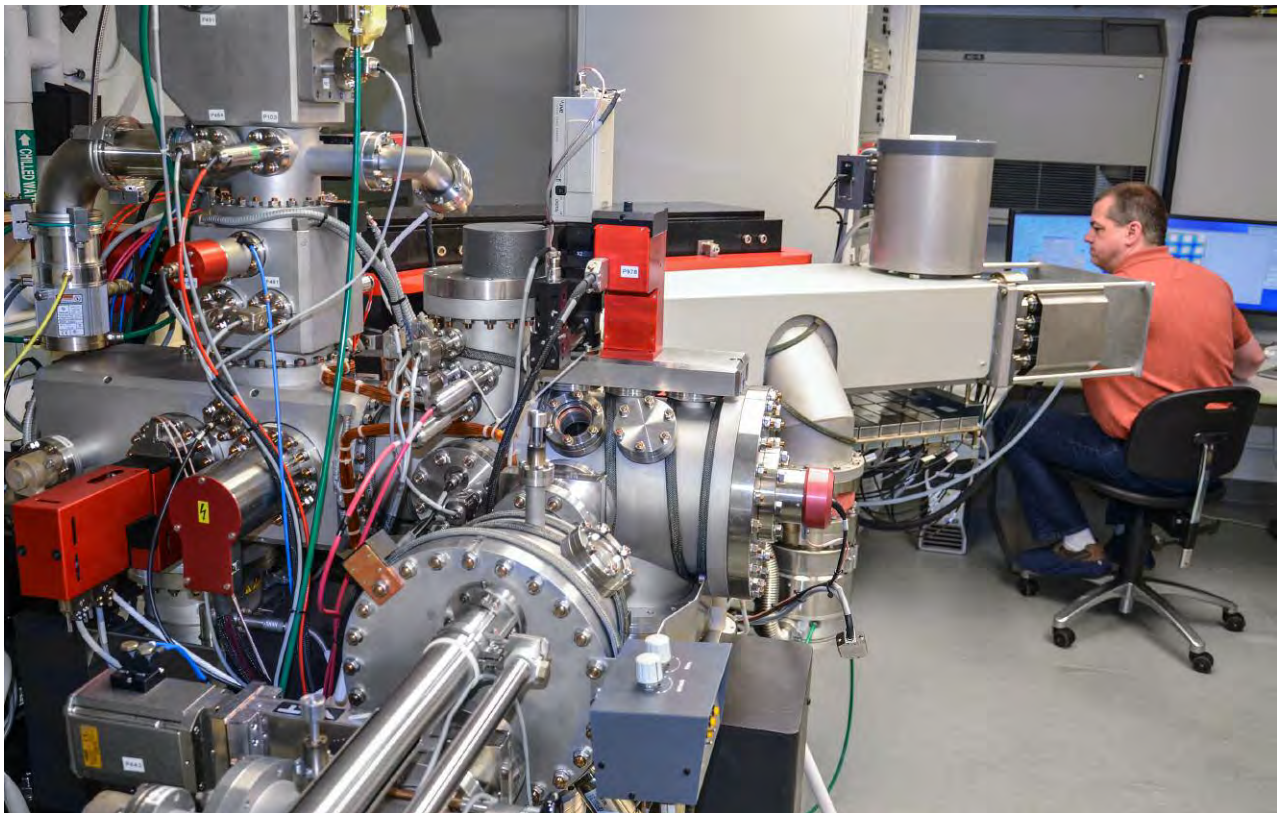

Figure 9. A secondary ion mass spectrometry (SIMS) instrument at the Carnegie Institution for Science in Washington, DC. Photo by Duncan Pay.

oratories will not be adopting SIMS equipment anytime soon, as this instrumentation is extremely expensive, requires highly specialized technicians and facilities to run it, is slow, and has rigid sample requirements that make it difficult to run most of the material submitted to gem labs today. However, it is a very useful tool presently for detecting trace and very trace elements that are difficult or impossible to accurately measure with LA-ICP-MS due to mass interferences. For example, we are actively exploring the wide range of Si in ruby and sapphire (and what it can tell us about origin), which currently can only be accurately quantified to the ppma level with SIMS.

Isotopic Studies. Presently, gemological laboratories do not incorporate isotopic analysis into their origin determination, but in the future it could have a place. Stable isotope geochemistry deals with isotopic variations that arise from isotope exchange reactions or mass-dependent fractionations that take place during the physical and chemical processes responsible for the formation of gems. The magnitude and temperature dependence of isotopic fractionation factors between minerals and fluids permit reconstitution of the geological history of gems in terms of source of the element and origin of the fluids (Fallick et al., 1985). Generally, stable isotopes are measured by mass spectrometry (including LA-ICP-MS and SIMS). Natural variations in isotopic ratios for gem minerals have been reported for only five light elements, namely carbon (C) and nitrogen (N) for diamond; O for oxides; hydrogen (H), O, and boron (B) for silicates; and heavier elements such as copper (Cu) for turquoise and S for lapis lazuli (Giuliani and Fallick, 2018). The stable isotope signatures of gems such as emerald, ruby, sapphire, agates, turquoise, and garnet shed light on the nature of the fluids, the source of the elements responsible for their formation, and in some cases their geographic origin (Giuliani et al., 2000a,b).

Oxygen is a dominant element, and the two main stable isotopes ^{18}O and ^{16}O are used for geological and geographical determinations. The $^{18}O/^{16}O$ ratio is 2.0052×10^{-3}—that is, for one atom of ^{18}O there are on average 500 atoms of ^{16}O. This ratio varies as a function of the geological context and the physical and chemical conditions that prevailed during gem formation, namely: (1) the source of O—i.e., the O-isotopic composition of the gem host rock and/or

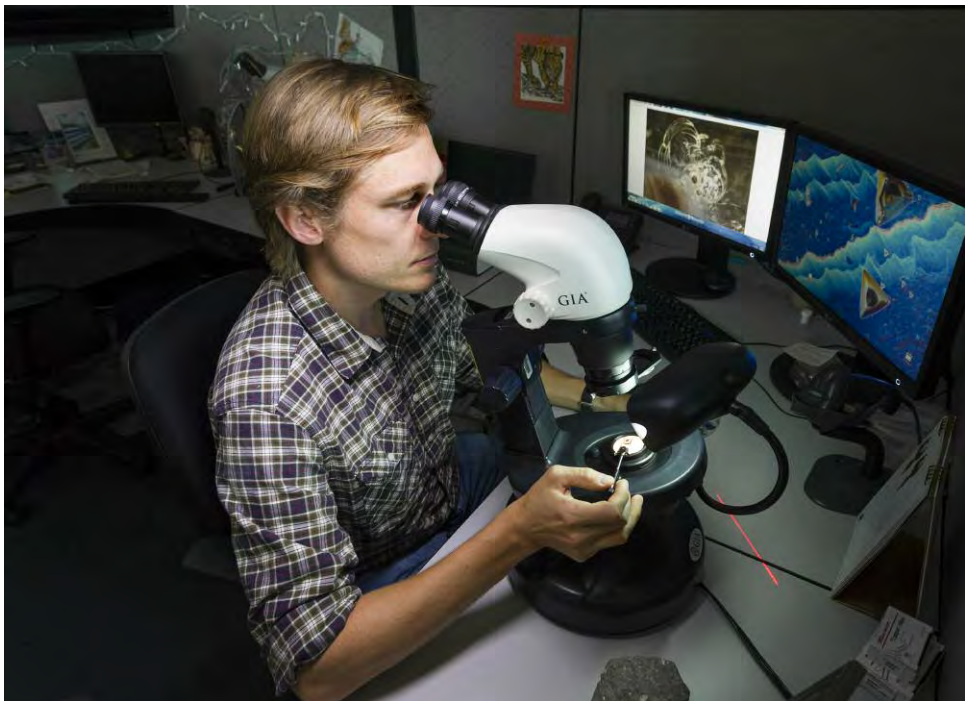

Figure 10. Careful microscopic observations of a stone's inclusion characteristics are an integral part of the origin determination process. Photo by Kevin Schumacher.

parental fluid; (2) the temperature of its formation; and (3) the intensity of the fluid-rock interaction in an open or closed geological system. The concentration of an isotope is usually given as a ratio—e.g., $\delta^{18}O$, in per mil, where the standard has a known isotopic composition. Data are reported in the conventional $\delta^{18}O$ notation as per mil (‰) relative to the Vienna Standard Mean Ocean Water (VSMOW), with $\delta^{18}O = (\{[^{18}O/^{16}O_{sample}]/[^{18}O/^{16}O_{standard}]\}\text{-}1) \times 10^3$. Isotopes have the same number of protons but different numbers of neutrons.

ANALYTICAL WORKFLOW FOR ORIGIN DETERMINATION AT GIA

When a gemstone is submitted to the GIA lab for an origin report, there is a workflow that routes the stone through a series of tests in order to collect sufficient data to establish the information contained on the report. The stone could be red, blue, or green; round brilliant, a cabochon, or square step cut—every origin call in the lab starts with identification, utilizing standard gemological testing, such as refractive index and specific gravity measurements to determine what the gem material is. The refractive index is measured on a standard gemological refractometer and specific gravity on a high-precision, well-calibrated scale that can measure a stone's weight suspended in water or on its own. Once the gem material is confirmed, further advanced testing may be used if an origin report is requested: Ruby, sapphire, emerald, alexandrite, Paraíba-type tourmaline, and red spinel are currently eligible for this service. Each material requires a specific decision making process when making a geographic origin determination.

Once a stone has been identified as one of the materials for which GIA offers origin reports and the service is requested, the origin determination process begins. In most cases, this starts with careful observations of the stone's inclusions using a standard gemological microscope (figure 10) with a variety of lighting conditions including darkfield, brightfield, fiber-optic illumination, and cross-polarized illumination. For some materials (especially blue sapphires, rubies, and emeralds) microscopic evidence constitutes much of the decision making process for an origin report. Microscopic observation also allows the gemologist to identify many synthetic stones that have unknowingly been submitted for origin reports. If needed, confocal Raman spectroscopy can be used to positively identify mineral inclusions in a stone (again, see figure 1). In order to correlate a stone's inclusion scene to a geographic origin, GIA gemologists have access to an extensive colored stone reference database. Over more than a decade, data from stones of known provenance collected through GIA's field gemology program (see Vertriest et al., 2019, pp. 490–511 of this issue) in the form of photomicrographs, trace element chemistry, and spectra have been entered in this database.

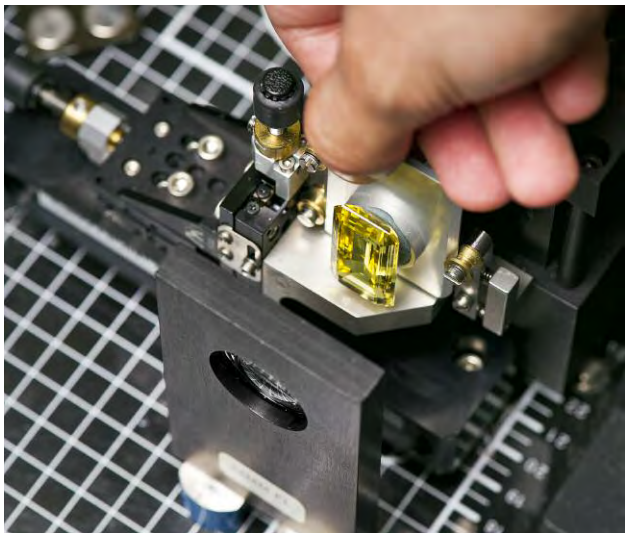

Figure 11. UV-Vis spectroscopy can provide additional evidence for some stones to narrow down the possible choices for a geographic origin determination. Photo by Kevin Schumacher.

Sometimes an inclusion scene can provide convincing evidence of a stone's geographic origin. Sometimes the gemologist is not so lucky and inclusions are ambiguous or absent in stones that are particularly clean. Regardless, microscopic evidence must be backed up with additional advanced testing. Emeralds and blue sapphires require UV-Vis-NIR spectroscopy (figure 11), where the presence or absence of certain absorption bands allows the separation of tectonic-metamorphic-related versus tectonic-magmatic-related emeralds, or metamorphic versus basalt-related blue sapphires (Saeseaw et al., 2019, pp. 614–646 of this issue; Palke et al., 2019a, pp. 536–579 of this issue). After microscopic observation and UV-Vis spectroscopy, if needed, the trace element chemistry of these stones is measured by LA-ICP-MS (figure 12). At this point, a ruby needing an origin determination can be separated into either the marble hosted ruby group or the so-called high-iron ruby group based on its concentration of Fe; see Palke et al. (2019b), pp. 580–612 of this issue. LA-ICP-MS measurement is also the safeguard for detecting Be-diffused corundum (Emmett et al., 2003). Rubies and sapphires that have undergone this extreme treatment are not eligible for the geographic origin determination service at GIA. Additionally, the trace element profiles of rubies and sapphires are measured at GIA using internally developed matrix-matched corundum standards (Stone-Sundberg et al., 2017, and box A of this paper). Once the trace element chemistry data is collected, it is compared to GIA's database of stones with known provenance. For some stones, the number of deposits has proliferated so much in recent years and the amount of data collected is extensive enough that it can be difficult to

Figure 12. LA-ICP-MS instrument used in the GIA laboratory as part of the geographic origin determination process. The instrument on the left is a Thermo Fisher iCap ICP-MS, while the Elemental Scientific Lasers NWR 213 laser ablation unit is in the center of the photo. Photo by Kevin Schumacher.

interpret an unknown sample's data on traditional two-dimensional plots. As mentioned in Palke et al. (2019a), pp. 536–579 of this issue, GIA employs a so-called selective plotting method to filter through the data and plot the unknown only against reference data with similar chemistry, making it much simpler to determine how to use the chemistry to assist in making an origin call.

At this point in the process, the full dataset has been collected for the submitted stone and a final decision must be made, taking into account all of the information available. In GIA laboratories, each stone and its corresponding data are always examined by at least two gemologists. If there are any discrepancies in their origin conclusions, the matter is discussed more fully, potentially involving additional gemologists, and all the gemologists involved must come together to reach an agreeable final decision. Ideally the evidence provided is sufficient to guide the geographic origin call to a specific location; however, in some cases when inclusion data or trace element chemistry are ambiguous, an inconclusive call is warranted. Once the gemologists have come to a conclusion on a geographic origin call, the stone can be finalized, an origin report is issued, and the stone is returned to its owner.

APPLICATION OF ANALYTICAL METHODS FOR GEOGRAPHIC ORIGIN DETERMINATION

Using traditional gemological techniques and advanced analytical instrumentation to collect robust and reliable data on gemstones can be extremely challenging. Often the biggest hurdle is to adapt analytical instruments originally designed for scientific specimens so that they analyze faceted gemstones in a nondestructive manner. However, sometimes the bigger challenge is to then take the information collected on a gemstone and synthesize the data in such a way as to aid in geographic origin determination. The following section provides a review of previous work approaching the origin determination problem using advanced analytical methods, with some examples of how the data produced has been used to deduce geographic origin for certain gemstones. Additionally, this special issue contains five articles that will detail GIA's methodology for geographic origin determination for blue sapphire, ruby, emerald, Paraíba-type tourmaline, and alexandrite (see the five gemstone-specific origin articles in this issue). These articles highlight the specific data collected for each material and the procedures that GIA gemologists follow for taking that data and making an origin call.

Corundum. Origin determination of corundum, especially blue sapphires, is challenging (Hainschwang and Notari, 2015; Palke et al., 2019a,b, pp. 536–579 and pp. 580–612 of this issue). To begin with, a number of microscopic features are common to corundum from many deposits. Therefore, inclusion characteristics must be considered very carefully in using this information to make an origin call, or to know when the inclusion information is too ambiguous to be used in origin determination. The most common inclusion in corundum is epitaxial rutile that is crystallographically aligned to the host corundum. Twinning is also a common feature observed globally in corundum along with boehmite intersection tubules associated with the intersection of twinning planes.

Blue sapphires from igneous sources such as Thailand, Cambodia, Ethiopia, Nigeria, and Australia may reveal inclusions that reflect their host rock and growth environment. Colorless feldspar crystals are one of the more common minerals observed in blue sapphires from igneous sources, but other mineral inclusions such as pyrochlore and columbite can be encountered, along with glassy melt inclusions that are highly indicative of igneous origin.

Sapphires from metamorphic deposits such as those in Myanmar, Sri Lanka, or some localities in Madagascar often contain negative crystals (voids with the crystallographic shape of the host corundum) that are filled with carbon dioxide fluid along with diaspore and sometimes graphite. Other solid minerals that are sometimes present are black cubes of uraninite, phlogopite mica, green spinel, or carbonate crystals. (Note that specific criteria used to distinguish blue sapphires based on their inclusion characteristics will be presented in a later article; Palke et al., 2019a, pp. 536–579 of this issue.)

Rarely does a single inclusion type narrow down a particular geographic origin. One notable exception is tourmaline and pargasite in sapphires from Kashmir. However, such inclusions are generally rare and cannot always be counted on to assist in an origin determination.

Rubies often contain inclusions that are representative of the geologic conditions or host rock that is responsible for their formation. For example, rubies from marble deposits often contain rounded grains of protogenetic calcite. They may also contain other mineral inclusions common to such an environment, includ-

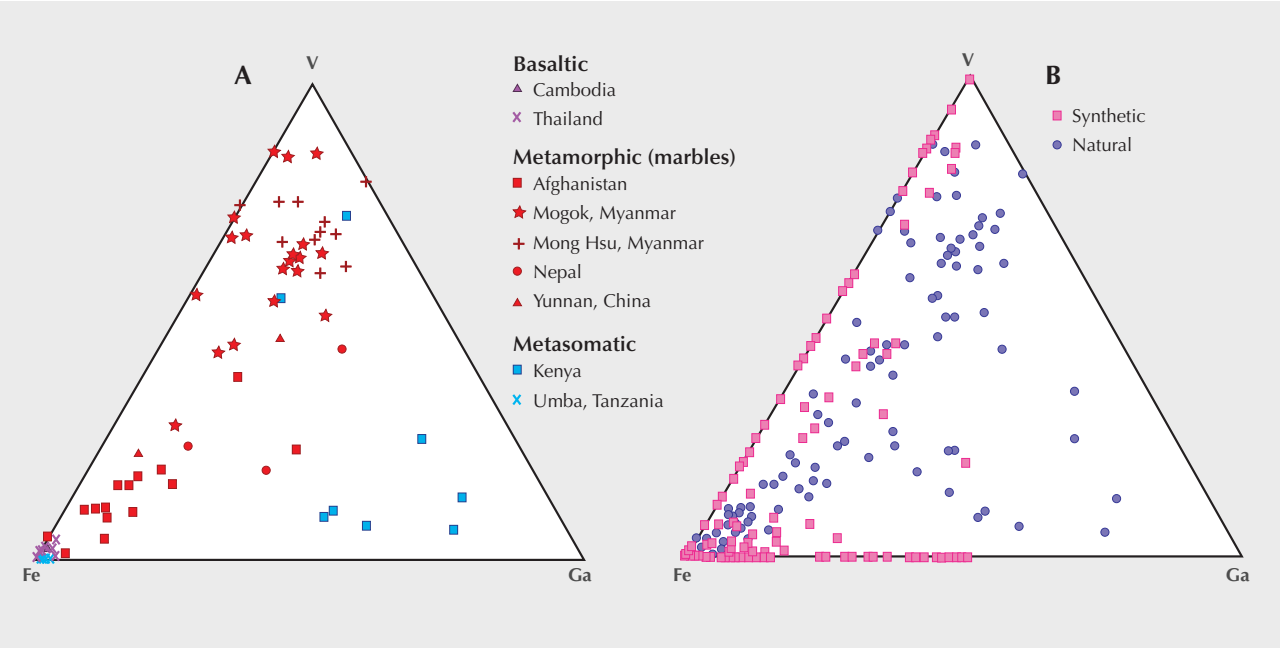

Figure 13. Chemical compositions of natural and synthetic rubies (from Giuliani et al., 2014a; modified from Muhlmeister et al., 1998). Gallium (Ga)-V-Fe diagrams (in wt.%) for (A) natural ruby from different deposits, and (B) natural versus synthetic ruby.

ing graphite, apatite, phlogopite, or rutile. Rubies from basalt-related sources such as Thailand and Cambodia showcase an entirely different suite of inclusions that would not be present in stones from metamorphic or metasomatic deposits. Glassy melt inclusions are one of the most common and diagnostic inclusions for rubies of igneous origin, and these stones can also contain other minerals such as metal sulfides.

Rubies from metasomatic deposits such as those associated with amphibolites (for example, the Montepuez deposit in Mozambique) often host elongated rods of pargasite inclusions that reflect their geological genesis. (Note that specific criteria used to distinguish rubies of various geographic origins are presented in more detail in Palke et al. (2019b), pp. 580–612 of this issue.)

Trace elements are often used for origin determination of corundum because the species and concentrations are a function of (1) the source of the elements and (2) the genesis of the corundum-bearing deposits—i.e., crystallization from a magma (syenite) or from fluid-rock interaction through metamorphic reactions (amphibolite).

Origin determination of corundum based on chemical composition was initiated by Muhlmeister et al. (1998), who used energy-dispersive X-ray fluorescence to study trace elements in 283 natural and synthetic rubies from 14 localities and 12 manufacturers. They found that the Ti, V, Fe, and Ga contents, when considered together as a trace element signature, provided a means of separating nearly all synthetic from natural rubies. This signature could also be used to establish the geological environment in which a ruby formed, and thus imply a geographical origin (figure 13). In particular, they found that ruby from basalts (from Thailand and Cambodia) is Fe-rich and V- and Ga-poor, while marble-hosted ruby (from Afghanistan, Myanmar, Nepal, and China) is V-rich and Ga- and Fe-poor (except ruby from Afghanistan and some rubies from China, Nepal, and the Mogok mines in Myanmar). Metasomatic ruby found in different types of rocks and geological settings showed wide variation in trace element concentrations.

Peucat et al. (2007) analyzed corundum from different geological environments using LA-ICP-MS and proposed using the Fe, Ti, Cr, Ga, and Mg contents and ratios (such as Ga/Mg, Fe/Ti, Fe/Mg, and Cr/Ga) for origin determination of sapphires. In some cases, however, the use of these chemical diagrams is not useful for discriminating between geologic and geographic origin or either. Figure 14 shows the extreme diversity of trace element chemistry of plumasite-related sapphires from the Greek island of Naxos (Voudouris et al., 2019). They overlap the chemical domains of sapphires from Mogok, Umba, and Mer-

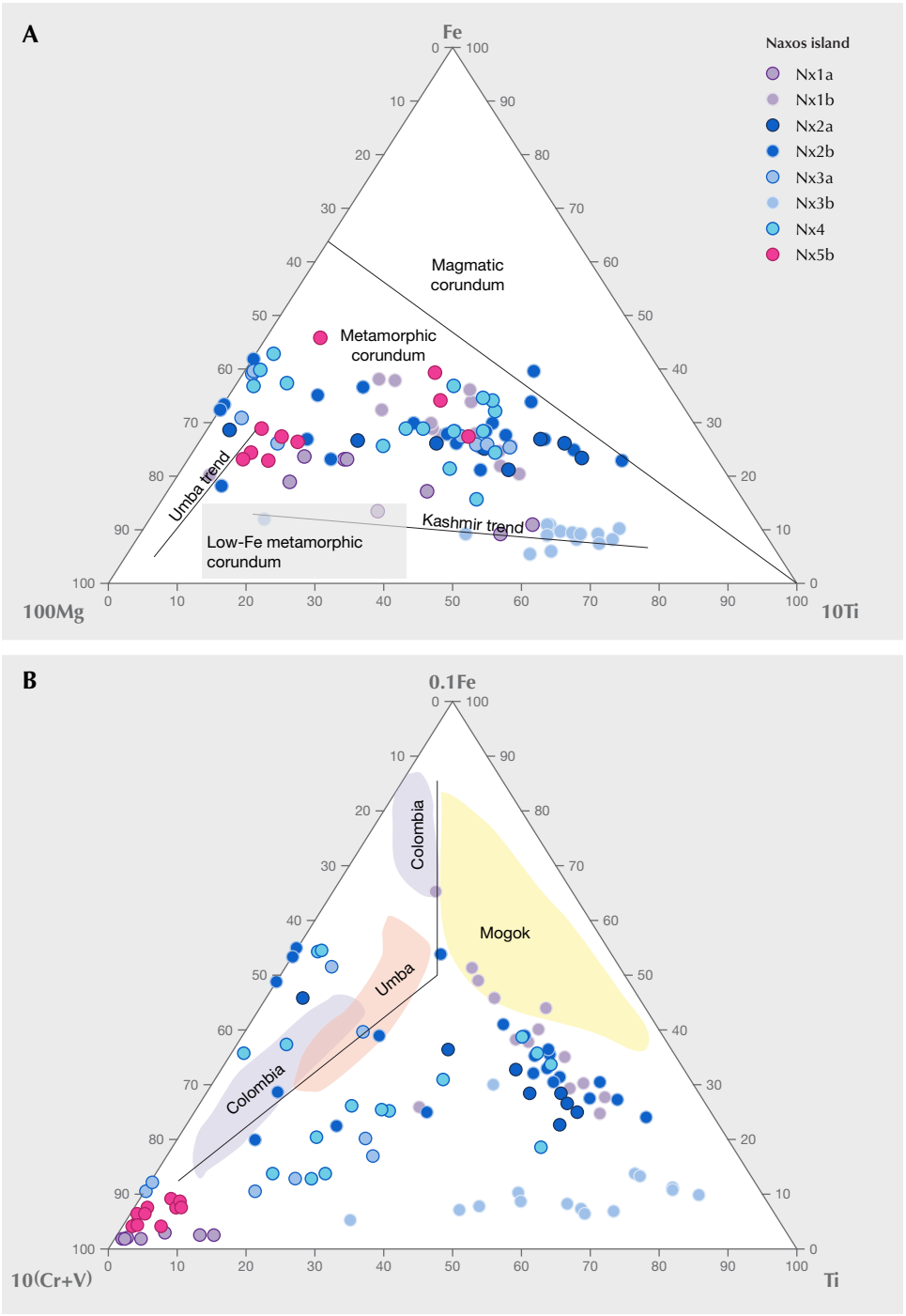

Figure 14. A: 100×Mg–Fe–10×Ti ternary discrimination diagram used for geological and geographical determination of blue sapphires. Modified from Voudouris et al. (2019). B: 0.1×Fe–10×(Cr + V)–Ti ternary diagram showing the chemical fields for blue sapphires from different deposits. Trace element data from Naxos sapphires are plotted as well to show how sapphires from a single geographic locale can overlap with several other important geologically distinct sapphire-producing regions.

caderes in Colombia, which are of different geological types. The Fe versus Ga/Mg diagram in figure 15 corroborates this conclusion, with the majority of Naxos sapphires scattered in the field of metamorphic sapphires, but with some blue and pink sapphires overlapping the field of sapphires from Yogo Gulch in Montana, which are magmatic. The Naxos case illustrates the complexity and ambiguity of the use of trace element chemistry. Observations of GIA's colored stone reference database for blue sapphires suggest the overlap in metamorphic and magmatic blue sapphires may be more extensive than previously known; see Palke et al. (2019a), pp. 536–579 of this issue. The application of the parameters from Peucat et al. (2007) to blue sapphires associated with alkali basalts permitted discrimination of: (1) magmatic

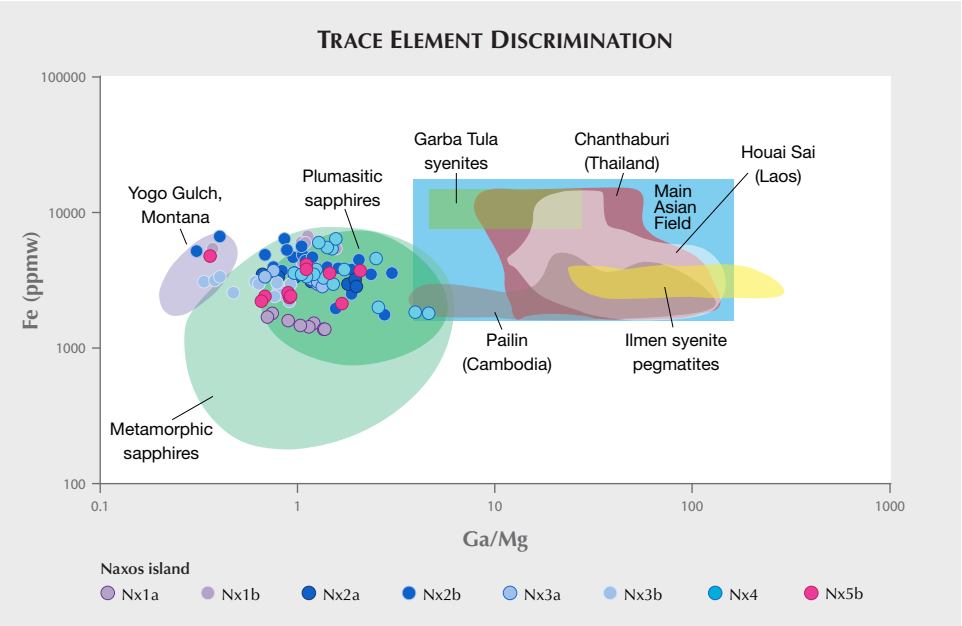

Figure 15. Ga/Mg versus Fe discrimination diagram for sapphires. From Voudouris et al. (2019).

blue sapphires that are Fe-rich (average 2000–11000 Fe ppmw), Ga-rich (>140 ppmw), and Mg-poor (<20 ppmw), with a Ga/Mg ratio >10; and (2) metamorphic pastel blue sapphires that are Fe-poor (average Fe <3000 ppmw), Ga-poor (<75 ppmw), and Mg-rich (>60 ppmw), with a low average Ga/Mg ratio (<10). The chemical parameters defined for the pastel blue sapphires are similar to those determined for blue sapphires from metamorphic areas such as Myanmar (Mogok), Sri Lanka, and Madagascar (Ilakaka). Using the Ga/Mg versus Fe diagram (figure 15), Voudouris et al. (2019) defined a field for sapphire-bearing plumasites formed via metasomatism of pegmatites.

Giuliani et al. (2012) proposed the use of the FeO – Cr_2O_3 – MgO – V_2O_3 versus FeO + TiO_2 + Ga_2O_3 diagram (figure 16) for the classification of primary deposits. This diagram uses Fe (FeO) as a major or minor trace element in corundum; the FeO content permits discrimination of the two prominent types of ruby: Fe-poor rubies in marbles and Fe-rich rubies in mafic-ultramafic rocks (Long et al., 2004). The second method used to discriminate ruby and sapphire is the addition (y-axis parameter) or subtraction from FeO (x-axis parameter) of trace elements associated prefer-

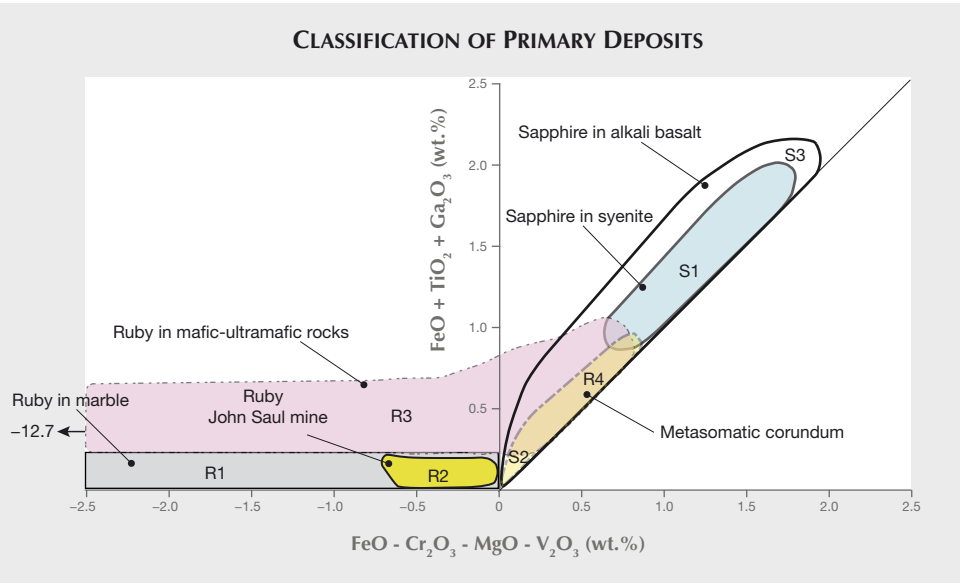

Figure 16. An FeO – Cr_2O_3 – MgO – V_2O_3 versus FeO + TiO_2 + Ga_2O_3 diagram (in wt.%) for classifying corundum deposits (Giuliani et al., 2010; 2014a,b). The R1 field corresponds to ruby in marble, R2 to ruby from the John Saul mine (Kenya), R3 to ruby from mafic and ultramafic rocks, R4 to ruby from metasomatites, S1 to sapphire from syenitic rocks, S2 to sapphire from metasomatites, and S3 to sapphire xenocrysts in alkali basalt and lamprophyre.

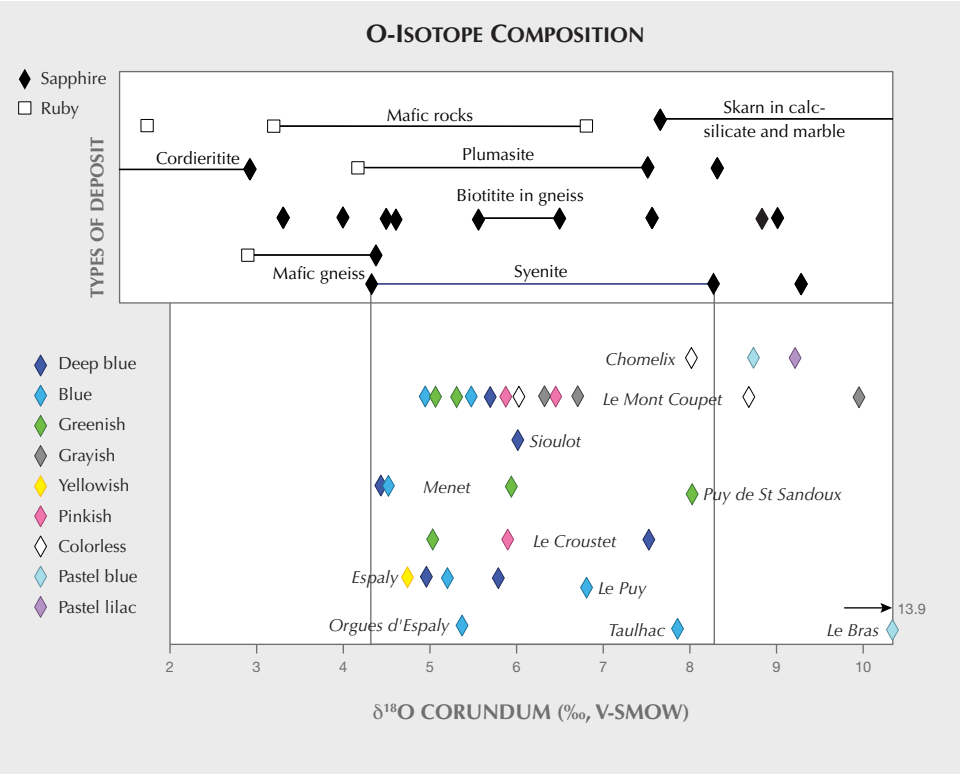

Figure 17. Oxygen isotope values of colored sapphires found in placers within the volcanic fields of the French Massif Central (Giuliani et al., 2009), with reference to the worldwide O isotopic database of corundum reported by Giuliani et al. (2005, 2007, 2009). The data are reported in the conventional delta notation ($\delta^{18}O$, expressed in per mil, ‰) relative to V–SMOW (Vienna Standard Mean Ocean Water).

entially with ruby (Cr_2O_3, V_2O_3, and MgO) or sapphire (TiO_2 and Ga_2O_3). The different types of corundum deposits are: *for ruby*, marble (R1), John Saul ruby mine (Kenya) type (R2), mafic and ultramafic rocks (R3), and metasomatites (R4); *for sapphire*, syenitic rocks (S1), metasomatites (S2), and xenocrysts in alkali-basalt and lamprophyre (S3). There is considerable overlap between the different domains (figure 16).

Oxygen makes up 47 wt.% of the composition of corundum. The two main stable isotopes are ^{18}O and ^{16}O, and data are reported in the conventional $\delta^{18}O$ notation ($^{18}O/^{16}O$ ratio) as per mil (‰) relative to Vienna Standard Mean Ocean Water (VSMOW). The $\delta^{18}O$ value in corundum presents an additional tool for deciphering its geological origin (Yui et al., 2003, 2006; Giuliani et al., 2005, 2007, 2009, 2014a; Zaw et al., 2006; Sutherland et al., 2009). As mantle and crustal rocks show distinct O isotope compositions, the $\delta^{18}O$ value permits investigation of the origin and source of corundum. Giuliani et al. (2007, 2014a) outlined the following principal genetic groups using $\delta^{18}O$ values of sapphire and ruby and their host rocks: (1) *for ruby*: marble, desilicated pegmatite in marble, John Saul mine type, mafic-ultramafic rocks, mafic gneiss, and alkali basalt; (2) *for sapphire*: desilicated pegmatite and skarn vein in marble, syenite, desilicated pegmatite in mafic-ultramafic rocks, cordierite, biotite schist in gneiss, and alkali basalt and lamprophyres.

An example of the use of O-isotope composition to investigate geological origin is that of BGY (blue-green-yellow) sapphires associated with alkali basalts from the French Massif Central (Giuliani et al., 2009). The sapphire crystals are dominantly pastel blue, pastel lilac, and colorless, or they are blue, deep blue, greenish, grayish, yellowish, pinkish, and bronze-colored but milky. The O-isotope composition of the sapphires ranges from 4.4 to 13.9‰ (figure 17). Two distinct groups have been defined. The first shows a restricted isotopic range between 4.4 and 6.8‰ (n = 22; mean $\delta^{18}O = 5.6 \pm 0.7$‰), falling within the worldwide range defined for BGY sapphires related to basaltic gem fields ($3.0 < \delta^{18}O < 8.2$‰, n = 150), and overlapping the range defined for magmatic sapphires in syenite ($4.4 < \delta^{18}O < 8.3$‰, n = 29). The presence of inclusions of columbite-group minerals, pyrochlore, Nb-bearing rutile, and thorite in these sapphires provides an additional argument for a magmatic origin. A second group, with an isotopic range between 7.6 and 13.9‰ (n = 9), suggests a metamorphic sapphire source such as biotite schist in gneisses or skarns. These are metamorphic sapphires occurring in the granulite facies.

Emerald. Inclusions in emeralds can be used to determine geographic origin if they are from hydrothermal or schist-hosted environments. Hydrothermal emeralds, such as those from Colombia, often contain

rhombohedral crystals of calcite and brassy yellow grains of pyrite. Schist-hosted emeralds, such as those from Zambia, Russia, and Ethiopia, commonly contain biotite mica and skeletal exsolution products of ilmenite and hematite.

Fluid inclusions in hydrothermal emeralds are jagged in shape because they result from secondary healing of fractures while still in the growth environment. Schist-hosted emeralds commonly show elongated, blocky primary fluid inclusions that reflect the crystal structure of the host beryl. Until recently, three-phase (gas, liquid, solid) inclusions in emerald were considered a reliable indicator of Colombian origin. However, we now know that such inclusions are often seen in emeralds from other countries including Afghanistan (Panjshir Valley), China (Davdar), and Zambia (Musakashi) (Saeseaw et al., 2014, and references therein). Saeseaw et al. (2014) studied 84 samples from these deposits and Colombian deposits and reported that in most cases the combination of inclusion details, UV-Vis-NIR absorption data, and trace element chemistry can help determine the origin of emeralds with three- or multiphase inclusions.

Zwaan et al. (2012) studied emeralds from the Fazenda Bonfim region of Brazil and showed that they can be distinguished from those of other schist- and pegmatite-related commercial deposits, such as Kafubu in Zambia and Sandawana in Zimbabwe, by careful comparison of internal features and physical and chemical properties. They observed that the properties of the Fazenda Bonfim emeralds show the most overlap with emeralds from the Itabira district of Brazil, but can be differentiated by their significantly higher cesium (Cs) and generally lower sodium (Na) contents.

Schwarz and Klemm (2012) used LA-ICP-MS to obtain approximately 2,600 spot analyses of 40 major and trace elements from approximately 650 emerald samples from 21 different occurrences worldwide. They reported that the analyses provided a solid basis for genetic interpretations and (together with additional criteria) origin determination.

Schwarz (2015) continued with three case studies: Cordillera Oriental in Colombia, Santa Terezinha in Brazil, and Swat Valley in Pakistan. He noted that when the emeralds crystallized in very different geological-genetic environments (e.g., black shales in Colombia and phlogopite schists and carbonate-talc schists at Santa Terezinha), their mineralogical-gemological properties are also very different and they are easily distinguished. However, if the geological-genetic environment is the same or nearly identical for two deposits (as is the case with Santa Terezinha and Swat Valley), the stones from them can sometimes show overlapping features. The separation of emeralds from such deposits can be difficult or even impossible.

Conversely, Hainschwang and Notari (2015) reported that the geographic origin of emerald can usually be determined with very high probability. In some cases, growth features and inclusions alone are sufficient to declare a geographic origin, but for many stones a combination of spectroscopic and chemical testing is used. For the latter, they identified the most important elements as Cr, V, Fe, Ga, Sc, and Cs, and sometimes rare earth elements. They noted that most emeralds from Colombia have very low Fe and high Cr and V contents, while many other deposits that are commercially important, such as Kafubu in Zambia, produce emeralds with much higher Fe content and typically much more Cr than V.

Ochoa et al. (2015) used X-ray fluorescence and infrared and Raman spectroscopy to study 530 samples from 35 mines in Colombia and Afghanistan and Brazil. Average Fe and Sc concentrations and a ternary Fe-Cr-V diagram could be used to distinguish between Colombian emeralds and those from Afghanistan and Brazil. They also used the ternary Fe-Cr-V diagram and Cr/V ratio to distinguish samples from Chivor and Gachalá from other mines in Colombia. The Cr/V ratio was used to distinguish Colombian gems from Brazilian, while the infrared data were able to separate Colombian from Afghan and Brazilian emeralds.

Aurisicchio et al. (2018) analyzed 17 emerald crystals from different worldwide deposits with EMP and SIMS. They then used principal component analysis (PCA) to study the major and trace element data and were able to discriminate each deposit with high reliability. They were also able to distinguish between emeralds related to granitic-pegmatitic intrusions and those occurring in environments controlled by tectonic events. Finally, Saeseaw et al. (2019), pp. 614–646 of this issue, details how trace element chemistry from LA-ICP-MS is used in GIA laboratories to determine geographic origin for emeralds.

Because H_2O in the channels in beryl represents the original fluid composition from the time of formation (Aines and Rossman, 1984; Brown and Mills, 1986; Taylor et al., 1992), the δD (ratio of the two stable isotopes of hydrogen, ^1H and ^2H; the latter is deuterium, hence "D") in H_2O released from beryl can be used to determine the source of the fluids from which the beryl grew (figure 18). This has been done for beryl from a number of deposits (Fallick and Barros, 1987; Taylor et al., 1992; Arif et al., 1996; Giuliani et al., 1997a,b, 1998, 2000b). In addition,

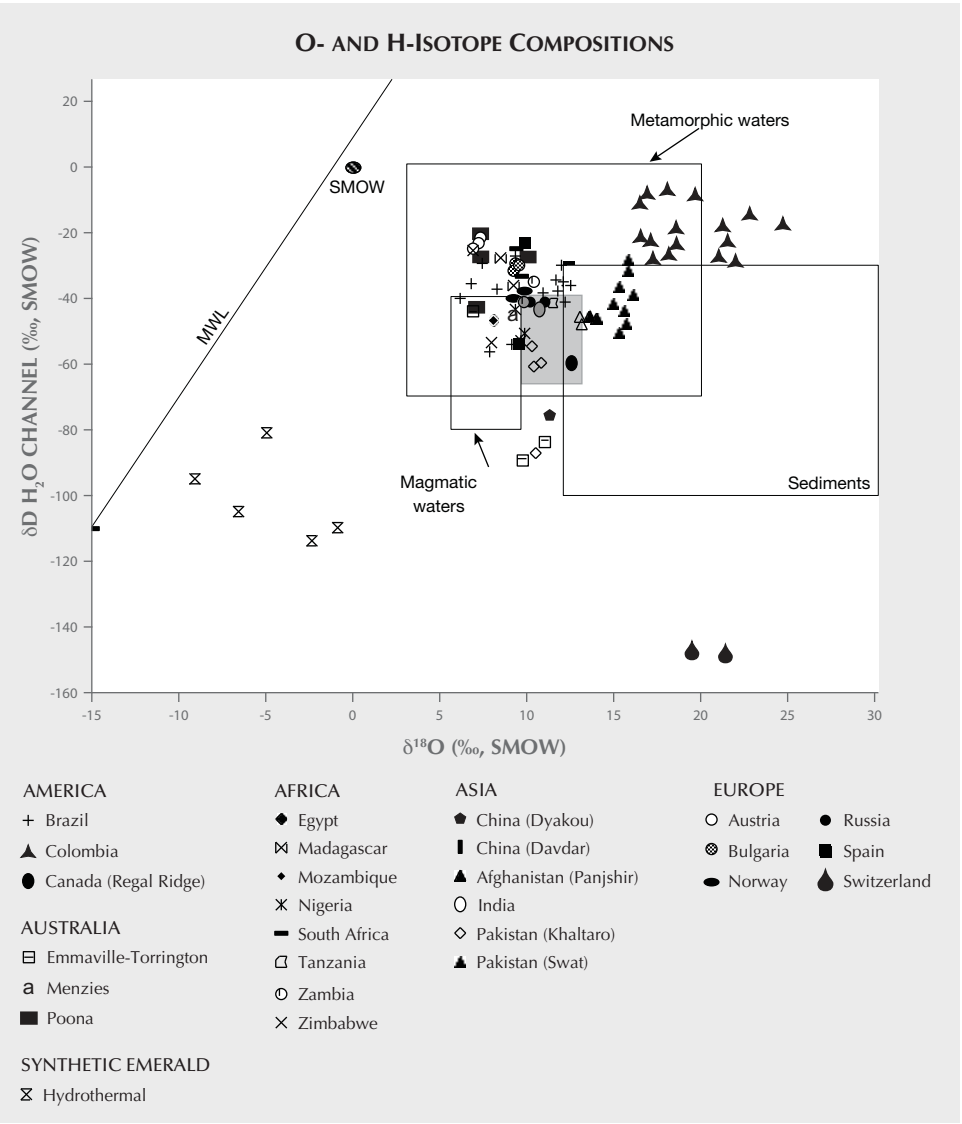

Figure 18. Channel $\delta^{18}O$ versus δD H_2O for emerald worldwide (Marshall et al., 2017 and references therein). The isotopic compositional fields are from Sheppard (1986), including the extended (Cornubian) magmatic water box (gray). MWL = Meteoric Water Line, SMOW = Standard Mean Ocean Water.

Giuliani et al. (2000a) used isotopic compositions of historical emerald artifacts to show that early artisans worked with emeralds originating from deposits supposedly discovered in the twentieth century, and that most of the high-quality emeralds cut in the eighteenth century in India originated from Colombia.

CONCLUSIONS

The last decade has seen unprecedented growth in the technological capacity of the modern gemological laboratory. Much of this technological advancement has resulted from the enormous pressure placed on gemological labs to provide geographic origin determination services for gemstones, especially corundum and emerald. The gem and jewelry industry often uses origin to set a stone's value. However, the geological forces that created many gems are sometimes apparently so similar across geographic localities that their physical and/or chemical properties can be difficult or essentially impossible to distinguish using the advanced instrumentation available to most gemological laboratories. GIA and other gemological research leaders are actively exploring the frontiers of new technology in analytical instrumentation to find additional criteria, such as isotopic measurements, photoluminescence analyses, and advanced statistical methods, to improve the accuracy of geographic origin determination. While there is hope in this regard, the geological origin for some stones and thus their physical properties are so similar that a definitive origin call cannot be made every time, even with the most advanced technological capabilities.

ABOUT THE AUTHORS

Dr. Groat is a professor in the Department of Earth, Ocean and Atmospheric Sciences at the University of British Columbia in Vancouver. Dr. Giuliani is a senior researcher at Université Paul Sabatier, GET/IRD and Université de Lorraine, CRPG/CNRS, Vandœuvre, France. Dr. Stone-Sundberg is a research scientist and technical editor of Gems & Gemology. *Mr. Sun is a research associate, Mr. Renfro is manager of colored stone identification, and Dr. Palke is a senior research scientist, at GIA in Carlsbad, California.*

ACKNOWLEDGMENTS

Authors LAG and GG would like to thank GIA for inviting us to coauthor this contribution.

REFERENCES

Abdalla H.M., Mohamed F.H. (1999) Mineralogical and geochemical investigations of beryl mineralisation, Pan-African belt of Egypt: Genetic and exploration aspects. *Journal of African Earth Sciences*, Vol. 28, No. 3, pp. 581–598, http://dx.doi.org/10.1016/S0899-5362(99)00033-0

Abduriyim A., Kitawaki H. (2006) Applications of laser ablation–inductively coupled plasma–mass spectrometry (LA-ICP-MS) to gemology. *G&G*, Vol. 42, No. 2, pp. 98–118, http://dx.doi.org/10.5741/GEMS.42.2.98

Aines R.D., Rossman G.R. (1984) The high-temperature behavior of water and carbon dioxide in cordierite and beryl. *American Mineralogist*, Vol. 69, No. 3-4, pp. 319–327.

Alexandrov P., Giuliani G., Zimmerman J.L. (2001) Mineralogy, age and fluid geochemistry of the Rila Emerald deposits, Bulgaria. *Economic Geology*, Vol. 96, No. 6, pp. 1469–1476, http://dx.doi.org/10.2113/gsecongeo.96.6.1469.

Andrianjakavah P.R., Salvi S., Béziat D., Rakotondrazafy A.F.M., Giuliani G. (2009) Proximal and distal styles of pegmatite-related metasomatic emerald mineralization at Ianapera, southern Madagascar. *Mineralium Deposita*, Vol. 44, No. 7, pp. 817–835, http://dx.doi.org/10.1007/s00126-009-0243-5

Arif M., Fallick A.E., Moon A.E. (1996) The genesis of emeralds and their host rocks from Swat, northwestern Pakistan: A stable-isotope investigation. *Mineralium Deposita*, Vol. 31, No. 4, pp. 255–268, http://dx.doi.org/10.1007/BF02280790

Artioli R., Rinaldi R., Stahl K., Zanazzi P.F. (1993) Structure refinements of beryl by single-crystal neutron and X-ray diffraction. *American Mineralogist*, Vol. 78, No. 7, pp. 762–768.

Aurisicchio C., Conte A.M., Medeghini L., Ottolini L., De Vito C. (2018) Major and trace element geochemistry of emerald from several deposits: Implications for genetic models and classification schemes. *Ore Geology Reviews*, Vol. 94, pp. 351–366, http://dx.doi.org/10.1016/j.oregeorev.2018.02.001

Beus A.A., Mineev D.A. (1972) *Some Geological and Geochemical Features of the Muzo-Coscuez Emerald Zone, Cordillera Oriental, Colombia*. Empresa Colombiana de Minas, Bogotá, 55 pp.

Brand A.A., Groat L.A., Linnen R.L., Garland M.I., Breaks F.W., Giuliani G. (2009) Emerald mineralization associated with the Mavis Lake pegmatite group, near Dryden, Ontario. *Canadian Mineralogist*, Vol. 47, No. 2, pp. 315–336, http://dx.doi.org/10.3749/canmin.47.2.315

Brown G.E. Jr., Mills B.A. (1986) High-temperature structure and crystal chemistry of hydrous alkali-rich beryl from the Harding pegmatite, Taos County, New Mexico. *American Mineralogist*, Vol. 71, No. 3-4, pp. 547–556.

Cesbron F., Lebrun P., Le Cléaćh J.M., Notari F., Grobon C., Deville J. (2002) *Corindon et spinelles: histoire, cristallochimie, minéralogie, gemmologie, gisements, utilisations, synthèse*. Minéraux et Fossiles, No. 15, CEDIM, Paris, 104 pp.

Conklin L.H. (2002) What is emerald – fact and opinion. *extra-Lapis English*, Vol. 2, pp. 72–73.

Emmett J.L., Scarratt K., McClure S.F., Moses T., Douthit T.R., Hughes R., Novak S., Shigley J.E. (2003) Beryllium diffusion of ruby and sapphire. *G&G*, Vol. 39, No. 2, pp. 84–135, http://dx.doi.org/10.5741/GEMS.39.2.84

Emmett J.L., Stone-Sundberg J., Guan Y., Sun Z. (2017) The role of silicon in the color of gem corundum. *G&G*, Vol. 53, No. 1, pp. 42–47, http://dx.doi.org/10.5741/GEMS.53.1.42

Fallick A.E., Barros J.G. (1987) A stable-isotope investigation into the origin of beryl and emerald from the Porangatu deposits, Goiás state, Brazil. *Chemical Geology: Isotope Geoscience Section*, Vol. 66, No. 3-4, pp. 293–300, http://dx.doi.org/10.1016/0168-9622(87)90048-0

Fallick A.E., Jocelyn T., Donnelly M., Guy M., Behan C. (1985) Origin of agates in volcanic rocks from Scotland. *Nature*, Vol. 313, No. 6004, pp. 672–674, http://dx.doi.org/10.1038/313672a0

Garstone J.D. (1981) The geological setting and origin of emeralds from Menzies, Western Australia. *Journal of the Royal Society of Western Australia*, Vol. 64, pp. 53–64.

Gavrilenko E.V., Pérez B.C. (1999) Characterisation of emeralds from the Delbegetey deposit, Kazakhstan. In C.J. Stanley et al., Eds., *Mineral Deposits: Processes to Processing Balkema.* Rotterdam, The Netherlands, pp. 1097–1100.

Gavrilenko E.V., Calvo Pérez B., Castroviejo Bolibar R., Garcia Del Amo D. (2006) Emeralds from the Delbegetey deposit (Kazakhstan): Mineralogical characteristics and fluid-inclusion study. *Mineralogical Magazine*, Vol. 70, No. 2, pp. 159–173, http://dx.doi.org/10.1180/0026461067020321

Giuliani G., Fallick A.E. (2018) Isotope signatures of gem minerals. *Wooshin*, Vol. 5, pp. 2–9.

Giuliani G., Groat L.A. (2019) Geology of corundum and emerald gem deposits: A review. *G&G*, Vol. 55, No. 4, pp. 464–489, http://dx.doi.org/10.5741/GEMS.55.4.464

Giuliani G., France-Lanord C., Zimmermann J.L., et al. (1997a) Fluid composition, δD of channel H_2O, and $\delta^{18}O$ of lattice oxygen in beryls: Genetic implications for Brazilian, Colombian, and Afghanistani emerald deposits. *International Geology Review*, Vol. 39, No. 5, pp. 400–424, http://dx.doi.org/10.1080/00206819709465280

Giuliani G., Cheilletz A., Zimmermann J.L., Ribeiro-Althoff A.M., France-Lanord C., Feraud G. (1997b) Les gisements d'émeraude du Brésil: genèse et typologie. *Chronique de la Recherche Minière*, Vol. 526, pp. 17–61.

Giuliani G., France-Lanord C., Coget P., Schwarz D., Cheilletz A., Branquet Y., Giard D., Martin-Izard A., Alexandrov P., Piat D.H. (1998) Oxygen isotope systematics of emerald: Relevance of its origin and geological significance. *Mineralium Deposita*, Vol 31, No. 5, pp. 513–519, http://dx.doi.org/10.1007/s001260050166

Giuliani G., Chaussidon M., Schubnel H.-J., et al. (2000a) Oxygen isotopes and emerald trade routes since antiquity. *Science*, Vol. 287, No. 5453, pp. 631–633, http://dx.doi.org/10.1126/science.287.5453.631

Giuliani G., Christian F., Cheilletz A., Coget P., Branquet Y., Laumonier B. (2000b) Sulfate reduction by organic matter in Colombian emerald deposits: Chemical and stable isotope (C, O, H) evidence. *Economic Geology*, Vol. 95, No. 5, pp. 1129–1153, http://dx.doi.org/10.2113/95.5.1129

Giuliani G., Fallick A.E., Garnier V., France-Lanord C., Ohnenstetter D., Schwarz D. (2005) Oxygen isotope composition as a tracer for the origins of rubies and sapphires. *Geology*, Vol.

33, No. 4, pp. 249–252, http://dx.doi.org/10.1130/G21261.1
Giuliani G., Ohnenstetter D., Garnier V, Fallick A.E., Rakotondrazafy A.F.M., Schwarz D. (2007) The geology and genesis of gem corundum deposits. In L.A. Groat, Ed., *Geology of Gem Deposits*, 1st ed. Mineralogical Association of Canada, Short Course Series 37, Yellowknife, Canada, pp. 23–78.
Giuliani G., Fallick A.E., Ohnenstetter D., Pegere G. (2009) Oxygen isotopes composition of sapphires from the French Massif Central: Implications for the origin of gem corundum in basaltic fields. *Mineralium Deposita*, Vol. 44, No. 2, pp. 221–231, http://dx.doi.org/10.1007/s00126-008-0214-2
Giuliani G., Lasnier B., Ohnenstetter D., Fallick A.E., Pégère G. (2010) Les gisements de corindon de France. *le Règne Minéral*, Vol. 93, pp. 5–22.
Giuliani G., Ohnenstetter D., Fallick A.E., Groat L., Feneyrol J. (2012) Geographic origin of gems linked to their geographical history. *InColor*, No. 19, pp. 16–27.
Giuliani G., Ohnenstetter D., Fallick A.E., Groat L., Fagan J. (2014a) The geology and genesis of gem corundum deposits. In L.A. Groat, Ed., *Geology of Gem Deposits*, 2nd ed. Mineralogical Association of Canada, Short Course Series 44, pp. 29–112.
Giuliani G., Caumon, G., Rakotosamizanany S., et al. (2014b) Classification chimique des corindons par analyse factorielle discriminante : application à la typologie des gisements de rubis et saphirs. *Revue de Gemmologie a.f.g.*, Vol. 188, pp. 14–22.
Giuliani G., Groat L.A., Marshall D., Fallick A.E., Branquet Y. (2019) Emerald deposits: A review and enhanced classification. *Minerals*, Vol. 9, No. 2, pp. 105–168, http://dx.doi.org/10.3390/min9020105
Graziani G., Gübelin E., Lucchesi S. (1983) The genesis of an emerald from the Kitwe District, Zambia. *Neues Jahrbuch für Mineralogie Monatschefte*, Vol. 1983, pp. 175–186.
Groat L.A., Marshall D.D., Giuliani G., et al. (2002) Mineralogical and geochemical study of the Regal Ridge showing emeralds, southeastern Yukon. *Canadian Mineralogist*, Vol. 40, No. 5, pp. 1313–1338, http://dx.doi.org/10.2113/gscanmin.40.5.1313
Groat L.A., Giuliani G., Marshall D.D., Turner D.J. (2008) Emerald deposits and occurrences: A review. *Ore Geology Reviews*, Vol. 34, No. 1-2, pp. 87–112, http://dx.doi.org/10.1016/j.oregeorev.2007.09.003
Gübelin E.J. (1958) Emeralds from Sandawana. *Journal of Gemmology*, Vol. 6, No. 8, pp. 340–354.
Hainschwang T., Notari, F. (2015) Standards and protocols for emerald analysis in gem testing laboratories. *InColor*, pp. 106–114.
Hammarstrom J.M. (1989) Mineral chemistry of emeralds and some minerals from Pakistan and Afghanistan: An electron microprobe study. In A.H. Kazmi, L.W. Snee, Eds., *Emeralds of Pakistan*. Van Nostrand Reinhold, New York, pp. 125–150.
Hänni H.A. (1994) Origin determination for gemstones: Possibilities, restrictions and reliability. *Journal of Gemmology*, Vol. 24, No. 3, pp. 139–148.
Hänni H.A., Klein H.H. (1982) Ein Smaragdvorkommen in Madagaskar. *Zeitschrift der Deutschen Gemmologischen Gesellschaft,* Vol. 21, pp. 71–77.
Hickman A.C.J. (1972) The Miku emerald deposit. *Geological Survey of Zambia, Economic Report,* Vol. 27, pp. 35.
Hughes R.W. (1997) *Ruby & Sapphire*. RWH Publishing, Boulder, Colorado, 512 pp.
Hughes R.W., Manorotkul W., Hughes E.B. (2017) *Ruby and Sapphire: A Gemologist's Guide*, RWH Publishing/Lotus Publishing, Thailand, 738 pp.
Kovaloff P. (1928) Geologist's report on Somerset emeralds. *South African Mining and Engineering Journal*, Vol. 39, pp. 101–103.
Kozlowski A., Metz P., Jaramillo H.A.E. (1988) Emeralds from Somondoco, Colombia: Chemical composition, fluid inclusion and origin. *Neues Jahrbuch für Mineralogie Abhandlungen*, Vol. 59, pp. 23–49.
Lake D.J., Groat L., Falck H., Cempirek J., Kontak D., Marshall D., Giuliani G., Fayek M. (2017) Genesis of emerald-bearing quartz veins associated with the Lened W-skarn mineralization, Northwest Territories, Canada. *Canadian Mineralogist*, Vol. 55, No. 4, pp. 561–593, http://dx.doi.org/10.3749/canmin.1700025
Leitmeier H. (1937) Das Smaragdvorkommen in Habachtal in Salzburg und seine Mineralien. *Zeitschrift für Kristallographie, Mineralogie und Petrographie*, Vol. 49, No. 4-5, pp. 245–368, http://dx.doi.org/10.1007/BF02945601
Long P.V., Vinh H.Q., Garnier V., et al. (2004) Gem corundum deposits in Vietnam. *Journal of Gemmology*, Vol. 29, No. 3, pp. 129–147.
Loughrey L., Marshall D., Jones P., Millsteed P., Main A. (2012) Pressure-temperature-fluid constraints for the Emmaville-Torrington emerald deposit, New South Wales, Australia: Fluid inclusion and stable isotope studies. *Open Geosciences*, Vol. 4, No. 2, pp. 287–299, http://dx.doi.org/10.2478/s13533-011-0056-9
Loughrey L., Marshall D., Ihlen P., Jones P. (2013) Boiling as a mechanism for colour zonations observed at the Byrud emerald deposit, Eidsvoll, Norway: Fluid inclusion, stable isotope and Ar-Ar studies. *Geofluids*, Vol. 13, No. 4, pp. 542–558, http://dx.doi.org/10.1111/gfl.12051
Marshall D.D., Groat L.A., Falck H., et al. (2004) The Lened emerald prospect, Northwest Territories, Canada: Insights from fluid inclusions and stable isotopes, with implications for Northern Cordilleran emerald. *Canadian Mineralogist*, Vol. 42, No. 5, pp. 1523–1539, http://dx.doi.org/10.2113/gscanmin.42.5.1523
Marshall D., Pardieu V., Loughrey L., Jones P., Xue G. (2012) Conditions for emerald formation at Davdar, China: Fluid inclusion, trace element and stable isotope studies. *Mineralogical Magazine*, Vol. 76, No. 1, pp. 213–226, http://dx.doi.org/10.1180/minmag.2012.076.1.213
Marshall D., Downes P.J., Ellis S., Greene R., Loughrey L., Jones, P. (2016) Pressure-temperature-fluid constraints for the Poona emerald deposits, Western Australia: Fluid inclusion and stable isotope studies. *Minerals*, Vol. 6, No. 4, pp. 130–152, http://dx.doi.org/10.3390/min6040130
Marshall D., Meisser N., Ellis S., Jones P., Bussy F., Mumenthaler T. (2017) Formational conditions for the Binntal emerald occurrence, Valais, Switzerland: Fluid inclusion, chemical composition and stable isotope studies. *Canadian Mineralogist*, Vol. 55, No. 4, pp. 725–741, http://dx.doi.org/10.3749/canmin.1600090
Martin H.J. (1962) Some observations on southern Rhodesian emeralds and chrysoberyl. *Journal of the Chamber of Mines*, Vol. 4, pp. 34–38.
Muhlmeister S., Fritsch E., Shigley J.E., Devouard B., Laurs B.M. (1998) Separating natural and synthetic rubies on the basis of trace-element chemistry. *G&G*, Vol. 34, No. 2, pp. 80–101, http://dx.doi.org/10.5741/GEMS.34.2.80
Nassau K. (1983) *The Physics and Chemistry of Color: The Fifteen Causes of Color*. John Wiley and Sons, New York, 480 pp.
Notari F., Grobon C.C. (2002) Gemmologie du corindon et du spinelle. In *Corindons et Spinelles*, Minéraux et Fossiles 15, Paris, France, pp. 48–59.
Ochoa C.J.C., Daza M.J.H., Fortaleche D., Jiménez J.F. (2015) Progress on the study of parameters related to the origin of Colombian emeralds. *InColor*, pp. 88–97.
Otero Muñoz G., Barriga Villalba A.M. (1948) *Esmeraldas de Colombia*. Banco de la Republica, Bogotá.
Ottaway T.L. (1991) The geochemistry of the Muzo emerald deposit, Colombia. M.Sc. thesis, University of Toronto.
Palke A.C., Saeseaw S., Renfro N.D., Sun Z., McClure S.F. (2019a) Geographic origin determination of blue sapphire. *G&G*, Vol. 55, No. 4, pp. 536–579, http://dx.doi.org/10.5741/GEMS.55.4.536
Palke A.C., Saeseaw S., Renfro N.D., Sun Z., McClure S.F. (2019b) Geographic origin determination of ruby. *G&G*, Vol. 55, No. 4, pp. 580–612, http://dx.doi.org/10.5741/GEMS.55.4.580
Peretti A., Günther D. (2002) The color enhancement of fancy sapphires with a new heat-treatment technique (Part A): Inducing color zoning by internal migration and formation of color centers. *Contributions to Gemology*, Vol. 11, pp. 1–48.
Petrusenko S., Arnaudov V., Kostov I. (1966) Emerald pegmatite from

the Urdini Lakes, Rila Mountains. *Annuaire de l'Université de Sofia Faculté de Géologie et Géographie*. Vol. 59, pp. 247–268.
Peucat J.J., Ruffault P., et al. (2007) Ga/Mg ratios as a new geochemical tool to differentiate magmatic from metamorphic blue sapphires. *Lithos*, Vol. 98, No. 1-4, pp. 261–274, http://dx.doi.org/10.1016/j.lithos.2007.05.001
Rondeau B., Fritsch E., Peucat J.J., Nordru F.S., Groat L.A. (2008) Characterization of emeralds from a historical deposit: Byrud (Eidsvoll), Norway. *G&G*, Vol. 44, No. 2, pp. 108–122, http://dx.doi.org/10.5741/GEMS.44.2.108
Saeseaw S., Pardieu V., Sangsawong S. (2014) Three-phase inclusions in emerald and their impact on origin determination. *G&G*, Vol. 50, No. 2, pp. 114–132, http://dx.doi.org/10.5741/GEMS.50.2.114
Saeseaw S., Renfro N.D., Palke A.C., Sun Z., McClure S.F. (2019) Geographic origin determination of emerald. *G&G*, Vol. 55, No. 4, pp. 614–646, http://dx.doi.org/10.5741/GEMS.55.4.614
Santiago J.S., Souza V.S., et al. (2018) Emerald from the Fazenda Bonfim deposit, northeastern Brazil: Chemical, fluid inclusions and oxygen isotope data. *Brazilian Journal of Geology*, Vol. 48, No. 3, pp. 457–472, http://dx.doi.org/10.1590/2317-4889201820170130
Schwarz D. (1991) Australian emeralds. *Australian Gemmologist*, Vol. 17, No. 12, pp. 488–497.
Schwarz D. (2015) The geographic origin determination of emeralds. *InColor*, pp. 98–105.
Schwarz D., Klemm L. (2012) Chemical signature of emerald. 34th International Geological Congress, Abstract 2812.
Schwarz D., Schmetzer K. (2002) The definition of emerald. *extraLapis English*, Vol. 2, pp. 74–78.
Schwarz D., Kanis J., Kinnaird J. (1996) Emerald and green beryl from central Nigeria. *Journal of Gemmology*, Vol. 25, No. 2, pp. 117–141.
Schwarz D., Pardieu V., Saul J.M., et al. (2008) Rubies and sapphires from Winza, central Tanzania. *G&G*, Vol. 44, No. 4, pp. 322–347, http://dx.doi.org/10.5741/GEMS.44.4.322
Sheppard S.M.F. (1986) Characterization and isotopic variations in natural waters. In J.W. Valley, H.P. Taylor, J.R. O'Neil, Eds., *Stable Isotopes in High Temperature Geological Processes*. Mineralogical Association of America, Chantilly, Virginia, Vol. 16, pp. 165–183.
Simpson E.S. (1948) *Minerals of Western Australia, Vol. 1*. Government Printer, Perth, Australia, pp. 195–207.
Stone-Sundberg J., Thomas T., Sun Z., Guan Y., Cole Z., Equall R., Emmett J.L. (2017) Accurate reporting of key trace elements in ruby and sapphire using matrix-matched standards. *G&G*, Vol. 53, No. 4, pp. 438–451, http://dx.doi.org/10.5741/GEMS.53.4.438
Sunagawa I., Bernhardt H.J., Schmetzer K. (1999) Texture formation and element partitioning in trapiche ruby. *Journal of Crystal Growth*, Vol. 206, No. 4, pp. 322–330, http://dx.doi.org/10.1016/S0022-0248(99)00331-0
Sutherland F.L., Zaw K., Meffre S., Giuliani G., Fallick A.E., Webb G.B. (2009) Gem-corundum megacrysts from east Australian basalt fields: Trace elements, oxygen isotopes and origins. *Australian Journal of Earth Sciences*, Vol. 56, No. 7, pp. 1003–1022, http://dx.doi.org/10.1080/08120090903112109
Taylor R.P., Fallick A.E., Breaks F.W. (1992) Volatile evolution in Archean rare-element granitic pegmatites: evidence from the hydrogen-isotopic composition of channel H_2O in beryl. *Canadian Mineralogist*, Vol. 30, pp. 877–893.
Vapnik Y., Sabot B., Moroz I. (2005) Fluid inclusions in Ianapera emerald, Southern Madagascar. *International Geology Review*, Vol. 47, No. 6, pp. 647–662, http://dx.doi.org/10.2747/0020-6814.47.6.647
Vapnik Y., Moroz I., Eliezri I. (2006) Formation of emeralds at pegmatite-ultramafic contacts based on fluid inclusions in Kianjavato emerald, Mananjary deposits, Madagascar. *Mineralogical Magazine*, Vol. 70, No. 2, pp. 141–158, http://dx.doi.org/10.1180/0026461067020320
Vertriest W., Palke A., Renfro N.D. (2019) Field gemology: Building a research collection and understanding the development of gem deposits. *G&G*, Vol. 55, No. 4, pp. 490–511, http://dx.doi.org/10.5741/GEMS.55.4.490
Vlasov K.A., Kutakova E.I. (1960) *Izumrudnye Kopi*. Moscow Akademiya Nauk SSGR. Moscow, Russia, 252 pp.
Voudouris P., Mavrogonatos C., Graham I., Giuliani G., et al. (2019) Gem corundum deposits of Greece: Geology, mineralogy and genesis. *Minerals*, Vol. 9, No. 1, pp. 49–90, http://dx.doi.org/10.3390/min9010049
Wang W., Hall M., Shen A.H., Breeding C.M. (2006) Developing corundum standards for LA-ICP-MS trace-element analysis. *G&G*, Vol. 42, No. 3, pp. 105–106.
Yui T.F., Zaw K., Limkatrun P. (2003) Oxygen isotope composition of the Denchai sapphire, Thailand: A clue to its enigmatic origin. *Lithos*, Vol. 67, No. 1-2, pp. 153–161, http://dx.doi.org/10.1016/S0024-4937(02)00268-2
Yui T.F., Wu C.-M., Limkatrun P., et al. (2006) Oxygen isotope studies on placer sapphire and ruby in the Chanthaburi-Trat alkali basaltic gemfield, Thailand. *Lithos*, Vol. 86, No. 3-4, pp. 197–211, http://dx.doi.org/10.1016/j.lithos.2005.06.002
Zambonini F., Caglioto V. (1928) Ricerche chimiche sulla rosterite di San Piero in Campo (Isola d'Elba) e sui berilli in generale. *Gazzetta Chimica Italiana*, Vol. 58, pp. 131–152.
Zaszczak J.A. (2013) Word to the wise: Raman spectroscopy in the identification and study of minerals. *Rocks & Minerals*, Vol. 88, No. 2, pp. 184–189, http://dx.doi.org/10.1080/00357529.2013.763698
Zaw K., Sutherland F.L., Dellapasqua F., et al. (2006) Contrasts in gem corundum characteristics, eastern Australian basaltic fields: Trace elements, fluid/melt inclusions and oxygen isotopes. *Mineralogical Magazine*, Vol. 70, No. 6, pp. 669–687, http://dx.doi.org/10.1180/0026461067060356
Zwaan J.C. (2006) Gemmology, geology and origin of the Sandawana emerald deposits, Zimbabwe. *Scripta Geologica*, Vol. 131, pp. 1–211.
Zwaan J.C., Seifert A.V., Vrána S., Laurs B.M., Anckar B., Simmons W.B., et al. (2005) Emeralds from the Kafubu area, Zambia. *G&G*, Vol. 41, No. 2, pp. 116–148, http://dx.doi.org/10.5741/GEMS.41.2.116
Zwaan J.C., Jacob D.E., Häger T., et al. (2012) Emeralds from the Fazenda Bonfim region, Rio Grande do Norte, Brazil. *G&G*, Vol. 48, No. 1, pp. 2–17, http://dx.doi.org/10.5741/GEMS.48.1.2

Geographic Origin Determination Of Blue Sapphire

Aaron C. Palke, Sudarat Saeseaw, Nathan D. Renfro, Ziyin Sun, and Shane F. McClure

Geographic origin determination, one of the most pressing issues facing modern gemological laboratories, is especially challenging for blue sapphire. Reliable origin determination requires careful analysis of a stone's inclusions and trace element chemistry as well as spectroscopic data. Some stones have characteristic inclusion scenes or trace element chemistry that make it easy to determine their origin, but in many cases there is significant overlap for blue sapphire from distinct geographic localities. The most commonly encountered inclusions are rutile silk and particle clouds. In some stones the silk or clouds may take on a distinct appearance and the origin may be accurately determined. But in many cases the evidence presented by inclusions within a stone is ambiguous. This contribution outlines the methods and criteria used at GIA for geographic origin determination of blue sapphire.

The twentieth century witnessed a surge of discoveries of blue sapphire deposits around the world. As the gem trade has evolved alongside these developments, geographic origin determination has become a major consideration in buying and selling sapphires. In some cases, the value of a stone can depend strongly on its origin, such as the Kashmir sapphires shown in figure 1. The trade largely relies on reputable gemological laboratories to make these origin determinations, which are based on comparison with extensive reference collections (see Vertriest et al., 2019, pp. 490–511 of this issue) and advanced analytical methods (see Groat et al., 2019, pp. 512–535 of this issue). After more than a decade of efforts by GIA's field gemology and research departments to acquire reliable samples in the field and collect reference data, blue sapphire remains one of the greatest challenges when it comes to origin determination. The following sections will detail the origin data GIA has collected for blue sapphire and describe the laboratory's methodology for using this data in geographic origin determination.

In Brief

- Geographic origin can have a significant impact on the value of fine blue sapphires.
- Origin determination for metamorphic blue sapphires relies heavily on their inclusions, while there is significant overlap in their trace element chemistry.
- Basalt-related blue sapphires tend to have largely overlapping inclusions, but trace element chemistry is more useful in origin determination.

SAMPLES AND ANALYTICAL METHODS

The sapphires included in this study are almost exclusively from GIA's reference collection, which was built over more than 10 years by GIA's field gemology department. Stones in GIA's reference collection were obtained by gemologists from reliable sources and collected as close to the mining source as possible (see Vertriest et al., 2019, pp. 490–511 of this issue). When necessary, the data from the reference collection were supplemented by stones from the personal collections of the authors of this study or from GIA's museum collection. The trace element data were collected from 606 samples total for metamorphic sapphires and 342 samples total for basalt-related sapphires: 124 from Sri Lanka, 263 from Madagascar, 219 from Myanmar (formerly Burma), 72 from Nigeria, 67 from Australia, 72 from Thailand, 46 from Cambodia, and 85 from Ethiopia. In modern times it has not been possible to collect Kashmir sapphires through the field gemology program. Therefore, data presented here for Kashmir sapphires are from observations on historic stones and collections with verifiable provenance or those that could be independently verified through multiple lines of evidence.

See end of article for About the Authors and Acknowledgments.
Gems & Gemology, Vol. 55, No. 4, pp. 536–579,
http://dx.doi.org/10.5741/GEMS.55.4.536

Figure 1. A matched pair of Kashmir sapphires, approximately 7 carats total. Photo by Robert Weldon/GIA; courtesy of Amba Gem Corporation.

Trace element chemistry was collected at GIA over the course of several years using two different laser ablation–inductively coupled plasma–mass spectrometry (LA-ICP-MS) systems. The ICP-MS used was either a Thermo Fisher X-Series II or iCAP Qc system, coupled to an Elemental Scientific Lasers NWR 213 laser ablation system with a frequency-quintupled Nd:YAG laser (213 nm wavelength with 4 ns pulse width). Ablation was carried out with 55 µm spot sizes, with fluence of 8–10 J/cm^2 and repetition rates of either 15 or 20 Hz. ^{27}Al was used as an internal standard at 529250 ppmw with custom-developed synthetic corundum used as external standards (Wang et al., 2006; Stone-Sundberg et al., 2017). Detection limits varied slightly through the course of the analyses but were generally 0.1–0.3 ppma Mg, 0.5–2.0 ppma Ti, 0.03–0.2 ppma V, 5–20 ppma Fe, and 0.03–0.07 ppma Ga. Trace element values are reported here in parts per million on an atomic basis rather than the more typical parts per million by weight unit used for trace elements in many geochemical studies. Units of ppma are the standard used in GIA laboratories for corundum, as they allow a simpler analysis of crystal chemical properties and an understanding of the color mechanisms of sapphire and ruby. Conversion factors are determined by a simple formula that can be found in table 1 of Emmett et al. (2003). The reference samples represent a diverse assemblage of stones in terms of their appearance and the presence/absence of silk, clouds, and otherwise included areas. Every effort was made to sample as many chemically distinct areas in heterogeneous samples as possible to ensure robust representation of silky, cloudy, and unincluded sapphire trace element chemistry.

Inclusions were identified, when possible, using Raman spectroscopy with a Renishaw inVia Raman microscope system. The Raman spectra of the inclusions were excited by a Modu-Laser Stellar-REN Arion laser producing highly polarized light at 514 nm and collected at a nominal resolution of 3 cm^{-1} in the 2000–200 cm^{-1} range. In many cases, the confocal capabilities of the Raman system allowed inclusions beneath the surface to be analyzed.

UV-Vis spectra were recorded with a Hitachi U-2910 spectrometer or a PerkinElmer Lambda 950 in the range of 190–1100 nm with a 1 nm spectral resolution and a scan speed of 400 nm/min. UV-Vis-NIR spectra are presented as absorption coefficient (a) in units of cm^{-1}, where $a = A \times 2.303/t$, with A = absorbance and t = path length in cm.

METAMORPHIC VS. BASALT-RELATED BLUE SAPPHIRE

Often the easiest approach in making a geographic origin determination is to simply exclude as many origins as possible, leaving only a few candidates for the final decision. Blue sapphire can be broadly separated into two groups based on geological conditions of formation, giving us "metamorphic" and "basalt-related" blue sapphire. Basalt-related blue sapphires are those that have been brought up from some unknown great depths in the earth as xenocrysts (foreign crystals) in volcanic eruptions of alkali basalts and related rocks. The sapphires themselves are presumed to have been in equilibrium with some other magma, which

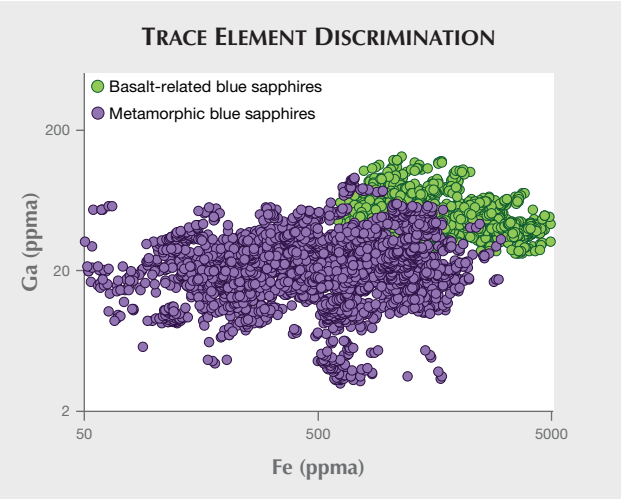

Figure 2. Representative plot of trace element chemistry of metamorphic and basalt-related blue sapphires from major world deposits showing values of Fe vs. Ga. Both groups tend to occupy their own characteristic ranges of trace element profiles, though there is overlap and trace element chemistry alone cannot fully separate these two groups.

would have been distinct from the host basalts (e.g., Graham et al., 2008; Giuliani and Groat, 2019, pp. 464–489 of this issue). Classical sources such as Australia, Thailand, and Cambodia have produced these sapphires for more than 100 years, but basalt-related sapphires are also found in some important newly discovered sources such as Nigeria and Ethiopia. In contrast, metamorphic sapphires are the product of cataclysmic tectonic events in which the earth's continents collided, forming massive mountainous terranes composed of high-grade metamorphic rocks in which the sapphires formed through solid-state recrystallization of preexisting rocks. There are many open questions about the exact geological conditions of formation in these deposits, but metamorphic sapphires are generally associated with marbles, gneisses, aluminous shales, or (in the case of Myanmar) syenite-like rocks associated with these high-grade metamorphic rocks (e.g., Stern et al., 2013; Giuliani et al., 2014). The classical sources of Sri Lanka, Myanmar, and Kashmir are included in the metamorphic sapphire group as well as the more modern source of Madagascar. Note that this work focuses on the methodology used to determine origin for classical metamorphic sapphires from Sri Lanka, Burma, Kashmir, and Madagascar, as well as basalt-related sapphires from Australia, Thailand, Cambodia, Nigeria, and Ethiopia. These sapphires represent the biggest challenges for origin determination. Origin determination is generally more straightforward for "non-classical" sapphire deposits such as those from Montana (United States) and Umba and Songea in Tanzania. These "non-classical" sapphires are not considered here for the sake of clarity and brevity.

While the metamorphic/basalt-related dichotomy may be oversimplifying what is almost certainly an extremely complex geological story (Giuliani and Groat, 2019, pp. 464–489 of this issue), making this distinction on an unknown sapphire can help narrow down the possible origins. Metamorphic and basalt-related blue sapphires tend to have different trace element profiles. Notably, metamorphic blue sapphires generally have lower Fe and Ga than basalt-related sapphires, which in some cases can be used to separate stones from these two groups. However, there is some overlap and the two groups cannot be completely separated (figure 2). Coarse separation is simplified using ultraviolet/visible/near-infrared (UV-Vis-NIR) spectroscopy. Figure 3 compares the UV-Vis-NIR spectrum of a metamorphic sapphire from Sri Lanka against that of a basalt-related sapphire from Australia. The spectra of the two samples share many similarities, including a broad absorption band at 580 nm (the Fe-Ti intervalence charge transfer band) and a series of narrow bands around 380–390 nm and 450 nm related to Fe^{3+} (Ferguson and Fielding, 1971; Krebs and Maisch, 1971; Hughes et al., 2017). The major difference is the presence of a broad band around 880 nm in basalt-related sapphires, which is always more intense than the 580 nm absorption band. The exact origin of the 880 nm band is still not well understood, although it is thought to be related to an Fe^{2+}-Fe^{3+} intervalence charge transfer mechanism, possibly with the involvement of Fe^{2+}-Fe^{3+}-Ti^{4+} clusters (Townsend, 1968; Fritsch and Rossman, 1988; Moon and Philips, 1994; Hughes et al., 2017). Obtaining a UV-Vis-NIR absorption spectrum is GIA's first step in geographic origin determination of sapphires, as it directs the unknown stone into one of two separate decision-making streams, each with its own unique set of reference data accumulated over more than a decade by GIA's field gemology program (Vertriest et al., 2019, pp. 490–511 of this issue). Note that there are reported instances of sapphires with metamorphic-type UV-Vis spectra altering to basalt-related-type UV-Vis spectra after heat treatment (e.g., figure 20 of Emmett and Douthit, 1993). However, this is considered uncommon based on years of experience of testing heated sapphires that can be clearly identified as metamorphic by microscopic observation. Additionally, trace element analysis can allow separation of most heated metamorphic sap-

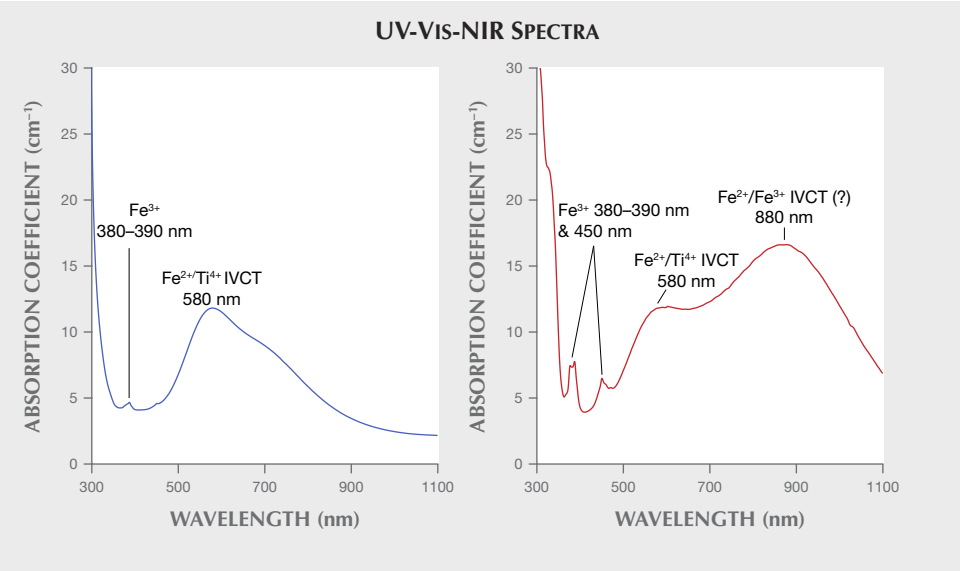

Figure 3. UV-Vis-NIR absorption spectra of a metamorphic-type sapphire from Sri Lanka (left) and a basalt-related-type sapphire from Australia (right). Both spectra are of the o-ray.

phires that start down the wrong decision stream based on their UV-Vis spectra.

INTERNAL FEATURES: METAMORPHIC SAPPHIRES

Metamorphic blue sapphire poses one of the biggest challenges in geographic origin determination. A hundred years ago it was much less of a problem, when the only major sources of these sapphires were Kashmir, Myanmar, and Sri Lanka. At that time, these sapphires were thought to have more or less diagnostic appearances and inclusion suites. A significant obstacle to metamorphic sapphire origin determination came about in the last 25 years, when Madagascar started producing large volumes of sapphires that could overlap with any of the three classical metamorphic sources (Kiefert et al., 1996; Schwarz et al., 1996; Gübelin and Peretti, 1997; Schwarz et al., 2000). Even without the arrival of Madagascar sapphires, it is not always possible to separate the three classical sources with 100% confidence. Adding further to the complication is the discovery in modern times of new mining sites within a single country, such as at Kataragama in Sri Lanka in 2012. The situation is all the more perilous given the dramatic difference in value between these origins: A fine, classical Kashmir sapphire (figure 4) can be sold for many times more than a Madagascar sapphire of exceptional quality and size (figure 5). In these circumstances, determining the geographic ori-

Figure 4. Kashmir sapphire weighing approximately 15 ct. Photo by Robert Weldon/GIA; courtesy of Amba Gem Corporation.

Figure 5. A 7.04 ct blue sapphire from Madagascar. Photo by Robert Weldon/GIA; courtesy of Mayer & Watt.

Figure 6. A 33.16 ct blue sapphire from Sri Lanka. Photo by Robert Weldon/GIA; courtesy of B&B Fine Gems.

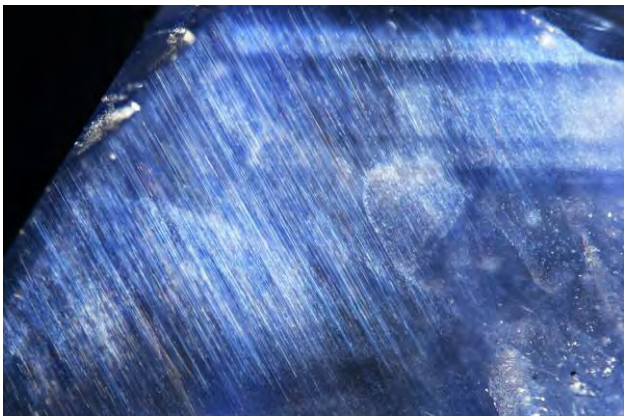

Figure 8. The long, slender rutile silk in this sapphire suggests its Sri Lankan origin. Photomicrograph by GIA; field of view 4.79 mm.

gin of metamorphic sapphires requires the utmost care and deliberation.

Typical Inclusion Scenes. For metamorphic blue sapphire, evidence of geographic origin largely comes from careful microscopic observations of inclusions. While certain mineral inclusions are sometimes considered diagnostic, such as tourmaline crystals in Kashmir sapphires, such inclusions are rare. For the most part, inclusion evidence comes in the form of the overall appearance of silk and clouds in metamorphic blue sapphire. While these more common inclusions may help to identify geographic origin, they should be used as supporting evidence in addition to chemical analysis as these features often overlap significantly. We will review the typical inclusion scenes expected for sapphires from Sri Lanka, Myanmar, Madagascar, and Kashmir. Additional reading on inclusions in metamorphic sapphires can be found in Atkinson and Kothavala (1983), Hänni (1990), Schwieger (1990), Kiefert et al. (1996), Schwarz et al. (1996), Gübelin and Peretti (1997), Schwarz et al. (2000), Gübelin and Koivula (2008), Kan-Nyunt et al. (2013), Krzemnicki (2013), Hughes et al. (2017), and Atikarnsakul et al. (2018).

Figure 9. Sri Lankan sapphires sometimes show irregular platelets, though they are not diagnostic. Photomicrograph by Ungkhana Atikarnsakul; field of view 1.73 mm.

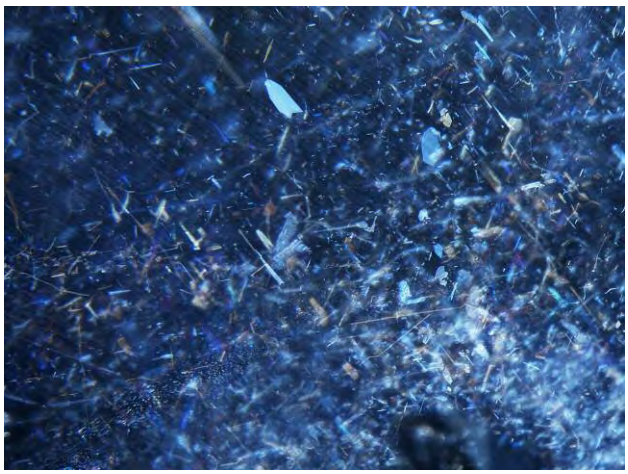

The Internal World of Sri Lankan Sapphires. Sri Lanka has been an important source of fine-quality blue sapphire (figure 6) for many millennia, throughout much of recorded human history. Cut stones are often fashioned from rough sapphires that formed as bipyramidal crystals (figure 7, facing page). Several photomicrographs depicting typical inclusions in Sri Lankan sapphires are shown in figures 8–12. The hallmark inclusion characteristic of Sri Lankan sapphires is long, slender rutile needles (figure 8). In Sri Lankan sapphire this long rutile silk is often relatively sparsely and evenly distributed, with single needles displaying exceptional continuity, sometimes traversing an entire stone. However, silk in Sri Lankan sapphires can also occur as thin, irregular platelets (figure 9) or as more densely packed particle clouds composed of typically shorter needles, but these are not necessarily suggestive of a Sri Lankan origin. Rectilinear, partially healed fractures are more common in

Figure 7. Rough bipyramidal sapphire crystal from Sri Lanka, weighing 10.4 grams (51.70 ct). Photo by Robert Weldon/GIA; courtesy of William Larson, Pala International.

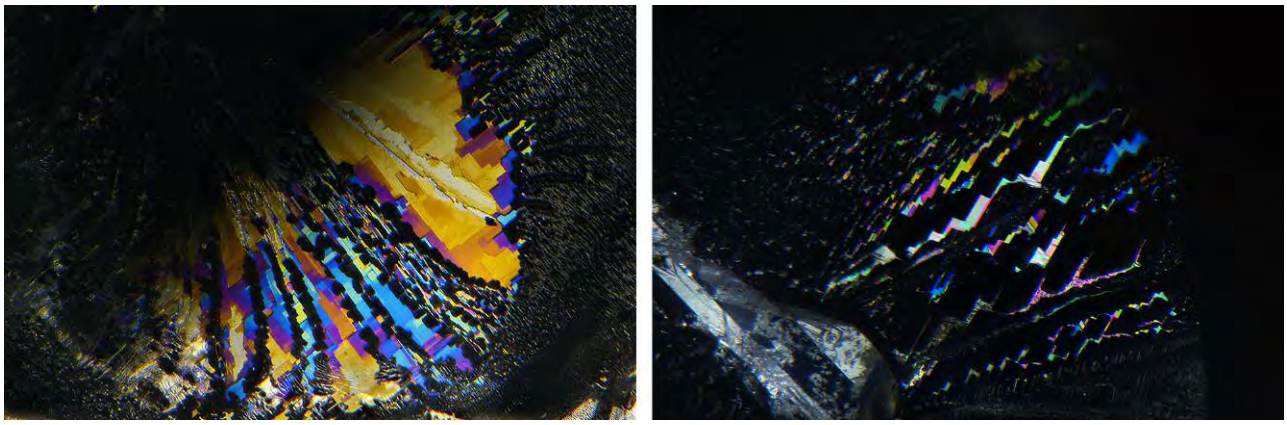

Figure 10. Rectilinear zigzag fingerprints, often exhibiting iridescent colors when viewed with fiber-optic illumination, are usually an indication of Sri Lankan origin. Photomicrographs by Nathan Renfro; field of view 1.38 mm (left) and 1.36 mm (right).

Sri Lankan sapphires than in sapphires from other sources (figure 10). These zigzag fingerprints are considered more indicative of a Sri Lankan origin, and their observation may influence geographic origin conclusion. The same is true for CO_2-filled negative crystals, which are found in metamorphic sapphires from many localities but are frequently associated with Sri Lanka in the minds of many gemologists and could give an initial impression of that origin (figure 11). Sri Lankan sapphires often have these negative crystals arranged in fingerprint-like planes. Similarly, green gahnospinel was once thought to be diagnostic of Sri Lankan sapphires. Although green spinel has now been seen in metamorphic sapphires from other deposits, it is still suggestive of Sri Lankan origin (figure 12). Unfortunately, green gahnospinels are rare inclusions. Pyrite inclusions, often in dark, round ball-like crystals, are also more common in Sri Lankan stones than from other deposits and can also be considered *suggestive* of Sri Lankan origin, but not definitive proof. Other mineral inclusions sometimes seen in Sri Lankan sapphire are mica, uraninite, calcite, and zircon. However, such mineral inclusions are also found in sapphires from other deposits and are not considered characteristic of a Sri Lankan origin. Sri Lankan sapphires often show color zoning as straight, alternating bands of blue and colorless zones, usually with sharp boundaries.

Figure 11. CO_2-filled negative crystals suggest a Sri Lankan origin for this sapphire. Photomicrograph by Jonathan Muyal; field of view 2.90 mm.

Figure 12. Green gahnospinel inclusions, which are not commonly encountered, can provide an initial indication of Sri Lankan origin, although these inclusions are not diagnostic. Photomicrograph by Nathan Renfro; field of view 1.87 mm.

Figure 13. Cushion-cut Burmese sapphire cut by Glenn Preuss, 1.85 ct. Photo by Robert Weldon/GIA; courtesy of Glenn Preuss.

Figure 14. Sapphire from Myanmar, approximately 8 ct. Photo by Robert Weldon/GIA; courtesy of Amba Gem Corporation.

The Internal World of Burmese Sapphires. Myanmar is another classical source of sapphires. The stones produced from the Mogok Stone Tract sometimes have an ill-gained reputation for being overly dark, while in reality Myanmar has produced many exceptional stones with vivid and bright blue hues that rival the colors of stones from the other classical sources (figures 13 and 14). While Sri Lankan sapphires have long, slender silk, Burmese sapphires are considered to be characterized by shorter, reflective rutile silk, sometimes occurring in an arrowhead pattern (figure 15). Note that despite these general differences, there is significant overlap in the nature of silk patterns in stones from Sri Lanka, Myanmar, and other sources. Additionally, many stones have silk or other inclusions that do not appear to be characteristic of any deposits. What follows is a description of the generally accepted characteristics of Burmese silk and other internal features.

The silk in Burmese sapphires can be densely packed in somewhat discrete bands (figures 16 and 17), and many Burmese sapphires have a mix of short

Figure 15. This Burmese sapphire contains typical inclusions of iridescent arrowhead silk. Photomicrograph by Charuwan Khowpong; field of view 1.75 mm.

Figure 16. The short, densely packed needles and longer, reflective and almost platelet-like silk seen here are typical of a Burmese origin. Photomicrograph by Ungkhana Atikarnsakul; field of view 2.89 mm.

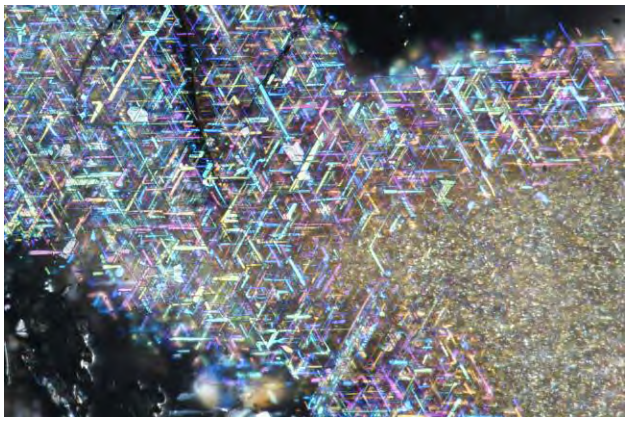

Figure 17. The coarse, iridescent platelet silk in this sapphire indicates its Burmese origin. Photomicrograph by Victoria Liliane Raynaud-Flattot; field of view 0.97 mm.

Figure 18. This inclusion scene with short to elongate iridescent silk could be used to help identify Burmese origin. Photomicrograph by Ungkhana Atikarnsakul; field of view 2.89 mm.

and long silk (figure 18). Often the silk has a straw-like nested pattern in which the lattice of silk is closely intergrown with itself (figure 19), although care may be needed to distinguish such an inclusion scene from the long silk sometimes seen in Sri Lankan sapphires. Rutile silk in Burmese sapphires tends to have a somewhat flattened aspect. The result is often wild displays of spectral colors due to a thin-film effect when using intense fiber-optic illumination from just the right angle (figures 15 and 17). Twinning is commonly observed in Burmese sapphires, especially with intersecting tubules sometimes filled with diaspore or other aluminum (oxy)hydroxides, and can be used as evidence supporting an origin determination (figure 20). Burmese sapphires typically have uniform color. When observed, color zoning is diffuse or "fuzzy," without the sharp boundaries seen in metamorphic sapphires from other deposits (figure 21). Mineral inclusions sometimes encountered in Burmese sapphires include calcite, mica, and zircon, although none of these are considered characteristic of a Burmese origin.

Figure 19. Straw-like, nested silk is typical of sapphires from Mogok, Myanmar, but could be mistaken for a Sri Lankan inclusion scene given the long rutile silk. Photomicrograph by GIA.

Figure 20. Twinning is a prominent feature in many Burmese sapphires and can provide useful supporting evidence for an origin determination. However, twinning alone is not diagnostic, and other corroborating evidence should be sought. Photomicrograph by Charuwan Khowpong; field of view 8.20 mm

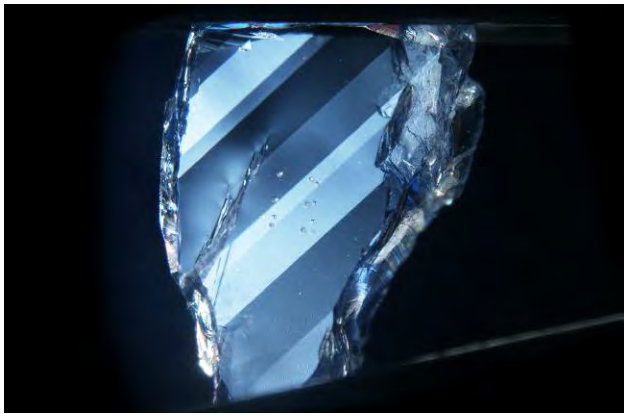

Figure 21. Color zoning is rarely observed in sapphires from Myanmar, but when present it is often gradational and diffuse (left). The same Burmese sapphire also shows typical inclusions of short, densely packed, and reflective rutile needles (right). Photomicrographs by Ungkhana Atikarnsakul; field of view 7.34 mm.

The Internal World of Kashmir Sapphires. The most highly sought-after sapphires are those bearing a Kashmir pedigree. Classical Kashmir sapphires (figures 22 and 23) often harbor characteristic inclusions that can be helpful in identifying them. It is widely known that Kashmir sapphires may also contain certain diagnostic mineral inclusions that can conclusively determine their origin. For instance, inclusions of tourmaline, pargasite (or hornblende), and elongate but often corroded zircon can generally be taken as

Figure 22. This blue Kashmir sapphire is a 3.08 ct cushion mixed cut. Photo by Robert Weldon/GIA; courtesy of Edward Boehm, RareSource.

Figure 23. Step-cut Kashmir sapphire, approximately 5 ct. Photo by Robert Weldon/GIA; courtesy of Amba Gem Corporation.

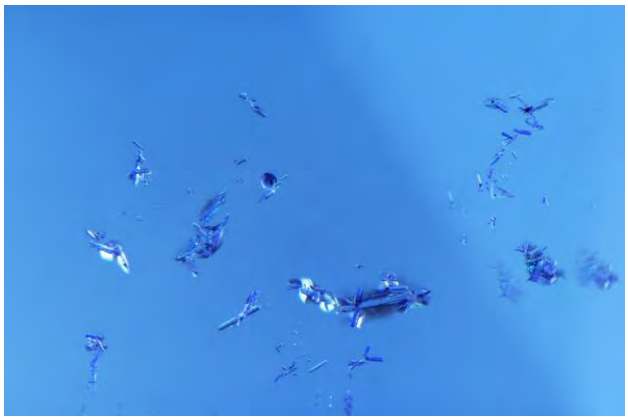

Figure 24. Clusters of elongate zircon inclusions are often seen in Kashmir sapphires. Photomicrograph by Jonathan Muyal; field of view 1.99 mm.

Figure 25. Elongate pargasite inclusions are diagnostic evidence of a Kashmir origin. Unfortunately, they are rarely seen. Photomicrograph by Jonathan Muyal; field of view 7.19 mm.

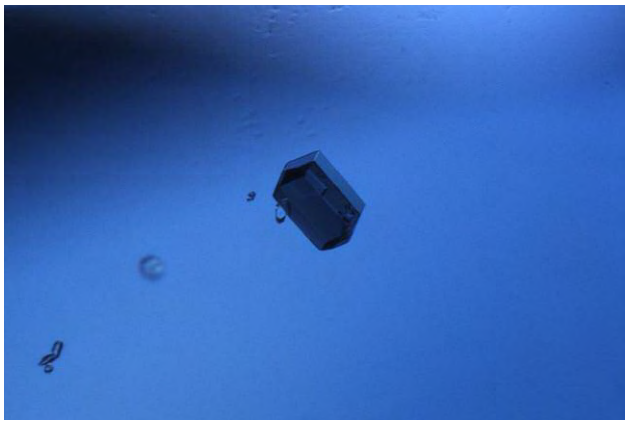

Figure 26. Tourmaline inclusions are considered diagnostic indicators of a Kashmir origin for a sapphire, but they are also very rare. Photomicrograph by Shane McClure; field of view 0.58 mm.

Figure 27. Patterned clouds including ladders (bottom left) and stringers (right) can indicate a Kashmir origin. Photomicrograph by Jonathan Muyal; field of view 7.19 mm.

Figure 28. Ladder inclusions are a form of patterned clouds considered characteristic of Kashmir sapphires. Photomicrograph by Jonathan Muyal; field of view 2.89 mm.

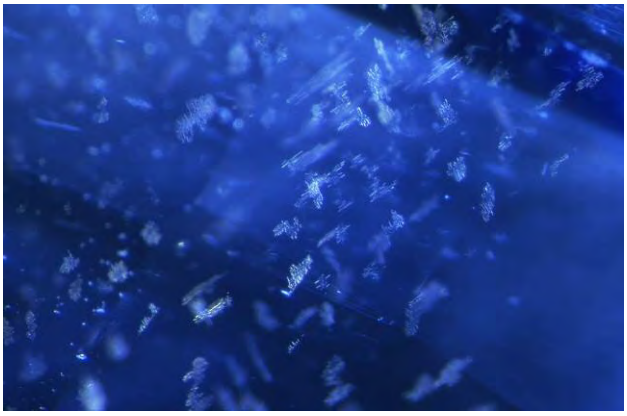

Figure 29. Snowflake-like inclusions are another form of patterned clouds that can suggest a Kashmir origin. Photomicrograph by Jonathan Muyal; field of view 3.57 mm.

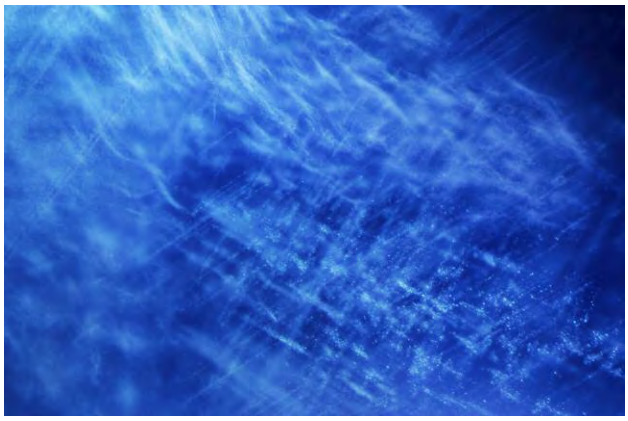

Figure 30. Patterned clouds provide evidence of this sapphire's Kashmir origin. Photomicrograph by Nathan Renfro; field of view 1.90 mm.

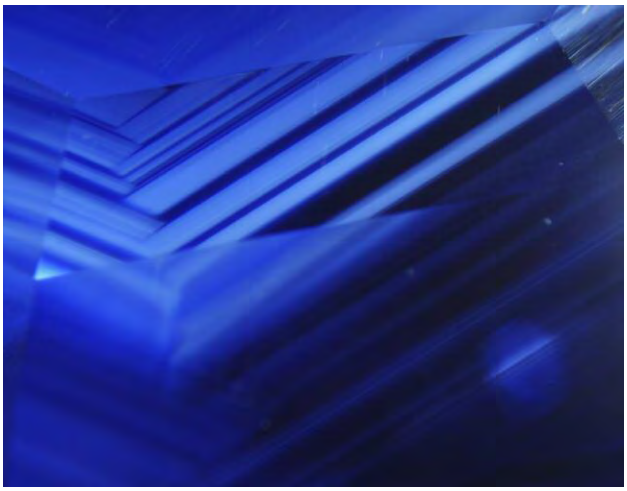

Figure 31. The dense, sharp-edged milky bands with a blocky, step-like hexagonal angle in this sapphire are evidence of its Kashmir origin. Photomicrograph by GIA.

evidence of a Kashmir provenance (figures 24–26). Unfortunately, such mineral inclusions are somewhat rare in fine Kashmir stones. What is left to decipher a Kashmir sapphire's origin, then, is often the same as with other sapphires: patterns of silk and particle clouds of varying textures. In particular, features often referred to as "patterned clouds" can be especially helpful with Kashmir sapphires (figures 27–30). Patterned clouds include so-called ladder, snowflake, and wavy stringer-like inclusions. Other helpful indicators of a Kashmir origin are dense, milky clouds arranged in well-defined hexagonal patterns. The term "milky" is used to describe clouds composed of submicroscopic particles that scatter light but cannot be resolved as individual particles in a microscope. These milky clouds often have what is described as a "blocky" pattern where the intersection of hexagonal bands occurs in a somewhat step-like pattern (figure 31). These milky bands are the cause of the sleepy, velvety texture so admired in fine Kashmir sapphires. Uraninite mineral inclusions are sometimes found in Kashmir sapphires but are not considered characteristic, as they are also found in stones from other deposits.

The Internal World of Madagascar Sapphires. Madagascar produces metamorphic sapphires (figure 32) from several geographically distinct deposits. Additionally, some of the mining areas such as Ilakaka are expansive secondary deposits in which the sapphires were likely derived from several distinct geological formations. For these reasons, Madagascar produces sapphires with a wider range of properties and inclusions than anywhere else. Moreover, the end result of this gemological diversity is that Madagascar sapphires can overlap (sometimes significantly) with metamorphic sapphires from all other major sources.

Figure 32. Blue sapphire from Madagascar, 11.16 ct. Photo by Robert Weldon/GIA.

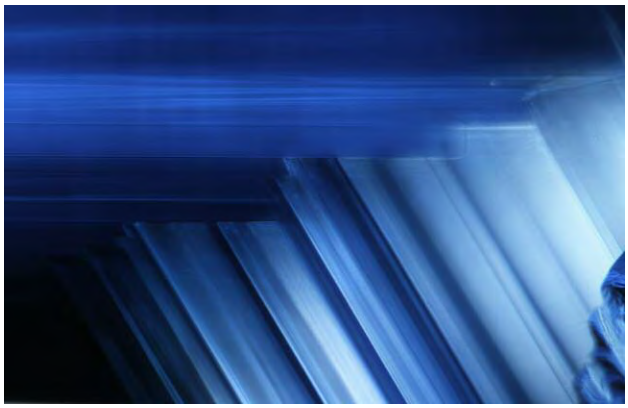

Figure 33. Banded, milky clouds composed of fine microscopic particles are common in Madagascar sapphires and are often one piece of evidence used to support a geographic origin determination. Photomicrograph by Victoria Liliane Raynaud-Flattot; field of view 1.05 mm.

Figure 34. Madagascar sapphires sometimes have milky cloud banding, which can be a useful tool to discern provenance. Photomicrograph by Ungkhana Atikarnsakul.

Nonetheless, some inclusion scenes are considered more characteristic of Madagascar sapphires and can be used to identify this origin. For instance, pronounced milky banding (figures 33 and 34) can often indicate a Madagascar origin. Milky clouds with unusual or chaotic geometric patterns, often occurring in finely repeating layers as so-called stacked milky clouds, can also suggest a sapphire was mined in Madagascar (figure 35). A highly experienced eye is sometimes needed to distinguish hexagonal milky bands in Kashmir sapphire from those seen in a small subset of Kashmir-like sapphires from Madagascar. In Kashmir sapphires, the intersection of these bands often has a stepped pattern (figure 31), while in Madagascar their intersection is often more irregular and chaotic (figure 34). Strong graining and intense color zoning, sometimes with a chaotic or irregular (but still geometric) pattern are occasionally seen (figure 36). Note as well that many Madagascar sapphires have clouds that appear milky in low magnification, but individual particles may become discernible at higher magnification in a gemological microscope (e.g., about 40× magnification). Such clouds should be called "particulate" clouds and not "milky" clouds. These are distinct from the classical Kashmir-like milky clouds. Finally, while etch tubes are

Figure 35. Madagascar sapphires often display bands of milky clouds with irregular geometric patterns and finely repeating layers as "stacked" milky clouds. Photomicrograph by Shane McClure.

Figure 36. Strong graining and intense, sharp color banding would support a Madagascar origin determination for this sapphire. Photomicrograph by Jonathan Muyal; field of view 4.79 mm.

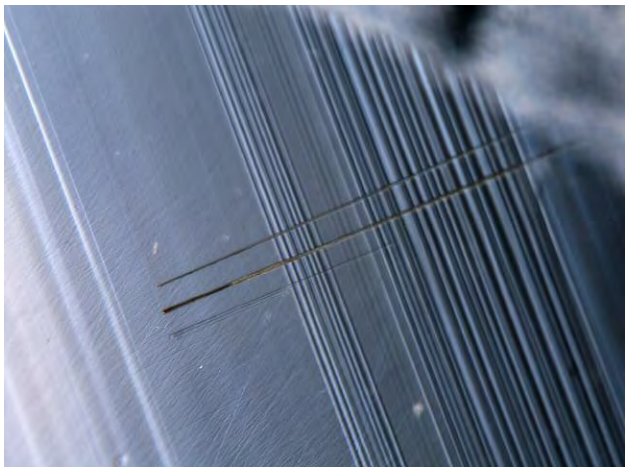

Figure 37. The etch tubes and strong graining in this sapphire could be used to support a Madagascar origin. Photomicrograph by Charuwan Khowpong; field of view 1.30 mm.

Figure 38. Finely alternating milky clouds in a Kashmir sapphire. Without the full hexagonal pattern, these milky clouds might be confused with an inclusion scene in a Madagascar sapphire. Photomicrograph by Jonathan Muyal; field of view 5.74 mm.

found in nearly all metamorphic sapphires, they tend to be more common in Madagascar stones (figure 37) and, taken together with other evidence, may lead to a geographic origin conclusion of Madagascar. Mineral inclusions sometimes found in Madagascar sapphires include calcite, uraninite, zircon, and mica, although none of these can be considered characteristic of a Madagascar origin, as they are found in sapphires from many of the metamorphic deposits.

Inclusion Scenes Gone Wrong. How would one determine the origin of a stone with the inclusion scene in figure 38? The dense, finely alternating milky clouds might give the initial impression of a Madagascar origin, but Kashmir cannot be ruled out. Milky clouds in Kashmir stones often have a blocky pattern in which the intersection of hexagonal bands occurs in a step-like pattern. However, this Kashmir sapphire shows only one set of these milky bands, precluding observation of this useful information. This brings up the challenge often faced in geographic origin determination. In every case we attempt to collect as many lines of evidence as possible to support an origin determination. If enough individual pieces of evidence point toward a specific origin, we can become more confident in making that call. In some cases, however, diagnostic inclusions are not observed in a certain stone, leaving only inclusions that are ambiguous due to overlapping inclusion characteristics between deposits.

For instance, the inclusions of two Sri Lankan sapphires in figures 39–42 show milky banding and/or hexagonal color banding that might initially be more suggestive of a Madagascar origin. If no other indicative inclusions are found, these stones could easily be victims of mistaken identity, with their Sri Lankan origin hidden away forever. Additional examples of Sri Lankan stones with potentially Madagascar-like inclusions such as pronounced milky clouds, strong graining, and angular, irregular color zoning are shown in figures 43 and 44.

By contrast, the longer, slender rutile silk in figures 45 and 46 might be taken as more suggestive of a Sri Lankan provenance, obscuring the true Mada-

Figure 39. The finely alternating bands of milky clouds in this Sri Lankan sapphire could, at first glance, be considered an indication of a Madagascar origin. Photomicrograph by Jonathan Muyal; field of view 4.67 mm.

Figure 40. These milky clouds in a Sri Lankan sapphire are reminiscent of an inclusion scene from Madagascar sapphires. Photomicrograph by Charuwan Khowpong; field of view 2.80 mm.

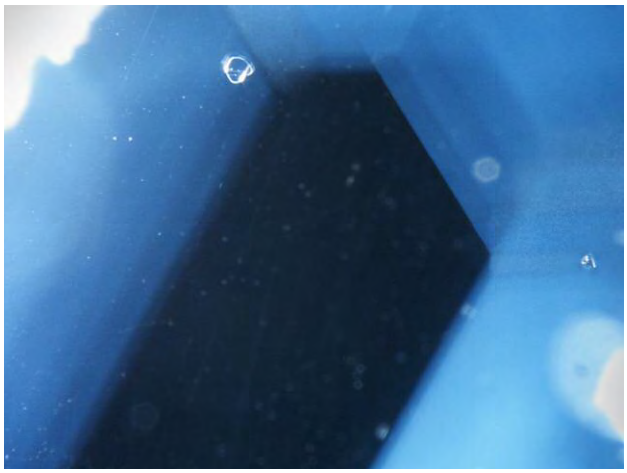

Figure 41. This Sri Lankan sapphire exhibits angular, milky clouds, which might also suggest a Madagascar origin. Photomicrograph by Ungkhana Atikarnsakul; field of view 3.10 mm.

gascar origin of these sapphires. Additionally, the rectilinear zigzag, partially healed fracture in figure 47 and the CO_2-filled negative crystal in figure 48 might lead to an incorrect conclusion of Sri Lankan origin for these sapphires, which have a known Madagascar or Burmese provenance, respectively. As mentioned above, Madagascar sapphires can sometimes harbor inclusion scenes that imitate almost any other source of metamorphic sapphires. The twinning and short, stubby reflective needles and arrowhead silk found in Madagascar sapphires shown in figures 49–51 might otherwise indicate a Burmese origin. Kashmir origin became especially troublesome in the lab once Madagascar sapphires were found with Kashmir-like features such as the patterned clouds shown in figures 52–54. Madagascar sapphires may also occasionally contain slightly elongate zircon inclusions, giving at least an initial impression of a Kashmir inclusion scene (figure 55). While the patterned clouds in Madagascar sapphires may have a different overall appearance than those found in Kashmir sapphires, there is enough potential overlap, especially on first examination, that these stones must be intensely scrutinized in the lab.

Figure 42. Some Sri Lankan sapphires have angular, banded milky clouds, color zoning, and graining, which under some circumstances would indicate a Madagascar origin. Photomicrograph by Ungkhana Atikarnsakul; field of view 1.38 mm.

Figure 43. With only these angular milky clouds as evidence, this sapphire might be mistaken for one from Madagascar and its Sri Lankan origin might not be uncovered. Photomicrograph by Charuwan Khowpong; field of view 2.56 mm.

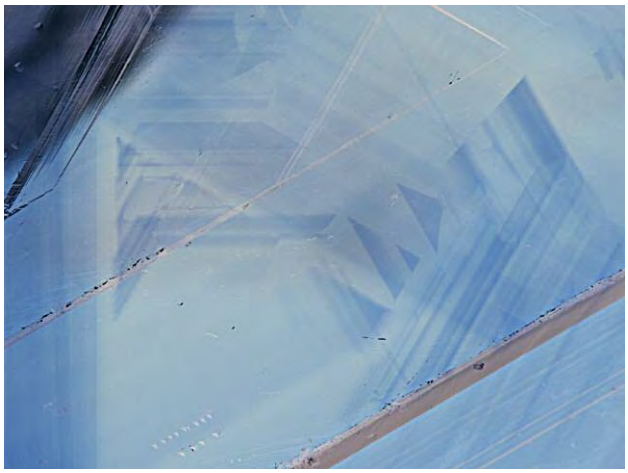

Figure 44. The chaotic, angular color zoning seen in this Sri Lankan sapphire is encountered more frequently in sapphires from Madagascar. Photomicrograph by GIA; field of view 8.20 mm.

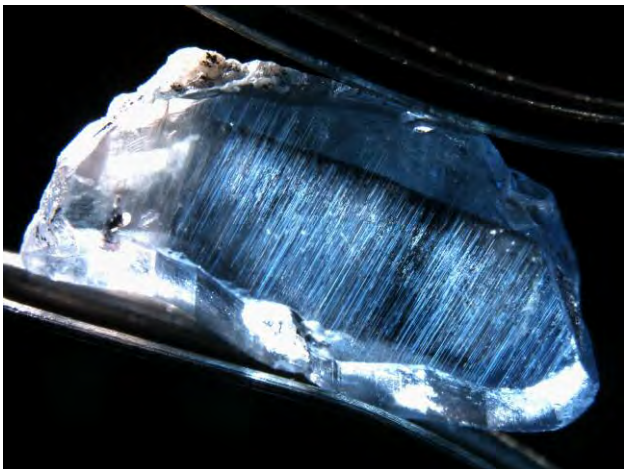

Figure 45. This sapphire from Madagascar could potentially be mistaken for a Sri Lankan sapphire because of the long, oriented rutile needles. Photomicrograph by Charuwan Khowpong; field of view 8.05 mm.

Figure 46. This Madagascar sapphire displays long, oriented rutile silk that could be erroneously taken as evidence of a Sri Lankan origin. Photomicrograph by GIA; field of view 3.10 mm.

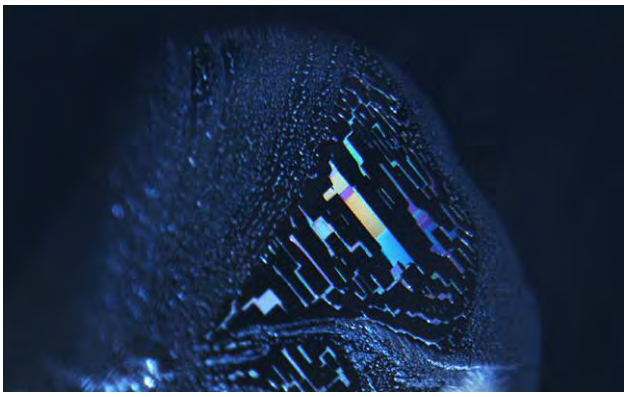

Figure 47. The rectilinear, zigzag healed fractures seen in this Madagascar sapphire could give the mistaken impression of an inclusion scene from a Sri Lankan sapphire. Photomicrograph by Ungkhana Atikarnsakul; field of view 2.62 mm.

Figure 48. While not diagnostic, the CO_2-filled negative crystal in this Burmese sapphire could give an initial impression of Sri Lankan origin. Photomicrograph by Victoria Raynaud-Flattot; field of view 1.20 mm.

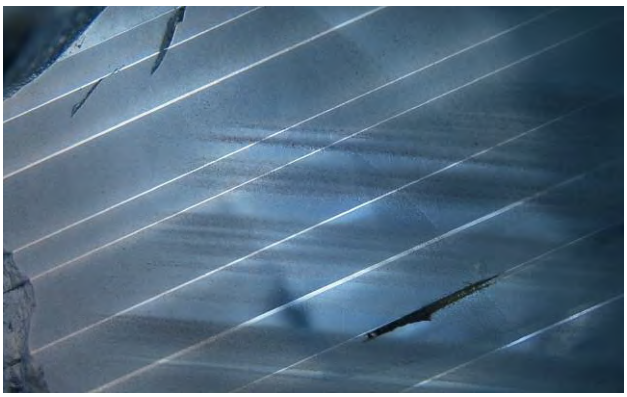

Figure 49. The twin planes displayed in this Madagascar sapphire could give the impression of Burmese origin. Photomicrograph by Charuwan Khowpong; field of view 3.96 mm.

Figure 50. Sapphires from Madagascar often have misleading inclusions such as the short, reflective silk shown here, which might seem to indicate a Burmese origin. Photomicrograph by Victoria Liliane Raynaud-Flattot; field of view 3.5 mm.

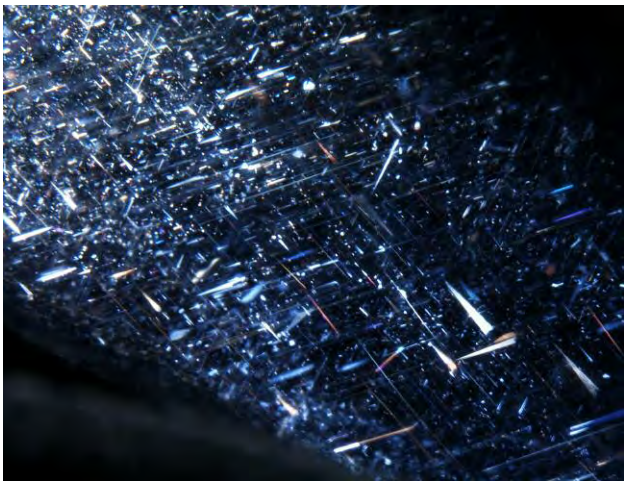

Figure 51. The arrowhead and platelet silk in this Madagascar sapphire are typically taken to be more indicative of a Burmese origin. Photomicrograph by Charuwan Khowpong; field of view 2.65 mm.

Figure 52. The patterned clouds in this Madagascar sapphire are larger and coarser than those typically found in Kashmir sapphires. Such inclusions must be intensely scrutinized to avoid confusion. Photomicrograph by Jonathan Muyal; field of view 2.90 mm.

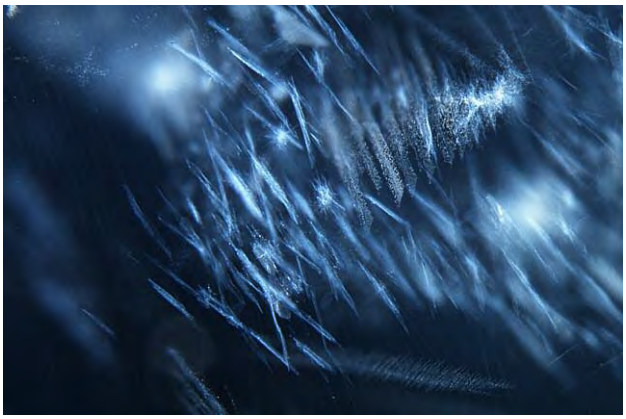

Figure 53. Madagascar sapphires may contain patterned clouds that initially suggest a Kashmir origin. It takes an experienced gemologist to make this separation. Photomicrograph by Charuwan Khowpong; field of view 1.95 mm.

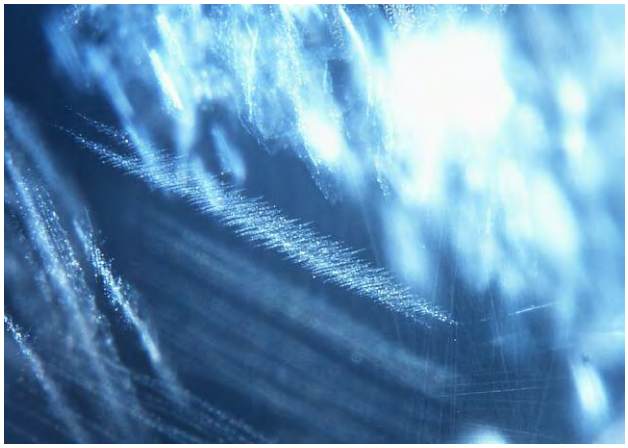

Figure 54. The patterned clouds in this Madagascar sapphires sometimes might give an initial impression of a Kashmir origin. Great care must be taken with these stones to avoid an erroneous origin call. Photomicrograph by Charuwan Khowpong; field of view 1.26 mm.

Burmese sapphires may go unrecognized on occasion when their inclusions are especially reminiscent of Madagascar or Sri Lankan sapphires (figures 56 and 57). However, sometimes the situation is not so dire. The Burmese sapphire in figure 57 may appear Sri Lankan at first glance with its long, slender, and

Figure 55. The slightly elongate zircon inclusions sometimes found in Madagascar sapphires can, at first glance, give the mistaken impression of a Kashmir origin. The trained eye of an experienced gemologist is needed to make this distinction confidently. Photomicrograph by Victoria Liliane Raynaud-Flattot; field of view 1.44 mm.

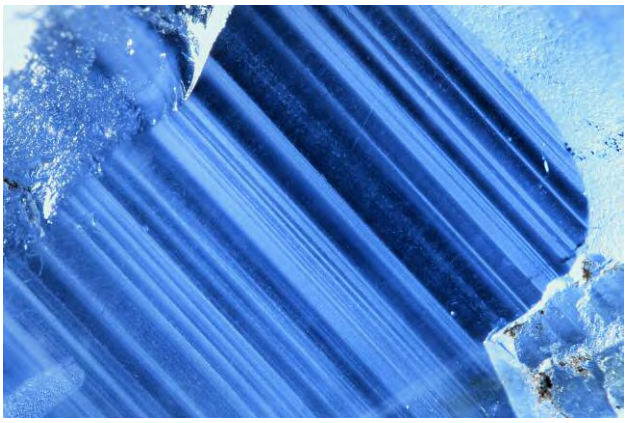

Figure 56. The banded milky clouds in this Burmese sapphire, while slightly coarser than those seen in Madagascar sapphires, are not a typical inclusion scene in sapphires from Myanmar. Photomicrograph by Ungkhana Atikarnsakul; field of view 0.70 mm.

loosely packed rutile silk. However, closer examination and the use of an intense fiber-optic light show reflective and shorter rutile needles and arrowhead silk, which are more suggestive of the stone's true Burmese origins.

INCLUSION SCENES IN BASALT-RELATED BLUE SAPPHIRE

If the UV-Vis-NIR spectrum of a blue sapphire shows a prominent absorption band at 880 nm, the stone is determined to be a basalt-related sapphire and an entirely different suite of origins are possible. At present, the main sources of gem-quality basalt-related sapphires that come through the lab include Australia, Thailand, Cambodia, Nigeria, and Ethiopia. Of course, there are other deposits where basalt-related blue sapphires are actively mined or have been in the recent past, including Cameroon, Laos, Vietnam, northern Madagascar, and China. However, these are expected to be less economically important in the global gem trade. While these stones are represented in GIA's reference collection and these sources can be considered for an origin call, there is a low probability

Figure 57. Long, slender rutile silk (left) might give an initial impression of a Sri Lankan sapphire. Upon closer examination, the reflective shorter silk on the right is more suggestive of the stone's true Burmese origin. Photomicrographs by Ungkhana Atikarnsakul; field of view 6.67 mm (left) and 3.07 mm (right).

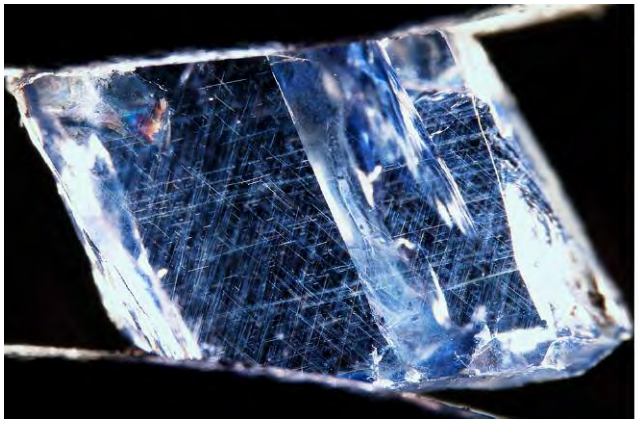

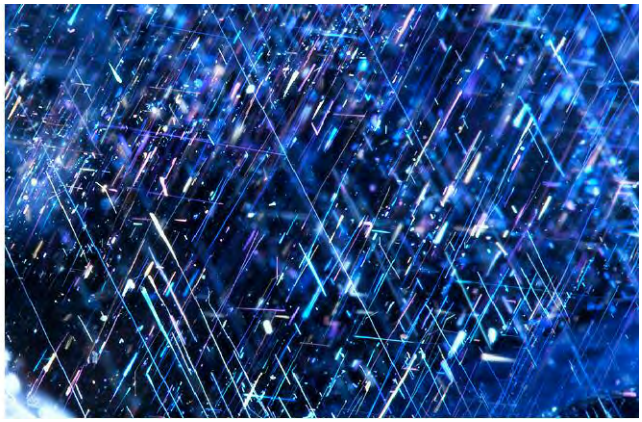

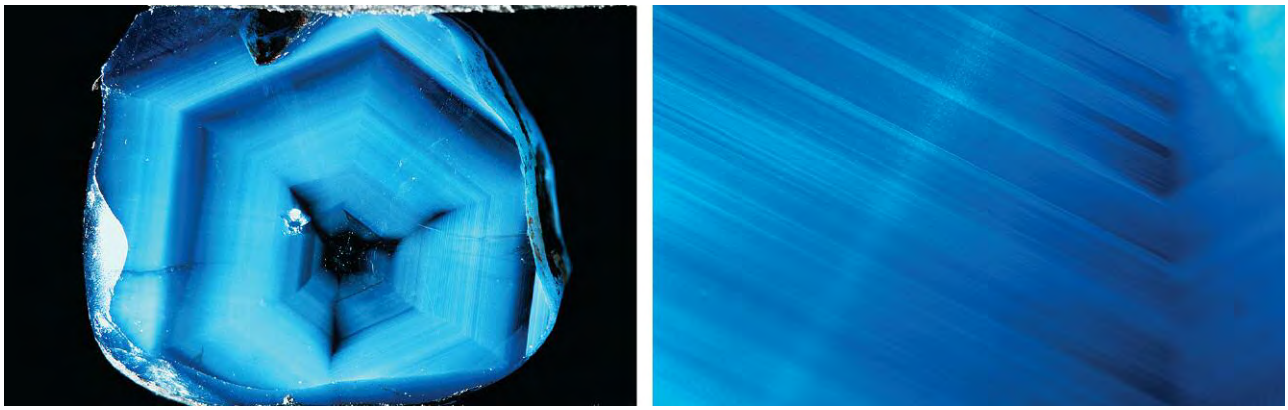

Figure 58. Dense, finely alternating milky bands are typical in Cambodian sapphires and can lend a Kashmir-like soft, sleepy appearance. Photomicrographs by Charuwan Khowpong; field of view 13.63 mm (left) and 1.36 mm (right).

of seeing them in a gemological laboratory, and their gemological properties will not be considered further here. The approach to geographic origin determination for basalt-related sapphires is slightly different than for metamorphic sapphires. Specifically, trace element chemistry tends to take on greater importance in making origin conclusions. Inclusion characteristics are still considered, but there tends to be far more overlap and similarities in inclusion scenes for basalt-related sapphires from various localities. However, the various sources of basalt-related stones do tend to have more distinct trace element profiles, allowing for successful origin determination in many cases. Nonetheless, there is still considerable overlap, and origin determination for basalt-related sapphires can be more challenging than for metamorphic sapphires. Additional information about the inclusion scenes in basalt-related sapphires can be found in Gunawardene and Chawla (1984), Sutherland et al. (2009), Sutherland and Abduriyim (2009), and Abduriyim et al. (2012).

Basalt-related sapphires from the classical mining area of Pailin, Cambodia, often have somewhat diagnostic inclusions. They typically have thick, dense bands of milky clouds arranged in hexagonal patterns (figure 58), reminiscent of those seen in Kashmir sapphires. The best Cambodian sapphires can resemble stones from Kashmir, with a similar sleepy and vel-

Figure 59. The pyrochlore in this Cambodian sapphire is distinguished from similar inclusions from other deposits by its deep, dark red color. Photomicrograph by Nathan Renfro; field of view 1.09 mm.

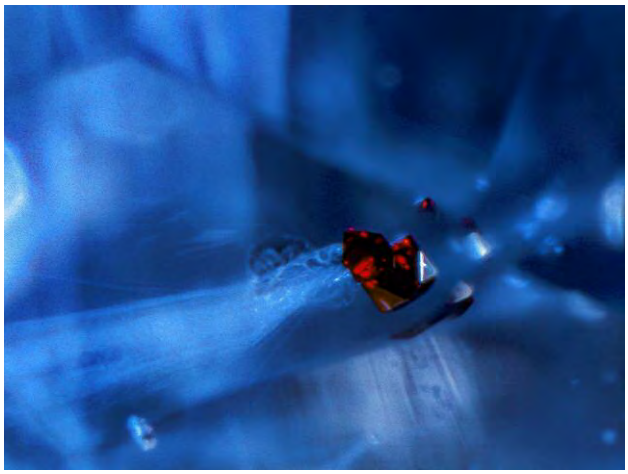

Figure 60. While pyrochlore inclusions are more prevalent in Cambodian sapphires, they can be found in basalt-related blue sapphires from any deposit, such as this sapphire from Australia. Photomicrograph by Nathan Renfro; field of view 1.60 mm.

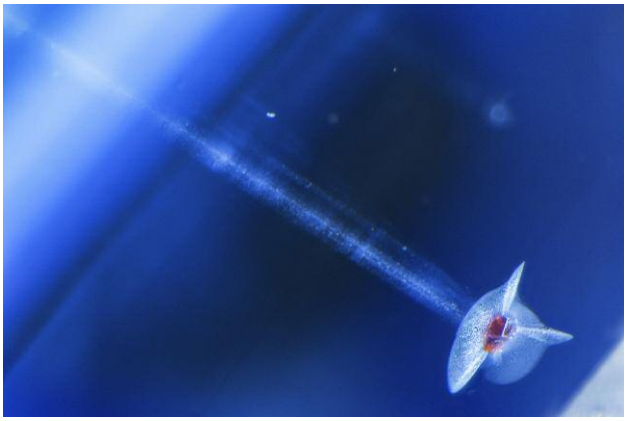

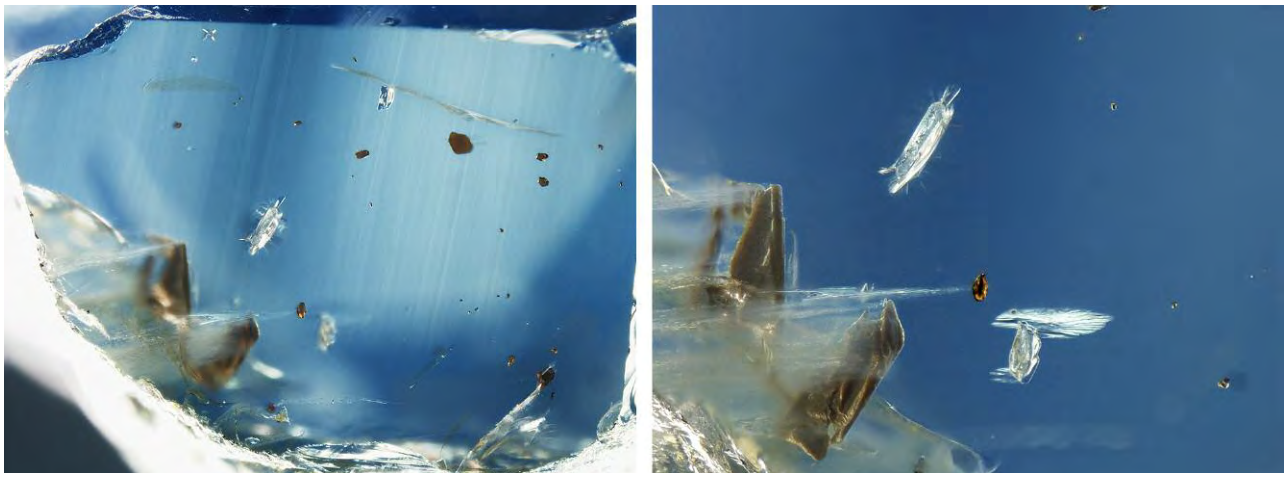

Figure 61. Pyrochlore in sapphires from Nigeria and some other basalt-related deposits tends to have a brownish orange color rather than the deep red of pyrochlore seen in Cambodian sapphires. However, making this distinction requires experience in studying stones of known provenance to gain an understanding of the color range for pyrochlore inclusions in each deposit. Photomicrographs by Jonathan Muyal; field of view 3.5 mm (left) and 1.53 mm (right).

vety appearance due to the presence of dense milky bands. In fact, the color of fine Cambodian stones can often be used as an indicator of origin on its own, as most other basalt-related sapphires take on a much darker blue color in contrast to the often bright, vivid, and saturated blues of Cambodian stones. Pyrochlore inclusions can also be helpful in identifying Cambodian sapphires. While pyrochlore can be found in basalt-related sapphires from many other deposits, the pyrochlore in Cambodian stones tends to take on a deeper red color (figure 59) rather than the more brownish orange color seen in stones from other deposits (figures 60–62).

However, these pyrochlore inclusions are not found in every Cambodian sapphire, so one is often left to observe various patterns of silk and milky clouds to ascertain provenance. Unfortunately, dense milky banding can also be seen in sapphires from most other basalt-related sapphire deposits (figures 63 and 64). The one (near) exception to this are the

Figure 62. Pyrochlore inclusions in Australian sapphires tend to have a more brownish orange color, making them distinguishable from Cambodian sapphires. Photomicrographs by GIA (left, field of view 0.90 mm) and Nathan Renfro (right, field of view 2.88 mm).

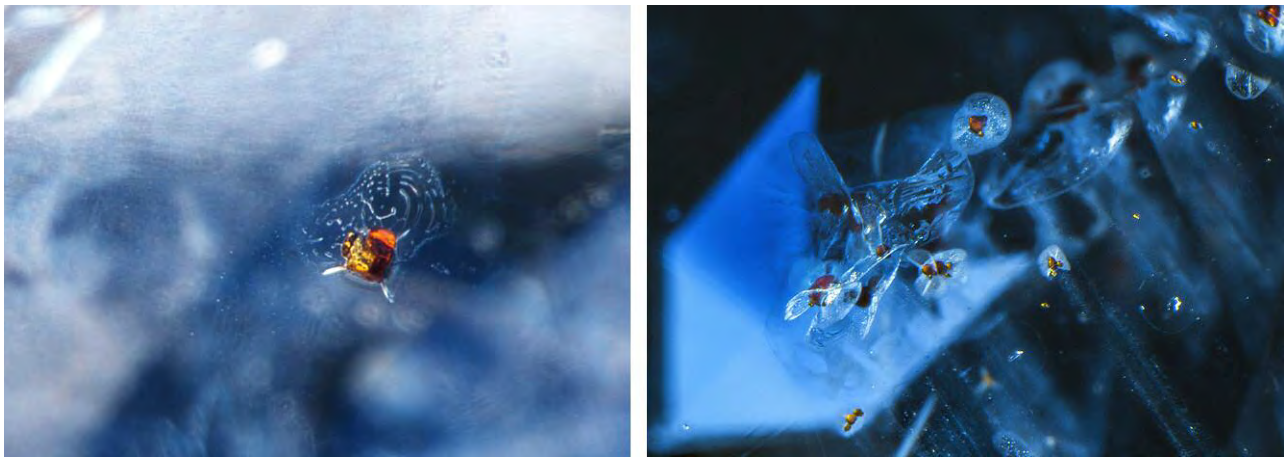

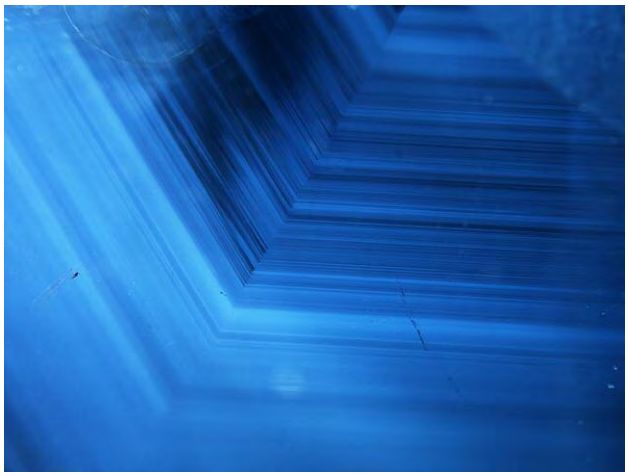

Figure 63. With basalt-related sapphires, inclusion evidence must be carefully considered in context with other available data. For instance, the milky banding in this Australian sapphire might give an initial impression of Cambodian origin. Photomicrograph by Charuwan Khowpong; field of view 3.89 mm.

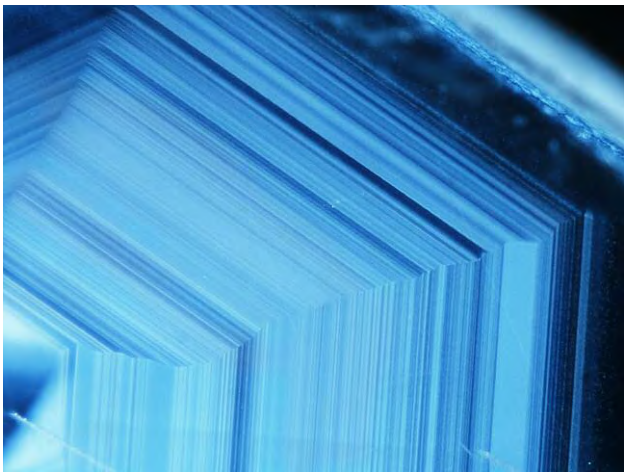

Figure 64. This Ethiopian sapphire exhibits dense, angular, milky banding, which is sometimes considered more characteristic of Cambodian sapphires. Photomicrograph by GIA; field of view 3.5 mm.

sapphires found right across the border from Pailin in Chanthaburi, Thailand. The Thai sapphires very rarely show milky banding, and when it is present the milky clouds tend to be more coarsely particulate in nature. More common in Thai sapphires are dense accumulations of coarse, short to long silk needles (figure 65). The coarse silk in Thai sapphires often occurs in discrete geometric patterns constrained by corundum's trigonal crystal lattice. Unfortunately, while coarser silk may be consistent with a Thai origin, this type of inclusion is also seen in sapphires from other basalt-related deposits such as Australia (figure 66) and Ethiopia (figure 67). The newly discovered deposit in Ethiopia actually represents one of the major difficulties with origin determination. While some inclusions that suggest an Ethiopian origin,

Figure 65. Thai sapphires seldom have the fine, milky bands of Cambodian sapphires. More frequently observed are finely alternating clouds of coarse silk composed of densely packed needles. Photomicrograph by Victoria Raynaud-Flattot; field of view 5.15 mm.

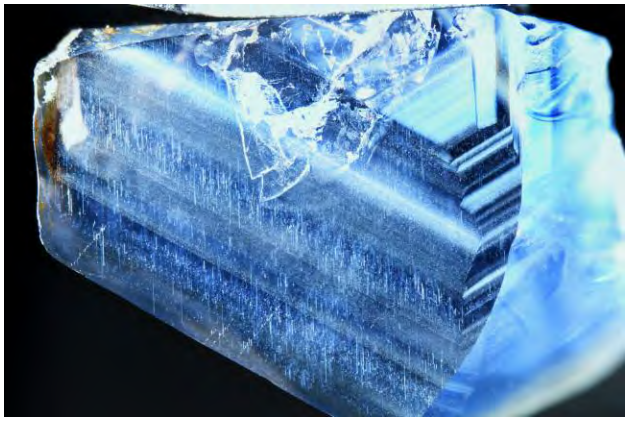

Figure 66. Australian sapphires contain a variety of inclusions. Some show coarse, long to short silk that can be very similar to that of Thai sapphires. Photomicrograph by Charuwan Khowpong; field of view 2.68 mm.

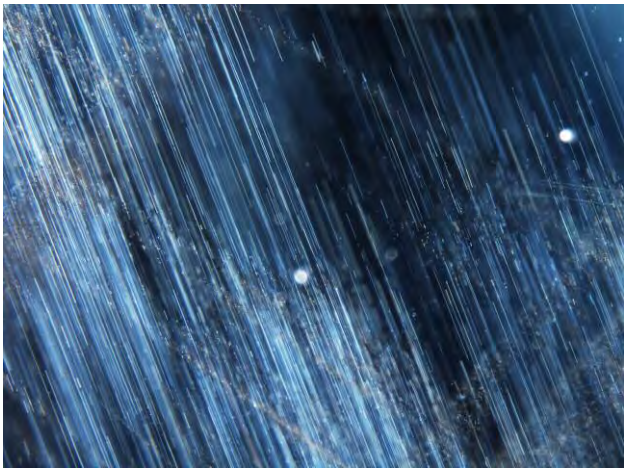

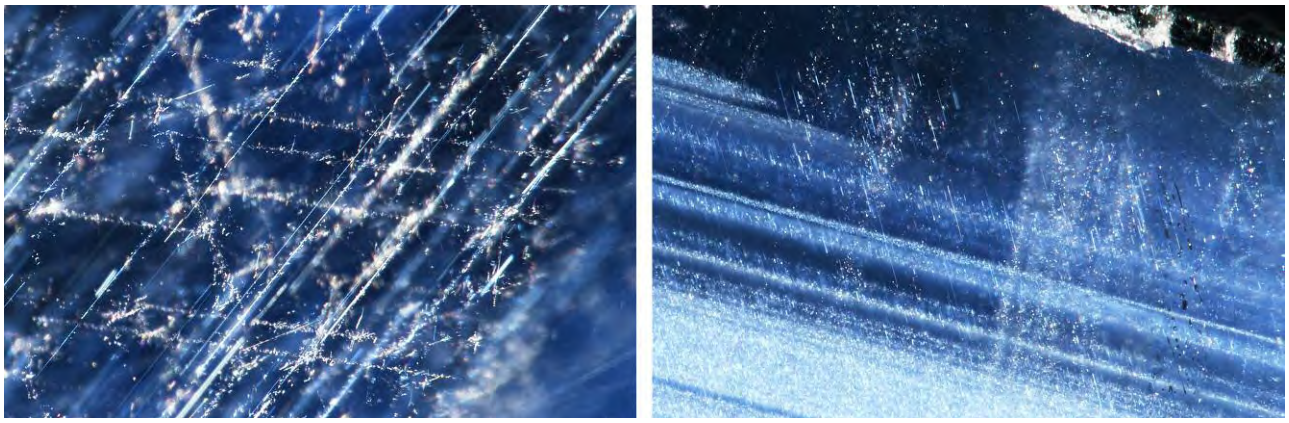

Figure 67. Coarse long and short needles can also be seen in sapphires from the new find in Ethiopia. Photomicrographs by Charuwan Khowpong; field of view 1.36 mm.

such as clusters of zircons (figure 68) or multiple intersecting twinned sectors (figure 69), the more common inclusions overlap with those from other deposits. As the number of possible deposits grows, so does the overlap between these deposits.

THE CHALLENGE OF ORIGIN DETERMINATION FOR HEATED BLUE SAPPHIRE

The foregoing discussion has demonstrated the difficulty of using common inclusions in blue sapphire to make origin determinations due to overlap in their internal characteristics. For the most part, the data presented are applicable only to unheated stones. An additional complicating factor is that most blue sapphires on the market have been heated—either to deepen the color of metamorphic sapphires or sometimes to lighten the color of overly dark basalt-related stones. The problem lies in the fact that deepening the blue color essentially destroys rutile silk, which in many stones is the only internal feature that can be used to support a geographic origin determination (figure 70). As the rutile inclusions dissolve, Ti internally diffuses into the corundum lattice, producing Fe-Ti pairs and, hence, blue coloration. Angular blue streaks inside the stone are all that remains of the silk. For this reason, geographic origin conclusions can be challenging, if not impossible, in heated blue sapphire. While the situation is complicated enough for unheated stones, extra caution and care must be

Figure 68. Clusters of euhedral zircons are sometimes encountered in Ethiopian sapphires. Photomicrograph by Charuwan Khowpong; field of view 0.83 mm.

Figure 69. While twinning occurs in many basalt-related sapphires, multiple intersecting twinned sectors are often seen in Ethiopian sapphires. Photomicrograph by Victoria Liliane Raynaud-Flattot; field of view 14.52 mm.

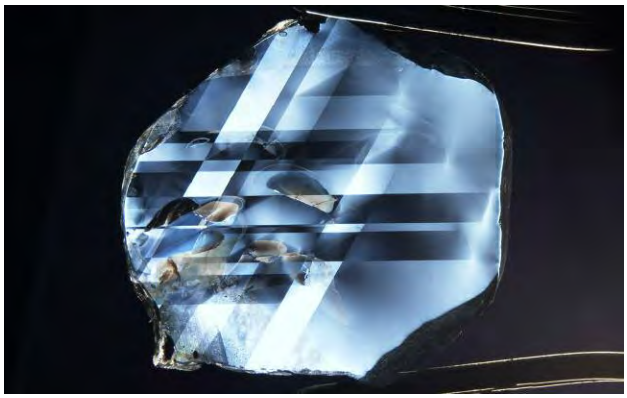

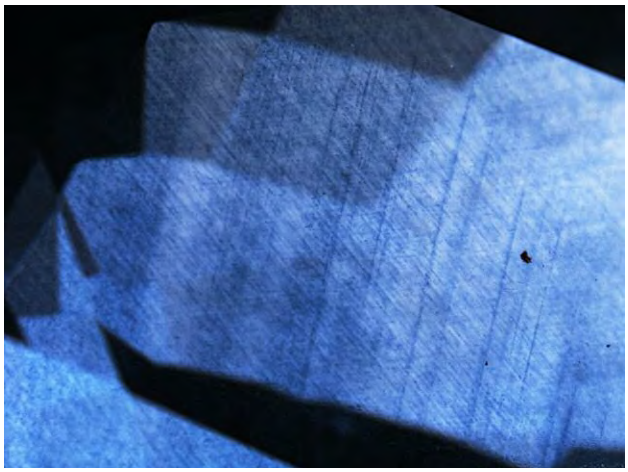

Figure 70. Heat treatment has dissolved the rutile silk in this Sri Lankan sapphire, nearly destroying the inclusion feature that would otherwise indicate the stone's provenance. Photomicrograph by GIA.

applied when attempting to identify the origin of heat-treated blue sapphire.

TRACE ELEMENT CHEMISTRY OF METAMORPHIC SAPPHIRES

Given the potential for overlapping properties for metamorphic sapphires from the major geographic deposits, reliable origin determinations can only come from consideration of multiple lines of evidence. Only when all available data are consistent with a single origin can the gemologist be satisfied with a geographic origin determination. While the origin of metamorphic blue sapphire is determined predominantly by inclusion scenes, trace element chemistry can play a supporting role and help increase confidence in an origin conclusion. Unfortunately, for metamorphic blue sapphires trace element chemistry is often of limited use. The problem is of a crystallographic nature. The physical properties that make corundum such a desirable gem material (high hardness and brilliance) are determined by its unique arrangement of aluminum and oxygen atoms. Unfortunately, corundum's crystal lattice is incredibly unforgiving when it comes to accepting foreign atoms into its structure. The result is that only a handful of trace elements are ever routinely found in sapphires and rubies, typically at very low concentrations. This list includes Mg, Ti, V, Cr, Fe, and Ga. Therefore, there is an extremely narrow range in trace element chemistry for sapphires from similar geological environments.

The reality of the situation is illustrated by the trace element plots shown in figure 71, from GIA's reference data for metamorphic blue sapphire. (Note that all trace element data are produced from LA-ICP-MS and reported in atomic parts per million; see Groat et al., 2019, pp. 512–535 of this issue.) The most striking aspect of these plots is the overwhelming amount of data included, representing nearly 10 years of unparalleled efforts in GIA's field gemology and research departments (the data are summarized in table 1). Also

TABLE 1. Generalized trace element profiles in ppma of metamorphic blue sapphire.

			Myanmar		
	Mg	**Ti**	**V**	**Fe**	**Ga**
Range	bdl–1510	6–1018	bdl–73	172–3041	5–82
Average	41	53	6	928	24
Median	31	39	3	763	21
			Sri Lanka		
	Mg	**Ti**	**V**	**Fe**	**Ga**
Range	bdl–390	4–1410	bdl–49	bdl–1070	4–51
Average	42	133	8	330	20
Median	33	66	5	261	19
			Madagascar		
	Mg	**Ti**	**V**	**Fe**	**Ga**
Range	bdl–167	bdl–1942	bdl–43	46–2717	3–92
Average	30	128	6	598	24
Median	21	60	5	460	22

**bdl = below the detection limit of the LA-ICP-MS analysis. Detection limits are provided in the Samples and Analytical Methods section, p. 537.*

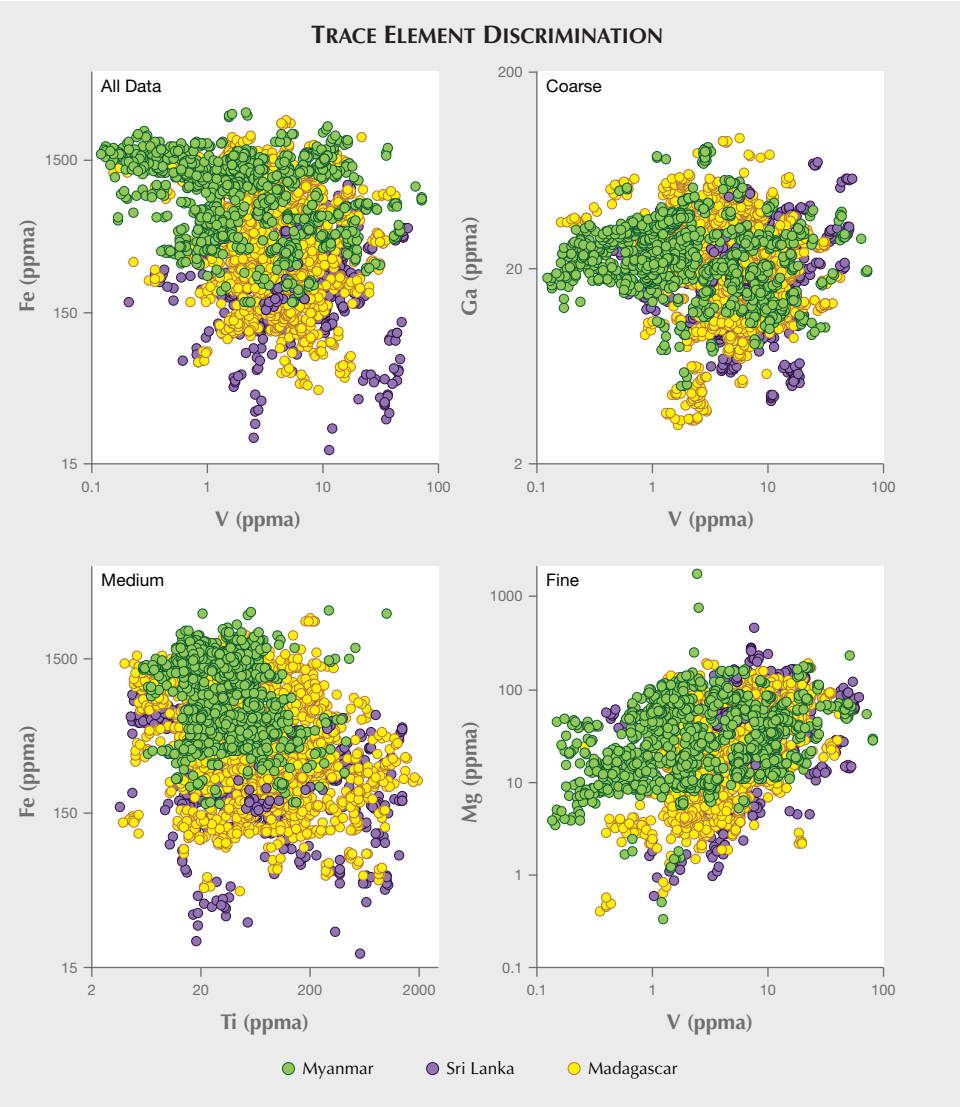

Figure 71. Trace element plots for metamorphic blue sapphire from GIA's field gemology reference collection.

worth noting is the high degree of overlap in much of the data for the major metamorphic blue sapphire deposits. There are clearly some areas in the plots that are uniquely occupied by sapphires from a specific origin such as some low-vanadium Burmese sapphires, some low-iron Sri Lankan stones, or Madagascar samples with low gallium and/or magnesium. However, most of the data occurs in a significantly overlapping field, and these plots clearly have limited value in origin determination. Also note that only three countries of origin are considered on these plots: Myanmar, Madagascar, and Sri Lanka. These chemical plots are also used for possible Kashmir stones and those from minor localities when appropriate, but in most cases these additional deposits are omitted from the plots in order to simplify the decision-making process. Typically, the sapphires are examined in the microscope before further advanced testing. If a stone has possible Kashmir inclusion features, the reference data for Kashmir sapphires can be added to the plots for comparison.

Part of the problem with these plots is their low dimensionality, as only two variables can be considered at one time and it is difficult to know if the overlap of certain data points on one plot could be cleared up by observing the same data on another plot. For instance, what if the Madagascar data that overlaps Sri Lanka on a Mg-Fe plot has much lower Ga than the specific Sri Lankan stones with overlapping Mg and Fe concentrations? This vast database would be much more useful if an unknown stone could be simultaneously compared against the entire trace element profile of the reference data. A new methodology used in the GIA laboratory involves tak-

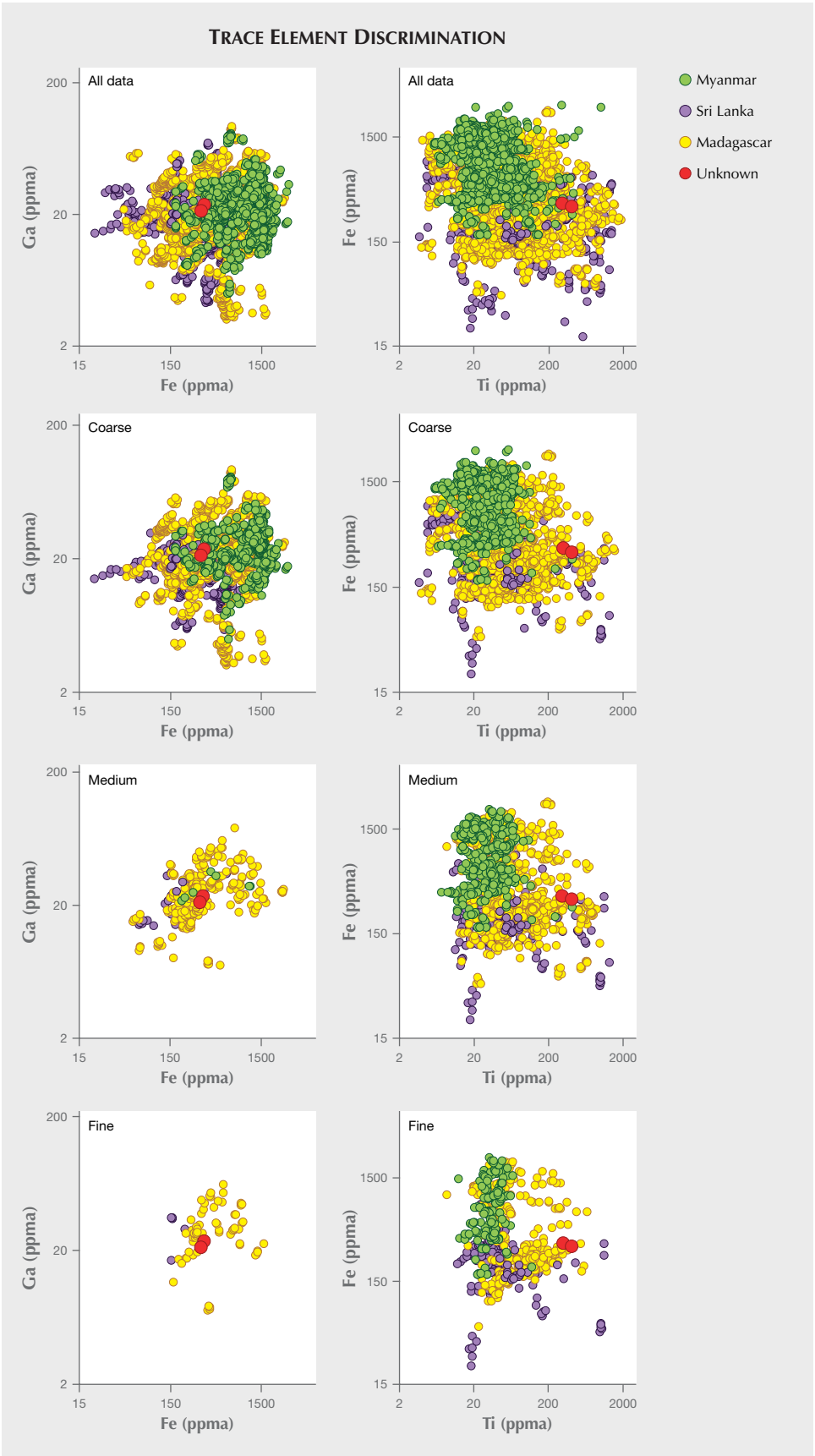

Figure 72. Trace element data on an unknown sapphire plotted with the selective plotting method used for origin determinations at GIA. With all *of the data plotted, the origin is impossible to ascertain. As reference data are selectively filtered progressively using the coarse, medium, and fine settings, the Madagascar origin becomes increasingly apparent.*

TABLE 2. An unknown sapphire and the compositional windows used in the selective plotting method (in ppma).

	Mg	Ti	V	Cr**	Fe	Ga
Unknown Sapphire*	34	359	3.0	1.0	337	22
Coarse Window	5–63	54–664	0–8	—	51–623	3–42
Medium Window	14–54	143–574	0–7	—	135–539	9–36
Fine Window	22–46	233–484	0–7	—	219–455	15–30

**Average of three LA-ICP-MS analyses*
***Cr not used in the selective plotting method*

ing the full trace element suite of an unknown stone and identifying only the reference data with similar chemistry. Then, the reference data with dissimilar chemistry are not shown in the plots. Not only does this mean the unknown is compared only against stones with similar chemistry, but it also clears up the plots by removing extraneous data, which greatly eases their use. Note that this method is essentially a variant of a well-established and widely used statistical classification procedure, the k-nearest neighbors technique (Cover and Hart, 1967; Dudani, 1976).

The mechanics of the method, which we call "selective plotting," are relatively straightforward. Three LA-ICP-MS analyses are collected on each sample, and when the three spots are close in value they are averaged. Then a compositional "window" is created around the averages for each element (Mg, Ti, V, Fe, and Ga for corundum) and any reference data within this window will be preserved in the plots while any data outside the window for any of the trace elements are not shown on the plots. GIA uses three different levels for the windows: fine, medium, and coarse. These windows are centered on the average of the trace element compositions of the unknown stone and opened up at plus or minus 35%, 60%, and 85%, respectively, of the average composition for each element. This method is explained more carefully in box A, and an example is shown in figure 72 with the data for the unknown stone shown in table 2, which also illustrates the methodology by listing the upper and lower boundaries of the coarse, medium, and fine windows created for the trace element profile of an unknown sapphire. Note that the method also uses a fixed lower boundary to prevent

TABLE 3. Trace element profiles of select blue metamorphic sapphires from distinct deposits showing essentially indistinguishable chemistry (in ppma).

Locality	Mg	Ti	V	Cr	Fe	Ga
Example 1						
Ratnapura, Sri Lanka	41	84	3.5	bdl*	171	20
Ilakaka, Madagascar	48	90	1.8	bdl*	167	17
Example 2						
Ratnapura, Sri Lanka	46	53	3.8	1.4	161	20
Ilakaka, Madagascar	45	50	5.4	4.0	148	17
Example 3						
Elahera, Sri Lanka	77	73	4.0	bdl*	251	17
Ilakaka, Madagascar	70	71	9.3	2.8	282	19
Example 4						
Kashmir	25	104	3.0	bdl*	305	18
Ilakaka, Madagascar	29	115	4.4	bdl*	293	18
Example 5						
Kashmir	45	61	6.0	bdl*	244	16
Ilakaka, Madagascar	48	65	3.1	bdl*	265	15

**bdl = below the detection limit of the analysis. Detection limits are provided in the Samples and Analytical Methods section, p. 537.*

BOX A: DEMONSTRATING THE SELECTIVE PLOTTING METHOD

As demonstrated in the body of this article, the use of trace element chemistry to decipher a stone's geographic origin is exceptionally challenging given the often significant apparent or actual overlap in data for reference stones of known provenance. For many years now, as more and more reference data are accumulated, GIA has turned an eye toward the use of advanced statistical methods for origin determination. In particular, the use of the linear discriminant analysis (LDA) technique has been explored and implemented at various stages of testing. While LDA is an established technique that has proven success in some applications, it has not yet been rolled out in a major way in the lab. The output from techniques such as LDA is often simply an origin call with values being reported for somewhat abstract parameters used in the statistical analysis. The result is that it can often be very difficult for the gemologist to interpret the output from these statistical techniques and to determine the accuracy of the resulting origin call. For this reason, GIA has sought additional statistical tools that can be more readily deciphered and understood in a gemological laboratory setting.

The selective plotting method described in the body of this article can be a powerful tool for comparing the full trace element profile of an unknown stone against reliable reference data in a complete and thorough manner. The method is essentially a variant of a well-established and widely used statistical classification procedure, the k-nearest neighbors technique (Cover and Hart, 1967; Dudani, 1976). The k-nearest neighbors technique has found application in many other fields of science such as biomedicine (Bullinger et al., 2008; Zuo et al., 2013; Rahman et al., 2015).

The selective plotting method is a way to determine which reference stones with known provenance are the closest match in their overall trace element profiles. Ideally the five elements considered for corundum could be plotted together. Of course, only three dimensions can be considered at a time, and 3D plots can be difficult to interpret. By filtering the reference data against the unknown, the output of the selective plotting method is a series of 2D plots with the unknown stone plotted against only those reference stones that have overall similar chemistry in all five dimensions (Mg, Ti, V, Fe, and Ga). If the selective plotting method shows the unknown stone in a field of reference stones of only one origin, this can be taken as a piece of evidence in the overall origin determination process, along with data from inclusions and spectroscopy. The basic question in the selective plotting method is "have we ever analyzed reference stones of known provenance from locality X (but not locality Y or Z) with similar overall trace element profiles as the unknown stone?" One potential complicating factor is the presence of chemical heterogeneity in many blue sapphires. However, the reliability of this method depends on the robustness of the reference database. At GIA all the reference stones of known provenance are sampled extensively in various sectors including colorless and blue color zones or included and unincluded zones. Therefore, the chemical heterogeneity seen in blue sapphires is fully built into the selective plotting method and is not a problem as long as the reference database is thorough and representative of the gem corundum seen in the trade. Of course, no gemological reference database can ever be perfect; however, GIA's field gemology department is ensuring the ever-increasing accuracy of origin determination through active collection of reliable reference stones as close to the

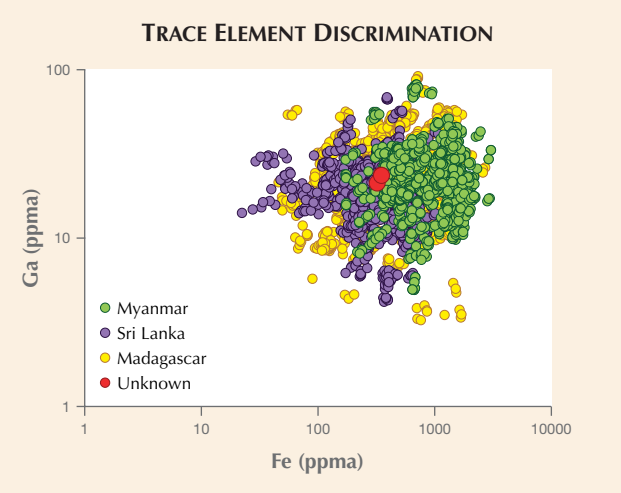

Figure A-1. Plot of Fe vs. Ga for metamorphic blue sapphire from Myanmar (green), Sri Lanka (purple), and Madagascar (yellow), with an unknown stone in red.

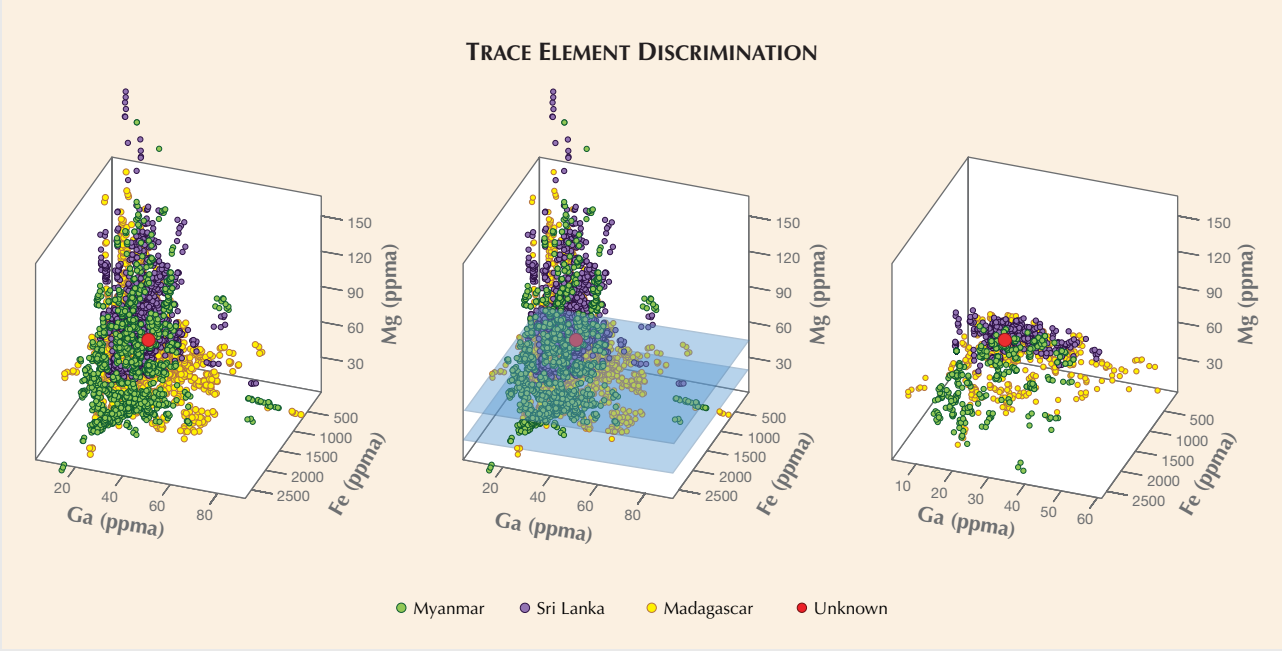

Figure A-2. Left: Three-dimensional Fe-Ga-Mg plot of metamorphic blue sapphires from Myanmar (green), Sri Lanka (purple), and Madagascar (yellow), with an unknown stone in red. Center: A window is drawn around the unknown from 22 to 46 ppma Mg. Right: The reference data outside this window are subsequently not shown in the plot.

mines as possible (Vertriest et al. 2019, pp. 490–511 of this issue).

In this box we will work through an example to demonstrate the method. We use the chemistry of the unknown sapphire in table 2 of the main text, which is shown in the Fe-Ga plot in figure A-1. We start by first selectively filtering out the reference data with dissimilar Mg values. The Fe-Ga plot is expanded to three dimensions in figure A-2, left. Then a window is drawn around the unknown stone from 22 to 46 ppma Mg in figure A-2, center. Finally, any reference data outside this window are not shown in figure A-2, right.

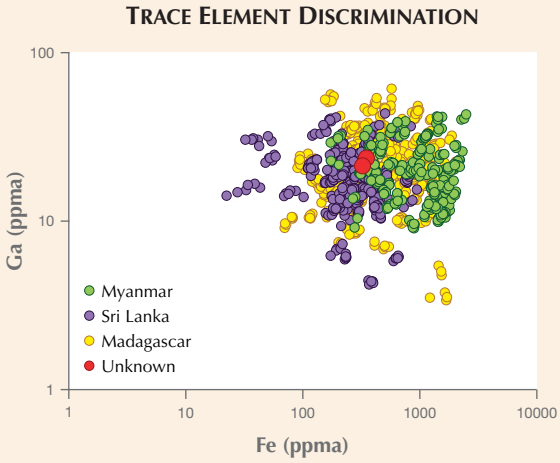

Figure A-3. Plot of Fe vs. Ga for metamorphic blue sapphire from Myanmar (green), Sri Lanka (purple), and Madagascar (yellow), with an unknown stone in red but with the removal of the reference data with dissimilar Mg values, as in figure A-2.

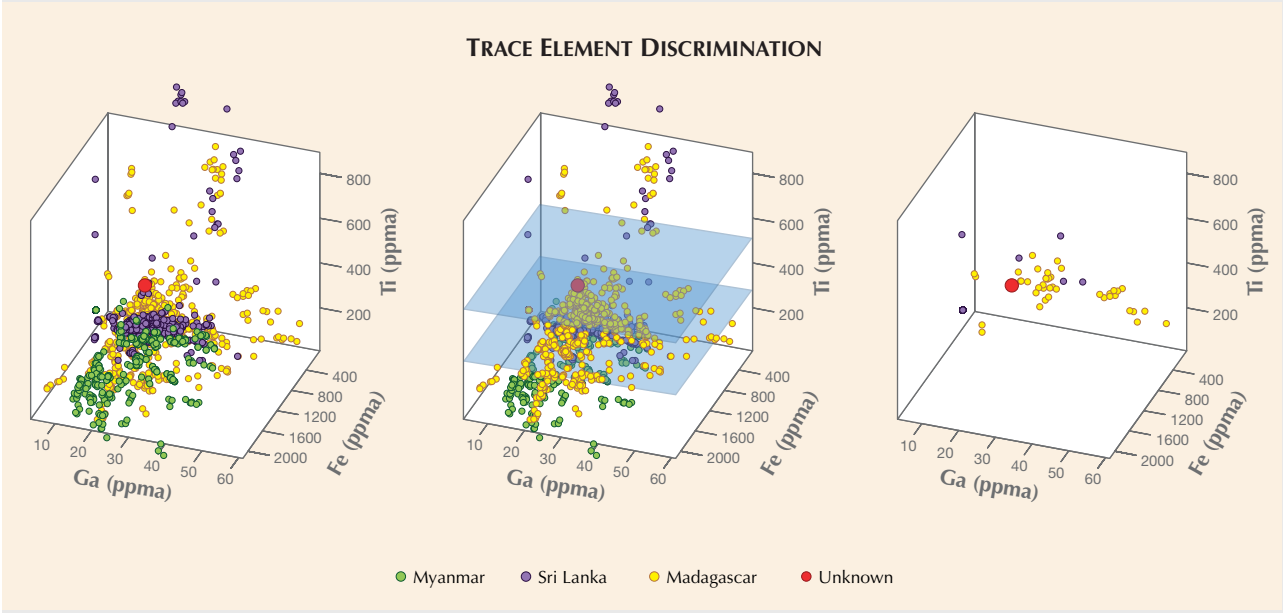

Figure A-4. Left: Three-dimensional Fe-Ga-Ti plot of metamorphic blue sapphires from Myanmar (green), Sri Lanka (purple), and Madagascar (yellow), and an unknown stone in red, after initial filtering of the data by removal of reference data with dissimilar Mg values as in figure A-2. Center: A window is drawn around the unknown from 233 to 484 ppma Ti. Right: The reference data outside this window are subsequently not shown.

Figure A-3 shows the unknown stone in the two-dimensional Fe-Ga plot compared against the reference data that have been selectively filtered to not show stones with dissimilar Mg values, as illustrated in figure A-2. With this selectively filtered reference data, the Fe-Ga plot is expanded into three dimensions with the addition of Ti in figure A-4, left. We follow the same procedure as for Mg, and a window is drawn around the unknown stone from 233 to 484 ppma Ti in figure A-4, center. Finally, in figure A-4, right, any reference data outside this window are not shown.

Figure A-5 shows the unknown stone in the two-dimensional Fe-Ga plot compared against the reference data that have been selectively filtered to avoid showing stones with dissimilar Mg and Ti values, as illustrated in figures A-2 and A-4, respectively. With this selectively filtered reference data, the Fe-Ga plot is expanded into three dimensions with the addition of V in figure A-6, left. We follow the same procedure as for Mg and Ti, and a window is drawn around the unknown stone from 0 to 7 ppma V in figure A-6, center. Finally, in figure A-6, right, any reference data outside this window are not shown.

Figure A-5. Plot of Fe vs. Ga for metamorphic blue sapphire from Sri Lanka (purple) and Madagascar (yellow), with an unknown stone in red after the removal of the reference data with dissimilar Mg and Ti values, as in figures A-2 and A-4, respectively.

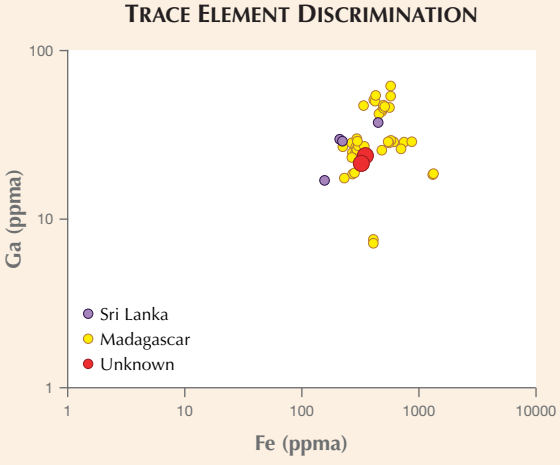

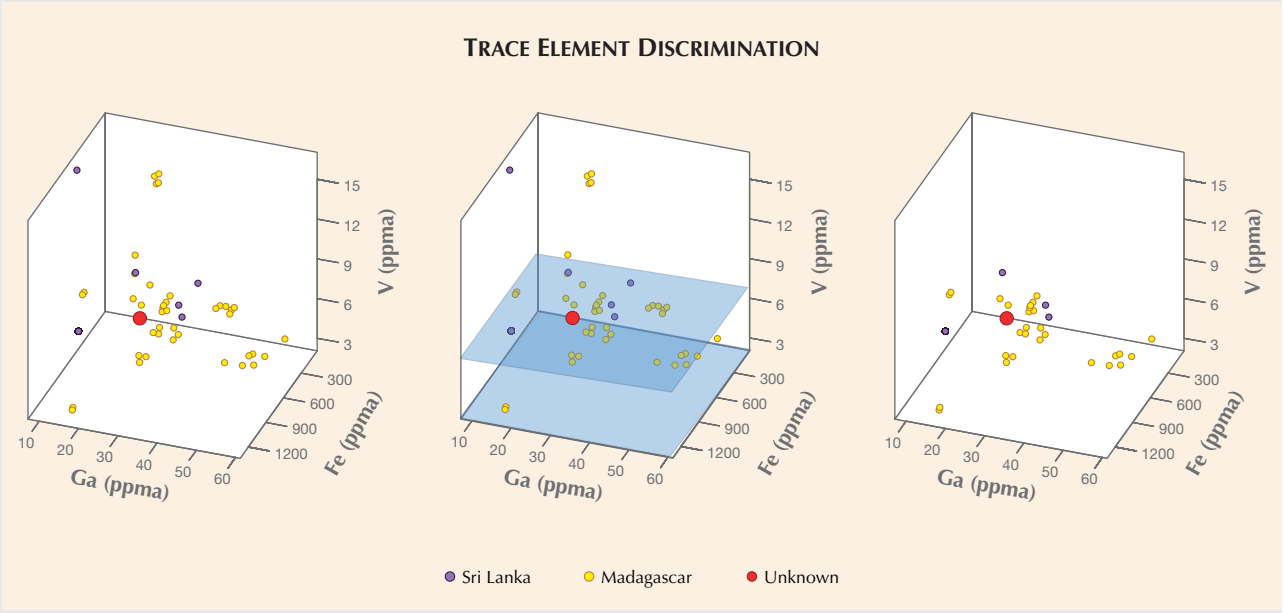

Figure A-6. Left: Three-dimensional Fe-Ga-V plot of metamorphic blue sapphires from Sri Lanka (purple) and Madagascar (yellow), and an unknown stone in red, after filtering of the data by removal of reference data with dissimilar Mg and Ti values, as in figures A-2 and A-4, respectively. Center: A window is drawn around the unknown from 0 to 7 ppma V. Right: The reference data outside this window are subsequently not shown.

The unknown stone is compared against the final, fully filtered reference data set in figure A-7, demonstrating the stone's closer similarity to Madagascar reference data than with either Sri Lanka or Myanmar. Note that in practice, more plots are generated in the same way, with 10 pairwise combinations of the five major corundum trace elements: Mg, Ti, V, Fe, and Ga. Note also that while the final plot in figure A-7 contains many fewer data than the unfiltered plot in figure A-1, the selective plotting method is not making fewer comparisons with the reference database and no reference data are "thrown out" or otherwise removed from the decision-making process. The selective plotting method still compares the unknown against the full reference database, but only those stones with similar multi-dimensional trace element profiles are chosen to be compared against the unknown in the two-dimensional plots. In a way, the technique is a method for taking complicated multi-dimensional data and reducing it to readily comprehensible two-dimensional plots. It could be termed, in essence, quasi-multidimensional two-dimensional plotting.

Figure A-7. Plot of Fe vs. Ga for metamorphic blue sapphire from Sri Lanka (purple) and Madagascar (yellow), with an unknown stone in red after the removal of the reference data with dissimilar Mg, Ti, and V values, as in figures A-2, A-4, and A-6.

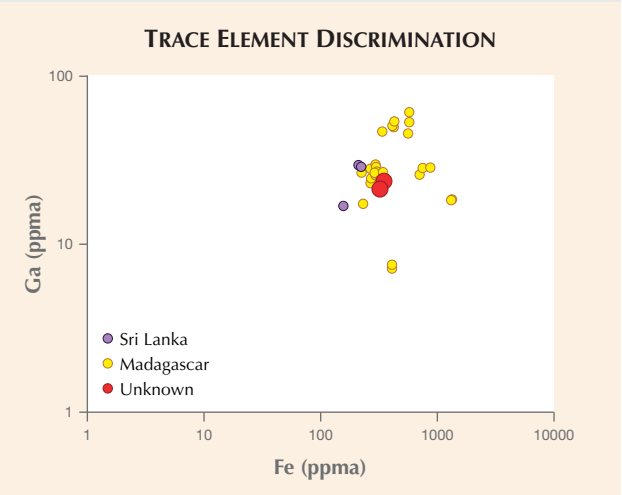

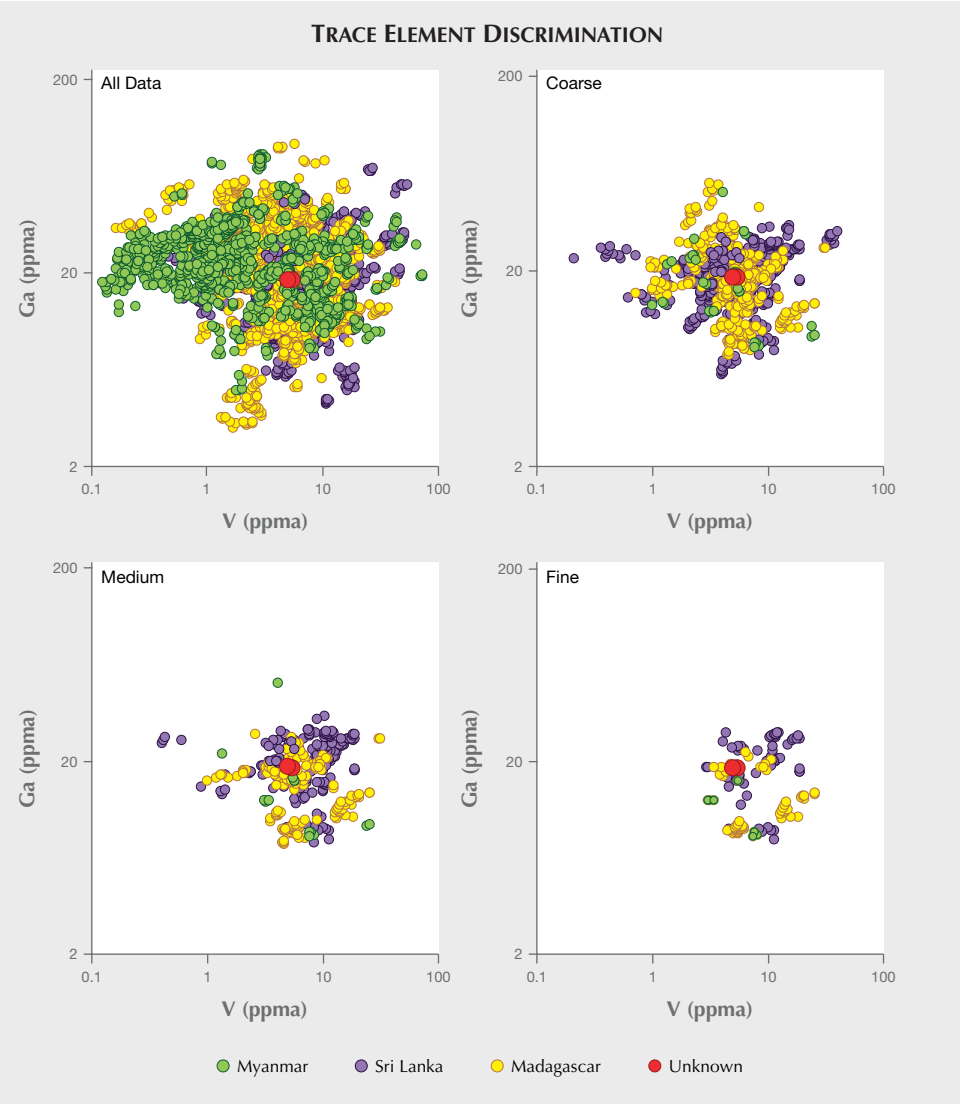

Figure 73. While the selective plotting method works well in some cases, for many metamorphic blue sapphires there is simply too much overlap to allow separation based on trace element chemistry, as illustrated by this unknown sapphire. Selective plotting uses coarse, medium, and fine windows to filter out dissimilar reference data, making the plots easier to interpret.

the trace element windows from closing too much. In this case, the element V is affected by this lower boundary for the window, which is set at 4 ppma. Also note that prior experience has suggested that Cr is not an effective discriminant element for sapphire, so it is not used in any of the plots or involved in the selective plotting method. As the window is increasingly closed (figure 72), fewer data are shown in the plot and the data shown have chemistry closer to that of the unknown. Going from coarse to fine, Madagascar appears to be a much more likely origin, which was not at all obvious without the use of selective plotting.

Of course, selective plotting has its limitations as well. For one thing, it is obvious that some sapphires from different geographic localities have nearly identical trace element profiles. Several such examples are shown in table 3 (see p. 561). Clearly there is no novel methodology or sophisticated statistical analysis that can separate stones with virtually identical trace element profiles. While selective plotting does help in many cases to get an indication of origin from trace element chemistry, in other cases the overlap is simply too great (figure 73). As always, if trace element chemistry is ambiguous and there is no definitive evidence from the inclusion scene, a gemological laboratory is obligated to issue a finding of "inconclusive" origin. Nonetheless, the selective plotting method has been blind tested in the laboratory at GIA on samples with known provenance collected through GIA's field gemology program. While the origin conclusions for the stones tested do not take into account inclusion evidence, in the cases when the selective plotting method does indicate a

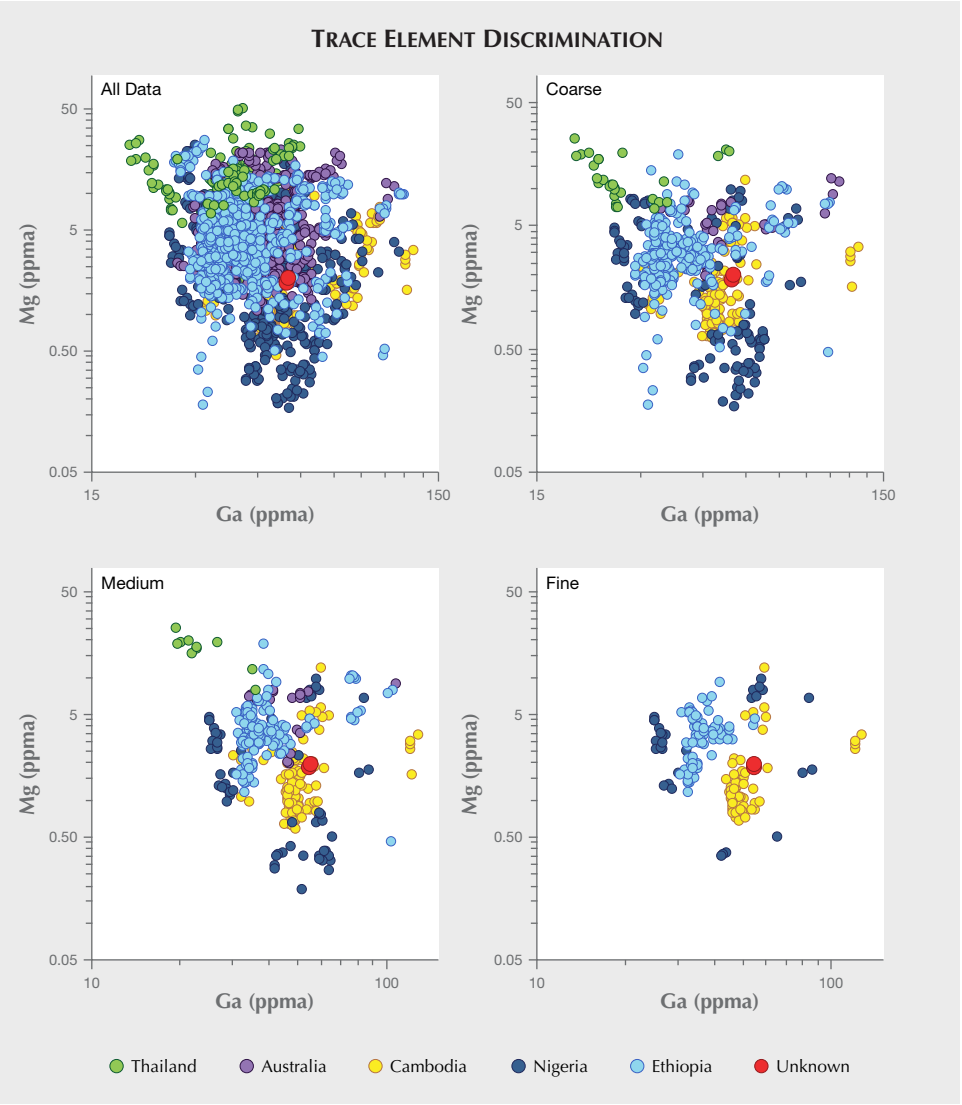

Figure 74. The use of the selective plotting method described in this article can be very helpful in elucidating the origin of basalt-related blue sapphire. This unknown Cambodian sapphire's provenance is slowly uncovered as the reference data are selectively filtered. The selective plotting uses coarse, medium, and fine windows to filter out dissimilar reference data, making the plots easier to interpret.

specific origin, the correct origin is assigned with a high level of accuracy using only trace element data and the selective plotting method.

TRACE ELEMENT CHEMISTRY OF BASALT-RELATED SAPPHIRE

While inclusions are not as useful for origin determination of basalt-related sapphires, trace element chemistry often plays a greater role (see table 4 for a summary of trace element data). GIA uses the same selective plotting technique as described above for metamorphic blue sapphire. An example of this method is shown in figure 74. (Note that all trace element data are produced from LA-ICP-MS; see Groat et al., 2019, pp. 512–535 of this issue.) The selective plotting method does seem to produce significantly more accurate origin determinations for basalt-related blue sapphire than for metamorphic blue sapphires. As with most geographic origin determinations, however, there will almost always be overlap, and in many cases the trace element chemistry evidence is ambiguous (figure 75). For basalt-related blue sapphires, ambiguous trace element data typically lead to an "inconclusive" origin call because of the often indistinct nature of their inclusions.

CONCLUSIONS

After more than 10 years, GIA's field gemology and research departments have produced an enormous amount of data on the gemological properties of blue sapphire from major deposits around the world. Despite these efforts, the inescapable conclusion seems to be that there is often significant overlap between stones from distinct geographic localities,

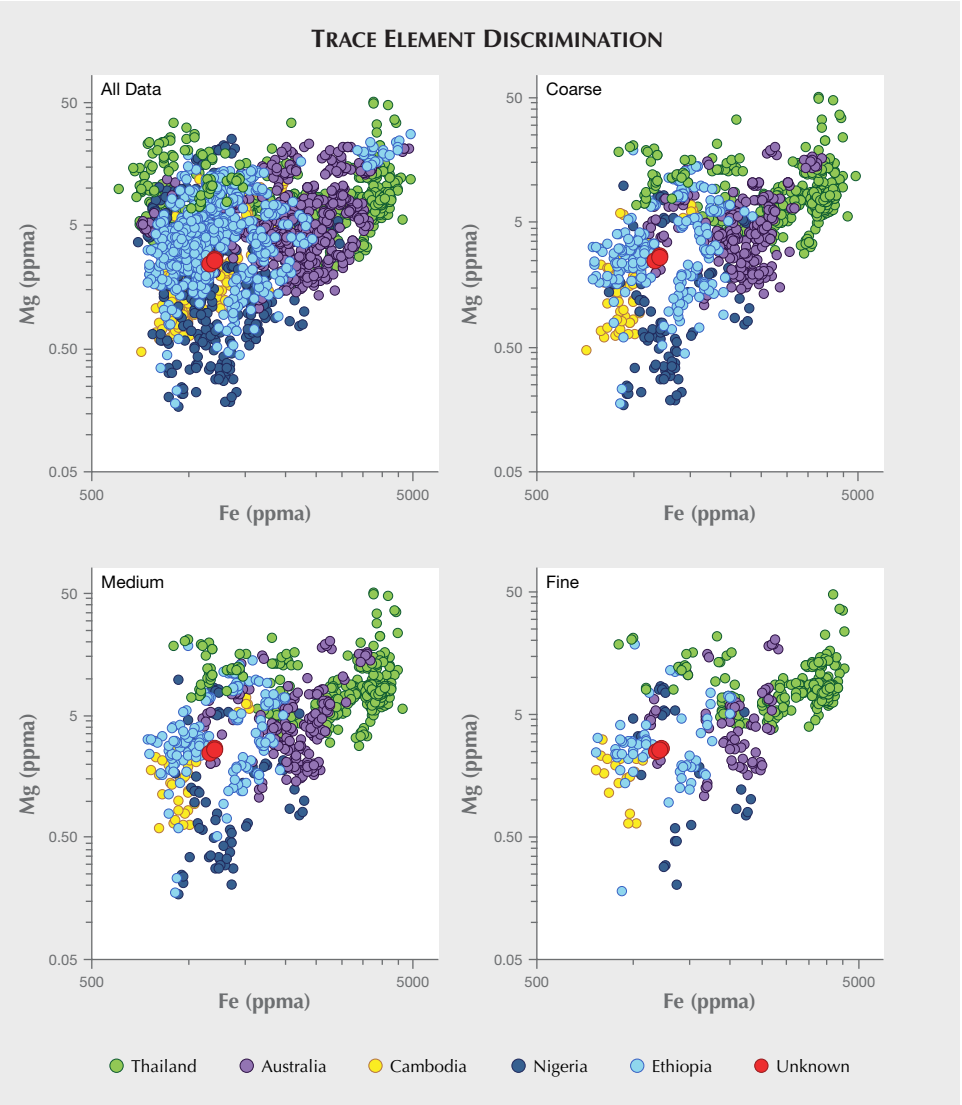

Figure 75. Given the sometimes overlapping properties of basalt-related sapphires, for some stones no amount of data processing can extract an origin determination from the data, as with this unknown sapphire. The selective plotting uses coarse, medium, and fine windows to filter out dissimilar reference data, making the plots easier to interpret.

which makes it difficult—if not impossible in some cases—to make origin determination for every blue sapphire. Inclusions and trace element chemistry can be helpful in some cases. Some blue sapphires have diagnostic mineral inclusions or distinctive patterns of silk that help trace the stone to a specific geographic locale. Especially for the metamorphic blue sapphires, stones from Sri Lanka (figure 76), Myanmar, Kashmir, or Madagascar often have characteristic inclusions that allow conclusive origin determination. Many of the criteria used to reach a conclusion on a gem's origin have come from years of experience of senior gemologists looking at stones. Our confidence in making many of these origin determinations stems from observation of reference stones collected by GIA's field gemology department that have corroborated the criteria developed over many years. For basalt-related sapphires especially, comparison with reliable trace element chemistry from field gemology reference samples may show that a stone matches with only one possible mining site, confirming its origin. But many stones—especially high-end stones, which tend to be very clean—may have ambiguous inclusion scenes or so few inclusions as to hinder origin determination. Or a stone's trace element profile may closely match reference data from two or more distinct geographic localities. While geographic origin determination for blue sapphire will remain a major focus of further research at GIA in order to refine and improve our methods, clearly no amount of additional data or collection of more reliable samples will resolve some of these cases where the overlap in data precludes an origin determination.

TABLE 4. Generalized trace element profiles in ppma of basalt-related blue sapphire.

Australia					
	Mg	**Ti**	**V**	**Fe**	**Ga**
Range	bdl–22	bdl–1316	bdl–10	716–4893	27–113
Average	6	109	4	2272	47
Median	5	46	4	2222	45
Thailand					
	Mg	**Ti**	**V**	**Fe**	**Ga**
Range	2–50	5–200	bdl–27	613–4966	19–60
Average	9	32	4	2575	38
Median	8	24	2	2638	38
Cambodia					
	Mg	**Ti**	**V**	**Fe**	**Ga**
Range	bdl–12	3–579	2–22	529–2245	30–128
Average	2	105	6	1137	56
Median	2	57	4	1015	50
Nigeria					
	Mg	**Ti**	**V**	**Fe**	**Ga**
Range	bdl–25	bdl–681	bdl–11	628–2961	25–116
Average	2	97	1	1202	50
Median	0	47	0	1095	49
Ethiopia					
	Mg	**Ti**	**V**	**Fe**	**Ga**
Range	bdl–27	4–852	bdl–17	748–4966	26–119
Average	5	66	6	1283	42
Median	4	46	6	1128	38

**bdl = below the detection limit of the LA-ICP-MS analysis. Detection limits are provided in the Samples and Analytical Methods section, p. 537.*

Figure 76. This ring contains a 4.93 ct Sri Lankan sapphire. Photo by Orasa Weldon; courtesy of Leslie Weinberg Designs.

Case Study 1: Sri Lankan Blue Sapphire

Figure CS 1-1. A 4.81 ct unheated blue sapphire considered for geographic origin determination. Photo by Diego Sanchez.

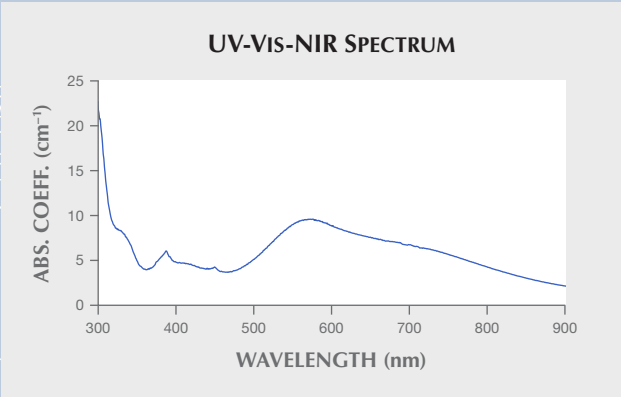

Figure CS 1-2. The UV-Vis-NIR absorption spectrum indicates a metamorphic origin, narrowing down the options for the stone's provenance to a smaller subset.

Under consideration in this case study is an unheated 4.81 ct mixed-cut oval blue sapphire (figure CS 1-1). The absence of an 880 nm band in the UV-Vis-NIR absorption spectrum indicates a metamorphic sapphire from Sri Lanka, Madagascar, Myanmar, or Kashmir (figure CS 1-2). Careful microscopic observation of the inclusions reveals long, fine rutile silk (figure CS 1-3) and several phlogopite mica crystals (figure CS 1-4), giving the distinct impression of a Sri Lankan origin. For added confidence, trace element analysis is needed (figure CS 1-5). Initially this stone plots in an area of extreme overlap between Sri Lanka, Madagascar, and Myanmar. In a case like this, a Sri Lankan origin determination might still be acceptable given that the trace element profile is at least consistent with our Sri Lankan sapphire reference data. However, using the selective plotting method introduced in this article, it can be seen that the overall trace element profile clearly matches the Sri Lankan reference data more than any other possible origin. Considering all the data collected on this stone, especially its inclusions and trace element profile, a Sri Lankan origin is determined.

Figure CS 1-3. Long, fine rutile silk gives an initial impression of a Sri Lankan origin. Photomicrograph by Nathan D. Renfro; field of view 2.85 mm.

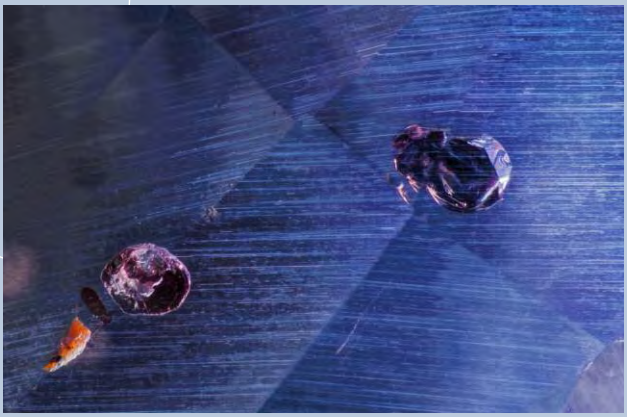

Figure CS 1-4. Fine, long silk and phlogopite mica inclusions suggest a Sri Lankan origin. Photomicrograph by Aaron C. Palke; field of view 1.49 mm.

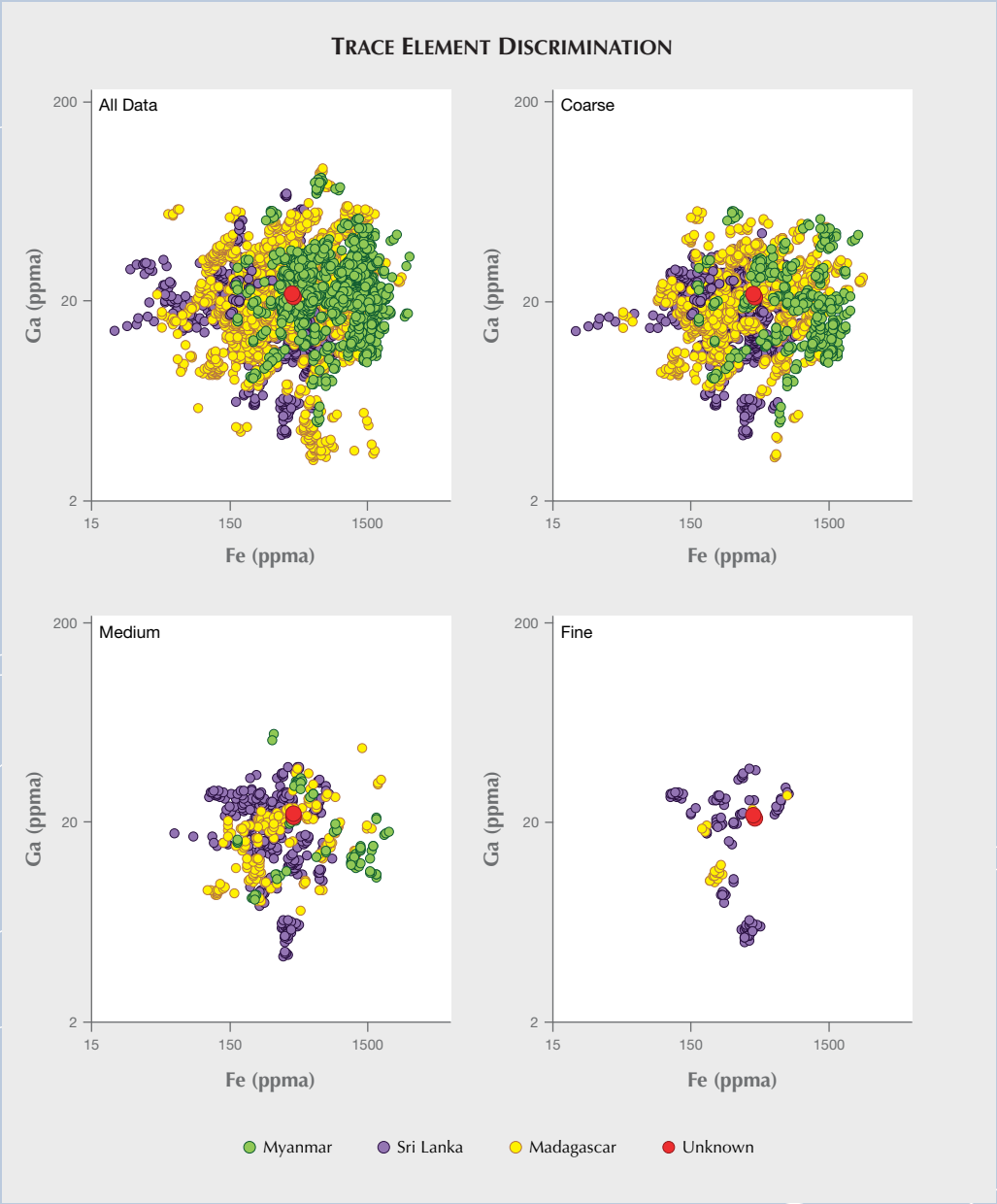

Figure CS 1-5. Trace element chemistry indicates a Sri Lankan origin for this stone (indicated by the red circle), supporting the information obtained from photomicroscopic observations of the inclusion scene.

Case Study 2: Inconclusive Metamorphic Blue Sapphire

Figure CS 2-1. A 2.83 ct unheated blue sapphire requiring a geographic origin determination. Photo by Diego Sanchez.

This case study involves an unheated 2.83 ct mixed-cut oval (figure CS 2-1). UV-Vis-NIR spectroscopy clearly indicates a metamorphic origin, which narrows down the possible origins to Sri Lanka, Myanmar, Madagascar, and Kashmir (figure CS 2-2). Microscopic observations of the inclusion characteristics shows the presence of reflective, iridescent elongate needles as well as planar, stacked clouds composed of coarse, oriented particulate silk (figure CS 2-3). At first glance, the stacked clouds are somewhat reminiscent of a Madagascar origin; however, the stacked clouds associated with a Madagascar origin are usually milky clouds composed of particles too small to be individually resolved using a microscope. The stacked clouds here do not suggest a Madagascar origin. The stone contains a CO_2 inclusion, which might initially suggest a Sri Lankan origin. However, this inclusion alone is not diagnostic (figure CS 2-4). Overall, the general inclusion scene is not indicative of any specific origin. In this case, trace element chemistry (figure CS 2-5) provides the final possible option for discerning geographic origin. Using GIA's full reference database, the stone plots in an overlapping region with Sri Lanka, Myanmar, and Madagascar. Even with the use of the selective plotting method, the overlap is not resolved. Unfortunately, an origin determination cannot be reached using the available data from inclusions, trace element chemistry, and spectroscopy. An "inconclusive" origin determination is the only option.

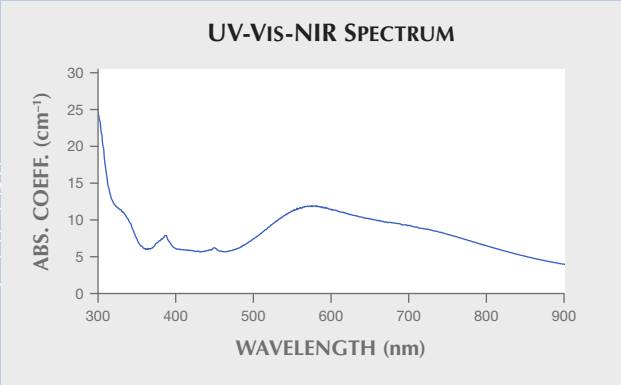

Figure CS 2-2. The UV-Vis-NIR absorption spectrum indicates a metamorphic origin, allowing the origin determination process to be narrowed down to a few possibilities.

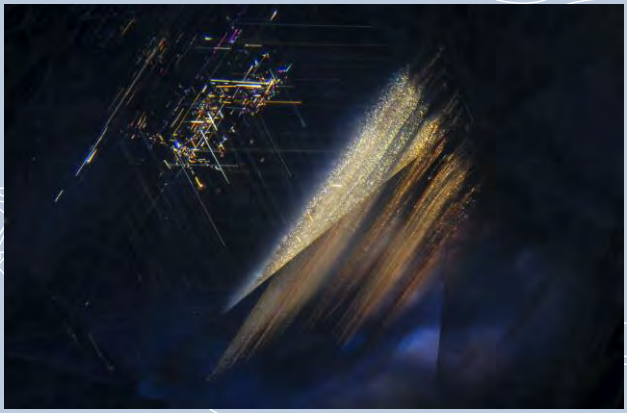

Figure CS 2-3. The sapphire has dense particulate clouds and coarse silk that show a thin-film interference effect. Photomicrograph by Aaron Palke; field of view 3.57 mm.

Figure CS 2-4. This sapphire contains a CO_2 fluid inclusion. Such inclusions might support a Sri Lankan origin but are not diagnostic. Photomicrograph by Nathan D. Renfro; field of view 2.88 mm.

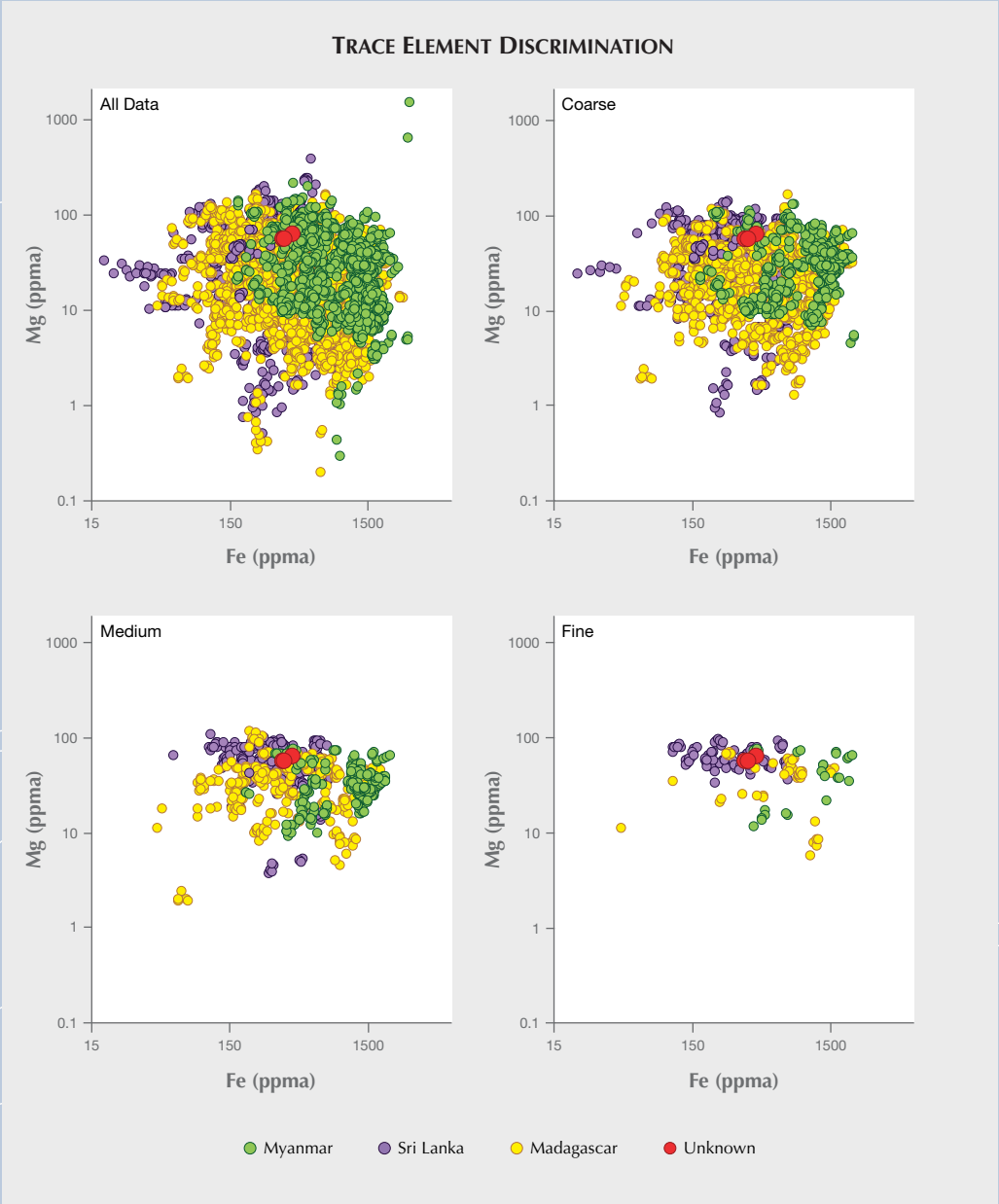

Figure CS 2-5. Trace element analysis fails to yield a distinct origin for the unknown blue sapphire (indicated by the red circle) from major metamorphic blue sapphire deposits. The selective plotting method was used to attempt to resolve this origin determination using coarse, medium, and fine filtering.

Case Study 3: Burmese Blue Sapphire

Figure CS 3-1. A 1.49 ct unheated blue sapphire undergoing the geographic origin determination process. Photo by Diego Sanchez.

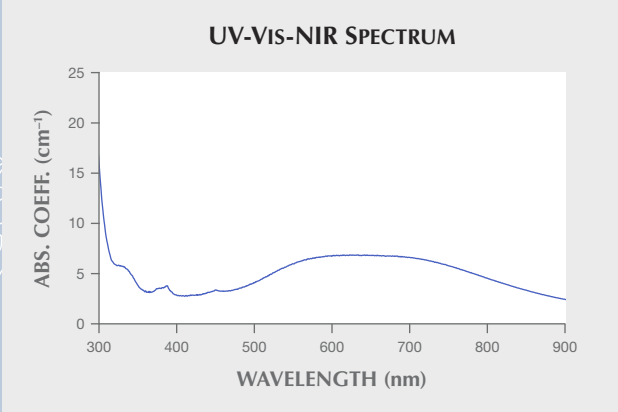

Figure CS 3-2. The UV-Vis-NIR absorption spectrum suggests a metamorphic origin, narrowing down the possible geographic origins.

For this case study, we will discuss the unheated 1.49 ct mixed-cut blue sapphire shown in figure CS 3-1. The first step in determining its geographic origin is to carefully analyze its UV-Vis-NIR spectrum (figure CS 3-2). The absence of an 880 nm absorption band reveals a metamorphic origin and narrows down the possible sources to Sri Lanka, Madagascar, Myanmar, and Kashmir. This sapphire can then be carefully studied in the microscope to search for clues in the inclusion scene. When an intense fiber-optic light is focused at a specific angle, vivid interference colors appear as the light reflects off short, stubby, and somewhat flattened rutile silk distributed throughout the sapphire (figure CS 3-3). This inclusion scene is highly reminiscent of features seen in Burmese sapphire from the GIA colored stone reference collection. The use of cross-polarized lighting reveals the presence of polysynthetic twinning, lending further credence to a Burmese origin (figure CS 3-4). The only remaining step is to check the trace element profile (figure CS 3-5) to ensure that its chemical fingerprint is consistent with our Burmese reference sapphires. The use of the selective plotting method corroborates the microscopic evidence and allows a Burmese origin to be assigned.

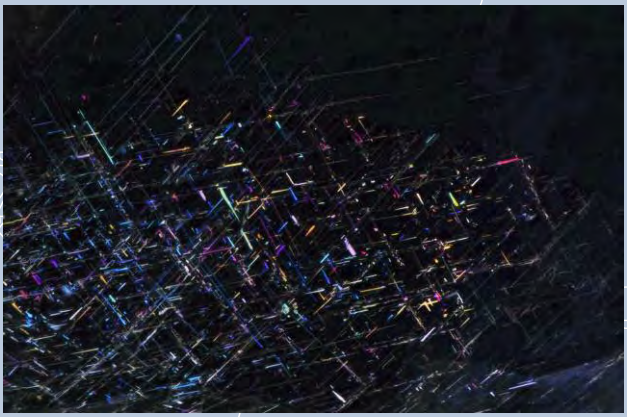

Figure CS 3-3. Short, iridescent platelet-like silk is suggestive of a Burmese origin. Photomicrograph by Aaron Palke; field of view 1.67 mm.

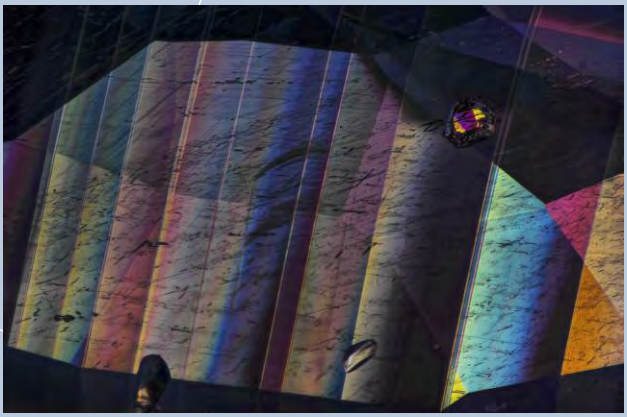

Figure CS 3-4. The twinning observed using cross-polarized light suggests a Burmese origin. Photomicrograph by Aaron Palke; field of view 2.34 mm.

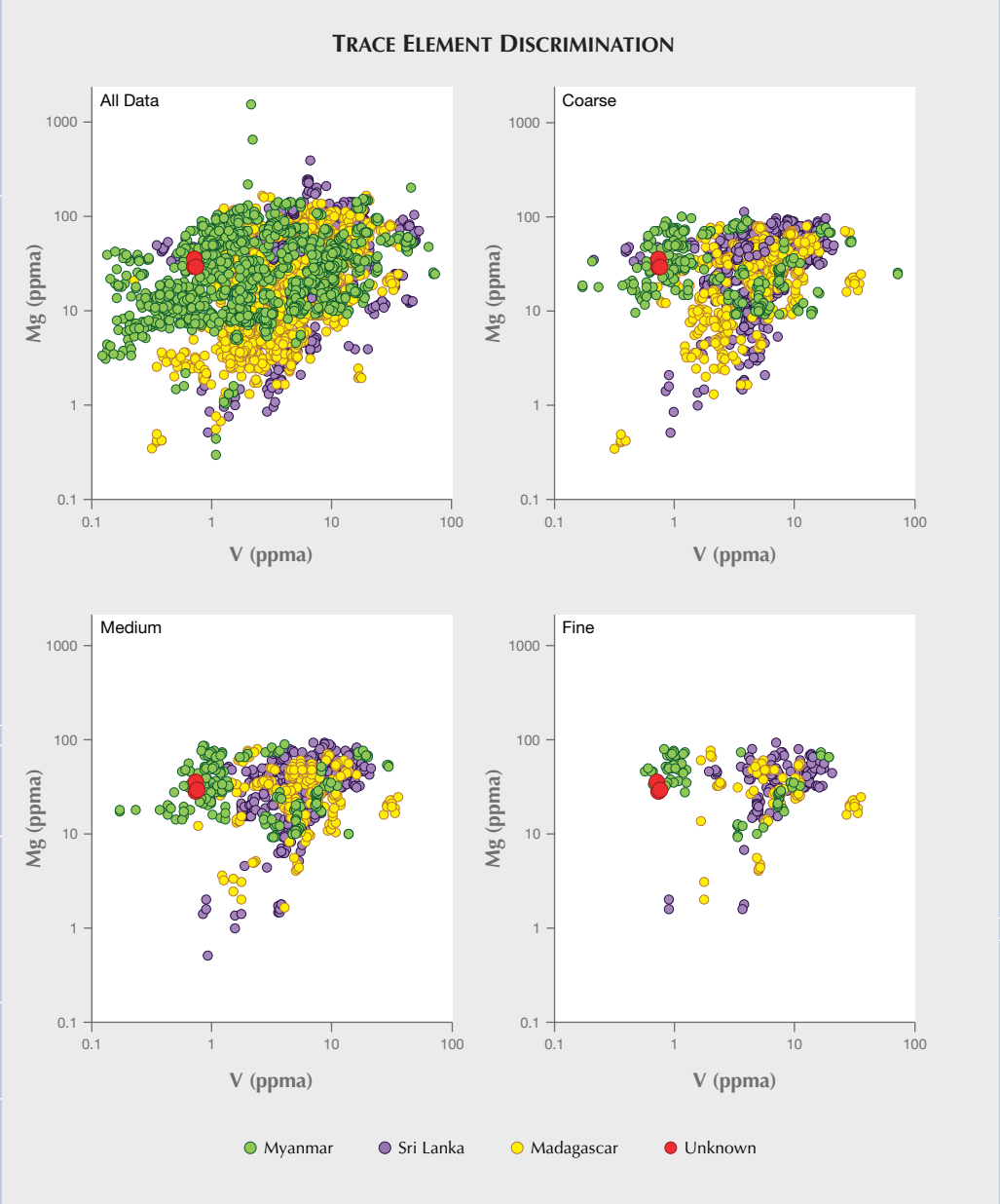

Figure CS 3-5. Trace element analysis of the unknown blue sapphire (indicated by the red circle) suggests a Burmese origin, corroborating evidence from microscopic observations.

Case Study 4: Inconclusive Blue Sapphire

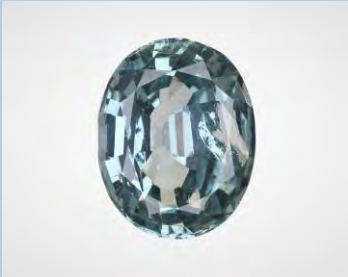

Figure CS 4-1. This blue sapphire case study involves a 5.74 ct unheated, mixed-cut oval. Photo by Diego Sanchez.

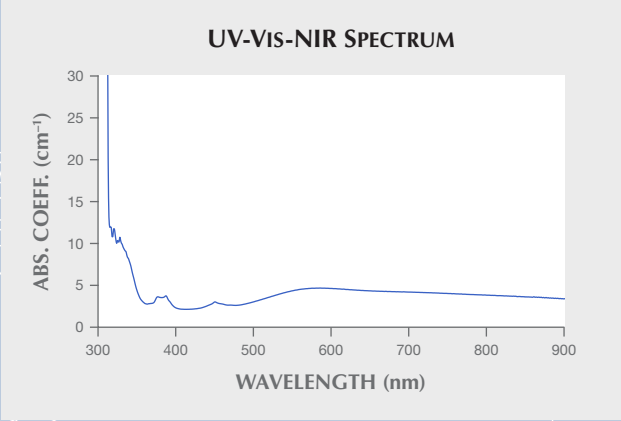

Figure CS 4-2. The UV-Vis-NIR absorption spectrum suggests a metamorphic origin, narrowing down the possible options for geographic origin.

In the final case study for this article, we will analyze the 5.74 ct unheated mixed-cut oval blue sapphire shown in figure CS 4-1. The UV-Vis-NIR absorption spectrum indicates a metamorphic origin, so we will consider Sri Lanka, Madagascar, Myanmar, and Kashmir as possible sources (figure CS 4-2). This unknown sapphire is quite clean. There is very little in the way of inclusion information that can provide a useful indication of origin. The only inclusion of note is the presence of graining throughout the sapphire (figure CS 4-3). Unfortunately, this inclusion feature does not provide much evidence one way or another about geographic origin. At this point, we can look for additional clues from trace element chemistry (figure CS 4-4). Even using the selective plotting method described in this article, the unknown sapphire plots in a region with considerable overlap of Sri Lanka, Madagascar, and Burmese reference stones. Considering the full body of evidence in this case, the only possible option is an "inconclusive" origin determination.

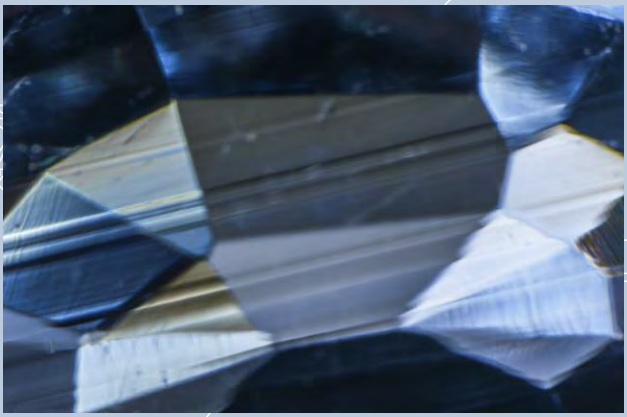

Figure CS 4-3. Microscopic observations provide little evidence of inclusions except for strong graining, shown in cross-polarized light. Photomicrograph by Nathan D. Renfro; field of view 4.80 mm.

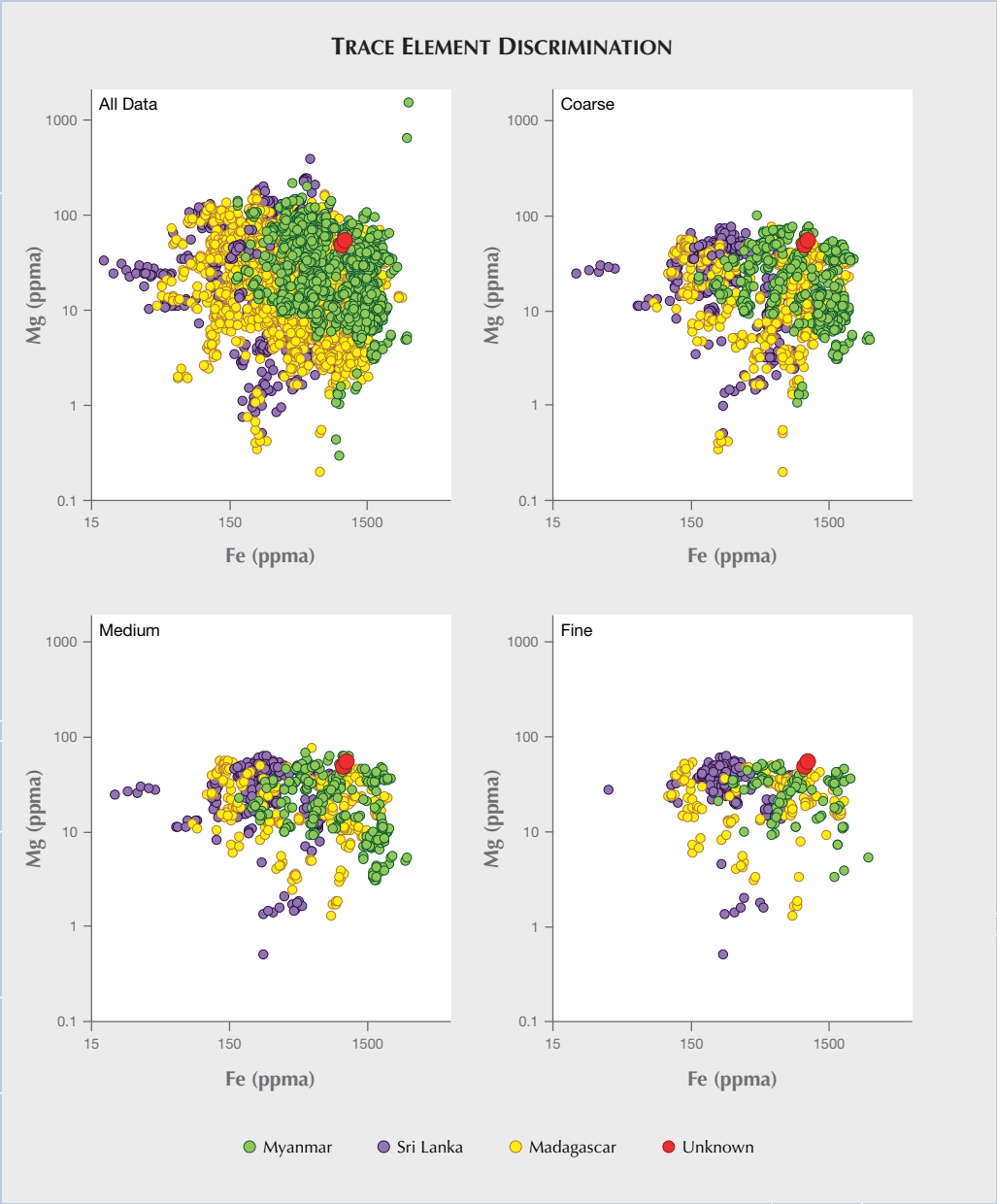

Figure CS 4-4. Trace element analysis of this unknown blue sapphire (indicated by the red circle) fails to match it conclusively to any reference stones of known provenance.

ABOUT THE AUTHORS

Dr. Palke is a senior research scientist, Mr. Renfro is manager of colored stone identification, Mr. Sun is a research associate, and Mr. McClure is global director of colored stone services, at GIA in Carlsbad, California. Ms. Saeseaw is senior manager of identification at GIA in Bangkok.

ACKNOWLEDGMENTS

The authors wish to express their gratitude for colleagues at GIA and elsewhere who have helped advance the knowledge of origin determination for sapphires and those that have otherwise helped in putting this article together, including Dino DeGhionno, Claire Malaquais, Philip Owens, Philip York, Nicole Ahline, John Koivula, Jennifer Stone-Sundberg, Barbara Dutrow, and John Valley among others. Terri Ottaway and McKenzie Santimer from the GIA Museum are also thanked for their support in the research efforts in the lab at GIA. We also thank James Day, Hanco Zwaan, and Jeffrey Keith for their thorough reviews of this manuscript and helpful comments and criticism.

REFERENCES

Abduriyim A., Sutherland F.L., Coldham T. (2012) Past, present and future of Australian gem corundum. *Australian Gemmologist*, Vol. 24, No. 10, pp. 234–242.

Atikarnsakul U., Vertriest W., Soonthorntantikul W. (2018) Characterization of blue sapphires from the Mogok Stone Tract, Mandalay region, Burma (Myanmar). *GIA Research News*, https://www.gia.edu/ongoing-research/characterization-blue-sapphires-from-mogok-stone-tract-mandalay-region-burma-myanmar

Atkinson D., Kothavala R.Z. (1983) Kashmir sapphire. *G&G*, Vol. 19, No. 2, pp. 64–76, http://dx.doi.org/10.5741/GEMS.19.2.64

Bullinger D., Fröhlich H., Klaus F., Neubauer H., Frickenschmidt A., Henneges C., Zell A., Laufer S., Gleiter C.H., Liebich H., Kammerer B. (2008) Bioinformatical evaluation of modified nucleosides as biomedical markers in diagnosis of breast cancer. *Analytica Chimica Acta*, Vol. 618, No. 1, pp. 29–34, http://dx.doi.org/10.1016/j.aca.2008.04.048

Cover T., Hart P. (1967) Nearest neighbor pattern classification. *IEEE Transactions on Information Theory*, Vol. 13, No. 1, pp. 21–27.

Dudani S.A. (1976) THe distance-weighted k-nearest-neighbor rule. *IEEE Transactions on Systems, Man, and Cybernetics*, No. 4, pp. 325–327.

Emmett J.L., Douthit T.R. (1993) Heat treating the sapphires of Rock Creek, Montana. *G&G*, Vol. 29, No. 4, pp. 250–272, http://dx.doi.org/10.5741/GEMS.29.4.250

Emmett J.L., Scarratt K., McClure S.F., Moses T., Douthit T.R., Hughes R., Novak S., Shigley J.E., Wang W., Bordelon O., Kane R.E. (2003) Beryllium diffusion of ruby and sapphire. *G&G*, Vol. 39, No. 2, pp. 84–135, http://dx.doi.org/10.5741/GEMS.39.2.84

Ferguson J.C., Fielding P.E. (1971) The origins of the colours of yellow, green and blue sapphires. *Chemical Physics Letters*, Vol. 10, No. 3, pp. 262–265, http://dx.doi.org/10.1016/0009-2614(71)80282-8

Fritsch E., Rossman G.R. (1988) An update on color in gems. Part 2: Colors involving multiple atoms and color centers. *G&G*, Vol. 24, No. 1, pp. 3–15, http://dx.doi.org/10.5741/GEMS.24.1.3

Giuliani G., Groat L.A. (2019) Geology of corundum and emerald gem deposits: A review. *G&G*, Vol. 55, No. 4, pp. 464–489, http://dx.doi.org/10.5741/GEMS.55.4.464

Giuliani G., Ohnenstetter D., Fallick A.E., Groat L., Fagan A.J. (2014) The geology and genesis of gem corundum deposits. In L.A. Groat, Ed., *Geology of Gem Deposits*, Mineralogical Association of Canada Short Course Series, Vol. 44, pp. 29–112.

Graham I., Sutherland L., Zaw K., Nechaev V., Khanchuk A. (2008) Advances in our understanding of the gem corundum deposits of the West Pacific continental margins intraplate basaltic fields. *Ore Geology Reviews*, Vol. 34, No. 1-2, pp. 200–215, http://dx.doi.org/10.1016/j.oregeorev.2008.04.006

Groat L.A., Giuliani G., Stone-Sundberg J., Renfro N.D., Sun Z. (2019) A review of analytical methods used in geographic origin determination of gemstones. *G&G*, Vol. 55, No. 4, pp. 512–535, http://dx.doi.org/10.5741/GEMS.55.4.512

Gübelin E.J., Koivula J.I. (2008) *Photoatlas of Inclusions in Gemstones*, Volume 3. Opinio Publishers, Basel, Switzerland, 672 pp.

Gübelin E.J., Peretti A. (1997) Sapphires from the Andranondambo mine in SE Madagascar: Evidence for metasomatic skarn formation. *Journal of Gemmology*, Vol. 25, No. 7, pp. 453–516.

Gunawardene M., Chawla S.S. (1984). Sapphires from Kanchanaburi Province, Thailand. *Journal of Gemmology*, Vol. 19, No. 3, pp. 228–239.

Hänni H.A. (1990) A contribution to the distinguishing characteristics of sapphire from Kashmir. *Journal of Gemmology*, Vol. 22, No. 2, pp. 67–75.

Hughes R.W., Manorotkul W., Hughes E.B. (2017) *Ruby & Sapphire: A Gemologist's Guide*. RWH Publishing/Lotus Publishing, Bangkok, 816 pp.

Kan-Nyunt H.-P., Karampelas S., Link K., Thu K., Kiefert L., Hardy P. (2013) Blue sapphires from the Baw Mar mine in Mogok. *G&G*, Vol. 49, No. 4, pp. 223–245, http://dx.doi.org/10.5741/GEMS.49.4.223

Kiefert L., Schmetzer K., Krzemnicki M.S., Bernhardt H.-J., Hänni H.A. (1996) Sapphires from Andranondambo area, Madagascar. *Journal of Gemmology*, Vol. 25, No. 3, pp. 185–210.

Krebs J.J., Maisch W.G. (1971) Exchange effects in the optical-absorption spectrum of Fe^{3+} in Al_2O_3. *Physical Review B*, Vol. 4, No. 3, pp. 757–769, http://dx.doi.org/10.1103/PhysRevB.4.757

Krzemnicki M.S. (2013) Kashmir sapphire. *SSEF Facette*, No. 20, pp. 6–9.

Moon A.R., Phillips M.R. (1994) Defect clustering and color in Fe, Ti: α-Al_2O_3. *Journal of the American Ceramic Society*, Vol. 77, No. 2, pp. 356–367, http://dx.doi.org/10.1111/j.1151-2916.1994.tb07003.x

Rahman S.A., Huang Y., Claassen J., Heintzman N., Kleinberg S. (2015) Combining Fourier and lagged *k*-nearest neighbor imputation for biomedical time series data. *Journal of Biomedical Informatics*, Vol. 58, pp. 198–207, http://dx.doi.org/10.1016/j.jbi.2015.10.004

Schwarz D., Petsch E.J., Kanis J. (1996) Sapphires from the Andranondambo region, Madagascar. *G&G*, Vol. 32, No. 2, pp. 80–99, http://dx.doi.org/10.5741/GEMS.32.2.80

Schwarz D., Kanis J., Schmetzer K. (2000) Sapphires from Antsiranana Province, northern Madagascar. *G&G*, Vol. 36, No. 3, pp. 216–233, http://dx.doi.org/10.5741/GEMS.36.3.216

Schwieger R. (1990) Diagnostic features and heat treatment of Kashmir sapphires. *G&G*, Vol. 26, No. 4, pp. 267–280,

http://dx.doi.org/10.5741/GEMS.26.4.267
Stern R.J., Tsujimori T., Harlow G., Groat L.A. (2013) Plate tectonic gemstones. *Geology*, Vol. 41, No. 7, pp. 723–726, http://dx.doi.org/10.1130/G34204.1
Stone-Sundberg J., Thomas T., Sun Z., Guan Y., Cole Z., Equall R., Emmett J.L. (2017) Accurate reporting of key trace elements in ruby and sapphire using matrix-matched standards. *G&G*, Vol. 53, No. 4, pp. 438–451, http://dx.doi.org/10.5741/GEMS.53.4.438
Sutherland F.L., Abduriyim A. (2009) Geographic typing of gem corundum: A test case from Australia. *Journal of Gemmology*, Vol. 31, No. 5-8, pp. 203–210.
Sutherland F.L., Giuliani G., Fallick A.E., Garland M., Webb G. (2009) Sapphire-ruby characteristics, West Pailin, Cambodia: Clues to their origin based on trace element and O-isotope analysis. *Australian Gemmologist*, Vol. 23, No. 9, pp. 329–368.
Townsend M.G. (1968) Visible charge transfer band in blue sapphire. *Solid State Communications*, Vol. 6, No. 2, pp. 81–83, http://dx.doi.org/10.1016/0038-1098(68)90005-7
Vertriest W., Palke A.C., Renfro N.D. (2019) Field gemology: Building a research collection and understanding the development of gem deposits. *G&G*, Vol. 55, No. 4, pp. 490–511, http://dx.doi.org/10.5741/GEMS.55.4.490
Wang W., Hall M., Shen A., Breeding C.M. (2006) Developing corundum standards for LA-ICP-MS trace-element analysis. *G&G*, Vol. 42, No. 3, pp. 105–106.
Zuo W.-L., Wang Z.-Y., Liu T., Chen H.-L. (2013) Effective detection of Parkinson's disease using an adaptive fuzzy *k*-nearest neighbor approach. *Biomedical Signal Processing and Control*, Vol. 8, No. 4, pp. 364–373, http://dx.doi.org/10.1016/j.bspc.2013.02.006

Geographic Origin Determination Of Ruby

Aaron C. Palke, Sudarat Saeseaw, Nathan D. Renfro, Ziyin Sun, and Shane F. McClure

Over the last several decades, geographic origin determination for fine rubies has become increasingly important in the gem trade. In the gemological laboratory, rubies are generally broken down into two groups based on their trace element chemistry: marble-hosted (low-iron) rubies and high-iron rubies. High-iron rubies are usually a straightforward identification based on their inclusions and trace element profiles. Marble-hosted rubies can be more challenging, with some deposits showing overlap in some of their inclusion scenes. But many marble-hosted rubies, especially Burmese stones from Mogok and Mong Hsu, can be accurately identified based on their internal features and trace element profiles. This contribution will outline the methods and criteria used at GIA for geographic origin determination for ruby.

The world ruby market has changed dramatically in modern times, especially in the last decade with the discovery and development of ruby mining in Mozambique (Chapin et al., 2015). As the gem trade has witnessed turbulent and dramatic changes in the ruby supply chain, the concept of geographic origin has become increasingly important to people buying and selling fine rubies. Often, the origin of a ruby plays an important role in the value placed on the stone, especially for exceptional quality rubies from Myanmar (figure 1). As with other colored gemstones, the ruby trade relies to a large extent on reputable gemological laboratories to make these origin determinations. In the second material-specific article of this series we delve into the world of rubies, their gemological properties, and characteristics that may aid in geographic origin determination. The following sections will detail the origin data GIA has collected for rubies and describe the methodology used in the lab to apply this data to geographic origin work.

SAMPLES AND ANALYTICAL METHODS

Rubies included in this study are predominantly from GIA's reference collection, which was assembled over more than 10 years by GIA's field gemology department. Stones in GIA's reference collection were obtained by skilled gemologists from reliable sources and were collected as close to the mining source as possible (see Vertriest et al., 2019, pp. 490–511 of this issue). When necessary, the data from the reference collection were supplemented by stones from the personal collections of the authors of this study or from GIA's museum collection. The trace element data were collected from 280 marble-hosted ruby samples and 219 high-iron samples: 65 samples from Myanmar, 93 from Vietnam, 74 from Afghanistan, 48 from Tajikistan, 34 from Cambodia, 7 from Thailand, 93 from Madagascar, and 85 from Mozambique.

Trace element chemistry was collected over the course of several years at GIA using two different laser ablation–inductively coupled plasma–mass spectrometry (LA-ICP-MS) systems. The ICP-MS used was either a Thermo Fisher X-Series II or iCAP

In Brief

- Geographic origin can have a significant impact on the value of fine rubies.
- Origin for marble-hosted rubies can often be determined from inclusions and trace element chemistry, but there are areas of overlap.
- Inclusions and trace element chemistry typically make origin determination for high-iron rubies much more straightforward.

See end of article for About the Authors and Acknowledgments.
Gems & Gemology, Vol. 55, No. 4, pp. 580–612,
http://dx.doi.org/10.5741/GEMS.55.4.580

Figure 1. Pair of ruby and diamond earrings from Mong Hsu, Myanmar, 6.04 carats total. Photo by Robert Weldon/GIA; courtesy of Robert E. Kane, Fine Gems International.

Qc system, coupled to an Elemental Scientific Lasers NWR 213 laser ablation system with a frequency-quintupled Nd:YAG laser (213 nm wavelength with 4 ns pulse width). Ablation was carried out with 55 µm spot sizes, with fluence of 8–10 J/cm^2 and repetition rates of either 15 or 20 Hz. ^{27}Al was used as an internal standard at 529250 ppmw with custom-developed synthetic corundum used as external standards (Wang et al., 2006; Stone-Sundberg et al., 2017). Detection limits varied slightly through the course of the analyses but were generally 0.1–0.3 ppma Mg, 0.5–2.0 ppma Ti, 0.03–0.2 ppma V, 5–20 ppma Fe, and 0.03–0.07 ppma Ga. Cr is not used in the laboratory as a discriminant element, after years of testing showed it is not useful for origin. Additionally, ruby/pink sapphire calls are made based on color and not Cr concentrations. Trace element values are reported here in parts per million on an atomic basis rather than the more typical parts per million by weight unit used for trace elements in many geo-

chemical studies. Units of ppma are the standard used in GIA laboratories for corundum, as this allows a more facile analysis of crystal chemical properties and an understanding of the color mechanisms of sapphire and ruby. Conversion factors are determined by a simple formula that can be found in table 1 of Emmett et al. (2003). The reference samples are diverse in terms of their appearance and presence/absence of silk, clouds, and otherwise included areas. Every effort was made to sample as many chemically distinct areas in heterogeneous samples as possible to ensure robust representation of silky, cloudy, and unincluded ruby trace element chemistry.

Inclusions were identified, when possible, using Raman spectroscopy with a Renishaw inVia Raman microscope system. The Raman spectra of the inclusions were excited by a Modu-Laser Stellar-REN Arion laser producing highly polarized light at 514 nm and collected at a nominal resolution of 3 cm^{-1} in the 2000–200 cm^{-1} range. In many cases, the confocal capabilities of the Raman system allowed inclusions beneath the surface to be analyzed.

UV-Vis spectra were recorded with a Hitachi U-2910 spectrometer or a PerkinElmer Lambda 950 in the range of 190–1100 nm with a 1 nm spectral resolution and a scan speed of 400 nm/min. UV-Vis-NIR spectra are presented as absorption coefficient (α) in units of cm^{-1} where $\alpha = A \times 2.303/t$, with A = absorbance and t = path length in cm.

MARBLE-HOSTED AND HIGH-IRON RUBIES

As with blue sapphires, the first step in making a geographic origin determination for rubies is to make a broad division into two groups—in this case, marble-hosted rubies and so-called high-iron rubies. The first group encompasses rubies from the legendary mines in Mogok in what is now Myanmar, as well as more modern deposits in Vietnam, Tajikistan, Afghanistan, and Mong Hsu in Myanmar. These marble-hosted ruby deposits are mostly located in Southeast and Central Asia and were formed during the Himalayan orogeny. During this geological event, platform carbonates (limestones) that formed in the warm shallow sea between the Indian and Asian plates were buried and subjected to extreme temperatures and pressures when these two plates collided. Fluids and molten salts that circulated through the marbles formed in this process were responsible for mobilizing aluminum and chromium in these rocks and forming ruby (Garnier et al., 2008; Giuliani and Groat, 2019, pp. 464–489 of this issue).

On the other hand, "high-iron ruby" is a catchall term used to describe the second group of rubies, which can be distinguished by their distinctive trace element chemistry. Rubies in this group have much more diverse geological origins, ranging from basalt-related rubies such as those found in Thailand and Cambodia to more metamorphic or metasomatic rubies found in Mozambique and Madagascar. The common thread, geologically speaking, seems to be that rubies in this group probably were derived from similar geological formations, which was most likely (ultra)mafic or basic intrusive igneous rocks (Mercier et al., 1999; Smith et al., 2016; Fanka and Sutthirat, 2018; Sutthirat et al., 2018; Palke et al., 2018). It was these iron-rich rocks that imparted their characteristic trace element profiles on the rubies (see Giuliani and Groat, 2019, pp. 464–489 of this issue, for more detailed discussion of the geology of these deposits).

Unfortunately, there is no spectroscopic test available to easily distinguish between these two groups of rubies as there is for metamorphic and magmatic blue sapphires. In many cases, a glance through the microscope can easily make this separation, as typical inclusion scenes tend to be different between the two groups. Intensity of fluorescence can also be an indicator: The iron in the "high-iron" group tends to inhibit fluorescence, and typically these rubies do not fluoresce as strongly as the marble-hosted rubies. In order to improve the accuracy of a geographic origin conclusion, however, trace element chemistry is important to consider as well. The marble-hosted rubies generally have iron concentrations below 200 ppma, with very few stones above 400 ppma, while iron contents in the high-iron rubies are mostly above 400 ppma. Assessing all the available data allows easy separation of rubies from these two groups in most cases, simplifying geographic origin determination by significantly reducing the number of potential locations. Those stones falling in between these two groups, with an iron content between 200 and 400 ppma, need to be considered very carefully, as several origins are possible in these cases.

GEOGRAPHIC ORIGIN DETERMINATION: MARBLE-HOSTED RUBY INCLUSIONS

In many cases, the geographic origin of marble-hosted rubies is difficult to identify in the laboratory. Historically, things would have been simpler. For hundreds if not thousands of years, the mining town of Mogok in Burma (now Myanmar) was practically the sole source of this group of rubies (Themelis,

Figure 2. Matched pair of Burmese rubies from Mogok, approximately 4 carats total. Photo by Robert Weldon/GIA; courtesy of Amba Gem Corporation.

Figure 3. Burmese ruby from Mogok, approximately 4 ct. Photo by Robert Weldon/GIA; courtesy of Amba Gem Corporation.

2008). The Afghan ruby mines at Jegdalek have had some production for several hundred years, but the output has never matched Mogok's in terms of quantity or quality (Garnier et al., 2008; Hughes et al., 2017). However, Mogok rubies started to see much more competition starting in the twentieth century with new finds of marble-hosted rubies in Vietnam, Tajikistan, and another deposit in Myanmar at Mong Hsu. Because all of these rubies were formed in the same geological event under similar geological conditions, their inclusion scenes and especially their trace element chemistry can sometimes be similar to those from the legendary deposit in Mogok.

For many stones coming through GIA's lab, inclusion scenes and trace element chemistry are enough to accurately determine a geographic origin. This is usually the case for Burmese rubies from Mogok and Mong Hsu, which often have typical inclusions. However, the reality of the situation is that in some cases a stone may not contain a diagnostic inclusion scene and the trace element chemistry may be ambiguous. In these situations, an "inconclusive" origin determination is the only appropriate answer. In the following sections we will lay out the exact criteria currently employed by GIA for making geographic origin determinations for marble-hosted rubies. Additional information about these rubies can be found in the following references: Kane et al. (1991), Brown (1992), Hughes (1994); Peretti et al. (1995), Smith (1998), Bowersox et al. (2000), Schwarz and Schmetzer (2001), Long et al. (2004a,b,c), Gübelin and Koivula (2008), Sorokina et al. (2015), and Hughes et al. (2017).

Typical Inclusion Scenes. Inclusion scenes often supply the bulk of the evidence in ascertaining geographic origin for marble-hosted rubies. Unfortunately, there are not any "diagnostic" mineral inclusions for rubies. All marble-hosted rubies can contain inclusions of calcite, apatite, and other common solid minerals. More often, the defining inclusion scenes are composed of characteristic patterns of silk, milky clouds, and patterned clouds. In the following sections we will offer examples of typical inclusion scenes for marble-hosted rubies from Myanmar, Vietnam, Afghanistan, and Tajikistan.

The Internal World of Burmese Rubies. Rubies come from two separate deposits in Myanmar: the historic Mogok region and the more recent Mong Hsu deposit. In general, Mogok has produced more important, finer-quality rubies (figures 2 and 3) while Mong Hsu has mostly supplied commercial-grade material. In the following sections, the inclusion scenes of Mogok and Mong Hsu rubies will be considered independently.

Several photomicrographs depicting typical inclusion scenes in Mogok rubies are shown in figures 4–9. The silk in Mogok rubies often occurs as nested concentrations of fine, long to short rutile needles (figure 4). These nests of silk often occur near the center of the stone, sometimes accompanied by inclusions of calcite and other minerals (figure 5). Silk in Mogok rubies often occurs as short reflective rutile needles with a flattened aspect, possibly exhibiting an arrowhead shape due to twinning of the rutile (figures 6–8). However, longer silk is also common in Mogok rubies (figures 4 and 5). Note that unlike many rubies from other deposits, Mogok rubies usually do not require heat treatment to optimize their color. This means that silk in these stones generally

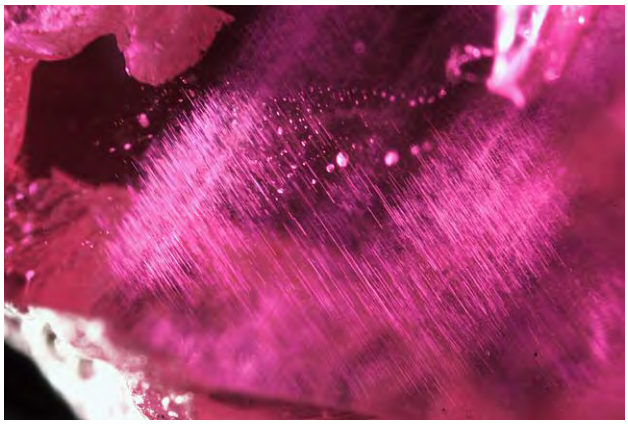

Figure 4. Dense concentrations of silk and rounded crystal inclusions suggest a Mogok, Myanmar, origin for this ruby. Photomicrograph by Charuwan Khowpong; field of view 2.37 mm.

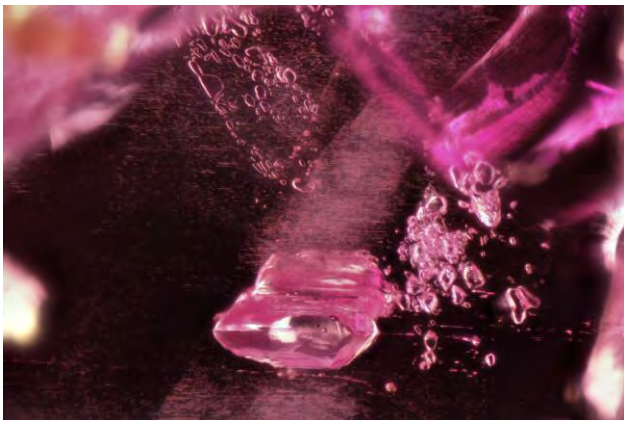

Figure 5. Dense concentrations of silk accompanied by rounded calcite crystals suggest a Burmese origin. Photomicrograph by Jonathan Muyal; field of view 1.99 mm.

stays intact. While heat treatment of blue sapphires tends to destroy evidence of origin in the form of silk patterns, this is rarely the case for the silk seen in Mogok rubies. Another inclusion scene suggestive of a Mogok origin is distinctive roiled graining, which is likely caused by turbulent and rapid crystal growth when the rubies formed (figure 9). Distinct red and colorless zoning is often associated with this graining. Note that Burmese rubies from Mogok can often be identified by characteristic inclusion scenes such as iridescent short needles or nested silk, though there may be borderline cases where the inclusions are not conclusively Mogok but might still indicate such an origin (see the "Inclusion Scenes Gone Wrong" section below).

The ruby deposits in Mong Hsu were discovered only recently, in the later part of the twentieth century. Luckily, Mong Hsu rubies tend to have characteristic inclusion scenes that allow them to be easily separated from rubies from Mogok and other marble-hosted rubies. Because dark blue zones and fractures are so common in Mong Hsu rubies in their natural state, most stones from this deposit are heat treated at high temperatures. Unheated Mong Hsu rubies are

Figure 6. Shorter rutile silk with a flattened aspect, typical of Mogok rubies, creates vivid iridescence when viewed with intense fiber-optic illumination. Photomicrograph by Charuwan Khowpong; field of view 1.12 mm.

Figure 7. Short, reflective platelet-like silk is characteristic of Mogok rubies. Photomicrograph by GIA; field of view 1.31 mm.

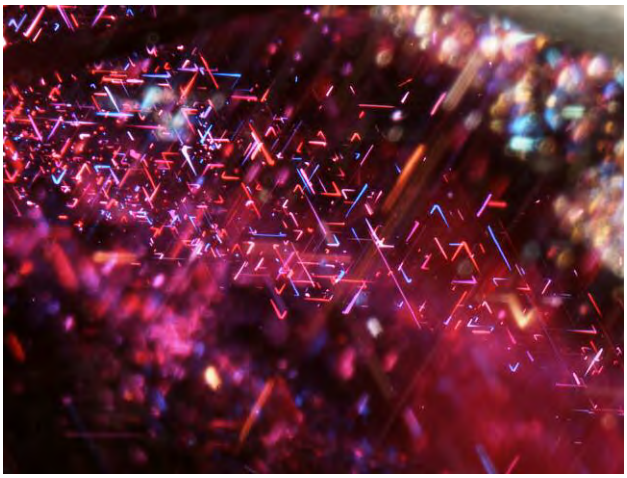

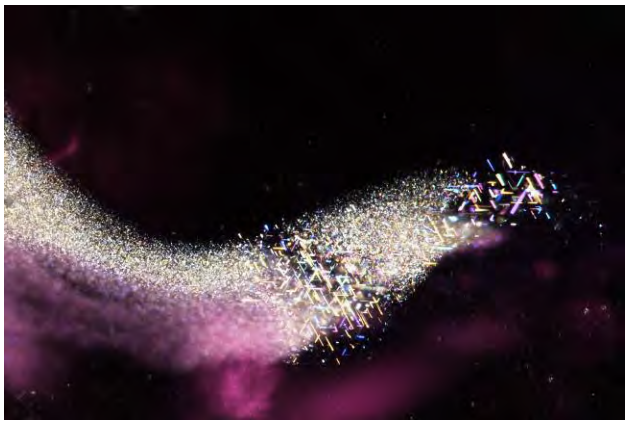

Figure 8. A mixture of flattened rutile needles is accompanied by a fine dusting of particulate silk in this Mogok ruby. Photomicrograph by Charuwan Khowpong; field of view 1.75 mm.

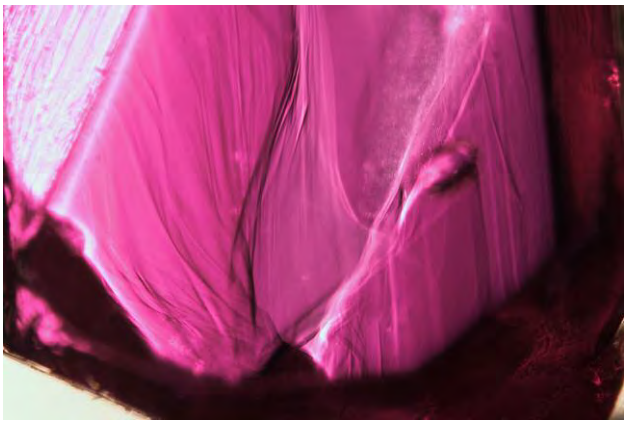

Figure 9. Roiled graining is consistent with a Mogok origin in this ruby. Photomicrograph by Charuwan Khowpong; field of view 2.83 mm.

Figure 10. This deep blue hexagonal core is a telltale sign of an unheated Mong Hsu ruby's provenance. However, unheated Mong Hsu rubies are rarely encountered in the trade. Photomicrograph by Jonathan Muyal; field of view 4.79 mm.

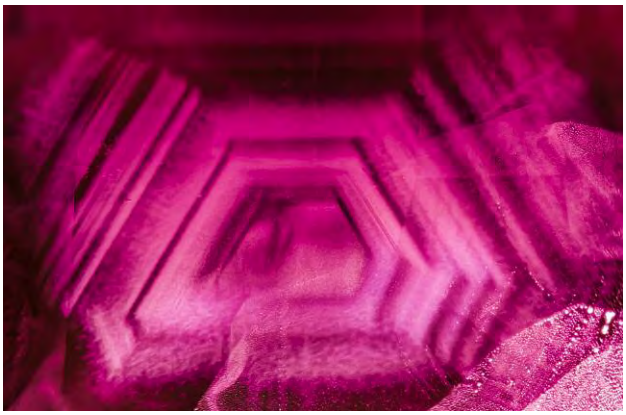

Figure 11. Heated Mong Hsu rubies are often identified by dense hexagonal white clouds in their cores. Photomicrograph by Nathan Renfro; field of view 2.97 mm.

often distinguished by a dark blue core (figure 10). However, unheated material from Mong Hsu is rare. More commonly seen is a white, cloudy core produced by the heat treatment process (figure 11). Patterned clouds such as ladders and snowflake inclusions are typical of Mong Hsu rubies (figures 12 and 13). Stepped, angular graining is occasionally seen in Mong Hsu rubies as well (figure 14). More recently, flux-as-

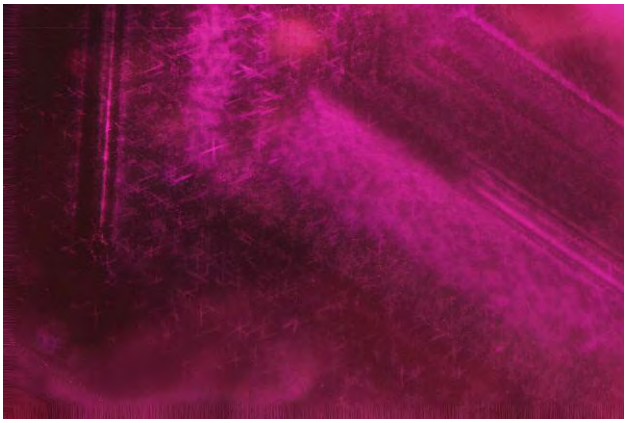

Figure 12. Snowflake inclusions and other types of patterned clouds are typical inclusions in heated Mong Hsu rubies. Photomicrograph by Jonathan Muyal; field of view 4.10 mm.

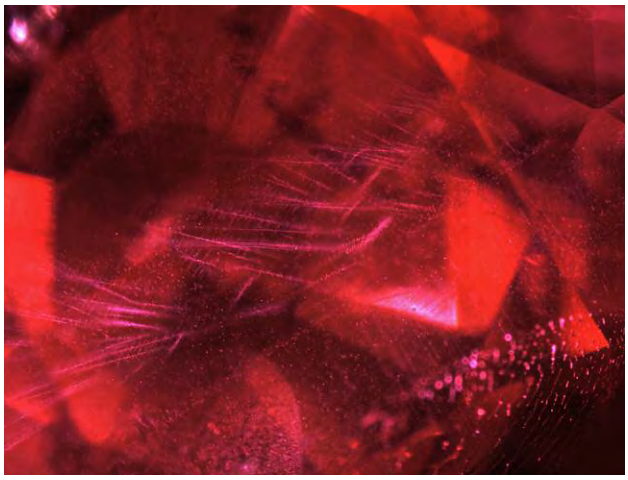

Figure 13. Ladder- and streamer-like inclusions provide an indication of this ruby's Mong Hsu origin. Photomicrograph by GIA; field of view 4.68 mm.

Figure 14. Stepped, angular graining can be seen in Mong Hsu rubies. Photomicrograph by GIA.

sisted heating of rubies has been widely used with Mong Hsu rubies, and flux-healed fractures are prevalent in much of the material on the market. Solid mineral inclusions are rare in these rubies.

The Internal World of Vietnamese Rubies. The ruby deposits in Vietnam, discovered in the late twentieth century, have yielded fine rubies of exceptional quality (figures 15 and 16), rivaling those from the famed Mogok Valley (Kane et al., 1991; Brown, 1992; Khoi et al., 2011). As with most marble-hosted rubies, there tends to be significant overlap in their properties between various geographic localities, especially when it comes to trace element chemistry (see the "Trace Element Chemistry" section below). However, Vietnamese rubies may have distinctive inclusion scenes that help in determining their provenance. Especially characteristic is the presence of dense, angular milky banding (figures 17 and 18). Coarse, patterned clouds such as snowflake and ladder inclusions are relatively common in Vietnamese rubies and tend to be larger than those found in Mong Hsu rubies (figure 18). Coarse, oriented silk is also seen in some Vietnamese rubies, sometimes resembling the silk in Mogok rubies, although their inclusion scenes can usually be distinguished by the experienced gemologist. Vietnamese rubies often have blue color zoning that can be somewhat irregu-

Figure 15. A 1.32 ct Vietnamese ruby. Photo by Orasa Weldon.

Figure 16. A 1.34 ct Vietnamese ruby. Photo by Robert Weldon/GIA.

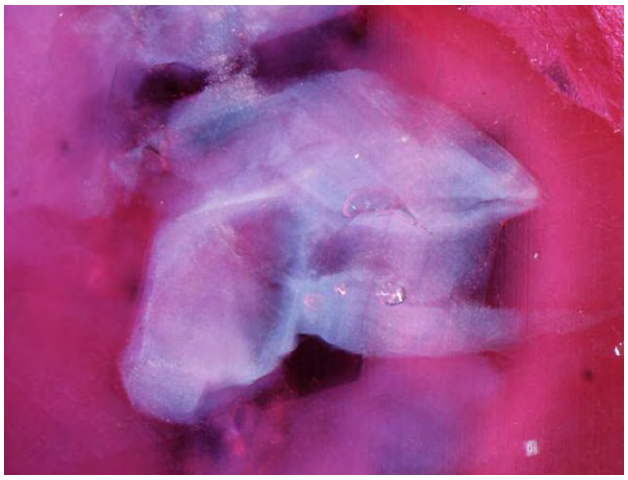

Figure 17. Dense, milky clouds distinguish this Vietnamese ruby from the rubies found in Mogok, Myanmar. Photomicrograph by GIA; field of view 1.75 mm.

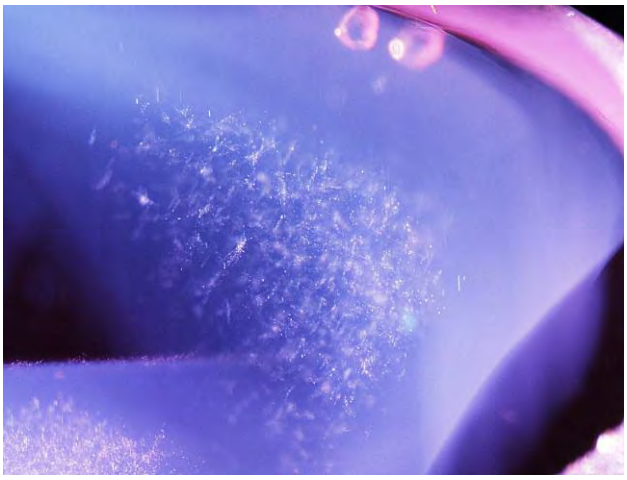

Figure 18. Coarse, patterned clouds and milky clouds provide strong evidence of this ruby's Vietnamese origin. Intense fiber-optic illumination produces the bluish coloration in this photo due to light scattering. Photomicrograph by GIA; field of view 2.33 mm.

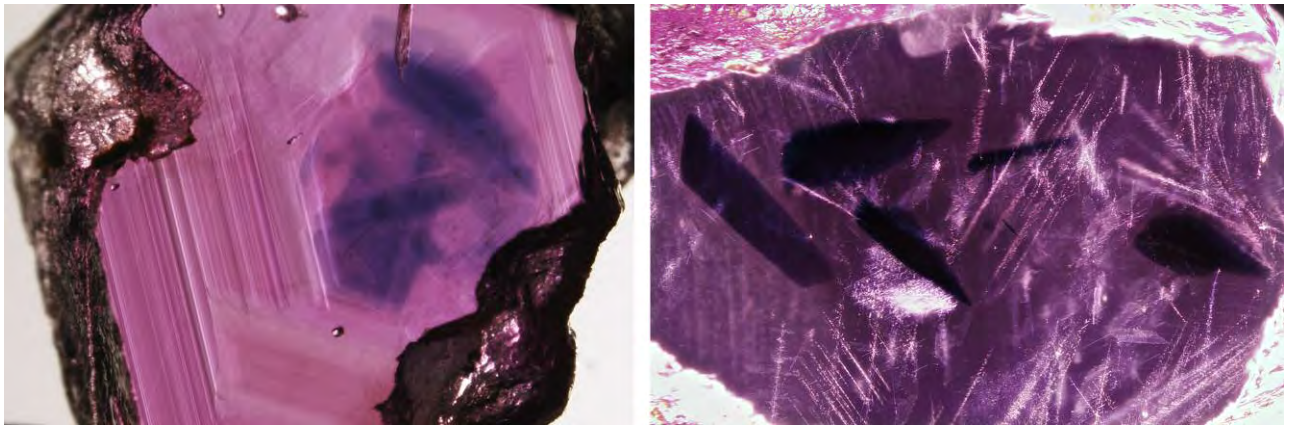

Figure 19. Blue color zoning is common in Vietnamese rubies. Photomicrographs by GIA (left, field of view 7 mm) and Jonathan Muyal (right, field of view 3.57 mm).

lar in nature (figure 19), as well as roiled growth patterns in some stones. Heat treatment is often used in an attempt to remove blue color zoning in these rubies, but this is often at a low enough temperature that a stone's silk may not be dramatically affected. Rounded mineral crystals can also be seen in Vietnamese rubies, although these are not considered diagnostic (figure 20).

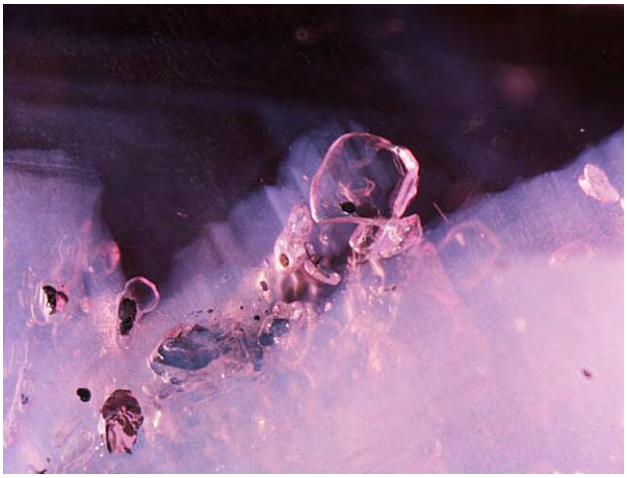

Figure 20. Rounded mineral inclusions similar to those found in rubies from Mogok can be seen in Vietnamese rubies. In this example, the Vietnamese origin is corroborated by dense, milky clouds. Photomicrograph by GIA; field of view 1.4 mm.

Figure 21. Short, thin rutile needles are also characteristic of Afghan rubies and may offer an indication of origin, along with other corroborating gemological data. Photomicrograph by Charuwan Khowpong; field of view 1.02 mm.

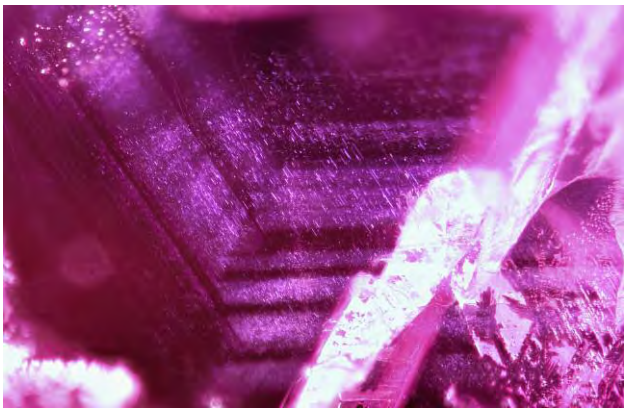

Figure 22. Fine particulate clouds arranged in a hexagonal pattern are often seen in Afghan rubies. Photomicrograph by Jonathan Muyal; field of view 1.8 mm.

The Internal World of Afghan Rubies. The ruby mines near Jegdalek in Afghanistan are considered one of the classic sources from the ancient world, believed to date back around 800 years (Bowersox et al., 2000). However, supplies have always been limited, especially for rubies with high clarity that could compete with fine rubies from Myanmar. The dominant inclusions in much of the material available are fractures and fingerprints. Unfortunately, high-quality material with sufficient clarity has been difficult to obtain, which has limited thorough study of the characteristic inclusions in this material. The following discussion will detail the information gathered so far by GIA's field gemology program. Afghan rubies can sometimes be distinguished by characteristic fine rutile needles (figure 21) and fine particulate clouds, often found in angular or hexagonal patterns (figure 22), which are distinct from the milky clouds found in Vietnamese rubies or the coarser and needle-like silk seen in Mogok rubies. Planar milky clouds can also be found in Afghan rubies (figure 23), but they tend to be fainter than those seen in Vietnamese rubies and are not easily observed without fiber-optic illumination. Stringer-type inclusions formed of small dusty particulates are sometimes seen in Afghan rubies (figure 24), but they are also found in rubies from

Figure 23. Afghan rubies can contain faint planar milky bands. Photomicrograph by Charuwan Khowpong; field of view 2.00 mm.

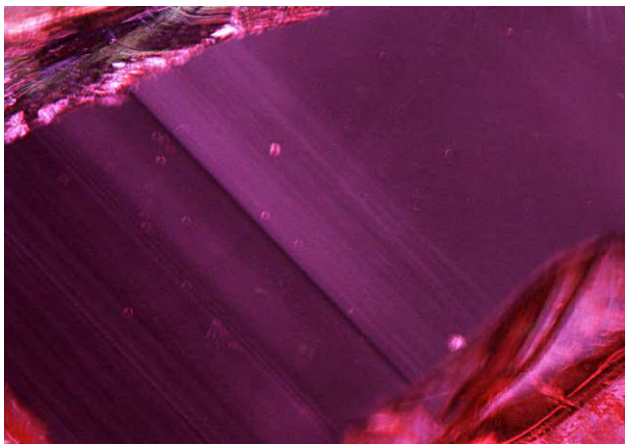

Figure 24. Stringer inclusions are also common in Afghan rubies. Photomicrograph by Charuwan Khowpong; field of view 3.1 mm.

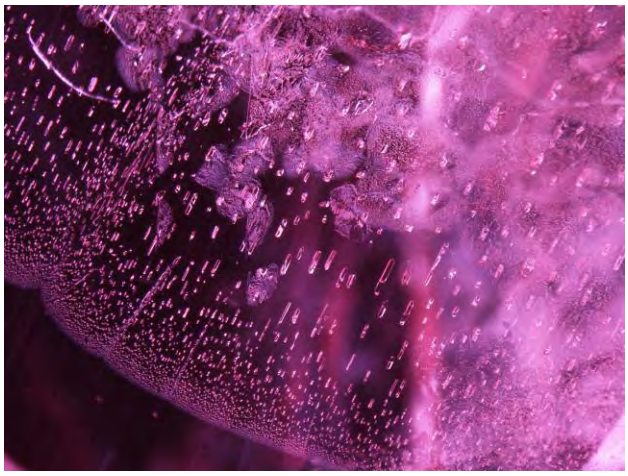

Figure 25. Fluid-filled fingerprints are often present in rubies from Afghanistan. Photomicrograph by GIA; field of view 3.1 mm.

Figure 26. A 17.14 ct Tajik ruby. Photo by Robert Weldon/GIA; courtesy of Arthur Groom.

Tajikistan. Fluid-filled fingerprints are also seen in Afghan rubies and (figure 25).

The Internal World of Tajik Rubies. Tajik rubies are another relative newcomer to the world ruby mining scene (figure 26). Discovered in the 1970s by Soviet geologists, only small quantities have been produced from the Snezhnoe deposit in southern Tajikistan near the Chinese border (Smith et al., 1998; Sorokina et al., 2015). Further, much of what is produced has been heavily included, lower-quality material. Nonetheless, some very fine rubies are known to have been sourced from Snezhnoe. Tajik rubies can be difficult to separate from other marble-hosted deposits, partly due to the relative lack of diagnostic inclusions. Much like Afghan rubies, the dominant inclusions are fractures and healed fissures (fingerprints). Also notable, and indicative of a Tajik origin, are so-called rosettes or haloes surrounding small crystal inclusions (figure 27). Blue color zoning is also frequently seen in Tajik rubies (figure 28). It can be distinguished from similar features observed in Vietnamese rubies by the angular

Figure 27. Small crystal inclusions with surrounding "rosettes" or haloes point to these rubies' Tajik origin. Photomicrographs by GIA; field of view 1.00 mm (left and right).

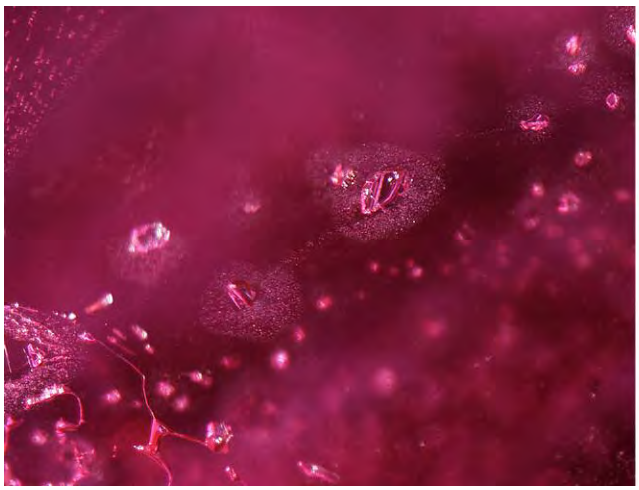

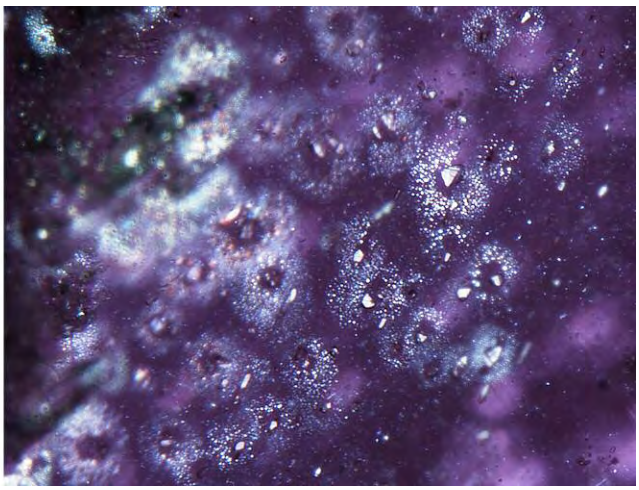

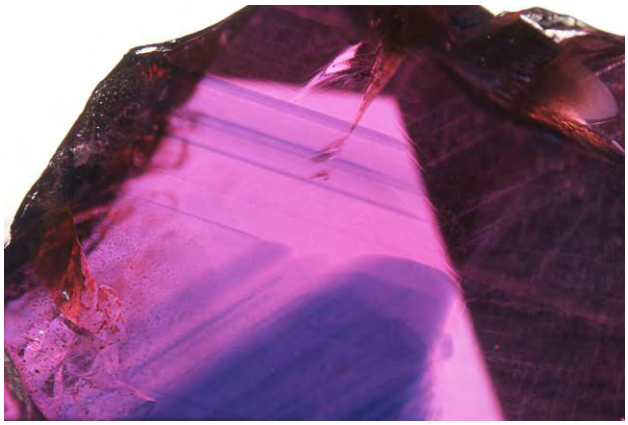

Figure 28. Blue color zoning in Tajik rubies is generally distinguished from similar features in Vietnamese rubies by its angular and more regular morphology. Photomicrograph by GIA; field of view 6.20 mm.

Figure 30. Small, often dusty groups of particles without a well-defined geometric pattern can be observed in Tajik rubies, but they may be difficult to distinguish from those seen in Afghan rubies. Photomicrograph by Charuwan Khowpong; field of view 2.5 mm.

and very planar nature of the blue zones, in contrast to the more irregular blue zoning in Vietnamese rubies. Tourmaline crystal inclusions seem to be a diagnostic mineral inclusion in Tajik rubies (figure 29). These tourmaline inclusions are often found in small, irregular clusters that include mica and graphite inclusions. Also observed are fine, dusty distributions of particles (figure 30) and sometimes stringer inclusions composed of fine particulate matter (figure 31). However, similar features are seen in Afghan rubies.

Inclusion Scenes Gone Wrong. With geographic origin determinations for marble-hosted rubies, one encounters the same problem as with metamorphic blue sapphires: The gems from these deposits were mostly formed in the same geological orogenic event, from very similar geological formations, and likely at similar conditions of pressure, temperature, and chemistry. For this reason, there tends to be significant overlap in their gemological properties, namely inclusions and trace element chemistry. Care needs to be taken, especially with Vietnamese and Mogok rubies, as occasionally their inclusion scenes overlap. Importantly, Vietnamese rubies can sometimes be found with patterns of rutile silk that might give the initial impression of a Mogok origin. Inclusion

Figure 29. Tourmaline inclusions are sometimes found in Tajik rubies and can be used as an indication of their origin. Tourmaline is often observed as clusters accompanied by mica and graphite (right). Photomicrographs by Charuwan Khowpong; field of view 1.10 mm (left) and 1.69 mm (right).

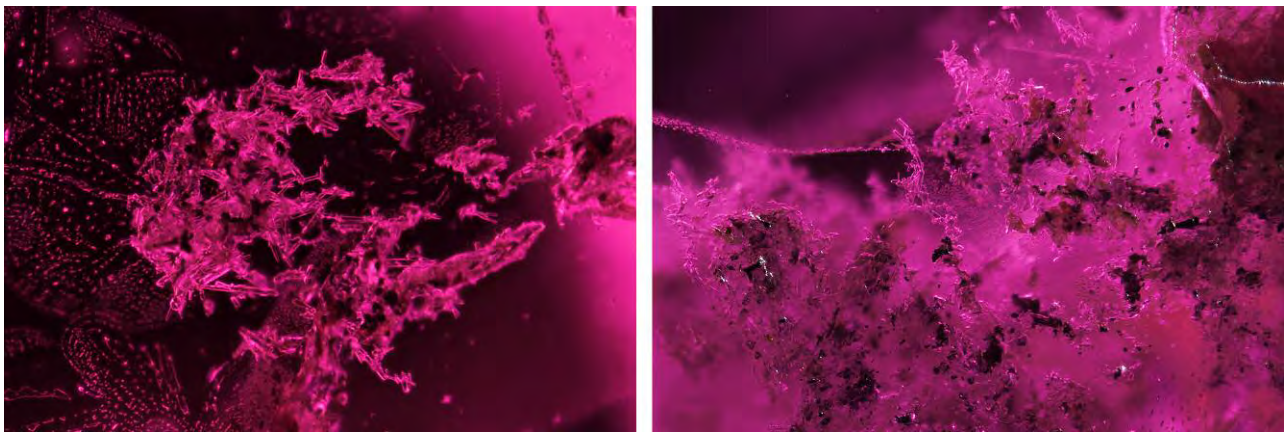

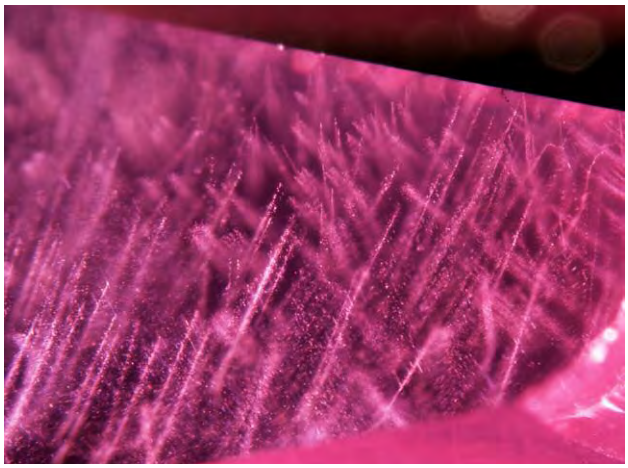

Figure 31. Stringer inclusions composed of minute particles can be seen in Tajik rubies as well as those from Afghanistan. Photomicrograph by Vararut Weeramonkhonlert; field of view 3.1 mm.

Figure 33. The dense, intergrown, and nested nature of the rutile silk might suggest a ruby mined in the Mogok Valley, potentially masking its true Vietnamese origin. Photomicrograph by GIA.

scenes suggestive of Mogok rubies, composed of short to long well-defined needles of rutile silk (sometimes densely packed and intergrown) can occasionally be found in rubies from Vietnam (figures 32 and 33). Additionally, the roiled graining considered characteristic of Mogok rubies can also occasionally be found in Vietnamese rubies (figure 34). Observation of dense milky clouds, if present, might help to resolve overlap and indicate a Vietnamese origin. Other potentially conflicting inclusion scenes include the presence of patterned clouds in Tajik and Afghan rubies that might give an initial impression of a Vietnamese ruby (figures 35 and 36). Whenever possible, additional gemological evidence should be sought out to corroborate an origin conclusion. For instance, milky clouds might suggest a Vietnamese origin or arrowhead rutile needles might indicate a Mogok origin. However, it bears emphasizing that the gemological world is not perfect. Not every faceted stone will contain inclusion scenes that are diagnostic of a particular locality. Moreover, many stones do not have inclusion scenes that are even suggestive of one origin over another. A marble-hosted ruby may lack milky or patterned clouds and

Figure 32. The short to long well-defined rutile silk in these Vietnamese rubies might give a mistaken impression of Burmese origin. Photomicrographs by GIA; field of view 1.10 mm (left) and 0.97 mm (right).

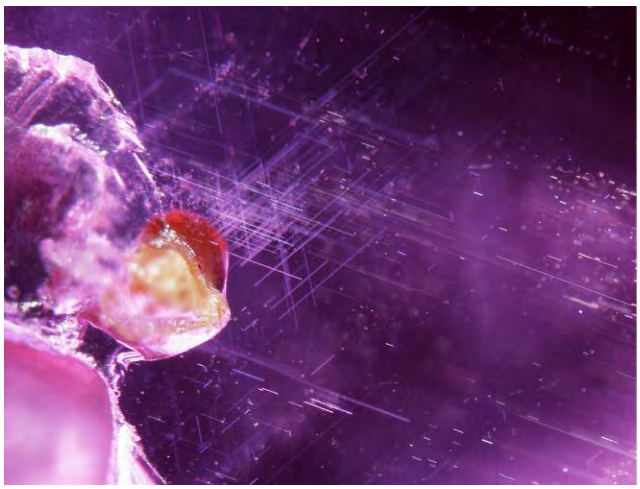

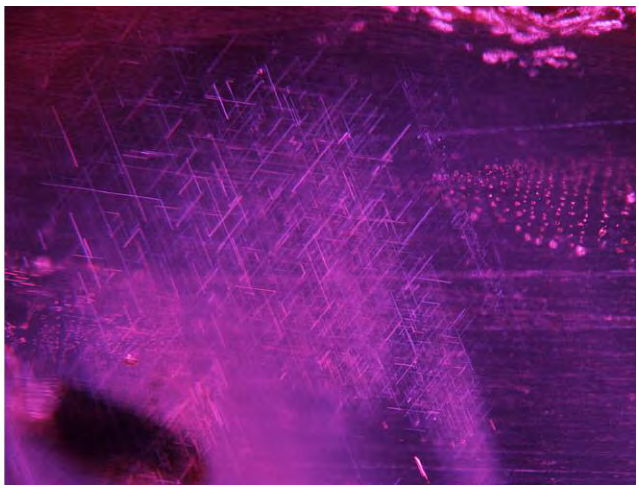

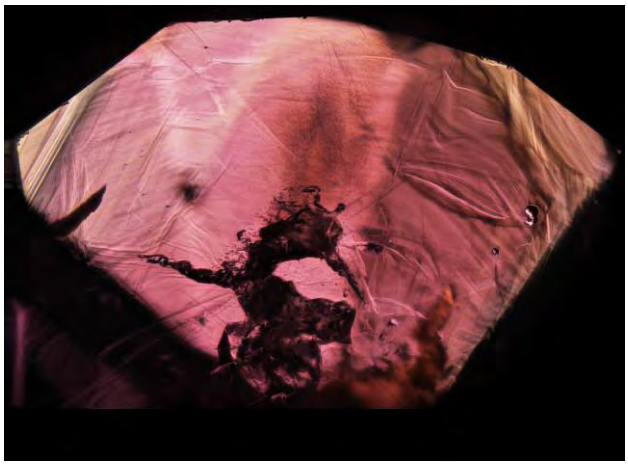

Figure 34. Roiled graining, sometimes suggestive of a Mogok origin, is occasionally observed in rubies from Vietnam. Photomicrograph by Jonathan Muyal; field of view 2.90 mm.

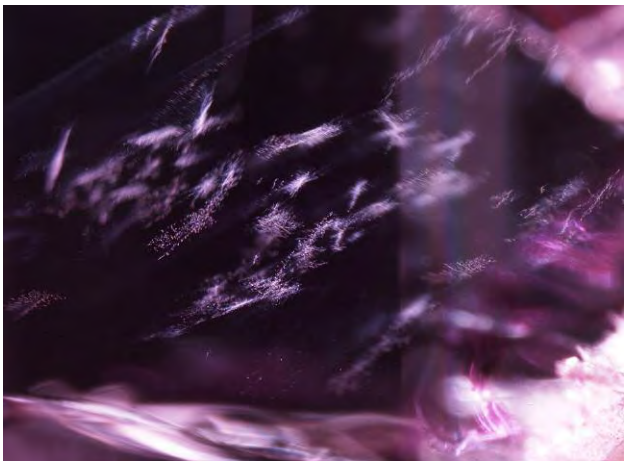

Figure 35. The snowflake-like patterned clouds in this Afghan ruby might otherwise suggest a Vietnamese origin. Other gemological evidence would be needed to issue a conclusive origin determination. Photomicrograph by Charuwan Khowpong; field of view 2.04 mm.

contain only coarse rutile silk that is not particularly nested and dense, and not iridescent. In this case, the inclusion scene could give the impression of either a Burmese or Vietnamese origin, offering scant evidence to indicate one origin over another. In these cases, the only clear choice is to offer an "inconclusive" origin determination. Unfortunately, there will always be stones for which laboratories will be obligated to issue "inconclusive" calls due to the lack of any diagnostic piece of evidence pointing toward a specific conclusion.

Figure 36. The patterned clouds in this Tajik ruby might also suggest a Vietnamese origin in the absence of any additional origin evidence. Photomicrograph by GIA; field of view 6.30 mm.

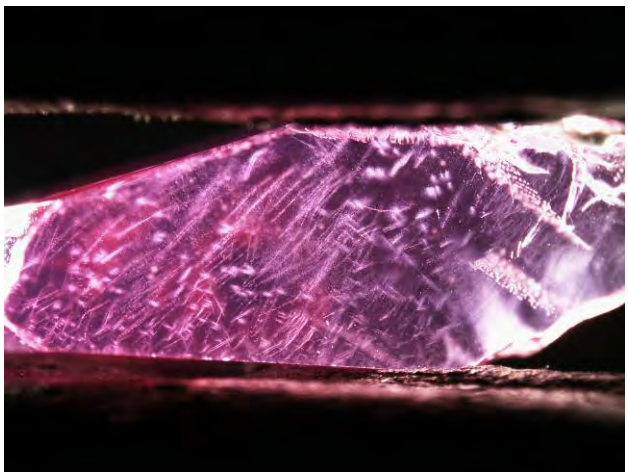

High-Iron Ruby Inclusions. If trace element analysis places a stone in the high-iron ruby group, the geographic origin determination process follows a different path from marble-hosted rubies, with a distinct set of possible provenances. These are rubies from Thailand and Cambodia, Madagascar, Mozambique, and smaller deposits in Tanzania, Kenya, and Greenland. Fortunately, "high-iron ruby" is more of a broad catchall term with relatively loose implications about geological conditions of formation. For instance, high-iron rubies from Mozambique and Madagascar formed during high-pressure and high-temperature regional metamorphism, while those mined near the Thai/Cambodian border are basalt-related and, in some ways, more geologically akin to classic magmatic blue sapphires. The common thread seems to be the rubies' derivation from similar host rocks. While there are many open questions about their exact geological genesis, high-iron rubies are generally considered to have been derived from what were originally basic or (ultra)mafic igneous rocks. Nonetheless, variations in the specific geological circumstances surrounding ruby genesis have produced differences in their gemological properties, allowing for straightforward origin determination in most cases.

Rubies from most of the high-iron ruby deposits (Mozambique, Madagascar, and Thailand/Cambodia) can often be separated based only on inclusions, but even if microscopic observations fail to produce a conclusion, trace element chemistry can almost always provide the final piece of evidence. In the following section we will describe typical inclusion scenes for

Figure 37. A 3.90 ct Cambodian ruby. Photo by Orasa Weldon.

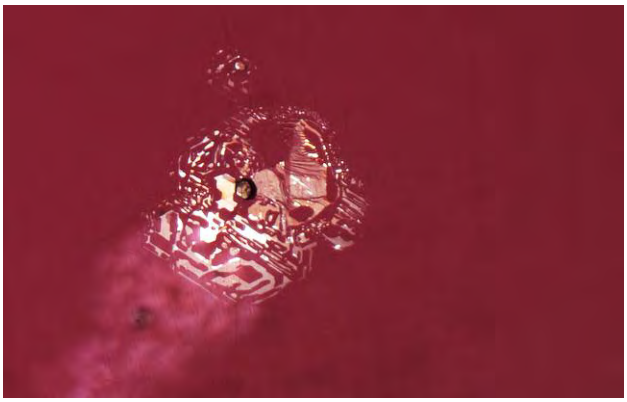

Figure 38. The geometric, partially healed decrepitation halo surrounding this negative crystal provides evidence of Cambodian provenance. Photomicrograph by Jonathan Muyal; field of view 0.95 mm.

the major high-iron ruby deposits. Additional information can be obtained from the following references (Schwarz and Schmetzer, 2001; Gübelin and Koivula, 2008; Pardieu et al., 2012; Hughes et al., 2015, 2017; Vertriest and Saeseaw, 2019).

The Internal World of Thai/Cambodian Rubies. Rubies were mined in the ancient kingdom of Siam, along the present-day Thai/Cambodian border, for hundreds of years (figure 37). Until relatively recently, these Siamese rubies were the only serious alternative to those mined in Mogok. Back then it would have been straightforward to separate them from Mogok rubies, and even today the Thai/Cambodian rubies are easy to identify. Note, however, that rubies from the Chanthaburi-Trat area in Thailand are virtually identical to those found just across the border in Pailin, Cambodia, as the mining area is essentially one single deposit that straddles this geographic border (Sangsawong et al., 2017). One of the most striking microscopic features of Thai/Cambodian rubies is their lack of any rutile silk. The most prominent features are negative crystals, melt inclusions, and voids with partially healed decrepitation haloes that show geometric patterns and iridescent colors when using fiber-optic illumination (figures 38 and 39). These haloes are all oriented in the same crystallographic direction and are very transparent when light is not being reflected off them. When the correct angle is found in the microscope, they all

Figure 39. The thin-film decrepitation haloes in Thai/Cambodian rubies tend to show iridescent interference colors when viewed with fiber-optic light. Photomicrographs by Jonathan Muyal (left, field of view 2.90 mm) and John I. Koivula (right, field of view 4.10 mm).

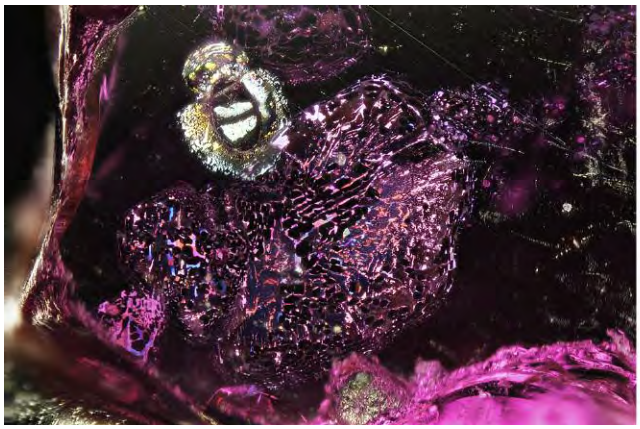

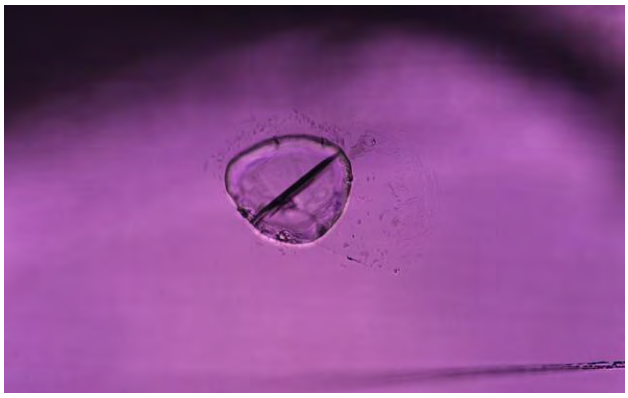

Figure 40. Diopside inclusions are a characteristic, if rarely encountered, inclusion in Thai/Cambodian rubies. Photomicrograph by Aaron Palke; field of view 0.71 mm.

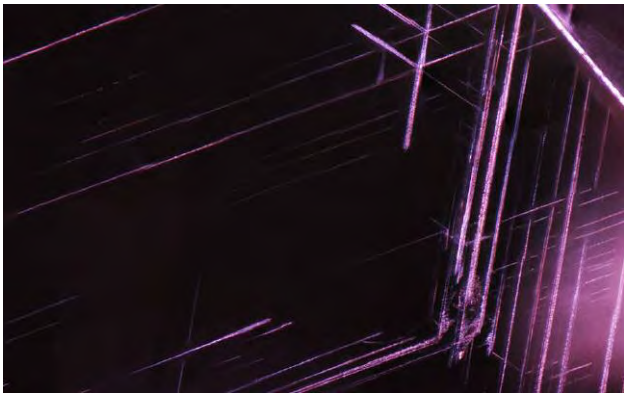

Figure 41. Twinning is relatively common in Thai/Cambodian rubies, and the intersection tubules between twinned domains are often filled with diaspore or other aluminum (oxy)hydroxides. Photomicrograph by Jonathan Muyal; field of view 1.03 mm.

light up at once, sometimes with colorful displays of iridescence. Also seen are similar reflective platelet-type inclusions, which are ostensibly not centered around a larger parent inclusion. Solid mineral inclusions are relatively uncommon but include diopside and rarely garnet or pyrrhotite (figure 40). Twinning is prevalent in Thai/Cambodian rubies, and the intersection tubules between twinned sectors are often filled with diaspore or other aluminum (oxy)hydroxides (figure 41). Note that Thai/Cambodian stones can almost always be identified in the lab by their signature inclusion scenes.

The Internal World of Mozambique Rubies. The rise of Mozambique in the early twenty-first century completely upended the global ruby market. Never before had such vast quantities of high-quality ruby (figure 42) been so freely available to the gem and jewelry industry. This could have resulted in a significant problem for the gemological laboratories had the Mozambique ruby not been fairly straightforward to identify (Vertriest and Saeseaw, 2019). In many cases, a Mozambique origin can be concluded based on observations of inclusion scenes, but additional evidence is always sought in the form of trace element chemistry, which almost always closes the case (see the "High-Iron Ruby Trace Element Chemistry" section below). Common mineral inclusions in Mozambique rubies are grayish green amphiboles (figure 43) and hexagonal mica booklets with stress fracture fringes (figure 44). Sulfide and spinel inclusions are also observed (figure 45). Mozambique rubies also can contain angular particulate clouds (figure 44, left), but they are more frequently identified by their characteristic fields of reflective, platelet-like particles (figures 46 and 47). Like the haloes seen in Thai/Cambodia rubies, these platelets are all oriented in the same crystallographic direction

Figure 42. Mozambique ruby, approximately 5 ct. Photo by Robert Weldon/GIA; courtesy of Amba Gem Corporation.

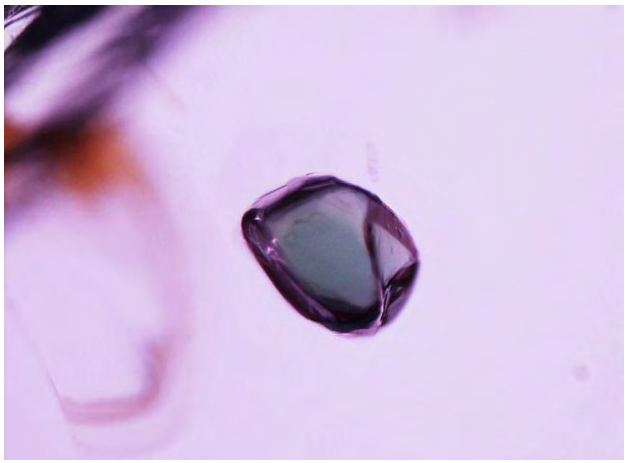

Figure 43. Grayish green amphiboles are one of the more common mineral inclusions in Mozambique rubies. Photomicrograph by Jonathan Muyal; field of view 1.32 mm.

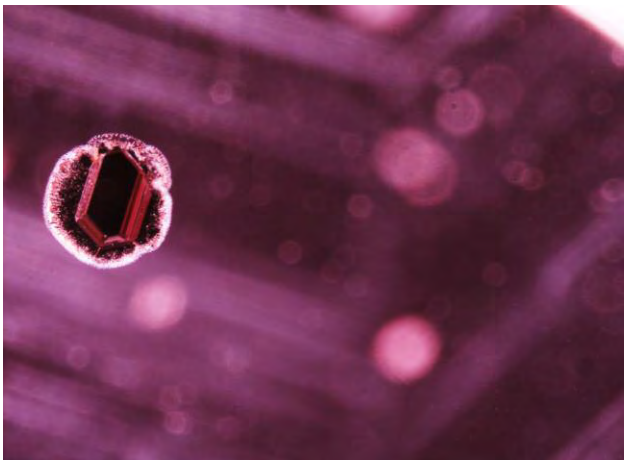

Figure 45. Sulfides are occasionally found as inclusions in Mozambique rubies. Photomicrograph by Jonathan Muyal; field of view 1.70 mm.

and may be difficult to see until that direction is found. Then they will all become visible at once. As with the rest of the high-iron rubies, Mozambique rubies can generally be identified in the lab by their inclusion scenes and trace element chemistry.

The Internal World of Madagascar Rubies. Madagascar rubies are the other East African newcomer in the ruby market (Schwarz and Schmetzer, 2001; Pardieu et al., 2012; Hughes et al., 2015). While they have never reached the commercial importance of Mozambique and much of the production is commercial grade, some exceptional ruby has been derived from Madagascar. Gemologically and geologically, Madagascar's rubies are most similar to those from Mozambique. Muscovite inclusions are occasionally encountered in rubies from Madagascar (figure 48) as well as amphibole, which may generally have a distinctive morphology with longer, more prismatic rod-like crystals (figure 49). However, the more common and characteristic inclusion in rubies from Madagascar is zircon, especially widely distributed clusters of small, rounded zircons (figures 50 and 51). Blocky and prismatic orange, brown, or black

Figure 44. Muscovite inclusions with concentrically centered tension fractures are a common sight in Mozambique rubies. Photomicrographs by Jonathan Muyal; field of view 1.99 mm (left) and 1.26 mm (right).

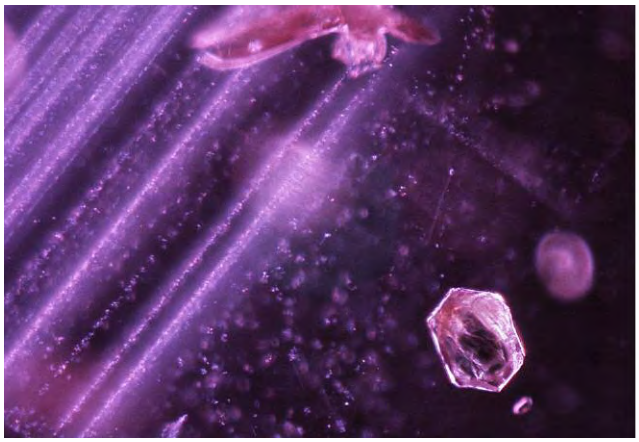

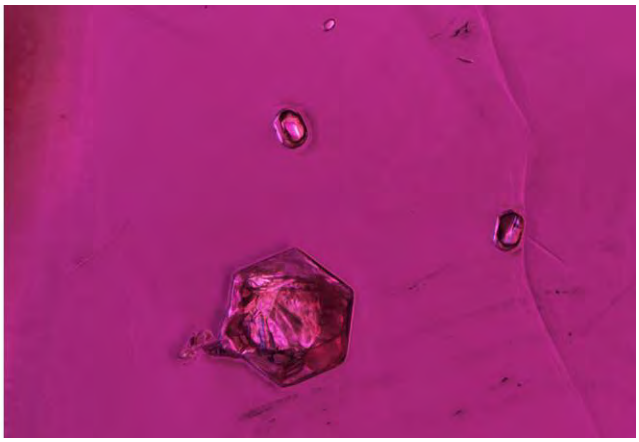

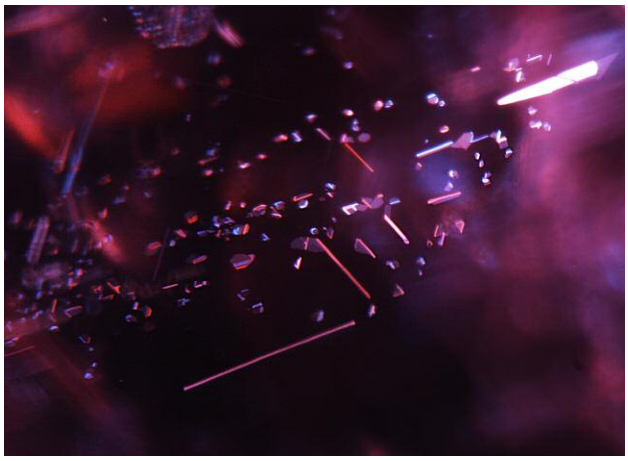

Figure 46. Platelet inclusions are one of the telltale signs of a Mozambique ruby. Photomicrograph by B. Kongsomart; field of view 0.70 mm.

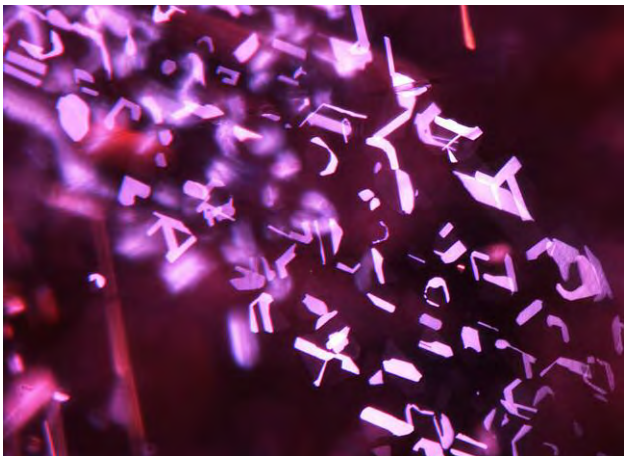

Figure 47. The field of platelet inclusions here is solid evidence of this ruby's Mozambique provenance. Photomicrograph by GIA; field of view 0.82 mm.

rutile inclusions can also be encountered and suggest a Madagascar provenance (figure 52). Particle clouds may be encountered as well, often composed of short needles and fine particulates, but sometimes mixed with long needles (figure 53). The particle clouds usually show a well-defined hexagonal arrangement, and there is the possibility of confusion with similar features seen in Mozambique rubies. Occasionally Madagascar rubies also host angular milky clouds, a feature not characteristic of the other major high-iron ruby deposits. Madagascar rubies are generally easy to identify in the laboratory based on their inclusion scenes and trace element chemistry.

Figure 48. Muscovite inclusions, as seen in this Madagascar ruby, can also be found in Mozambique rubies. These inclusions alone should not be used to determine a ruby's geographic origin. Photomicrograph by GIA; field of view 0.97 mm.

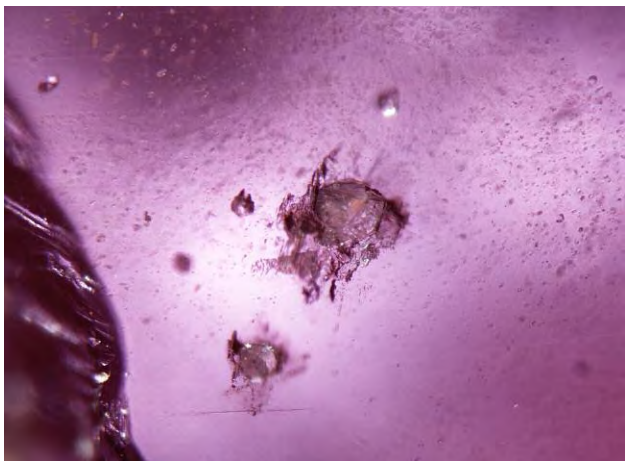

Trace Element Chemistry of Marble-Hosted Ruby. When attempting to use trace elements to discern a marble-hosted ruby's origin, one has the same problem encountered with metamorphic blue sapphires:

Figure 49. Amphibole inclusions are found in Mozambique as well as Madagascar rubies (shown here). In Madagascar rubies, amphibole tends to take on an elongate, rod-like morphology, although similar morphology can be encountered in Mozambique stones. Care should be taken when using these inclusions as an indicator of origin. Photomicrograph by Victoria Liliane Raynaud-Flattot; field of view 1.04 mm.

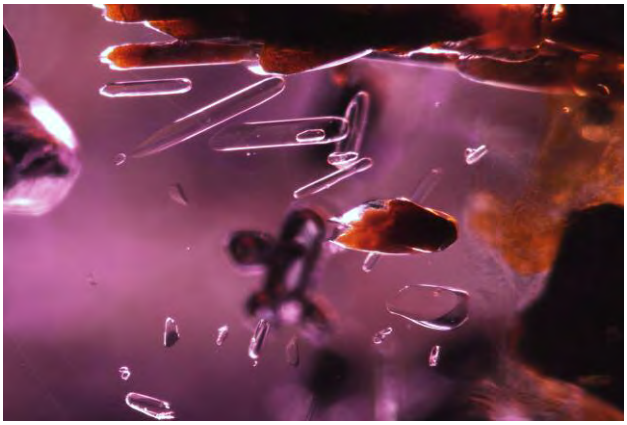

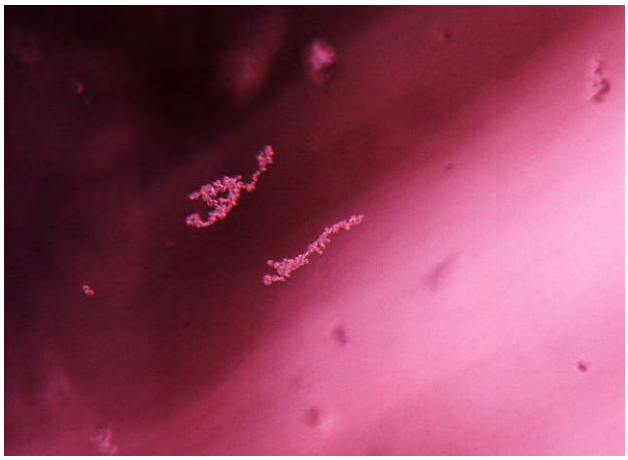

Figure 50. Clusters of small, rounded zircon crystals support a conclusive geographic origin determination for this Madagascar ruby. Photomicrograph by Patcharee Wongrawang; field of view 0.86 mm.

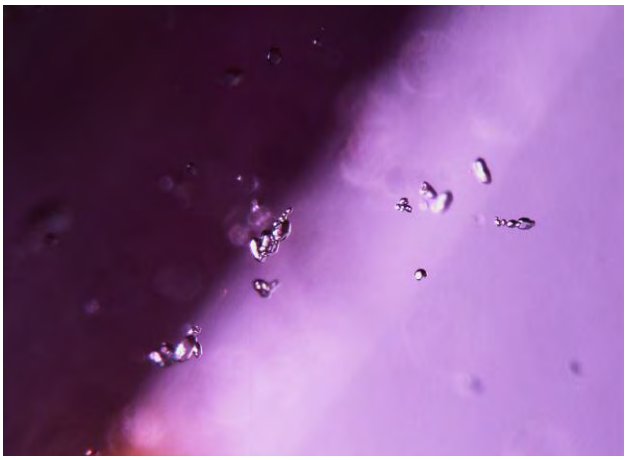

Figure 51. Madagascar rubies are often identified by clusters of small zircon crystals. Photomicrograph by Patcharee Wongrawang; field of view 1.56 mm.

The very similar geological conditions of formation for these rubies creates very little deviation in their trace element profiles. When the compositional data are plotted together for the major economic deposits, separation can seem almost hopeless. The selective plotting method developed for blue sapphires (see Palke et al., 2019, pp. 536–579 of this issue) is also applied to origin determinations for marble-hosted rubies using the same suite of trace elements (Mg, Ti, V, Fe, and Ga). The ranges of trace element profiles seen in marble-hosted rubies can be found in table 1. By filtering out reference data with dissimilar trace element profiles and comparing an unknown stone only against reference stones that match the unknown, the trace element plots are greatly simplified, making it easier to interpret the data. In some cases, the selective plotting method is very useful for marble-hosted rubies and can provide evidence of a stone's provenance that would not have been obvious otherwise (figure 54). (Note that all trace element

Figure 52. Blocky, euhedral rutile crystal inclusions are a common sight in Madagascar ruby. Photomicrograph by Patcharee Wongrawang; field of view 1.95 mm.

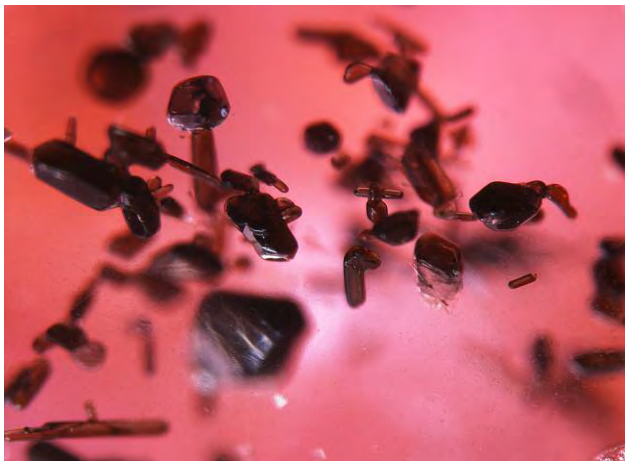

Figure 53. Hexagonal particulate clouds composed of short and long rutile silk are a frequent observation in Madagascar rubies. Photomicrograph by Patcharee Wongrawang; field of view 1.20 mm.

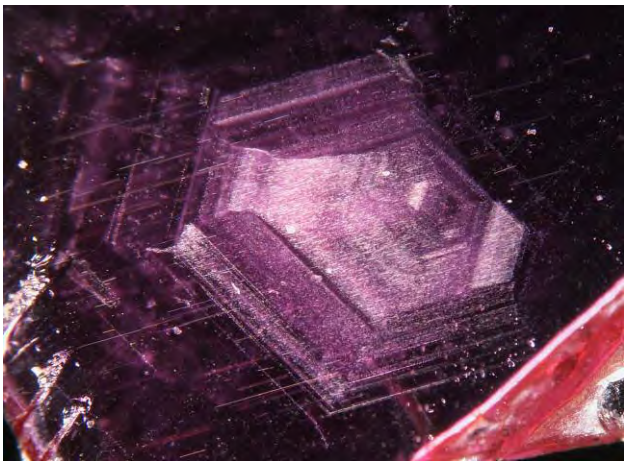

TABLE 1. Generalized trace element profiles in ppma of marble-hosted rubies.

	Myanmar (Mogok)				
	Mg	**Ti**	**V**	**Fe**	**Ga**
Range	5–75	7–80	48–1089	bdl–301	2–51
Average	40	45	212	35	18
Median	40	44	158	22	17
	Myanmar (Mong Hsu)				
	Mg	**Ti**	**V**	**Fe**	**Ga**
Range	6–68	5–997	51–229	bdl–28	8–23
Average	23	247	123	2	15
Median	19	176	112	bdl	16
	Vietnam				
	Mg	**Ti**	**V**	**Fe**	**Ga**
Range	1–130	bdl–1214	2–214	bdl–471	1–122
Average	33	132	43	54	21
Median	24	60	27	24	20
	Afghanistan				
	Mg	**Ti**	**V**	**Fe**	**Ga**
Range	7–380	9–486	4–135	bdl–1128	5–35
Average	33	68	34	124	14
Median	27	42	30	105	12
	Tajikistan				
	Mg	**Ti**	**V**	**Fe**	**Ga**
Range	6–58	bdl–579	24–112	bdl–155	14–28
Average	15	127	38	36	21
Median	13	91	34	bdl	20

**bdl = below the detection limit of the LA-ICP-MS analysis. Detection limits are provided in the Samples and Analytical Methods section, p. 581.*

data are produced from LA-ICP-MS; see Groat et al., 2019, pp. 512–535 of this issue.) But as with metamorphic blue sapphires, in some cases there is simply too much overlap in the trace element data and no amount of statistical analysis or variation in plotting the data will help (figure 55). Unfortunately, this is the limitation of geographic origin determination imposed by the forces of nature and geology that created these fine stones. An "inconclusive" call is always warranted if the gemological evidence does not produce any clear indication of origin. Note that for the sake of clarity the plots shown here include only the major marble-hosted ruby deposits, while some smaller deposits (especially from East Africa) are not included. In laboratory practice, the trace element data for these deposits can be considered as possibilities if there is other corroborating evidence.

Trace Element Chemistry of High-Iron Ruby. Stones in the high-iron ruby group are much easier to separate than marble-hosted rubies by using multiple lines of evidence. Even in cases where microscopy alone cannot determine a ruby's provenance, which is fairly uncommon, the addition of trace element analysis almost always results in an accurate origin conclusion. The full range of trace element profiles for high-iron rubies can be found in table 2. Several trace element plots are shown in figure 56, illustrating how the use of only a few trace elements can almost always separate high-iron rubies from the major mining areas. (Note that all trace element data are produced from LA-ICP-MS; see Groat et al., 2019, pp. 512–535 of this issue.) The selective plotting method used for blue sapphires and marble-hosted rubies at GIA (see Palke et al., 2019, pp. 536–579 of this issue) is sometimes

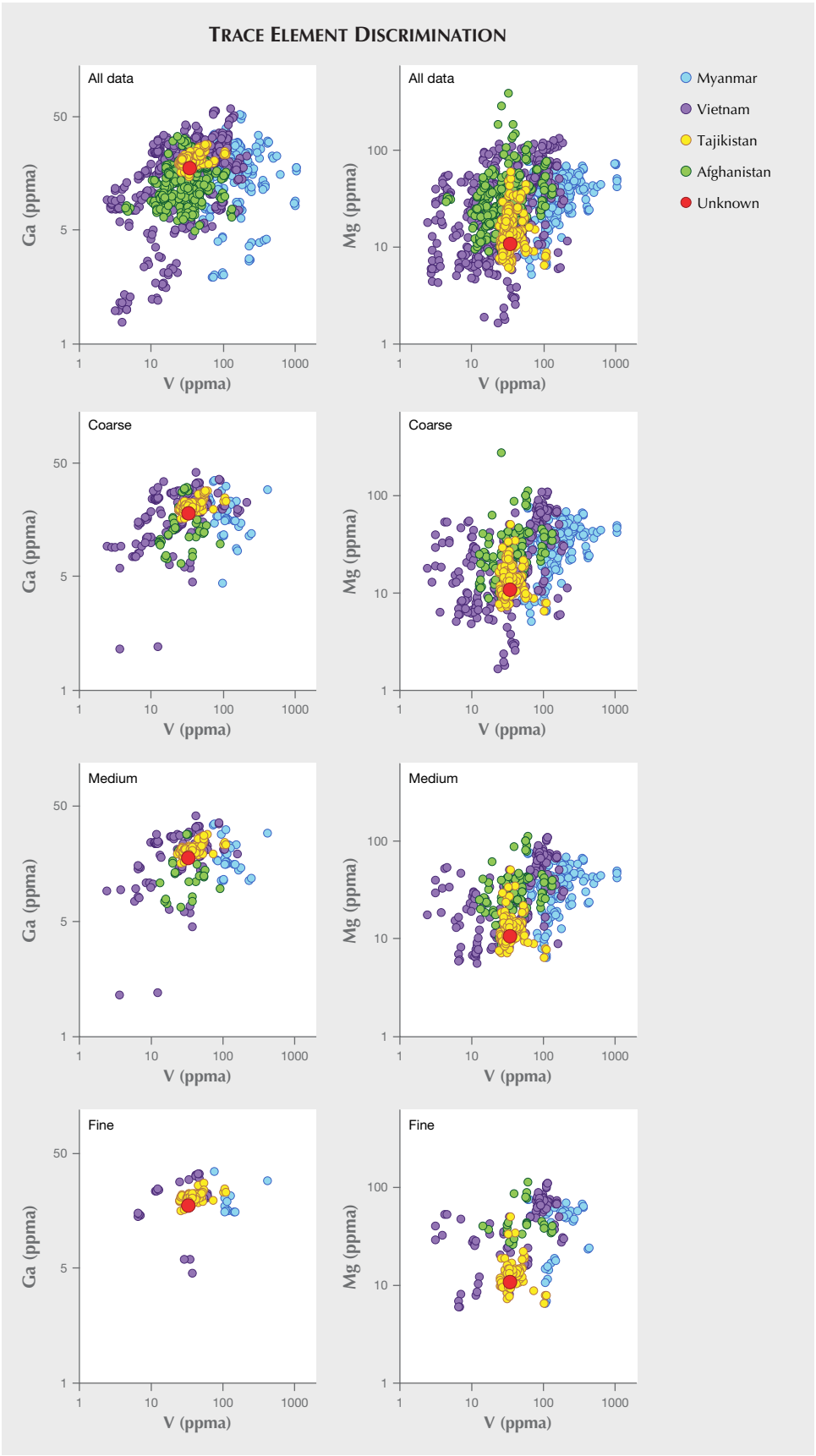

Figure 54. Trace element plots for marble-hosted rubies showing data for Myanmar, Vietnam, Afghanistan, and Tajikistan, as well as an unknown ruby. The trace element profile of an unknown marble-hosted ruby (indicated by the red circle in each plot) may not provide much information when plotted against the full dataset from GIA's field gemology reference collection. In some cases, however, the "selective plotting" method used in GIA's laboratory may help to make sense of this data, providing more evidence of a stone's origin, as with this Tajik ruby. Selective plotting uses coarse, medium, and fine windows to filter out dissimilar reference data, making the plots easier to interpret.

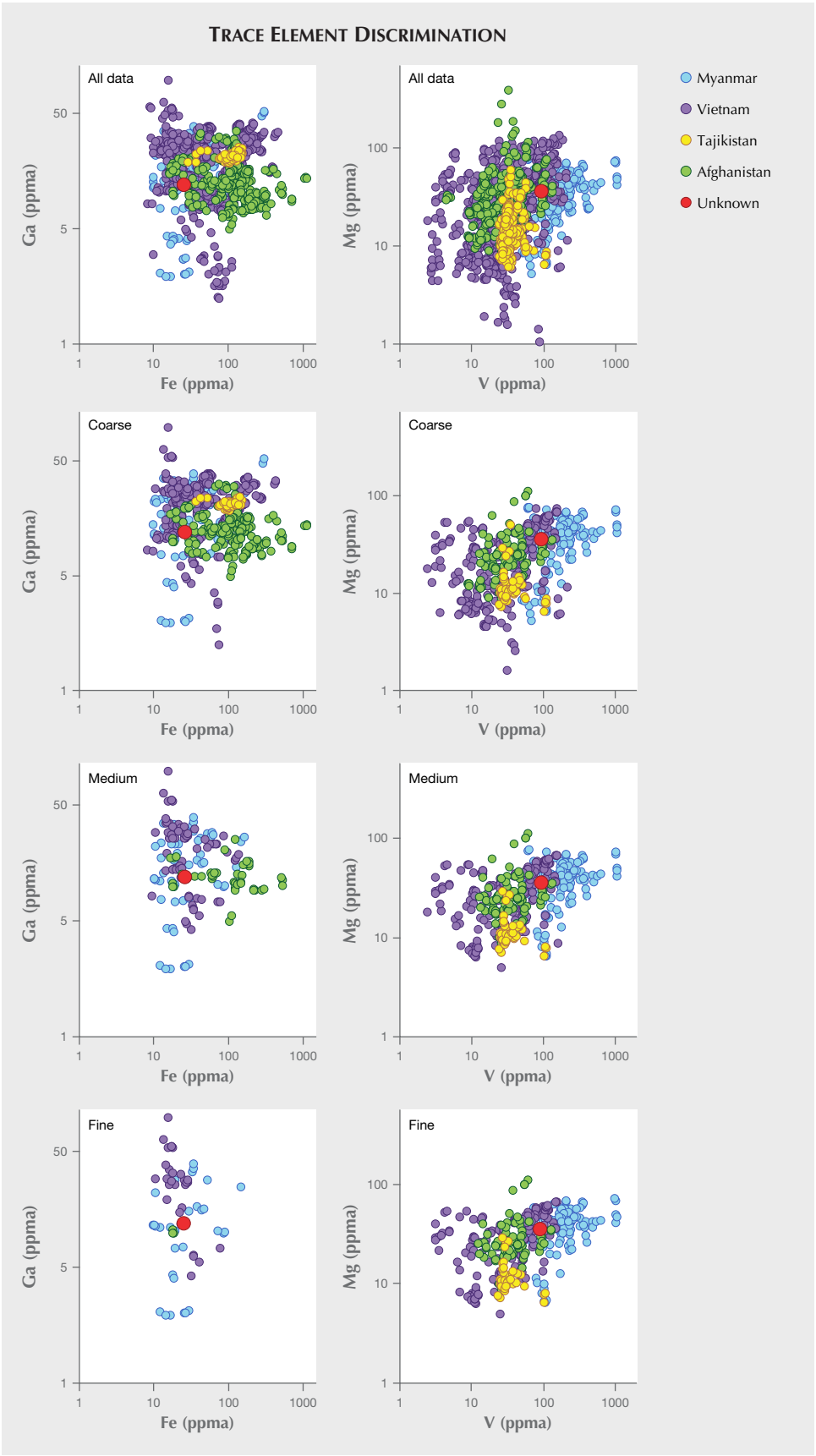

Figure 55. Trace element plots for marble-hosted rubies showing data for Myanmar, Vietnam, Afghanistan, and Tajikistan, as well as an unknown stone. While the selective plotting method is useful in some cases, many marble-hosted rubies have such overlapping trace element profiles, which renders the trace element data useless in origin determination. This unknown ruby (indicated by the red circles) is a prime example. The selective plotting uses coarse, medium, and fine windows to filter out dissimilar reference data, making the plots easier to interpret.

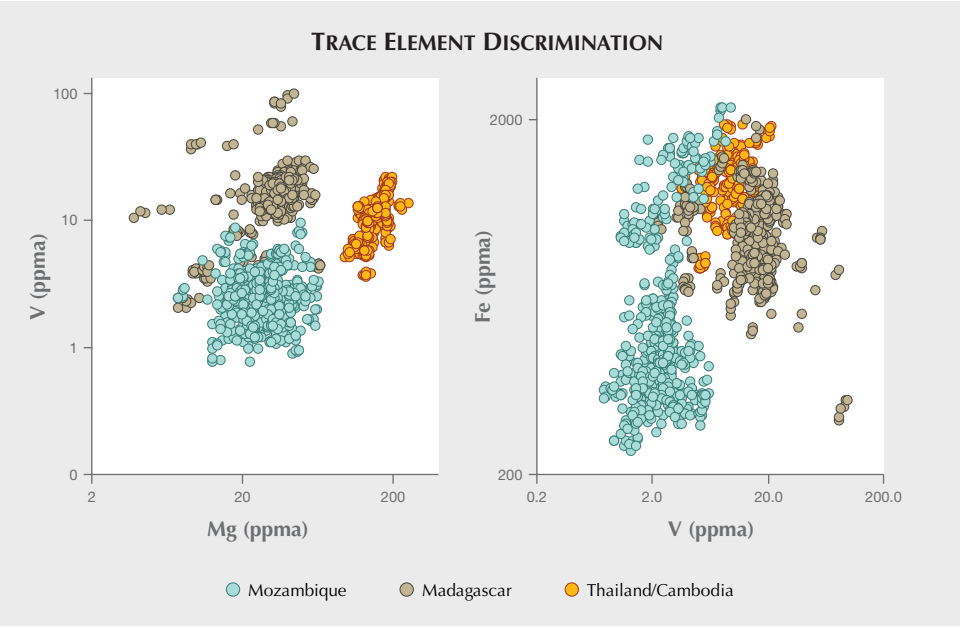

Figure 56. High-iron rubies from Mozambique, Madagascar, and Thailand/Cambodia, among others, are much easier to separate using trace element chemistry. The vast majority can be separated without needing the selective plotting method used at GIA for blue sapphires and other rubies.

used for high-iron rubies as well, but in most cases it is not necessary. Note that for the sake of clarity, these plots show only the major high-iron ruby deposits, while some smaller deposits such as those in Tanzania, Kenya, and Greenland are not included. In laboratory practice, the trace element data for these

TABLE 2. Generalized trace element profiles in ppma of high-iron rubies.

Cambodia					
	Mg	**Ti**	**V**	**Fe**	**Ga**
Range	97–258	32–138	5–22	818–1935	5–11
Average	154	77	11	1317	9
Median	151	74	11	1325	9
Thailand					
	Mg	**Ti**	**V**	**Fe**	**Ga**
Range	126–181	36–89	4–14	756–1442	5–10
Average	143	54	8	1089	8
Median	138	51	7	1183	7
Madagascar					
	Mg	**Ti**	**V**	**Fe**	**Ga**
Range	bdl–67	4–434	2–100	284–1994	5–30
Average	32	42	17	933	15
Median	33	34	15	887	15
Mozambique					
	Mg	**Ti**	**V**	**Fe**	**Ga**
Range	8–65	bdl–59	bdl–10	231–2154	5–14
Average	29	21	3	622	8
Median	27	20	2	431	7

**bdl = below the detection limit of the LA-ICP-MS analysis. Detection limits are provided in the Samples and Analytical Methods section, p. 581.*

deposits can be considered as possibilities if there is other corroborating evidence. Additional information about these deposits can be found in Thirangoon (2009), Smith et al. (2016), and Hughes et al. (2017).

CONCLUSIONS

The twentieth and twenty-first centuries have seen dramatic changes in the world ruby market. The rapid increase in ruby sources across the world has largely benefited the gem-consuming public by making these precious stones more accessible over a wide range of price points. However, as the gem industry has come to incorporate geographic origin in determining the value of these stones (e.g., the Burmese ruby and sapphire in figure 57), this diversification of ruby sources has proven to be a great challenge for gemological laboratories. Through 10 years of efforts, GIA's field gemology and research departments have amassed world-class collections of rubies from the major world sources. The data collected on these reference stones has been crucial in allowing GIA to make origin determinations with the utmost confidence and integrity (even when the origin call is necessarily "inconclusive"). Nonetheless, the data and methods used at GIA for making ruby origin determinations, as described in this article, demonstrate the oftentimes precarious nature of origin determination in gemological laboratories.

Many stones present characteristic inclusion scenes that lead to a straightforward origin decision. This is often the case with rubies from Thailand, Mozambique, Madagascar, and rubies from some of the marble-hosted deposits, especially those from Myanmar (figure 58). Rubies from the other marble-hosted deposits such as Vietnam, Afghanistan, and Tajikistan are generally more challenging. Trace element chemistry can be useful, especially for so-called high-iron rubies. Unfortunately, and especially for marble-hosted rubies, trace element chemistry can often be ambiguous.

The use of the "selective plotting" method described herein may help in making sense of this trace element data, but it is hardly a cure-all. In cases where the inclusion scenes and trace element evidence are ambiguous, the only possible determination is an "inconclusive" origin. Future research and field gemology efforts will focus on advancing our understanding of ruby origin determination and refining the methods used in the laboratory at GIA. However, it is almost certain that there will always be rubies with a lack of characteristic origin data to support an origin conclusion. While further work may help us reduce the number of "inconclusive" calls, the overlap in gemological properties for many of our reference stones makes it unlikely that this number will ever reach zero.

Figure 57. A 2.58 ct cushion-cut ruby and a 4.47 ct cushion-cut blue sapphire, both of Burmese origin. Photo by Robert Weldon/GIA; courtesy of Bear Essentials.

Figure 58. This necklace contains approximately 50 carats of rubies, including 28 oval and numerous square and rectangular rubies. All the rubies are of Burmese origin with no evidence of heat. Photo by Robert Weldon/GIA; courtesy of Ronny Levy, Period Jewels Inc.

Case Study 1: Burmese Ruby

In the first ruby case study, we consider the 2.21 ct ruby shown in figure CS 1-1. LA-ICP-MS analysis measures an Fe concentration of 28 ppma, placing this stone in the marble-hosted ruby group and narrowing down the possible origins to Myanmar, Vietnam, Afghanistan, and Tajikistan. The next step is to make careful observations of its inclusion characteristics. Viewed through the microscope, this stone exhibits nested, straw-like silk that is strongly reminiscent of classic rubies from Mogok, Myanmar (figure CS 1-2). Also seen are large crystalline inclusions of apatite and other minerals, which support a Burmese origin (figure CS 1-3). While the inclusion evidence points strongly toward a Burmese origin, trace element chemistry should be considered carefully as well. Without using the selective plotting method described in this article and in Palke et al. (2019, pp. 536–579 of this issue), this unknown stone plots in a field of overlapping Myanmar and Vietnam reference data (figure CS 1-4). However, filtering the data using the selective plotting method narrows down this field and shows a clear match with other Burmese rubies in the GIA colored stone reference collection. Taking all the data together, we can confidently assign a Burmese origin to this stone.

Figure CS 1-1. A 2.21 ct mixed-cut ruby considered for geographic origin determination. Photo by Diego Sanchez.

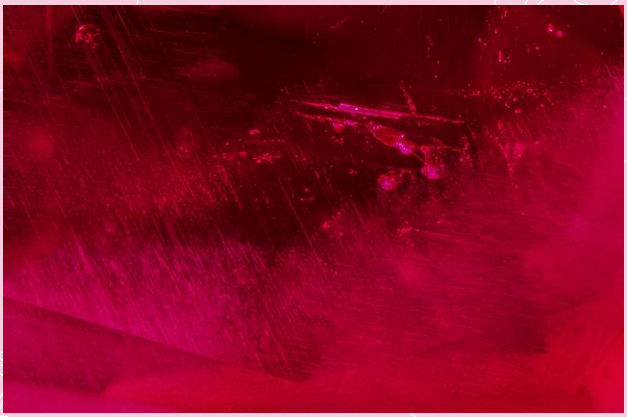

Figure CS 1-2. Nested straw-like silk and crystalline inclusions strongly suggest a Burmese origin. Photomicrograph by Aaron Palke; field of view 4.48 mm.

Figure CS 1-3. A crystalline inclusion of apatite is consistent with Burmese origin. Photomicrograph by Aaron Palke; field of view 2.84 mm.

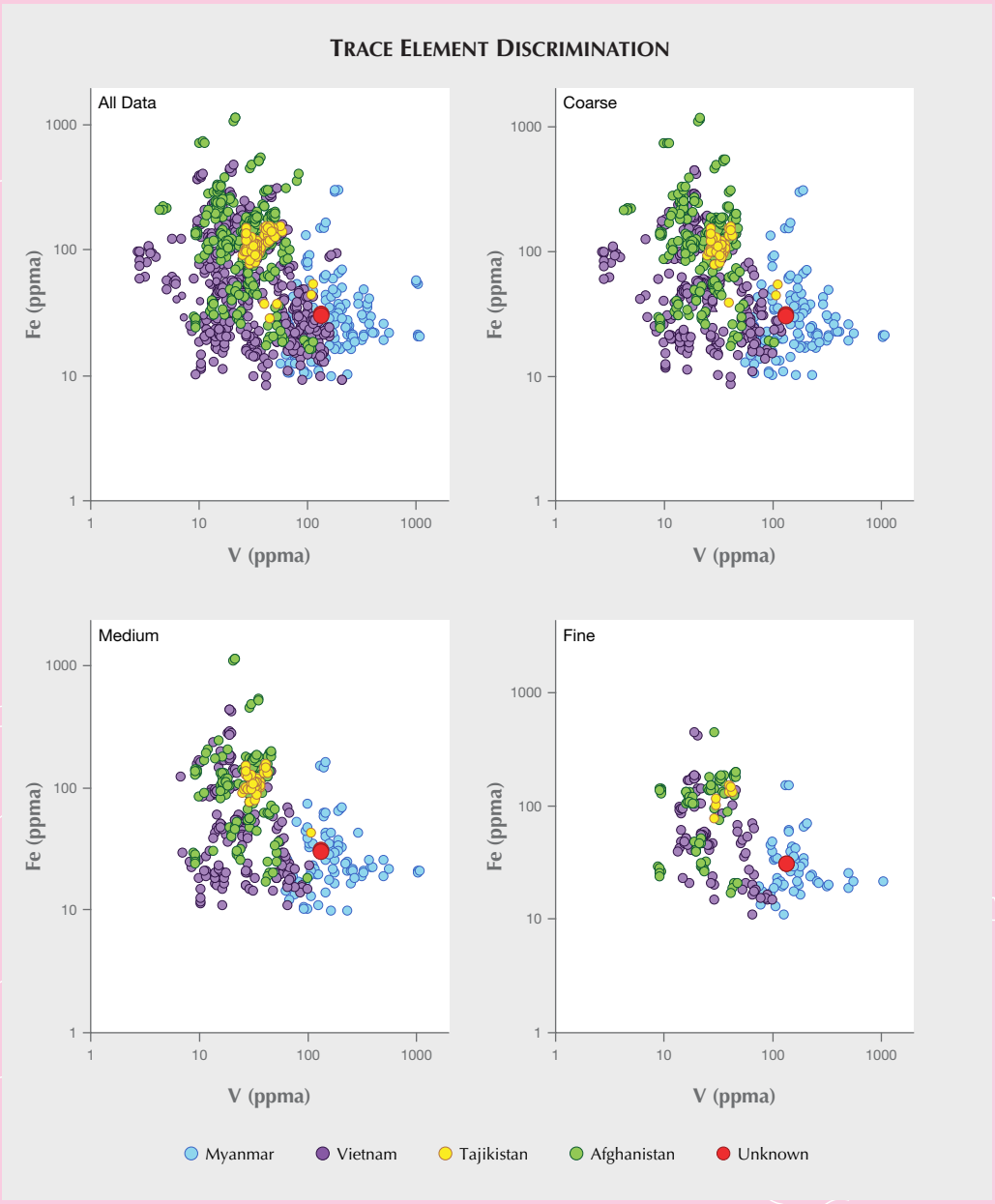

Figure CS 1-4. Trace element analysis supports a Burmese origin for this ruby (indicated by the red circle).

Case Study 2: Tajik Ruby

In this case study we investigate the 0.16 ct step-cut ruby shown in figure CS 2-1. Precise measurement of the trace element profile indicates an Fe concentration of 41 ppma, placing it in the marble-hosted ruby group. This essentially simplifies the origin determination problem to a choice between Myanmar, Vietnam, Afghanistan, and Tajikistan. Observation of the inclusion scenes in marble-hosted rubies can help narrow down this field even further and can often lead to a conclusive origin determination. Among the inclusions observed in this stone are crystals with rosette-like haloes (figure CS 2-2), polyphase aggregated solid inclusions, and clusters of slender tourmaline crystals (figure CS 2-3). All of these features are indicative of a Tajik origin. Additional corroborating evidence can be sought in the stone's trace element fingerprint. Figure CS 2-4 shows representative trace element plots of the unknown ruby against GIA's marble-hosted ruby database. The use of the selective plotting method allows clearer interpretation of the trace element data and shows this stone is more consistent with the Tajik ruby reference data than any other source. Taken together, the data collected for this stone allows a Tajik origin determination.

Figure CS 2-1. The 0.16 ct ruby under consideration in this geographic origin determination case study. Photo by Diego Sanchez.

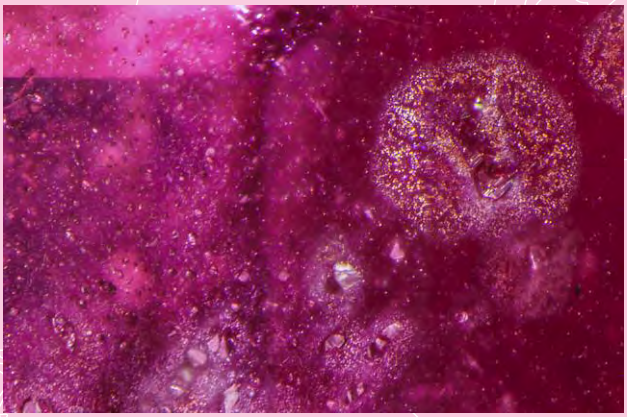

Figure CS 2-2. The rosette-like fringe around this inclusion is suggestive of a Tajik origin. Photomicrograph by Nathan D. Renfro; field of view 1.10 mm.

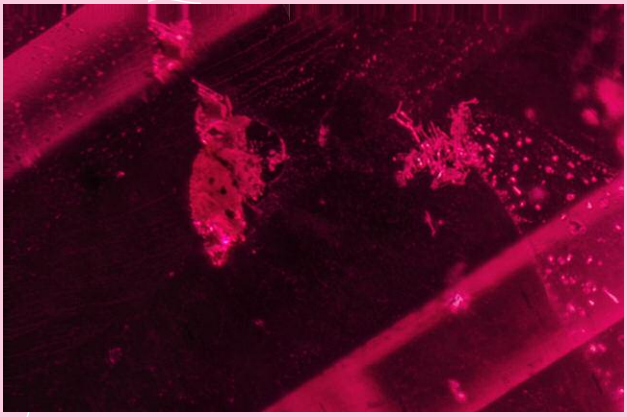

Figure CS 2-3. Clusters of slender tourmaline crystals (upper right) and polyphase, aggregate solid inclusions (left) corroborate a Tajik origin determination. Photomicrograph by Aaron C. Palke; field of view 1.77 mm.

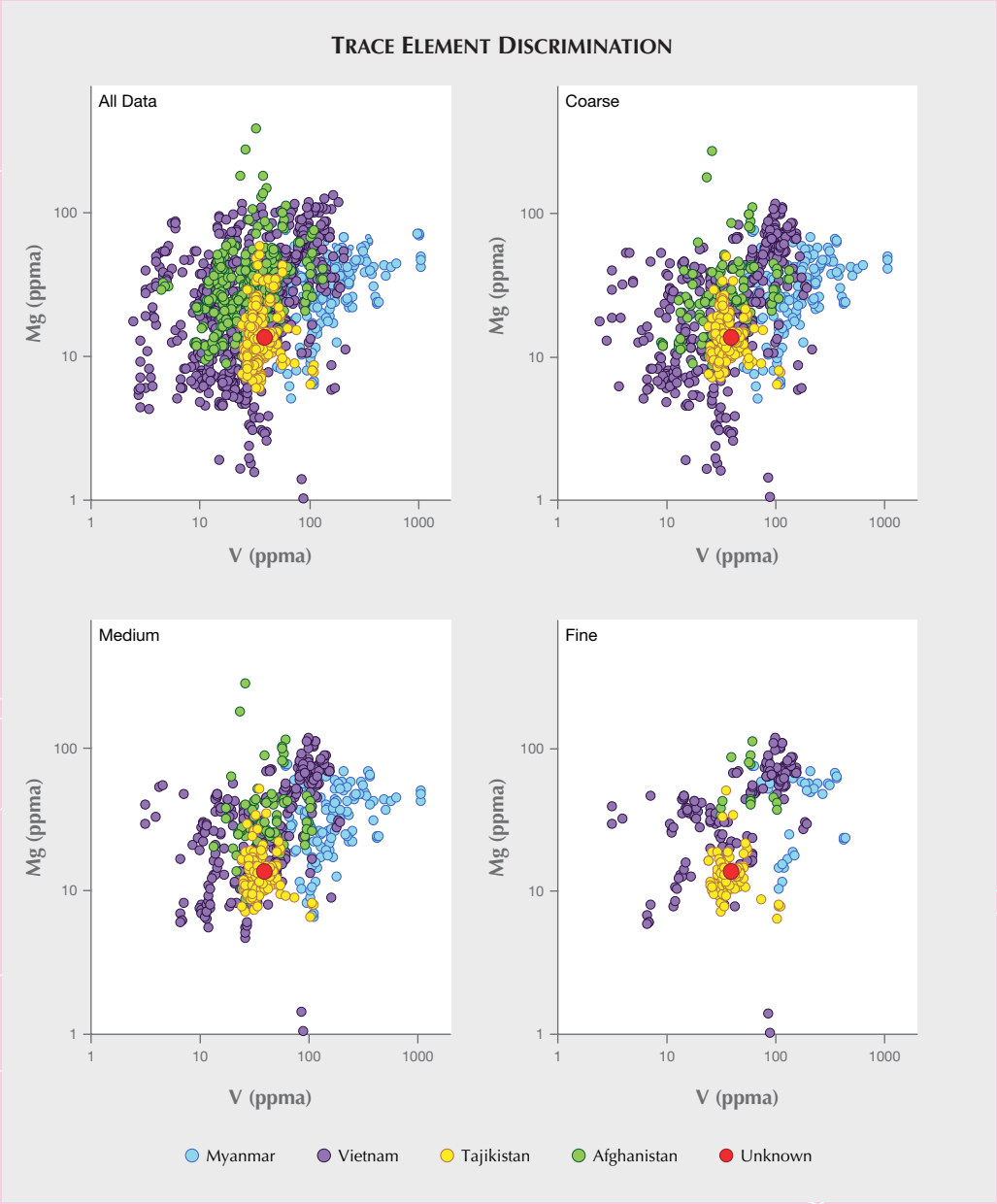

Figure CS 2-4. Trace element analysis of this unknown ruby (indicated by the red circle) favors a Tajik origin.

Case Study 3: Madagascar Ruby

For the third case study, we will consider the 0.39 ct ruby shown in figure CS 3-1. Its Fe concentration was measured at 2720 ppma, so the unknown stone belongs to the so-called high-iron ruby group. The most likely geographic origins, therefore, include Mozambique, Madagascar, and Thailand/Cambodia. Microscopic observation provides the gemologist with an inclusion scene such as the one seen in figure CS 3-2. With an intense fiber-optic light at just the right angle, the reflective rutile silk in the stone lights up and provides the first clue to origin. Similar inclusion scenes can be seen in both Mozambique and Madagascar rubies, but rutile silk like this is never found in Thai/Cambodian rubies. However, the observation of zircon clusters provides strong evidence of a Madagascar origin for this stone (figure CS 3-3). Advanced testing involving precise measurement of the trace element signature using LA-ICP-MS is required as additional evidence to support an origin determination. The representative trace element plot shown in figure CS 3-4 confirms a Madagascar origin.

Figure CS 3-1. This case study considers a 0.39 ct ruby for geographic origin determination. Photo by Diego Sanchez.

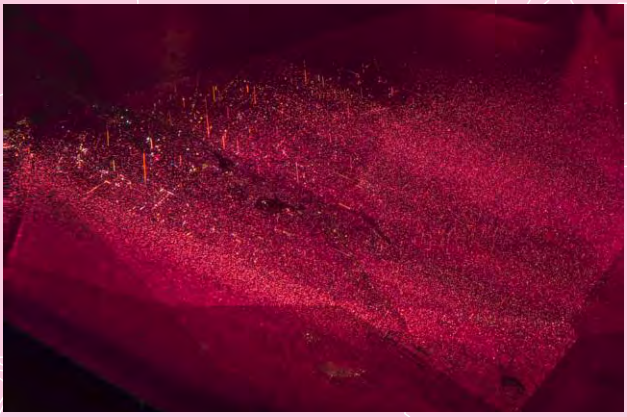

Figure CS 3-2. Particulate clouds and short, iridescent silk are not characteristic of any unique origin. Photomicrograph by Aaron C. Palke; field of view 3.97 mm.

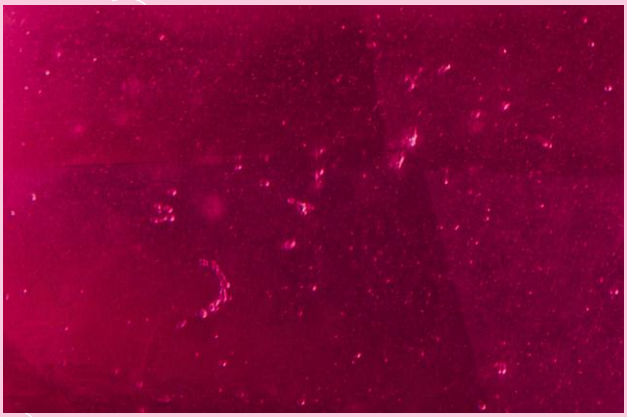

Figure CS 3-3. The zircon clusters in this ruby strongly indicate a Madagascar origin. Photomicrograph by Nathan D. Renfro; field of view 1.02 mm.

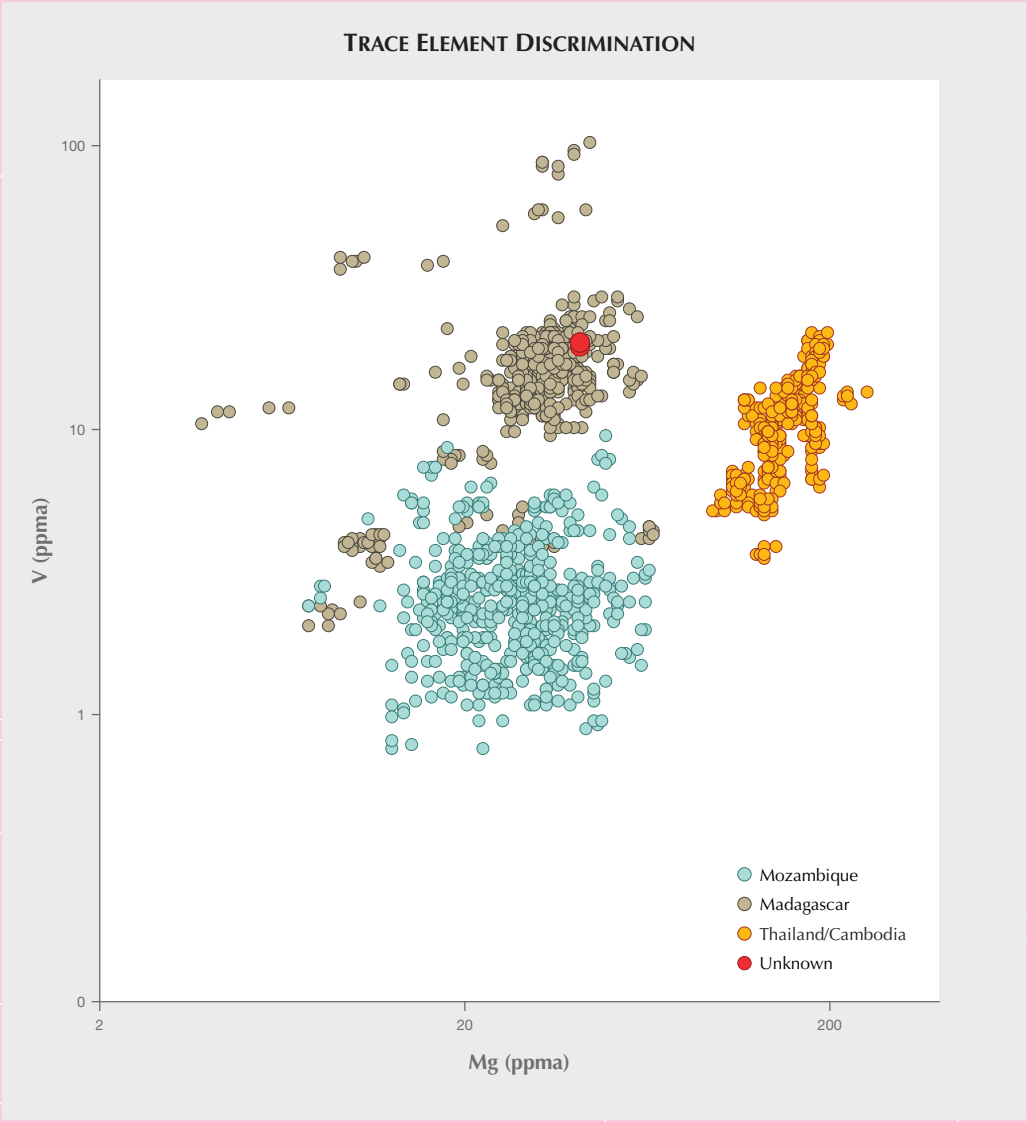

Figure CS 3-4. Trace element analysis of this unknown ruby (indicated by the red circle) indicates a Madagascar origin.

Case Study 4: Inconclusive Ruby

The final case study involves a 0.22 ct ruby (figure CS 4-1). Trace element analysis measured an Fe concentration of 449 ppma, placing it in the high-iron ruby group. The main geographic locales to be considered, then, are Mozambique, Madagascar, and Thailand/Cambodia. The next step in uncovering this unknown ruby's origin is careful observation of inclusions in the gemological microscope. While this stone is not especially clean, unfortunately it contains no particularly diagnostic or indicative inclusions. The main inclusion feature is a fingerprint-like veil of fluid inclusions (figure CS 4-2). Regardless, the geographic origin of many high-iron rubies can be confidently determined by trace element analysis, even when there are no useful inclusions to be found. However, this stone remains a mystery even after precisely measuring its trace element fingerprint using LA-ICP-MS (figure CS 4-3). The chemical data plot outside the defined fields for any reference rubies from known deposits. While the selective plotting method does seem to display some affinity for Madagascar as a possible source, the unknown stone is still outside the range from our reference collection. Given that there is also no inclusion evidence to corroborate a Madagascar origin, the best option is an "inconclusive" origin determination.

Figure CS 4-1. A 0.22 ct ruby is the focus of geographic origin determination in this case study. Photo by Diego Sanchez.

Figure CS 4-2. No diagnostic inclusions are observed. The only inclusion features identified are fingerprint-like fields of fluid inclusions. Photomicrograph by Nathan D. Renfro; field of view 2.05 mm.

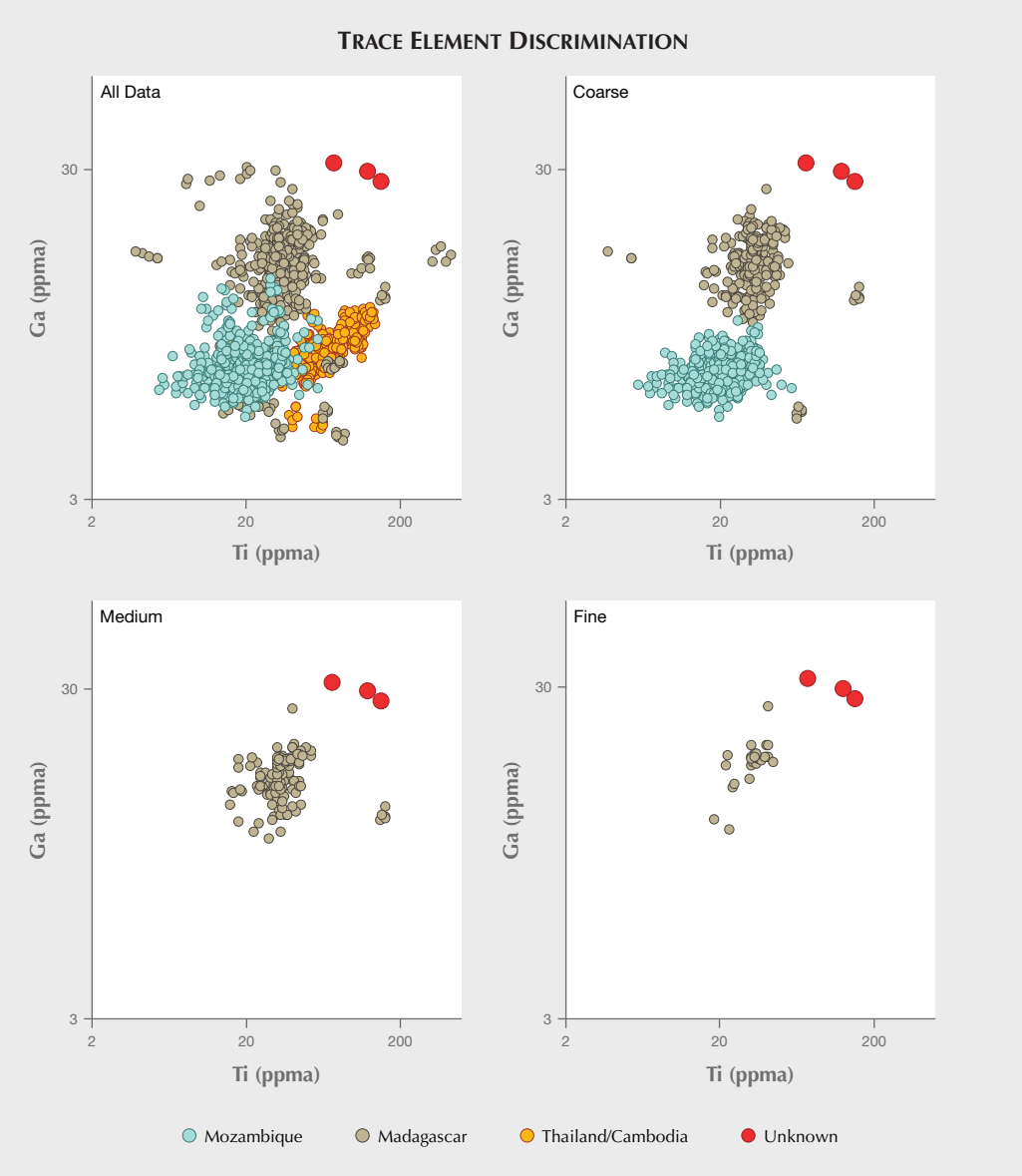

Figure CS 4-3. Trace element analysis of this unknown ruby (indicated by the red circle) fails to produce a unique match with any of the reference data for stones of known provenance.

ABOUT THE AUTHORS

Dr. Palke is a senior research scientist, Mr. Renfro is manager of colored stone identification, Mr. Sun is a research associate, and Mr. McClure is global director of colored stone services, at GIA in Carlsbad, California. Ms. Saeseaw is senior manager of identification at GIA in Bangkok.

ACKNOWLEDGMENTS

The authors wish to express their gratitude for colleagues at GIA and elsewhere who have helped advance the knowledge of origin determination for rubies and who have otherwise helped put this article together, including Dino DeGhionno, Claire Malaquais, Philip Owens, Philip York, Nicole Ahline, John Koivula, Jennifer Stone-Sundberg, Barbara Dutrow, and John Valley, among others. Terri Ottaway and McKenzie Santimer from the GIA Museum are also to be thanked for their support in the research efforts in the lab at GIA. We also thank Lin Sutherland, Hanco Zwaan, and Ahmadjan Abduriyim for their thorough reviews of this manuscript and helpful comments and criticism.

REFERENCES

Bowersox G.W., Foord E.E., Laurs B.M., Shigley J.E., Smith C.P. (2000) Ruby and sapphire from Jegdalek, Afghanistan. *G&G*, Vol. 36, No. 2, pp. 110–126, http://dx.doi.org/10.5741/GEMS.36.2.110

Brown G. (1992) Vietnamese ruby: A discriminatory problem for gemmologists. *Australian Gemmologist*, Vol. 18, No. 2, pp. 43–46.

Chapin M., Pardieu V., Lucas A. (2015) Mozambique: A ruby discovery for the 21st century. *G&G*, Vol. 51, No. 1, pp. 44–54, http://dx.doi.org/10.5741/GEMS.51.1.44

Emmett J.L., Scarratt K., McClure S.F., Moses T., Douthit T.R., Hughes R., Novak S., Shigley J.E., Wang W., Bordelon O., Kane R.E. (2003) Beryllium diffusion of ruby and sapphire. *G&G*, Vol. 39, No. 2, pp. 84–135, http://dx.doi.org/10.5741/GEMS.39.2.84

Fanka A., Sutthirat C. (2018) Petrochemistry, mineral chemistry, and pressure-temperature model of corundum-bearing amphibolite from Montepuez, Mozambique. *Arabian Journal for Science and Engineering*, Vol. 43, pp. 3751–3767.

Garnier V., Giuliani G., Ohnenstetter D., Fallick A.E., Dubessy J., Banks D., Vinh H.Q., Lhomme T., Maluski H., Pecher A., Bakhsh K.A., Long P.V., Trinh P.T., Schwarz D. (2008) Marble-hosted ruby deposits from Central and Southeast Asia: Towards a new genetic model. *Ore Geology Reviews*, Vol. 34, No. 1-2, pp. 169–191, http://dx.doi.org/10.1016/j.oregeorev.2008.03.003

Giuliani G., Groat L.A. (2019) Geology of corundum and emerald gem deposits: A review. *G&G*, Vol. 55, No. 4, pp. 464–489, http://dx.doi.org/10.5741/GEMS.55.4.464

Groat L.A., Giuliani G., Stone-Sundberg J., Renfro N.D., Sun Z. (2019) A review of analytical methods used in geographic origin determination of gemstones. *G&G*, Vol. 55, No. 4, pp. 512–535, http://dx.doi.org/10.5741/GEMS.55.4.512

Gübelin E.J., Koivula J.I. (2008) *Photoatlas of Inclusions in Gemstones*, Volume 3. Opinio Publishers, Basel, Switzerland, 672 pp.

Hughes R.W. (1994) The rubies and spinels of Afghanistan. *Journal of Gemmology*, Vol. 24, No. 4, pp. 256–267.

Hughes R.W., Manorotkul W., Hughes E.B. (2015) Let it bleed: New rubies from Madagascar. http://www.lotusgemology.com/index.php/library/articles/322-blood-red-rubies-from-madagascar-lotus-gemology.

Hughes R.W., Manorotkul W., Hughes B.E. (2017) *Ruby & Sapphire: A Gemologist's Guide*. RW Publishing/Lotus Publishing, Bangkok, 816 pp.

Kane R.E., McClure S.F., Kammerling R.C., Khoa N.D., Mora C., Repetto S., Khai N.D., Koivula J.I. (1991) Rubies and fancy sapphires from Vietnam. *G&G*, Vol. 27, No. 3, pp. 136–155, http://dx.doi.org/10.5741/GEMS.27.3.136

Khoi N.N., Sutthirat C., Tuan D.A., Nam V.N., Minh N.T., Nhung N.J. (2011) Ruby and sapphire from the Tan Huong–Truc Lau area, Yen Bai Province, northern Vietnam. *G&G*, Vol. 47, No. 3, pp. 182–196, http://dx.doi.org/10.5741/GEMS.47.3.182

Long P.V., Vinh H.Q., Garnier V., Giuliani G., Ohnenstetter D. (2004) Marble-hosted ruby from Vietnam. *Canadian Gemmologist*, Vol. 25, No. 3, pp. 83–95.

Long P.V., Vinh H.Q., Garnier V., Giuliani G., Ohnenstetter D., Lhomme T., Schwarz D., Fallick A., Dubessy J., Trinh P.T. (2004) Gem corundum deposits in Vietnam. *Journal of Gemmology*, Vol. 29, No. 3, pp. 129–147.

Long P.V., Vinh H.Q., Nghia N.X. (2004) Inclusions in Vietnamese Quy Chau ruby and their origin. *Australian Gemmologist*, Vol. 22, pp. 67–71.

Mercier A., Rakotondrazafy M., Ravolomiandrinarivo B. (1999) Ruby mineralization in southwest Madagascar. *Gondwana Research*, Vol. 2, No. 3, pp. 433–438, http://dx.doi.org/10.1016/S1342-937X(05)70281-1

Palke A.C., Wong J., Verdel C., Avila J.N. (2018) A common origin for Thai/Cambodian rubies and blue and violet sapphires from Yogo Gulch, Montana, U.S.A.? *American Mineralogist*, Vol. 103, No. 3, pp. 469–479, http://dx.doi.org/10.2138/am-2018-6164

Palke A.C., Saeseaw S., Renfro N.D., Sun Z., McClure S.F. (2019) Geographic origin determination of blue sapphire. *G&G*, Vol. 55, No. 4, pp. 536–579, http://dx.doi.org/10.5741/GEMS.55.4.536

Pardieu V., Rakotosaona N., Noverraz M., Bryl L.P. (2012) Ruby and sapphire rush near Didy, Madagascar. *GIA Research News*, https://www.gia.edu/ongoing-research/ruby-and-sapphire-rush-near-didy-madagascar

Peretti A., Schmetzer K., Bernhardt H.J., Mouawad F. (1995) Rubies from Mong Hsu. *G&G*, Vol. 31, No. 1, pp. 2–26, http://dx.doi.org/10.5741/GEMS.31.1.2

Sangsawong S., Vertriest W., Saeseaw S., Pardieu V. (2017) A study of rubies from Cambodia and Thailand. *GIA Research News*, https://www.gia.edu/gia-news-research/study-rubies-cambodia-thailand

Schwarz D., Schmetzer K. (2001) Rubies from the Vatomandry area, eastern Madagascar. *Journal of Gemmology*, Vol. 27, No. 7, pp. 409–416.

Smith C.P. (1998) Rubies and pink sapphires from the Pamir Range in Tajikistan, former USSR. *Journal of Gemmology*, Vol. 26, No. 2, pp. 103–109.

Smith C.P., Fagan A.J., Bryan C. (2016) Ruby and pink sapphire from Aappaluttoq, Greenland. *Journal of Gemmology*, Vol. 35, No. 4, pp. 294–306.

Sorokina E.S., Litvinenko A.K., Hofmeister W., Häger T., Jacob D.E., Nasriddinov Z.Z. (2015) Rubies and sapphires from Snezhnoe, Tajikistan. *G&G*, Vol. 51, No. 2, pp. 160–175, http://dx.doi.org/10.5741/GEMS.51.2.160

Stone-Sundberg J., Thomas T., Sun Z., Guan Y., Cole Z., Equall R.,

Emmett J.L. (2017) Accurate reporting of key trace elements in ruby and sapphire using matrix-matched standards. *G&G*, Vol. 53, No. 4, pp. 438–451, http://dx.doi.org/10.5741/GEMS.53.4.438
Sutthirat C., Hauzenberger C., Chualaowanich T., Assawincharoenkij T. (2018) Mantle and deep crustal xenoliths in basalts from the Bo Rai ruby deposit, eastern Thailand: Original source of basaltic ruby. *Journal of Asian Earth Sciences*, Vol. 164, pp. 366–379, http://dx.doi.org/10.1016/j.jseaes.2018.07.006
Themelis T. (2008) *Gems & Mines of Mogok*. A&T Publishers, USA, 352 pp.
Thirangoon K. (2009) Ruby and pink sapphire from Aappaluttoq, Greenland. *GIA Research News*, https://www.gia.edu/gia-news-research-nr32309
Vertriest W., Saeseaw S. (2019) A decade of ruby from Mozambique: A review. *G&G*, Vol. 55, No. 2, pp. 162–183, http://dx.doi.org/10.5741/GEMS.55.2.162
Vertriest W., Palke A.C., Renfro N.D. (2019) Field gemology: Building a research collection and understanding the development of gem deposits. *G&G*, Vol. 55, No. 4, pp. 490–511, http://dx.doi.org/10.5741/GEMS.55.4.490
Wang W. Hall M., Shen A.H., Breeding C.M. (2006) Developing corundum standards for LA-ICP-MS trace-element analysis. *G&G*, Vol. 42, No. 3, pp. 105–106.

THANK YOU, REVIEWERS

GEMS & GEMOLOGY requires each manuscript submitted for publication to undergo a rigorous peer review process, in which each paper is evaluated by at least three experts in the field prior to acceptance. This is essential to the accuracy, integrity, and readability of *G&G* content. In addition to our dedicated Editorial Review Board, we extend many thanks to the following individuals who devoted their valuable time to reviewing manuscripts in 2019.

Non-Editorial Board Reviewers

Raquel Alonso-Perez • Troy Ardon • Mikko Åström • Roy Bassoo • Kenny Befus • K.C. Bell • Richard Berg • Emily Cahoon • Robert Coenraads • James Day • Emily Dubinsky • Ekaterina Gerasimova • Ronnie Geurts • Al Gilbertson • Darrell Henry • Don Hoover • Jeffrey Keith • Mandy Krebs • Yan Liu • Taijin Lu • Yun Luo • Dan Marshall • Daniela Mascetti • Hollie McBride • Claudio Milisenda • Jack Ogden • Vincent Pardieu • Stuart Robertson • Sudarat Saeseaw • Alberto Scarani • Kenneth Scarratt • Karl Schmetzer • Jeremy Shepherd • Steve Shirey • Russ Shor • Ziyin Sun • Lin Sutherland • David Brian Thompson • Lisbet Thoresen • Rebecca Tsang • Rachelle Turnier • John Valley • Wim Vertriest • Xiaodong Xu • Alexander Zaitsev

Geographic Origin Determination Of Emerald

Sudarat Saeseaw, Nathan D. Renfro, Aaron C. Palke, Ziyin Sun, and Shane F. McClure

The gem trade has grown to rely on gemological laboratories to provide origin determination services for emeralds and other fine colored stones. In the laboratory, this is mostly accomplished by careful observations of inclusion characteristics, spectroscopic analysis, and trace element profile measurements by laser ablation–inductively coupled plasma–mass spectrometry (LA-ICP-MS). Inclusions and spectroscopy can often separate Colombian emeralds from other sources (although there is some overlap between Colombian, Afghan, and Chinese [Davdar] emeralds). For non-Colombian emeralds, trace element analysis by LA-ICP-MS is needed in addition to information from the stone's inclusions. The relative chemical diversity of emeralds from worldwide deposits allows confidence in origin determination in most cases. This contribution outlines the methods and criteria used at GIA for geographic origin determination for emerald.

When the Spanish conquistadors first brought Colombian emeralds (figures 1 and 2) onto the international market, they became a global sensation in their day. Emeralds from Central Asia and Egypt were known at the time, but the world had likely never seen emeralds of such high quality and size. Traders soon developed distribution channels that brought the Colombian material all the way from the royal courts in Europe to the powerful Moguls of India (Giuliani et al., 2000).

The nineteenth and twentieth centuries saw all of this change as new mines sprang up around the world to challenge the famed Colombian emeralds. Most notable in terms of high-quality production were Brazil, Russia, and Zambia, but smaller deposits have been uncovered in Madagascar and Ethiopia and elsewhere. As the market has evolved alongside these developments, geographic origin has come to be an important factor for fine-quality emeralds. The demand for emerald origin determination was initially driven by the proliferation of sources. However, this expansion and diversification of emerald sources has also complicated origin determination. As the number of sources grows, so does the overlap in their characteristics. The following sections will detail the specific criteria used in the laboratory at GIA to make geographic origin conclusions for emeralds, as well as potential areas of overlap and how these are dealt with.

In Brief

- Emerald origin determination can be challenging due to the number of deposits and their often similar inclusion scenes.
- Emeralds can be classified as hydrothermal/metamorphic or schist-hosted based on UV-Vis-NIR spectroscopy and inclusions.
- Hydrothermal/metamorphic emeralds, including those from Colombia, have jagged fluid inclusions but can easily be separated by trace element chemistry.
- For schist-hosted emeralds, a combination of trace element chemistry and microscopic observations of inclusions is required for a conclusive origin determination.

SAMPLES AND ANALYTICAL METHODS

Emeralds included in this study are dominantly from GIA's reference collection, which was assembled over more than a decade by GIA's field gemology department. Stones in GIA's reference collection were obtained from reliable sources and collected as close to the mining source as possible; see Vertriest et al. (2019), pp. 490–511 of this issue. When necessary, the data from the reference collection was supplemented

See end of article for About the Authors and Acknowledgments.
Gems & Gemology, Vol. 55, No. 4, pp. 614–646,
http://dx.doi.org/10.5741/GEMS.55.4.614

Figure 1. An 88.4 g emerald crystal from Coscuez, Colombia. Photo by Robert Weldon/GIA; courtesy of the Roz and Gene Meieran Collection.

by stones gathered by the authors of this study outside of the field gemology program or borrowed from GIA's museum collection. The trace element data was obtained from 298 samples total, with 36 from Zambia (25 from Kafubu and 11 from Musakashi), 34 from Colombia, 36 from Afghanistan, 22 from Madagascar, 64 from Russia, 49 from Brazil, 32 from Ethiopia, and 25 from China (Davdar). Emeralds from Madagascar are much less frequently encountered in the lab. Therefore, these deposits are included in the trace element section here, but their inclusions are not described for the sake of brevity and clarity. More

Figure 2. Colombian emerald from Chivor, 4.50 ct. Photo by Robert Weldon/GIA.

information about specific mines within these countries can be found in Vertriest et al. (2019), pp. 490–511 of this issue.

Trace element chemistry was collected at GIA over the course of several years using two different LA-ICP-MS systems. The ICP-MS was either a Thermo Fisher X-Series II or iCAP Qc system, coupled to an Elemental Scientific Lasers NWR 213 laser ablation system with a frequency-quintupled Nd:YAG laser (213 nm wavelength with 4 ns pulse width). Ablation was carried out with 55 µm spot sizes with fluence of 8–10 J/cm^2 and repetition rates of either 7, 10, or 20 Hz. ^{29}Si was used as an internal standard at 313500 ppm using NIST 610 and 612 as external standards. Repeat analyses on samples from single locations over time have verified the consistency of the analyses with these various setups. Accuracy is estimated to be within 10–20% for most elements analyzed, based on comparisons with electron microprobe data on a small selection of samples.

Inclusions were identified, when possible, using Raman spectroscopy with a Renishaw inVia Raman microscope system. The Raman spectra of the inclusions were excited by a Stellar-REN Modu Ar-ion laser producing highly polarized light at 514 nm and collected at a nominal resolution of 3 cm^{-1} in the 2000–200 cm^{-1} range. In many cases, the confocal capabilities of the Raman system allowed inclusions beneath the surface to be analyzed.

UV-Vis spectra were recorded with a Hitachi U-2910 spectrometer or a PerkinElmer Lambda 950 in the range of 190–1100 nm with a 1 nm spectral resolution and a scan speed of 400 nm/min. When possible, polarized spectra of oriented samples were collected to obtain o- and e-ray absorption spectra. UV-Vis-NIR spectra are presented either as relative absorbance with no units or absorption coefficient (α) in units of cm^{-1} where $\alpha = A \times 2.303/t$, with A = absorbance and t = path length in cm.

RESULTS

UV-Vis-NIR Spectroscopy in Emerald Origin Determination. As with rubies and sapphires, emerald's geographic origin determination starts with a coarse separation into one of two groups based on their geological conditions of formation: hydrothermal/metamorphic and schist-hosted/magmatic-related (the Type II tectonic metamorphic-related and Type I tectonic magmatic-related groups from Giuliani et al., 2019; Giuliani and Groat, 2019, pp. 464–489 of this issue). This distinction also roughly corresponds to a separation between Colombian emeralds (or those emeralds that might have Colombian-like features) and essentially everything else. The hydrothermal/metamorphic group contains emeralds from Colombia, Afghanistan, and China (Davdar), while the schist-hosted/magmatic group includes emeralds from Zambia (Kafubu), Russia, Ethiopia, and Brazil, among others. In many cases, this separation can be made based on gemological properties. Hydrothermal/metamorphic emeralds often have jagged multiphase inclusions, whereas schist-hosted emeralds generally have blocky or irregular multiphase inclusions. The difference in appearance is likely related to variations in the way the fluids were originally entrapped as well as post-entrapment healing and evolution of the inclusions while the emeralds were held at high temperature and pressure before being exhumed to the earth's surface (e.g., Giuliani et al., 2019).

But advanced analytical techniques are often more reliable than relying solely on inclusions. Schist-hosted emeralds generally have much higher Fe content than hydrothermal/metamorphic emeralds. This chemical distinction is most easily seen using UV-Vis-NIR spectroscopy. Representative UV-Vis-NIR o-ray spectra of hydrothermal/metamorphic emeralds are shown in figure 3 (top). The most prominent features in this group are the Cr^{3+} broad absorption bands at about 430 and 600 nm and the sharp Cr^{3+} band at around 683 nm. A typical Colombian UV-Vis-NIR spectrum is characterized by the absence of any absorption bands in the near-IR region at wavelengths

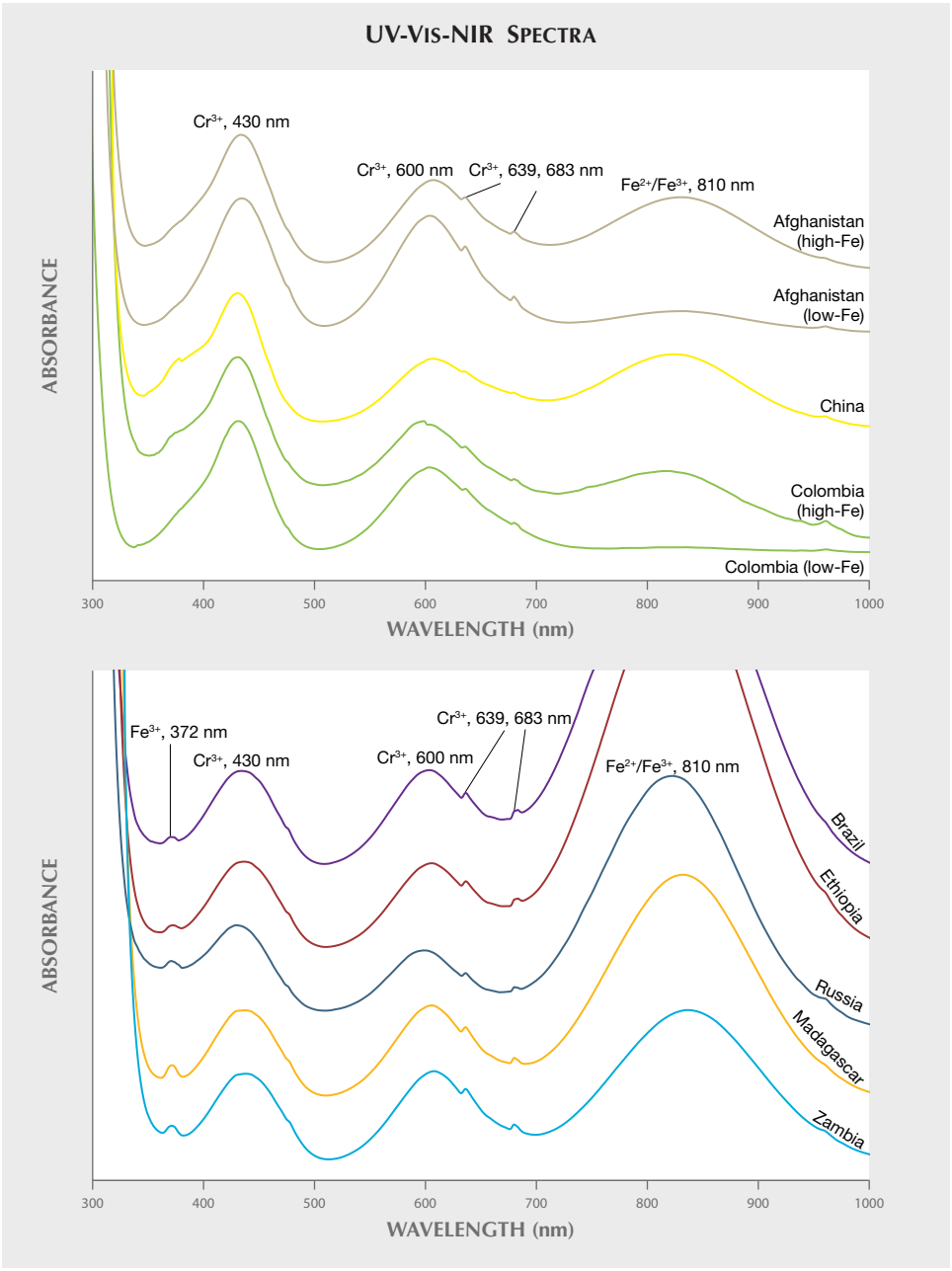

Figure 3. Top: Representative UV-Vis-NIR spectra of metamorphic/hydrothermal emeralds. The low-Fe and high-Fe Colombian emeralds have 200 and 1900 ppm Fe, respectively, while the low-Fe and high-Fe Afghan emeralds have 1100 and 2400 ppm Fe, respectively. Bottom: Representative UV-Vis-NIR spectra of schist-hosted emeralds. All spectra are o-ray spectra and have been renormalized in order to compare the relative intensities of absorption features and, hence, absolute intensities cannot be compared between spectra. The spectra are also offset by various amounts in order to facilitate comparison.

greater than 700 nm (bottom spectrum in figure 3, top). Other members of the hydrothermal/metamorphic emerald group (i.e., Davdar, China, and Afghanistan), which generally have higher concentrations of Fe, usually show a noticeable to significant absorption band at 810 nm caused by Fe^{2+}, possibly enhanced by nearby Fe^{3+}. This feature has traditionally been used to separate Colombian emeralds from those from all other deposits (e.g., Saeseaw et al., 2014). However, as shown in figure 3 (top), there is some overlap between some Colombian emeralds and other members of the hydrothermal/metamorphic group. On average, Colombian emeralds have lower Fe content than stones from any other deposit. However, the few stones at the higher range of Fe content for Colombian emeralds have a noticeable Fe^{2+} absorption band at 810 nm. Similarly, while Afghan emeralds tend to have higher Fe content than most Colombian stones, at their lower Fe concentration range some stones may show only a slight Fe-related absorption at 810 nm, which could be mistaken for a classic Colombian emerald spectrum. Great care must be

taken in interpreting UV-Vis-NIR spectra to identify possible Colombian emeralds, and multiple lines of evidence, including trace element chemistry, must be used to accurately ascertain a Colombian origin.

Due to their much higher Fe content, schist-hosted emeralds are easy to separate from Colombian and other hydrothermal/metamorphic stones based on their o-ray UV-Vis-NIR absorption spectra (figure 3, bottom). The most obvious distinction is the significantly increased intensity of the Fe-related 810 nm absorption band in schist-hosted emeralds. Additionally, these higher-iron emeralds also tend to have a more prominent Fe^{3+} absorption band at 372 nm than the hydrothermal/metamorphic emeralds. As with the hydrothermal/metamorphic group, making geographic origin determinations for schist-hosted emeralds requires the use of multiple lines of evidence including UV-Vis-NIR analysis, trace element chemistry, and microscopic observation of a stone's inclusions.

Microscopic Internal Inclusions. Emeralds, even top-quality material, tend to be fairly heavily included. Fluid inclusions, partially healed fissures, needles, and/or solid mineral crystals are frequently encountered. Inclusions are an extremely important tool for geographic origin determination as well as separating natural and synthetic emeralds. However, there are several areas of overlap. Emeralds from some deposits may have inclusion scenes that resemble those seen in other important deposits. Some stones may lack any diagnostic inclusions, making it impossible to provide an origin opinion if there is no definitive trace element data. Gemologists often classify emerald into two broad groups based on fluid inclusions: jagged or blocky. This also corresponds roughly to the hydrothermal/metamorphic and schist-hosted classification presented above. Most fluid inclusions in emerald are multiphase, but it is often difficult to observe all the distinct phases in an inclusion using a gemological microscope. Jagged fluid inclusions usually appear to be composed of a liquid, a gas, and one or more solid phases. Sometimes there is even more than one liquid phase present as well. Regardless, when there are clearly observed solid, liquid, and gas phases present, these are typically referred to as three-phase inclusions. Blocky fluid inclusions often appear to be composed of only two phases, a liquid and a gas. However, there is often a solid phase present in these inclusions, which is hard to observe due to similarity in refractive index between the solid and fluid. Sometimes the use of cross-polarized light reveals hidden solid crystals in these fluid inclusions. Additional information about the internal features of emeralds from major world deposits can be found in the following references: Giuliani et al. (1993, 2019), Vapnik et al. (2006), Groat et al. (2008), Marshall et al. (2012), Zwaan et al. (2012), Saeseaw et al. (2014), and Vertriest and Wongrawang (2018).

Geographic Origin Determination of Hydrothermal/Metamorphic Emeralds. Colombian emeralds are the most economically important from the hydrothermal/metamorphic type of deposit, and jagged fluid inclusions are their hallmark features. Such fluid inclusions are typically elongate, with jagged sawtooth edges. Unfortunately, emeralds from other hydrothermal/metamorphic deposits such as Afghanistan and China may have similar jagged fluid inclusions. Among the mineral inclusions found in these emeralds are calcite, pyrite with various morphologies, albite, and carbonate minerals. This section will document the internal features of emeralds from Colombia, Afghanistan, and China. Emeralds from a minor deposit at Musakashi in Zambia will also be mentioned briefly at the end of this section. Further information on the inclusion scenes in emeralds from these deposits can be found in Bowersox et al. (1991), Bosshart (1991), and Saeseaw et al. (2014).

The Internal World of Colombian Emeralds. Colombian emeralds (figure 4) have long been held in high esteem for their rich green color and for the history

Figure 4. Matched pair of Colombian emeralds with no oil, approximately 10 carats total. Photo by Robert Weldon/GIA; courtesy of Amba Gem Corporation.

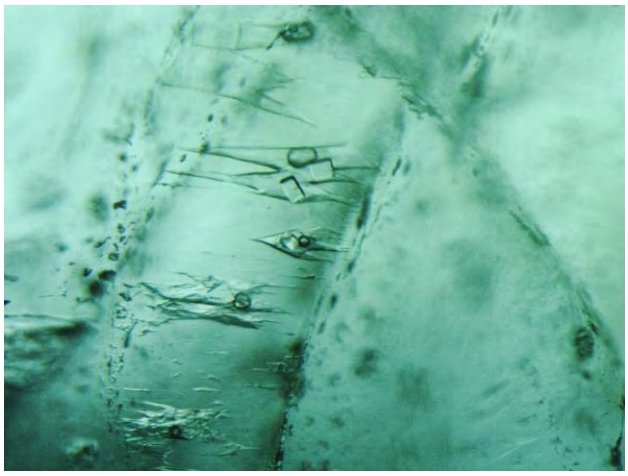

Figure 5. Small jagged inclusions in Colombian emeralds. Photomicrograph by Sudarat Saeseaw; field of view 0.9 mm.

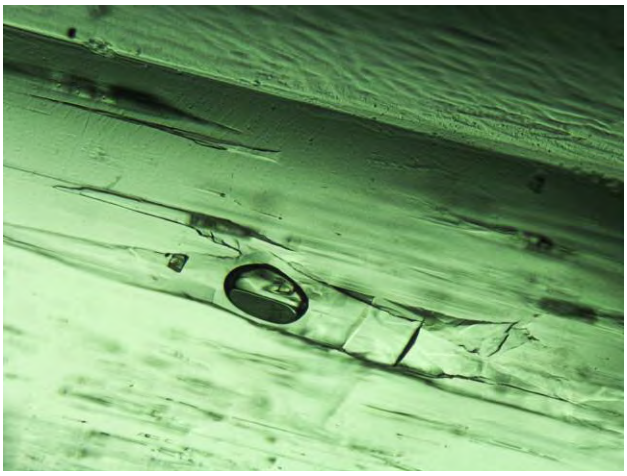

Figure 6. This large jagged multiphase inclusion is characteristic of Colombian emerald. Photomicrograph by Charuwan Khowpong; field of view 1 mm.

and legends associated with these stones. The most readily identifiable feature of Colombian emeralds are classic three-phase jagged fluid inclusions. These contain a gas bubble and a cubic crystal (typically halite and/or sylvite) and generally range in size from 100 µm to 1 mm (figures 5 and 6). However, as mentioned above, jagged fluid inclusions can be seen in emeralds from other deposits such as Afghanistan and China (see also Saeseaw et al., 2014). Large jagged fluid inclusions (greater than about 500 µm) are unique to Colombia and can be taken as diagnostic evidence of origin. However, when only smaller jagged fluid inclusions are observed, care must be taken to ascertain a stone's origin and additional supporting evidence should be sought out. *Gota de aceite* is a growth feature sometimes seen in Colombian emeralds that can be used as a strong indication of origin (figure 7). Similar growth features are sometimes observed in emeralds from other sources such as Zambia, but it is by far most common in emeralds from Colombia. This growth feature's name is Spanish for "drop of oil," in reference to the roiled and turbid appearance it lends. Gota de aceite grows parallel to the basal faces, often in planes that do not extend throughout the stone. Common solid inclusions in Colombian emeralds are carbonates, pyrite (figure 8),

Figure 7. Unique gota de aceite *growth features in Colombian emerald. Photomicrograph by Patcharee Wongrawang; field of view 0.9 mm.*

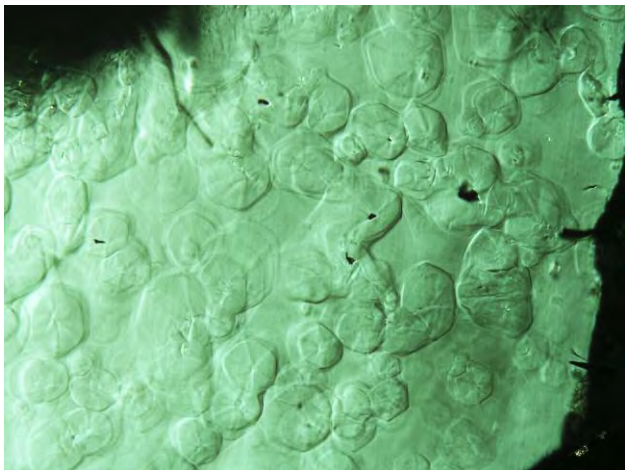

Figure 8. Group of pyrite crystals and rhombohedral carbonate crystal in Colombian emerald. Photomicrograph by Patcharee Wongrawang; field of view 1.6 mm.

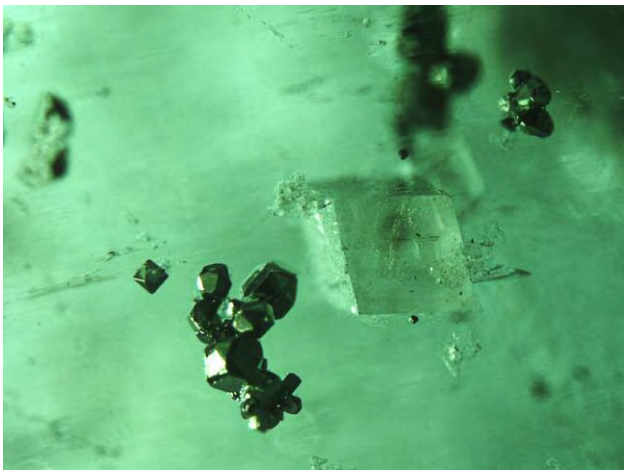

Figure 9. Emeralds from Afghanistan: a 23.43 ct emerald-cut stone from Zarajet and an emerald crystal measuring approximately 31.7 mm long. Photo by Robert Weldon/GIA; courtesy of Himalayan Gems & Jewelry.

quartz, feldspar, and small black particles from the surrounding black shales (Giuliani et al., 2019; Giuliani and Groat, 2019, pp. 464–489 of this issue). However, most of these minerals are also found in other emerald deposits. Similar to Kashmir sapphires, Colombian emeralds also have one very rare mineral inclusion that has never been seen in emeralds from other deposits: parisite (Gübelin and Koivula, 2008). When observed, it can be considered a diagnostic indicator of Colombian origin; unfortunately, this inclusion is not frequently encountered.

The Internal World of Afghan Emeralds. While Afghan emeralds have never held the market share of their Colombian brethren, many fine stones have been produced from the mines in the Panjshir Valley (figure 9). As for their internal characteristics, multiphase fluid inclusions are the most common inclusion in Afghan emeralds. They often have an elongate, needle-like shape and host several daughter minerals (figures 10 and 11), which can distinguish them from Colombian and Chinese emeralds. Daughter minerals in fluid inclusions in emeralds are

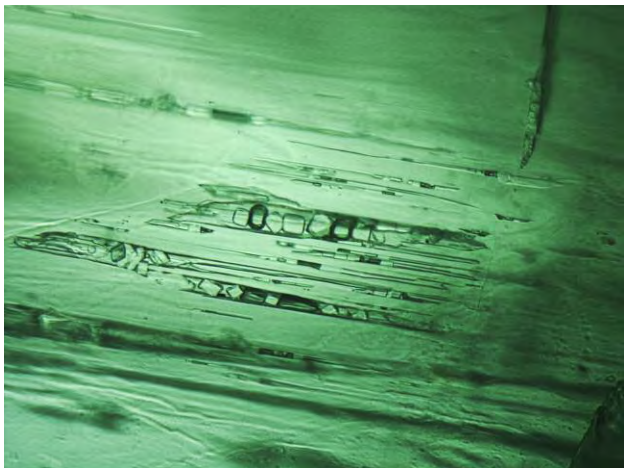

Figure 10. Elongate needle-like multiphase inclusions containing several daughter crystals and a gas bubble are typically seen in Afghan emeralds. Photomicrograph by Charuwan Khowpong; field of view 0.7 mm.

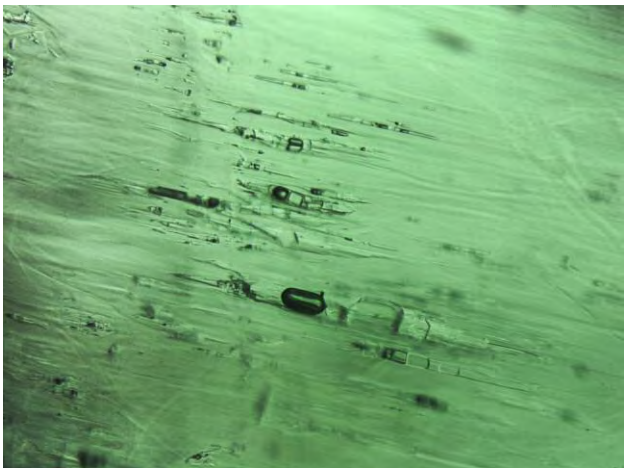

Figure 11. Needle-like multiphase inclusions lie parallel to each other in Afghan emerald. Photomicrograph by Charuwan Khowpong; field of view 0.9 mm.

often assumed to be halite when they have a cubic habit; however, when there are several daughter minerals, as in the inclusions in Afghan emeralds, their exact identity is often hard to determine, even with the use of confocal Raman spectroscopy. The typical inclusion scene in these emeralds from the Panjshir Valley consists of small jagged fluid inclusions (figures 12 and 13), similar to those seen in Colombian emeralds, and scarce crystalline inclusions. Solid inclusions, when present, include pyrite, limonite, beryl, carbonate minerals, and feldspar.

The Internal World of Chinese Emeralds. The deposit at Davdar, China, was discovered late in the twentieth century. The geology of Davdar is not well understood, but it is reported that this deposit shares some similarities with other metamorphic deposits (Giuliani et al., 2019). Fluid inclusions in these emeralds have a jagged shape and are composed of a rounded gas bubble and a cubic crystal (figures 14–17). They are often small and can resemble those seen in emeralds from Colombia and Afghanistan. While there is likely very little production from the Chinese mines

Figure 12. Small jagged inclusions in Afghan emerald. Photomicrograph by Nattida Ng-Pooresatien; field of view 0.7 mm.

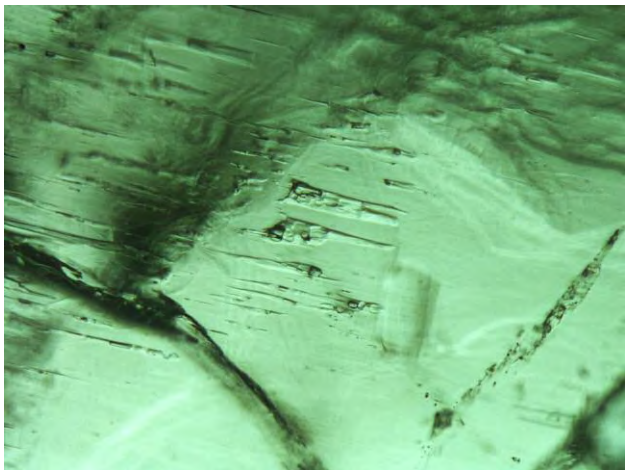

Figure 13. Irregular jagged inclusions in Afghan emerald. Photomicrograph by Nattida Ng-Pooresatien; field of view 0.9 mm.

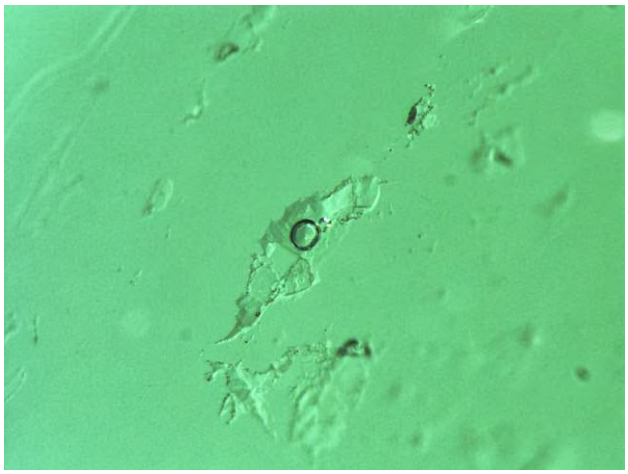

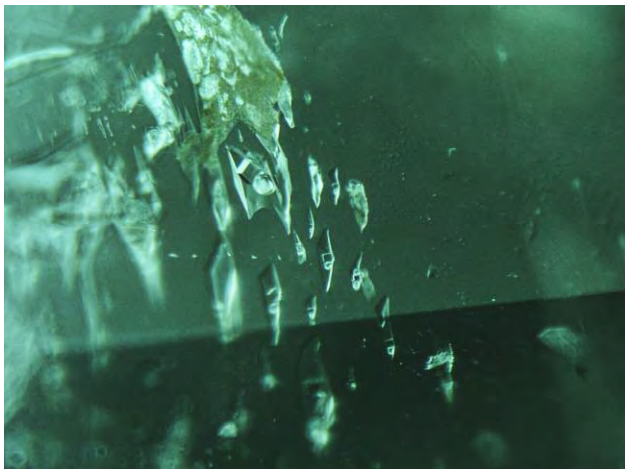

Figure 14. Jagged fluid inclusions with a transparent cubic crystal and a gas bubble in emerald from China. Photomicrograph by Sudarat Saeseaw; field of view 0.7 mm.

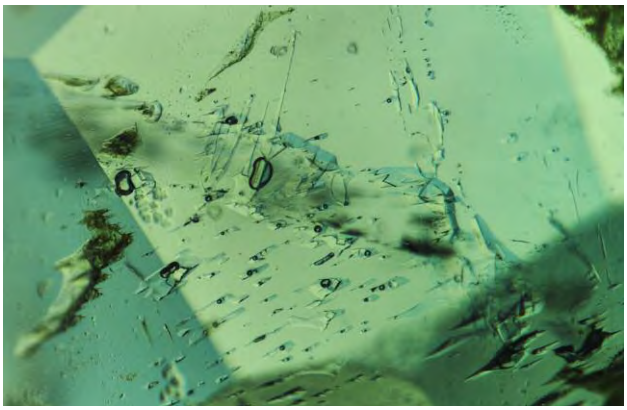

Figure 15. Jagged fluid inclusions in Chinese emerald. Photomicrograph by Charuwan Khowpong; field of view 1.05 mm.

reaching the market, their potential for overlap with Colombian emeralds makes it important to be aware of their identifying characteristics to avoid potential problems in origin determination.

Inclusion Scenes Gone Wrong. Many Colombian emeralds are easily identified by large jagged inclusions (figure 6) or gota de aceite growth features (figure 7). Multiphase inclusions containing numerous daughter crystals (figure 10) are considered conclusive evidence of an Afghan origin. However, it can be complicated in smaller or less-included stones where there may not be much information available to the microscopist. For example, the inclusion scenes of two Afghan emeralds in figures 18 and 19 showed jagged edges with a rounded gas bubble and cubic crystal(s). These inclusions could easily be misinterpreted as Colombian. Similarly, emeralds from a minor deposit in Zambia at Musakashi can also have jagged three-phase inclusions similar to those seen in Colombian emeralds, making it necessary to search for further evidence (figures 20 and 21). As with the Chinese emerald deposit at Davdar, few stones have emerged from Musakashi. Nonetheless, it is important to be aware of this potential overlap in properties. UV-Vis-NIR analysis can be helpful to

Figure 16. Elongate jagged inclusions in emerald from China. Photomicrograph by Nattida Ng-Pooresatien; field of view 0.7 mm.

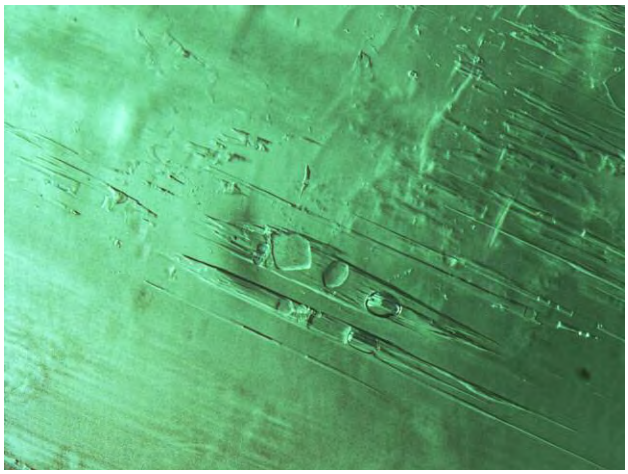

Figure 17. Irregular multiphase inclusions in Chinese emerald. Photomicrograph by Nattida Ng-Pooresatien; field of view 0.7 mm.

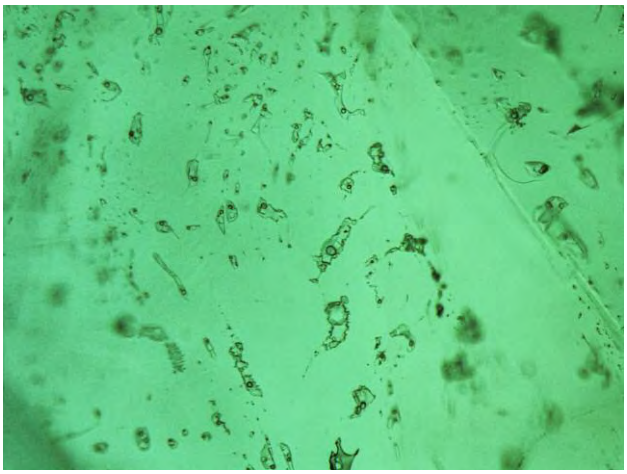

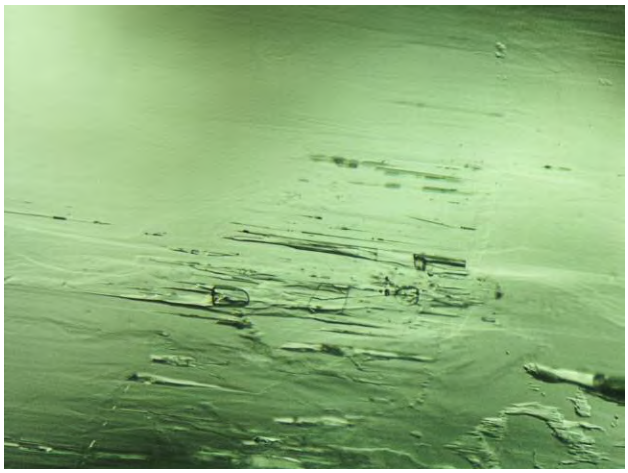

Figure 18. Jagged multiphase inclusions in an Afghan emerald appear similar to features seen in some Colombian emeralds. Photomicrograph by Nattida Ng-Pooresatien; field of view 0.8 mm.

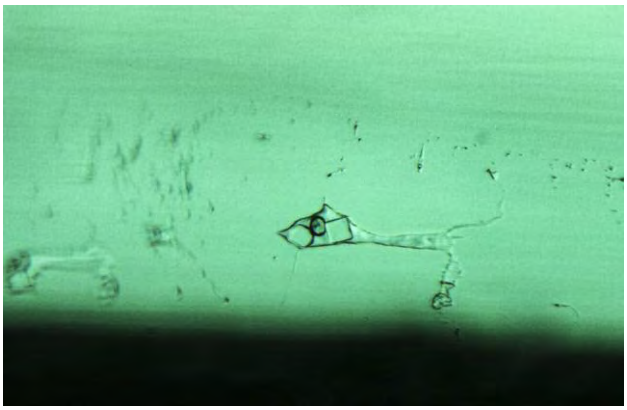

Figure 19. Irregularly shaped multiphase inclusion hosting a small gas bubble and several crystals in an Afghan emerald. Photomicrograph by GIA; field of view 0.3 mm.

separate between Colombian and Afghan, Chinese, or Musakashi emerald. Many Afghan, Chinese, and Musakashi emeralds have obvious Fe-related absorption bands distinguishing them from Colombian stones. However, there will be some overlap in the high-Fe Colombian emeralds and the low-Fe Afghan and Chinese emeralds, both of which may show minor Fe-related absorption bands. For these borderline cases, chemical analysis is needed for a conclusive result.

Geographic Origin Determination for Schist-Hosted Emeralds. Schist-hosted emerald deposits are the result of magmatic processes, including pegmatitic events. Emeralds formed in these deposits through interaction of pegmatites or other magmatic bodies with mafic, ultramafic, and/or metamorphic country rocks. This type of emerald includes important sources such as Zambia (Kafubu), Brazil, Russia, and Ethiopia. These emeralds tend to have a darker green color than Colombian, Afghan, and Chinese emeralds owing to their generally higher iron content. However, some lower-iron schist-hosted emeralds, especially those from Russia, may have lighter-toned colors. Schist-hosted emeralds often have blocky fluid inclusions that can be either two-phase, three-phase,

Figure 20. Jagged three-phase fluid inclusions in an emerald from Musakashi, Zambia. Photomicrograph by Charuwan Khowpong; field of view 0.7 mm.

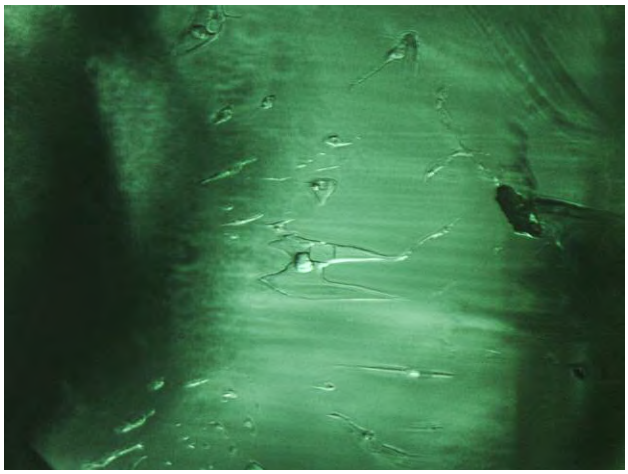

Figure 21. Jagged three-phase fluid inclusions in an emerald from Musakashi, Zambia. Photomicrograph by Charuwan Khowpong; field of view 0.7 mm.

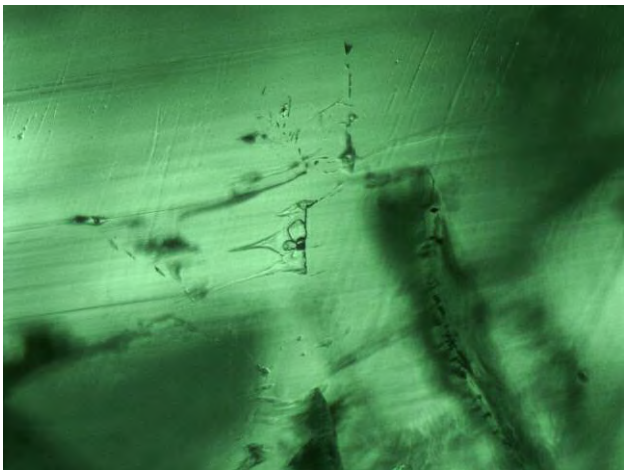

Figure 22. Zambian emeralds at 8.14 ct (left) and 1.76 ct (right). Photo by Robert Weldon/GIA; courtesy of Mark Kaufman, Kaufman Enterprises.

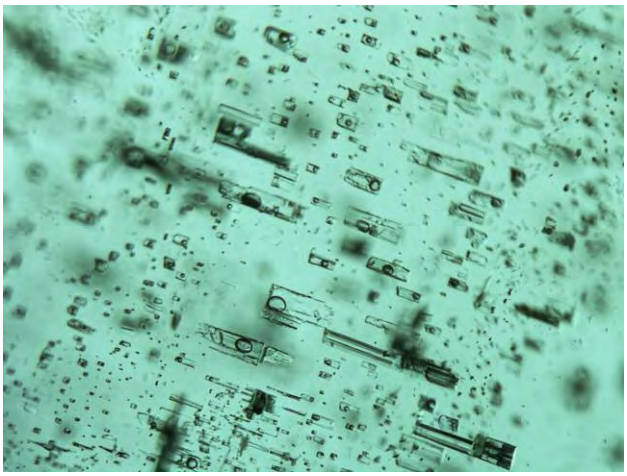

Figure 23. Blocky fluid inclusions are common in Zambian emeralds, seen perpendicular to the optic axis of the host. Photomicrograph by Nattida Ng-Pooresatien; field of view 1.1 mm.

or multiphase. The most common solid crystal inclusion is mica, which occurs in a variety of forms and colors. Mica can be formed before the emerald (i.e., protogenetic) or at the same time as the host crystal (syngenetic). Other mineral inclusions can also be found: dendritic black inclusions and quartz, carbonate minerals, talc, pyrite, emerald, chlorite, and spinel. The following sections will describe typical inclusion scenes for each origin. Note that emeralds from Madagascar would be included in the schist-hosted group. However, these emeralds are much less frequently encountered in the lab and so they are not included in the discussion of inclusion scenes. Nonetheless, origin determination of Madagascar emeralds will be considered later in the trace element chemistry section. Further information on the inclusion scenes in schist-hosted emeralds can be found in Cassedanne and Sauer (1984), Hänni et al. (1987), Zwaan et al. (2005), Saeseaw et al. (2014), Vertriest and Wongrawang (2018), and Palke et al. (2019a).

The Internal World of Zambian Emeralds from Kafubu. Zambian emeralds (figure 22) are found in the Kafubu area in the southern part of the historically important copper mining area known as the Copperbelt. Emerald mineralization occurs at the phlogopite-biotite contact zone between pegmatites and a talc-magnetite schist. Zambian emerald fluid inclusions are typically blocky (figure 23) or irregularly shaped (figure 24) multiphase inclusions. Mica is a common inclusion in Zambian emeralds from Kafubu, occurring with a brownish color and rounded shape (figure 25) or in pseudo-hexagonal green platelets (figure 26). Black platelets, or dendritic inclusions composed of oxide minerals such as magnetite, hematite, or ilmenite (figure 27), can be seen in Zambian and other schist-hosted emeralds. Elongate amphibole crystals are also observed occasionally in Zambian emeralds (figure 28). Other minerals such as apatite, pyrite, talc, barite, albite, and calcite have also been reported (Saeseaw et al., 2014).

The Internal World of Brazilian Emeralds. Emeralds have been discovered in several Brazilian localities including Carnaíba and Socotó (Bahia), Santa Terezinha (Goiás), and Itabira (Minas Gerais). This article will focus on production from Itabira, or the Belmont

Figure 24. Irregularly shaped multiphase inclusions in emeralds from Kafubu, Zambia, as seen parallel to the optic axis. Photomicrograph by Nattida Ng-Pooresatien; field of view 2 mm.

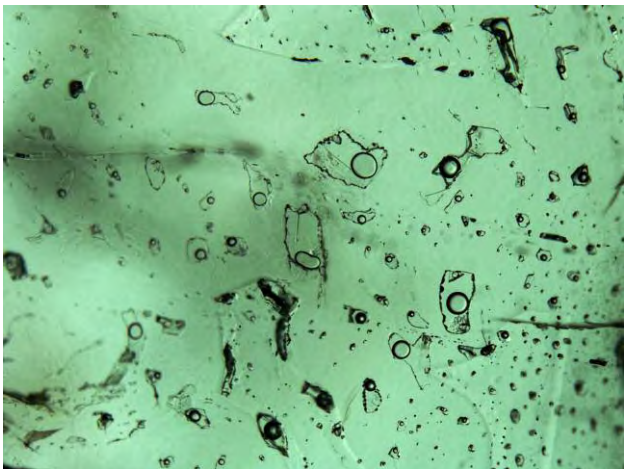

Figure 25. Brownish micas are common in Zambian emerald but can also be found in emerald from other deposits. Photomicrograph by Nattida Ng-Pooresatien; field of view 1.3 mm.

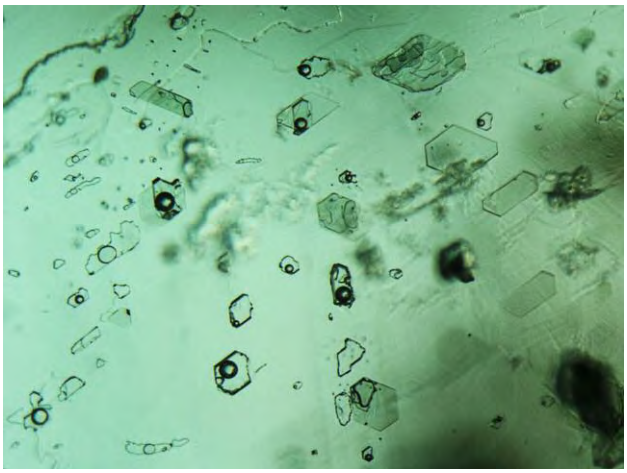

Figure 26. Pseudo-hexagonal fluid inclusions and greenish mica are common in Zambian emerald. Photomicrograph by Nattida Ng-Pooresatien; field of view 0.9 mm.

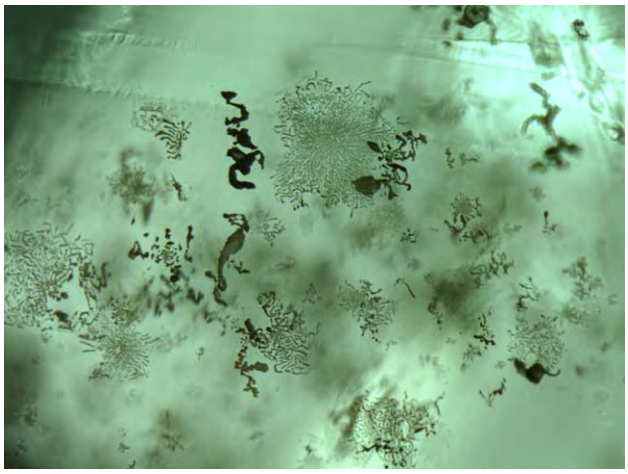

Figure 27. Opaque thin platelets showing dendritic inclusions are seen in Zambian and other schist-hosted emeralds. Photomicrograph by Nattida Ng-Pooresatien; field of view 1.0 mm.

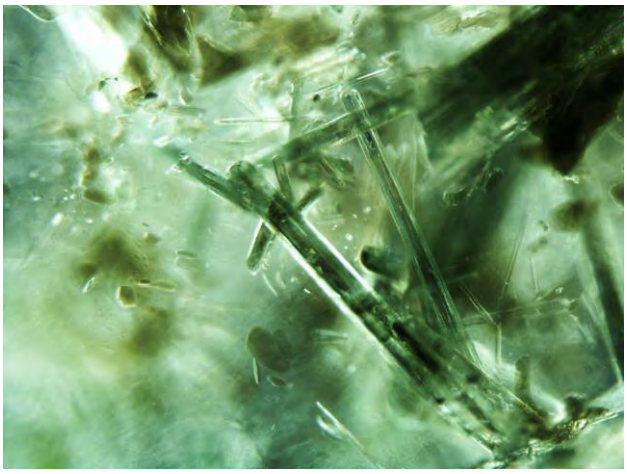

Figure 28. Greenish rod-like inclusions identified as amphibole in Zambian emerald. Photomicrograph by Nattida Ng-Pooresatien; field of view 1.6 mm.

mine, as it is the main producer of Brazilian emerald today. Characteristic inclusions for emeralds from Belmont include blocky fluid inclusions and parallel tiny tubes described as "rain-like" (figure 29) that, if dense enough, can occasionally produce chatoyancy. The fluid inclusions typically show a blocky shape (figure 30) and may have multiple liquid/gas/solid phases apparent within (figure 31). Some irregular

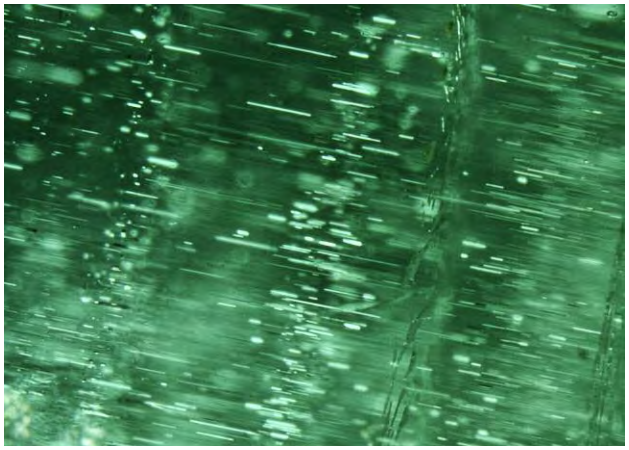

Figure 29. Cloud of fine elongate tubes with various fillings form a rain-like inclusion in a Brazilian emerald. Photomicrograph by Charuwan Khowpong; field of view 1.30 mm.

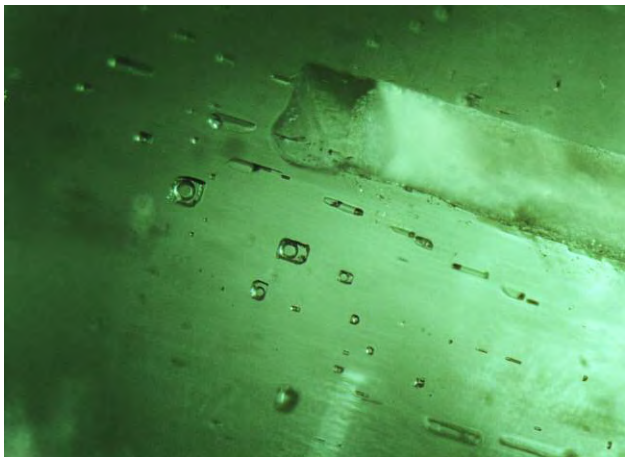

Figure 30. This Brazilian emerald contains blocky and rectangular fluid inclusions and a tube filled with aggregate calcite. Photomicrograph by Charuwan Khowpong; field of view 0.80 mm.

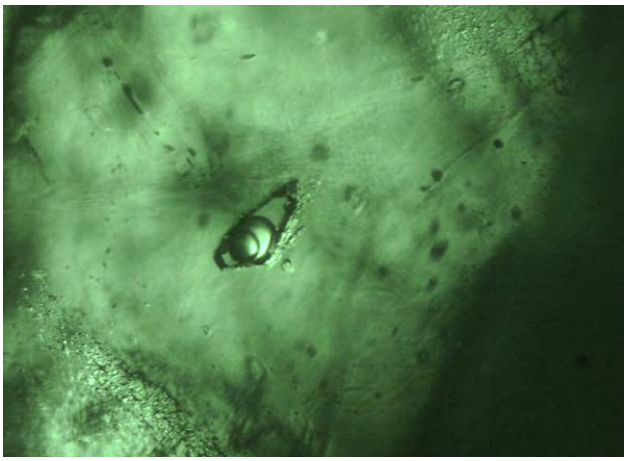

Figure 31. Irregular three-phase inclusion (liquid/liquid/gas) with immiscible liquids and a gas bubble in a Brazilian emerald. Photomicrograph by Charuwan Khowpong; field of view 1.00 mm.

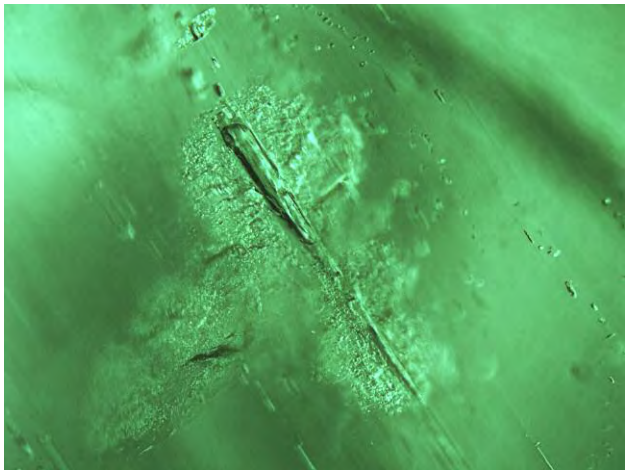

Figure 32. Elongate three-phase inclusion with concentric equatorial fractures in a Brazilian emerald. Photomicrograph by Patcharee Wongrawang; field of view 1.30 mm.

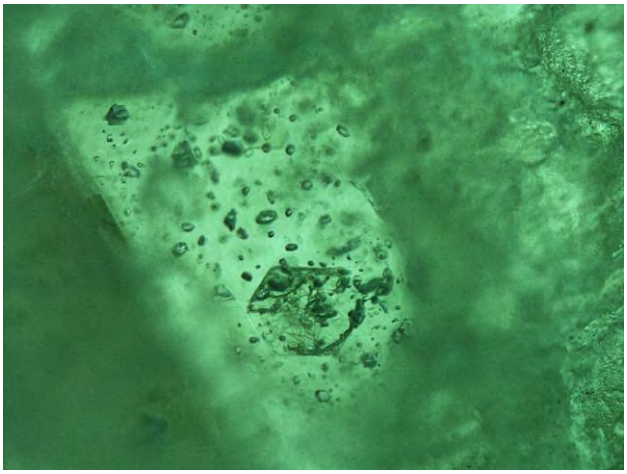

Figure 33. Brownish mica flakes (syngenetic) showing a nearly ideally formed pseudo-hexagonal shape in a Brazilian emerald. Photomicrograph by Charuwan Khowpong; field of view 0.70 mm.

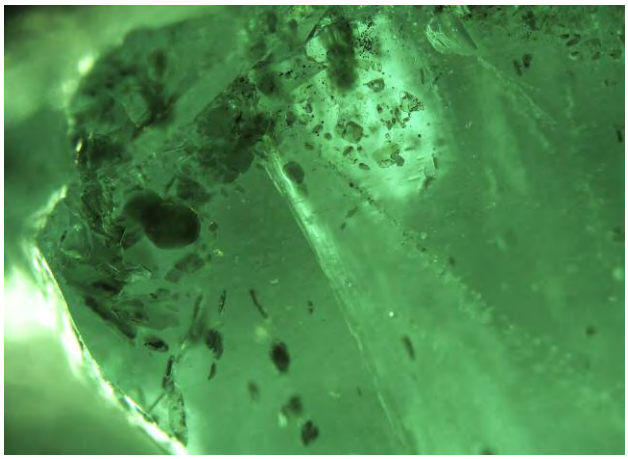

fluid inclusions in Brazilian emeralds may have concentric equatorial fractures (figure 32). Mica can be found as both syngenetic pseudo-hexagonal (figure 33) and protogenetic rounded brown crystals (figure 34). Other solid mineral inclusions such as quartz, magnetite, chromite spinel, calcite, or pyrite can also be observed, similar to other deposits of schist-hosted emerald.

Figure 34. Crystals of rounded dark brownish biotite-phlogopite mica flakes in a Brazilian emerald. Photomicrograph by P. Wongrawang; field of view 2.70 mm.

Figure 35. Left to right: Ethiopian emeralds weighing 2.00, 9.72, and 4.13 ct. Photo by Robert Weldon/GIA; courtesy of Mayer & Watt.

Figure 36. Ethiopian emerald weighing 4.12 ct. Photo by Robert Weldon/GIA; courtesy of Mayer & Watt.

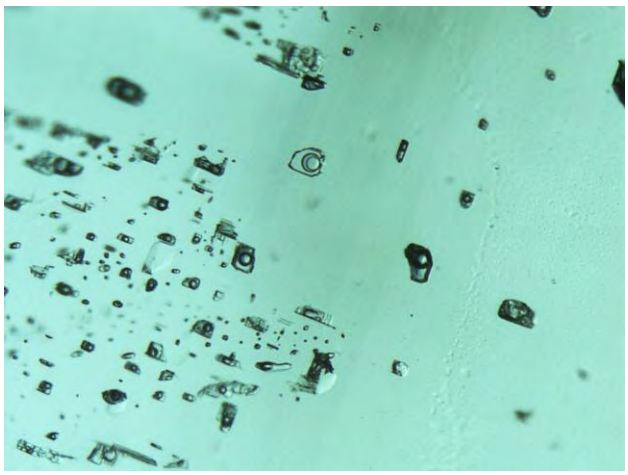

Figure 37. Blocky and irregular fluid inclusions in an Ethiopian emerald. Photomicrograph by Jonathan Muyal; field of view 1.44 mm.

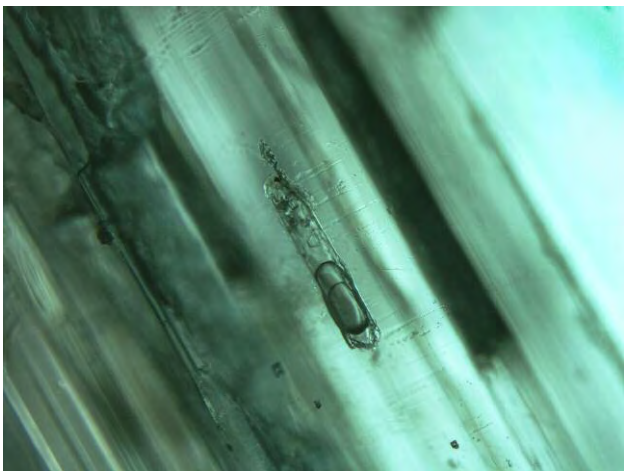

Figure 38. Fluid inclusion with two separate liquids and a gas bubble in an Ethiopian emerald. Photomicrograph by Jonathan Muyal; field of view 0.72 mm.

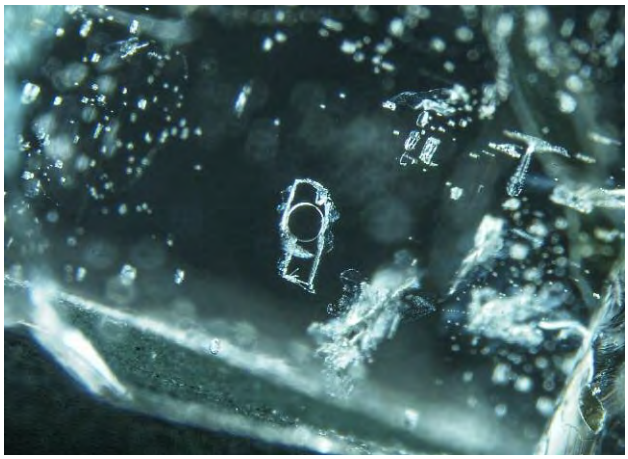

Figure 39. Irregular fluid inclusion with large gas bubble in an Ethiopian emerald. Photomicrograph by Ungkhana Atikarnsakul; field of view 2.0 mm.

The Internal World of Ethiopian Emeralds. In late 2016, emerald was discovered in Ethiopia near the village of Shakiso (figures 35 and 36). Their fluid inclusions often reveal blocky, elongate, or irregular multiphase inclusions (figures 37–39) and nail-like growth blockage inclusions (figure 40). The blocky inclusions are very similar to those seen in emeralds from Zambia (Kafubu), Brazil, and Russia. Some fluid inclusions in Ethiopian stones contain two separate liquid phases, one gas bubble, and often solid crystals

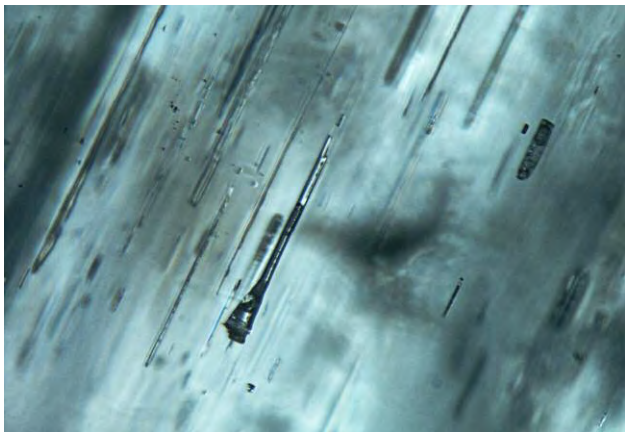

Figure 40. Elongate fluid inclusion originating around a mineral inclusion, resembling "nail head spicules" in an Ethiopian emerald. Photomicrograph by Ungkhana Atikarnsakul; field of view 0.8 mm.

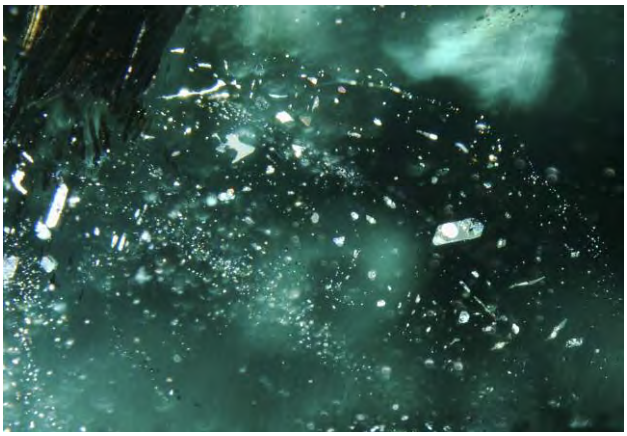

Figure 41. Scattered thin films in an Ethiopian emerald. Photomicrograph by Ungkhana Atikarnsakul; field of view 2.0 mm.

(liquid/liquid/gas) (figures 37–39). When these stones are examined in a microscope using an intense incandescent light, one of the fluids can evaporate and merge with the gas, which has been identified by Raman spectroscopy as a CO_2 gas. Some inclusions may also have granular fringes (figure 39). Minute particles and iridescent thin films (figure 41) are seen occasionally and can be confused with inclusion scenes more typical of Russian emerald. Internal growth features are typically straight with angular color zoning following crystal prism faces. Some stones exhibit roiled growth (figure 42) that is distinct from the gota de aceite growth seen in Colombian emeralds. Other mineral inclusions such as brown mica platelets, clinochlore, magnetite spinel, calcite, quartz, and talc can be observed in Ethiopian emerald.

Figure 42. Roiled internal growth in an Ethiopian emerald. Photomicrograph by Ungkhana Atikarnsakul; field of view 2.7 mm.

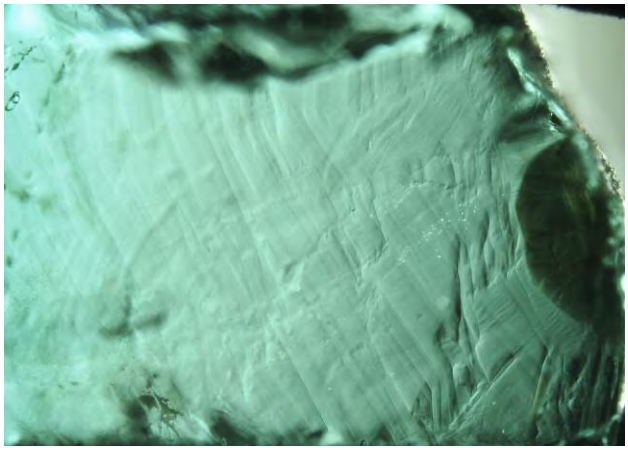

The Internal World of Russian Emeralds. Fine emeralds have been produced from the Ural Mountains since the mid-nineteenth century, placing Russia as one of the classic sources. Russian emeralds can harbor unique inclusion scenes. Iridescent thin films that lie parallel to the basal pinacoid are especially indicative of origin (figure 43). Fluid inclusions take on different forms including elongate (figure 44), irregularly edged multiphase (figures 45 and 46), to blocky (figure 47), although blocky fluid inclusions are uncommon in Russian emeralds. Some fluid inclusions also have patchy, granular fringes (figure 48). Long needles or growth tube inclusions can also be found (figure 49). Brown mica (figure 50) and rod-shaped or needle-like amphibole crystals have been observed. Russian emerald typi-

Figure 43. Plane of numerous interference thin films aligned parallel to the basal pinacoid in a Russian emerald. Photomicrograph by Charuwan Khowpong; field of view 1.40 mm.

Figure 44. Elongate fluid inclusion with a small solid inclusion at the end in a Russian emerald. Photomicrograph by Suwasan Wongchacree; field of view 1.20 mm.

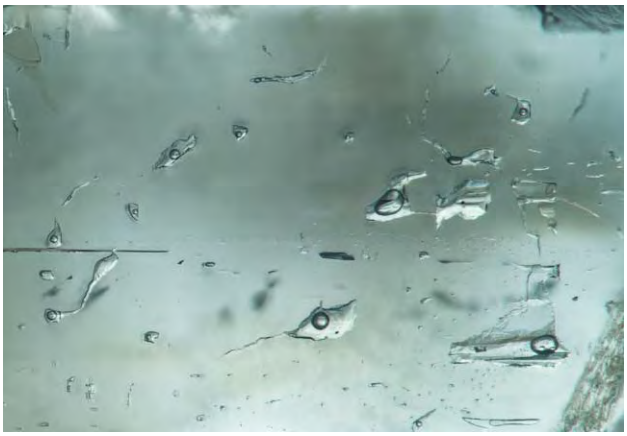

Figure 45. Irregularly shaped two- and three-phase inclusions in a Russian emerald. Photomicrograph by Suwasan Wongchacree; field of view 1.05 mm.

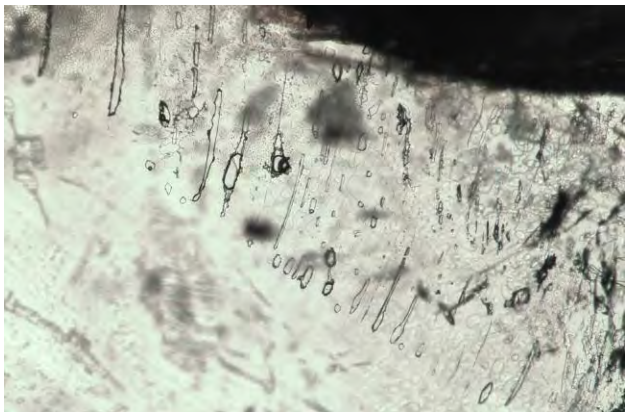

Figure 46. Irregularly shaped fluid inclusions in a Russian emerald. Photomicrograph by Charuwan Khowpong; field of view 1.75 mm.

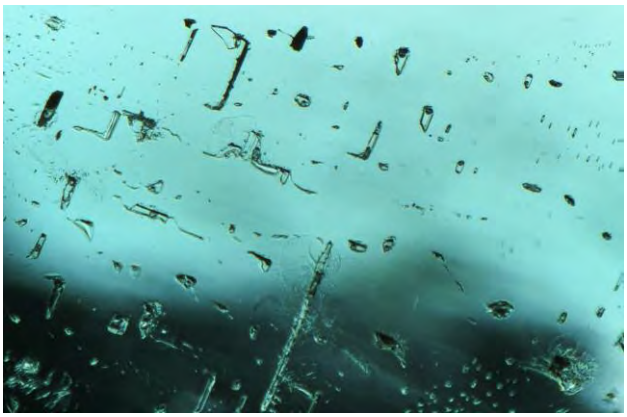

Figure 47. Blocky and irregular fluid inclusions in a Russian emerald. Photomicrograph by Aaron Palke; field of view 1.26 mm.

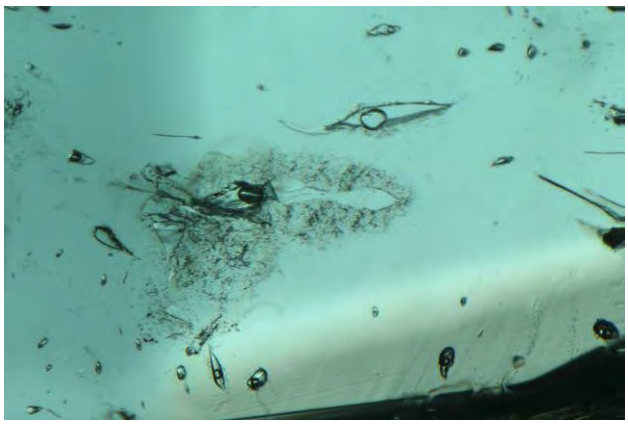

Figure 48. Irregular fluid inclusions with granular fringes in a Russian emerald. Photomicrograph by Aaron Palke; field of view 1.26 mm.

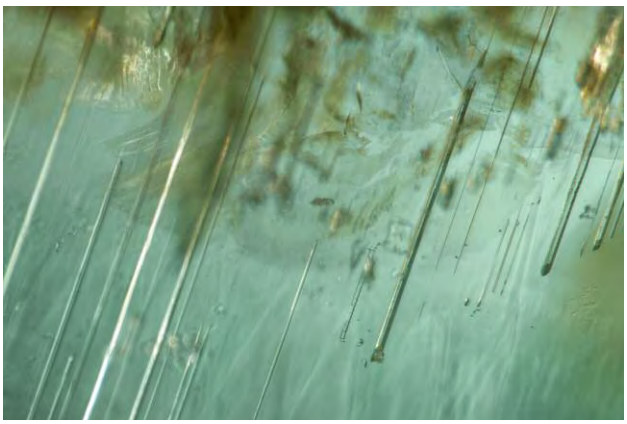

Figure 49. Long growth tubes in a Russian emerald. Fiber-optic illumination. Photomicrograph by Suwasan Wongchacree; field of view 1.05 mm.

Figure 50. Lath-shaped brown inclusions identified as phlogopite mica in a Russian emerald. Photomicrograph by Suwasan Wongchacree; field of view 1.40 mm.

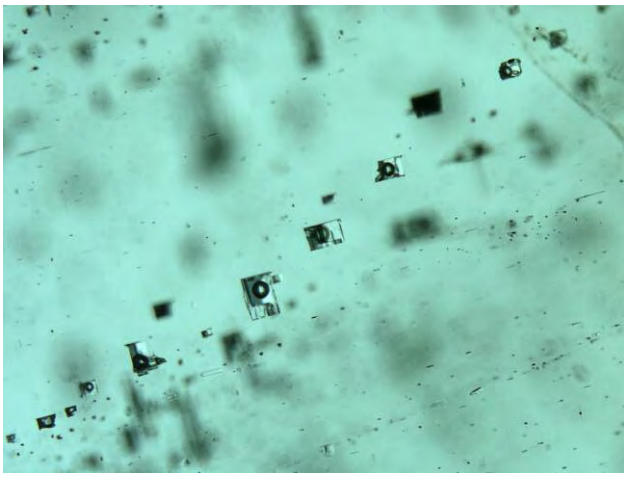

Figure 51. Rectangular blocky fluid inclusions typically seen in Zambian emeralds. Photomicrograph by Nattida Ng-Pooresatien; field of view 1.1 mm.

cally has few inclusions, and origin determination can be challenging.

Inclusion Scenes Gone Wrong. Owing to their similar geological genesis, emeralds from Zambia (Kafubu), Brazil, Russia, and Ethiopia may be difficult to distinguish. Making an accurate origin determination requires an experienced gemologist with a robust reference database to compare against unknown stones. Reaching an origin conclusion is easier when the stone has abundant inclusions as opposed to a clean stone. However, every emerald must be observed carefully, as stones from geographically disparate deposits can have similar inclusion scenes. For example, how would you determine origin on these blocky inclusions shown in figures 51 and 52? One is from Zambia and the other from Ethiopia. Irregular fluid inclusions that might have once given an impression of Zambian origin (again, see figure 24) are now also occasionally found in Ethiopian emerald (figure 53). Elongate or thin rod-like fluid inclusions were first seen in Brazilian stones, but similar inclusions have been found in emeralds from Ethiopia and Russia (figure 54). Similarly, rain-like inclusions were once considered diagnostic for Brazilian emerald but can now be observed in Ethiopian and Russian emer-

Figure 52. Blocky fluid inclusions in Ethiopian emerald might lead to misinterpretation as Zambian origin. Photomicrograph by Ungkhana Atikarnsakul; field of view 1.1 mm.

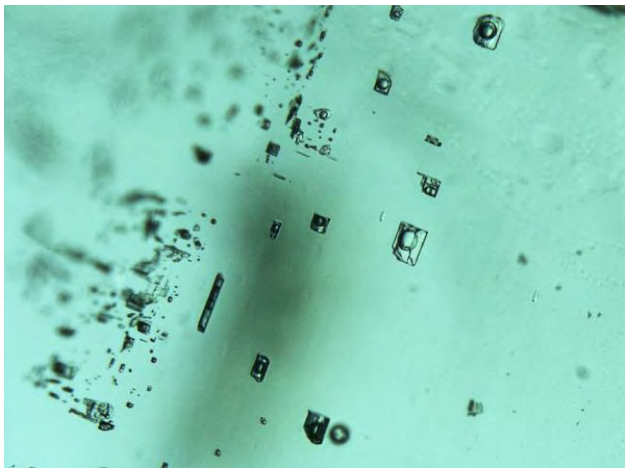

Figure 53. Irregular fluid inclusions in this Ethiopian emerald were initially interpreted as an indicator of Zambian origin. Photomicrograph by Ungkhana Atikarnsakul; field of view 1.3 mm.

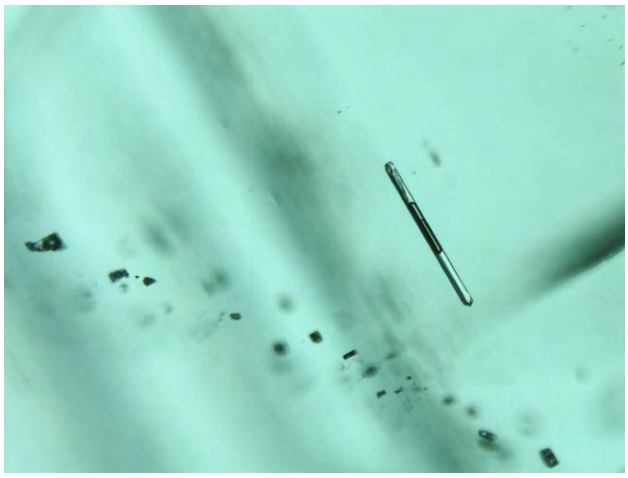

Figure 54. Elongate fluid inclusions in emerald from Ethiopia. These can be also seen in Brazilian and Russian emerald. Photomicrograph by Ungkhana Atikarnsakul; field of view 1.1 mm.

Figure 55. Parallel fine needles in Russian emerald resemble inclusions seen in Brazilian stones. Photomicrograph by Suwasan Wongchacree; field of view 1.05 mm.

alds as well (figure 55). Clusters of brownish mica are common inclusions in all of these schist-hosted emeralds (figure 56). In this class there are no mineral inclusions that can be used to indicate origin. In many cases it is impossible to give an origin opinion based on microscopy. For emeralds from schist-host rock, UV-Vis-NIR analysis is not useful in separation as they all display similar spectra. In this case, chemical analysis by LA-ICP-MS is required to make an accurate origin determination.

Trace Element Chemistry. Trace element analysis is a much more powerful tool for origin determination of emeralds than it is for gem corundum. This likely has its roots in the respective crystalline structures. Beryl has several unique crystal sites of varying sizes and geometry into which trace elements can substitute. This allows easier incorporation and greater variety of substitutional trace elements than for corundum, which has only one crystallographic site that can accept foreign elements. Therefore, emeralds appear to be more sensitive to slight changes in their geological environment, which can impart unique trace element signatures for stones from different geographic localities. Given the overlapping inclusion scenes for emeralds from the deposits discussed here, trace element chemistry analysis is crucial for making accurate origin calls. Several examples of trace element plots used in the GIA laboratory for emerald origin determination are shown in figure 57, and table 1 gives the general ranges and averages of the trace elements used in origin determination at GIA. Commonly used trace elements include Li, K, V, Cr, Fe, Rb, and Cs. Colombian emeralds tend to be the purest chemically, possessing generally lower concentrations of the alkalis Li, K, Rb, and Cs as well as Fe. The other hydrothermal/metamorphic emeralds from Afghanistan and China are more enriched in these trace elements, allowing them to be clearly separated from Colombian stones. The most characteristic feature of the schist-hosted emeralds is their enrichment in Fe relative to the hydrothermal/metamorphic group. However, most schist-hosted emeralds also have much higher concentrations of the alkali metals, and members of this group can be generally differentiated from each other by their dis-

Figure 56. Cluster of brownish phlogopite mica crystals in Ethiopian emerald. These can also be seen in other schist-hosted emeralds. Photomicrograph by Ungkhana Atikarnsakul; field of view 4.0 mm.

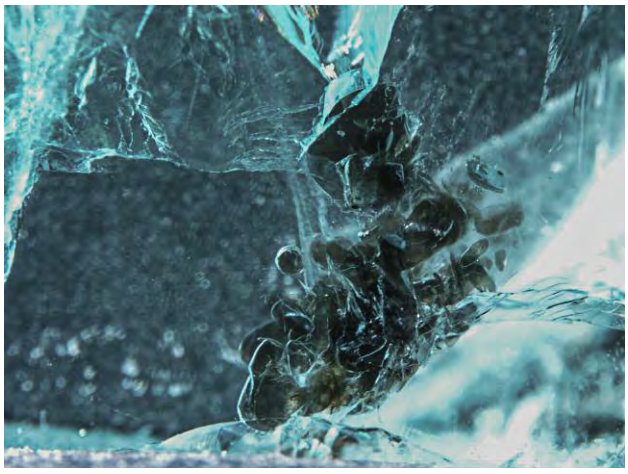

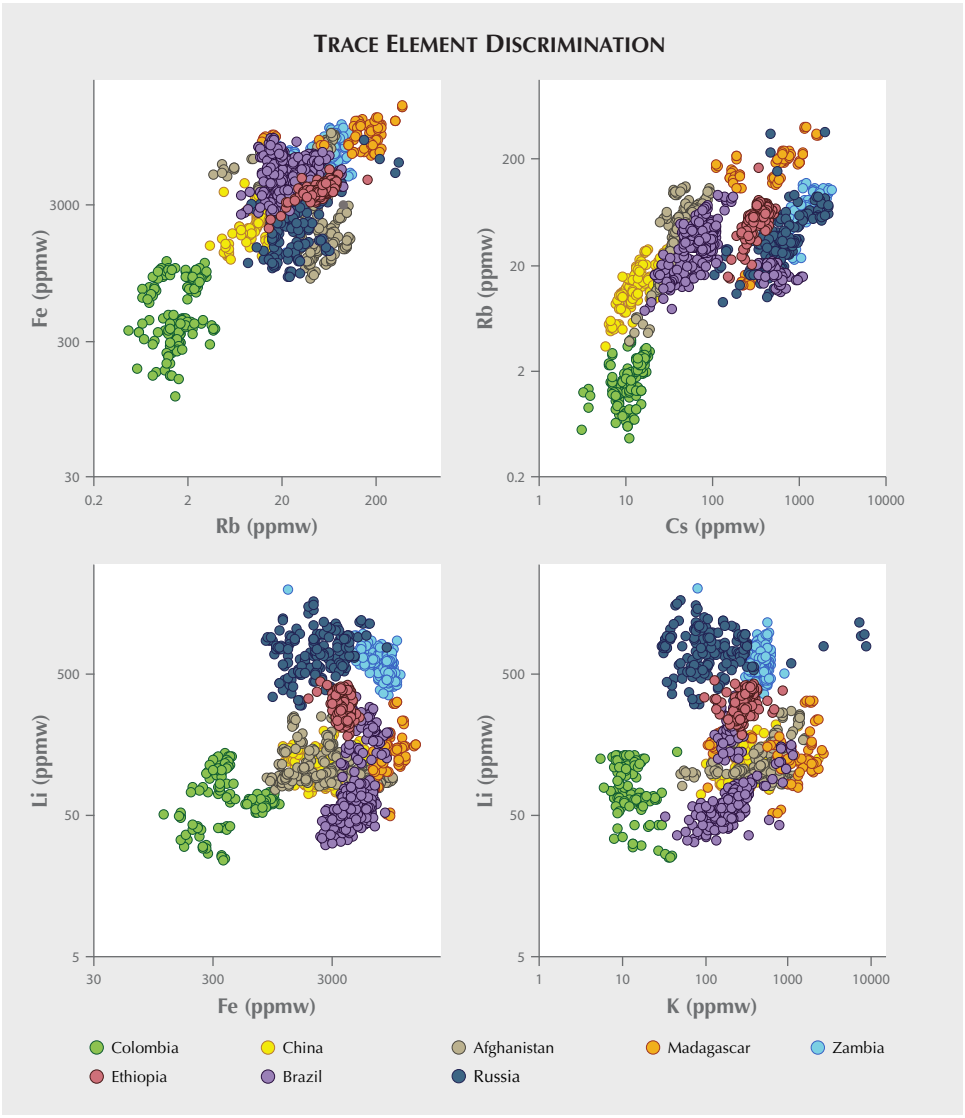

Figure 57. Typical trace element plots used for origin determination of emeralds.

tinctive trace element profiles. For instance, Russian emeralds tend to have lower Fe and higher Li; Zambian emeralds from Kafubu tend to have high Cs, Fe, and Li; Madagascar emeralds tend to have high K and Fe; Ethiopian emeralds tend to be moderately enriched in most trace elements; and Brazilian stones tend to occupy the lower range of many of the trace elements.

Despite these general trace element profiles, there is still significant overlap when considering only one or two trace elements at a time. However, the selective plotting method employed by GIA for blue sapphires and rubies is also routinely used to provide greater confidence in emerald origin determination based on trace element chemistry; see Palke et al. (2019b), pp. 536–579 of this issue, for a discussion of this method. Essentially, selective plotting makes for an easier comparison between an unknown stone and the vast accumulation of reference data available by filtering out data with dissimilar trace element profiles and comparing only against reference stones that match the full trace element signature of the unknown stone. Elements used in the selective plotting method include Li, K, Fe, Rb, and Cs. The use of selective plotting often allows trace element data to be interpreted more easily and provides greater confidence in origin determination based on these data (figure 58). In most cases trace element chemistry provides solid evidence about a stone's origin, but sometimes there is still too much overlap in the trace element data (figure 59). When trace element data and inclusion information are ambiguous or contradictory, an "inconclusive" origin determination is always warranted.

TABLE 1. Generalized trace element profiles of major world emerald deposits in ppmw.

Hydrothermal/Metamorphic Emeralds					
Colombia					
	Li	**K**	**Fe**	**Rb**	**Cs**
Range	24.2-139	bdl-359	117-2030	bdl-4.92	3.17-19.0
Average	62.9	17.7	553	2.03	10.9
Median	61.0	14.3	414	1.96	10.7
Afghanistan					
	Li	**K**	**Fe**	**Rb**	**Cs**
Range	78.2-268	51.7–1590	849–9820	3.87–110	11.3–97.0
Average	115	639	3780	46.9	46.2
Median	99.7	625	3120	44.1	43.6
China (Davdar)					
	Li	**K**	**Fe**	**Rb**	**Cs**
Range	68.6–332	91.8–1320	1170–6430	3.47–31.5	5.96–41.2
Average	114	314	2711	15.1	16.3
Median	110	303	2470	14.6	13.8
Schist-Hosted Emeralds					
Brazil					
	Li	**K**	**Fe**	**Rb**	**Cs**
Range	31.3–359	33.2–1150	2460–9120	7.42–91.8	16.8–1130
Average	80.8	231	5120	31.4	148
Median	59.4	205	5035	30.0	79.7
Ethiopia					
	Li	**K**	**Fe**	**Rb**	**Cs**
Range	183–446	98.6–889	1970–5320	14.7–166	151–544
Average	310	307	3841	56.9	345
Median	306	306	3870	58.0	351
Madagascar					
	Li	**K**	**Fe**	**Rb**	**Cs**
Range	50.3–320	107–2660	6720–15800	12.7–395	110–1670
Average	144	1200	9400	157	555
Median	127	1220	8990	174	541
Russia					
	Li	**K**	**Fe**	**Rb**	**Cs**
Range	300–1640	bdl–8830	864–8800	9.10–361	107–2180
Average	751	319	2613	39.9	714
Median	723	108	2330	28.5	521
Zambia (Kafubu)					
	Li	**K**	**Fe**	**Rb**	**Cs**
Range	360–1140	305–890	4620–11600	17.4–116	375–2430
Average	604	500	8139	65.9	1344
Median	600	513	8410	72.6	1480
Detection Limits (ppmw)					
	Li	**K**	**Fe**	**Rb**	**Cs**
Range	0.016–0.71	0.27–3.15	0.71–5.57	0.003–0.040	0.005–0.99

**bdl = below the detection limit of the LA-ICP-MS analysis*

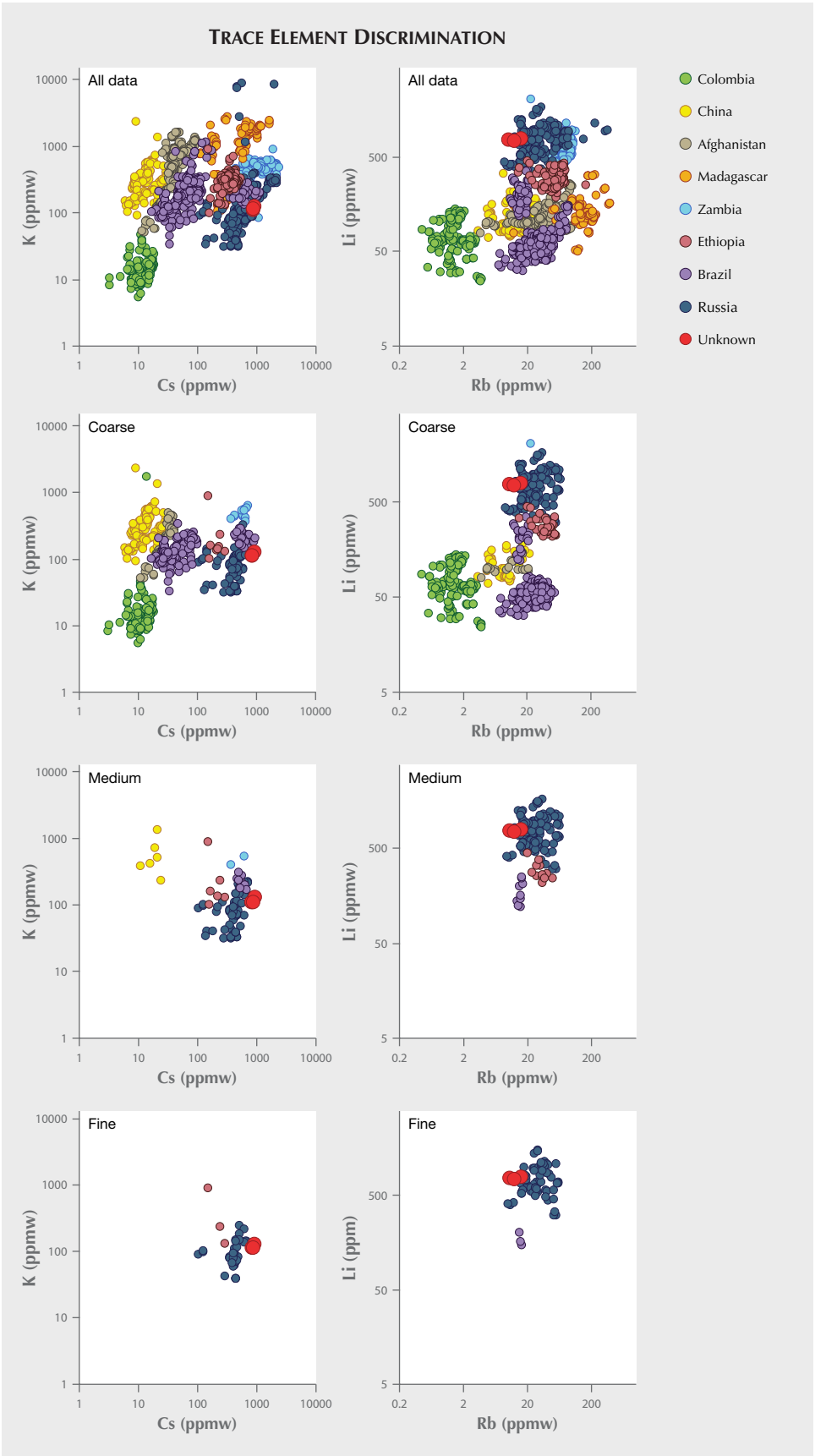

Figure 58. Example of a Russian emerald's origin determined using the selective plotting method (the unknown stone shown as a red circle). The trace element profile of an unknown emerald can be easier to interpret through the selective plotting method used by GIA. Selective plotting uses coarse, medium, and fine windows to filter out dissimilar reference data, making the plots easier to interpret.

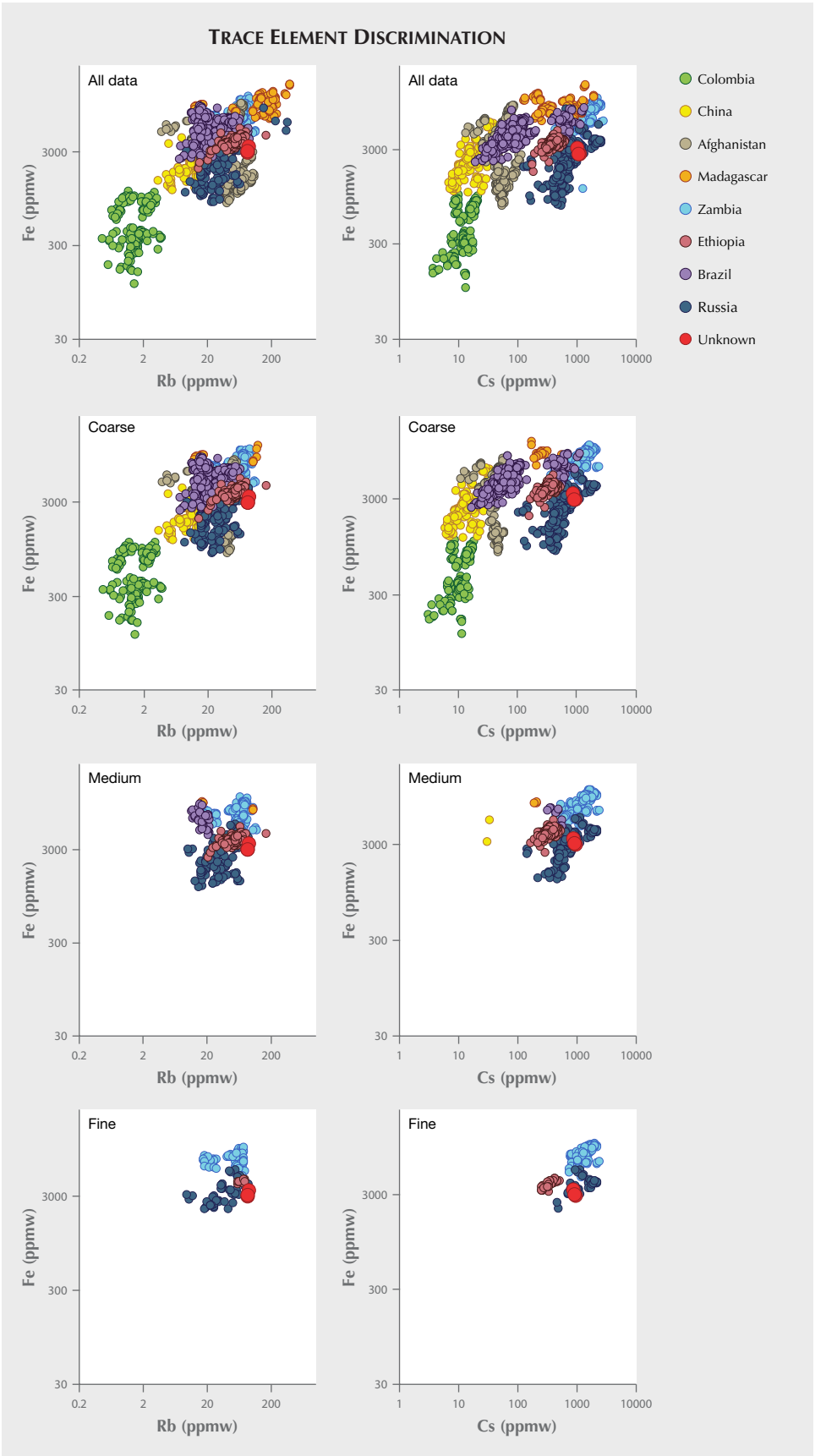

Figure 59. An example of an emerald with an "inconclusive" origin (analyses shown as red circles). Even with the selective plotting method, there may still be too much overlap in the data and an "inconclusive" origin would be warranted.

Figure 60. This ring contains a 12.09 ct sugarloaf cabochon emerald. Photo by Robert Weldon/GIA; courtesy of Pioneer Gems.

Figure 61. The emeralds in this bracelet, 48.91 carats total, are from the Chivor mine in Colombia. Photo by Robert Weldon/GIA; courtesy of Pioneer Gems.

CONCLUSIONS

With the proliferation of sources across the world in the twenty-first century, emerald origin determination has become an increasingly important service offered by gemological laboratories. At GIA, origin determinations are supported by years of meticulous efforts by the field gemology department in assembling a robust reference collection and collecting data on these samples (Vertriest et al., 2019, pp. 490–511 of this issue). This continual accumulation of information has forced the laboratory to adapt its methods and criteria for origin determination to keep up with the evolution of the world emerald market (figures 60 and 61). Given the finding of jagged three-phase fluid inclusions in low-Fe emeralds from Afghanistan and China, any stone that gives an initial impression of a Colombian origin must be carefully scrutinized to avoid inaccurate origin conclusion. The rise of Ethiopian emerald in the last few years has also forced the lab to come to terms with these new stones and their inclusion scenes, which can overlap with Brazilian, Russian, and Zambian emeralds. The lab has also had to understand the increased likelihood of seeing Russian emeralds from the Mariinsky (Malysheva) mine near Ekaterinburg in the Russian Urals. For any non-Colombian emeralds, trace element chemistry is always needed to support an origin determination, given the potential for overlap in their internal features. And yet, despite the years of experience collecting and analyzing data and documenting changes to the emerald mining scene, there are still some stones for which the lab is obligated to issue "inconclusive" origin opinions. Most of the time this is due to a trace element profile that does not match any of the reference data or because of ambiguous or contradictory inclusion scenes. Efforts by the laboratory and the field gemology department will be crucial to closing gaps in our knowledge and keeping on top of further developments in the world of emeralds—whatever the future may hold.

Case Study 1: Zambian Emerald

In the first emerald case study, we will analyze the 0.57 ct step-cut emerald shown in figure CS 1-1. The first step in determining this stone's geographic origin is to collect a UV-Vis-NIR absorption spectrum. The absorption spectrum (figure CS 1-2) shows a pronounced 850 nm absorption band in the near-infrared region. This identifies the stone as a schist-hosted emerald, essentially narrowing the options for its geographic origin to Zambia, Brazil, Russia, Ethiopia, and Madagascar. Microscopic observation shows a field of blocky fluid inclusions (figure CS 1-3), typical for schist-hosted emeralds. At this point, trace element chemistry is required to ensure an accurate origin determination. Representative trace element plots using data from LA-ICP-MS measurements are shown in figure CS 1-4. Use of the selective plotting method (see Palke et al., 2019b, pp. 536–579 of this issue) clearly shows that this stone is consistent with a Zambian origin. Taken together, the analytical data collected allows a conclusive origin determination of Zambia.

Figure CS 1-1. This 0.57 ct step-cut emerald is at the center of this origin determination case study. Photo by Diego Sanchez.

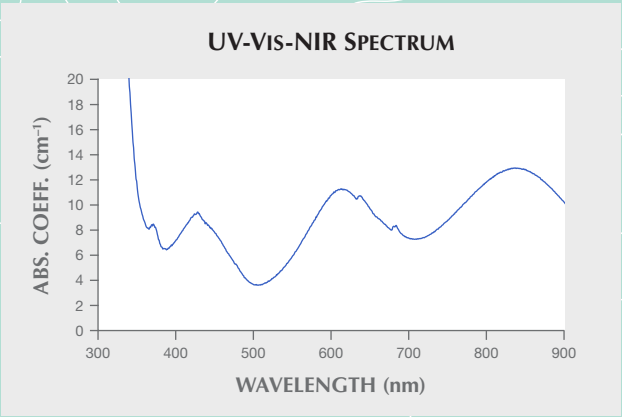

Figure CS 1-2. UV-Vis-NIR absorption spectroscopy indicates a schist-hosted deposit such as Zambia, Ethiopia, or Brazil.

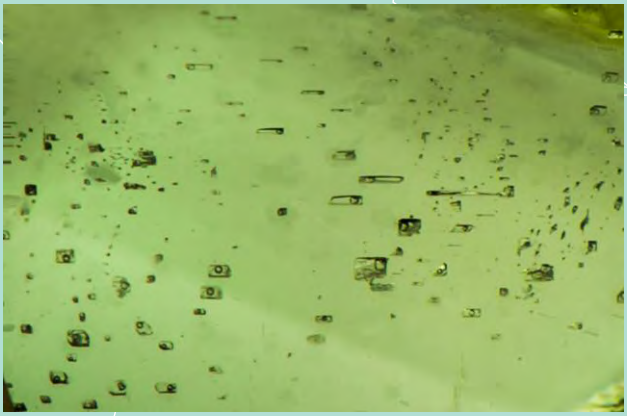

Figure CS 1-3. Blocky fluid inclusions also indicate a schist-hosted deposit such as Zambia, Ethiopia, or Brazil. Photomicrograph by Aaron Palke; field of view 1.72 mm.

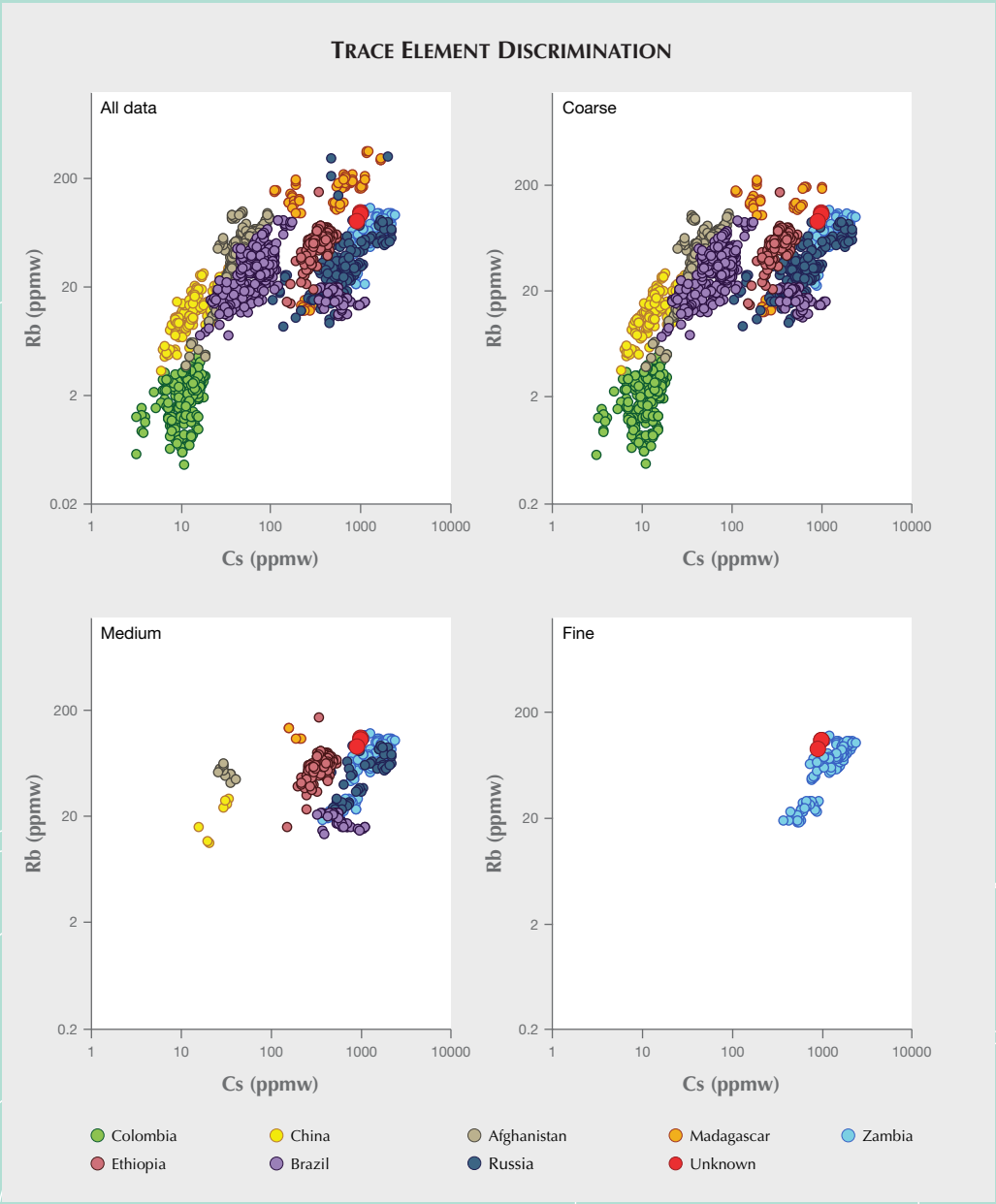

Figure CS 1-4. Trace element analysis supports a Zambian origin. The selective plotting method was used with coarse, medium, and fine filters.

Case Study 2: Colombian Emerald

The 2.04 ct step-cut emerald shown in figure CS 2-1 is the focus of this case study. The origin determination procedure starts with the stone's UV-Vis-NIR spectrum (figure CS 2-2). There is only a very slight rise in the absorption spectrum beyond 700 nm and into the near-infrared region. This indicates a very likely Colombian origin, though an Afghan or Chinese origin cannot be completely ruled out, as some emeralds from those locales show similar UV-Vis-NIR spectra. The most noteworthy inclusions are jagged fluid inclusions, which also give a distinct impression of Colombian pedigree (figure CS 2-3). Once again, this information must be considered carefully as some emeralds from China, Afghanistan, and Zambia (Musakashi) can show somewhat similar inclusions. Therefore, trace element analysis is needed. Representative trace element plots (figure CS 2-4) clearly indicate a Colombian origin. Note that the selective plotting method was not employed here and is generally not needed for Colombian emeralds.

Figure CS 2-1. This case study involves the origin determination process for a 2.04 ct step-cut emerald. Photo by Diego Sanchez.

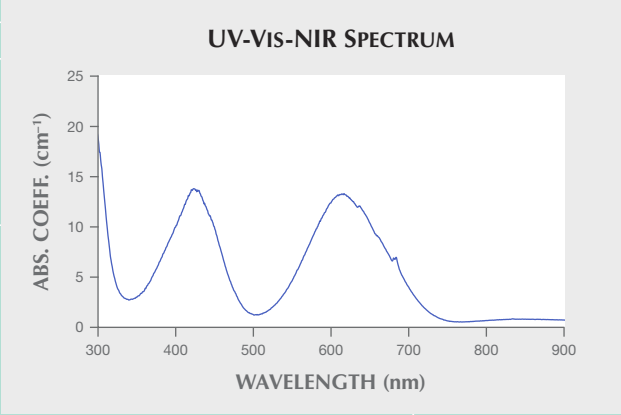

Figure CS 2-2. UV-Vis-NIR absorption spectroscopy suggests an origin in a metamorphic-related deposit such as Colombia, Afghanistan, or China.

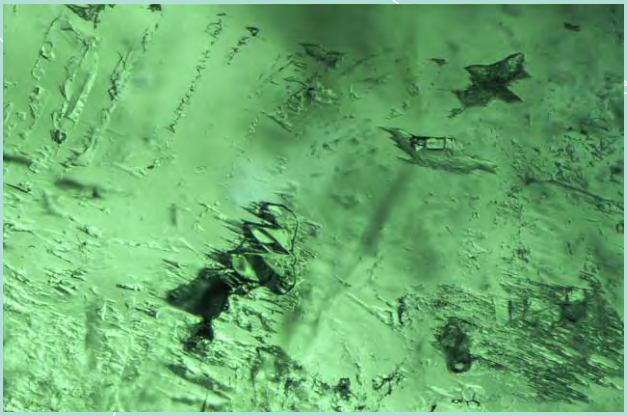

Figure CS 2-3. Jagged fluid inclusions strongly indicate a Colombian origin. Photomicrograph by Nathan Renfro; field of view 1.31 mm.

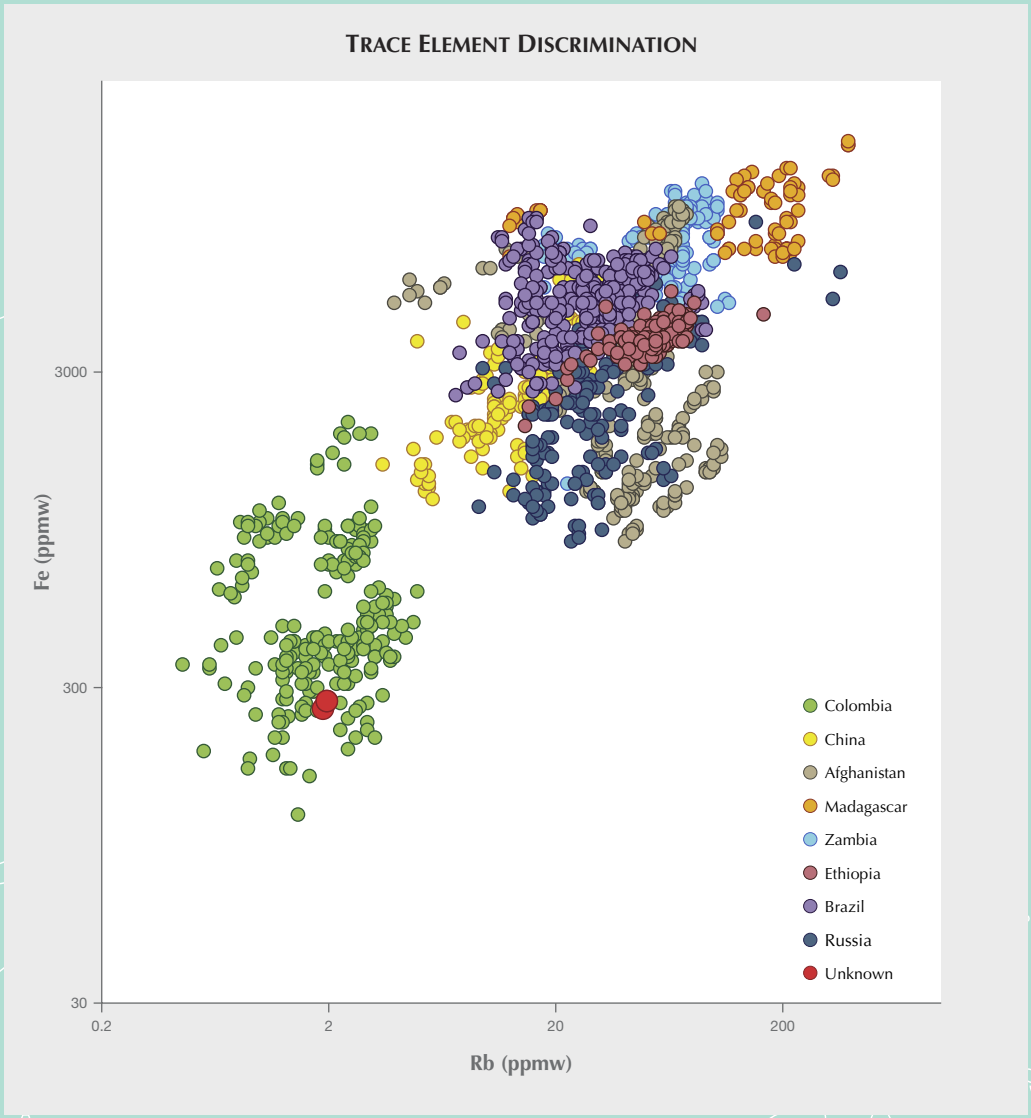

Figure CS 2-4. Trace element analysis corroborates a Colombian origin for this emerald, shown as the red circle.

Case Study 3: Inconclusive Emerald

Figure CS 3-1 shows a 1.05 ct step-cut emerald under consideration for a geographic origin determination. GIA's standard procedure for emerald origin determination is to start by collecting a UV-Vis-NIR absorption spectrum (figure CS 3-2). The rise in absorption beyond 700 nm and into the near-infrared clearly indicates that this stone belongs to the schist-hosted emerald group. Therefore, the origins we will consider are Zambia, Brazil, Russia, Ethiopia, and Madagascar. Microscopic observations of the inclusion characteristics reveal irregularly shaped fluid inclusions, which are typical of many schist-hosted emeralds but do not clearly indicate any specific origin (figure CS 3-3). Finalizing the geographic origin determination on this stone requires trace element chemistry measurements. Figure CS 3-4 shows representative trace element plots in comparison with reference stones of known provenance from GIA's colored stone reference collection. Unfortunately, this stone does not seem to uniquely match any specific geographic location. Without the use of selective plotting, the Fe-Li plot seems to suggest a Madagascar origin. However, other plots show that this stone lies outside the field of the Madagascar reference data. Therefore, with the reference collection data we have so far and with the application of selective plotting, Madagascar does not appear to be a viable option. With more reference data, hopefully stones such as this one will be able to match to data. Until then, given the ambiguity in the data, the only possible option today for this emerald is an "inconclusive" origin call.

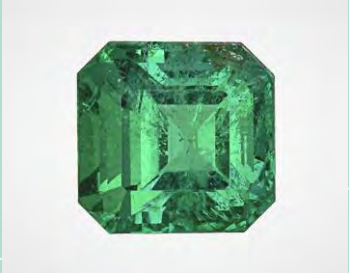

Figure CS 3-1. This 1.05 ct step-cut emerald is the focus of this origin determination case study. Photo by Diego Sanchez.

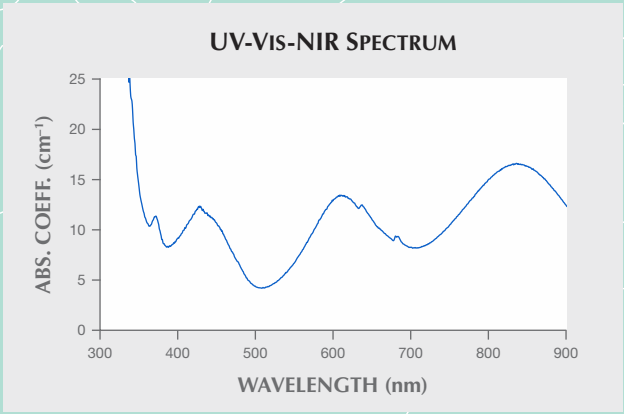

Figure CS 3-2. UV-Vis-NIR absorption spectroscopy indicates a schist-hosted deposit such as Zambia, Russia, Ethiopia, Brazil, or Madagascar.

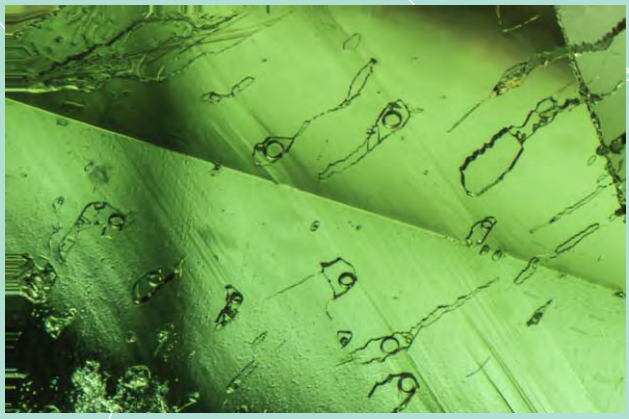

Figure CS 3-3. Irregular fluid inclusions also suggest a schist-hosted emerald deposit such as Zambia, Russia, Ethiopia, Brazil, or Madagascar. Photomicrograph by Aaron Palke; field of view 2.37 mm.

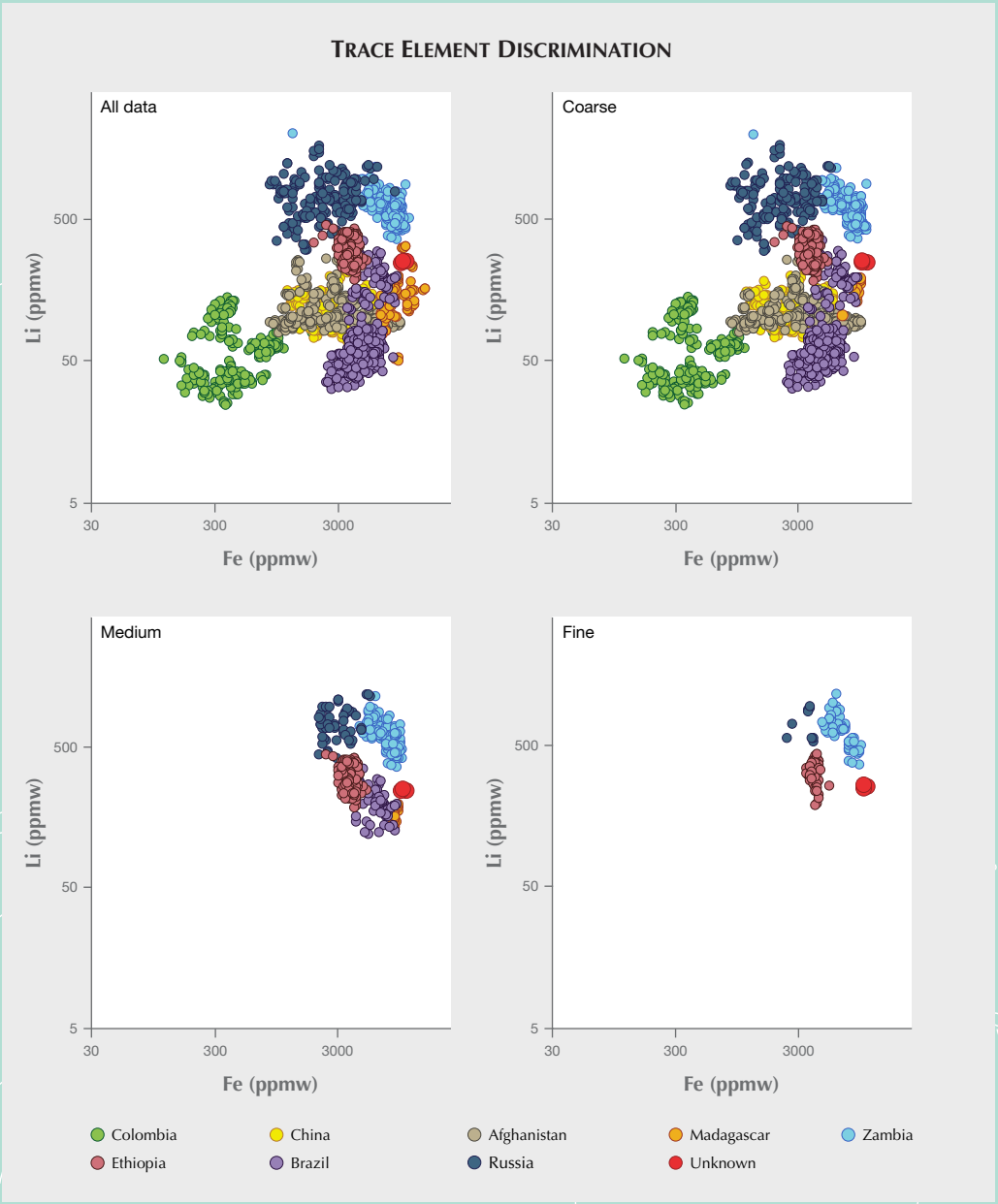

Figure CS 3-4. Trace element analysis of this unknown emerald (shown as the red circle) failed to conclusively match it with reference data of stones with known provenance. The ultimate origin call would be "inconclusive." The selective plotting method was used with coarse, medium, and fine filters.

Case Study 4: Zambian Emerald

In this case study we examine the 1.04 ct step-cut emerald shown in figure CS 4-1. The UV-Vis-NIR absorption spectrum shows a significant rise beyond 700 nm, leading to a large peak in the near-infrared region (figure CS 4-2). This allows clear assignment of this stone to the schist-related emerald group. Hence, the main geographic origins to consider are Zambia, Brazil, Russia, Ethiopia, and Madagascar. Microscopic examination shows abundant rectangular, blocky fluid inclusions (figure CS 4-3), an inclusion scene consistent with most schist-hosted emeralds. However, the observation of such inclusions alone cannot lead to an accurate origin call. To finalize the origin determination, we need accurate trace element analysis. Figure CS 4-4 shows representative trace element plots from LA-ICP-MS measurements. Use of the selective plotting method demonstrates a clear correlation with Zambian emeralds from GIA's colored stone reference collection. Along with the spectroscopic and inclusion data, this allows a confident conclusion of Zambian origin.

Figure CS 4-1. The origin determination process for a 1.04 ct emerald is the subject of this case study. Photo by Diego Sanchez.

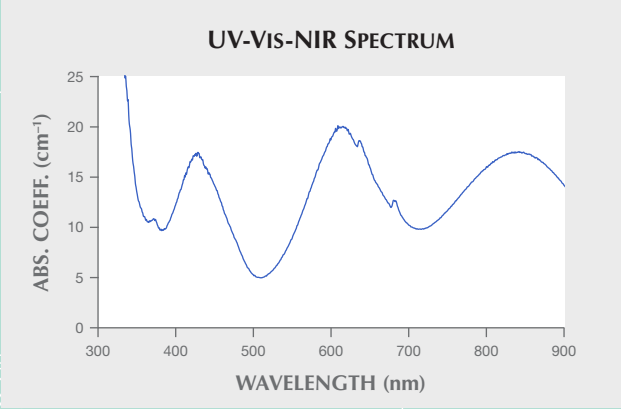

Figure CS 4-2. UV-Vis-NIR absorption spectroscopy provides evidence of a schist-hosted emerald that did not originate in Colombia.

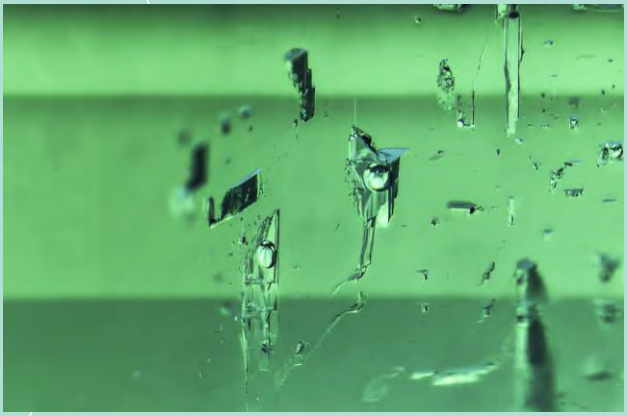

Figure CS 4-3. Blocky fluid inclusions point to a schist-related emerald deposit, indicating an origin of Zambia, Ethiopia, or Brazil. Photomicrograph by Nathan Renfro; field of view 1.89 mm.

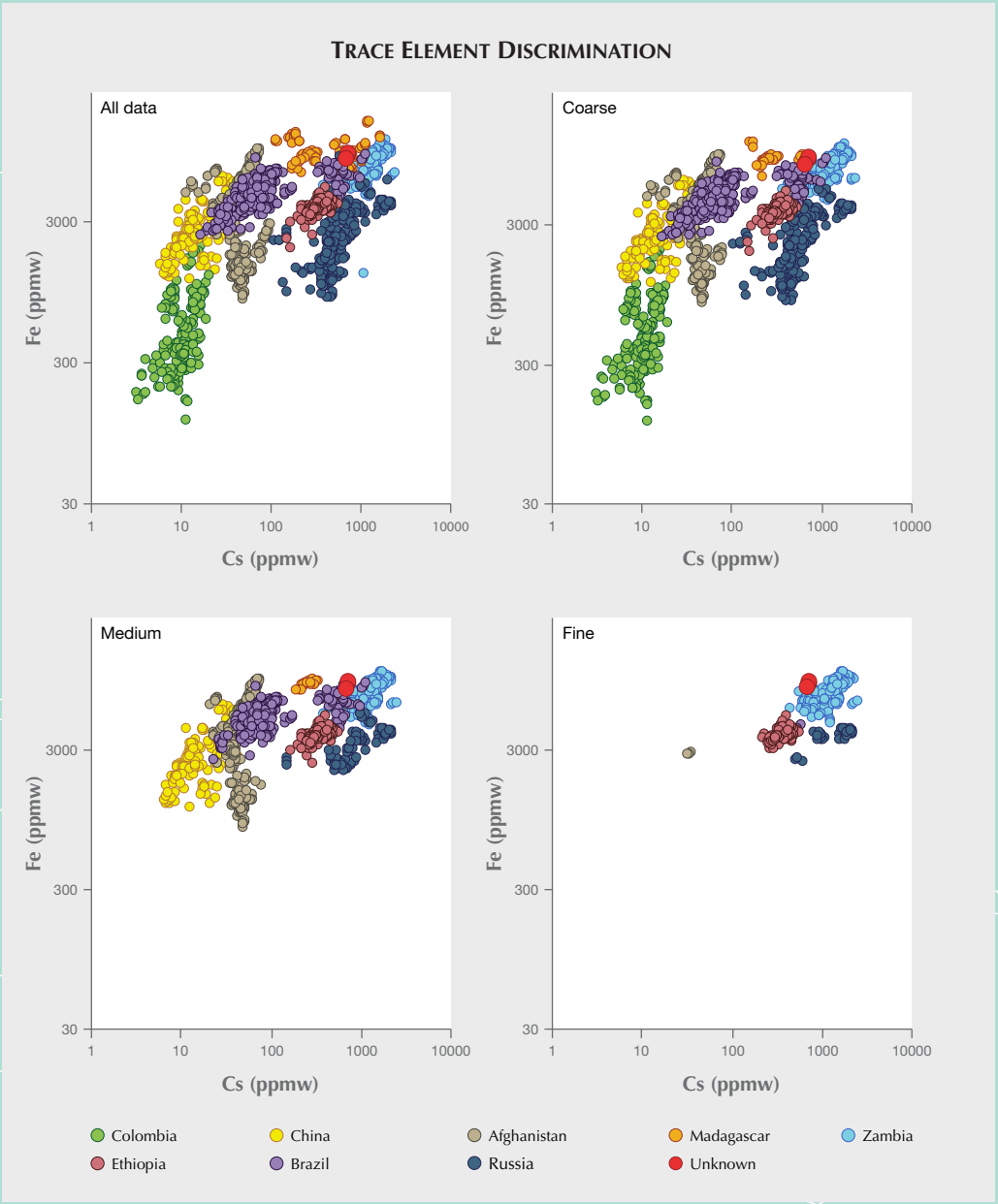

Figure CS 4-4. Trace element analysis provides conclusive evidence of Zambian origin. The selective plotting method was used with the coarse, medium, and fine filters.

ABOUT THE AUTHORS

Ms. Saeseaw is senior manager of identification at GIA in Bangkok. Dr. Palke is a senior research scientist, Mr. Renfro is manager of colored stone identification, Mr. Sun is a research associate, and Mr. McClure is global director of colored stone services, at GIA's laboratory in Carlsbad, California.

ACKNOWLEDGMENTS

The authors would like to thank GIA colleagues in Bangkok and Carlsbad for their valuable assistance. We also thank James Day and Raquel Alonso-Perez and an anonymous reviewer for their thorough and helpful peer reviews which greatly strengthened this manuscript.

REFERENCES

Bosshart G. (1991) Emeralds from Colombia (Part 2). *Journal of Gemmology*, Vol. 22, No. 7, pp. 409–438.

Bowersox G., Snee L.W., Foord E.E., Seaf II R.R. (1991) Emeralds of the Panjshir Valley, Afghanistan. *G&G*, Vol. 27, No. 1, pp. 26–39, http://dx.doi.org/10.5741/GEMS.27.1.26

Cassedanne J.P., Sauer D.A. (1984) The Santa Terezinha de Goiás emerald deposit. *G&G*, Vol. 20, No. 1, pp. 4–13, http://dx.doi.org/10.5741/GEMS.20.1.4

Giuliani G., Groat L.A. (2019) Geology of corundum and emerald gem deposits: A review. *G&G*, Vol. 55, No. 4, pp. 464–489, http://dx.doi.org/10.5741/GEMS.55.4.464

Giuliani G., Cheilletz A., Dubessy J., Rodriguez C.T. (1993) Chemical composition of fluid inclusions in Colombian emerald deposits. *Proceedings of the Eighth Quadrennial IAGOD Symposium*, pp. 159–168.

Giuliani G., Chaussidon M., Schubnel H.-J., Piat D.H., Rollion-Bard C., France-Lanord C., Giard D., de Narvaez D., Rondeau B. (2000) Oxygen isotopes and emerald trade routes since antiquity. *Science*, Vol. 287, No. 5453, pp. 631–633, http://dx.doi.org/10.1126/science.287.5453.631

Giuliani G., Groat L.A., Marshall D., Fallick A.E., Branquet Y. (2019) Emerald deposits: A review and enhanced classification. *Minerals*, Vol. 9, No. 2, p. 105, http://dx.doi.org/10.3390/min9020105

Groat L.A., Giuliani G., Marshall D.D., Turner D.B. (2008) Emerald deposits and occurrences: A review. *Ore Geology Reviews*, Vol. 34, No. 1-2, pp. 87–112, http://dx.doi.org/10.1016/j.oregeorev.2007.09.003

Gübelin E.J., Koivula J.I. (2008) *Photoatlas of Inclusions in Gemstones,* Volume 3. Opinio Publishers, Basel, Switzerland, 672 pp.

Hänni H.A., Schwarz D., Fischer M. (1987) The emeralds of the Belmont mine, Minas Gerais, Brazil. *Journal of Gemmology*, Vol. 20, No. 7, pp. 446–456.

Marshall D., Pardieu V., Loughrey L., Jones P., Xue G. (2012) Conditions for emerald formation at Davdar, China: Fluid inclusion, trace element and stable isotope studies. *Mineralogical Magazine*, Vol. 76, No. 1, pp. 213–226, http://dx.doi.org/10.1180/minmag.2012.076.1.213

Palke A.C, Lawley F.J., Vertriest W., Wongrawang P., Katsurada Y. (2019a) The Russian emerald saga: The Mariinsky Priisk mine. *InColor*, No. 44, pp. 36–46.

Palke A.C., Saeseaw S., Renfro N.D., Sun Z., McClure S.F. (2019b) Geographic origin determination of blue sapphires. *G&G*, Vol. 55, No. 4, pp. 536–579, http://dx.doi.org/10.5741/GEMS.55.4.536

Saeseaw S., Pardieu V., Sangsawong S. (2014) Three-phase inclusions in emerald and their impact on origin determination. *G&G*, Vol. 50, No. 2, pp. 114–132, http://dx.doi.org/10.5741/GEMS.50.2.114

Vapnik Y., Moroz I., Roth M., Eliezri I. (2006) Formation of emeralds at pegmatite-ultramafic contacts based on fluid inclusions in Kianjavato emerald, Mananjary deposits, Madagascar. *Mineralogical Magazine*, Vol. 70, No. 2, pp. 141–158, http://dx.doi.org/10.1180/0026461067020320

Vertriest W., Wongrawang P. (2018) A gemological description of Ethiopian emeralds. *InColor*, No. 40, pp. 72–73.

Vertriest W., Palke A., Renfro N.D. (2019) Field gemology: Building a research collection and understanding the development of gem deposits. *G&G*, Vol. 55, No. 4, pp. 490–511, http://dx.doi.org/10.5741/GEMS.55.4.490

Zwaan J.C., Seifert A.V., Vrana S., Laurs B.M., Anckar B., Simmons W.B., Falster A.U., Lustenhouwer W.J., Muhlmeister S., Koivula J.I., Garcia-Guillerminet H. (2005) Emeralds from the Kafubu area, Zambia. *G&G*, Vol. 41, No. 2, pp. 116–148, http://dx.doi.org/10.5741/GEMS.41.2.116

Zwaan J.C., Jacob D.E., Hager T., Cavalcanti M.T.O., Kanis J. (2012) Emeralds from the Fazenda Bonfim region, Rio Grande do Norte, Brazil. *G&G*, Vol. 48, No. 1, pp. 2–17, http://dx.doi.org/10.5741/GEMS.48.1.2

Not all gems come from under the ground.

The Gemological Institute of America® supports communities where gems are mined, working with the Nelson Mandela Centre of Memory to build libraries in Africa and helping artisanal miners understand the quality of their discoveries with our Gem Guide. These initiatives help make it possible for regional populations to take a more active role in the industry and ultimately help their community look forward to a brighter future. Our contributions are one of the many reasons why GIA® is the world's foremost authority on diamonds, colored stones and pearls.

Learn more about the many facets of GIA at GIA.edu

GIA®

The World's Foremost Authority in Gemology™

Ensuring the Public Trust Through Nonprofit Service Since 1931

BENEFICIATION EDUCATION INSTRUMENTS LABORATORY RESEARCH

Geographic Origin Determination Of Paraíba Tourmaline

Yusuke Katsurada, Ziyin Sun, Christopher M. Breeding, and Barbara L. Dutrow

Vivid blue to green copper-bearing tourmalines, known as Paraíba tourmalines, are recovered from deposits in Brazil, Nigeria, and Mozambique. These tourmalines are sought after for their intense colors. Prices are based, in part, on the geographic origin of a stone, and determining provenance is thus an important aspect for Paraíba tourmaline. However, their geographic origin cannot be established by standard gemological testing and/or qualitative chemical analyses. GIA has established sophisticated criteria requiring quantitative chemical analyses to determine geographic origin for these tourmalines. These criteria were based on several hundred samples from known sources spanning the three countries. Highly accurate and precise quantitative elemental concentrations for Cu, Zn, Ga, Sr, Sn, and Pb are acquired with laser ablation–inductively coupled plasma–mass spectrometry (LA-ICP-MS). These data can then be plotted as a function of elemental concentration for accurate geographic origin determination.

Copper-bearing gem tourmaline—recognizable by its vivid neon blue to green color—has been one of the most popular colored gemstones on the market for the nearly three decades since its debut (figures 1 and 2). It was first discovered in the state of Paraíba in northeastern Brazil in the late 1980s, and subsequently found in the neighboring state of Rio Grande do Norte (Fritsch et al., 1990; Shigley et al., 2001; Furuya, 2007). These gems became known as Paraíba tourmalines after the locality of their discovery. In the early twenty-first century, similarly colored gem-quality tourmalines were discovered in Nigeria and Mozambique (figures 3 and 4; Smith et al., 2001; Abduriyim and Kitawaki, 2005).

In the gem market, Brazilian Paraíba tourmalines are typically more highly valued than their African counterparts. While top-quality Brazilian Paraíba tourmalines tend to have more intense color, there is significant overlap in the color range for all localities. Additionally, standard gemological tests cannot definitively separate stones from these three localities. As a result, there is market demand for gemological laboratories to offer origin determination for copper-bearing tourmalines.

The most recent Laboratory Manual Harmonisation Committee (LMHC) definition of "Paraíba" tourmaline is "a blue (electric blue, neon blue, violet blue), bluish green to greenish blue, green (or yellowish green) tourmaline, of medium-light to high saturation and tone (relative to this variety of tourmaline), mainly due to the presence of copper (Cu) and manganese (Mn) of whatever geographical origin" (LMHC, 2012). This definition, widely accepted in the gem industry and at GIA, clearly

In Brief

- Geographic origin can have a significant impact on the value of Paraíba tourmaline.
- Quantitative chemical analysis with LA-ICP-MS provides a robust tool for origin determination.
- The trace elements Cu, Zn, Ga, Sr, Sn, and Pb are the most useful discriminators for Paraíba tourmaline origin.
- In limited cases where there are no matching reference data, an "inconclusive" origin determination would be required.

See end of article for About the Authors and Acknowledgments.
Gems & Gemology, Vol. 55, No. 4, pp. 648–659,
http://dx.doi.org/10.5741/GEMS.55.4.648

Figure 1. Faceted and polished copper-bearing tourmalines, ranging from 0.39 to 1.47 ct, from Brazil's Paraíba State. Photo by Robert Weldon/GIA; courtesy of Gerhard Becker.

Figure 2. This 2.87 ct Paraíba tourmaline is from Brazil. Photo by Robert Weldon/GIA; courtesy of David Bindra, B&B Fine Gems.

Figure 4. A 29.34 ct Paraíba tourmaline from Mozambique. Photo by Robert Weldon/GIA; courtesy of the Granada Gallery.

mentions not only the color appearance but also the chemical elements causing the color. Iron (Fe) can also cause a blue coloration in tourmaline, such as the variety commonly termed indicolite (Faye et al., 1968; Mattson and Rossman, 1987). However, the bright blue color characteristic of Paraíba tourmaline is caused by Cu (Rossman et al., 1991) and easily surpasses the intensity and hue of indicolite's Fe-related blues. Many years of trace element analyses at GIA have demonstrated that Cu occurs in many gem tourmalines in the range of single-digit parts per million by weight (ppmw) to tens of ppmw concentrations. However, such low levels of Cu will not produce the Paraíba-like color; at least several hundred ppmw Cu are required for that. Merkel and Breeding (2009) noted that peaks near 700 and 900 nm in visible and near-infrared absorption spectra can be useful in assessing the contribution of Cu when the stone also contains Fe. Mn, another element mentioned by the LMHC definition, can create purple and pinkish hues when in combination with Cu, thus impacting the color appearance of Paraíba tourmaline.

Figure 3. This 19.90 ct Paraíba tourmaline is from Nigeria. Photo by Robert Weldon/GIA.

Because standard gemological properties and microscopic observations (e.g., mineral and fluid inclusions, fracture patterns, growth tubes) are not conclusive in distinguishing geographic origin for Paraíba tourmaline, other methods must be used. Quantitative chemical analyses of minor and trace elements have been collected and presented herein for Brazilian, Nigerian, and Mozambican material as used for locality determination (e.g., Shigley et al., 2001; Breeding et al., 2007; Laurs et al., 2008). Com-

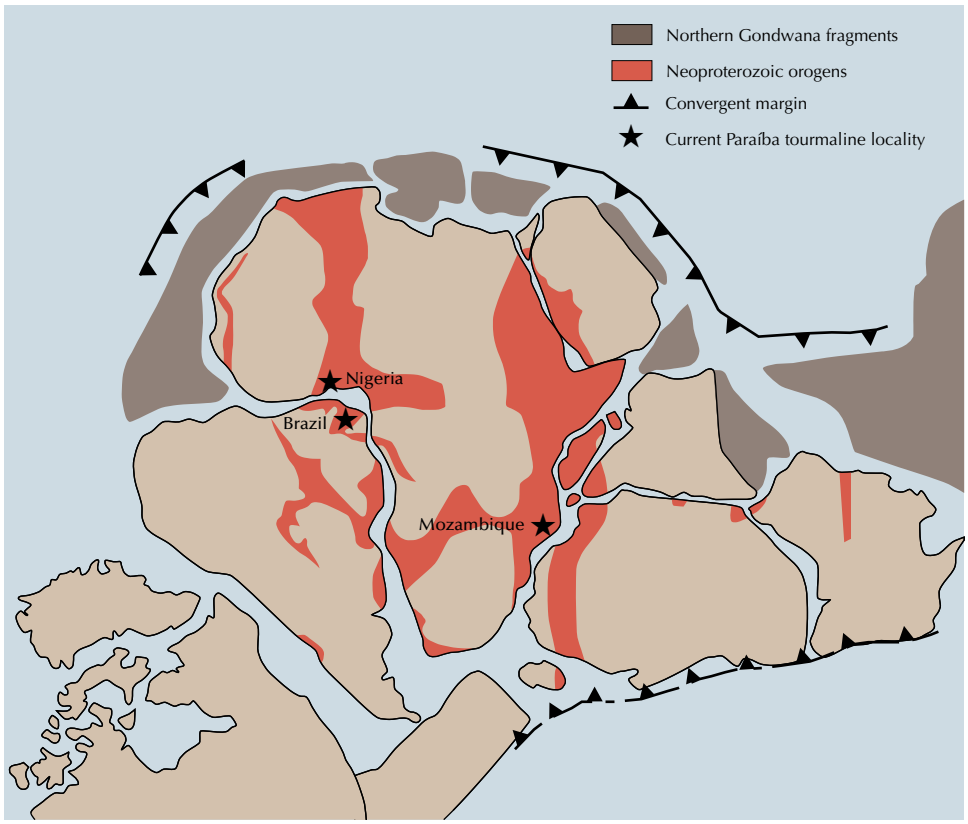

Figure 5. Overview of the Brasiliano–Pan-African orogeny (shown as Neoproterozoic orogens) in the Gondwana supercontinent (540 Ma) and locations of current Paraíba tourmaline sources. Modified from Kröner and Stern (2004).

parative studies of chemical data have also been carried out and discussed for the purpose of origin determination by several authors (Abduriyim et al., 2006; Peretti et al., 2009; Okrusch et al., 2016). For GIA's lab service of Paraíba tourmaline origin determination, we have established an analytical and calculation protocol that utilizes major, minor, and trace element data obtained by LA-ICP-MS on reference samples from known localities.

PARAÍBA TOURMALINE GEOGRAPHIC LOCALITIES: A BRIEF SUMMARY

Most of Brazil's Paraíba tourmaline mining sites are primary deposits in pegmatites that intruded quartzites or metaconglomerates between 530 and 480 million years ago (Ma) (Beurlen et al., 2011). Nigerian and Mozambican mines occur as secondary deposits where the tourmalines are recovered from alluvium rather than the original host rock (e.g., Laurs et al., 2008; Milisenda, 2018a). Paraíba tourmaline's microscopic inclusions and gemological properties, however, are similar among the deposits on both continents, suggesting a very similar geological formation for copper-bearing tourmalines collected from primary and secondary deposits.

The regional geology of northeastern Brazil and western Nigeria primarily consists of igneous and metamorphic rocks related to the Brasiliano–Pan-African orogeny that occurred 650 to 480 Ma. In Mozambique, the tourmaline host rocks are pegmatites that intruded around 500 Ma, during or after the East African orogeny, which involved the agglomeration of landmasses and continental collision that formed the Gondwana supercontinent (Kröner and Stern, 2004; figure 5).

Brazilian copper-bearing tourmaline was formed by direct crystallization from a hydrous melt, rich in boron and lithium with an unusual concentration of copper, at the early stage of pegmatite formation in the quartz core and prior to the appearance of secondary lepidolite and other late hydrothermal minerals (e.g., Beurlen et al., 2011). The origin of the copper in Brazilian Paraíba tourmaline localities is still an open question, but some researchers have attributed it to copper enrichment of the host pegmatites or pegmatite-independent hydrothermal activity (Beurlen et al., 2011 and references therein). Laurs et al. (2008) discussed the alluvial paleoplacer deposit origin of Mozambican materials, and Pezzotta (2018) proposed a residual alluvial origin from field observations. The lack of copper-rich tourma-

line in pegmatites located in the upstream area of Mozambique's Paraíba tourmaline mines leaves the copper source unknown. Further field study is necessary to better understand the source of copper in Mozambican Paraíba tourmalines.

MATERIALS AND METHODS

GIA's Paraíba tourmaline reference samples comprise a range of stones collected by researchers directly from the mines (Shigley et al., 2001; Laurs et al., 2008; Hsu, 2018); borrowed from personal and museum collections (some established before the discovery of the African mines, thus certifying that the stones are Brazilian); or obtained from highly trusted dealers specializing in tourmaline from particular sources (see the table 1 footnote for details). The GIA reference data comes from 151 samples from Brazil, 116 elbaite and 17 liddicoatite samples from Mozambique, and 17 samples from Nigeria.

For the past decade, GIA has chemically analyzed copper-bearing tourmaline samples by LA-ICP-MS. Two instruments have been used to collect this chemical data (with great care in calibrating the instruments to ensure that the data are internally consistent). A Thermo Fisher X-series II ICP-MS coupled with a New Wave Research UP-213 laser ablation unit was used initially, with National Institute of Standards and Technology (NIST) 610 and 612 references used for external calibration. Ablation was achieved using a 55 µm diameter laser spot size, a fluence of around 10 J/cm^2, and a 15 Hz repetition rate. ^{11}B was initially selected as an internal standard, although for comparison with data collected later the analyses were reprocessed with ^{29}Si as the internal standard. Between 2014 and 2017, the LA-ICP-MS systems at GIA were upgraded to those currently in place, including a Thermo Fisher iCAP Qc ICP-MS coupled with an Elemental Scientific Lasers NWR213 laser ablation system. With this upgrade, data for most of the reference stones were recollected in order to ensure internal consistency of data collected on client stones using the new system. At the same time, data processing protocols were revised, with ^{29}Si used as an internal standard and U.S. Geological Survey glasses GSD-1G, GSE-1G, and NIST 610 as external standards. Ablation is currently achieved using a 55 µm diameter laser spot size, a fluence of around 10 J/cm^2, and a 20 Hz repetition rate. The isotopes routinely measured include ^{23}Na, ^{24}Mg, ^{27}Al, ^{29}Si, ^{39}K, ^{43}Ca, ^{51}V, ^{53}Cr, ^{55}Mn, ^{57}Fe, ^{63}Cu, ^{66}Zn, ^{69}Ga, ^{88}Sr, ^{118}Sn, and ^{206}Pb.

TABLE 1. Paraíba tourmaline samples used in this study.

Origin	Species[a]	Number of samples tested
Brazil[b]	Elbaite	151
Nigeria[c]	Elbaite	17
Mozambique[d]	Elbaite	116
Mozambique[e]	Liddicoatite	17

[a]*F cannot be determined using LA-ICP-MS. Therefore, only hydroxyl end members are shown.*
[b]*Brazilian samples include mine-collected stones from the states of Paraíba and Rio Grande do Norte, stones from Shane McClure's personal collection and GIA collections that were acquired prior to the discovery of African sources, and stones provided by Hussain Rezayee and Chico Bank.*
[c]*Nigerian samples include stones obtained directly from local miners and provided to GIA by Bill Barker, William Larson, and Hussain Rezayee.*
[d]*Mozambican samples include stones obtained directly from local miners and provided to GIA by Bill Barker, Blue Sheppard, William Larson, and Hussain Rezayee.*
[e]*Mozambican liddicoatite samples are those reported in Katsurada and Sun (2017).*

To date, results obtained from the two different standards sets, instruments, and operating conditions have not varied in the overall values of the trace elements used for discrimination. As a result, we have combined the data acquired from both old and new LA-ICP-MS systems for presentation. Both data sets for the elements selected in this study show a close overlap.

DISCRIMINATION DIAGRAMS FOR REFERENCE SAMPLES

Major Elements. Tourmaline is a supergroup mineral because of the large number of species under that classification. Overall, it is a complex boron-aluminum cyclosilicate mineral. The generalized formula can be written as $XY_3Z_6(T_6O_{18})(BO_3)_3V_3W$, with the primary occupancies of X = Na^+, Ca^{2+}, K^+, vacancy; Y = Fe^{2+}, Mg^{2+}, Mn^{2+}, Al^{3+}, Li^+, Fe^{3+}, Cr^{3+}, Ti^{4+}; Z = Al^{3+}, Fe^{3+}, Mg^{2+}, Cr^{3+}; T = Si^{4+}, Al^{3+}, B^{3+}; B = B^{3+}; V = OH^-, O^{2-}; W = OH^-, F^-, O^{2-} (Henry et al., 2011). The majority of gem-quality tourmaline is elbaite or fluor-elbaite, followed by solid solutions of dravite and uvite[1]. While most Paraíba tourmalines are elbaites, in 2010 copper-bearing liddicoatite[1] appeared in the market (Karampelas and Klemm,

[1]elbaite = $Na(Li_{1.5}Al_{1.5})Al_6Si_6O_{18}(BO_3)_3(OH)_3OH$
fluor-elbaite = $Na(Li_{1.5}Al_{1.5})Al_6Si_6O_{18}(BO_3)_3(OH)_3F$
dravite = $NaMg_3Al_6Si_6O_{18}(BO_3)_3(OH)_3OH$
fluor-uvite = $CaMg_2(Al_5Mg)Si_6O_{18}(BO_3)_3(OH)_3F$
fluor-liddicoatite = $Ca(Li_2Al)Al_6Si_6O_{18}(BO_3)_3(OH)_3F$
Note: While uvite and liddicoatite exist only as the fluor-dominant species listed above, the common names are used for simplicity.

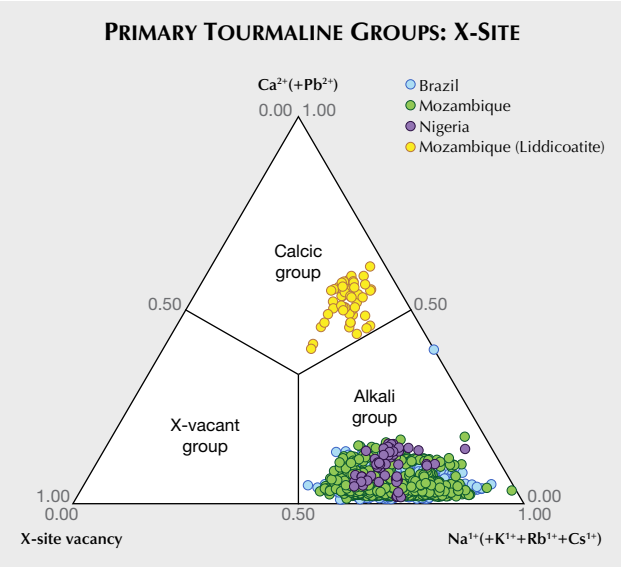

Figure 6. Ternary diagram displaying the primary tourmaline groups based on X-site occupancy of copper-bearing elbaite samples from GIA's reference collection and copper-bearing liddicoatite samples reported in Katsurada and Sun (2017). From Henry et al. (2011).

2010). Because calcium (Ca) is the dominant cation in the X-site for liddicoatites, they are easily distinguished based on major element analyses. Cu^{2+} in copper-bearing tourmaline is considered to be located in the Y-site (e.g., Ertl et al., 2013).

The normalization method established by Sun et al. (2019) allows for the accurate calculation of tourmaline stoichiometry from LA-ICP-MS analyses, with the exception of the fluor- and oxy-species. A ternary diagram of X-site composition of reference samples shows that there are two different primary groups for the Paraíba tourmalines: alkali and calcic groups (figure 6). Based on Y-site (Li-dominant) occupancy, the species are determined as elbaite and (fluor-)liddicoatite species.

Minor/Trace Elements. Among the minor and trace element concentrations measured, Cu, Zn, Ga, Sr, Sn, and Pb proved to be the most useful discriminators for Paraíba tourmaline geographic origin determination. The ranges, averages, and associated standard deviations of the concentration of these six elements for different localities are summarized in table 2. Brazilian samples have higher Cu (approximately 11400 ppmw on average, compared to less than 2000 ppmw for their African counterparts), but light-colored stones may have lower Cu concentration (figure 7A, B, and F). Nigerian samples have higher Sr (approxi-

TABLE 2. Generalized trace element profiles of Paraíba tourmalines in parts per million weight (ppmw).

	Brazil					
	Cu	**Zn**	**Ga**	**Sr**	**Sn**	**Pb**
Range	119–38800	bdl–33400	38.4–281	bdl–48.9	bdl–1610	0.62–1360
Average	11400	4640	115	1.12	4.95	40.1
Median	10900	1070	109	0.51	bdl	26.1
	Mozambique					
	Cu	**Zn**	**Ga**	**Sr**	**Sn**	**Pb**
Range	193–5720	bdl–633	170–701	bdl–34.7	bdl–48.8	5.91–244
Average	1850	29.2	361	0.43	5.40	37.1
Median	1640	3.00	363	0.11	5.02	11.1
	Nigeria					
	Cu	**Zn**	**Ga**	**Sr**	**Sn**	**Pb**
Range	736–2780	1.66–2900	94.0–181	6.53–159	bdl–22.5	42.1–1180
Average	1550	386	131	73.0	3.10	611
Median	1500	24.9	124	72.8	1.88	616
	Mozambique (Liddicoatite)					
	Cu	**Zn**	**Ga**	**Sr**	**Sn**	**Pb**
Range	1330–2980	bdl–33.4	242–465	0.70–4.21	14.8–43.2	404–819
Average	1830	0.80	346	3.07	25.6	625
Median	1570	bdl	351	3.20	25.1	644
Detection limits (ppmw)	0.029–0.60	0.013–0.97	0.006–0.30	0.001–0.090	0.013–1.13	0.001–0.45

**bdl = below the detection limit of the LA-ICP-MS analysis*

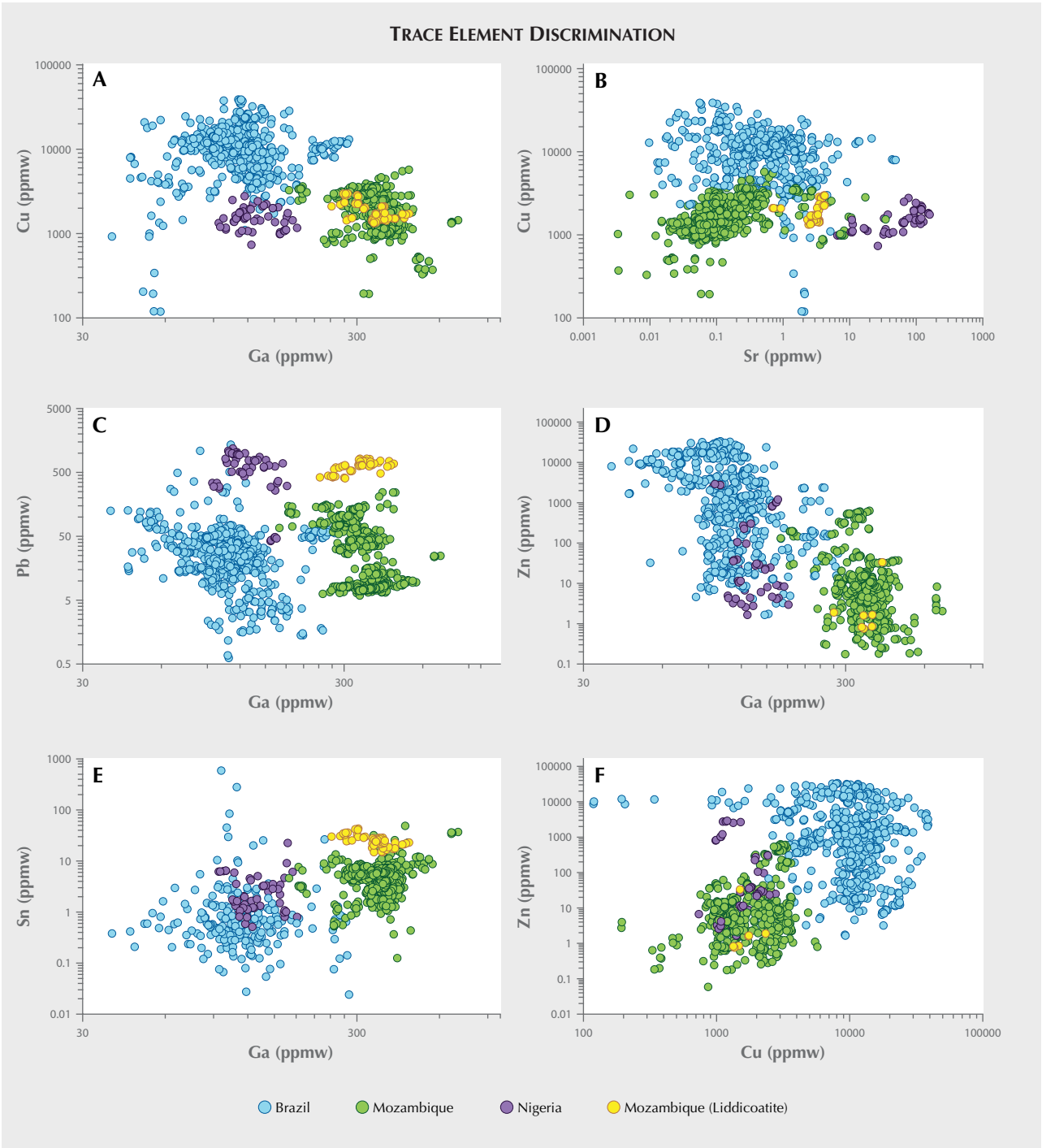

Figure 7. Diagrams displaying the concentration for selected elements used to discriminate localities: (A) Cu-Ga, (B) Cu-Sr, (C) Pb-Ga, (D) Zn-Ga, (E) Sn-Ga, and (F) Zn-Cu.

mately 73 ppmw on average, compared to less than 4 ppmw elsewhere) and higher Pb (approximately 611 ppmw on average, compared to less than 50 ppmw for Brazilian and Mozambican elbaite samples); see figure 7B and C. Mozambican samples generally show higher Ga (both elbaite and liddicoatite are approximately 361 ppmw on average, compared to around 100 ppmw for other localities); see figure 7A, C, D, and E. High Zn (>1000 ppm) is limited to Brazilian samples, but Zn values below 1000 ppmw are not

helpful discriminators (figure 7D and F). Most of the Nigerian samples contain high Sr and Pb (figure 7B and C). Any single pair of certain elements is insufficient to determine the geographic origin, but the *combination* of these elemental discriminators provides a robust tool for origin determination. In general, the results presented here are comparable to those in previous studies (e.g., Abduriyim et al., 2006; Peretti et al., 2009; Okrusch et al., 2016).

Using GIA's reference data, four selected case studies for origin determination are shown in box A. Although most Paraíba tourmaline origin determinations are as straightforward as these case studies, some stones cannot be separated clearly, as some plot in overlapping locality fields and are not easily distinguished. When data plot in the middle of overlapping ranges for many element pairs, a definitive locality origin cannot be concluded. Such an example is shown as Case 4 in box A.

DISCUSSION

Geographic origin can be conclusively and accurately determined for the vast majority of Paraíba tourmalines based on their trace element profiles, allowing this service to be offered for Paraíba tourmaline in the gem and jewelry market, such as the fine-color Brazilian stones in figure 8. Nonetheless, there are some cases where an "inconclusive" call is warranted when the trace element profiles are ambiguous or contradictory. There are three reasons for the ambiguity:

1. From time to time the laboratory examines Paraíba tourmalines that do not seem to match the trace element profiles of any stones in GIA's reference collection. Obtaining reference samples with reliable provenance that match these unknown stones is currently a priority of GIA's field gemology department; see Vertriest et al. (2019), pp. 490–511 of this issue.
2. New chemical discriminators may be needed. Statistical approaches such as discriminant analysis or multivariate statistics may provide additional mechanisms to evaluate the certainty of the locality determination and reduce "inconclusive" calls.
3. Chemical zoning in tourmaline may complicate interpretations. Color zoning is common in cuprian tourmaline and has been studied with electron probe microanalysis and LA-ICP-MS. In these studies, trace element concentrations correlate with color in naturally zoned samples (e.g., Laurs et al., 2008; Peretti et al., 2009). It is possible that the limits of chemical zoning of Paraíba tourmaline have not been included in the original fields for localities. Ideally, potential chemical zoning should be known before conducting LA-ICP-MS analysis so that all of the compositions can be captured. In tourmaline, however, chemical zoning may not include chromophores and may not be visually recognizable.

Figure 8. Brazilian Paraíba tourmalines with exceptional color, ranging from 2.59 ct to 3.68 ct. Photo by Robert Weldon/GIA; courtesy of the Dr. Edward J. Gübelin Collection.

BOX A: CASE STUDIES OF TYPICAL RESULTS

Examples of geographic origin determination for typical stones from Brazil, Nigeria, and Mozambique are shown in Cases 1–3. These stones were examined by GIA. Photographs and weights of the samples used for these case studies are shown in figure A-1. Three spots on each stone were analyzed by LA-ICP-MS; the results are listed in table A-1. Cases 1, 2, and 3 plotted in the typical ranges for Brazil, Mozambique, and Nigeria, respectively (see figure A-2). These three cases represent the vast majority of stones submitted to the laboratory whose origin can be easily concluded based on trace element chemistry as determined by the described procedures.

Occasionally the laboratory examines stones, such as the one in Case 4 (figure A-1), that do not match any of the data in GIA's reference database. The trace element profile of this stone based on three LA-ICP-MS analyses did not plot in the known trace element ranges for any established Paraíba tourmaline localities. While the origin of most Paraíba tourmalines examined by GIA can be easily established using trace element chemistry, inevitably a small number fall into this zone between two localities in compositional spaces that are completely devoid of reference data. These stones were clearly unearthed from some mine in the world, likely in any of the three Paraíba tourmaline localities. Despite efforts to obtain reliable reference stones that match these questionable tourmaline compositions, we are unable to identify the origin of these stones. Consequently, the only possible origin determination for these questionable cases is "inconclusive."

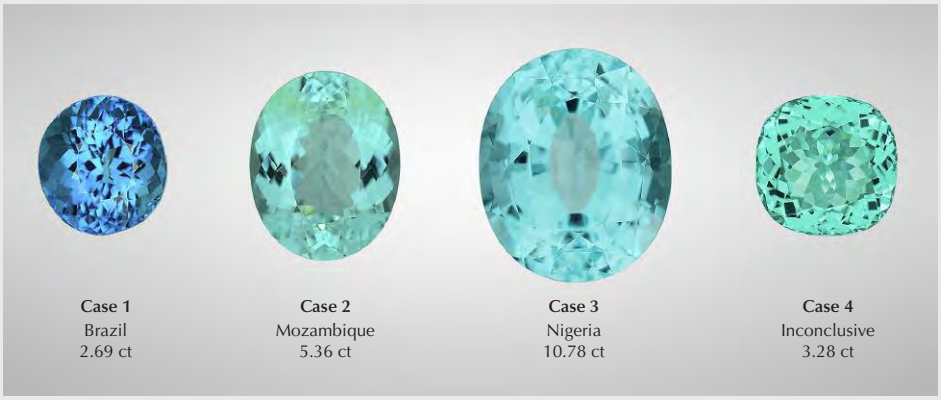

Figure A-1. Photos and weights of the stones from Cases 1, 2, 3, and 4. LA-ICP-MS identified their origin as Brazil, Mozambique, Nigeria, and "inconclusive," respectively.

TABLE A-1. Concentration of selected elements (in ppmw) for Cases 1–4.

	Cu	Zn	Ga	Sr	Sn	Pb	Results
Case 1, Spot 1	17120	71.3	78.1	0.57	0.21	31.2	Brazil
Case 1, Spot 2	17150	73.8	77.7	0.55	0.27	31.8	Brazil
Case 1, Spot 3	16930	72.2	76.3	0.62	0.24	31.6	Brazil
Case 2, Spot 1	1810	2.80	348	0.61	3.78	102	Mozambique
Case 2, Spot 2	1800	3.08	356	0.62	3.93	106	Mozambique
Case 2, Spot 3	1750	3.05	340	0.61	3.76	105	Mozambique
Case 3, Spot 1	1510	480	141	130	16.9	451	Nigeria
Case 3, Spot 2	1440	550	138	129	16.2	414	Nigeria
Case 3, Spot 3	1370	1030	137	132	18.4	433	Nigeria
Case 4, Spot 1	6230	8.06	253	10.3	0.47	233	Inconclusive
Case 4, Spot 2	6400	8.14	277	10.5	0.28	256	Inconclusive
Case 4, Spot 3	6420	8.31	271	10.3	0.35	246	Inconclusive
Detection limits (ppmw)	0.029–0.60	0.013–0.97	0.006–0.30	0.001–0.090	0.013–1.13	0.013–1.13	

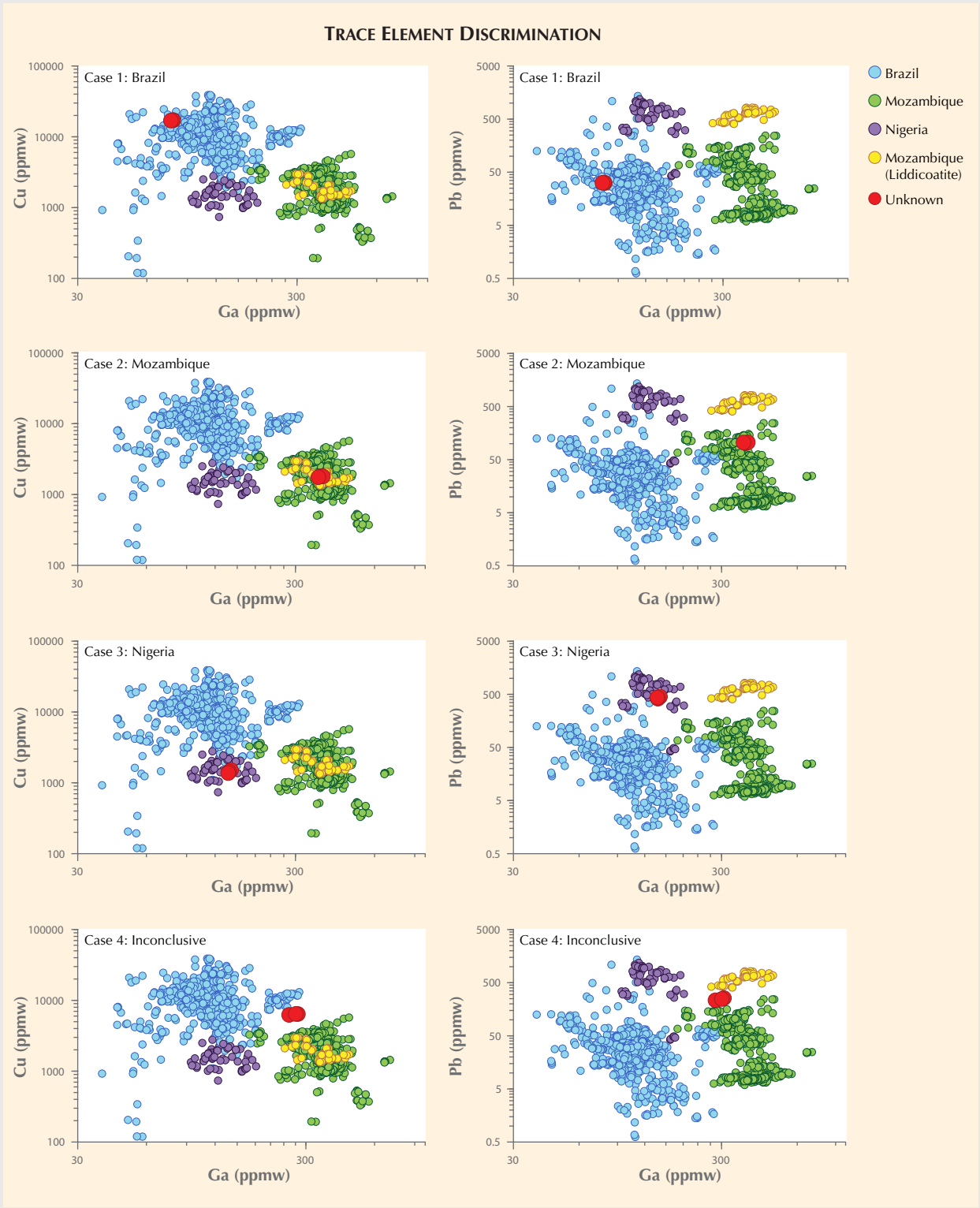

Figure A-2. Elemental concentrations from LA-ICP-MS analyses, plotted in Cu-Ga and Pb-Ga diagrams. Four case studies are shown for typical stones from Brazil (Case 1), Mozambique (Case 2), and Nigeria (Case 3), as well as an example of a stone whose trace element profile would require an "inconclusive" origin determination (Case 4).

As noted earlier, liddicoatite can also be found in the Paraíba tourmaline market. Katsurada and Sun (2017) reported that the origin of the copper-bearing liddicoatite was unknown at the time of publication. Subsequently the source was identified as Maraca, Mozambique (Milisenda and Müller, 2017). For the purpose of Paraíba tourmaline origin determination, if the LA-ICP-MS analyses identify a cuprian tourmaline as liddicoatite, the stone's origin is conclusively Mozambique.

Copper-bearing tourmalines are reported to occur in various colors, including pink, purple, violet, blue, and green (e.g., Laurs et al., 2008). Heat treatment is known to improve the color of cuprian tourmaline by changing the valence state of manganese ions from trivalent (Mn^{3+}) to divalent (Mn^{2+}), consequently reducing Mn^{3+} absorption in the visible range. This change can remove the purple and pink components of some stones, resulting in blue to green colors consistent with the Paraíba designation. Unfortunately, heat treatment is not always detectable. Appearance of a pink halo around tube-like inclusions, called "pink sleeves," has been used as evidence of an unheated stone (Koivula et al., 2009). However, these features can remain in heated samples (S.F. McClure, pers. comm., 2017). Therefore, the colors of Paraíba tourmalines should always be considered to be potentially modified by heat treatment. One possible avenue of future research would be to study the trace element signatures of the various colors of Paraíba tourmaline, but of course this is complicated by the prevalence of heat treatment in most stones.

Different approaches have been proposed for determination of origin. These techniques include, in part, using isotopic compositions of boron and lithium (Shabaga et al., 2010; Ludwig et al., 2011), photoluminescence spectra (Milisenda, 2018b), and laser-induced breakdown spectroscopy (LIBS) with multivariate statistics (Dutrow et al., 2019). These approaches may be helpful as additional techniques to enhance chemical fingerprinting and facilitate origin determination.

CONCLUSIONS

Based on GIA's database containing more than 300 Paraíba tourmaline samples with known provenance, geographic origin determinations can be made using a variety of minor/trace element data when collected by highly precise and accurate methods. In the modern gemological laboratory, the weight of the origin determination rests overwhelmingly on trace element analysis by LA-ICP-MS. Paraíba tourmalines from Brazil, Mozambique, and Nigeria can, in most cases, be identified by their unique fingerprints of concentrations of trace elements such as Sr, Cu, Zn, Ga, Sn, and Pb. Additionally, the more recent find of Paraíba tourmaline belonging to the liddicoatite species can be identified through major element analysis. However, in a few cases "inconclusive" origin determinations may result when their trace element profiles do not match with any reference samples of known provenance. By improving the database with additional reference samples and conducting further research on analytical methods and statistical analyses, fewer Paraíba tourmalines will require an "inconclusive" call.

ABOUT THE AUTHORS

Dr. Katsurada is a senior staff gemologist at GIA in Tokyo. Mr. Sun is a research associate, and Dr. Breeding is a senior research scientist, at GIA in Carlsbad, California. Dr. Dutrow is the Williams Distinguished Alumni professor at Louisiana State University in Baton Rouge and a GIA governor.

ACKNOWLEDGMENTS

Thorough and thoughtful peer reviews by Professor Darrell Henry at Louisiana State University, Dr. Claudio Milisenda at DSEF German Gem Lab, and an anonymous reviewer greatly improved the manuscript. Dr. Aaron Palke provided timely and important feedback. We thank Bill Barker, William Larson, Hussain Rezayee, Shane McClure, Chico Bank, Blue Sheppard, and the GIA Museum for providing many of the reference samples for this study. This paper benefited from National Science Foundation funding to BD (grant number EAR-1551434).

REFERENCES

Abduriyim A., Kitawaki H. (2005) Gem News International: Cu- and Mn-bearing tourmaline—More production from Mozambique. *G&G*, Vol. 41, No. 4, pp. 360–361.

Abduriyim A., Kitawaki H., Furuya M., Schwarz D. (2006) "Paraíba"-type copper-bearing tourmaline from Brazil, Nigeria, and Mozambique: Chemical fingerprinting by LA-ICP-MS. *G&G*, Vol. 42, No. 1, pp. 4–21, http://dx.doi.org/10.5741/GEMS.42.1.4

Beurlen H., de Moura O.J.M., Soares D.R., Da Silva M.R.R., Rhede D. (2011) Geochemical and geological controls on the genesis of gem-quality "Paraíba tourmaline" in granitic pegmatites from northeastern Brazil. *Canadian Mineralogist*, Vol. 49, No. 1, pp. 277–300, http://dx.doi.org/10.3749/canmin.49.1.277

Breeding C.M., Rockwell K., Laurs B.M. (2007) Gem News International: New Cu-bearing tourmaline from Nigeria. *G&G*, Vol. 43, No. 4, pp. 384–385.

Dutrow B.L., Farnsworth-Pinkerton S., Henry D.J., McMillan N.J., Niepagen N. (2019) Copper-bearing tourmaline sources: Evidence from laser-induced breakdown spectroscopy (LIBS) and electron microprobe analyses (EMP). Geological Society of America Abstracts with Programs, p. 51.

Ertl A., Giester G., Schüssler U., Brätz H., Okrusch M., Tillmanns E., Bank H. (2013) Cu- and Mn-bearing tourmalines from Brazil and Mozambique: Crystal structures, chemistry and correlations. *Mineralogy and Petrology*, Vol. 107, No. 2, pp. 265–279, http://dx.doi.org/10.1007/s00710-012-0234-6

Faye G.H., Manning P.G., Nickel E.H. (1968) The polarized optical absorption spectra of tourmaline, cordierite, chloritoid and vivianite: Ferrous-ferric electronic interaction as a source of pleochroism. *American Mineralogist*, Vol. 53, No. 7-8, pp. 1174–1201.

Fritsch E., Shigley J.E., Rossman G.R., Mercer M.E., Muhlmeister S.M., Moon M. (1990) Gem-quality cuprian-elbaite tourmalines from São José da Batalha, Paraíba, Brazil. *G&G*, Vol. 26, No. 3, pp. 189–205, http://dx.doi.org/10.5741/GEMS.26.3.189

Furuya M. (2007) Copper-bearing tourmalines from new deposits in Paraíba State, Brazil. *G&G*, Vol. 43, No. 3, pp. 236–239, http://dx.doi.org/10.5741/GEMS.43.3.236

Henry D.J., Novák M., Hawthorne F.C., Ertl A., Dutrow B.L., Uher P., Pezzotta F. (2011) Nomenclature of the tourmaline-supergroup minerals. *American Mineralogist*, Vol. 96, No. 5–6, pp. 895–913, http://dx.doi.org/10.2138/am.2011.3636

Hsu T. (2018) Paraíba tourmaline from Brazil: The neon-blue burn. *InColor*, No. 39, pp. 42–50.

Karampelas S., Klemm L. (2010) Gem News International: "Neon" blue-to-green Cu- and Mn-bearing liddicoatite tourmaline. *G&G*, Vol. 46, No. 4, pp. 323–325.

Katsurada Y., Sun Z. (2017) Cuprian liddicoatite tourmaline. *G&G*, Vol. 53, No. 1, pp. 34–41, http://dx.doi.org/10.5741/GEMS.53.1.34

Koivula J.I., Nagle K., Shen A.H., Owens P. (2009) Solution-generated pink color surrounding growth tubes and cracks in blue to blue-green copper-bearing tourmalines from Mozambique. *G&G*, Vol. 45, No. 1, pp. 45–47, http://dx.doi.org/10.5741/GEMS.45.1.44

Kröner A., Stern R.J. (2004) Pan-African orogeny. *Encyclopedia of Geology*, Vol. 1, Elsevier, Amsterdam, pp. 1–12, http://dx.doi.org/10.1016/B0-12-369396-9/00431-7

Laboratory Manual Harmonisation Committee (LMHC) (2012) LMHC Information Sheet #6: "Paraíba tourmaline" Version 7, https://static1.squarespace.com/static/5bfbb7e6cc8fed3bb9293bf3/t/5bfe92a90e2e72555d61eec3/1543410345434/LMHC+Information+Sheet_6_V7_2012.pdf

Laurs B.M., Zwaan J.C., Breeding C.M., Simmons W.B., Beaton D., Rijsdijk K.F., Befi R., Falster A.U. (2008) Copper-bearing (Paraíba-type) tourmaline from Mozambique. *G&G*, Vol. 44, No. 1, pp. 4–30, http://dx.doi.org/10.5741/GEMS.44.1.4

Ludwig T., Marschall H.R., Pogge von Strandmann P.A.E., Shabaga B.M., Fayak M., Hawthorne F.C. (2011) A secondary ion mass spectrometry (SIMS) re-evaluation of B and Li isotopic compositions of Cu-bearing elbaite from three global localities. *Mineralogical Magazine*, Vol. 75, No. 4, pp. 2485–2494, http://dx.doi.org/10.1180/minmag.2011.075.4.2485

Mattson S.M., Rossman G.R. (1987) Fe^{2+}-Fe^{3+} interactions in tourmaline. *Physics and Chemistry of Minerals*, Vol. 14, pp. 163–171, http://dx.doi.org/10.1007/BF00308220

Merkel P.B., Breeding C.M. (2009) Spectral differentiation between copper and iron colorants in gem tourmalines. *G&G*, Vol. 45, No. 2, pp. 112–119, http://dx.doi.org/10.5741/GEMS.45.2.112

Milisenda C.C. (2018a) Paraíba tourmaline revisited. *InColor*, No. 39, pp. 34–41.

Milisenda C.C. (2018b) Gemstones and photoluminescence. *G&G*, Vol. 54, No. 3, p. 258.

Milisenda C.C., Müller S. (2017) REE photoluminescence in Paraíba type tourmaline from Mozambique. Abstract Proceedings, 35th International Gemmological Conference, Windhoek, Namibia, pp. 71–73.

Okrusch M., Ertl A., Schüssler U., Tillmanns E., Brätz H., Bank H. (2016) Major- and trace-element composition of Paraíba-type tourmaline from Brazil, Mozambique and Nigeria. *Journal of Gemmology*, Vol. 35, No. 2, pp. 120–139.

Peretti A., Bieri W.P., Reusser E., Hametner K., Günther D. (2009) Chemical variations in multicolored "Paraíba-type" tourmalines from Brazil and Mozambique: Implications for origin and authenticity determination. *Contributions to Gemology*, Vol. 9, pp. 1–77.

Pezzotta F. (2018) Mozambique Paraíba tourmaline deposits—an update. *InColor*, No. 39, pp. 52–56.

Rossman G.R., Fritsch E., Shigley J.E. (1991) Origin of color in cuprian elbaite from São José da Batalha, Paraíba, Brazil. *American Mineralogist*, Vol. 76, pp. 1479–1484.

Shabaga B.M., Fayak M., Hawthorne F.C. (2010) Boron and lithium isotopic compositions as provenance indicators of Cu-bearing tourmalines. *Mineralogical Magazine*, Vol. 74, No. 2, pp. 241–255, http://dx.doi.org/10.1180/minmag.2010.074.2.241

Shigley J.E., Cook B.C., Laurs B.M., de Oliveira Bernardes M. (2001) An update on "Paraíba" tourmaline from Brazil. *G&G*, Vol. 37, No. 4, pp. 260–276, http://dx.doi.org/10.5741/GEMS.37.4.260

Smith C.P., Bosshart G., Schwarz D. (2001) Gem News International: Nigeria as a new source of copper-manganese-bearing tourmaline. *G&G*, Vol. 37, No. 3, pp. 239–240.

Sun Z., Palke A.C., Breeding C.M., Dutrow B.L. (2019) A new method for determining gem tourmaline species by LA-ICP-MS. *G&G*, Vol. 55, No. 1, pp. 2–17, http://dx.doi.org/10.5741/GEMS.55.1.2

Vertriest W., Palke A.C., Renfro N.D. (2019) Field gemology: Building a research collection and understanding the development of gem deposits. *G&G*, Vol. 55, No. 4, pp. 490–511, http://dx.doi.org/10.5741/GEMS.55.4.490

Geographic Origin Determination Of Alexandrite

Ziyin Sun, Aaron C. Palke, Jonathan Muyal, Dino DeGhionno, and Shane F. McClure

The gem and jewelry trade has come to place increasing importance on the geographic origin of alexandrite, as it can have a significant impact on value. Alexandrites from Russia and Brazil are usually more highly valued than those from other countries. In 2016, GIA began researching geographic origin of alexandrite with the intent of offering origin determination as a laboratory service. Unfortunately, collecting reliable samples with known provenance can be very difficult. Alexandrite is often recovered as a byproduct of mining for other gemstones (e.g., emerald and corundum), so it can be difficult to secure reliable parcels of samples because production is typically erratic and unpredictable. The reference materials studied here were examined thoroughly for their trace element chemistry profiles, characteristic color-change ranges under daylight-equivalent and incandescent illumination, and inclusion scenes. The data obtained so far allow us to accurately determine geographic origin for alexandrites from Russia, Brazil, Sri Lanka, Tanzania, and India. Future work may help to differentiate alexandrites from other localities.

After the discovery of a gem mineral with unusual color-change behavior in the Russian Ural Mountains during the early 1830s, Swedish mineralogist Nils Adolf Erik Nordenskiöld named this new gem alexandrite in 1834 in honor of the future Czar Alexander II (Kozlov, 2005). This immediately created a royal and romantic aura around this variety of chrysoberyl. The most coveted alexandrites exhibit a lush green to greenish blue color in daylight and a warm, bright red shade in candlelight (Levine, 2008); some fine Brazilian and Indian alexandrite examples are shown in figures 1–3 and 6. This phenomenal color change is caused by the presence of trace Cr^{3+} substituting for Al^{3+} in the chrysoberyl crystal structure. Alexandrite is routinely described as "emerald by day, ruby by night." It is a stone of duality—green or red, cool or warm, day or night (Levine, 2008). Because of its rare and attractive color-change phenomenon, alexandrite has been highly sought after and is one of the most valuable gemstones in the trade.

Alexandrite, particularly fine-quality material, is also very scarce; it has generally been a byproduct of mining other major colored stones. Overall production statistics are hard to evaluate. It has been mined in Russia (Kozlov, 2005; Schmetzer, 2010), Tanzania (Gübelin, 1976; Schmetzer and Malsy, 2011b) and Zimbabwe (Brown and Kelly, 1984; Schmetzer et al., 2011) as a byproduct of emerald mining, and in Brazil (Proctor, 1988; Cassedanne and Roditi, 1993; Voynick, 1988) and India (Newlay and Pashine, 1993; Patnaik and Nayak, 1993; Panjikar and Ramchandran,1997; Voynick, 1988; Valentini, 1998) along with cat's-eye and nonphenomenal chrysoberyl, as

In Brief

- Geographic origin can significantly affect alexandrite's value.
- Collecting reliable alexandrite samples with known provenance can be very difficult because production is typically erratic and unpredictable.
- Trace element chemistry data obtained from LA-ICP-MS are the primary consideration in determining its geographic origin.
- Color-change behavior and inclusions are used as secondary factors to support the geographic origin determination.

See end of article for About the Authors and Acknowledgments.
Gems & Gemology, Vol. 55, No. 4, pp. 660–681,
http://dx.doi.org/10.5741/GEMS.55.4.660

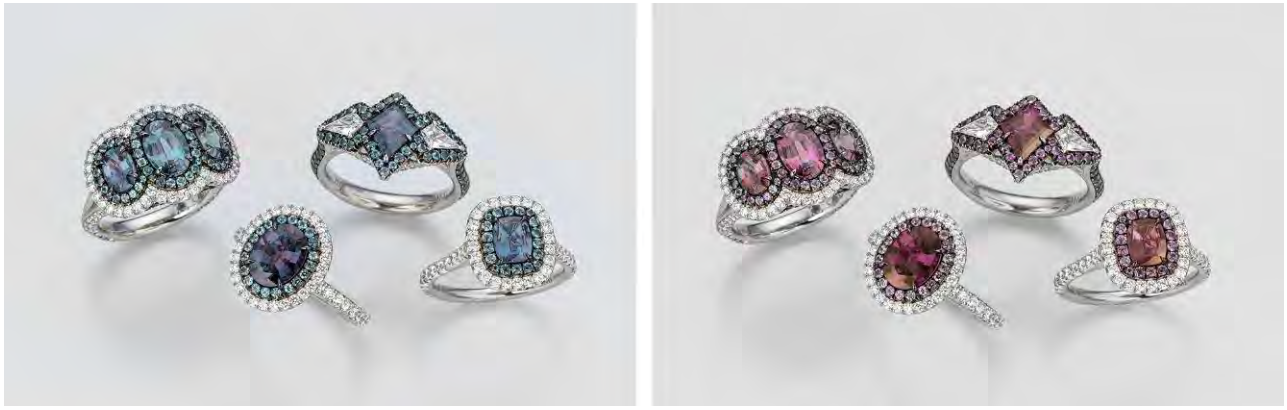

Figure 1. A group of rings featuring alexandrite from Brazil. Top row, left to right: A three-stone alexandrite ring with a 1.35 ct center oval flanked by two smaller ovals with a combined weight of 1.29 carats and a ring with a 1.32 ct kite-shaped center stone flanked by two kite-shaped diamonds weighing a total of 0.32 carats. Bottom row, left to right: Rings featuring a 1.71 ct oval and a 0.72 ct cushion-cut alexandrite. The designs also feature melee-cut alexandrites of unknown provenance and diamonds. The image on the left was photographed in daylight-equivalent lighting, the image on the right in incandescent light. Detailed procedures for photographing the alexandrites shown in this article are provided in appendixes 2 and 3, online at https://www.gia.edu/doc/WN19-Alexandrite-Appendixes2-3.pdf. Photos by Robert Weldon/GIA; courtesy of Omi Privé.

well as other pegmatitic minerals. In Sri Lanka (Zwaan, 1982; Zoysa, 1987, 2014), it is mined as a byproduct of corundum, cat's-eye and nonphenomenal chrysoberyl, and other minerals. The supply of alexandrite in the U.S. market has been low since the 1990s, as the supplies from the initial rush in Brazil presumably started drying up (Costanza, 1998). However, demand for the gemstone has stayed high in the U.S., especially for large stones with high clarity and intense and distinctive color change (again, see figures 1–3 and 6). The situation has changed somewhat recently, with new production from Sri Lanka, Brazil, and Tanzania (Jarrett, 2015).

With the development of these modern sources and the subsequent rapid changes in the alexandrite supply chain, there is growing demand from the gem trade for geographic origin determination for fine alexandrite. Origin is increasingly important, as it is often used as a factor in establishing a stone's value. Stones from Russia or Brazil can easily command a higher price than alexandrite from Tanzania and Zimbabwe with the same attributes. Because of all of

Figure 2. This ring features a 0.72 ct Brazilian cushion-cut alexandrite with a strong color-change effect, and the design uses additional alexandrite melee and diamonds as accents. The loose oval alexandrite below the ring weighs 4.13 ct and hails from India. The image on the left was photographed in daylight-equivalent lighting, the image on the right in incandescent light. Photos by Robert Weldon/GIA; courtesy of Omi Privé.

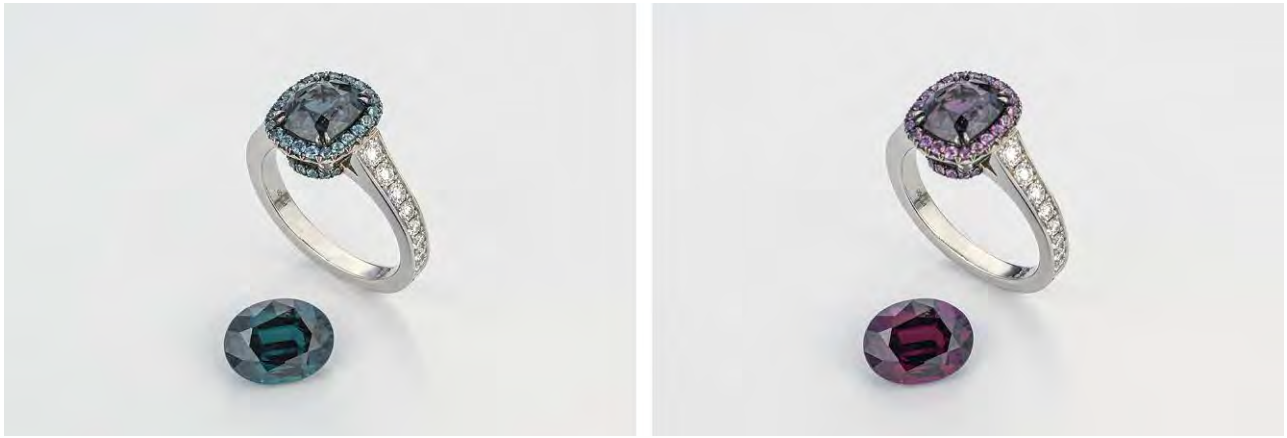

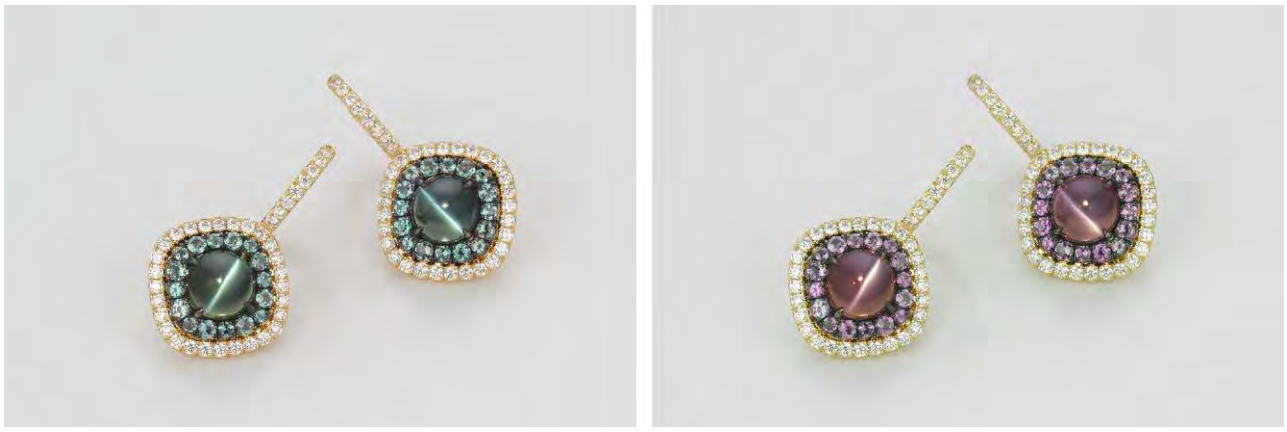

Figure 3. This matched pair of cat's-eye alexandrites from Brazil exhibits double phenomena (color change and chatoyancy) and weighs a total of 2.43 carats. The design also features alexandrite and diamond melee accents. The image on the left was photographed with daylight-equivalent lighting and the image on the right with incandescent light. Pinpoint light was used to reveal the stones' chatoyancy. Photos by Robert Weldon/GIA; courtesy of Omi Privé.

these market factors, in 2016 GIA initiated a research project centered around alexandrite geographic origin determination. Since then, many samples have gone through the laboratories and had their characteristic chemistry, colors, and inclusions carefully documented. Reference stones with reliable provenance were obtained from multiple sources. The data collected on stones from a single country from various sources were generally found to be self-consistent, which corroborates the validity of the origin determination criteria developed. GIA announced the origin determination service in early 2019 and will continue to develop its alexandrite database to ensure the most accurate identification and origin reporting for the jewelry trade.

ALEXANDRITE GEOGRAPHIC LOCALITIES: A BRIEF SUMMARY

Russia. The original locality for alexandrite remains one of the most highly valued sources (Kozlov, 2005; Schmetzer, 2010). Alexandrites from Russia are generally a byproduct of emerald mining from metamorphic mica-schist veins in ultramafic host rocks. The micaceous rocks are called "glimmerites" because of the glowing sheen of the micas.

Russian production began in the 1830s but waned in the twentieth century when mining emphasis shifted to beryllium, and it lapsed with the fall of the Soviet Union in 1991. Recent efforts have been undertaken to increase Russian alexandrite production. There are a few important deposits: Mariinskoye (Malyshevskoye); Cheremshanskoye; Sretenskoye (Sverdlovskoye), where the first Russian emeralds were discovered; Krasnobolotnoye, where the largest and most beautiful Russian alexandrites were found in 1839; and Krasnoarmeiskoye. Of these, the Mariinskoye deposit has historically had the largest mining operation.

Sri Lanka. Sri Lanka is one of the world's most important gemstone localities (Zwaan, 1982; Zoysa, 1987, 2014). The main gem-bearing areas are the Ratnapura district in Sabaragamuwa Province, Elahera in Central Province, Okkampitiya in Uva Province, and the Kataragama area in Southern Province. The chrysoberyl occurrences are more frequently found in and around Morawaka and Deniyaya in Southern Province. All of these gems occur in alluvial deposits underlain by Precambrian metamorphic rocks, and their original source remains unknown. There was little reliable information available on the amount and value of the gem material recovered in Sri Lanka until 1923, when the discovery of fine-quality alexandrites in Ratnapura's Pelmadulla deposits was reported. There was a constant supply of Sri Lankan alexandrite in the market until the end of the 1980s, when production dropped (Proctor, 1988).

Most Sri Lankan alexandrites have a weaker color change than Russian and Brazilian stones (see the loose stones in figure 4), although finer-quality material can show color change from saturated green to

Figure 4. The ring on the far left features a heart-shaped alexandrite from India. The second ring is mounted with an oval-shaped alexandrite—possibly from Madagascar—and melee-cut diamonds. All loose faceted stones are from Sri Lanka. The stones range from 4.01 to 22.99 ct. The image on the left was taken under an LED light source simulating daylight-equivalent lighting, while the right-hand image was taken under an LED light source simulating incandescent illumination. Photos by Kevin Schumacher; courtesy of LC Gem Collection Inc.

red. However, Sri Lankan alexandrites often achieve large sizes with high clarity, and stones up to 600 ct have been examined by GIA.

Brazil. In the 1980s, as Russia's Uralian deposits were producing little and supplies from Sri Lanka were drying up, the pegmatite district in Minas Gerais, Brazil, became for a time the world's major alexandrite producer (Koivula, 1987a,b; Proctor, 1988; Cassedanne and Roditi, 1993).

From 1846 until the 1980s, the Americana and Santana Valleys, near the city of Padre Paraíso in the Teófilo Otoni–Marambaia pegmatite districts, accounted for approximately 95% of the chrysoberyl and cat's-eye chrysoberyl found in Minas Gerais. But fine alexandrites from the Americana, Santana, Gil, and Barro Preto Valleys were rare. Brazil's foremost source of fine alexandrite was the Malacacheta region in the northeast of Minas Gerais State. Alexandrite was mined there from 1975 to 1988, with peak production in the early 1980s. In 1987, the Lavra de Hematita alexandrite deposit was discovered. This marked the greatest discovery of Brazilian alexandrite. To date, Hematita has yielded tens of kilos of alexandrite that are generally larger and cleaner than those from Malacacheta, including some faceted gems weighing up to 30 ct that exhibit extraordinary color change. A few locations in the adjacent states of Bahia and Espírito Santo also produce alexandrite, albeit with an overall lower quality in terms of color, clarity, size, or some combination.

Most of the finest cyclical twinned alexandrite mineral specimens in today's market come from Brazil (see figure 5). Brazilian alexandrites have a distinct color change that is often comparable to that of the finest Russian stones (see figure 6), but with a higher clarity, larger size, and much greater availability. Brazil also produces some of the world's finest cat's-eye alexandrite, such as the pair in figure 3 that exhibit a distinct color change and a sharp eye.

India. In the religions associated with Southeast Asia and the Indian subcontinent—Hinduism, Jainism, and Buddhism—cat's-eye chrysoberyl holds a place of distinction among the Navratnas (a combination of nine sacred gemstones) (Brunel, 1972). Chrysoberyl has been mined in five Indian states—Kerala, Madhya Pradesh, Odisha (formerly Orissa), Andhra Pradesh, and Tamil Nadu—since the 1980s and '90s. Alexandrite is found there either in pegmatites intruding granitic rock or in biotite schists developed along the contact zone of pegmatites and peridotites (Soman and Nair, 1985; Patnaik and Nayak, 1993; Newlay and Pashine, 1993; Panjikar and Ramchandran, 1997; Valentini, 1998).

Indian alexandrites usually have a weaker color change than Russian and Brazilian material (see the ring mounted with a heart-shaped stone in figure 4). However, stones with good color change and clarity are comparable to the finest Russian and Brazilian specimens. The 4.13 ct loose oval in figure 2, repre-

Figure 5. A cyclical twinned Brazilian alexandrite mineral specimen, 4.13 cm in the longest dimension, shows distinct color change from green to red under daylight-equivalent lighting and incandescent illumination, respectively. The image on the left was taken under an LED light source simulating daylight-equivalent lighting, while the image on the right was taken under an LED light source simulating incandescent illumination. Photos by Kevin Schumacher; courtesy of John I. Koivula.

senting top-quality Indian alexandrite, exhibited saturated blue-green color under daylight and saturated red under incandescent light. Many small Indian cat's-eye alexandrites with weak color change are fairly common in today's market, but Indian cat's-eye alexandrite with distinct color change and sharp eyes are rare.

Tanzania. Alexandrite has come mainly from two mining areas in Tanzania: Lake Manyara in the north and Tunduru in the south (Gübelin, 1976; Johnson and Koivula, 1996, 1997; Henricus, 2001; Schmetzer and Malsy, 2011b; Jarrett, 2015). Lake Manyara is a primary deposit where alexandrite has been found in a phlogopite-bearing schist. Alexandrite from Tunduru has been mined from a secondary alluvial deposit. Alexandrite from Lake Manyara (figure 7) entered the market in the 1960s, with significant production into the early 1980s. Johnson and Koivula reported a wide variety of gem materials, including alexandrite, from Tunduru at the Tucson show in 1996. Since then, the area has been known for producing large quantities of alexandrite, and material from Tunduru was available in the U.S. market in 2015 according to Michael Couch of Michael Couch & Associates (Jarrett, 2015). In the early 2000s, emerald and alexandrite were reported from Mayoka, just outside Manyara National Park, by Abe Suleman, a director of the International Colored Gemstone Association and a member of the Tanzania Mineral Dealers Association (Henricus, 2001), but environmental concerns stopped mining activities in late 2000 and little material was produced.

A chameleon brooch mounted with beautiful rough alexandrite crystals from Lake Manyara on its back and small faceted alexandrites on its legs and tail changes from blue green to violet when viewing under daylight and incandescent light, as seen in figure 7.

Figure 6. A suite of fine Brazilian alexandrite exhibiting the finest color change seen in this material. The left image was taken under an LED light source simulating daylight-equivalent lighting, while the right photo was taken under an LED light source simulating incandescent illumination. Photos by Robert Weldon/GIA; courtesy of Evan Caplan.

Minor Alexandrite Geographic Localities. *Zimbabwe.* Alexandrite has been recovered from the Novello deposit of Zimbabwe's Masvingo district (Schmetzer, 2011). It is located in a phlogopite-bearing host rock with surrounding serpentinite. Peak production was in the 1960s and 1970s and yielded larger, mostly non-facet-grade material. The material is considered very dark and only suitable for faceting small stones with

Figure 7. Rough and faceted alexandrite from Lake Manyara, Tanzania. The left image was taken under an LED light source simulating daylight-equivalent lighting, while the right photo was taken under an LED light source simulating incandescent illumination. Photos by Robert Weldon/GIA; courtesy of Omi Privé.

intense color change. The deposit is believed to still produce alexandrite.

Madagascar. Alexandrite originating from phlogopite-bearing host rocks comes from primary emerald deposits in the Mananjary region of Madagascar (Schmetzer and Malsy, 2011a). The other deposit, in the Ilakaka region (Hänni, 1999; Milisenda et al., 2001), is a secondary deposit where different varieties of chrysoberyl—including alexandrite—have been found. Occasionally, large alexandrite crystals of gem quality have been recovered in the Lake Alaotra region.

Myanmar. In Myanmar (formerly Burma), the pegmatites in the western part of the Mogok Valley in Sakangyi or Barnardmyo, and the alluvial placers in the Mogok Stone Tract near Mogok, Kyatpyin, and Barnardmyo, have produced gem-quality alexandrite ("Alexandrite world occurrences...," n.d.). Burmese alexandrites usually fluoresce intense red under long- and short-wave UV radiation due to lack of iron.

Australia. Dowerin is the first recorded alexandrite occurrence in Western Australia, known since 1930. The deposit has yielded many small crystals (Bevan and Downes, 1997; Downes and Bevan, 2002).

United States. In recent years, small chrysoberyl crystals with weak color change were reported from a mine at La Madera Mountain in Rio Arriba County, New Mexico ("Alexandrite world occurrences & mining localities," n.d.).

Zambia. Some Zambian alexandrite with similar characteristics to Zimbabwean stones has appeared in the market. No reliable information is currently available.

MATERIALS AND METHODS

Reference Samples. GIA's research project on alexandrite origin started in early 2016, with suites of alexandrites from both Russia and Brazil. Almost all Russian material came from Warren Boyd, who acquired them as a mining consultant at the Malysheva emerald and alexandrite mine from 1992 to 2007. There are four different sources for the Brazilian alexandrites. Seventeen specimens came from Evan Caplan, who acquired them from a source directly connected to a mine owner in Brazil. Fifteen of the Brazilian gems came from Nilam Alawdeen, who later provided three Sri Lankan and two Indian stones during this project. Spectrum Fine Jewelry & Exotic Gems supplied 140 Brazilian alexandrites. Four additional samples came from the GIA Museum. It is very likely that all the Brazilian material came from the Hematita deposit in Minas Gerais.

A few months later, eight Sri Lankan, twenty-one Tanzanian, and two Indian alexandrites were provided to the lab by LC Gem Collection Inc., a Sri Lanka–based gem company. Gem dealer Chandika Thambugala submitted nine Sri Lankan stones to the lab. The GIA Museum was also able to provide thirteen Sri Lankan, four Indian, and five Tanzanian gems. In some cases, all that was known about a specimen was the country of origin; specific mines were unknown. However, the Tanzanian stones were very likely from Lake Manyara. An additional 18 Indian stones were provided by Lance Davidson. Field gemologist Vincent Pardieu provided us with some stones from his personal collection: three Madagascar alexandrites bought in Madagascar; nine Zambian stones bought in Mahesak, Thailand, from a trustworthy source; and one Burmese sample purchased from the trade in Mogok. Five Zimbabwean stones came from two different sources: Two were borrowed from the personal collection of Yusuke Katsurada, a senior gemologist and scientist in GIA's Tokyo laboratory, and the GIA Museum provided the other three. Detailed reference sample provenance is listed in appendix 1, table 1, online at https://www.gia.edu/doc/WN19-Alexandrite-Appendix1.pdf.

Procedures for Alexandrite Identification in GIA Laboratories. When an alexandrite first arrives at the GIA laboratory, we ask a question even more fundamental than geographic origin: Is this a natural alexandrite? Fourier-transform infrared spectroscopy (FTIR) is performed on every alexandrite to distinguish natural from synthetic material (Stockton and Kane, 1988) and to identify imitations. Natural alexandrites are then sent for laser ablation–inductively coupled plasma–mass spectrometry (LA-ICP-MS); see Groat et al. (2019), pp. 512–535 of this issue. This method is used to acquire trace element chemistry for geographic origin determination, if origin service is requested by the client.

After advanced analysis, the stone is given to a preliminary gemologist for standard gemological testing and identification. The stone is examined under a standard GIA desktop microscope for inclu-

sions that would be indicative of a natural or synthetic origin. Photomicrographs are taken and Raman spectroscopy is performed if there are crystalline inclusions that might aid in origin determination (see Groat et al., 2019, pp. 512–535 of this issue). The colors exhibited by the alexandrite are also considered as possible evidence of origin. A stone's warm and cool colors are also recorded in GIA's database with careful photographic documentation under standardized conditions (see below). The stone is then sent to a more senior gemologist to further check all the physical and chemical properties to confirm the stone's identity and complete the identification and origin determination.

Photography. *GIA Digital Imaging for Color-Change Stones.* GIA has a set of standardized procedures for photographing color-change stones to ensure consistency in appearance reproduction. The image of an alexandrite is captured using a variety of high-quality cameras and lenses in a specially made light box produced by the GIA instrument department. An LED light with a color temperature around 6500 K is used as a daylight-equivalent light source, while an LED light with a color temperature around 2700 K is used as an incandescent light source. The final printed images are viewed in a controlled lighting environment and compared to the actual stone. Slight color adjustments are made with Adobe Photoshop software if needed, using a monitor that is maintained and color calibrated using GretagMacbeth calibration software.

Photomicrography of Inclusions. Photomicrographs are taken using various Nikon microscopes, including an Eclipse LV100, SMZ1500, and SMZ10 (Renfro, 2015a,b). Photographs of the inclusion scenes are captured using Nikon DS-Ri2 digital cameras. Various lighting environments including darkfield, brightfield, and fiber-optic illumination are used to highlight specific internal features. Image stacking (Renfro, 2015a) is sometimes employed to maximize the depth of field of an image.

Raman Spectroscopy. Raman spectra are collected with a Renishaw inVia Raman microscope system. The Raman spectra of the inclusions are collected using a Stellar-REN Modu Ar-ion laser producing highly polarized light at 514 nm at a nominal resolution of 3 cm^{-1} in the 2000–200 cm^{-1} range. Each inclusion spectrum is accumulated three times at 20× or 50× magnification. In many cases, the confocal capabilities of the Raman system allow inclusions beneath the surface to be analyzed.

FTIR. Fourier-transform infrared spectra are collected using a Thermo Fisher Nicolet 6700 FTIR spectrometer equipped with an XT-KBr beam splitter and a mercury-cadmium-telluride (MCT) detector operating with a 4× beam condenser accessory. The beam is transmitted through the stone. The spectra are collected at a nominal resolution of 4 cm^{-1} with 1.928 cm^{-1} data spacing. Each stone is scanned 128 times to achieve a high signal-to-noise ratio.

LA-ICP-MS. Trace element chemistry is acquired using a Thermo Fisher iCAP Qc ICP-MS coupled with an Elemental Scientific Lasers NWR213 laser ablation system. It incorporates a Nd:YAG laser rod that emits light with a wavelength of 1064 nm in the infrared and a frequency quintupler system to generate a 213 nm ($^1/_5$ of 1064 nm) ultraviolet wavelength that is used to ablate samples. Ablation is achieved using a 55 µm diameter circular spot size, a fluence (energy density) of approximately 10 J/cm^2, and a 20 Hz repetition rate. National Institute of Standards and Technology (NIST) Standard Reference Material (SRM) 610 (http://georem.mpch-mainz.gwdg.de/sample_query.asp; Jochum et al., 2005) is used as an external standard. ^{27}Al is used as an internal standard, with a value of 425000 calculated and rounded from pure chrysoberyl. A similar method was used in works done by Malsy and Schmetzer (Schmetzer, 2010; Schmetzer and Malsy, 2011b; Schmetzer et al., 2011).

RESULTS AND DISCUSSION

Trace Element Chemistry of Alexandrite from Different Countries. In general, trace element chemistry is the most important factor in determining a geographic origin for alexandrite. By carefully examining our reference datasets, we concluded that Mg, Fe, Ga, Ge, and Sn are the five best discriminators to distinguish different geographic locations (figure 8). B, V, and Cr were also good discriminators for separating alexandrites among some countries (see figures 9 and 10), but must be considered as an addition to the first five with specific criteria. The generalized trace element profiles are listed in table 1. The results described herein and shown in figures 8–10 are generally consistent with the results previously reported by Malsy and Schmetzer.

Using any two of the five discriminators (Mg, Fe,

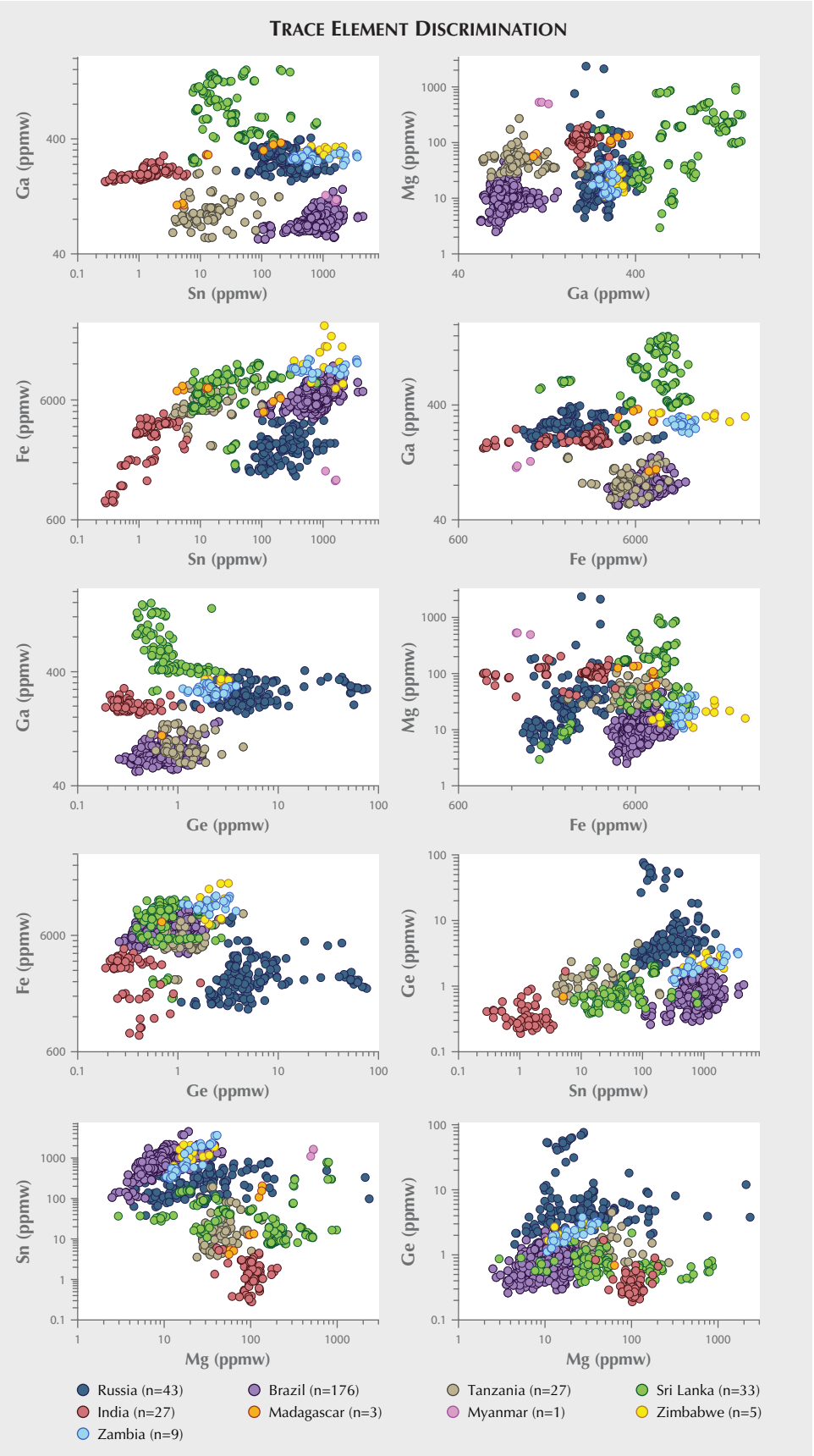

Figure 8. Plots of Mg, Fe, Ga, Ge, and Sn concentration in alexandrite reference stones from different countries. Ten plots were generated by plotting any two elements against each other. The origin of most alexandrite samples can be confidently ascertained using these 10 plots.

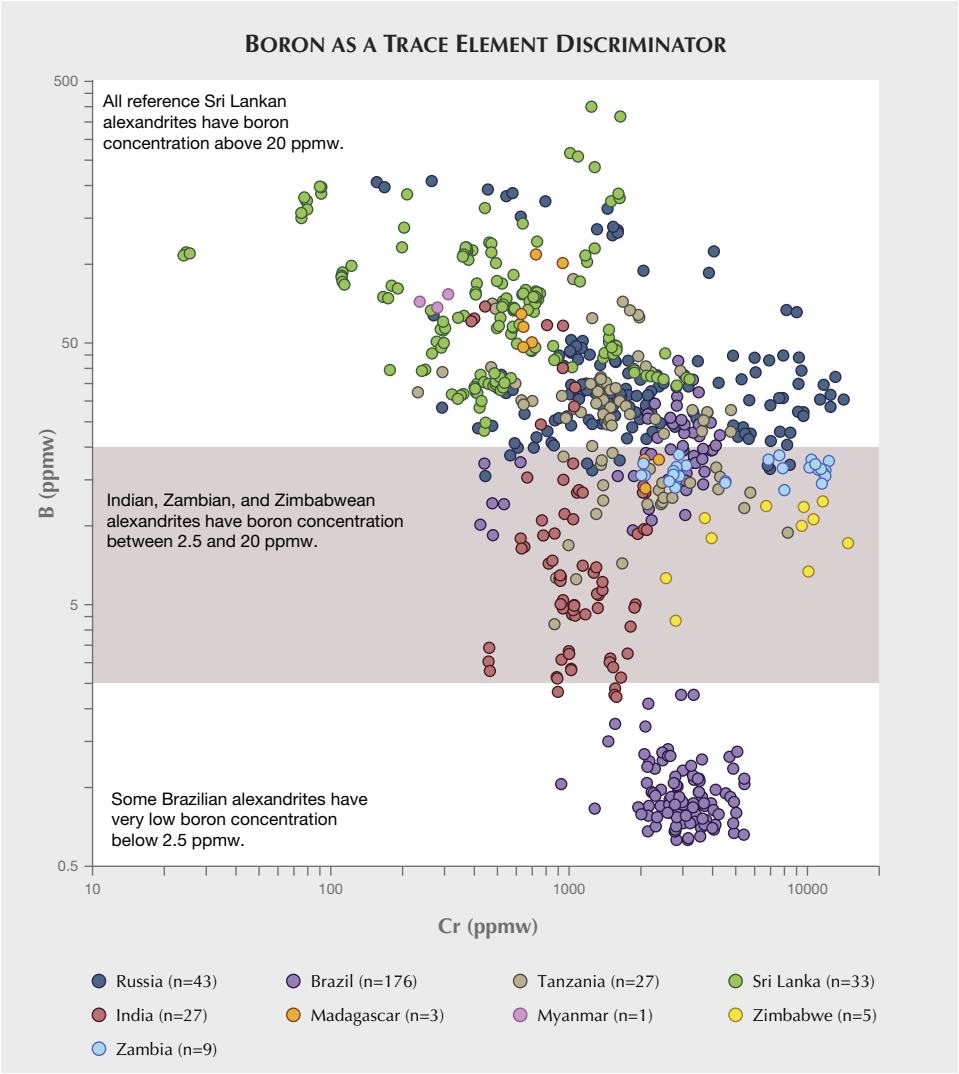

Figure 9. Boron can be used to separate Sri Lankan alexandrite from Indian, Zambian, and Zimbabwean samples. Some Brazilian stones have the lowest boron concentrations among all countries.

Ga, Ge, and Sn) to plot against each other, 10 plots can be generated (figure 8). Alexandrites from different countries have their own characteristic chemistry.

Mg—Indian and Tanzanian alexandrites have high Mg concentrations, while Brazilian, Zambian, and Zimbabwean stones have low Mg concentration. Russian and Sri Lankan stones have wide ranges of Mg concentrations that overlap with every other source.

Fe—Zambian and Zimbabwean stones have relatively high Fe concentration, while Tanzanian, Brazilian, and Sri Lankan specimens have medium Fe concentration. Russian and Indian stones have the lowest Fe concentrations.

Ga—Sri Lankan stones have the highest gallium concentration. Indian, Russian, Zambian, and Zimbabwean material falls in a middle range, while Tanzanian and Brazilian alexandrites have the lowest Ga concentrations.

Ge—Russian alexandrites have the highest germanium concentrations, while Sri Lankan, Indian, Brazilian, and Tanzanian stones have the lowest. Zambian and Zimbabwean stones have medium Ge concentrations.

Sn—Russian, Brazilian, Zambian, and Zimbabwean alexandrites have higher Sn concentrations, while Indian specimens have lower amounts. Sri Lankan and Tanzanian stones have similar Sn concentrations in the middle range.

In addition to these five discriminators, B, V, and Cr are very useful for some specific cases. These three elements can further validate geographic origin

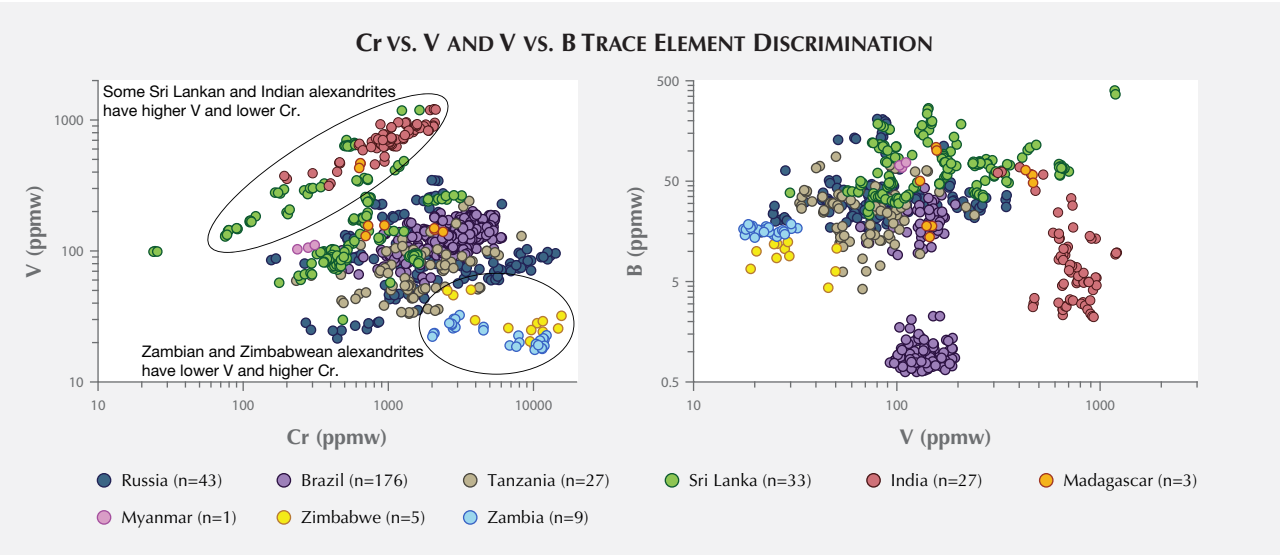

Figure 10. Cr-V and V-B plots prove very useful in validating the origin of Indian, Zambian, and Zimbabwean alexandrites. The Indian stones, along with some of the Sri Lankan specimens, have the highest V/Cr ratios. The Zambian and Zimbabwean stones have the lowest V/Cr ratios.

conclusions (figures 9 and 10). Boron can be used to distinguish Sri Lankan alexandrite from Indian, Zambian, Zimbabwean, and some of the low-boron Brazilian stones (figure 9). According to our reference database, all Sri Lankan alexandrites collected so far have boron concentrations above 20 ppmw, while almost all Indian, Zambian, and Zimbabwean alexandrites have boron concentrations between 2.5 and 20 ppmw, and some Brazilian alexandrites have the lowest boron concentrations, below 2.5 ppmw (figure 9). Besides boron, the chromophores vanadium and chromium are also very important in separating Indian, Zambian, and Zimbabwean alexandrites from material from other localities (figure 10). According to our reference database, some Sri Lankan and all Indian alexandrites have the highest V/Cr ratio among all reference stones (indicated by the black oval in the top left of the plot in figure 10). Zambian and Zimbabwean alexandrites have the lowest V/Cr ratio among all reference stones (indicated by the black oval in the bottom right of the plot in figure 10).

Selective Plotting for Alexandrite Geographic Origin Determination. We have found that the use of the "selective plotting" method can greatly enhance the accuracy of origin determination for alexandrite (figure 11). The method essentially involves plotting data for the unknown client stone only against reference data with similar full trace element profiles; see Palke et al. (2019), pp. 536–579 of this issue. In this method, discrete "windows" are selectively created around the trace element data of the client stone, and only reference data within these windows are plotted while everything else is filtered out. This results in plots that are much easier to read and accurately interpret. A few examples are shown in figure 11. The plots after discrimination usually point to simple and definite results.

Characteristic Color Change of Alexandrite from Different Countries. Anyone who is familiar with alexandrite is well aware that material from different countries has different characteristic color-change behaviors. Many dealers have a good sense of where a specimen comes from through visual observation under daylight and incandescent lighting conditions. After examining hundreds of alexandrites, we can provide some examples of typical color-change pairings of alexandrite from different countries (figure 12). The images are from stones submitted to GIA at the five different global identification laboratories; each origin was confirmed by analyzing their trace element profiles as measured by LA-ICP-MS. While there is usually a range in the warm/cool color pairs seen for alexandrite from a single locality, each local-

TABLE 1. Generalized trace element profiles of alexandrite samples in ppmw.

Russia								
	B	**Mg**	**V**	**Cr**	**Fe**	**Ga**	**Ge**	**Sn**
Range	15.5–208	4.47–3140	21.5–347	156–14200	1390–8610	171–406	1.08–76.4	37.9–1550
Average	45.0	93.0	102	3090	2780	263	10.3	324
Median	31.4	26.1	84.0	1640	2480	255	4.55	244
Sri Lanka								
	B	**Mg**	**V**	**Cr**	**Fe**	**Ga**	**Ge**	**Sn**
Range	23.1–400	2.95–987	29.8–1190	24.1–3200	1720–12200	246–1580	bdl–2.70	7.35–785
Average	81.6	170	211	702	7680	731	0.55	57.9
Median	68.5	123	146	526	8090	638	0.55	29.3
Brazil								
	B	**Mg**	**V**	**Cr**	**Fe**	**Ga**	**Ge**	**Sn**
Range	bdl–42.7	2.50–46.7	56.8–201	424–6050	4180–11500	53.3–145	bdl–2.55	87.4–4470
Average	2.17	11.9	136	2960	6350	72.8	0.70	871
Median	bdl	11.1	137	2870	6270	69.9	0.69	821
India								
	B	**Mg**	**V**	**Cr**	**Fe**	**Ga**	**Ge**	**Sn**
Range	bdl–68.9	38.4–203	314–1210	192–2120	829–4610	168–284	bdl–1.68	0.28–6.01
Average	10.8	104	722	1090	2900	199	0.30	1.69
Median	5.68	102	714	1020	3250	195	0.28	1.33
Tanzania								
	B	**Mg**	**V**	**Cr**	**Fe**	**Ga**	**Ge**	**Sn**
Range	4.21–87.8	24.0–270	33.2–241	232–8270	2470–9210	54.9–212	bdl–4.48	3.56–192
Average	28.3	53.3	76.1	1990	5620	94.1	0.84	22.9
Median	26.7	47.1	69.2	1500	5390	85.8	0.79	14.2
Zimbabwe								
	B	**Mg**	**V**	**Cr**	**Fe**	**Ga**	**Ge**	**Sn**
Range	bdl–12.4	10.9–38.3	19.1–50.6	2550–15600	7480–25000	269–343	bdl–3.19	338–2110
Average	7.87	20.5	31.2	8700	14100	313	1.78	1200
Median	8.97	19.4	28.1	9650	12700	317	2.04	1080
Zambia								
	B	**Mg**	**V**	**Cr**	**Fe**	**Ga**	**Ge**	**Sn**
Range	13.7–18.7	10.6–40.9	17.6–32.4	2010–12300	9050–13100	228–317	1.12–3.8	305–3630
Average	16.2	21.5	23.2	6720	11000	276	2.19	1270
Median	16.3	18.0	22.6	6860	10900	277	2.04	668
Madagascar								
	B	**Mg**	**V**	**Cr**	**Fe**	**Ga**	**Ge**	**Sn**
Range	13.9–109	56.2–136	130–468	630–2380	4770–7840	106–338	bdl–0.69	4.16–205
Average	53.4	97.4	249	1200	6850	248	0.077	57.7
Median	50.3	97.2	156	726	7280	289	bdl	12.7
Myanmar								
	B	**Mg**	**V**	**Cr**	**Fe**	**Ga**	**Ge**	**Sn**
Range	68.3–76.8	495–531	103–111	236–311	1270–1530	114–129	bdl–bdl	1100–1640
Average	72.3	519	107	276	1360	120	bdl	1440
Median	71.9	530	106	280	1290	118	bdl	1580
Detection limits (ppmw)								
	B	**Mg**	**V**	**Cr**	**Fe**	**Ga**	**Ge**	**Sn**
Range	0.091–0.15	0.014–0.034	0.008–0.021	0.15–0.26	0.87–1.63	0.007–0.031	0.037–0.11	0.026–0.065

**bdl = below the detection limit of the LA-ICP-MS analysis*

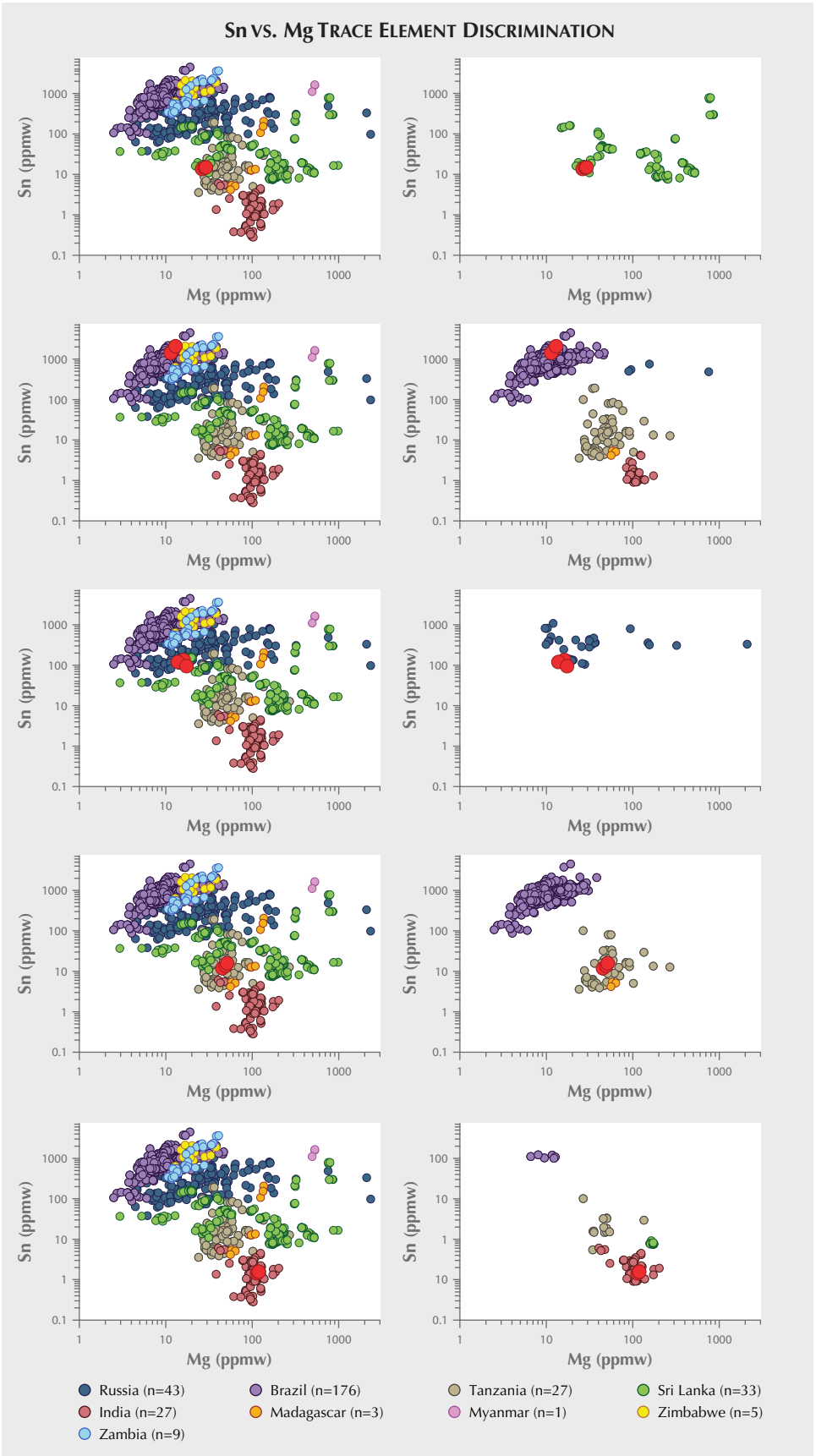

Figure 11. The left column shows Sn-Mg plots before discrimination for alexandrite from (top to bottom) Sri Lanka, Brazil, Russia, Tanzania, and India. The right column shows the same Sn-Mg plots after application of the selective plotting method. This method leaves in reference data that are similar to unknown stones and filters out irrelevant information, making these plots much easier to interpret accurately.

ity does tend to have its own specific range, and the different colors seen are generally helpful in narrowing down the origin. The color types for each country in figure 12 were determined based on both colorimetric analyses of the images and visual observations by gemologists.

Sri Lankan alexandrites usually have a yellowish green component in daylight-equivalent lighting and a brownish or orangy component with incandescent illumination. Brazilian alexandrites tend to have a bluish green component in daylight-equivalent lighting and a reddish purple to purple component under incandescent light. The color-change characteristics of alexandrites from other countries are not as well known, because of the limits of our current image database.

Geographic origin determinations should never be based on color alone; trace element chemistry is the primary factor in establishing origin. However, color can support the origin determination derived from trace element chemistry. The authors grouped all types of alexandrite color-change pairings into the following general categories (corresponding to types in figure 12):

1. **Sri Lanka – Cool**
   Even though Sri Lankan alexandrites typically have brownish to grayish overtones, some lack these overtones and fall into the Cool category. In lighter-toned stones, hue changes from green or bluish green in daylight to purplish red or grayish purple in incandescent light. Saturation is low to medium in fine-quality stones, with a medium to dark tone.

2. **Sri Lanka – Warm**
   Specimens in the Warm category exhibit the typical brownish to grayish overtones that characterize many Sri Lankan alexandrites. Daylight hues are generally yellowish compared to other alexandrites, ranging from yellowish green to brownish yellow to the occasional pure green. In incandescent light, they usually appear brownish, with yellowish brown, orangy brown, brownish pink, brownish purple, brownish yellow, and brownish red hues. Saturation is generally low to medium, with medium to dark tones.

3. **Brazil**
   Top Brazilian stones are generally considered to exhibit the finest color change of any alexandrites. Most tend to have a bluish component to their daylight color. Their hues are greenish blue to blue-green to pure green in daylight and red-purple to purple in incandescent light. These colors are often vivid, with medium to high saturation and medium to dark tone.

4. **Russia**
   Russian alexandrite can exhibit some of the finest colors in top-quality material. Hues are generally pure green to bluish green to green-blue in daylight and purple-red to purple in incandescent light. Stones tend to have medium to high saturation, with medium to dark tone.

5. **Tanzania**
   Tanzanian alexandrite is capable of producing superb color change. Hue tends to range from bluish green to greenish blue in daylight and red-purple to purple in incandescent light. Tanzanian stones typically have medium to high saturation and medium to dark tone.

6. **India**
   Hue for Indian alexandrite tends to range from green to bluish green in daylight, changing to purplish violet, purple, brownish purple, or red-purple in incandescent light. Indian stones typically have low to medium saturation and medium to dark tone.

Inclusions in Alexandrite from Different Countries. Geological environment not only controls the presence of certain trace elements and their concentration but also impacts the inclusions an alexandrite contains. GIA has captured photomicrographs of inclusions in alexandrite and is using them to support the origin determinations made by chemistry and color.

Brazil. Metal sulfides have frequently been found in Brazilian alexandrites (figure 13A and B) and are almost diagnostic for this origin in the authors' opinion, although alabandite, a metal sulfide with similar appearance to the inclusions in figure 13A and B, was reported by Gübelin and Koivula (1986) in a non-color-change Sri Lankan chrysoberyl. Minute particles sometimes group together to form fingerprints (figure 13C) and wispy clouds (figure 13D). Crystals of fluorite (figure 13E) and mica crystals and flakes (possibly phlogopite or biotite, figure 13F) are also observed occasionally. Other researchers have also reported fluorite, phlogopite, and biotite and

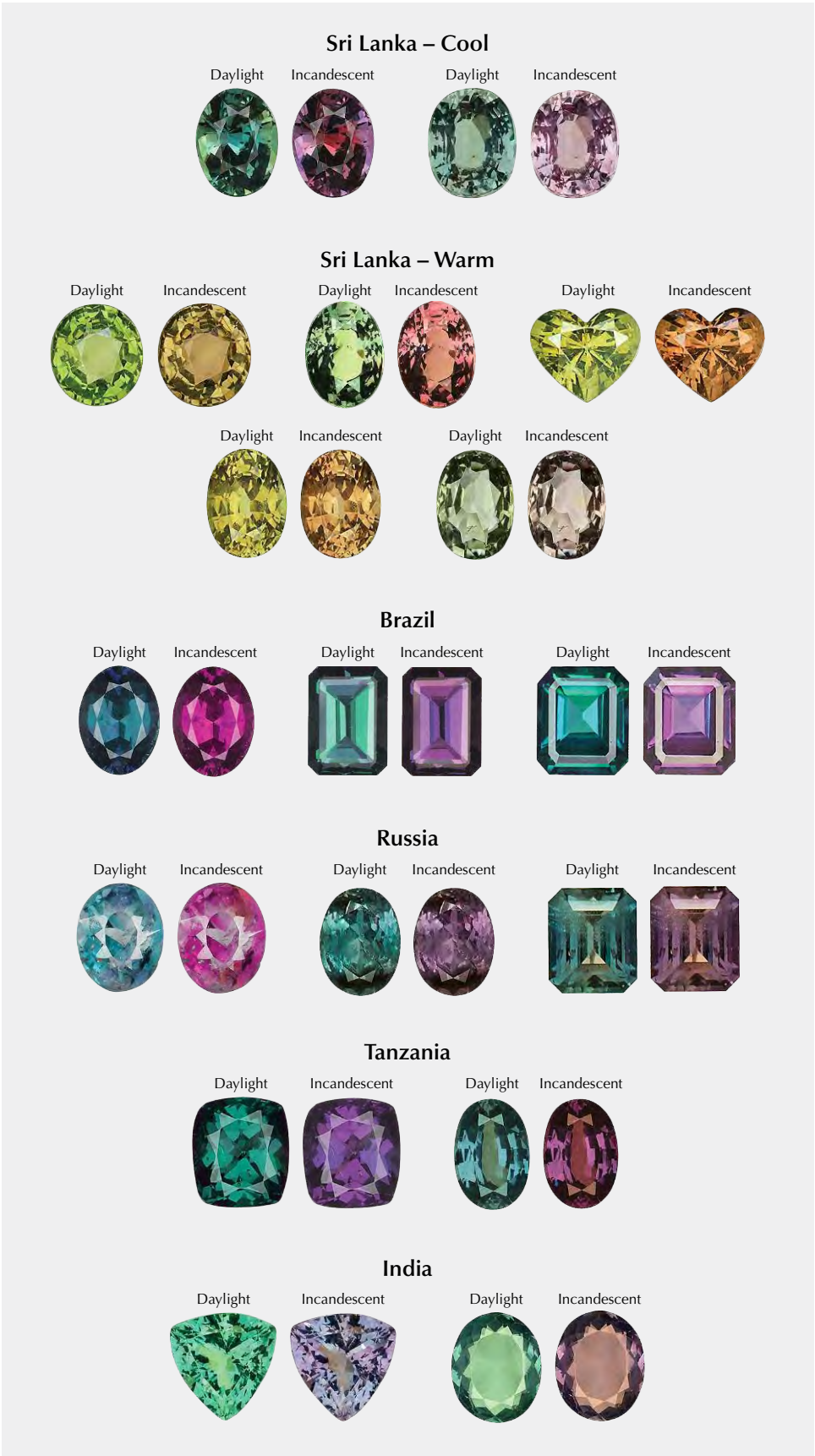

Figure 12. Characteristic color-change pairings of alexandrite from different countries. The photos were selected from GIA's digital imaging database of production stones, which were taken using GIA digital imaging procedures and printed on GIA alexandrite reports.

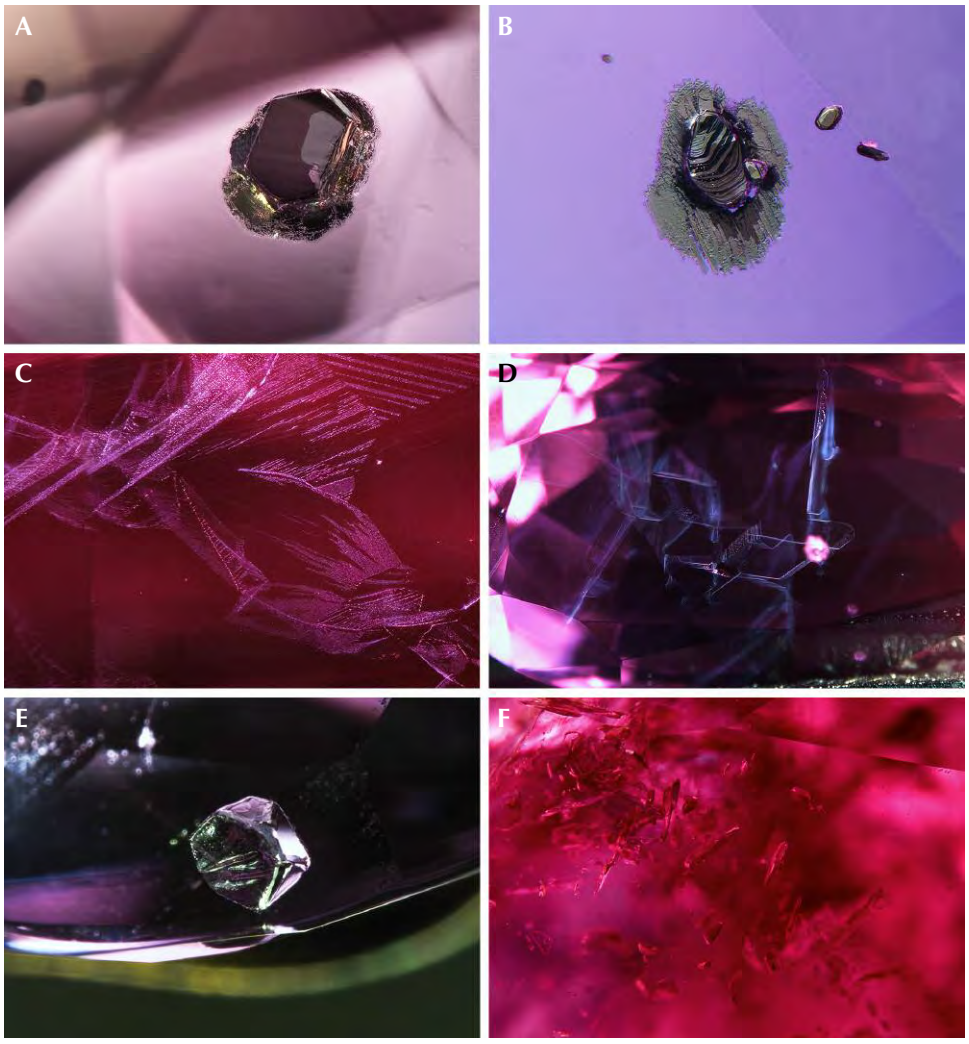

Figure 13. Inclusions in Brazilian alexandrite. A: A metal sulfide crystal inclusion surrounded by a melted/decrepitated halo under diffused fiber-optic illumination. B: Chalcopyrite crystal surrounded by melted/decrepitated halo under darkfield and oblique fiber-optic illumination. C: Silk, bands, and fingerprints composed of minute particles under oblique fiber-optic illumination. D: Clouds/fingerprints composed of minute particles under darkfield and oblique fiber-optic illumination. E: Rounded fluorite crystal inclusions under diffused illumination. F: Mica crystals under darkfield illumination. Fields of view: 1.99 mm (A), 1.42 mm (B), 2.34 mm (C), 7.19 mm (D), 0.55 mm (E), and 2.00 mm (F). Photomicrographs by Jonathan Muyal (A, C), Tyler Smith (B, D, E), and Makoto Miura (F).

additionally calcite, apatite, albite, and two-phase and multiphase fluid inclusions in Brazilian alexandrites (Gübelin and Koivula, 1986; Proctor, 1988; Koivula and Kammerling, 1988).

Sri Lanka. Sri Lankan stones submitted to GIA are usually clean, but the identification team has still documented many inclusions. Strong brown color zoning has only been observed in Sri Lankan stones and may be diagnostic of this origin (figure 14A), although additional observations are needed to confirm this. Under fiber-optic illumination, these brown color zones are populated with reflective milky clouds (figure 14B). Very rarely, elongate prismatic sillimanite crystals (figure 14C) and euhedral feldspar crystals (figure 14D) have been observed. Fingerprints (figure 14E and F) formed by two-phase and multiphase fluid inclusions are normal. Minute particles may group together to form flake-like clouds (figure 14G). Occasionally, tubes with brownish oxide stains (figure 14H) can also be observed. Additionally, green mica, quartz crystals, and slender rod-like crystals of columbite, spessartine, ilmenite, and alabandite have previously been observed in Sri Lankan alexandrites and non-color-change chrysoberyls (Gübelin and Koivula, 1986).

Russia. In our limited observations of inclusions in Russian alexandrite, phlogopite mica has been seen forming flattened, rounded, unevenly shaped crystals (figure 15A) and clusters of cotton-like inclusions (figure 15B). Very rarely, corroded and rounded fluorite crystals (figure 15C) and prismatic rod-like tourmaline crystals (figure 15D) have been observed. Both inclusions were first reported in Russian alexandrites. Tourmaline crystals, chemically identified as

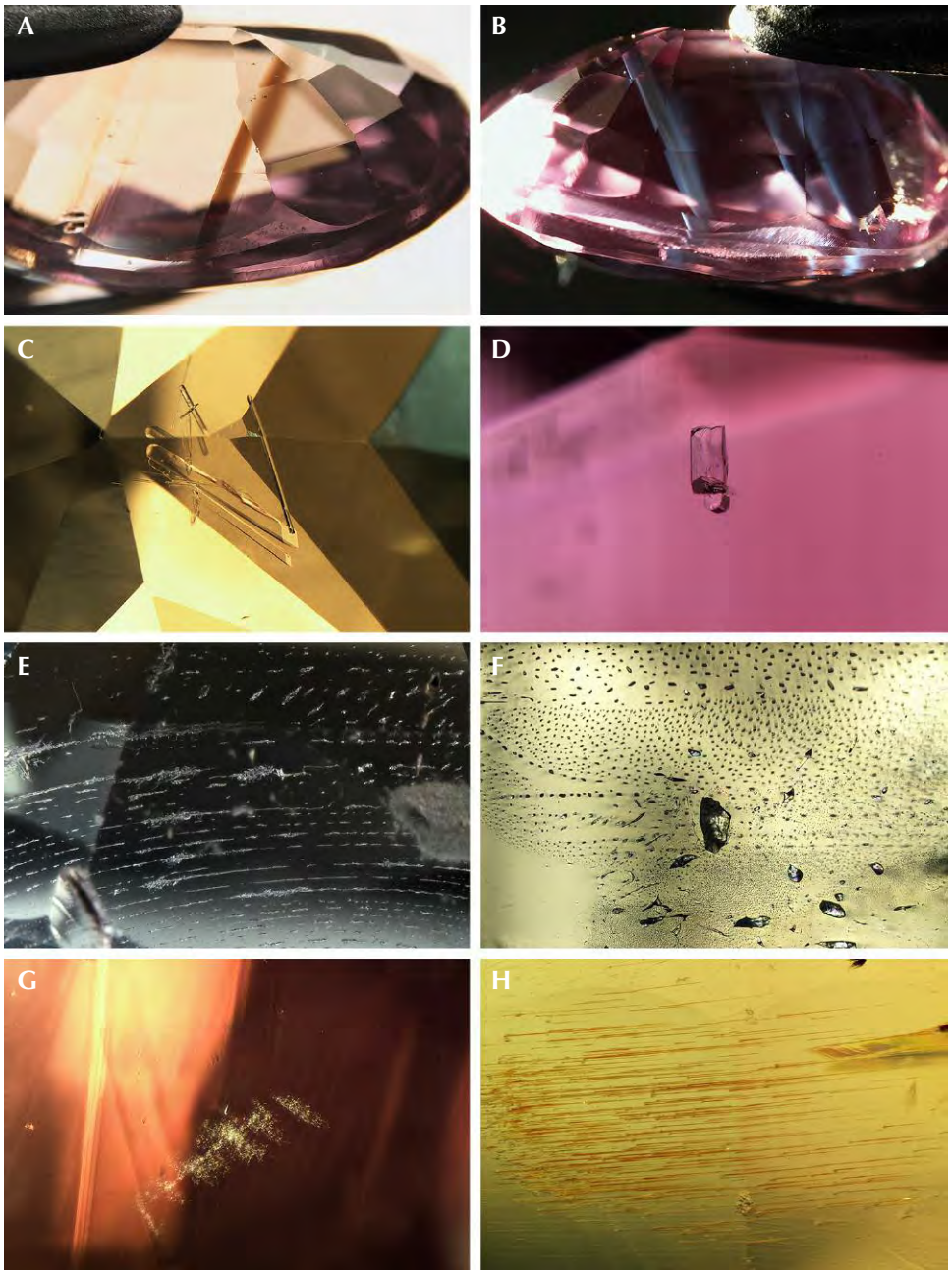

Figure 14. Inclusions in Sri Lankan alexandrite. A: Brown color zoning and strong parallel graining under brightfield illumination. B: The same brown color zoning in (A) becomes milky bands under darkfield and oblique fiber-optic illumination. C: Well-formed prismatic sillimanite crystals under darkfield and oblique fiber-optic illumination. D: Euhedral feldspar crystal under diffused illumination. E: Fingerprints formed by parallel lines of fluids and tiny crystals under darkfield and diffused fiber-optic illumination. F: Irregularly shaped crystals and fingerprints composed of two-phase and multiphase fluid inclusions under darkfield illumination. G: Flake-like cloud of particles under oblique fiber-optic illumination. H: Tubes with brownish oxide stains under diffused fiber-optic illumination. Fields of view: 7.19 mm (A), 7.19 mm (B), 2.90 mm (C), 1.99 mm (D), 2.90 mm (E), 3.57 mm (F), 1.44 mm (G), and 1.99 mm (H). Photomicrographs by Tyler Smith (A–D) and Jonathan Muyal (E–H).

dravite by LA-ICP-MS (Sun et al., 2019), may be diagnostic of the origin, although additional observations are needed to confirm this. Sometimes it is not difficult to see pseudo-hexagonal growth sections shown in different colors under brightfield illumination between crossed polarizers (figure 15E). Graphite film, resembling a spaceship in figure 15F, has been occasionally observed in Russian material. Rounded cotton-like clouds composed of tiny particles (figure 15G) show unique texture and may be diagnostic. Planes of fluid inclusions (figure 15H) have also been observed. Further work is underway to collect additional information on reliably sourced Russian alexandrite. Mica (e.g., phlogopite and biotite) and amphibole inclusions are most commonly observed in Russian alexandrites (Gübelin and Koivula, 1986).

Tanzania. For alexandrite from Tanzania, inclusions of actinolite crystals, mica, monazite, xenotime, and rounded metamict zircon have been observed (Gübe-

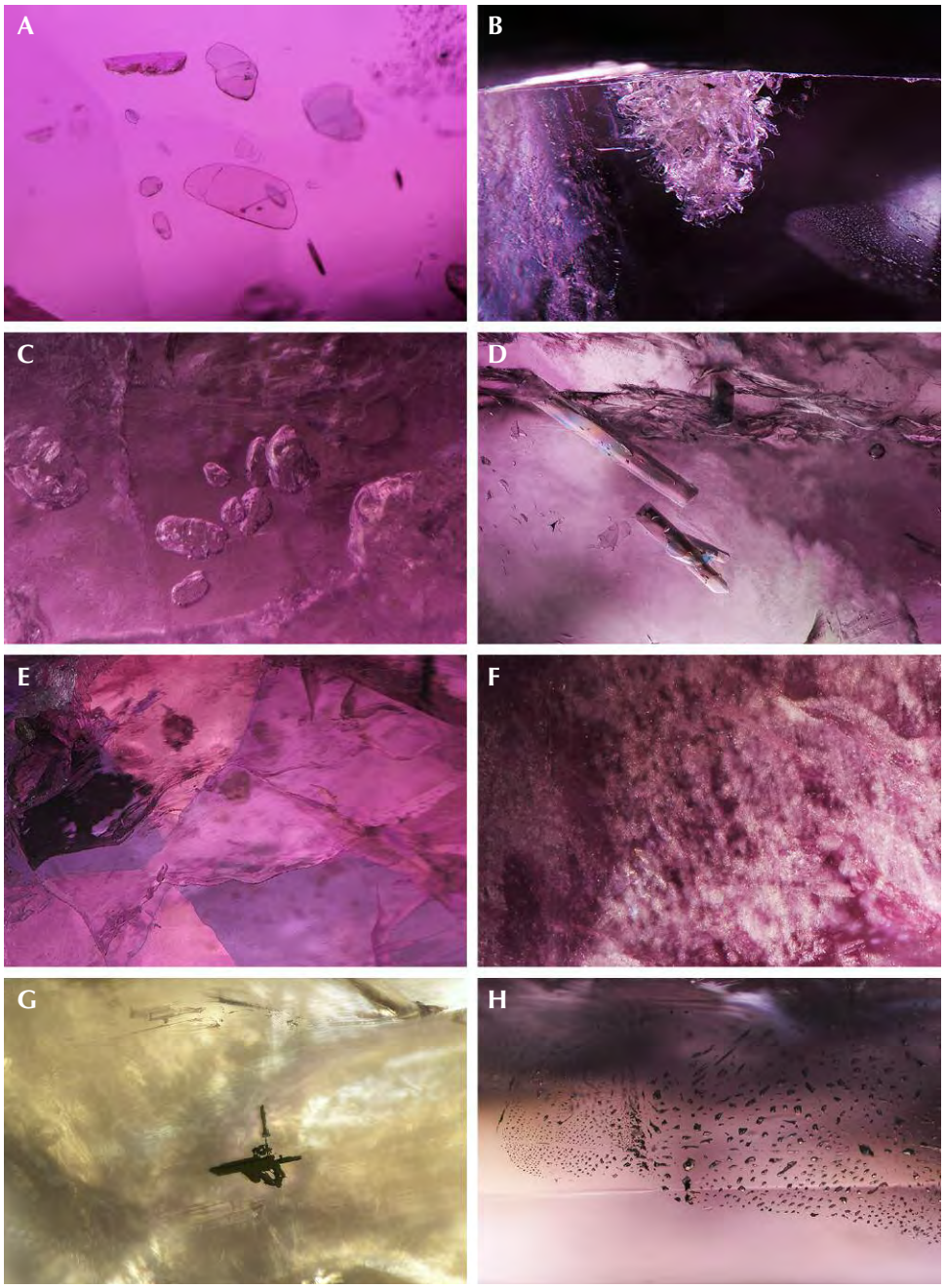

Figure 15. Inclusions in Russian alexandrite. A: Rounded, unevenly shaped flat transparent phlogopite crystals under darkfield illumination. B: A dense cluster of colorless, bladed phlogopite crystals breaks the surface of the stone under darkfield and oblique fiber-optic illumination. C: Corroded and rounded fluorite crystals under diffused illumination. D: Prismatic rod-like tourmaline crystals under brightfield illumination between crossed polarizers. E: Pseudo-hexagonal growth sections shown in different colors under brightfield illumination between crossed polarizers. F: Graphite film under darkfield illumination. G: Rounded cotton-like clouds under oblique fiber-optic illumination. H: Minute two-phase and multiphase fluid fingerprints under diffused illumination. Fields of view: 0.80 mm (A), 1.99 mm (B), 1.26 mm (C), 1.44 mm (D), 3.57 mm (E), 0.72 mm (F), 4.79 mm (G), and 1.44 mm (H). Photomicrographs by Makoto Miura (A), Tyler Smith (B), and Jonathan Muyal (C–H).

lin and Koivula, 1986). Currently, there are only a few images of crystals and fingerprint-like inclusions in GIA's production database. Groups of prismatic apatite crystals (figure 16A, B, and C) and nests of fine silk (figure 16D) have been observed in one Tanzanian alexandrite.

India. Fingerprint-like inclusions in Indian alexandrite are usually composed of tiny needles and oval and round reflective particles (figure 17A, B, and C). This feature may be diagnostic of the origin, although additional observations are needed to confirm this. Occasionally, zircon crystals (figure 17D) with tension fissures have been observed. Figure 17E shows two adjacent crystals with unknown identity; the larger one shows a metallic luster. Groups of elongate negative crystals (figure 17F) are also observed sometimes in Indian alexandrite. Additionally, mica flakes (biotite, muscovite, etc.) are often observed (Panjikar and Ramchandran, 1997). Quartz

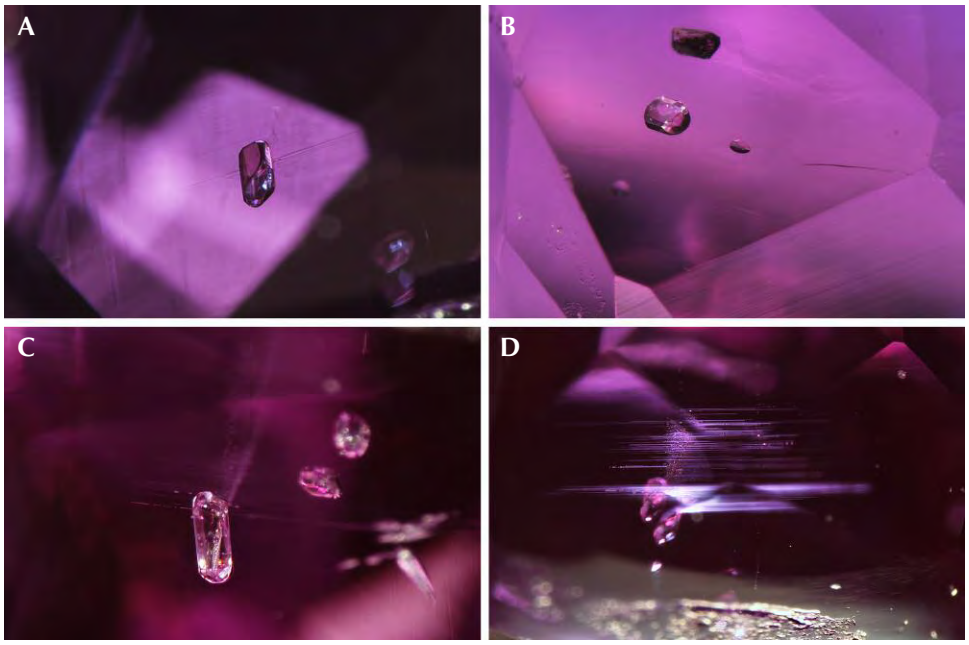

Figure 16. Inclusions in Tanzanian alexandrite. A: Prismatic apatite crystal with slightly rounded edges and uneven termination. B: Large colorless apatite crystal on the left and smaller, slightly tapered phlogopite crystal on the right. C: Apatite crystal with faint needles and particles. D: Nest of fine silk and small platelets. The "X" is an artifact from the facet junctions. Fields of view: 1.99 mm (A), 1.76 mm (B), 1.76 mm (C), and 2.90 mm (D). Photomicrographs by Tyler Smith; oblique fiber-optic and darkfield illumination.

and apatite crystals (Patnaik and Nayak, 1993) are sometimes randomly scattered or in isolation. Needles of rutile and colorless sillimanite can also be observed (Panjikar and Ramchandran, 1997).

Other Localities. GIA lacks inclusion information on alexandrite from Madagascar, Zimbabwe, Zambia, and Myanmar. The field gemology team is actively working to expand GIA's reference collection for these stones.

CONCLUSIONS

Determining alexandrite's geographic origin is a complicated process that requires careful examination of a wide range of physical and chemical properties. In order to make a final determination, we evaluate a combination of the three most important characteristics: trace element chemistry, color-change behavior under daylight-equivalent lighting and incandescent illumination, and inclusions. Of these three characteristics, trace element chemistry obtained from LA-ICP-MS is the primary consideration. Color and inclusions are used as secondary factors to support the origin determination derived from trace element chemistry.

The trace elements Mg, Fe, Ga, Ge, and Sn are the five best discriminators to distinguish alexandrite from the major producing countries of Russia (figure 18), Sri Lanka, Brazil, India, and Tanzania. B, V, and Cr are good discriminators for separating alexandrites among some countries, but they must be considered as a complement to the first five trace elements with specific criteria, rather than on their own.

Most Sri Lankan alexandrites have a yellowish green component in daylight-equivalent lighting and a brownish or orangy component in incandescent illumination. Brazilian alexandrites have a bluish green component in daylight-equivalent lighting and a purple to purplish red component in incandescent illumination. The color characteristics of alexandrites from other sources are less well known at the moment, but this remains an area of active research.

Sulfides with metallic luster may be diagnostic inclusions for Brazilian alexandrites. Prismatic rod-like tourmaline crystals and rounded cotton-like clouds composed of tiny particles may be diagnostic for Russian alexandrites. Fingerprint-like inclusions composed of tiny needles and oval and round reflective particles may be unique to Indian alexandrites. Strong brown color zoning is a good indication of Sri Lankan origin. Characterization of inclusion scenes in alexandrite from the various localities is an active area of research in this project, and future work may help identify additional microscopic indicators of a stone's origin.

Alexandrite origin is an ongoing project for the GIA research and identification department. One of the largest efforts on this front is to add samples obtained by GIA's field gemology team to our reference database. It can be difficult to find reliable alexandrite samples from secondary deposits such as Sri Lanka,

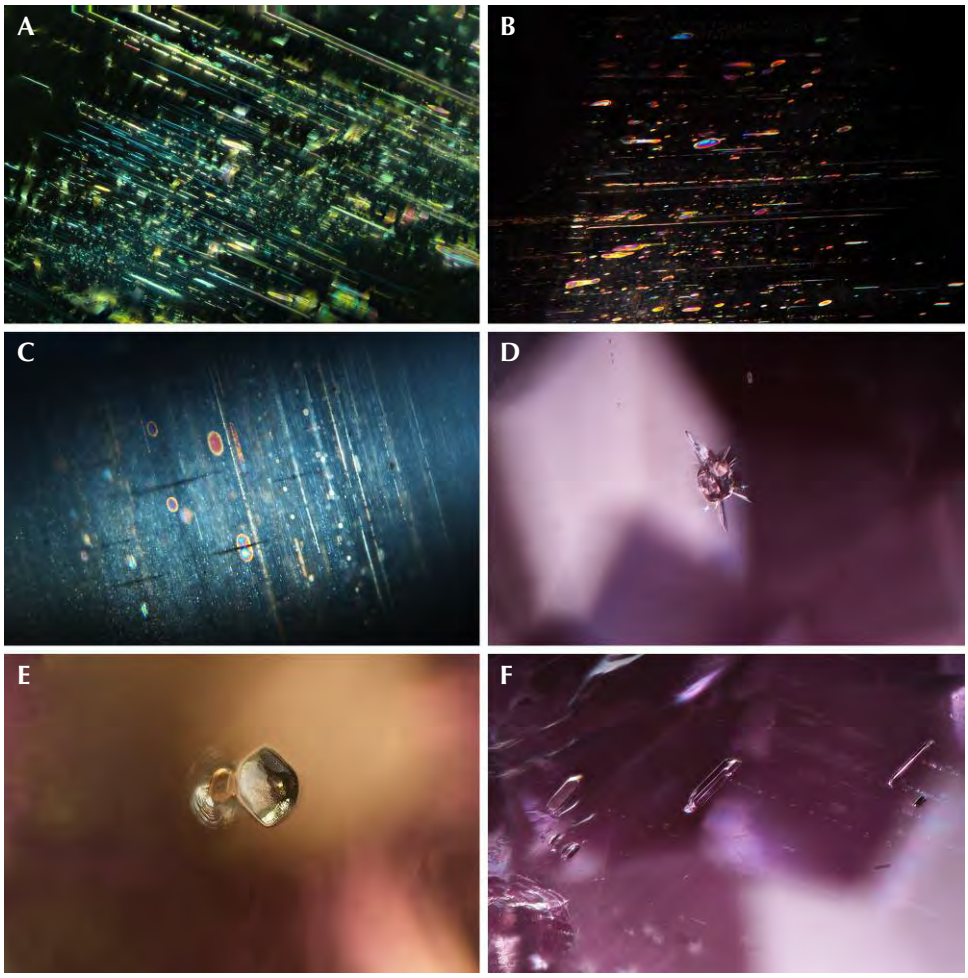

Figure 17. Inclusions in Indian alexandrite. A: Needles and tiny oval-shaped reflective particles under oblique fiber-optic and darkfield illumination. B: Needles and tiny oval reflective particles under darkfield illumination. C: Needles, a minute and large reflective oval, and round particles under darkfield illumination. D: Zircon crystal inclusion surrounded by tension fissures under darkfield illumination. E: Large unknown crystal with metallic luster and adjacent small crystal with halo-like tension fissure under darkfield illumination. F: Elongate negative crystals under diffused illumination. Fields of view: 0.72 mm (A), 1.26 mm (B), 2.41 mm (C), 1.26 mm (D), 1.44 mm (E), and 1.58 mm (F). Photomicrographs by Jonathan Muyal (A, B, D, E, F) and Makoto Miura (C).

Tunduru in Tanzania, or Ilakaka in Madagascar. That is why our reference data were obtained from trusted members of the trade or the GIA Museum. As this new origin service evolves, future efforts of the field gemology team will focus on obtaining samples from these sources as material becomes available. Addi-

Figure 18. Russian alexandrite in daylight-equivalent light (left) and incandescent light (right). The twinned crystal from Malysheva measures 32.35 mm, and the faceted stone weighs 2.61 ct. Photos by Robert Weldon/GIA; courtesy of William Larson.

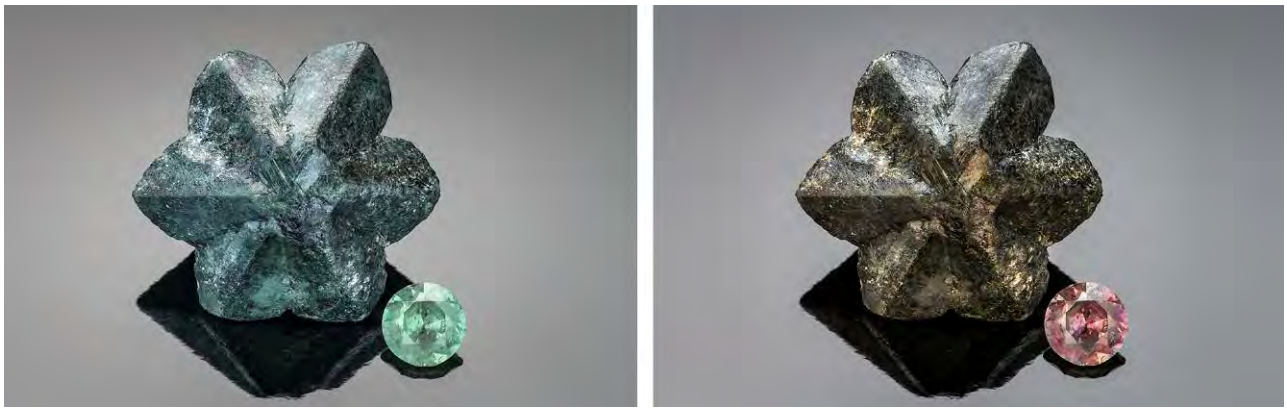

tionally, the internal crystal growth pattern and morphology of rough crystals have been used as factors for geographic origin determination by other researchers (Schmetzer, 2011; Schmetzer and Malsy, 2011a,b). These two areas can enhance our current methods and are worth investigating. Third, different deposits within a country can contain crystals with very different morphologies, producing material with varying trace element chemistries that show different colors and inclusions. Further work will be needed to collect additional data on stones from all major locations in order to delineate the differences, not only for alexandrite from different geographic locations but also for alexandrite from a single source. In this there is a truth that applies to all gemological laboratories, no matter how mature and well established: We must remain vigilant and continue expanding the state of our gemological knowledge if we are to uncover the story of any precious stone that passes through our hands.

ABOUT THE AUTHORS

Mr. Sun is a research associate, Dr. Palke is a senior research scientist, Mr. Muyal is a former staff gemologist, Mr. DeGhionno is senior manager of colored stone services, and Mr. McClure is global director of colored stone services at GIA's laboratory in Carlsbad, California.

ACKNOWLEDGMENTS

The authors deeply thank Omi Privé for providing high-end alexandrite jewelry and faceted stones for photography. Evan Caplan, John Koivula, and LC Gem Collection Inc. are greatly thanked for providing high-end faceted alexandrite and rough mineral specimens for photography. Warren Boyd, Evan Caplan, Vincent Pardieu, Chandika Thambugala, Nilam Alawdeen, Yusuke Katsurada, Lance Davidson (Davidson Inc.), LC Gems Collection Inc., and Spectrum Fine Jewelry & Exotic Gems are thanked for providing alexandrite stones for chemical analysis and taking photomicrographs of inclusions to build our reference database. We are deeply grateful to Robert Weldon and Kevin Schumacher for their alexandrite photos. Robison McMurtry and Diego Sanchez provided GIA's digital imaging procedures for color-change stones. Many thanks are owed to Yusuke Katsurada, Makoto Miura, Sudarat Saeseaw, Vararut Weeramonkhonlert, Daniel Girma, Tyler Smith, Virginia Schneider, Mei Mei Sit, Sze Ling Wong, Chun Fai Chow, Nathan D. Renfro, Claire Malaquias, and Christopher M. Breeding for constant support and contributions on sample testing and data collection and the important suggestions they provided throughout the project.

REFERENCES

Alexandrite world occurrences & mining localities (n.d.) Alexandrite Tsarstone Collectors Guide, https://www.alexandrite.net/localities/index.html

Bevan A.W.R., Downes P.J. (1997) Alexandrite chrysoberyl from Dowerin, Western Australia: Revisited. *Australian Gemmologist*, Vol. 19, No. 11, pp. 460–463.

Brown G., Kelly S.M.B. (1984) Alexandrite-chrysoberyl from Zimbabwe. *Australian Gemmologist*, Vol. 15, No. 8, pp. 275–278.

Brunel F. (1972) *Jewellery of India: Five Thousand Years of Tradition*. National Book Trust, New Delhi, 82 pp.

Cassedanne J., Roditi M. (1993) The location, geology, mineralogy and gem deposits of alexandrite, cat's-eye and chrysoberyl in Brazil. *Journal of Gemmology*, Vol. 23, No. 6, pp. 333–354.

Costanza F. (1998) Supplies of alexandrite are scarcer than ever. *National Jeweler*, Vol. 42, No. 5, pp. 16–18.

Downes P.J., Bevan A.W.R. (2002) Chrysoberyl, beryl and zincian spinel mineralization in granulite-facies Archaean rocks at Dowerin, Western Australia. *Mineralogical Magazine*, Vol. 66, No. 6, pp. 985–1002, http://dx.doi.org/10.1180/0026461026660072

Groat L.A., Giuliani G., Stone-Sundberg J., Renfro N.D., Sun Z. (2019) A review of analytical methods used in geographic origin determination of gemstones. *G&G*, Vol. 55, No. 4, pp. 512–535, http://dx.doi.org/10.5741/GEMS.55.4.512

Gübelin E.J. (1976) Alexandrite from Lake Manyara, Tanzania. *G&G*, Vol. 15, No. 7, pp. 203–209.

Gübelin E.J., Koivula J.I. (1986) *Photoatlas of Inclusions in Gemstones, Vol. 2*. Opinio Publishers, Basel, Switzerland, 829 pp.

Hänni H.A. (1999) …. And other gems from near Ilakaka. *G&G*, Vol. 35, No. 2, p. 150.

Henricus J. (2001) New gem rush in Tanzania. *Jewellery News Asia*, No. 197, pp. 78–80.

Jarrett D. (2015) The story behind the stone: Another source, another phenomenon. *Mid-America Jewelry News*, Nov. 1, p. 22, https://midamericajewelrynews.com/columnists/diana-jarrett/3135-the-story-behind-the-stone-another-source-another-phenomenon

Jochum K.P., Nohl U., Herwig K., Lammel E., Stoll B., Hofmann A.W. (2005) GeoReM: A new geochemical database for reference materials and isotopic standards. *Geostandards and Geoanalytical Research*, Vol. 29, No. 3, pp. 333–338, http://dx.doi.org/10.1111/j.1751-908X.2005.tb00904.x

Johnson M.L., Koivula J.I. (1996) Gem News: Gem materials from the new locality at Tunduru, Tanzania. *G&G*, Vol. 32, No. 1, pp. 58–59.

——— (1997) Gem News: Tunduru-Songea gem fields in southern Tanzania. *G&G*, Vol. 33, No. 4, p. 305.

Koivula J.I. (1987a) Gem News: Brazilian alexandrites. *G&G*, Vol. 23, No. 2, p. 123.

——— (1987b) Gem News: More on Brazilian alexandrites. *G&G*, Vol. 23, No. 4, pp. 238–240.

Koivula J.I., Kammerling R.C. (1988) Gem News: Inclusions identified in new Brazilian alexandrites. *G&G*, Vol. 24, No. 1, p. 59.
Kozlov Y.S. (2005) *Alexandrite*. Nauka Publishers, Moscow, 144 pp.
Levine G.B. (2008) Gemology: Alexandrite—It's magic. *Adornment*, Vol. 7, No. 2, p. 7.
Milisenda C.C., Henn U., Henn J. (2001) New gemstone occurrences in the south-west of Madagascar. *Journal of Gemmology*, Vol. 27, No. 7, pp. 385–394.
Newlay S.K., Pashine J.K. (1993) A note on the finding of rare gemstone alexandrite in Madhya Pradesh. In *National Seminar on Gemstones*, Society of Geoscientists and Allied Technologists, Bhubaneswar, India, December 11–12, pp. 88–89.
Palke A.C., Saeseaw S., Renfro N.D., Sun Z., McClure S.F. (2019) Geographic origin determination of blue sapphire. *G&G*, Vol. 55, No. 4, pp. 536–579, http://dx.doi.org/10.5741/GEMS.55.4.536
Panjikar J., Ramchandran K.T. (1997) New chrysoberyl deposits from India. *Indian Gemmologist*, Vol. 7, No. 1/2, pp. 3–7.
Patnaik B.C., Nayak B.K. (1993) Alexandrite occurrence in Orissa. In *National Seminar on Gemstones,* Society of Geoscientists and Allied Technologists, Bhubaneswar, India, December 11–12, p. 87.
Proctor K. (1988) Chrysoberyl and alexandrite from the pegmatite districts of Minas Gerais, Brazil. *G&G*, Vol. 24, No. 1, pp. 16–32, http://dx.doi.org/10.5741/GEMS.24.1.16
Renfro N. (2015a) Digital photomicrography for gemologists. *G&G*, Vol. 51, No. 2, pp. 144–159, http://dx.doi.org/10.5741/GEMS.51.2.144
——— (2015b) The application of differential interference contrast microscopy to gemmology. *Journal of Gemmology*, Vol. 34, No. 7, pp. 616–620.
Schmetzer K. (2010) *Russian Alexandrites*. Schweizerbart Science Publishers, Stuttgart, Germany, 141 pp.
——— (2011) Measurement and interpretation of growth patterns in chrysoberyl, including alexandrite. *Journal of Gemmology*, Vol. 32, No. 5-8, pp. 129–144.
Schmetzer K., Malsy A.-K. (2011a) Natural alexandrite with an irregular growth pattern: A case study. *Journal of the Gemmological Association of Hong Kong*, Vol. 32, pp. 68–75, http://www.gahk.org/journal/Alexandrite_for%20web_v1.pdf
——— (2011b) Alexandrite and colour-change chrysoberyl from the Lake Manyara alexandrite-emerald deposit in northern Tanzania. *Journal of Gemmology*, Vol. 32, No. 5-8, pp. 179–209.
Schmetzer K., Stocklmayer S., Stocklmayer V., Malsy A.-K. (2011) Alexandrites from the Novello alexandrite-emerald deposit, Masvingo District, Zimbabwe. *Australian Gemmologist*, Vol. 24, No. 6, pp. 133–147.
Soman K., Nair N.G K. (1985) Genesis of chrysoberyl in the pegmatites of southern Kerala, India. *Mineralogical Magazine*, Vol. 49, No. 354, pp. 733–738.
Stockton C.M., Kane R.E. (1988) The distinction of natural from synthetic alexandrite by infrared spectroscopy. *G&G*, Vol. 24, No. 1, pp. 44–46, http://dx.doi.org/10.5741/GEMS.24.1.44
Sun Z., Palke A.C., Breeding C.M., Dutrow B.L. (2019) A new method for determining gem tourmaline species by LA-ICP-MS. *G&G*, Vol. 55, No. 1, pp. 2–17, http://dx.doi.org/10.5741/GEMS.55.1.2
Valentini P. (1998) Current mining report for India. *ICA Gazette*, pp. 8–10.
Voynick S. (1998) Cat's-eye chrysoberyl. *The Guide*, Vol. 17, No. 1, pp. 13–15.
Zoysa E.G. (1987) An account of chrysoberyl-bearing pegmatite near Pattara, Sri Lanka. *Journal of Gemmology*, Vol. 20, No. 7/8, pp. 486–489.
Zoysa G. (2014) Geology and gem deposits of Sri Lanka. *InColor*, No. 27, pp. 38–41.
Zwaan P.C. (1982) Sri Lanka: The gem island. *G&G*, Vol.18, No. 2, pp. 62–71, http://dx.doi.org/10.5741/GEMS.18.2.62

What's Next?

Shane F. McClure, Thomas M. Moses, and James E. Shigley

Here at the end we are left with the question "What's next?" Geographic origin determination is likely here to stay. In fact, like it or not, it may expand to other gemstones. As to which gemstones that will be, it depends entirely on whether or not there is a demand for this service. The reason? It takes a lot of time, effort, and expense to develop criteria for any gemstone, but if there is a significant demand for it, there is reason to pursue it.

Take demantoid garnet as an example. It is a small market because of availability, but there is a demand for demantoid from Russia versus other deposits, and there are not that many deposits known in the world. Therefore, this is a reasonable service to offer. Some laboratories already do.

On the other hand, we have occasionally been asked if we could do geographic origin on amethyst. Whether amethyst carries enough value to justify the expense is not for the laboratories to say. However, amethyst comes from so many locations around the world that the cost of developing such a service would be prohibitive in relation to the market value of amethyst. It is also quite likely that for this same reason the overlap of properties would be so severe as to make separation impossible.

CAN WE IMPROVE THIS SERVICE?

Since geographic origin is here to stay, one of our primary focuses should be to improve how it's done. It is safe to say that everyone involved would like nothing more than to make it less of an opinion and improve the overall consistency.

How do we do that? The most significant way is to pursue advances in technology or to try to adapt technologies that have been developed for other industries. Some examples of techniques that are currently being researched for gemstone applications are:

- Isotopic analysis
- Ultraviolet fluorescence mapping
- Ultraviolet fluorescence spectroscopy
- Raman mapping
- Photoluminescence spectroscopy
- Cathodoluminescence spectroscopy

It is important to note that adapting instrumentation to work with gemstones is usually not easy. Sample holders might need to be designed and built, sample chambers might need to be modified, and different procedures might need to be developed, all because we might be attempting to use an instrument in a way it was not originally designed for.

None of these instruments were developed with valuable, relatively fragile test subjects in mind. When scientists in other fields want to test a sample, they are usually not concerned about the worth of that sample. Typically the samples they use have little intrinsic value. If an X-ray powder diffraction analysis is needed, a piece of the sample may be ground to dust and that powder used for analysis. Obviously this won't work for faceted gemstones. To solve this problem, one of GIA's famous gemologists of the past, Charles Fryer, developed a technique that used a scraper made of a diamond mounted on a brass rod that was used to remove a microscopic amount of material from the girdle of a faceted stone. This powder was mounted on a tiny glass fiber to obtain a diffraction pattern with no weight loss and no eye-visible damage to the stone. The advent of Raman spectroscopy made this technique almost obsolete.

Progress also defines new and ever challenging limitations in analysis. The typical instrument for chemical analysis of gemstones prior to about 2003 was EDXRF (energy-dispersive X-ray fluorescence spectroscopy). While it is a good technique that is completely nondestructive and more of a bulk sampling method, which is a plus in many cases, it cannot detect elements lighter than sodium on the periodic table, it is difficult to achieve truly quantitative results, and it typically has much higher detection limits than mass spectrometry techniques.

In 2003, when the beryllium treatment of sapphire was finally understood, the need for chemical analysis of lighter elements at low concentrations became necessary. The technique called LA-ICP-MS (laser ablation–inductively coupled plasma–mass

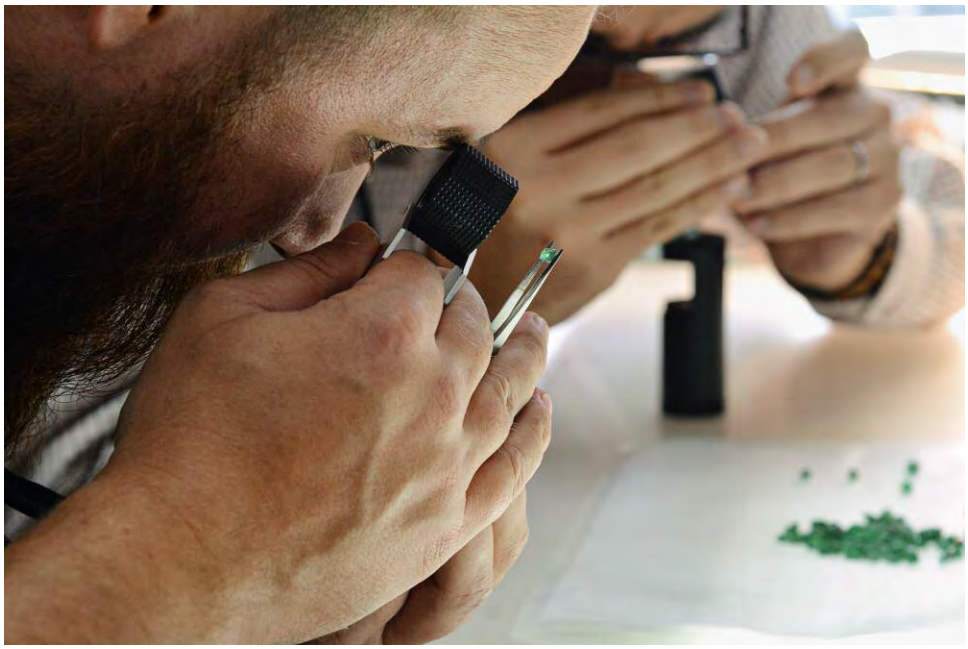

Wim Vertriest examines emeralds at the Mariinsky Priisk (formerly Malysheva) mine in the Ural Mountains of Russia. Photo by Aaron Palke.

spectrometry) allows true quantitative analysis of almost all the elements on the periodic table at very low concentrations. The drawbacks: The instrument is expensive to buy and maintain. It takes skilled personnel to operate and maintain it and to correctly analyze the data that come from it. Also, it is a micro-sampling technique that only analyzes material from a small spot on the stone, so multiple spots are necessary to get an accurate picture of a stone's chemistry.

Accurate, repeatable data for such a machine highly depends on the standards one uses. Poor standards will produce poor results. GIA felt it necessary to produce in-house corundum standards for testing rubies and sapphires since a great many of these stones are tested in the laboratory. These standards did not exist previously and took a great deal of time and expense to create.

This is just one example of the problems faced by gemological researchers. Sometimes there just isn't any information available on a given subject. When beryllium was discovered as a treatment in corundum, it quickly became clear that almost no data existed concerning this element in this material. Everything we know today had to be collected and analyzed subsequent to the advent of this treatment.

How do we know or learn about techniques or instrumentation that might be out there somewhere waiting to be discovered? We go outside the usual gemological sources and try to connect with bright young students, and universities and other institutions that are performing research that might cross over to our needs. To this end, GIA has an active postdoctoral program and an internship program in which we hope to find young talent with fresh ideas who might be interested in the world of gemstones. We also reach out and work with well-established ge-

False-color mapping of Cr^{3+} luminescence intensity reveals growth features in this Sri Lankan sapphire at a high level of resolution. This information is not evident in the color zoning of the stone.

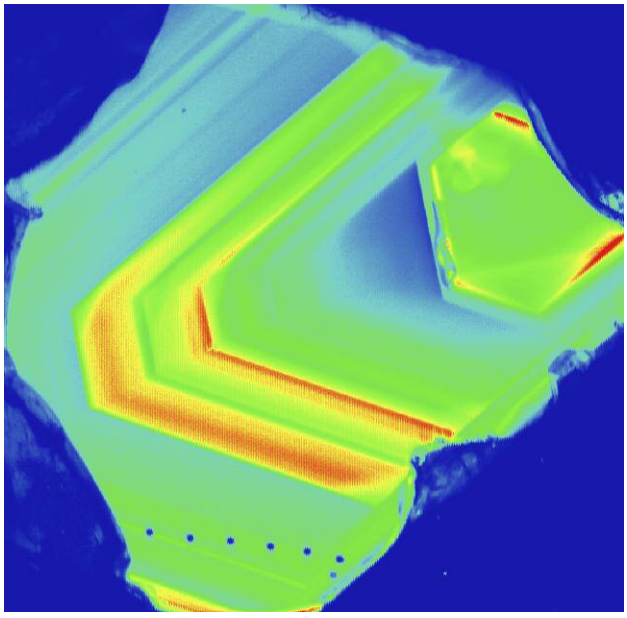

A GIA field gemology team visiting a dealer in Mogok, Myanmar. Photo by Robert Weldon/GIA.

ologists, mineralogists, physicists, and others in major institutions such as Caltech, the Smithsonian Institution, the Carnegie Institution, and universities in Louisiana, Wisconsin, and elsewhere.

TIMES ARE CHANGING

The whole concept and need for geographic origin determination of colored stones has until recently been largely focused on the monetary value of a gemstone based on its provenance. This has been the case for a long time.

However, we are forced to recognize that the use of this kind of information is no longer limited to value alone. It cannot be denied that geographic origin has become important in other ways. In 2019 the United States government stated that they are watching the jewelry industry and considering passing regulations that will require jewelers to have knowledge of where the materials they sell originated. This is not because they are concerned about the value of stones being sold. They are concerned about terrorism and money laundering. It may soon be required that all jewelers have documentation declaring the source of their gemstones and precious metals.

The other concern is that the millennial generation—the young adults of the world—are less concerned with value and "sparkle" than with the social and economic impact of what they buy. Is it ethical, is it sustainable, is it damaging to the environment, is child labor being used to produce it? These and other questions are important to them. The jewelry industry needs to pay attention, and geographic origin determination will play a significant role in providing some answers.

Finally, we should ask ourselves if geographic origin and all the other services and information the industry provides the jewelry-buying public are really in the public's best interest. This is a difficult but important question to answer. GIA's mission is to ensure the public trust in gems and jewelry, and we firmly believe that it is necessary to continually ask ourselves if what we do is in the best interest of the public. We also must reconcile industry wishes with the limitations of science in determining the geographic origin of a gemstone.

Mr. McClure is global director of colored stone services, Mr. Moses is chief laboratory and research officer, and Dr. Shigley is a distinguished research fellow, at the Gemological Institute of America.

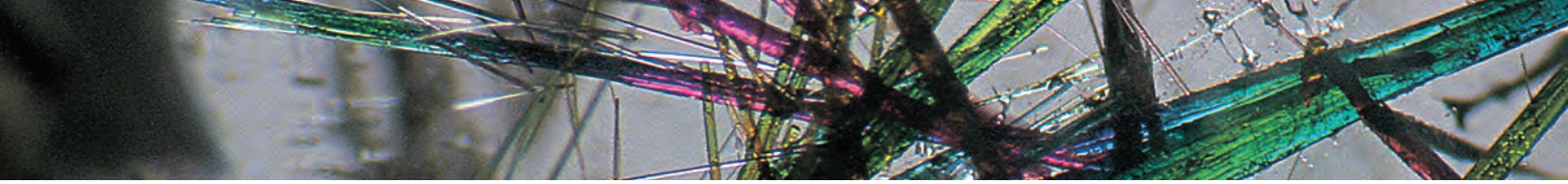

GIA®

Liddicoat Postdoctoral Research Fellowships in Mineralogy, Materials Science and Gemology at GIA

GIA (Gemological Institute of America®) invites qualified candidates to apply for the Richard T. Liddicoat Postdoctoral Research Fellowships at its Carlsbad, California and New York City locations. The one- to two-year fellowships encourage early career scientists to pursue full-time academic research in mineralogy, geology, physics, materials science and other fields related to gemology – the study of diamonds, colored gemstones, pearls and their treatment. Fellows are expected to conduct creative, independent, publishable research and collaborate with GIA scientists, outside research institutions and universities.

The fellowship includes a competitive annual stipend ($60,000+), research funding and approved travel subsidies. Benefits include health, dental and vision, and potential reimbursement of relocation expenses.

The start date of each fellowship is flexible, but accepted candidates should begin by Jan. 31, 2021. Applicants must have received their Ph.D. in a relevant field by the start date, and preferably within the last three years.

Applications are due by April 30, 2020. For more information visit **GIA.edu/research-careers**

Evan Smith, Ph.D.

GIA Research Fellow Unveils Clues About Earth's Mantle

In a recent study published in *Science* magazine (Dec. 16, 2016), GIA Postdoctoral Research Fellow Evan Smith and coauthors uncovered clues about Earth's deep mantle by examining the distinct characteristics of large, exceptional gem diamonds known as "CLIPPIR" diamonds. Not normally available for research, inclusions found in these cut diamond pieces led to two breakthrough discoveries.

Established in 1931, GIA is the world's foremost authority on diamonds, colored gemstones and pearls. A public benefit, nonprofit institute with locations in 13 countries, GIA is the leading source of research knowledge, standards and education in gems and jewelry. Visit **GIA.edu**

CARLSBAD NEW YORK ANTWERP BANGKOK DUBAI GABORONE HONG KONG
JOHANNESBURG LONDON MUMBAI RAMAT GAN SURAT TAIPEI TOKYO